Rhodes University
Grahamstown

Synthesis and Characterisation of Novel Platinum(II) Complexes: Potential Chemotherapeutic Drugs

A thesis submitted in fulfilment of the requirements for the degree of

DOCTOR OF PHILOSOPHY

by

MICHAEL STEVEN DATT

January 2001

To my late grandfather, Lorie Rabenowitz

ABSTRACT

The present study involves the preparation of novel mixed-ligand platinum(II) complexes in the hope of expanding the range of platinum(II) complexes that exhibit anticancer activity and which are less toxic and have a broader spectrum of activity than cisplatin and its analogues. To this end, *N*-(3-*R*-benzoyl)-*N',N'*-diethylthiourea, *N*-(3-*R*-benzoyl)-*N'*-morpholinothiourea, *N*-(3-*R*-benzoyl)-*N',N'*-di(2-hydroxyethyl)thiourea (R = NO_2, Cl, H, CH_3, OCH_3), *N,N*-diethyl-*N'*-menthyloxycarbonylthiourea and *N*-menthyloxycarbonyl-*N'*-morpholinothiourea ligands, and their corresponding mixed-ligand platinum(II) complexes of the type [PtCl(L)(RR'SO)], were synthesised and characterised by elemental analyses, IR, ^{1}H and ^{195}Pt NMR spectroscopy and, in some cases, X-ray crystallography. Dimethylsulfoxide complexes were prepared using all the ligands, while complexes containing unsymmetrically substituted sulfoxides were prepared using the *N*-benzoyl-*N',N'*-diethylthiourea and *N,N*-diethyl-*N'*-(-)-(3*R*)-menthyloxycarbonylthiourea ligands only. The molecular structures of *cis*-(S,S)-[PtCl(DMSO)(L)] (where L = *N*-benzoyl-*N',N'*-diethylthioureato, *N*-(+)-(3*S*)-menthyloxycarbonyl-*N'*-morpholinothioureato), *cis*-(S,S)-[Pt(*N*-benzoyl-*N',N'*-diethylthioureato)Cl(MPSO)] and *cis*-[Pt(*N*-benzoyl-*N',N'*-diethylthioureato)$_2$] were determined by X-ray crystallography. The X-ray crystal structure of *N,N*-diethyl-*N'*-(-)-(3*R*)-menthyloxycarbonylthiourea was also determined. The spectroscopic and crystallographic data are consistent with complexes containing a (S,O)-chelated ligand and a sulfur-bonded sulfoxide ligand. However, the ^{1}H and ^{195}Pt NMR studies showed that the alkoxycarbonylthioureato complexes exist as geometric isomers with the sulfoxide coordinated either in a *cis*-(S,S) or *trans*-(S,S) arrangement with respect to the sulfur donor atom of the chelated ligand, whereas the acylthioureato complexes yielded only *cis*-(S,S)-[PtCl(L)(RR'SO)] complexes.

The difference in the coordination chemistry of the acylthiourea and alkoxycarbonylthiourea ligands was examined further by treatment of the [PtCl(DMSO)(L)] complexes, where L = *N*-benzoyl-*N',N'*-diethylthioureato, *N*-benzoyl-*N'*-morpholinothioureato, *N,N*-diethyl-*N'*-(-)-(3*R*)-menthyloxycarbonylthioureato and *N*-(+)-(3*S*)-menthyloxycarbonyl-*N'*-morpholinothioureato, with PPh_3 to give the corresponding [PtCl(L)(PPh_3)] and $[Pt(L)(PPh_3)_2]^+$ complexes. ^{31}P NMR studies of these complexes reveal that the alkoxycarbonylthioureato ligands bind less strongly than the acylthioureato ligands, which is consistent with the crystallographic studies. The morpholine derivatives of the acylthioureato and alkoxycarbonylthioureato ligand systems also appear to bind less tightly than the diethyl derivatives. The weaker binding properties of the alkoxycarbonylthioureato ligands might be a possible explanation for the observed geometric isomerisation of these complexes, with the mechanism of isomerisation involving a chelate ring-

opening step. Furthermore, crystallographic and ^{31}P NMR studies suggest that the acylthioureato carbonyl oxygen donor atom is relatively softer and therefore has a greater *trans*-influence than the carbonyl oxygen donor atom of the alkoxycarbonylthioureato ligand.

The substitution kinetics of the chloride and sulfoxide leaving groups by azide, iodide, thiocyanate, triphenylphosphine, 2-mercaptobenzimidazole, 4-(dimethylamino)pyridine and thiourea, from selected *cis*-(S,S)-[PtCl(*N,N*-dialkyl-*N'*-(3-*R*-benzoyl)thioureato)(RR'SO)] complexes, in methanol, were evaluated to determine if variation of the electronic properties of the chelated ligand and variation of the sulfoxide have a significant influence on the reactivity of these complexes. Two consecutive reactions were observed. It was found that neutral nucleophiles initially substitute the dimethylsulfoxide, while anionic nucleophiles substituted the chloride ligand. For all the nucleophiles studied, the first substitution step was evaluated, except for triphenylphosphine and 4-(dimethylamino)pyridine, where the second step was also evaluated. The overall order of reactivity for the first substitution step was; N_3^- < DMAP < I^- < SCN^- < MBI < thiourea < PPh_3, with the rate varying three orders of magnitude. The substitution of the dimethylsulfoxide ligand by PPh_3 from *cis*-(S,S)-[Pt(*N*-benzoyl-*N',N'*-diethylthioureato)Cl-(DMSO)] to form *cis*-(S,P)-[Pt(*N*-benzoyl-*N',N'*-diethylthioureato)Cl(PPh_3)] was confirmed by X-ray crystallography. In general, manipulation of the chelating moiety, as well as interchanging the sulfoxide did not alter the reactivity of these complexes to a great extent.

The anticancer activity of all the platinum(II) sulfoxide complexes were evaluated against a HeLa cell line, of which three complexes, *cis*-(S,S)-[PtCl(DMSO)(*N,N*-diethyl-*N'*-(3-nitrobenzoyl)-thioureato)], *cis*-(S,S)-[PtCl(DMSO)(*N*-morpholino-*N'*-(3-nitrorobenzoyl)thioureato)] and *cis*-(S,S)-[PtCl(DMSO)(*N*-(3-methoxybenzoyl)-*N'*-morpholinothioureato)] exhibited a concentration dependent anti-proliferative effect, but were less potent than cisplatin. These three complexes displayed a similar dose response in a MCF-7 cell line. Preliminary morphology studies with the three biologically active complexes in a HeLa cell line suggest that they induce cell death by apoptosis.

Preliminary pBR322 plasmid DNA binding studies of selected [Pt(acylthioureato)Cl(RR'SO)] complexes clearly indicate that these complexes have a different mode of binding to DNA than cisplatin.

TABLE OF CONTENTS

CHAPTER 3

SYNTHESIS AND CHARACTERISATION OF *N*-ACYL-*N'*,*N'*-DIALKYLTHIOUREA AND *N*-ALKOXYCARBONYL -*N'*,*N'*-DIALKYL-THIOUREA LIGAND SYSTEMS

CHAPTER 4: PART A
SYNTHESIS AND CHARACTERISATION OF
[Pt(ACYLTHIOUREATO)Cl(RR'SO)] COMPLEXES

CHAPTER 4: PART B
SYNTHESIS AND CHARACTERISATION OF
[Pt(ALKOXYCARBONYLTHIOUREATO)Cl(RR'SO)] COMPLEXES

CHAPTER 4: PART C
COMPARISON OF THE COORDINATION CHEMISTRY OF ALKOXYCARBONYLTHIOUREA AND ACYLTHIOUREA LIGAND SYSTEMS

CHAPTER 5
SUBSTITUTION REACTION KINETICS OF ACYLTHIOUREATO PLATINUM(II) SULFOXIDE COMPLEXES

PART A: ANIONIC NUCLEOPHILES

PART B: NEUTRAL NUCLEOPHILES

ACKNOWLEDGEMENTS

I would like to express my sincere appreciation to my supervisor Dr Cheryl Sacht for her guidance and enthusiasm throughout this study. I am sure that the training that I have received will give me a competitive advantage in my future endeavors.

A number of people have made valuable contributions to my research and have assisted in the preparation of this thesis for which I would like to express my appreciation.

- Dr L. Parolis for training me on the NMR and for her assistance in acquiring some of the multinuclear NMR spectra.
- Dr S. Otto and Prof A. Roodt for the crystal structure determinations.
- Prof A. Roodt and Dr S. Otto for their supervision in the kinetic studies.
- Mr H. Engelbrecht for his assistance in acquiring some of the kinetic data.
- Prof J. Seegers and Dr M. –L. Lottering for carrying out the cytotoxicity and morphology studies.
- Prof E. R. Freed-Isserow, Prof M. E. Brown, Emmanuel Lamprecht and Edith Antunes for proof reading this thesis.
- Christopher Gray for assistance with Sigma Plot and HPLC.
- I would like to thank the past members of the Bioinorganic Chemistry Group with whom I have had the pleasure of working. Thank you Lowri, Kerry, Patrick, Richard, Brian, Valerie and Babalwa.
- To my mother and Candice Platt for their support and encouragement throughout this thesis.

I would like to sincerely thank the staff and students of Rhodes University, Chemistry Department for their support, encouragement and friendship throughout the years.

The National Research Foundation (NRF) and Rhodes University provided financial support during my postgraduate research for which I am extremely grateful.

LIST OF PUBLICATIONS

The following publications have resulted from this thesis to date.

1. Synthesis, characterisation and coordination chemistry of novel chiral *N,N*-dialkyl-*N'*-menthyloxycarbonylthioureas. Crystal and molecular structures of *N,N*-diethyl-*N'*-(-)-(3*R*)-menthyloxycarbonylthiourea and *cis*-(S,S)-[Pt(L)Cl(DMSO)] [where HL = *N*-(+)-(3*S*)-menthyloxycarbonyl-*N'*-morpholino-thiourea or *N*-benzoyl-*N',N'*-diethylthiourea].
   C. Sacht, M. S. Datt, S. Otto, A. Roodt, *J. Chem. Soc., Dalton Trans*., 2000, 4579.

2. Synthesis and characterisation of mixed-ligand platinum(II)-sulfoxide complexes, [PtCl(DMSO)(L)], for potential use as chemotherapeutic agents (HL = *N,N*-dialkyl-*N'*-(3-*R*-benzoyl)thiourea).
   C. Sacht, M. S. Datt, *Polyhedron*, 2000, **19**, 1347.

3. Chiral and achiral platinum(II) complexes for potential use as chemotherapeutic agents: crystal and molecular structures of *cis*-[Pt(L^1)$_2$] and [Pt(L^1)Cl(MPSO)] [HL^1 = *N,N*-diethyl-*N'*-benzoylthiourea].
   C. Sacht, M. S. Datt, S. Otto, A. Roodt, *J. Chem. Soc., Dalton Trans*., 2000, 727.

LIST OF FIGURES

LIST OF TABLES

LIST OF ABBREVIATIONS

DMSO	Dimethylsulfoxide
MPSO	Methylphenylsulfoxide
(*S*)-MTSO	(*S*)-Methyltolylsulfoxide
(*R*)-MTSO	(*R*)-Methyltolylsulfoxide
Ph_2SO	Diphenylsulfoxide
MeBzSO	Methylbenzylsulfoxide
Bz_2SO	Benzylsulfoxide
^{i}PrSO	Isopropylsulfoxide
en	Ethylenediamine
Me_4en	*N,N,N',N'*-Tetramethylethylenediamine
dach	1,2-diaminocyclohexane
damch	1,2-bis(aminomethyl)cyclohexane
dien	1,5-diamino-3-azapentane
bipy	2,2'-Bipyridine
phen	1,10-Phenanthroline
quin	Quinoline
isoquin	Isoquinoline
Tz	Thiazole
pic	Picoline or 4-methylpyridine
py	Pyridine
RR'SO	Sulfoxide
5'-GMP	5'-Guanosine monophosphate
5'-AMP	5'-Adenosine monophosphate
5'-TMP	5'-Thymosine monophosphate
5'-CMP	5'-Cytidine monophosphate
DNA	Deoxyribose nucleic acid
A	Adenine
C	Cytosine
T	Thymine
G	Guanine
am	Primary or secondary amine

TIPT	2,4,6-Triisopropylbenzenethiol
sacac	Monothioacetylacetonate
Bzsac	3-Mercapto-1-phenyl-but-2-en-1-onate
TSA	Thiosalicylic acid
acac	Acetylacetonate
NaOAc	Sodium acetate
Å	Angstrom
T	Temperature
K	Kelvin
°C	Degree celsius
R	Universal gas constant, rate constant, alkyl group
NMR	Nuclear magnetic resonance
HMBC	Heteronuclear multiple bond correlation
HMQC	Heteronuclear multiple quantum coherence
FTIR	Fourier transform infrared
DSC	Differential scanning calorimetry
HPLC	High performance liquid chromatography
TLC	Thin-layer chromatography
mp	Melting point
DMAP	4-(Dimethylamino)pyridine
PPh_3	Triphenylphosphine
MBI	2-Mercaptobenzimidazole
HL1a	*N*-Benzoyl-*N',N'*-diethylthiourea
HL1b	*N*-(3-Chlorobenzoyl)-*N',N'*-diethylthiourea
HL1c	*N,N*-Diethyl-*N'*-(3-nitrobenzoyl)thiourea
HL1d	*N,N*-Diethyl-*N'*-(3-methoxybenzoyl)thiourea
HL1e	*N,N*-Diethyl-*N'*-(3-methylbenzoyl)thiourea
HL1f	*N,N*-Adipoylbis(*N',N'*-diethylthiourea)
HL2a	*N*-Benzoyl-*N'*-morpholinothiourea
HL2b	*N*-(3-Chlorobenzoyl)-*N'*-morpholinothiourea
HL2c	*N*-Morpholino-*N'*-(3-nitrobenzoyl)thiourea
HL2d	*N*-(3-Methoxybenzoyl)-*N'*-morpholinothiourea
HL2e	*N*-(3-Methylbenzoyl)-*N'*-morpholinothiourea

HL3a	*N*-Benzoyl-*N',N'*-di(2-hydroxyethyl)thiourea
HL3b	*N*-(3-Chlorobenzoyl)-*N',N'*-di(2-hydroxyethyl)thiourea
HL3c	*N,N*-Di(2-hydroxyethyl)-*N'*-(3-nitrobenzoyl)thiourea
HL3d	*N,N*-Di(2-hydroxyethyl)-*N'*-(3-methoxybenzoyl)thiourea
HL3e	*N,N*-Di(2-hydroxyethyl)-*N'*-(3-methylbenzoyl)thiourea
HL4	*N,N*-Diethyl-*N'*-(-)-(3*R*)-menthyloxycarbonylthiourea
HL5	*N,N*-Diethyl-*N'*-(+)-(3*S*)-menthyloxycarbonylthiourea
HL6	*N*-(-)-(3*R*)-Menthyloxycarbonyl-*N'*-morpholinothiourea
HL7	*N*-(+)-(3*S*)-Menthyloxycarbonyl-*N'*-morpholinothiourea
^{3}J(PtH)	Vicinal platinum-hydrogen coupling constant
^{1}J(PtP)	One bond platinum-phosphorus coupling constant
^{2}J(PP)	Geminal phosphorus-phosphorus coupling constant
Hz	Hertz
$\Delta S^{\neq}$	Enthropy of activation
$\Delta H^{\neq}$	Enthalpy of activation
$\Delta G^{\neq}$	Gibbs free energy of activation
k	Rate constant
K_{eq}	Equilibrium constant
h	Planck's constant
TMS	Tetramethylsilane
$CDCl_3$	Deuterated chloroform
DMSO-d_6	Deuterated dimethylsulfoxide
N–N	Diimine or chelating amine
NA	Nucleic acid
AA	Amino acid

CHAPTER 1

INTRODUCTION

1.1 Introduction

This study is concerned with the synthesis and characterisation of novel platinum(II) complexes for potential use as anticancer drugs. Accordingly, the introduction of this study will cover a brief overview of cancer and the treatment of cancer, as well as an account of the mechanism of action of platinum(II) anticancer drugs and their current status.

1.2 Cancer and its treatment

Cancer is not a single disease but a group of many diseases affecting different organ systems of the body. It is associated with the uncontrolled, accelerated growth of cells and the spread of aberrant cells from their site of origin. [1] Most cancers are initiated by specific genetic mutations. [2, 3] These mutations affect the factors controlling cell division either by stimulating cell division or by deactivating the processes that control cell division in the cell cycle. [3–5] The cell cycle is controlled by a sequence of interacting proteins that induces and coordinates the duplication of the cell contents and cell division. Therefore, a mutation of the genes coding structural or regulatory proteins for cell division may result in the transformation of a normal cell into a tumour cell. [2, 3, 6, 7] In normal cells, growth and division are regulated by at least two types of genes: proto-oncogenes, which promote growth, and tumour suppressor genes, which retard cell division. The initiation of tumour formation can be caused by two events: the transformation of a proto-oncogene into an oncogene (a gene whose expression causes a tumour) and/or the inactivation of a tumour suppressor gene. Cancers can be caused by chemical carcinogens (which cause local changes in nucleotide sequences); by ionizing radiation, such as X-rays (which cause chromosome breaks and translocations); or by viruses (which introduce foreign DNA into a cell). [3]

A benign tumour is not necessarily life-threatening, unlike cancerous or malignant tumours that invade nearby tissue and transform normal cells into cancerous cells. Cancers can be clinically defined by their tissue of origin. The origin may be epithelial, mesenchymal, or they may originate in the bone marrow. Tumours of epithelial origin are described as carcinomas, e.g. basal cell carcinoma of the skin, while those of

glandular epithelium origin are described as adenocarcinomas, e.g. colon adenocarcinomas. Tumours of mesenchymal origin are known as sarcomas, e.g. osteosarcomas, whereas leukemias are derived from haematopoietic cells of the bone marrow. Each cancer has its own particular characteristics and requires its own individual course of treatment. [3]

The treatment of localised or solid tumours initially involves the surgical removal of the tumour and some of the surrounding tissue. Modern protocols generally combine surgery and radiation therapy because radiation can destroy any microscopic cancer cells that may remain in the lymph nodes and in the surrounding tissue following surgical removal of the primary and secondary growths. Unfortunately, ionizing radiation is known to cause cancer under certain conditions, thus the application of radiation therapy is limited. The efficiency of radiation therapy has been greatly enhanced by the development of radiation sensitizers that increase the damaging effects of radiation to the "sensitized" cells without an increase in radiation dose. Examples of radiation sensitizers used clinically are 5-fluorouracil, metronidazole and razoxane (Figure 1.1). [8]

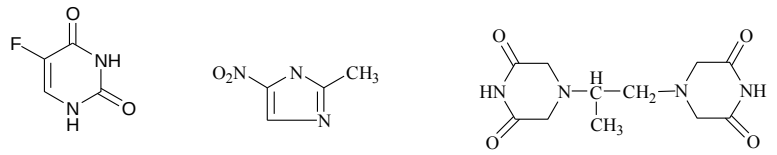

5-Fluorouracil Metronidazole Razoxane

Figure 1.1: Examples of some radiation sensitizers. [8]

Alternative methods of cancer treatment include the use of radiopharmaceuticals and photodynamic therapy. Radiopharmaceuticals have a high specificity for tumour cells and deliver radiation (β-particles) *in situ* to cancer cells, with minimal damage to surrounding tissue. [9] Photodynamic therapy makes use of hematoporphyrin derivatives (HPD) and dyes. HPD derivatives are cleared from tumour cells at a slower rate than from normal tissue due to the lower activity of lymphatic drainage from tumours. This results in the selective accumulation of the drug in the tumour cells. To destroy the tumour, red light from a tunable laser is directed at the tumour, generating singlet oxygen radicals, which destroy the tumour cells selectively. The singlet oxygen radicals chemically destroy membrane proteins, sterols, and unsaturated lipids, and this leads to a

change in cell permeability and cytolysis. Red light is chosen due to its penetrating power in human tissue and to the fact that it is not absorbed by chromophores present in normal tissue. It is thus especially effective in damaging or destoying tumours. [10, 11]

The problem of metastasis and disseminated forms of cancers, such as leukemia, led to the development of chemotherapeutic agents that may target cancer cells directly. Modern chemotherapeutic drugs can be generally divided into several categories: alkylating agents (e.g. chlorambucil), carcinolytic antibiotics (e.g. actinomycin D), antimetabolites (e.g. 5-fluorouracil), mitotic inhibitors (e.g. vinblastine) and hormonal agents (e.g. mitotane). [12]

1.3 Metal-based chemotherapeutic agents

The use of inorganic complexes as chemotherapeutic agents has a long history, dating back centuries. A few examples of the diverse therapeutic uses of inorganic complexes are: the use of gold complexes for the treatment of arthritis, silver salts as topical antibacterials and gallium for the treatment of hypercalcemia of malignancy. [13, 14] In 1931, Collier and Krauss described the first systematic studies in the field of tumour-inhibiting metal complexes. They proposed that the "effect of the heavy metal on experimental murine cancer is not only due to the metal alone, but also to the structure of the compounds and the type of compounds". [15]

The use of inorganic complexes in cancer treatment was limited until the serendipitous discovery of the antitumour activity of platinum coordination compounds by Rosenberg in 1960's, such as *cis*-diamminedichloroplatinum(II), commonly known as cisplatin (Figure 1.2). Before the discovery of the anticancer activity of cisplatin, anticancer research tended towards the screening and testing of organic-based drugs, because heavy metals were regarded as potential carcinogens and non-selective poisons. [15]

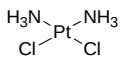

Figure 1.2: Structure of *cis*-diamminedichloroplatinum(II), commonly known as cisplatin.

The success of cisplatin stimulated further research in the search for other metal-based anticancer drugs. Today, complexes of rhodium, copper, tin, ruthenium, germanium, gallium, gold, molybdenum and titanium, which show significant anticancer activity, have been reported (Figure 1.3). [13–26]

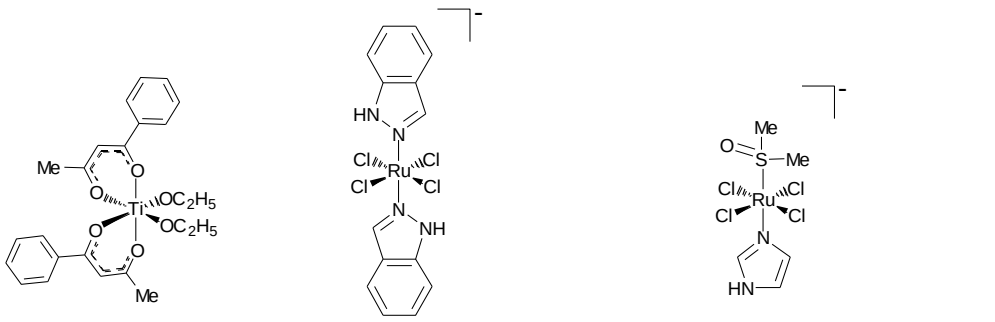

[$Ti(Bzac)_2(OEt)_2$] *trans*-[$RuCl_4(indazole)_2$]$^-$ *trans*-[$RuCl_4(DMSO)(imidazole)$]$^-$

Figure 1.3: Examples of metal complexes exhibiting anticancer activity. The [$Ti(Bzac)_2(OEt)_2$] complex is commonly known as Budotitane. Bzac = 1-phenylbutane-1,3-dionato. [14, 15, 26]

1.3.1 Platinum(II) complexes in cancer chemotherapy

Cisplatin (Figure 1.2) was first synthesised in 1844 by Michele Peyrone, and was only discovered to have anticancer activity by Barnett Rosenberg in 1969. Rosenberg was examining the influence of an electric field applied across platinum electrodes on an aerobic solution of *E. coli* growing in the presence of ammonium chloride. Bacterial cells were noted to grow up to 300 times their normal length, but no cell division was observed. The experimental conditions favoured the formation of ammoniumhexachloroplatinate(IV), [$PtCl_6(NH_4)_2$], which was photochemically converted to *cis*-diamminetetrachloroplatinum(IV), *cis*-[$PtCl_4(NH_3)_2$], which inhibits cell division. Rosenberg then synthesised a range of simple platinum complexes, one of which was cisplatin. Only the *cis*-bis(am(m)ine)Pt(II) and Pt(IV) complexes were found to be biologically active, while the *trans*-isomers were inactive. Since the *cis*-isomers inhibited cell division without killing the bacterial cells, it was thought that these compounds might inhibit tumour cell division with little toxicity to the host. [15, 27]

Cisplatin qualified for clinical trials in 1971 and, following FDA (US Food and Drug Administration) approval in 1979, is used routinely for the successful treatment of testicular carcinomas and significantly increases the life expectancy of patients with

ovarian carcinomas, oropharyngeal carcinomas, bronchogenic carcinomas, lymphoma, osteosarcoma, melanoma and neuroblastoma. [15, 28]

Although cisplatin has proved to be a valuable drug for the treatment of a number of cancers, it does have several drawbacks. It is highly toxic (nausea, nephrotoxicity (dose-limiting), ototoxicity), has a limited spectrum of activity and, after prolonged use and/or even a single treatment, resistance (acquired or intrinsic) towards the drug can develop. [29] Because of these problems, thousands of platinum complexes have been prepared and screened in search of complexes with lower toxicity and drug resistance than cisplatin, but only a few have passed clinical trials. [15] Carboplatin, *cis*-diammine-1,1'-cyclobutanedicarboxylatoplatinum(II), (Figure 1.4) was the first second-generation cisplatin analogue to pass clinical trials. It is used clinically for the treatment of ovarian, small-cell lung, bladder and cervical cancers. Carboplatin displays similar activity to cisplatin, but is less toxic, however myelosuppression and thrombocytopenia are dose limiting. [15, 30] Some examples of second- and third-generation cisplatin analogues that have been prepared are shown in Figure 1.4. Second-generation complexes differ from cisplatin by having different leaving groups, for example carboxylates, while the third-generation complexes have different amines. [29] A structure-activity relationship was formulated for these classical cisplatin analogues. It was thought that for a platinum complex to show biological activity it must have two amines in a *cis* geometry (with at least one NH group) and leaving groups with a weaker *trans*-effect than the amine. This structure-activity relationship is, however, no longer valid because *trans* complexes and complexes that are not structurally similar to cisplatin or its analogues have been found to exhibit significant anticancer activity. [31]

1.3.1.1 Mode of action of cisplatin

A wide range of biological molecules are available as potential donors in biological systems, such as peptides, proteins, RNA, DNA and cellular membranes. Although it has been shown that DNA is the active target, it is important to remember that the activity of a drug is the net result of a process characterised by a sequence of interactions with cellular constituents that occur at specific sites and at specific times. A large number of review articles cover the interactions of platinum complexes with DNA and other biologically relevant molecules. [27, 29, 31–47, 48]

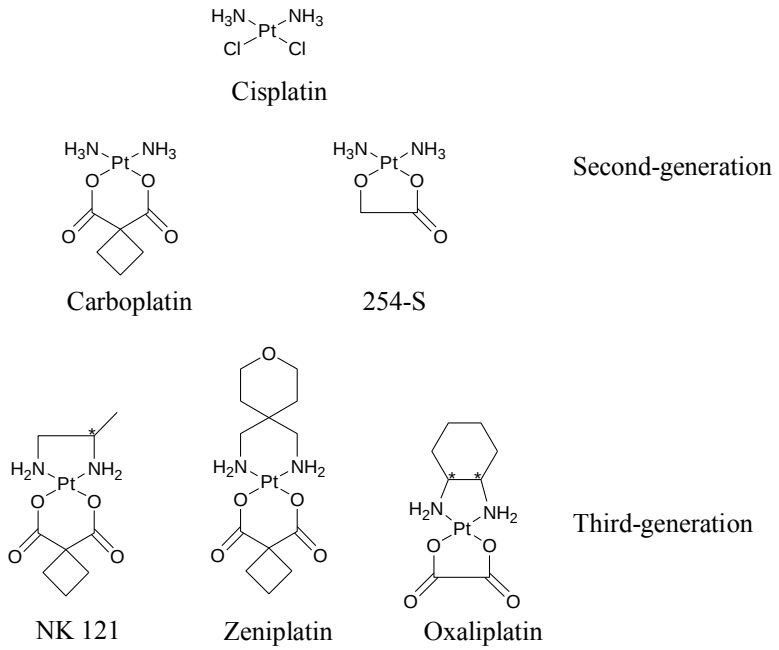

Figure 1.4: Structures of some second- and third-generation cisplatin analogues. [13, 29]

Cisplatin has two labile chloride ligands that are inert to substitution outside the cell, due to a high extracellular concentration (100 mM) of chloride ions. [29] The neutral complex diffuses through the cell membrane where it is activated by the stepwise hydrolysis of the chloride ligands to form a positively charged aqua species. A ^{195}Pt study by Bancroft *et al*. showed that the dominant species is most likely *cis*-$[PtCl(H_2O)(NH_3)_2]^+$, with the hydrolysis of the chloride ligands being the rate-determining step in the reaction of cisplatin with DNA. [49] Platinum is a soft donor and has a strong kinetic preference for class B donor atoms, therefore, the bound water molecules can then undergo competitive exchange for sulfur and nitrogen donor atoms associated with peptides, proteins and DNA. Platinum binds irreversibly to DNA and the platinum-DNA adducts have been shown to correlate with the bioactivity of the complexes. The biological activities of the various platinum-DNA lesions are also different, for example the d(GpG) adduct inhibits several DNA and RNA polymerases more efficiently than the d(ApG) adduct, but the d(ApG) adduct is more mutagenic than the d(GpG) lesion. [50]

Hence, studies on the mechanism of cisplatin-DNA interactions have been carried out to gain insight into the empirically derived structure-activity relationships for this class of anticancer agent. The research has focussed on determining the structure of these specific

DNA adducts and comparison of the information obtained with their antineoplastic activity, because an understanding of these interactions at a molecular level may lead to the development of new anticancer drugs.

1.3.1.2 DNA-binding studies

The products of the reactions of various platinum complexes with purines, pyrimidines, nucleosides, nucleotides and short oligonucleotides, have been determined by X-ray crystallography [50–60] and NMR spectroscopy. [50, 52–71] These model studies indicate that platinum complexes have a preference for coordination to the nucleobases, in particular to the N7 donor atom of guanine. The structures of these models of platinum-DNA interactions have made a significant contribution to the understanding of platinum binding specificity and kinetics. Although these simple nucleobase, nucleoside and nucleotide models cannot be used as accurate models of the bifunctional, intrastrand binding of cisplatin to DNA, because they lack the constraints imposed by the DNA sugar-phosphate backbone, they have provided the knowledge base that is required to interpret the more involved, and biologically relevant, oligonucleotide studies.

As shown in Table 1.1, the major cisplatin-DNA adduct that is formed is the GpG 1,2-intrastrand N7, N7 cross-link, which makes up 55–65% of all lesions. The structure of the major 1,2-intrastrand cross-link between adjacent guanines that involves coordination to the N7 positions in a series of oligonucleotides, has been determined by X-ray crystallography [59, 60, 72–75] and NMR spectroscopy. [62, 76–80] These studies, together with gel electrophoresis studies, indicate that the resulting platinated DNA was unwound and bent towards the major groove, in which hydrogen bonding between the complementary strands of the platinated DNA are still present. [27, 81–85] The second most abundant adduct is the ApG 1,2-intrastrand N7, N7 cross-link which accounts for 25–35% of all lesions. [86, 87] No binding was found to occur at a GpA sequence. These observations are important, because the ApG and GpA sites are chemically identical. [31] In the coordination of cisplatin with the trinucleotide ApGpA, both ApG and GpA adducts are observed. [31] The non-formation of the GpA adduct in duplex DNA must therefore be due to structural features associated with the DNA, which are responsible for introducing sequence specific binding of the drug.

Table 1.1: Percentage of various adducts formed by the reaction of *cis*-$[PtCl_2(NH_3)_2]$ and $[PtCl_2(en)_2]$ with DNA. [88]

cis-$[PtCl_2(NH_3)_2]$		$[PtCl_2(en)_2]$	
GpG	55–65%	GpG	57–62%
ApG	25–35%	ApG	5–10%
GpNpG	6%	GpNpG	13–18%
G-Pt-G	< 5%	G-Pt-G	< 5%

Molecular mechanics calculations and investigations of platinum(II) ApG adduct crystal structures have indicated the presence of a hydrogen bond between the ammine group on the 5' side of the adduct and a phosphate group, as well as between the ammine group on the 3' side and the exocyclic oxygen-6 atom of guanine. In the GpA adduct, there is a highly unfavourable interaction between the ammine ligand on the 3' side and the exocyclic NH_2-group of adenine. The loss of hydrogen bonding and the mutual repulsion of the ammine and amino group contribute to the destabilisation of the GpA adduct. This is thought to be the reason for the sequence selective binding to ApG and not to GpA sites. [31] Both molecular modeling and NMR studies of short oligonucleotide fragments have revealed that transplatin cannot form an analogous intrastrand cross-links. [33] It thus appears that one or both the ApG and GpG lesions are important for the antineoplastic activity of cisplatin.

As seen from the relative amounts of cisplatin-DNA adducts, cisplatin binding to DNA is sequence selective. [89] Selectivity for platinum binding to duplex DNA is not only governed by the stability of the final complex (GpG > ApG > GpA), but also by the stability and ease of formation of the first platination binding step. Platinum binding to DNA is controlled kinetically, and the final binding site is determined by the first binding step. [41, 66, 90, 91] Chottard *et al.* [92] evaluated the effect of the nucleobase adjacent to the guanine and the factors affecting the rate of the first binding step. Two adjacent guanines accelerated the first step in the platination of guanine in XpG and GpX dinucleotides (X = G, A, C) by *cis*-$[Pt(H_2O)_2(NH_3)_2]^{2+}$. The rate of platination decreases in the order: 3' GpG > CpG >ApG and 5' GpG > GpC > GpA. The 3' and 5' indicate which guanine is being platinated. This observation was explained in terms of the stability of the first platinated intermediate and the ease of approach of the drug to the guanine-N7 site.

Molecular modeling indicates that the neighbouring guanine stabilises the five-coordinate intermediate by means of a hydrogen bond connecting the oxygen-6 atom with a non-leaving water ligand. Similar results were obtained for the platination of a wide range of oligonucleotides with cisplatin and its hydrolysis products. The platinum binding is dependent on the neighbouring bases, with adjacent guanines being the most reactive. Initial binding to adenine was generally not observed. Competition reactions of four mononucleoside monophosphates with cisplatin and transplatin indicated that the relative order of nucleophilicity of the nucleotides decrease in the order, GMP > AMP >> CMP > UMP, at 25°C and pH 7. This confirms the kinetic preference for the guanosine site. [27] The first binding step is thought to occur via the *cis*-$[PtCl(H_2O)(NH_3)_2]^+$ species. The presence of chloride arrests the monoadduct-to-diadduct conversion, suggesting that chelation to form the bifunctional DNA adduct occurs via hydrolysis of the remaining chloride ligand to form a reactive aqua-monoadduct. [41]

The preferential binding of platinum to the guanine-N7 site, over that of cytosine-N3, adenine-N1, N7 in DNA, is also due, in part, to the higher basicity of guanine, compared to adenine and cytosine, and the availability of these sites for coordination in DNA. Calculations of electrostatic potentials indicate that the carbonyl group on guanine enhances the basicity of the G-N7 site, while the amino group in adenine decreases the relative basicity of the A-N7 site. The adenine and cytosine sites are also less available for metal binding than the more exposed guanine-N7 site in the major groove. [27]

The biological activity of a platinum drug cannot be explained solely on the basis of its ability to bind and damage DNA. For example, the platinum complex, transplatin, binds to DNA and blocks replication but is ineffective as a chemotherapeutic agent. This suggests that stereochemical differences in the platinated DNA adduct are responsible for the biological activity of these complexes. These differences have been found to affect replication, transcription, repair and protein recognition of the platinated DNA. Both gel electrophoretic mobility shift assays and expression library screening of human cells with cisplatin-modified DNA have revealed the existence of proteins that bind specifically to the 1,2-d(GpG) and 1,2-d(ApG) intrastrand adducts. These structure-specific recognition proteins (SSRPs) have a 75 amino acid sequence in common, known as the high mobility

group (HMG) domain, which is thought to be the source of specificity for platinated DNA. [88, 93–95]

A number of proteins contain this domain, including the non-histone chromosomal proteins, HMG1 and HMG2, as well as many transcription factors. The HMG1 protein recognises the d(GpG) and d(ApG) 1,2-intrastrand cross-links made by cisplatin. It is thought that the binding of HMG domain proteins to the two major DNA adducts formed by cisplatin may prevent repair of these lesions, because cells that do not have these proteins (due to genetic mutations) are more sensitive to cisplatin. Huang *et al*. have shown that HMG domain proteins selectively inhibit the excision repair of the 1,2-d(GpG) cisplatin cross-link, but not the 1,3-(GpTpG) cross-link, protecting them from repair and thereby preserving their ability to block replication of DNA required for tumour cell proliferation. [93] Recently Lippard and coworkers made a significant contribution to the understanding of the binding specificity of HMG domain proteins with cisplatin adducts by determining the X-ray crystal structure of a HMG1 domain A protein from a rat bound to a 16 base-pair DNA fragment containing a single *cis*-[$Pt(NH_3)_2${d(GpG)-N7,N7}] intrastrand cross-link. [96] The DNA in the complex is bent towards the major groove with an overall curvature of 61°. The HMG domain protein binds with its concave surface contacting the minor groove of the DNA duplex. An interesting feature of the crystal structure is that platinated guanine residues are destacked, exposing their hydrophobic surfaces in the minor groove, with the phenyl ring of phenylalanine 37 projected into this hydrophobic crevice.

1.3.1.3 Consequences of protein and peptide binding

Sulfur-containing proteins have also been shown to play an important role in the transport and toxicological properties of platinum complexes. The binding to sulfur-containing molecules is thought to be responsible for the inactivation of the platinum drugs, for the development of resistance and for the toxic side-effects exhibited by these drugs. The therapeutic efficacy of cisplatin is limited by nephrotoxicity, which is associated with the binding to sulfur-containing enzymes and proteins found in the kidney. [47] Consequently, a large amount of research has focussed on the importance of platinum-sulfur binding and its implications for future drug design.

Typical sulfur-containing biomolecules which can react with platinum are albumin, metallothionine, glutathionine, cysteine and methionine. [46, 47, 97–100] Complexes of methionine and platinum(II) have been identified in the urine of patients receiving cisplatin. Incubation of methionine with cisplatin *in vivo* has also been shown to reduce nephrotoxicity, while the cytotoxicity against cancer cells is maintained. A substantial amount of research has therefore been carried out to identify and study the coordination chemistry of these complexes. [101–123] The complex [Pt(*L*-met-S,N)$_2$] exists in aqueous solution as a mixture of *cis*- and *trans*-isomers which undergo interconversion. These complexes are unreactive and are considered to be a non-toxic form of platinum. Methionine, glutathione and other sulfur-containing molecules have a kinetic preference for platinum over nucleobases at neutral pH. These platinum complexes undergo intermolecular and intramolecular transfers from the sulfur donor atom to the nucleobase. Reactions of platinum complexes with sulfur nucleophiles are kinetically favoured, while the platinum-nucleobase adducts are thermodynamically favoured products. [47, 124–126]

Cisplatin reacts with methionine to yield multiple products and as a result [PtCl(dien)]Cl and [PtCl$_2$(en)] have been used as model compounds for studying the competitive reactions involving nucleobases and sulfur-containing compounds. These model complexes form relatively stable products with sulfur donor ligands and were therefore used to evaluate the transfer of platinum from the sulfur-containing product to nucleobases. [101, 107, 127]

Intramolecular migration

The first example of migration from a thioether to guanine was shown by the reaction of [PtCl(dien)]Cl with *S*-guanosyl-*L*-homocysteine (SGH), (Figure 1.5). Coordination to the thioether donor atom was observed, with subsequent intramolecular transfer of the platinum to the N7 donor atom of guanine. On addition of a further equivalent of platinum, both the sulfur donor and guanine sites are platinated. [128] The migration of the [Pt(dien)]$^{2+}$ complex illustrates the thermodynamic lability of the platinum-methionine bond in the presence of a strong nucleophile. If the reaction is repeated with *S*-adenosyl-*L*-homocysteine (SAH), the adenosyl group remains unplatinated even in the presence of excess platinum. In order to evaluate the intramolecular migration at a higher pH value, the free amino group of the cysteine moiety had to be avoided. Hence, two methionine-

nucleotide models were prepared, Met-d(TpG)$^-$ and Met-d(TpGpG)$^{2-}$. These model compounds have the added advantage of closely mimicking the methionine residues of proteins and the phosphodiester backbone has a closer resemblance to that of natural DNA. [129]

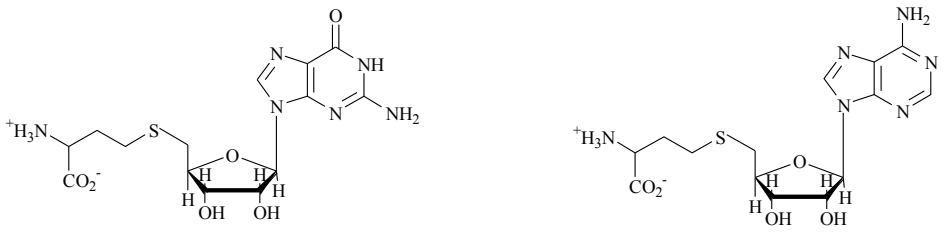

S-Guanosyl-*L*-homocysteine (SGH) *S*-Adenosyl-*L*-homocysteine (SAH)

Figure 1.5: Structures of *S*-guanosyl-*L*-homocysteine (SGH) and *S*-adenosyl-*L*-homocysteine (SAH). [128]

The reactions of Met-d(TpG)$^-$ with [PtCl(dien)]Cl and [PtCl$_2$(en)] were evaluated at pH 7. Rapid coordination of the platinum complexes to the thioether site was observed with subsequent migration to the N7 site of guanine. With the bifunctional complex, [PtCl$_2$(en)], no migration was observed, but ring-closure occurred to form the stable [Pt(en){Met-d(TpG)-S,N7}]$^+$ complex. [129] The reaction of [PtCl(dien)]Cl with Met-d(TpGpG)$^{2-}$ initially resulted in platination of the sulfur donor atom at a similar rate to that observed for Met-d(TpG)$^-$, yielding the [Pt(dien){Met-d(TpGpG)}-S] complex. Over a period of time the platinum migrated and coordinated to the N7 donor atom of the 3'- and 5'-guanines to give the monofunctional complex [{Pt(dien)}$_2${Met-d(TpGpG)}-N7(5'G),N7(3'G)]$^{2+}$ complex. [47]

Intermolecular migration

The reactions of cisplatin, [PtCl(dien)]Cl and [PtCl$_2$(en)] with methionine in the presence of 5'-GMP and GpG have been evaluated by Sadler and coworkers. [104, 130, 131] They showed that the intermolecular displacement of sulfur-bound methionine by 5'-GMP and GpG occurs readily, and that the intermolecular migration is specific for guanine because no reaction is observed with 5'-AMP, 5'-CMP and 5'-TMP. The substitution of methionine by 5'-GMP is about an order of magnitude slower than the intramolecular isomerisation of [Pt(dien)(guanosylhomocysteine-S)] reported by van Boom and Reedijk. [128] The presence of methionine was found to increase the rate of reaction of

cisplatin with 5'-GMP. The reaction of $[Pt(dien)(H_2O)]^{2+}$ with glutathione (GSH) and cysteine showed the expected kinetic preference for sulfur donor atoms over nitrogen donors, except that no coordination to 5'-GMP was noted, even in the presence of an excess of 5'-GMP. Competitive experiments between 5'-GMP and glutathione and S-methyl-glutathione show conclusively that thiols bind irreversibly to platinum, while the platinum-thioether bond is reversible. [124, 132] These results show that platinum binding to sulfur-containing amino acids, peptides and proteins plays an integral role in the activation, inactivation and transport of platinum drugs in the body. The data also lend support to the suggestion that thioether-containing proteins may act as a reservoir for platinum drugs in the body. [14, 47]

1.3.2 Non-classical platinum(II) complexes

Complexes that are not structurally related to cisplatin can be prepared by the variation of the non-leaving group and/or the leaving groups. The non-leaving ligands may influence the bioavailability and the specificity and reactivity of the metal ion towards biomolecules (e.g. sulfur-containing biomolecules) and thereby govern the toxicity and mode of action of the complex. The leaving groups will undergo exchange for more nucleophilic biomolecules and thereby infer a biological lesion, or the metal complex may require an exchange of one or more of the labile ligands by water to become activated. As mentioned previously, complexes that are not structurally similar to cisplatin or its analogues have been found to exhibit significant anticancer activity, and several are currently in various stages of clinical trials. [14, 31] This section will be concerned with providing an overview of non-classical platinum(II) complexes.

1.3.2.1 Sulfur-containing complexes

The use of dimethylsulfoxide as a leaving group for anticancer platinum(II) complexes was first proposed by Farrell *et al*. and this led to the preparation of a series of $[PtCl(diamine)(RR'SO)]^+$ complexes. [133] The $[PtCl(diamine)(RR'SO)]^+$ complexes are more water-soluble and less toxic than their chloride counterparts, and they maintain a high degree of biological activity. [134] These complexes are of interest as they are the first set of platinum complexes with sulfur donor ligands, as well as being one of the first

well-defined cationic species with good anticancer activity, thus violating the empirical structure-activity relationship set down initially for platinum complexes.

The antitumour activity of the $[PtCl(diamine)(RR'SO)]^+$ complexes (Figure 1.6) was found to be dependent on the nature of both the amine and the sulfoxide ligands. The *in vitro* efficacy for a limited series of $[PtCl(diamine)(RR'SO)]^+$ complexes was found to be in the order: damch > dach and Ph_2SO > MPSO > DMSO, where dach = 1,2-diaminocyclohexane and damch = 1,2-bis(aminomethyl)cyclohexane, with the more labile and sterically bulky sulfoxides being the most potent. The importance of the nature of the amine on the cytotoxicity is evident from the fact that these complexes are active in cisplatin-resistant cell lines, which is characteristic of most complexes containing the dach and damch moieties. By contrast, complexes of the type *cis*-$[Pt(am)_2Cl(RR'SO)]^+$, where am = mono-alicyclic amines or ammine groups, were found to be inactive. [134] The lability of the sulfoxide was also noted to be dependent on the nature of the amine, with the damch complexes being five to ten times more labile than the corresponding dach complexes. A dependence on the sulfoxide lability on the amine has also been noted in complexes of the type *trans*-$[Pt(am)_2Cl(RR'SO)]^+$, where am = NH_3, pyridine or picoline, in which the sulfoxide ligand is replaced more rapidly in the aromatic amine than in the ammine complexes. [135]

Farrell *et al*. also reported that the anticancer activity of the $[PtCl(diamine)(RR'SO)]^+$ complexes was dependent on the chirality of the sulfoxide leaving group, with the (*S*)-MTSO containing complexes being more potent than the (*R*)-MTSO stereoisomers. This represents the first demonstration of the effect of the chirality of the leaving group on biological activity, as well as the first use of a sulfur-containing leaving group.

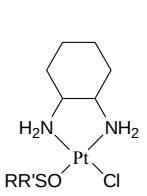

$[PtCl(dach)(RR'SO)]^+$

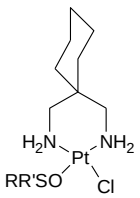

$[PtCl(damch)(RR'SO)]^+$

Figure 1.6: Examples of the first platinum(II) sulfoxide complexes prepared. [134]

To determine the mode of action of complexes of the type, $[PtCl(diamine)(RR'SO)]^+$, the binding of 5'-GMP and d(GpG) with $[PtCl(DMSO)(en)]^+$ was studied. It was found that the chloride ligand was initially substituted to give the $[Pt(DMSO)(en)(5'\text{-GMP-N7})]^{2+}$ and $[Pt(DMSO)(en)\{d(GpG)\text{-N7}\}]^{2+}$ complexes, respectively. Reaction of a further equivalent of 5'-GMP with $[Pt(DMSO)(en)(5'\text{-GMP-N7})]^{2+}$ yielded the $[Pt(en)(5'\text{-GMP-N7})_2]^{2+}$ complex. Similarly, bidentate coordination of the platinum ion to the other available N7 site of guanine in the $[Pt(DMSO)(en)\{d(GpG)\text{-N7}\}]^{2+}$ complex occurred to form the $[Pt(DMSO)(en)\{d(GpG)\text{-N7(1),N7(2)}\}]^{2+}$ complex. [136] The substitution pattern observed for the reaction of 5'-GMP and d(GpG) with $[PtCl(DMSO)(en)]^+$ is in agreement with the rates of hydrolysis determined by Farrell *et al*., in which the rate of sulfoxide hydrolysis was found to be substantially slower than chloride hydrolysis. [134] Based on these results, a mechanism of action of the $[PtCl(diamine)(RR'SO)]^{2+}$ complexes was proposed. Intracellular chloride hydrolysis was proposed to occur to form $[Pt(diamine)(H_2O)(RR'SO)]^{2+}$, which then reacts with DNA to give a sulfoxide-Pt-DNA intermediate. Subsequent activation and displacement by a neighbouring guanine base gives a bifunctional DNA adduct. The $[PtCl(diamine)(RR'SO)]^+$ complexes form the same products as $[PtCl_2(en)]$ on binding to nucleotides. [136] Thus, the range of antitumour activity of these complexes is therefore probably not related to a different overall mechanism, but may have its origins in the reactivity of these complexes with DNA and proteins. Further examples of platinum(II) sulfoxide complexes that have been reported in the literature as potential anticancer drugs or for kinetic studies on sulfoxide lability are listed in Table 1.2. Two reviews cover several aspects of sulfoxide coordination chemistry. [137, 138]

As discussed above, the incorporation of sulfur donor atoms (sulfoxides) as leaving groups in complexes of the type $[PtCl(diamine)(RR'SO)]^+$ has a distinct effect on the bioactivity of these complexes. The use of sulfur donors was thus extended to include thiourea and sulfide derivatives. [139, 140, 141] Two mononuclear complexes, $[PtCl(en)(SC(NMe_2))]^+$ and $[PtCl(dach)(SC(NMe_2))]^+$ and a dinuclear complex $[\{PtCl(en)\}_2\{\mu\text{-}(C_nH_{2n})(NMeCS(NMe_2)_2\text{-S,S'})\}]^+$, where n = 2, 6, were prepared (Figure 1.7). These thiourea derivatives unfortunately did not show significant cytotoxicity. Reactions with 5'-GMP indicated that only the chloride ligand was substituted. The thiourea ligand was kinetically inert, but had a profound effect on the hydrolytic

behaviour of the Pt–Cl bond. The low cytotoxicity of these complexes is probably due to the fact that only monofunctional adducts with double-stranded DNA can be formed. It is well known that monofunctional Pt-DNA adducts, such as those formed by $[PtCl(dien)]^+$, are ineffective in blocking DNA replication. The lack of activity of the thiourea derivatives, compared to the sulfoxide complexes, clearly demonstrates that the lability of the sulfur donor ligand is a pre-requisite for the bioactivity of complexes of the type $[PtCl(diamine)(S\text{-donor})]^+$. [140, 141]

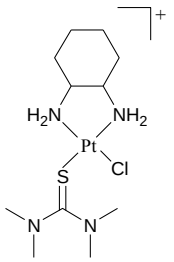

$[PtCl(dach)(SC(NMe_2)_2)]^+$

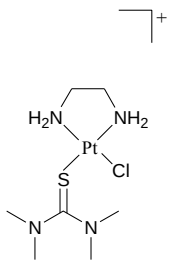

$[PtCl(en)(SC(NMe_2)_2)]^+$

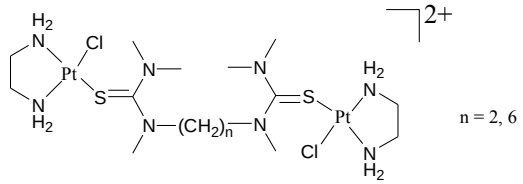

$[\{PtCl(en)\}_2\{(CH_2)_n(NMeCSNMe_2)_2\}]^{2+}$

Figure 1.7: Thiourea derivatives of $[PtCl(diamine)(S\text{-donor})]^+$ complexes. [140, 141]

Pasini *et al*. prepared complexes of the type $[Pt(diamine)(L\text{-}S,O)]^+$, where (L-S,O) represents the leaving group, which are bidentate (S,O)-chelates containing either sulfoxide or thioether sulfur donor atoms (Figure 1.8), to investigate the factors affecting the lability of the sulfur donor atoms. The Pt–O bonds were found to be more labile than the Pt–S bonds, and the Pt–S(sulfoxide) bonds were more labile than the Pt–S(thioether) bonds. [142, 143–145]

Table 1.2: Some platinum(II) sulfoxide complexes reported in the literature.

Complex	Other group	Sulfoxide	Ref.
$[PtCl_2(RR'SO)_2]$	-	numerous sulfoxides	135, 146–149
$[Pt(DMSO)_2(en)]^{2+}$	en	DMSO	150
$[Pt(diamine)(RR'SO)X]^+$	dach, damch	DMSO, MPSO, MTSO, Ph_2SO, MeBzSO, Bz_2SO	134
	en	DMSO	150, 151
	Me_4en	DMSO	152
	O-methylene-bis-aniline	DMSO	153
	1,4-diaminobutane	DMSO	151
$[Pt(dien)(DMSO)]^+$	dien	DMSO	154
$[Pt(am)Cl_2(RR'SO)]$	NH_3	DMSO, MeBzSO, MPSO	135
	alicyclic amines	DMSO	155
	1° and 2° amines	DMSO	156–159
$[PtCl_2(R\text{-}py)(RR'SO)]$	substituted-pyridines	DMSO	156, 160–162
$[PtCl(R\text{-}py)_2(RR'SO)]^+$	substituted-pyridines	DMSO	163
$[PtCl(R\text{-}py)(RR'SO)_2]^+$	substituted-pyridines	DMSO	163
$[Pt(am)(am')Cl(RR'SO)]^+$	alicyclic	DMSO	164, 155
	NH_3	DMSO	165
$[PtCl_2(quin)(RR'SO)]$	quinoline	MTSO	135
		DMSO, MPSO, MeBzSO	166
$[Pt(AA)(DMSO)X]^+$	amino-acids	DMSO	167–169
$[PtCl_2(NA)(RR'SO)]$	nucleic-acid	^{i}PrSO, DMSO	170–172
[Pt(DMSO)(en)(NA)]	nucleic-acid	DMSO	136
$[Pt(DMSO)(N\text{-}N)X]^+$	bipy, AMP, en	DMSO	173
$[Pt(DMSO)(N\text{-}N)(Me)]^+$	diimines	DMSO	174, 175
$[PtCl(DMSO)_2Me]$	-	DMSO	176
[Pt(am)Cl(DMSO)Me]	amines	DMSO	176
$[PtCl_2(DMSO)(RCN)]$	nitriles	DMSO	160, 177–179
$[Pt(alkene)Cl_2(RR'SO)]$	alkene	DMSO	179, 180
cis-$[PtCl_2(DMSO)(H_2O)]$	-	DMSO	181
[PtCl(DMSO)(salicylaldoxine)]	salicylaldoxine	DMSO	182

The [Pt(diamine)(L-S,O)]$^+$ complexes exhibited modest cytotoxicity, with the most reactive complexes being the most toxic. The bioactivity of these complexes is thought to occur via an intermediate ring-opened [PtCl(diamine)(L-S)]$^+$ complex, in which only the sulfur donor atom is coordinated. Their mode of action is thought to be similar to the [PtCl(diamine)(RR'SO)]$^+$ complexes discussed previously. [142]

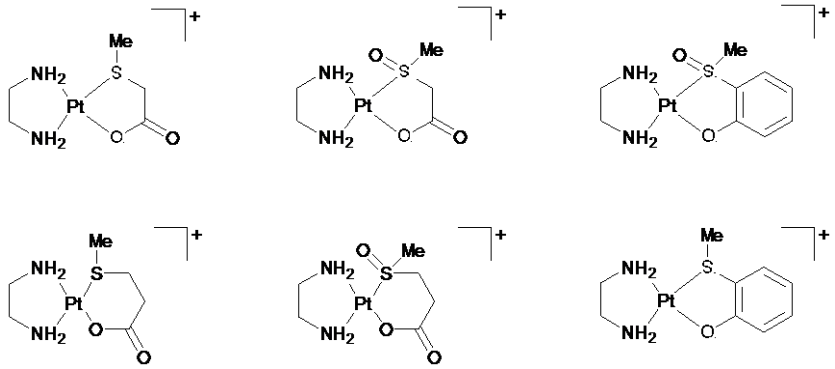

Figure 1.8: Examples of some sulfoxide and thioether complexes of the type [Pt(diamine)(L-S,O)]$^+$. [142, 143–145]

1.3.2.2 Active trans complexes

The *trans*-isomers of complexes of the type [Pt(am(m)ine)Cl_2], were generally considered to be biologically inactive, but when planar aromatic ligands, such as pyridine, were incorporated into the coordination sphere, the *trans* complexes were found to be more potent than the corresponding *cis*-isomers (Figure 1.9). [166, 183] DNA adducts formed by cisplatin, transplatin, *trans*-[$PtCl_2(py)_2$] and *cis*-[$PtCl_2(py)_2$] have been evaluated in order to explain the differences in biological activity of these complexes and how the incorporation of a planar aromatic molecule into the coordination sphere increases the bioactivity. The binding affinity of these complexes to DNA was found to decrease in the order, transplatin >> cisplatin >> *cis*-[$PtCl_2(py)_2$] > *trans*-[$PtCl_2(py)_2$]. The lower binding affinity of the pyridine derivatives may be due to the bulkiness of the planar ligands, as well as the loss of hydrogen bonding capabilities. The ability of these complexes to unwind supercoiled plasmid DNA decreases in the order, *trans*-[$PtCl_2(py)_2$] (ϕ = 17°) > cisplatin (ϕ = 13°) > transplatin (ϕ = 9–10°) > *cis*-[$PtCl_2(py)_2$] (ϕ = 4°). The *trans*-[$PtCl_2(py)_2$] complex is remarkably efficient at unwinding supercoiled DNA and has been shown to form different adducts with DNA. These adducts are characterised by enhanced interstrand cross-linking, large unwinding angles, sequence specificity for (GC)

sequences and an overall decrease in the rate of binding compared to transplatin. All these factors may contribute to the enhanced cytotoxicity of the *trans*-[$PtCl_2(py)_2$] complex. [184, 185] A similar increase in cytotoxicity was observed when the NH_3 groups in transplatin were replaced by γ-picoline (γ-pic), thiazole (Tz) and N-methylimidazole (N-MeIm), (Figure 1.9). [166, 183]

Farrell and coworkers have recently described two classes of complexes of the type [$PtCl_2(L)(L')$], incorporating planar aromatic ligands where, i) L = quinoline, L' = sulfoxide and ii) L = quinoline, isoquinoline and thiazole, L' = NH_3 (Figure 1.9). [166] The replacement of a single NH_3 of transplatin by a quinoline, to give *trans*-[$PtCl_2(NH_3)$(quinoline)], leads to a dramatic increase in activity, which is comparable with that of cisplatin. [30] In cisplatin-sensitive and -resistant L1210 cell lines, the *trans*-isomers exhibited greater activities than their *cis* counterparts. [166] For complexes of the type [$PtCl_2$(quinoline)(RR'SO)], the cytotoxicity was dependent on the nature of the sulfoxide. The more inert sulfoxides, such as dimethylsulfoxide, gave more cytotoxic complexes. The opposite trend was observed for the [PtCl(diamine)(RR'SO)]$^+$ complexes, in which the highest activity was found with the more labile sulfoxides. [134]

The DNA-binding properties of the *cis*-[$PtCl_2(NH_3)(L)$] complexes, where L = quinoline, have recently been evaluated by Farrell and coworkers. [67, 186–188] The quinoline ligand is not lost upon DNA binding and plays an important role in determining the conformational changes involved upon platination. The presence of the bulky quinoline ligand drastically slows the substitution of the chloride ligand relative to that in transplatin. The binding affinity of *trans*-[$PtCl_2(NH_3)$(quin)] for methionine is also drastically lower compared to that of transplatin. The slower rate of chloride substitution results in the quinoline-based compounds forming long-lived monofunctional adducts with DNA.

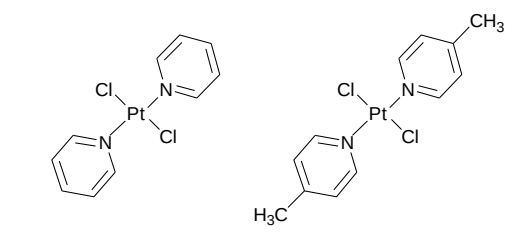

trans-[$PtCl_2(py)_2$]

trans-[$PtCl_2(\gamma\text{-pic})_2$]

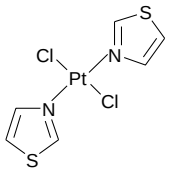

trans-[$PtCl_2(Tz)_2$]

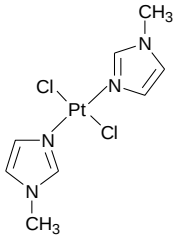

trans-[$PtCl_2(N\text{-MeIm})_2$]

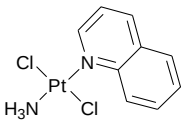

trans-[$PtCl_2(NH_3)(quin)$]

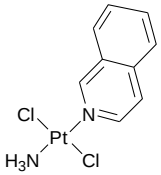

trans-[$PtCl_2(isoquin)(NH_3)$]

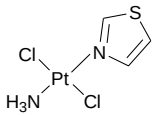

trans-[$PtCl_2(NH_3)(Tz)$]

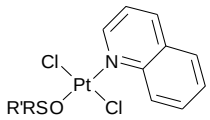

trans-[$PtCl_2(quin)(RR'SO)$]

Figure 1.9: Examples of *trans* complexes exhibiting significant cytotoxicity. [166, 183]

The quinoline-based complexes are also able to induce protein-associated DNA degredation in L1210 leukemia *in vitro*. As mentioned above, the replacement of an ammine ligand in transplatin with a quinoline does not only modulate the nucleotide-binding properties of the *trans* geometry, but also decreases its affinity towards sulfur donors such as methionine. The reduced overall reactivity of these platinum(II) complexes towards sulfur-containing amino acids may contribute to the efficacy of these drugs in cisplatin-resistant cells by altering the uptake and reactivity with endogenous thiols (glutathione) and the rate of DNA repair. [187, 188]

1.3.2.3 Complexes with bulky non-leaving groups

cis-Amminedichloro(2-methylpyridine)platinum(II), ZD0473 (Figure 1.10), was rationally designed to circumvent resistance by sterically hindering the binding of glutathione and other cellular thiols, while still retaining the ability to form cytotoxic lesions with DNA. ZD0473 is less reactive towards DNA than cisplatin, but, with time, platination occurs to the same level as with cisplatin. The crystal structure of ZD0473 indicates that the methyl group is directly above the platinum centre. This causes a decrease in the substitution kinetics of this complexes, with the rate of hydrolysis being two to three times slower than that of cisplatin. [14, 189] ZD0473 is active against cisplatin-

resistant cell lines and against an acquired cisplatin-resistant subline of a human ovarian carcinoma xenograph both by injection and oral administration. Across a panel of cisplatin-sensitive and -resistant human ovarian carcinoma xenographs, ZD0473 exhibited improved or comparable activity to that observed for an equitoxic dose and schedule of cisplatin. [28, 190] ZD0473 is currently in clinical trials. [14]

Other examples of platinum complexes with sterically crowded platinum centres are $[Pt(bmic)Cl_2]$ and $[Pt(bmi)Cl_2]$, where bmi = *N'*,*N'*-dimethyl-2,2'-biimidazole and bmic = bis-(*N*-methylimidazol-2-yl)carbinol, (Figure 1.10). $[Pt(bmic)Cl_2]$ and $[Pt(bmi)Cl_2]$ show different rates of chloride substitution by 5'-GMP, with the more bulky $[Pt(bmic)Cl_2]$ complex being less reactive but more cytotoxic than $[Pt(bmi)Cl_2]$. $[Pt(bmic)Cl_2]$ shows significant anticancer activity, while $[Pt(bmi)Cl_2]$ is inactive. These complexes may react in a similar fashion to ZD0473, because the increased bulk over the platinum centre hinders deactivation of $[Pt(bmic)Cl_2]$ by thiol-containing proteins. [191]

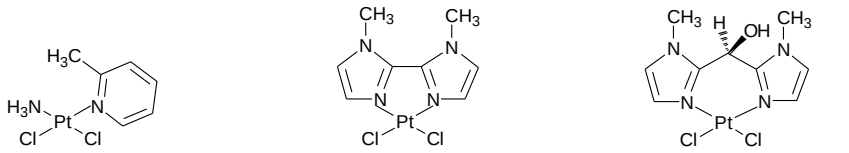

ZD0473 $[Pt(bmi)_2Cl_2]$ $[Pt(bmic)Cl_2]$

Figure 1.10: Structure of sterically crowded platinum(II) complexes that exhibit significant cytotoxicity. [189, 191]

1.3.2.4 Complexes with biologically active ligands

Several researchers have designed novel platinum complexes that contain biologically active ligands, in the hope that these complexes would be more potent than the parent complex. Examples of some of the biologically active ligands in use are: acridine, [192, 193] acridinecarboxamides, [194] ethidium bromide, [185, 195] acridine orange, [196–198] anthraquinones, [199] phenylquinolines, [200] sugars, [201, 202] estrogenic arylethylenediamines, [203–209] and chlorambucil. [212]

Denny *et al*. have prepared a series of complexes by attaching (1,2-diaminoethane)-dichloroplatinum(II) and (1,3-diaminopropane)dichloroplatinum(II) to anilinoacridine and

acridinecarboxamide (Figure 1.11). These complexes exhibited improved activity in cisplatin-resistant cell lines, compared to the parent platinum complexes, but no improvement relative to the carrier ligands was observed. The complexes attached at the 4-position rather than the 2-position were the most active. [193, 194] A similar structure-activity relationship was observed for a series of anthraquinone-containing complexes (Figure 1.11). The complexes attached at the 1-position had greater activity than complexes where attachment was at the 2-position. [199] Unfortunately, these classes of complexes with biologically active ligands have not resulted in any significant clinical advances. Although the results are interesting and encouraging, further research is required.

1.3.2.5 Multinuclear platinum(II) complexes

An extensive series of multinuclear platinum complexes with bridging linkers has been prepared. The chain length and the geometry of the leaving groups at the platinum centre have been shown to have a marked effect on the bioactivity of these complexes. Some of these complexes have shown activity in both cisplatin-sensitive and -resistant cell lines, which suggests that the mechanism of action of these complexes may be different to that of cisplatin. Bis(platinum) complexes (Figure 1.12) are very efficient at cross-linking DNA and are more reactive than their analogous monomers with DNA. [211–222]

An interesting feature of bis(platinum) complexes is that the ammine derivatives induce B $\rightarrow$ Z transitions in poly(dG–dC)·poly(dG–dC) DNA, whereas, if the ammine groups are substituted by pyridine or quinoline, a stabilisation of the B-form of DNA results. The incorporation of pyridine or quinoline ligands results in a decrease in cytotoxicity of the complexes relative to the monomers. [213, 214]

The most important of these multinuclear platinum(II) complexes is the 4+ charged trinuclear platinum complex BBR3464 (Figure 1.12). This complex exhibits a complete lack of cross-resistance to cisplatin-resistant cell lines and is significantly more potent than cisplatin *in vitro* in an osteosarcoma cell line. The increased potency has been attributed to increased cellular platinum uptake of BBR3464 relative to that of cisplatin and to the extent and unique mode of DNA binding of this complex. BBR3464 is an

excellent example, demonstrating that compounds which are structurally different to cisplatin and bind differently to DNA do exhibit a different spectrum of activity. [28, 211, 223]

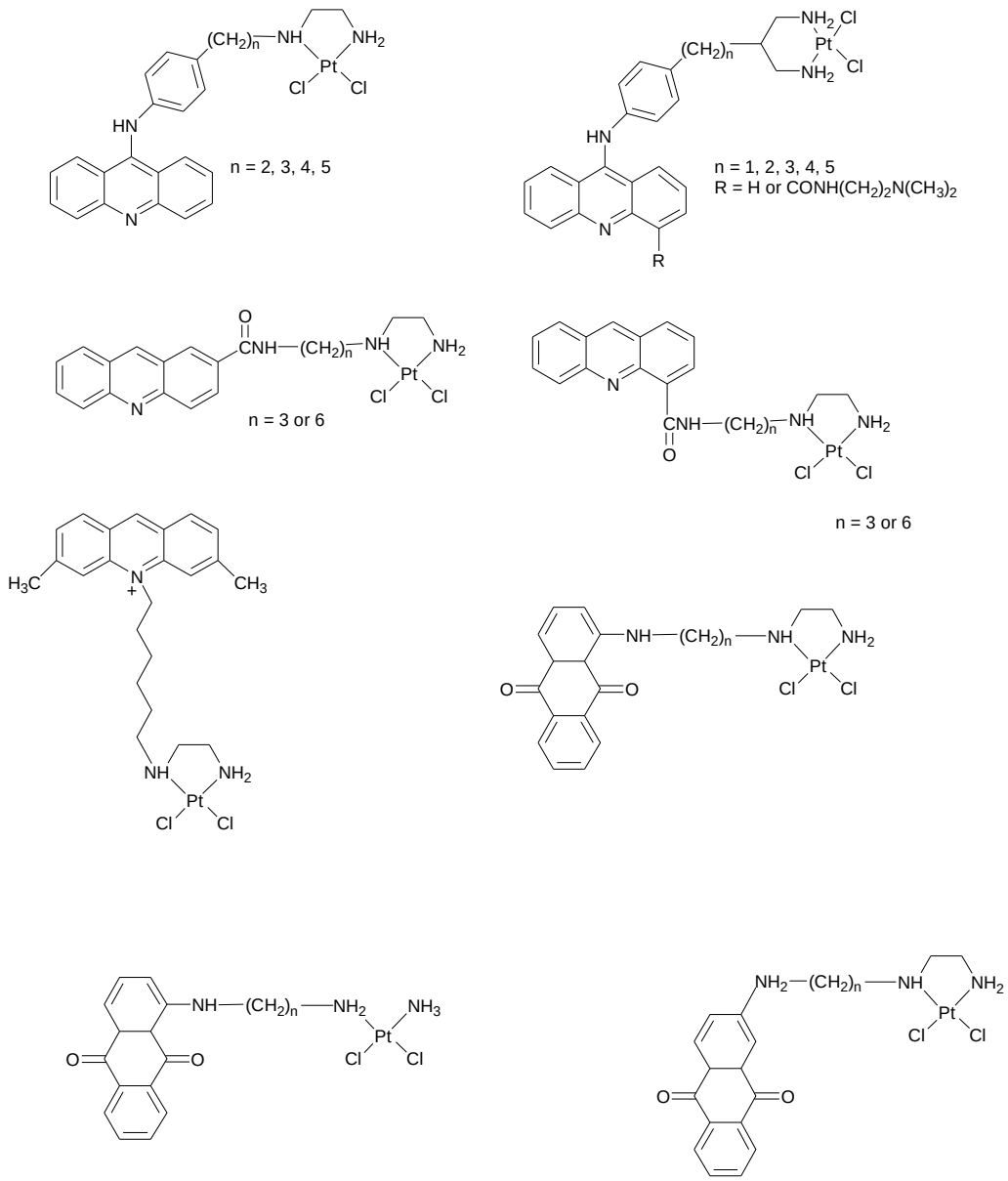

Figure 1.11: Examples of platinum complexes tethered to biologically active ligands. [193, 194, 199]

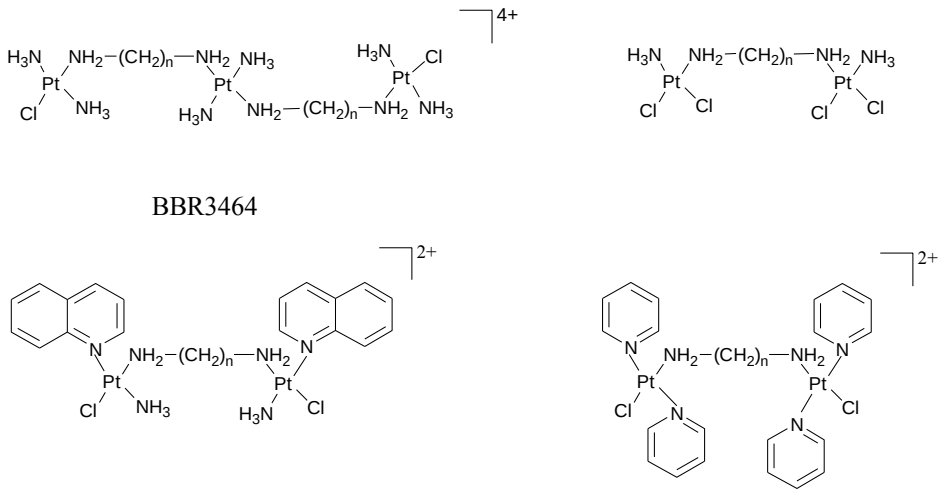

Figure 1.12: Structure of BBR3464 and some selected multinuclear platinum(II) complexes. [28, 186, 214, 221]

1.4 Objectives of study

As mentioned above, the synthesis of complexes that are not structurally similar to cisplatin and which show antineoplastic activity, has made a significant contribution to the development of novel platinum(II) chemotherapeutic agents. Hence, the present study involves the synthesis and characterisation of novel non-classical mixed-ligand platinum(II) complexes of the type [PtCl(L)(RR'SO)], where L = bidentate (S,O)-chelating ligands and RR'SO = sulfoxide, as potential covalent binders of DNA. The [PtCl(L)(RR'SO)] complexes were prepared in the hope of expanding the range of platinum complexes exhibiting anticancer activity that are less toxic and have a broader spectrum of activity than cisplatin and its analogues.

To achieve the objectives of the present study the following studies were carried out, as described in the following chapters:

1) *N*-(3-*R*-Benzoyl)-*N',N'*-(disubstituted)thiourea and *N,N*-(disubstituted)-*N'*-menthyl-oxycarbonylthiourea ligands have been synthesised and characterised, (Chapter 3).

2) A series of platinum(II) sulfoxide complexes of the type [Pt(acylthioureato)Cl(RR'SO)] and [PtCl(menthyloxycarbonylthioureato)(RR'SO)], have been synthesised and characterised, (Chapter 4).

3) The substitution kinetics of the [Pt(acylthioureato)Cl(RR'SO)] complexes were evaluated to determine the effect of the nature of the non-leaving and leaving groups on the reactivity of these complexes, (Chapter 5).

4) The *in vitro* biological activity of all the complexes were evaluated against a HeLa cell line, while selected complexes were further evaluated against a MCF-7 cell line. A preliminary morphology study was also carried out with the biologically active complexes in a HeLa cell line, to determine how these complexes induce cell death. Preliminary plasmid DNA binding studies with selected [Pt(acylthioureato)Cl(RR'SO)] complexes were carried out, using a gel mobility shift assay, to determine the mode of binding of these complexes to DNA. (Chapter 6).

1.5 References

1. S. P. Gupta, *Chem. Rev*., 1994, **94**, 1507.
2. K. B. Burck, E. T. Liu, J. W. Larrick, in *Oncogenes: An Introduction to the Concept of Cancer genes*, Springer-Verlag, New York, 1988.
3. B. Alberts, D. Bray, J. Lewis, M. Raff, K. Roberts, J. D. Watson, in *Molecular Biology of The Cell*, Garland Publishing, Inc., New York, 3rd edn., 1994.
4. J. B. Weitzman, M. Yaniv, *Nature*, 1999, **400**, 401.
5. W. C. Hahn, C. M. Counters, A. S. Lundberg, R. L. Beijersbergen, M. W. Brooks, R. A. Weinberg, *Nature*, 1999, **400**, 464.
6. A. W. Murray, *Nature*, 1992, **359**, 599.
7. L. H. Hartwell, M. B. Kastan, *Science*, 1994, **266**, 1821.
8. W. O. Foye, S. K. Sengupta, in *Principles of Medicinal Chemistry*, ed. W. O. Foye, T. L. Lemke, D. A. Williams, Williams & Wilkins, London, 4th edn., 1995, ch. 37, pp. 822–845.
9. J. R. Dilworth, S. J. Parrott, *Chem. Soc. Rev*., 1998, **27**, 43.
10. F. Dall'Acqua, G. Jori, in *Principles of Medicinal Chemistry*, ed. W. O. Foye, T. L. Lemke, D. A. Williams, Williams & Wilkins, London, 4th edn., 1995, ch. 41, pp. 893–907.
11. T. J. Dougherty, C. J. Gomer, B. W. Henderson, G. Jori, D. Kessel, M. Korbelik, J. Moan, Q. Peng, *J. Natl. Cancer Inst*., 1998, **90**, 889.
12. A. Gringauz, in *Introduction to Medicinal Chemistry: How Drugs act and Why*, Wiley-VCH, New York, 1997, ch. 4, pp. 93–139.
13. M. J. Abrams, B. A. Murrer, *Science*, 1993, **261**, 725.
14. Z. Guo, P. J. Sadler, *Angew. Chem. Int. Ed*., 1999, **38**, 1512.
15. B. K. Keppler, in *Metal Complexes in Cancer Chemotherapy*, VCH, New York, 1993.
16. O. M. Ni Dhubhghaill, W. R. Hagen, B. K. Keppler, K. –G, Lipponer, P. J. Sadler, *J. Chem. Soc., Dalton Trans*., 1994, 3305.
17. R. A. Vilaplana, F. González-Vílchez, E. Gutierrez-Puebla, C. Ruiz-Valero, *Inorg. Chim. Acta*, 1994, **224**, 15.
18. L. Y. Kuo, M. G. Kanatzidis, M. Sabat, A. L. Tipton, T. J. Marks, *J. Am. Chem. Soc*., 1991, **113**, 9027.

19. H. T. Chifotides, K. R. Dunbar, J. H. Matonic, N. Katsaros, *Inorg. Chem*., 1992, **31**, 4628.
20. D. T. Hill, G. R. Girard, F. L. McCabe, R. K. Johnson, P. D. Stupik, J. H. Zhang, W. M. Reiff, D. S. Eggleston, *Inorg. Chem*., 1989, **28**, 3529.
21. B. Moubaraki, K. S. Murray, J. D. Ranford, J. J. Vittal, X. Wang, Y. Xu, *J. Chem. Soc., Dalton Trans*., 1999, 3573.
22. D. L. Banville, W. D. Wilson, L. G. Marzilli, *Inorg. Chem*., 1985, **24**, 2479.
23. H. Tamura, H. Imai, J. Kuwahara, Y. Sugiura, *J. Am. Chem. Soc*., 1987, **109**, 6870.
24. S. J. Berners-Price, R. K. Johnson, C. K. Mirabelli, L. F. Faucette, F. L. McCabe, P. J. Sadler, *Inorg. Chem*., 1987, **26**, 3383.
25. E. Alessio, G. Mestroni, G. Nardin, W. M. Attia, M. Calligaris, G. Sava, S. Zorzet, *Inorg. Chem*., 1988, **27**, 4099.
26. A. Galeano, M. R. Berger, B. K. Keppler, *Arzneim. –Forsch./Drug Res*., 1992, **42(I)**, 821.
27. S. E. Sherman, S. J. Lippard, C*hem. Rev*., 1987, **87**, 1153.
28. E. Wong, C. M. Giandomenico, *Chem. Rev*., 1999, **99**, 2451.
29. J. Reedijk, C*hem. Commun.*, 1996, 801.
30. C. F. J. Barnard, M. J. Cleare, P. C. Hydes, *Chem. Brit*., 1986, 1001.
31. T. W. Hambley, *Coord. Chem. Rev*., 1997, **166**, 181.
32. E. L. M. Lempers, J. Reedijk, *Adv. Inorg. Chem*., 1991, **37**, 175.
33. W. I. Sundquist, S. J. Lippard, *Coord. Chem. Rev.*, 1990, **100**, 293.
34. K. Wang, J. Lu, R. Li, *Coord. Chem. Rev.*, 1996, **151**, 53.
35. A. L. Pinto, S. J. Lippard, *Biochim. Biophys. Acta*, 1885, **780**, 167.
36. J. Reedijk, *Pure Appl. Chem.*, 1987, **59**, 181.
37. A. Pasini, F. Zunino, *Angew. Chem*., 1987, **26**, 615.
38. B. Lippert, *Prog. Inorg. Chem*., 1989, **37**, 1.
39. N. Farrell, in *Transition Metal Complexes as Drugs and Chemotherapeutic Agents*, Kluwer Academic Publishers, Netherlands, 1989.
40. P. Banerjee, *Coord. Chem. Rev*., 1999, **190–192**, 19.
41. J. Kozelka, F. Legendre, F. Reeder, J. –C. Chottard, *Coord. Chem. Rev*., 1999, **190–192**, 61.
42. B. Lippert, *Coord. Chem. Rev*., 1999, **182**, 263.
43. J. Reedijk, *Inorg. Chim. Acta*, 1992, **198–200**, 873.

44. A. Iakovidis, N. Hadjiliadis, *Coord. Chem. Rev*., 1994, **135/136**, 17.
45. S. G. Chaney, A. Sancar, *J. Natl. Cancer Inst*., 1996, **88**, 1346.
46. M. Gosland, B. Lum, J. Schimmelpfennig, J. Baker, M. Doukas, *Pharmacotherapy*, 1996, **16**, 16.
47. J. Reedijk, *Chem. Rev*., 1999, **99**, 2499
48. E. R. Jamieson, S. J. Lippard, *Chem. Rev*., 1999, **99**, 2467.
49. D. P. Bancroft, C. A. Lepre, S. J. Lippard, *J. Am. Chem. Soc*., 1990, **112**, 6860.
50. G. Schröder, J. Kozelka, M. Sabat, M. –H. Fouchet, R. Beyerle-Pfnür, B. Lippert, *Inorg. Chem*., 1996, **35**, 1647.
51. M. Grehl, B. Krebs, *Inorg. Chem*., 1994, **33**, 3877.
52. B. Longato, G. Bandoli, G. Trovó, E. Marasciulo, G. Valle, *Inorg. Chem*., 1995, **34**, 1745.
53. G. Schröder, B. Lippert, M. Sabat, C. J. L. Lock, R. Faggiani, B. Song, H. Sigel, *J. Chem. Soc*., *Dalton Trans*., 1995, 3767.
54. E. G. Talman, W. Brüning, J. Reedijk, A. L. Spek, N. Veldman, *Inorg. Chem*., 1997, **36**, 854.
55. K. J. Barnham, C. J. Bauer, M. I. Djuran, M. A. Mazid, T. Rau, P. J. Sadler, *Inorg. Chem*., 1995, **34**, 2826.
56. D. Holthenrich, M. Krumm, E. Zangrando, F. Pichierri, L. Randaccio, B. Lippert, *J. Chem. Soc*., *Dalton Trans*., 1995, 3275.
57. B. Lippert, C. J. L. Lock, R. A. Speranzini, *Inorg. Chem*., 1981, **20**, 808.
58. A. Schreiber, M. S. Lüth, A. Erxleben, E. C. Fusch, B. Lippert, *J. Am. Chem. Soc*., 1996, **118**, 4124.
59. M. Coll, S. E. Sherman, D. Gibson, S. J. Lippard, A. H. –J. Wang, *J. Biomol. Struct. Dyns*., 1990, **8**, 315.
60. S. E. Sherman, D. Gibson, A. H. –J. Wang, S. J. Lippard, *J. Am. Chem. Soc*., 1988, **110**, 7368.
61. V. Aletras, N. Hadjiliadis, B. Lippert, *Polyhedron*, 1992, **11**, 1359.
62. J. H. J. den Hartog, C. Altona, J. –C. Chottard, J. –P. Girault, J. –Y. Lallemand, F. A. A. M. de Leeuw, A. T. M. Marcelis, J. Reedijk, *Nucleic Acid Res*., 1982, **10**, 4715.
63. T. W. Hambley, E. C. H. Ling, B. A. Messerle, *Inorg. Chem*., 1996, **35**, 4663.
64. P. –C. Kong, F. D. Rochon, *Chem. Commun*., 1975, 599.
65. M. Maeda, N. Abiko, H. Uchida, T. Sasaki, *J. Med. Chem*., 1984, **27**, 444.

66. F. Reeder, J. Kozelka, J. C. Chottard, *Inorg. Chem*., 1996, **35**, 1413.
67. U. Bierbach, N. Farrell, *Inorg. Chem*., 1997, **36**, 3657.
68. P. –C. Kong, D. Iyamuremye, F. D. Rochon, *Bioinorganic Chemistry*, 1976, **6**, 83.
69. J. L. van der Veer, H. van den Elst, J. Reedijk, *Inorg. Chem*., 1987, **26**, 1536.
70. M. Schmülling, B. Lippert, R. van Eldik, *Inorg. Chem*., 1994, **33**, 3276.
71. V. Aletras, N. Hadjiliadis, A. Lymberopoulou-Karaliota, I. Rombeck, B. Lippert, *Inorg. Chim. Acta*, 1994, **227**, 17.
72. S. E. Sherman, D. Gibson, A. H. –J. Wang, S. J. Lippard, *Science*, 1985, **230**, 412.
73. P. M. Takahara, C. A. Frederick, S. J. Lippard, *J. Am. Chem. Soc*., 1996, **118**, 12309.
74. P. M. Takahara, A. C. Rosenzweig, C. A. Frederick, S. J. Lippard, *Nature*, 1995, **377**, 649.
75. G. Admiraal, J. L. van der Veer, R. A. G. de Graaff, J. H. J. den Hartog, J. Reedijk, *J. Am. Chem. Soc*., 1987, **109**, 592.
76. M. J. Bloemink, R. J. Heetebrij, K. Inagaki, Y. Kidani, J. Reedijk, *Inorg. Chem*., 1992, **31**, 4656.
77. J. H. J. den Hartog, C. Altona, J. H. van Boom, G. A. van der Marel, C. A. G. Haasnoot, J. Reedijk, *J. Biomol. Struct. Dyns*., 1985, **2**, 1137.
78. F. Herman, J. Kozelka, V. Stoven, E. Guittet, J. –P. Girault, T. Huynh-Dinh, J. Igolen, J. –Y. Lallemand, J. –C. Chottard, *Eur. J. Biochem*., 1990, **194**, 119.
79. J. H. J. den Hartog, C. Altona, J. H. van Boom, G. A. van der Marel, C. A. G. Haasnoot, J. Reedijk, *J. Am. Chem. Soc*., 1984, **106**, 1528.
80. B. Van Hemelryck, E. Guittet, G. Chottard, J. –P. Girault, T. Huynh-Dinh, J. –Y. Lallemand, J. Igolen, J. –C. Chottard, *J. Am. Chem. Soc*., 1984, **106**, 3037.
81. G. L. Cohen, W. R. Bauer, J. K. Barton, S. J. Lippard, *Science*, 1979, **203**, 1014.
82. H. M. Ushay, T. D. Tullius, S. J. Lippard, *Biochemistry*, 1981, **20**, 3744.
83. M. Howe-Grant, K. C. Wu, W. R. Bauer, S. J. Lippard, *Biochemistry*, 1976, **15**, 4339.
84. J. A. Rice, D. M. Crothers, A. L. Pinto, S. J. Lippard, *Proc. Natl. Acad. Sci. USA*, 1988, **85**, 4158.
85. N. Poklar, D. S. Pilch, S. J. Lippard, E. A. Redding, S. U. Dunham, K. J. Breslauer, *Proc. Natl. Acad. Sci. USA*, 1996, **93**, 7606.
86. A. M. J. Fichtinger-Schepman, J. L. van der Veer, J. H. J. den Hartog, P. H. M. Lohman, J. Reedijk, *Biochemistry*, 1985, **24**, 707.

87. P. G. Yohannes, G. Zon, P. W. Doetch, L. G. Marzilli, *J. Am. Chem. Soc*., 1993, **115**, 5105.

88. S. J. Lippard, NATO ASI Series *Bioinorganic Chemistry: An Inorganic Perspective of Life*, ed. D. P. Kessissoglou, Kluwer Academic Publishers, The Netherlands, 1995, 131–140.

89. G. L. Cohen, J. A. Ledner, W. R. Bauer, H. M. Ushay, C. Caravana, S. J. Lippard, *J. Am. Chem. Soc*., 1980, **102**, 2487.

90. F. Gonnet, F. Reeder, J. Kozelka, J. –C. Chottard, *Inorg. Chem*., 1996, **35**, 1653.

91. F. Reeder, J. Kozelka, J. –C. Chottard, *Inorg. Chem*., 1998, **37**, 3964.

92. A. Laoui, J. Kozelka, J. –C. Chottard, *Inorg. Chem*., 1988, **27**, 2751.

93. J. –C. Huang, D. B. Zamble, J. T. Reardon, S. J. Lippard, A. Sancar, *Proc. Natl. Acad. Sci. USA*, 1994, **91**, 10394.

94. P. M. Pil, S. J. Lippard, *Science*, 1992, **256**, 234.

95. E. N. Hughes, B. N. Engelsberg, P. C. Billings, *J. Biol. Chem*., 1992, **267**, 13520.

96. U. –M. Ohndorf, M. A. Rould, Q. He, C. O. Pabo, S. J. Lippard, *Nature*, 1999, **399**, 708.

97. L. Trynda-Lemiesz, H. Kozowski, B. K. Keppler, *J. Inorg. Biochem*., 1999, **77**, 141.

98. T. G. Appleton, J. W. Connor, J. R. Hall, P. D. Prenzler, *Inorg. Chem*., 1989, **28**, 2030.

99. G. Natarajan, R. Malathi, E. Holler, *Biochem. Pharmacol*., 1999, **58**, 1625.

100. T. Rau, R. Alsfasser, A. Zahl, R. van Eldik, *Inorg. Chem*., 1998, **37**, 4223.

101. R. E. Norman, J. D. Ranford, P. J. Sadler, *Inorg. Chem*., 1992, **31**, 877.

102. O. Heudi, A. Cailleux, P. Allain, *J. Inorg. Biochem*., 1998, **71**, 61.

103. P. d. S. Murdoch, J. D. Ranford, P. J. Sadler, S. J. Berners-Price, *Inorg. Chem*., 1993, **32**, 2249.

104. K. J. Barnham, M. I. Djuran, P. d. S. Murdoch, J. D. Ranford, P. J. Sadler, *J. Chem. Soc., Dalton Trans*., 1995, 3721.

105. Y. Chen, Z. Guo, P. d. S. Murdoch, E. Zang, P. J. Sadler, *J. Chem. Soc., Dalton Trans*., 1998, 1503.

106. P. d. S. Murdoch, J. D. Ranford, P. J. Sadler, S. J. Berners-Price, *Inorg. Chem*., 1993, **32**, 2249.

107. T. Grochowski, K. Samochocka, *J. Chem. Soc., Dalton Trans*., 1992, 1145.

108. T. G. Appleton, J. W. Connor, J. R. Hall, *Inorg. Chem*., 1988, **27**, 130.

109. J. A. Galbraith, K. A. Menzel, E. M. A. Ratilla, N. M. Kostic, *Inorg. Chem*., 1987, **26**, 2073.
110. D. D. Gummin, E. M. A. Ratilla, N. M. Kostic, *Inorg. Chem*., 1986, **25**, 2429.
111. Z. Guo, G. Faraglia, S. Sitran, *Transition Met. Chem*., 1995, **20**, 91.
112. S. Suvachittanont, R. van Eldik, *J. Chem. Soc., Dalton Trans*., 1995, 2027.
113. C. A. McAuliffe, *J. Chem. Soc*. (A), 1967, 641.
114. Y. Y. Davidson, S. –C. Chang, R. E. Norman, *J. Chem. Soc., Dalton Trans*., 1995, 77.
115. A. Caubet, V. Moreno, E. Molins, C. Miravitlles, *J. Inorg. Biochem*., 1992, **48**, 135.
116. C. Wilson, M. L. Scudder, T. W. Hambley, H. C. Freeman, *Acta Crystallogr*., *Sect. C*, 1992, **48**, 1012.
117. H. C. Freeman, M. L. Golomb, *Chem. Commun*., 1970, 1523.
118. A. F. M. Siebert, W. S. Sheldrick, *J. Chem. Soc., Dalton Trans*., 1997, 385.
119. M. Calaf, A. Caubet, V. Moreno, M. Font-Bardia, X. Solans, *J. Inorg. Biochem*., 1995, **59**, 63.
120. K. J. Barnham, M. I. Djuran, P. d. S. Murdoch, J. D. Ranford, P. J. Sadler, *Inorg. Chem*., 1996, **35**, 1065.
121. Z. Guo, T. W. Hambley, P. d. S. Murdoch, P. J. Sadler, U. Frey, *J. Chem. Soc., Dalton Trans*., 1997, 469.
122. B. T. Khan, K. Annapoorna, S. Shamsuddin, K. Najmuddin, *Polyhedron*, 1992, **11**, 2109.
123. K. Samochocka, M. Kruszewski, I. Szumiel, *Chem. -Biol. Interact*., 1997, **105**, 145.
124. R. N. Bose, S. Moghaddas, E. L. Weaver, E. H. Cox, *Inorg. Chem*., 1995, **34**, 5878.
125. E. L. M. Lempers, J. Reedijk, *Inorg. Chem*., 1990, **29**, 217.
126. M. I. Djuran, E. L. M. Lempers, J. Reedijk, *Inorg. Chem*., 1991, **30**, 2648.
127. T. G. Appleton, J. W. Connor, J. R. Hall, *Inorg. Chem*., 1988, **27**, 130.
128. S. S. G. E. van Boom, J. Reedijk, *Chem. Commun*., 1993, 1397.
129. J. –M. Teuben, S. S. G. E. van Boom, J. Reedijk, *J. Chem. Soc., Dalton Trans*., 1997, 3979.
130. K. J. Barnham, M. I. Djuran, P. d. S. Murdoch, P. J. Sadler, *Chem. Commun*., 1994, 721.

131. K. J. Barnham, Z. Guo, P. J. Sadler, *J. Chem. Soc., Dalton Trans*., 1996, 2867.
132. S. S. G. E. van Boom, B. W. Chen, J. M. Teuben, J. Reedijk, *Inorg. Chem*., 1999, **38**, 1450.
133. N. Farrell, *Chem. Commun*., 1982, 331.
134. N. Farrell, D. M. Kiley, W. Schmidt, M. P. Hacker, *Inorg. Chem*., 1990, **29**, 397.
135. K. Lövqvist, Ph.D. Dissertation, Lund University, Sweden, 1996.
136. E. L. M. Lempers, M. J. Bloemink, J. Reedijk, *Inorg. Chem*., 1991, **30**, 201.
137. J. A. Davies, *Adv. Inorg. Chem. Radiochem*., 1981, **24**, 115.
138. M. Calligaris, O. Carugo, *Coord. Chem. Rev*., 1996, **153**, 83 and references therein.
139. A. R. Khokhar, S. S. Al-Baker, C. Shah, *J. Coord. Chem*., 1995, **36**, 7.
140. U. Bierbach, T. W. Hambley, N. Farrell, *Inorg. Chem*., 1998, **37**, 708.
141. U. Bierbach, J. D. Roberts, N. Farrell, *Inorg. Chem*., 1998, **37**, 717.
142. A. Pasini, P. Perego, M. Balconi, M. Lupatini, *J. Chem. Soc., Dalton Trans*., 1995, 579.
143. A. Pasini, G. D'Alfonso, C. Manzotti, M. Moret, S. Spinelli, M. Valsecchi, *Inorg. Chem*., 1994, **33**, 4140.
144. A. Pasini, C. Fiore, *Inorg. Chim. Acta*, 1999, **285**, 249.
145. A. Pasini, M. Moroni, *J. Chem. Soc., Dalton Trans*., 1997, 1093.
146. L. Antolini, U. Folli, D. Iarossi, L. Schenetti, F. Taddei, *J. Chem. Soc., Perkin Trans. 2*, 1991, 955.
147. R. Melanson, F. D. Rochon, *Acta Crystallogr*., *Sect. C*, 1987, **43**, 1869.
148. S. G. de Almeida, J. L. Hubbard, N. Farrell, *Inorg. Chim. Acta*, 1992, **193,** 149.
149. F. P. Fanizzi, G. Natile, M. Lanfranchi, A. Tiripicchio, *Inorg. Chim. Acta*, 1997, **264**, 11.
150. S. Lanza, D. Minniti, R. Romeo, M. L. Tobe, *Inorg. Chem*, 1983, **22**, 2006.
151. O. Clement, A. W. Roszak, E. Buncel, *Inorg. Chim. Acta*, 1996, **253**, 53.
152. G. Alibrandi, R. Romeo, L. M. Scolaro, M. L. Tobe, *Inorg. Chem*., 1992, **31**, 5061.
153. W. Lesueur, A. J. Rogers, C. Floriani, A. Chiesi-Villa, C. Rizzoli, *Inorg. Chem*., 1998, **37**, 44.
154. R. Romeo, D. Minniti, G. Alibrandi, L. De Cola, M. L. Tobe, *Inorg. Chem*., 1986, **25**, 1944.
155. P. D. Braddock, R. Romeo, M. L. Tobe, *Inorg. Chem*., 1974, **13**, 1170.

156. R. Romeo, M. L. Tobe, *Inorg. Chem.*, 1974, **13**, 1991.
157. E. W. Neuse, A. G. Perlwitz, J. S. Field, N. Ramesar, *Transition Met. Chem*., 1995, **20**, 62.
158. G. Caldwell, E. W. Neuse, A. G. Perlwitz, J. S. Field, N. Ramesar, *Transition Met. Chem*., 1995, **20**, 200.
159. R. Melanson, F. D. Rochon., *Acta Crystallogr*., *Sect. B*, 1978, **34**, 941.
160. V. K. Belsky, V. E. Konovalov, V. Yu. Kukushkin, *Acta Crystallogr*., *Sect. C*, 1991, **47**, 292.
161. R. Melanson, F. D. Rochon., *Acta Crystallogr*., *Sect B*, 1977, **33**, 3571.
162. F. Caruso, R. Spagna, L. Zambonelli, *Acta Crystallogr*., *Sect B*, 1980, **36**, 713.
163. L. G. Marzilli, Y. Hayden, M. D. Reily, *Inorg. Chem*., 1986, **25**, 974.
164. W. I. Sundquist, K. J. Ahmed, L. S. Hollis, S. J. Lippard, *Inorg. Chem*., 1987, **26**, 1524.
165. J. –M. Delafontaine, P. Khodadad, P. Toffoli, N. Rodier, *Acta Crystallogr*., *Sect. C*, 1985, **41**, 702.
166. M. van Beusichem, N. Farrell, *Inorg. Chem.*, 1992, **31**, 634.
167. L. E. Erickson, I. E. Burgeson, E. Eidsmoe, R. G. Larsen, *Inorg. Chem*., 1989, **28**, 1315.
168. T. Komorita, A. Fuyuhiro, K. Tanimoto, K. Yamauchi, K. Fujita, *Bull. Chem. Soc. Jpn*., 1995, **68**, 1593.
169. J. S. Kerrison, P. J. Sadler, *Chem. Commun*., 1977, 861.
170. R. Melanson, F. D. Rochon, *Inorg. Chem*., 1978, **17**, 679.
171. M. D. Reily, K. Wilkowski, K. Shinozuka, L. G. Marzilli, *Inorg. Chem*., 1985, **24**, 37.
172. C. J. L. Lock, R. A. Speranzini, G. Turner, J. Powell, *J. Am. Chem. Soc*., 1976, **98**, 7865.
173. G. Annibale, L. Canovese, G. Chessa, L. Cattalini, M. L. Tobe, *J. Chem. Soc*., *Dalton Trans*., 1990, 401.
174. R. Romeo, G. Arena, L. M. Scolaro, M. R. Plutino, *Inorg. Chim. Acta*, 1995, **240**, 81.
175. R. Romeo, L. M. Scolaro, N. Nastasi, G. Arena, *Inorg. Chem*., 1996, **35**, 5087.
176. R. Romeo, L. M. Scolaro, N. Nastasi, B. E. Mann, G. Bruno, F. Nicolò, *Inorg. Chem*., 1996, **35**, 7691.
177. F. D. Rochon, P. C. Kong, R. Melanson, *Inorg. Chem*., 1990, **29**, 1352.

178. V. K. Belsky, V. E. Konovalov, V. Yu. Kukushkin, A. I. Moiseev, *Inorg. Chim. Acta*, 1990, **169**, 101.
179. V. Yu. Kukushkin, V. K. Belsky, V. E. Konovalov, G. A. Kirakosyan, L. V. Konovalov, A. I. Moiseev, V. M. Tkachuk, *Inorg. Chim. Acta*, 1991, **185**, 143.
180. R. G. Ball, N. C. Payne, *Inorg. Chem*., 1977, **16**, 1871.
181. F. D. Rochon, P. C. Kong, R. Melanson, *Inorg. Chem*., 1990, **29**, 2708.
182. Y. N. Kukushkin, V. K. Krylov, S. F. Kaplan, M. Calligaris, E. Zangrando, A. J. L. Pombeiro, V. Yu. Kukushkin, *Inorg. Chim. Acta*, 1999, **285**, 116.
183. N. Farrell, T. T. B. Ha, J. –P. Souchard, F. L. Wimmer, S. Cros, N. P. Johnson, *J. Med. Chem*., 1989, **32**, 2241.
184. Y. Zou, B. Van Houten, N. Farrell, *Biochemistry*, 1993, **32**, 9632.
185. M. V. Keck, S. J. Lippard, *J. Am. Chem. Soc*., 1992, **114**, 3386.
186. M. Kharatishvili, M. Mathieson, N. Farrell, *Inorg. Chim. Acta*, 1997, **255**, 1.
187. U. Bierbach, N. Farrell, *JBIC*., 1998, **3**, 570.
188. U. Bierbach, Y. Qu, T. W. Hambley, J. Peroutka, H. L. Nguyen, M. Doedee, N. Farrell, *Inorg. Chem*., 1999, **38**, 3535.
189. Y. Chen, Z. Guo, J. A. Parkinson, P. J. Sadler, *J. Chem. Soc., Dalton Trans*., 1998, 3577.
190. J. Holford, S. Y. Sharp, B. A. Murrer, M. Abrams, L. R. Kelland, *Br. J. Cancer*, 1998, **77**, 366.
191. M. J. Bloemink, H. Engelking, S. Karentzopoulos, B. Krebs, J. Reedijk, *Inorg. Chem*., 1996, **35**, 619.
192. V. Murray, H. Motyka, P. R. England, G. Wickham, H. H. Lee, W. A. Denny, W. D. McFadyen, *Biochemistry*, 1992, **31**, 11812.
193. B. D. Palmer, H. H. Lee, P. Johnson, B. C. Baguley, G. Wickham, L. P. G. Wakelin, W. D. McFadyen, W. A. Denny, *J. Med. Chem*., 1990, **33**, 3008.
194. H. H. Lee, B. D. Palmer, B. C. Baguley, M. Chin, W. D. McFadyen, G. Wickham, D. Thorsbourne-Palmer, L. P. G. Wakelin, W. A. Denny, *J. Med. Chem*., 1992, **35**, 2983.
195. W. I. Sundquist, D. P. Bancroft, L. Chassot, S. J. Lippard, *J. Am. Chem. Soc*., 1988, **110**, 8559.
196. B. E. Bowler, L. S. Hollis, S. J. Lippard, *J. Am. Chem. Soc*., 1984, **106**, 6102.
197. B. E. Bowler, S. J. Lippard, *Biochemistry*, 1986, **25**, 3031.

198. B. E. Bowler, K. J. Ahmed, W. I. Sundquist, L. S. Hollis, E. E. Whang, S. J. Lippard, *J. Am. Chem. Soc*., 1989, **111**, 1299.

199. D. Gibson, N. Mansur, K. F. Gean, *J. Inorg. Biochem*., 1995, **58**, 79.

200. Y. Mikata, M. Yokoyama, K. Mogami, M. Kato, I. Okura, M. Chikira, S. Yano, *Inorg. Chim. Acta*, 1998, **279**, 51.

201. N. D. Sachinvala, H. Chen, W. P. Niemczura, E. Furusawa, R. E. Cramer, J. J. Rupp, I. Ganjian, *J. Med. Chem*., 1993, **36**, 1791.

202. T. Tsubomura, M. Ogawa, S. Yano, K. Kobayashi, T. Sakurai, S. Yoshikawa, *Inorg. Chem*., 1990, **29**, 2622.

203. R. Gust, K. Niebler, H. Schönenberger, *J. Med. Chem*., 1995, **38**, 2070.

204. P. J. Bednarski, *J. Inorg. Biochem*., 1995, **80**, 1.

205. R. Köckerbauer, P. J. Bednarski, *J. Inorg. Biochem*., 1996, **62**, 281.

206. R. Gust, H. Heinrich, R. Krauser, H. Schönenberger, *Inorg. Chim. Acta*, 1999, **285**, 184.

207. H. Brunner, F. Maiterth, B. Treittinger, *Inorg. Chim. Acta*, 1992, **198–200**, 79.

208. R. Gust, H. Schönenberger, J. Kritzenberger, K. –J. Range, U. Klement, T. Burgemeister, *Inorg. Chem*., 1993, **32**, 5939.

209. R. Gust, M. Gelbcke, B. Angermaier, H. Bachmann, R. Krauser, H. Schönenberger, *Inorg. Chim. Acta*, 1997, **264**, 145.

210. D. Christodoulou, C. M. Giandomenico, M. J. Abrams, S. Martelluci, L. Kelland, K. Harrap, presented in part at the 5th International Symposium on Applied Bioinorganic Chemistry, Corfu, April, 1999.

211. P. Perego, C. Caserini, L. Gatti, N. Carenini, S. Romanelli, R. Supino, D. Colangelo, I. Viano, R. Leone, S. Spinelli, G. Pezzoni, C. Manzotti, N. Farrell, F. Zunino, *Mol. Pharmacol*., 1999, **55**, 528.

212. H. Rauter, R. Di Domenico, E. Menta, A. Oliva, Y. Qu, N. Farrell, *Inorg. Chem*., 1997, **36**, 3919.

213. M. Kharatishvili, M. Mathieson, N. Farrell, *Inorg. Chim. Acta*, 1997, **255**, 1.

214. N. Farrell, T. G. Appleton, Y. Qu, J. D. Roberts, A. P. Soares Fontes, K. A. Skov, P. Wu, Y. Zou, *Biochemistry*, 1995, **34**, 15480.

215. P. K. Wu, M. Kharatishvili, Y. Qu, N. Farrell, *J. Inorg. Biochem*., 1996, **63**, 9.

216. P. K. Wu, Y. Qu, B. Van Houten, N. Farrell, *J. Inorg.Biochem*., 1994, **54**, 207.

217. M. J. Bloemink, J. Reedijk, N. Farrell, Y. Qu, A. I. Stetsenko, *Chem. Commun*., 1992, 1002.

218. E. Schuhmann, J. Altman, K. Karaghiosoff, W. Beck, *Inorg. Chem*., 1995, **34**, 2316.

219. G. Zhao, H. Lin, P. Yu, H. Sun, S. Zhu, Y. Chen, *Chem. -Biol. Interact*., 1998, **116**, 19.

220. N. Farrell, Y. Qu, L. Feng, B. Van Houten, *Biochemistry*, 1990, **29**, 9522.

221. N. P. Farrell, S. G. de Almeida, K. A. Skov, *J. Am. Chem. Soc*., 1988, **110**, 5018.

222. Y. Qu, S. G. de Almeida, N. Farrell, *Inorg. Chim. Acta*, 1992, **201**, 123.

223. V. Brabec, J. Kašpárková, O. Vrána, O. Nováková, J. W. Cox, Y. Qu, N. Farrell, *Biochemistry*, 1999, **38**, 6781.

CHAPTER 2

GENERAL PHYSICAL METHODS

2.1 Instrumentation and physical methods

The following instruments and experimental methods were used throughout this study for the identification and characterisation of the compounds prepared.

Elemental analyses

Elemental analyses for % C, H, N and S were carried out at the microanalytical unit at the University of Cape Town, South Africa.

Melting point determination

All melting points were determined on a Reichert hot-stage microscope and are uncorrected.

Infrared spectroscopy

Infrared (IR) spectra were recorded as KBr disks on a Perkin-Elmer FTIR Spectrum 2000, between 4000 and 250 cm^{-1}. The infrared data are reported as follows: position of signal (cm^{-1}), intensity of band (w = weak, vw = very weak, m = moderate, s = strong, vs = very strong) and shape of band (br = broad, sh = sharp, pr = pair and shld = shoulder).

Thin-layer chromatography

Thin-layer chromatography (TLC) was performed on silica sheets $60F_{254}$ (Merck, Darmstadt). Reverse phase TLC was performed on glass backed RP-$C18F_{254}S$ plates (Techware).

Flash chromatography

Flash chromatography was performed on silica gel 60 (Merck, Darmstadt).

Molecular exclusion chromatography

Molecular exclusion chromatography was performed using Lipophilic Sephadex LH-20 (Sigma).

Polarimetry

The optical rotations of chiral compounds was determined using a Perkin-Elmer 141 Polarimeter, with dry acetone as solvent at 25°C.

Differential scanning calorimetry

Differential scanning calorimetry (DSC) was performed on a Perkin-Elmer Delta series 7 instrument, under a nitrogen atmosphere. The temperature range for the DSC experiments was 50–250°C.

High performance liquid chromatography

High performance liquid chromatography (HPLC) was performed with a Spectro-Physics P100 isocratic pump, Whatman Partisil 10 Column (NP), Waters 401 Differential Refractometer, Rikadenki chart recorder (5 mm/min.; 10 mV) and rheodyne injector.

NMR spectroscopy

^{1}H (400 MHz), ^{13}C (100 MHz), Dept-135, COSY, HMBC and HMQC NMR spectra were recorded on a Bruker 400 AMX or Avance pulse Fourier transform spectrometer using standard pulse sequences. Unless otherwise stated, the probe temperature for all experiments was 30 ± 1°C. All samples were prepared using deuterated solvents purchased from Aldrich Chemical Company and 5 mm NMR tubes were used throughout. Chemical shifts are reported in parts per million (ppm) relative to the central line of the solvent resonance of known shifts relative to TMS, and coupling constants are reported in hertz (Hz). The chemical shift data are reported as follows: chemical shift (ppm); number of protons; multiplicity, s = singlet, d = doublet, t = triplet, m = multiplet; assignment.

^{195}Pt NMR spectra were recorded using 70–150 KHz spectral widths and 13 μs pulses with 1 s pulse delay. Between 2048 and 16 000 transients, with a line broadening factor of 10 Hz, gave good spectra. All ^{195}Pt chemical shifts are quoted relative to an external standard [H_2PtCl_6 (500 mg in 1 ml 30% (v/v) D_2O/1 M HCl)].

^{31}P-{^{1}H} NMR spectra were recorded using 130 KHz spectral widths and 15.5 μs pulses with 1 s pulse delay. Between 32 and 17 000 transients, with a line broadening factor of 1 Hz, gave good spectra. All ^{31}P chemical shifts are reported relative to an external standard (85% H_3PO_4).

Due to the extensive use of ^{195}Pt (I = ½, 33.7%) and ^{31}P (I = ½, 100%) NMR spectroscopy in this study, the theoretical aspects of ^{195}Pt and ^{31}P NMR spectroscopy will now be discussed.

Background Theory

The use of ^{195}Pt and ^{31}P NMR spectroscopy has become routine for the identification and characterisation of compounds containing these NMR active nuclei. The ^{1}H and ^{13}C NMR spectra of mixtures of complexes tend to be complicated, while the corresponding ^{195}Pt and ^{31}P NMR spectra are relatively simple and easier to interpret. The ^{195}Pt chemical shift is very sensitive to the coordination sphere around the metal centre and small changes in the molecular structure or geometry of the complex generally result in significantly different chemical shifts for the different species. [1, 2]

No accurate predictions of ^{195}Pt and ^{31}P chemical shifts are possible, but for ^{195}Pt some qualitative generalisations have been made in the literature. [1, 2]

i) Chemical shifts move to higher fields in the order: P > As > S > N > Cl^- > O.
ii) The signals for platinum(II) complexes often appear at higher fields compared to those for the corresponding platinum(IV) complexes.
iii) The ^{195}Pt NMR chemical shift of the *cis*-isomers of complexes of the type [$PtCl_2L_2$] are generally upfield with respect to the *trans*-isomers, where L = phosphine or sulfide.

Both solvent and temperature affect the ^{195}Pt and ^{31}P chemical shifts, therefore, conclusions based on small differences in the ^{195}Pt and ^{31}P chemical shifts, must be drawn from measurements made in the same solvent and at the same temperature.

If NMR active nuclei (^{1}H, ^{13}C and ^{31}P) are spin-spin coupled to the platinum centre, one- to three-bond coupling constants, commonly called satellites, may be observed, which may aid in the identification and characterisation of these complexes. For example, the presence of ^{3}J(PtH) coupling of the methyl protons resonances of a sulfoxide with a platinum nucleus are indicative of a sulfur-bonded sulfoxide. [3]

The one-bond coupling constant is defined as follows:

$$J(\mathrm{A},\mathrm{B}) = (\text{constant})\gamma_{\mathrm{A}}\gamma_{\mathrm{B}}\left|\Psi(0)\right|^{2}_{\mathrm{A}}\left|\Psi(0)\right|^{2}_{\mathrm{B}}\pi_{\mathrm{AB}}$$

where γ is the gyromagnetic ratio, $|\Psi(0)|^2$ describes the valence *s* electron densities at the nuclei A and B and π_{AB} is the mutual polarisability of nuclei A and B. Nuclei with small γ and $|\Psi(0)|^2$ values have smaller ^{1}J(PtL) coupling constants than nuclei with larger γ values. For example, ^{1}J(PtP) coupling constants are an order of magnitude larger than ^{1}J(PtN) coupling constants. The ^{1}J(PtP) coupling constants are sensitive to changes in the ligand *trans* to the phosphorus atom and are hardly affected by a change in the nature of the *cis* neighbour and therefore have been used to determine the *trans*-influence of various groups *trans* to the phosphines. [4] The *trans*-influence of a ligand Y in a metal complex has been defined as the extent that Y weakens the bond *trans* to itself in the ground state. [5] The ^{1}J(PtP) coupling constants provide information on the *s*-orbital contribution and therefore extreme care must be taken in extrapolating to other types of metal-ligand bonding, for example, dπ–dπ backbonding. [1, 4]

Chemically non-equivalent phosphorus atoms couple with one another as well as the platinum atom and appear as two sets of doublets with satellites. The ^{1}J(PtP) coupling constant varies according to the *trans*-influence of the ligand opposite to the Pt–P bond. The general trend observed is that phosphorus atoms *trans* to each other have ^{1}J(PtP) values of approximately 2200–2400 Hz, whereas phosphorus atoms *cis* to each other have ^{1}J(PtP) values in the range 3200–3600 Hz. [4, 6, 7]

2.2 References

1. P. S. Pregosin, *Coord. Chem. Rev*., 1982, **44**, 247.
2. P. S. Pregosin, in *Studies in Inorganic Chemistry 13, Transition Metal Nuclear Magnetic Resonance*, ed. P. S. Pregosin, Elsevier, New York, 1991.
3. J. H. Price, A. N. Williamson, R. F. Schramm, B. B. Wayland, *Inorg. Chem*., 1972, **11**, 1280.
4. T. G. Appleton, H. C. Clark, L. E. Manzer, *Coord. Chem. Rev*., 1973, **10**, 335.
5. A. Pidcock, R. E. Richards, L. M. Venanzi, *J. Chem. Soc*. (A), 1966, 1707.
6. P. S. Pregosin, R. W. Kunz, in *NMR Basic Principles and Progress: ^{31}P and ^{13}C NMR of Transition Metal Complexes*, ed. P. Diehl, E. Fluck, R. Kosfeld, Springer-Verlag, New York, 1979.
7. *Phosphorus–31 NMR Spectroscopy in Stereochemical Analysis: Organic Compounds and Metal Complexes*, ed. J. G. Verkade, L. D. Quin, VCH, Weinheim, 1987.

CHAPTER 3

SYNTHESIS AND CHARACTERISATION OF *N*-ACYL-*N'*,*N'*-DIALKYLTHIOUREA AND *N*-ALKOXYCARBONYL-*N'*,*N'*-DIALKYL-THIOUREA LIGAND SYSTEMS

3.1 Introduction

The general structures of *N*-acyl-*N'*-alkylthioureas (**1**) and *N*-acyl-*N',N'*-dialkylthioureas (**2**) and *N*-alkoxycarbonyl-*N',N'*-dialkylthioureas (**3**) are shown in Figure 3.1. *N*-Acyl-*N'*-alkylthiourea and *N*-acyl-*N',N'*-dialkylthioureas have been used extensively for the solvent extraction and preconcentration [1, 2] of platinum group metals, as well as the selective coordination and separation of the softer 2nd and 3rd row transition metals. [3–30]

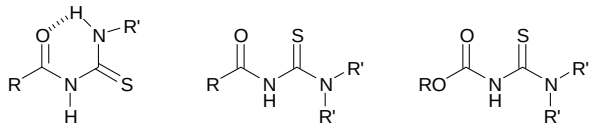

(**1**) (**2**) (**3**)

Figure 3.1: Schematic representation of *N*-acyl-*N'*-alkylthiourea (**1**), *N*-acyl-*N',N'*-dialkylthiourea (**2**) and *N*-alkoxycarbonyl-*N',N'*-dialkylthiourea (**3**).

Crystal structure determinations of a number of *N*-acyl-*N'*-alkylthioureas (**1**) [31–39] and *N*-acyl-*N',N'*-dialkylthioureas (**2**) [13, 15, 40–46] have shown that (**1**) and (**2**) are structurally different. A characteristic feature of *N*-acyl-*N'*-alkylthioureas (**1**) is the presence of an intramolecular hydrogen bond between the thioamide NH and the carbonyl oxygen atom (Figure 3.1). The intramolecular hydrogen bond is present in solution [13, 47, 48] and in the solid state. [31–39] In this respect, the *N*-acyl-*N'*-alkylthioureas (**1**) are structurally similar to the monothio-β-diketones (Figure 3.2). The structural differences between (**1**) and (**2**) have a distinct effect on the coordination chemistry of these ligand systems towards platinum group metals. *N*-Acyl-*N'*-alkylthioureas generally act as unidentate sulfur donors, because coordination of the carbonyl group is prohibited by an intramolecular hydrogen bond between the carbonyl group and the thioamide proton. *N*-Benzoyl-*N'*-propylthiourea is an elegant example of this unidentate coordination of a potentially bidentate ligand. Coordination of this ligand to Pt(II) yields complexes of the type *cis*/*trans*-$[PtCl_2(HL\text{-}S)_2]$, where (HL-S) represents the sulfur coordinated *N*-benzoyl-*N'*-propylthiourea. [13, 39] The unidentate coordination of *N*-acyl-*N'*-alkylthiourea ligands is comparable to that observed for thiourea. [49] There are two reported cases of *N*-aroyl-*N'*-phenylthiourea ligands coordinating tridentately to nickel [2] and rhodium. [50] For example, treatment of $[RhCl(CO)_2]_2$ with *N*-benzoyl-*N'*-phenylthiourea (L^2) followed by a slight excess of PPh_3 leads to the formation of $[(PPh_3)_2(CO)Rh(\mu\text{-}L^2\text{-}$

κN':κO,S)Rh(PPh$_3$)(CO)]·(CH$_3$)$_2$CO, in which one rhodium atom is coordinated to the carbonyl and thiocarbonyl donor atoms and the second rhodium metal centre is bound to the amidic nitrogen atom of the doubly deprotonated *N*-benzoyl-*N'*-phenylthiourea ligand.

Thiourea Monothio-β-diketone

Figure 3.2: Schematic representation of thiourea and monothio-β-ketones. [49]

N-Acyl-*N',N'*-dialkylthioureas can act as either unidentate or bidentate ligands, depending on the the pH. [47, 48] For bidentate chelation, deprotonation of the acidic amide proton must occur for the carbonyl oxygen to coordinate to the metal centre. If the amide proton is not removed, the ligand will bind monodentately via the sulfur donor atom. [47] Structural studies have revealed that *N*-acyl-*N',N'*-dialkylthioureas generally form complexes with a *cis* configuration. [11, 12, 22, 26, 51] Recently Koch *et al*. reported the first crystal structure of a *trans*-[Pt(*N*-acyl-*N',N'*-dialkylthioureato)$_2$] complex, *trans*-[Pt(*N,N*-dibutyl-*N'*-naphthoylthioureato)$_2$], which was isolated as the minor product. [52]

Tetradentate 3,3,3',3'-tetraalkyl-1,1'-aryldicarbonylbis(thiourea) and 3,3,3',3'-tetra-alkyl-1,1'-alkanedioylbis(thiourea) ligands have also been prepared. [11, 22, 23] The general structure of these tetradentate acylthiourea ligands is shown in Figure 3.3.

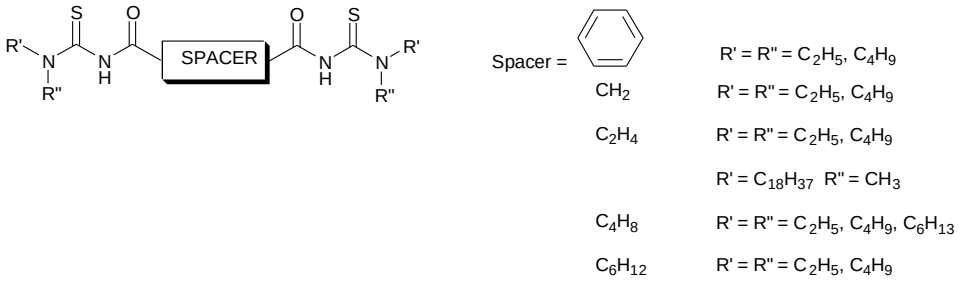

Figure 3.3: General structure of tetradentate *N*-acyl-*N',N'*-dialkylthiourea ligands. [11, 22, 23]

Hoyer *et al*. reported the crystal structure of a Ni$_3$L$_3$ complex where L = 3,3,3',3'-tetraethyl-1,1'-terephthaloylbis(thiourea). [53] A series of 3,3,3',3'-tetraalkyl-1,1'-alkane-dicarbonylbis(thiourea) ligands was prepared by König *et al*. for the selective extraction and separation of Ni(II), Cu(II), Pd(II) and Pt(II). [23]

N,N-Dialkyl-*N'*-ethoxycarbonylthioureas have a similar coordination chemistry to *N*-acyl-*N',N'*-dialkylthioureas, in that they coordinate to Co(II), Cu(II) and Ni(II) bidentately via the carbonyl and thiocarbonyl donor atoms. [54] *N*-Ethoxycarbonyl-, *N*-butoxycarbonyl- and *N*-methoxycarbonyl-*N'*-(*p*-nitrophenyl)thioureas have a similar coordination chemistry to *N*-acyl-*N'*-alkylthioureas, as they were found to bind monodentately via the thiocarbonyl to Cu(I). [55, 56] *N*-Ethoxycarbonyl-*N',N'*-diethylthiourea has been used for the separation of a wide range of transition metals using high performance thin-layer chromatography. [57] No X-ray crystal structures of *N*-alkoxycarbonyl-*N',N'*-dialkyl-thioureas and their metal complexes have been reported.

Interest in acylthiourea ligand systems stems from their ease of preparation and the fact that the acyl and thiourea groups can be readily varied. [13, 18, 58] For example, fluorescent or electrochemically active groups have been incorporated into these ligand systems. Electrochemical molecular recognition is a growing research area at the interface of electrochemistry and supramolecular chemistry. One of the aims of this research is the development of selective and sensitive probes for charged and neutral guest species. Beer and coworkers have prepared a number of redox-active thiourea receptors, containing a ferrocene moiety that is capable of anionic recognition. [59] It was found that the thiourea and urea derivatives interacted favourably with guest species, but the *N*-alkyl-*N'*-ferrocenoylthioureas (Figure 3.4) did not act as sensors for anionic guest species. The absence of redox-activity at this ferrocene moiety is thought to be due to the intramolecular hydrogen bond between the carbonyl and the thioamide proton forcing the molecule into an unfavourable conformation. The synthesis of *N,N*-dialkyl-*N'*-ferrocenoylthioureas (Figure 3.4) and their metal complexes with nickel, cobalt, copper and manganese have recently been reported. [14, 15]

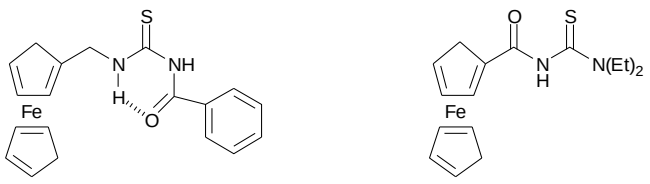

Figure 3.4: Structures of ferrocene acylthiourea ligands. [14, 15, 59]

The detection of metal ions in biomedical and environmental samples is very important. Unfortunately, only a few metal ions exhibit a natural luminescence. This necessitates

complexation with ligands with intrinsic luminescent properties, because fluorescence detection is very sensitive and selective and allows the detection of trace quantities of metal ions in solution. *N*-Acyl-*N',N'*-dialkylthioureas are known to bind selectively to class (b) metals. Hence, Schuster *et al*. have recently prepared acylthiourea ligands containing fluorescent moieties. [16, 17, 25] An anthracene-substituted benzoylthiourea, *N*-benzoyl-*N'*-methyl-*N'*-9-(methylanthracene)thiourea (**4**) and two pyrene substituted ligands, *N,N*-diethyl-*N'*-1-pyreneoylthiourea (**5**) and *N,N*-diethyl-*N'*-4-(1-pyrene)butyryl-thiourea (**6**) (Figure 3.5), have been prepared for the fluorometric determination of metal ions. The anthracene-substituted ligands were found to be very selective and sensitive sensors for Hg(II). [17] The pyrene ligands showed selective complexation in that Pd(II), Pt(II), Ru(III) and Rh(III) are complexed at pH-values < 2, whereas Ni(II), Zn(II) and Co(II) are complexed at higher pH-values. The fluorescent properties of the ligands were found to be dependent on the length of the methylene spacer group next to the pyrene moiety. [25] Studies are currently being carried out for the development of a multiple fibre optic sensor array based on laser-induced luminescence. 1-(9-Anthrylcarbonyl)-3,3-tetra-methylenethiourea has also recently been prepared. [40]

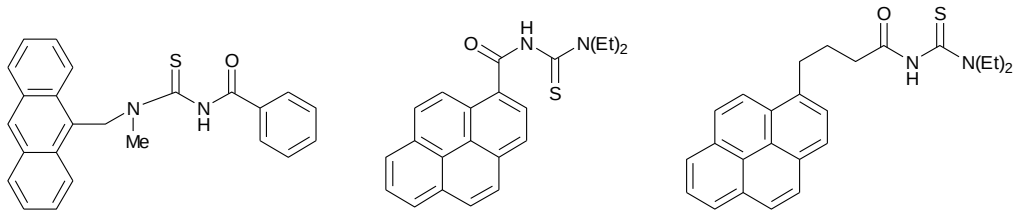

(**4**) (**5**) (**6**)

Figure 3.5: Luminescent *N*-benzoyl-*N'*-methyl-*N'*-9-(methylanthracene)thiourea (**4**), *N,N*-diethyl-*N'*-1-pyreneoylthiourea (**5**) and *N,N*-diethyl-*N'*-4-(1-pyrene)butyrylthiourea (**6**) ligands. [16, 17, 25]

N-Aryl-*N'*-benzoylthioureas have also been used as liquid crystals and as building blocks for heterometallic liquid crystal systems. Ferrocene derivatives of 4-alkoxy-substituted *N*-aryl-*N'*-benzoylthioureas (Figure 3.6) with increasing chain length have been prepared by Seshadri *et al*.. [60] These compounds exhibited enantiotropic smectic S_c and S_a phases while the presence of the nematic phase below the glass-transition temperature lends itself to possible applications in display devices.

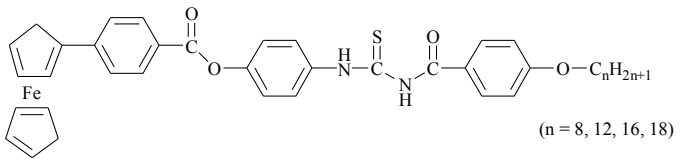

Figure 3.6: 4-Alkoxy-substituted *N*-aryl-*N'*-benzoylthioureas with liquid crystalline properties. [60]

A wide range of chiral *N*-acyl-*N',N'*-dialkylthioureas has been prepared by Djerassi *et al*. utilising chiral carboxylic acids. [61] Chirality has also been introduced into acylthiourea ligand systems through the thiourea moiety, via the incorporation of a chiral proline ethyl ester moiety. [46]

In the present study, *N,N*-dialkyl-*N'*-(3-*R*-benzoyl)thiourea, *N*-(3-*R*-benzoyl)-*N'*-morpholinothiourea, *N,N*-diethyl-*N'*-menthyloxycarbonylthiourea and *N*-menthyloxy-carbonyl-*N'*-morpholinothiourea ligand systems have been prepared. The hydrophilicity of the ligands and, therefore, the corresponding platinum(II) complexes, has been varied by altering the amine moiety with groups of varying degrees of water solubility (diethylamine, morpholine and di(2-hydroxyethyl)amine). The 3-R-benzoyl moiety, where R = NO_2, Cl, H, OCH_3 and CH_3, has been varied with groups having different electronic properties. Chiral ligands have also been prepared by incorporating a menthyloxycarbonyl group as the acyl moiety. By varying the electronic properties and the degree of water solubility, and by the incorporation of chiral groups, it may be possible to control the substitution reaction kinetics and bioavailability and/or the specific uptake of the corresponding platinum(II) complexes.

3.2 Ligand synthesis

In the present study, all the *N*-acyl-*N',N'*-dialkylthiourea, *N*-(3-*R*-benzoyl)-*N'*-morpholinothiourea, *N,N*-diethyl-*N'*-menthyloxycarbonylthiourea and *N*-menthyloxy-carbonyl-*N'*-morpholinothiourea ligand systems were prepared according to a modified method of Douglass and Dains, as described by the following overall equation (**3 – 1**). [62]

$$RCOCl + KSCN + HN(R')_2 \longrightarrow RCONHCSN(R')_2 \qquad (\mathbf{3-1})$$

The multi-step one pot synthesis involves nucleophilic attack of the isothiocyanate/thiocyanate anion at the carbonyl group of an acid chloride or chloroformate, to form the substituted isothiocyanate and thiocyanate, respectively. The reaction of the substituted isothiocyanate with a secondary amine yields the respective acylthiourea or alkoxycarbonylthiourea ligands.

The reaction of an acid chloride and alkyl chloroformate with the thiocyanate/isothiocyanate anion has been reported by Takamizawa *et al*., [63] and is outlined in Figure 3.7. Benzoyl chlorides and alkyl chloroformates show distinctly different reactivities towards the thiocyanate anion. [63] In acetone or other polar solvents, the thiocyanate anion exists in two forms **(7)** and **(8)**. [64] Electrophilic attack of the carbonyl carbon of the benzoyl chloride is equally possible at the sulfur and nitrogen sites and gives rise to the acylthiocyanate **(9)** and acylisothiocyanate **(10)**, respectively. On heating, total conversion of the acylthiocyanate to the acylisothiocyanate derivative is achieved because the carbonyl carbon of the acylthiocyanate isomer is relatively reactive and therefore reacts with an additional isothiocyanate anion to yield **(10)**. Alkyl chloroformates do not behave in this manner, because the carbonyl carbon of the alkoxycarbonylthiocyanate is relatively unreactive, hence both the alkoxycarbonyl-thiocyanate and alkoxycarbonylisothiocyanate products are isolated.

The reactions of carbonyl isothiocyanates with amines have been extensively investigated and have been shown to occur smoothly on heating in polar solvents, as well as solvents of low polarity. [64]

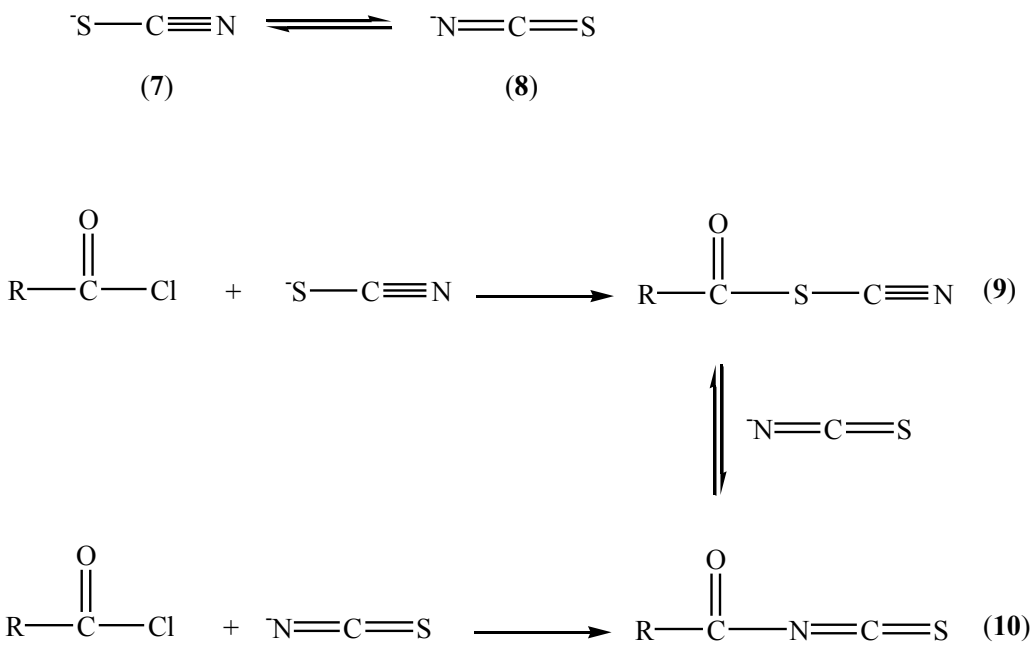

Figure 3.7: Outline of the mechanism involved in the reaction of an acid chloride with the thiocyanate/ isothiocyanate anion. Where RCOCl is a benzoyl chloride only the acylisothiocyanate **(10)** is obtained, but when an alkyl chloroformate is used, both the alkoxycarbonylthiocyanate **(9)** and alkoxycarbonyl-isothiocyanate **(10)** products are obtained. [63]

The structural formulae and atom numbering schemes adopted for NMR assignments of the *N,N*-dialkyl-*N'*-(3-*R*-benzoyl)thiourea, *N*-(3-*R*-benzoyl)-*N'*-morpholinothiourea, *N,N*-diethyl-*N'*-menthyloxycarbonylthiourea and *N*-menthyloxycarbonyl-*N'*-morpholino-thiourea ligands prepared in this study are shown in Figures 3.8 and 3.9. A detailed description of the ligand syntheses can be obtained in the experimental section (Section 3.5). The ligands **HL1b**, **HL1d** and **HL3a** were available in the laboratory and were therefore not prepared.

The syntheses of *N*-benzoyl-*N',N'*-di(2-hydroxyethyl)thiourea (**HL3a**), [13, 18] and *N,N*-adipoylbis(*N',N'*-diethylthiourea) (**HL1f**) [23] have been reported. The preparations of *N*-(3-*R*-benzoyl)-*N',N'*-diethylthioureas (**HL1a–d**) and *N*-(3-*R*-benzoyl)-*N'*-morpholino-thioureas (**HL2a–d**), where R = H, Cl, NO_2 and OCH_3, have also recently been described. [19, 20] The ligands **HL1e**, **HL2e**, **HL3b–e** and **HL4–7** depicted in Figure 3.8 and Figure 3.9 are all novel.

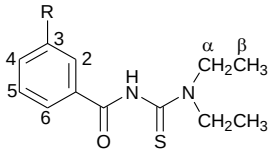

HL1a: R = H
HL1b: R = Cl
HL1c: R = NO_2
HL1d: R = OCH_3
HL1e: R = CH_3

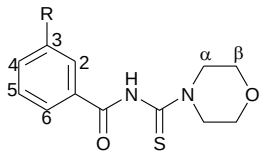

HL2a: R = H
HL2b: R = Cl
HL2c: R = NO_2
HL2d: R = OCH_3
HL2e: R = CH_3

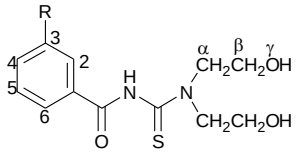

HL3a: R = H
HL3b: R = Cl
HL3c: R = NO_2
HL3d: R = OCH_3
HL3e: R = CH_3

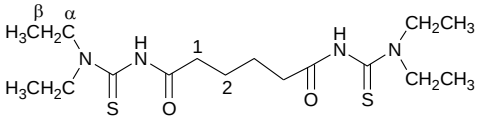

HL1f

Figure 3.8: Structural formulae and atom numbering scheme adopted for NMR assignments for *N*-acyl-*N',N'*-dialkylthiourea and *N*-acyl-*N'*-morpholinothiourea ligands.

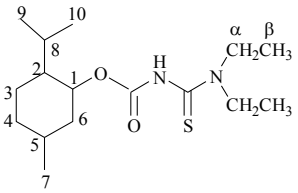

HL4 = (-)-menthyl
HL5 = (+)-menthyl

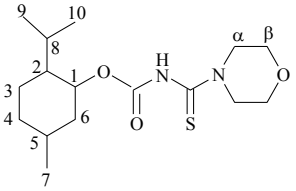

HL6 = (-)-menthyl
HL7 = (+)-menthyl

Figure 3.9: Structural formulae and atom numbering scheme adopted for NMR assignments for *N,N*-diethyl-*N'*-menthyloxycarbonylthiourea and *N*-menthyloxycarbonyl-*N'*-morpholinothiourea ligands.

3.3 Results and discussion

3.3.1 Synthesis of *N*-acyl-*N',N'*-dialkylthiourea and *N*-acyl-*N'*-morpholinothiourea ligands

The ligands were obtained in yields ranging from 19–77%. The ligands were purified by recrystallisation from ethanol and were characterised by elemental analyses and ^{1}H NMR and IR spectroscopy. The analytical and spectroscopic data are consistent with the proposed structural formulae given in Figure 3.8.

3.3.2 Characterisation of *N*-acyl-*N'*,*N'*-dialkylthiourea and *N*-acyl-*N'*-morpholino-thiourea ligands

The analytical data, principal infrared bands and ^{1}H NMR chemical shift data for the *N,N*-dialkyl-*N'*-(3-*R*-benzoyl)thiourea and *N*-(3-*R*-benzoyl)-*N'*-morpholinothiourea ligands are summarised in Tables 3.1, 3.2 and 3.3, respectively. For convenience, the ^{1}H NMR data for *N,N*-adipoylbis(*N',N'*-diethylthiourea) (**HL1f**) are given in the experimental section (Section 3.5).

Table 3.1: Analytical data for *N*-acyl-*N',N'*-dialkylthiourea and *N*-acyl-*N'*-morpholinothiourea ligands.

Compound	R-(C_6H_4)-	Mp/ °C	Yield/ %	Molecular Formula	Analytical data (% C/H/N/S)[a]
HL1a	H	97–98	55	$C_{12}H_{16}N_2OS$	61.0; 6.95; 11.9; 12.9 (61.0; 6.8; 11.9; 13.6)
HL1c	NO_2	119–121	62	$C_{12}H_{15}N_3O_3S$	51.7; 5.35; 14.8; 10.6 (51.2; 5.4; 15.9; 11.4)
HL1e	CH_3	96–97	55	$C_{13}H_{18}N_2OS$	62.4; 7.3; 11.2; 12.2 (62.4; 7.25; 11.2; 12.8)
HL1f	-[b]	97–99	19	$C_{16}H_{30}N_4O_2S_2$	51.3; 8.3; 15.1; 17.4 (51.3; 8.1; 15.0; 17.1)
HL2a	H	142–144	57	$C_{12}H_{14}N_2O_2S$	57.4; 5.7; 11.25; 12.6 (57.8; 5.7; 11.2; 12.9)
HL2b	Cl	152–154	49	$C_{13}H_{13}ClN_2O_2S$	51.0; 4.6; 9.6; 11.1 (50.6; 4.6; 9.8; 11.3)
HL2c	NO_2	153–155	45	$C_{12}H_{13}N_3O_4S$	48.7; 4.4; 14.2; 10.9 (48.8; 4.4; 14.2; 10.9)
HL2d	OCH_3	144–145	47	$C_{13}H_{16}N_2O_3S$	55.6; 5.7; 10.0; 11.3 (55.7; 5.7; 10.0; 11.4)
HL2e	CH_3	141–142	73	$C_{13}H_{16}N_20_2S$	59.1; 6.15; 10.6; 11.75 (59.1; 6.1; 10.6; 12.1)
HL3b	Cl	132–134	69	$C_{12}H_{15}ClN_2O_3S$	47.7; 5.1; 9.3; 10.6 (47.6; 5.0; 9.25; 10.6)
HL3c	NO_2	138–141	70	$C_{12}H_{15}N_3O_5S$	46.2; 4.85; 13.5; 9.9 (46.0; 4.8; 13.4; 10.2)
HL3d	OCH_3	103–106	77	$C_{13}H_{18}N_2O_4S$	53.1; 6.3; 9.4; 10.4 (52.3; 6.1; 9.4; 10.7)
HL3e	CH_3	136–138	75	$C_{13}H_{18}N_2O_3S$	56.1; 6.6; 9.5; 11.4 (55.3; 6.4; 9.9; 11.35)

[a] Required values are given in parentheses.

[b] *N,N*-adipoylbis(*N',N'*-diethylthiourea).

Table 3.2: Selected infrared absorptions for *N*-acyl-*N',N'*-dialkylthiourea and *N*-acyl-*N'*-morpholinothiourea ligands.

Compound	ν(C=O)/ cm^{-1}	ν(NH)/ cm^{-1}
HL1a	1678	3213
HL1c	1662	3285
HL1e	1646	3311
HL1f	1669	3251
HL2a	1667	3249
HL2b	1698	3257
HL2c	1699	3188
HL2d	1652	3136
HL2e	1657	3150
HL3b	1693	[a]
HL3c	1697	[a]
HL3d	1688	[a]
HL3e	1693	[a]

[a] Cannot be assigned due to overlapping with the OH peak.

Table 3.3: ^{1}H NMR data for *N,N*-dialkyl-*N'*-(3-*R*-benzoyl)thiourea and *N*-(3-*R*-benzoyl)-*N'*-morpholinothiourea ligands. The spectra were recorded at 30°C in $CDCl_3$, unless otherwise stated.

Ligand	R-Group	δH_2	δH_3	δH_4	δH_5	δH_6	δH_α	δH_β	δH_γ	δH_R	δH_{NH}
HL1a	H	7.823	7.461	7.563	7.461	7.823	4.018 3.606	1.322			8.238
HL1b [b]	Cl	7.816		7.539	7.410	7.692	4.016 3.594	1.222			8.165
HL1c	NO_2	8.654		8.170	7.662	8.418	3.987 3.595	1.322			8.774
HL1d [b]	OCH_3	7.324		7.065	7.324	7.324	3.993 3.580	1.300		3.815	8.428
HL1e	CH_3	7.639		7.355	7.355	7.608	4.026 3.605	1.328		2.403	8.176
HL2a	H	7.832	7.488	7.594	7.488	7.832	4.230 3.663	3.838			8.410
HL2b	Cl	7.828		7.565	7.431	7.696	4.228 3.644	3.835			8.361
HL2c	NO_2	8.681		8.181	7.712	8.443	4.232 3.659	3.844			8.577
HL2d	OCH_3	7.375		7.119	7.375	7.375	4.226 3.670	3.853		3.853	8.386
HL2e	CH_3	7.642		7.395	7.363	7.610	4.226 3.656	3.837		2.413	8.380
HL3a [a, b, c]	H	7.85	7.50	7.59	7.50	7.85	3.97 3.73	3.75 3.69	5.60 4.85		10.86
HL3b [a]	Cl	7.882		7.671	7.540	7.811	3.990 3.726	3.726	5.516 4.843		10.818
HL3c [a]	NO_2	8.659		8.279	7.792	8.435	4.007 3.735	3.735	5.538 4.857		11.129
HL3d [a]	OCH_3	7.438		7.162	7.438	7.438	3.985 3.742	3.742	5.624 4.840	3.814	10.829
HL3e [a]	CH_3	7.685		7.413	7.382	7.650	3.981 3.742	3.742	5.621 4.840	2.368	10.813

[a] Spectra were recorded in DMSO–d_6.

[b] These ligands were not prepared and were available in the laboratory and are included for comparison.

[c] Values obtained from ref. 13. The spectrum was recorded at 25°C.

3.3.2.1 ^{1}H NMR spectroscopy

The assignments of the ^{1}H NMR spectra of the *N*-(3-*R*-benzoyl)-*N',N'*-diethylthiourea, *N*-(3-*R*-benzoyl)-*N',N'*-di(2-hydroxyethyl)thiourea and *N*-(3-*R*-benzoyl)-*N'*-morpholinothiourea ligands were generally straightforward. The assignments of the aromatic protons and methylene protons were confirmed by 2–3 bond HMBC correlations to the carbonyl or thiocarbonyl carbon. The NMR assignments are based on the numbering scheme given in Figure 3.8. All the spectra are similar and a representative ^{1}H NMR spectrum, using *N*-(3-chlorobenzoyl)-*N'*-morpholinothiourea (**HL2b**) as an example, is shown in Figure 3.10.

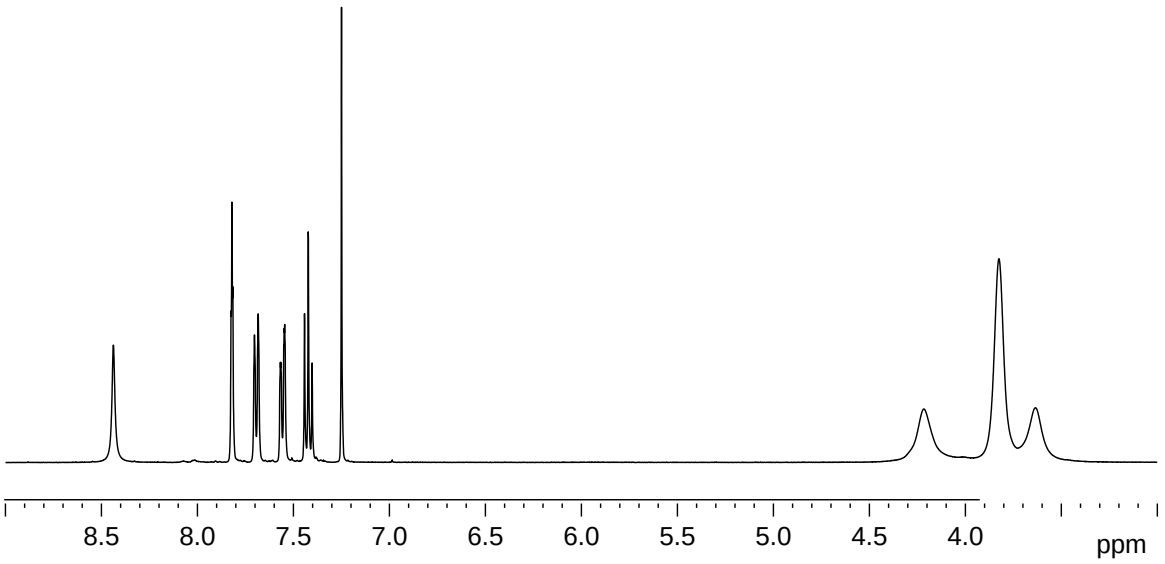

Figure 3.10: ^{1}H NMR spectrum of *N*-(3-chlorobenzoyl)-*N'*-morpholinothiourea (**HL2b**) at 30°C in $CDCl_3$.

The ^{1}H NMR spectra are characterised by a single NH signal in the 8–12 ppm region. Another notable feature of the ^{1}H NMR spectra of *N,N*-dialkyl-*N'*-(3-*R*-benzoyl)thiourea ligands is the observation of separate resonances for the methylene protons (H_α) of the respective amines. The magnetic inequivalence of the methylene protons is ascribed to the restricted rotation around the C–N bond between the thiocarbonyl and the amine nitrogen, due to the partial double bond character of this bond. [5] The partial double bond character has also been observed in related acylthiourea ligands and has been confirmed by X-ray crystallography. [13]

The ^{1}H NMR spectra of the *N*-(3-*R*-benzoyl)-*N',N'*-di(2-hydroxyethyl)thiourea ligands in DMSO-d_6 show inequivalent proton resonances for the hydroxyl protons. The lower field signal is broad and unresolved, while the upper field signal is a well-resolved triplet. This inequivalence of the hydroxyl protons is due to the presence of an intramolecular hydrogen bond between one hydroxyl moiety and the amide NH. [13]

The electron-withdrawing and electron-releasing properties of the R-groups and the amine moiety may possibly influence the acidity of the amide N–H bond, as the chemical shift of the NH proton signal is dependent on the R-group and the amine moiety. Notably, the NH proton chemical shifts of the 3-nitrobenzoylthiourea ligands (**HL1c**, **HL2c** and **HL3c**) are significantly deshielded with respect to the other ligand systems in that series. The NH proton chemical shifts of the morpholine ligands (**HL2a–e**) are significantly more deshielded than the diethyl derivatives (**HL1a–e**), which suggests that the N–H bonds of the morpholine ligands are more acidic than the diethyl derivatives. The pK_a values for **HL1a** and **HL2a** have been reported and are 10.87 and 10.68, respectively, which are consistent with the observed ^{1}H NMR data. [65] Unfortunately, no correlation between the R-group and the acidity of the amide N–H bond can be made because no pK_a values are available for *N,N*-dialkyl-*N'*-(3-*R*-benzoyl)thiourea and *N*-(3-*R*-benzoyl)-*N'*-morpholinothiourea ligands, where R = NO_2, Cl, OCH_3 and CH_3.

3.3.2.2 Infrared spectroscopy

The carbonyl stretching frequencies ν(C=O) and amide stretching frequencies ν(NH) are clearly visible and range from about 1650–1690 cm^{-1} and 3130–3200 cm^{-1}, respectively. The assignments were confirmed upon complexation, because deprotonation of the amide and coordination though the oxygen atom induces a large shift to higher frequencies of the ν(C=O) signal and a disappearance of the ν(NH) stretching frequency. The thioamide stretching frequencies, ν(C=S), could not be unambiguously assigned due to overlapping vibrations.

3.3.3 Synthesis of *N,N*-diethyl-*N'*-menthyloxycarbonylthiourea and *N*-menthyloxycarbonyl-*N'*-morpholinothiourea ligands

The ligands were obtained in yields ranging from 26–42%. The low yields of the alkoxycarbonylthiourea ligands may possibly be attributed to the lower reactivity of chloroformates with respect to acid chlorides, and the fact that the reaction of an alkyl chloroformate with the thiocyanate/isothiocyanate anion results in the formation of both the alkoxycarbonylisothiocyanate and an unreactive alkoxycarbonylthiocyanate. [63] Hence, only half the available chloroformate is converted to the required alkoxycarbonylisothiocyanate for reaction with a secondary amine to yield the desired *N*-alkoxycarbonyl-*N',N'*-dialkylthiourea or *N*-alkoxycarbonyl-*N'*-morpholinothiourea.

3.3.4 Characterisation of *N,N*-diethyl-*N'*-menthyloxycarbonylthiourea and *N*-menthyloxycarbonyl-*N'*-morpholinothiourea ligands

The alkoxycarbonylthiourea ligand systems were characterised using infrared (IR) spectroscopy, nuclear magnetic resonance (NMR) spectroscopy, polarimetry and elemental analyses. The structure of *N,N*-diethyl-*N'*-(-)-(3*R*)-menthyloxycarbonylthiourea (**HL4**) was also confirmed by X-ray crystallography. The analytical data, principal infrared bands and ^{1}H NMR chemical shift data for the *N,N*-diethyl-*N'*-menthyloxycarbonylthiourea and *N*-menthyloxycarbonyl-*N'*-morpholinothiourea ligands are summarised in Tables 3.4, 3.5 and 3.6, respectively. The optical rotations are given in Table 3.4.

The structural formulae and atom numbering scheme adopted for NMR assignments for the *N,N*-diethyl-*N'*-menthyloxycarbonylthiourea and *N*-menthyloxycarbonyl-*N'*-morpholinothiourea ligands are given in Figure 3.9. The elemental analyses and spectroscopic data of the *N,N*-diethyl-*N'*-menthyloxycarbonylthiourea and *N*-menthyloxycarbonyl-*N'*-morpholinothiourea ligands are consistent with the proposed structural formulae given in Figure 3.9.

Table 3.4: Analytical data for *N,N*-diethyl-*N'*-menthyloxycarbonylthiourea and *N*-menthyloxycarbonyl-*N'*-morpholinothiourea ligands.

Ligands	Mp/ °C	Yield/ %	$[\alpha]^{D}_{25}$/ °	Molecular Formula	Analytical Data (% C/H/N/S)[a]
HL4	88–90	26	- 42.4	$C_{16}H_{30}N_2O_2S$	60.6; 10.3; 9.0; 9.85 (61.1; 9.6; 8.9; 10.2)
HL5	89–90	32	+ 36.5	$C_{16}H_{30}N_2O_2S$	61.0; 10.3; 9.1; 10.2 (61.1; 9.6; 8.9; 10.2)
HL6	128–130	42	- 45.8	$C_{16}H_{28}N_2O_3S$:	58.9; 8.8; 8.55; 9.3 (58.5; 8.6; 8.5; 9.8)
HL7	127–129	42	+ 45.4	$C_{16}H_{28}N_2O_3S$:	59.0; 8.9; 8.4; 9.1 (58.5; 8.6; 8.5; 9.8)

[a] Required values are given in parentheses.

Table 3.5: Selected infrared absorptions for *N,N*-diethyl-*N'*-menthyloxycarbonylthiourea and *N*-menthyloxycarbonyl-*N'*-morpholinothiourea ligands.

Compound	ν(NH)/ cm^{-1}	δ(NH) + ν(C=O) / cm^{-1}	ν(C=O) + δ(NH)/ cm^{-1}
HL4	3179	1536	1737
HL5	3179	1536	1737
HL6	3209	1540	1737
HL7	3209	1540	1737

Table 3.6: ^{1}H NMR data for the *N,N*-diethyl-*N'*-menthyloxycarbonylthiourea and *N*-menthyloxycarbonyl-*N'*-morpholinothiourea ligands. The spectra were recorded at 30°C in $CDCl_3$.

Compound	δH_1	δH_2	δH_3	δH_4	δH_5	δH_6	δH_7	δH_8	δH_9	δH_{10}	δH_α	δH_β	δH_{NH}
HL4	4.575	1.341	1.676	1.676	1.466	2.038	0.906	1.898	0.783	0894	3.639	1.274	6.998
			1.030	0.854		1.030							
HL5	4.575	1.341	1.676	1.676	1.466	2.038	0.906	1.898	0.783	0894	3.639	1.274	6.998
			1.030	0.854		1.030							
HL6	4.557	1.349	1.671	1.671	1.460	2.002	0.894	1.868	0.760	0.894	3.785	3.785	7.346
			1.024	0.837		1.024							
HL7	4.557	1.349	1.671	1.671	1.460	2.002	0.894	1.868	0.760	0.894	3.785	3.785	7.346
			1.024	0.837		1.024							

3.3.4.1 Physical properties

The optical rotations of the menthyloxycarbonylthiourea ligands were determined and are in agreement with the sign observed for the respective menthyl chloroformate used.

3.3.4.2 ^{1}H NMR spectroscopy

The assignments of the ^{1}H NMR spectra of the *N,N*-diethyl-*N'*-menthyloxycarbonyl-thiourea and *N*-menthyloxycarbonyl-*N'*-morpholinothiourea ligands were done using 1D and 2D NMR experiments. The assignment of the menthyl resonances was aided by comparing them with standard spectra of menthol. [66, 67] A representative ^{1}H NMR spectrum is shown in Figure 3.11, using the *N,N*-diethyl-*N'*-(-)-(3*R*)-menthyloxy-carbonylthiourea ligand (**HL4**) as an example.

The ^{1}H NMR spectra are characterised by a single NH signal in the 6–8 ppm region. Another notable feature of the ^{1}H NMR spectra of the alkoxycarbonylthiourea ligands is the observation of a broad resonance for the methylene protons (H_{α}) of the respective amines. The magnetic inequivalence of the methylene protons is ascribed to restricted rotation around the C–N bond between the thiocarbonyl and the amine nitrogen, in a similar fashion to the *N,N*-dialkyl-*N'*-(3-*R*-benzoyl)thiourea and *N*-(3-*R*-benzoyl)-*N'*-morpholinothiourea ligands. The partial double bond character of the C–N bond is consistent with the crystallographic data obtained for *N,N*-diethyl-*N'*-(-)-(3*R*)-menthyl-oxycarbonylthiourea (**HL4**) shown in Figure 3.12.

3.3.4.3 Infrared spectroscopy

The thioamide stretching frequencies, ν(C=S), could not be unambiguously assigned due to overlapping vibrations. The amide stretching frequency ν(NH) is clearly visible and ranges from 3209–3179 cm^{-1}. The ester oxygen has a distinct effect on the dipole moment of the carbonyl bond. Comparing the *N,N*-dialkyl-*N'*-(3-*R*-benzoyl)thiourea with an *N*-alkoxycarbonyl-*N',N'*-dialkylthiourea, the strong electron-donating property of the alkoxycarbonyl group weakens the carbonyl dipole moment, shifting it to higher frequencies which allows vibrational coupling with the δ(NH) bend. This is evidenced by

intensity stealing by the δ(NH) bend from the ν(C=O) stretching frequency. The assignments of the carbonyl and amide stretching and bending frequencies were confirmed upon complexation, because deprotonation of the amide and coordination though the oxygen atom induce a large shift to higher frequencies of the ν(C=O) signal and a disappearance of the ν(NH) stretching frequency.

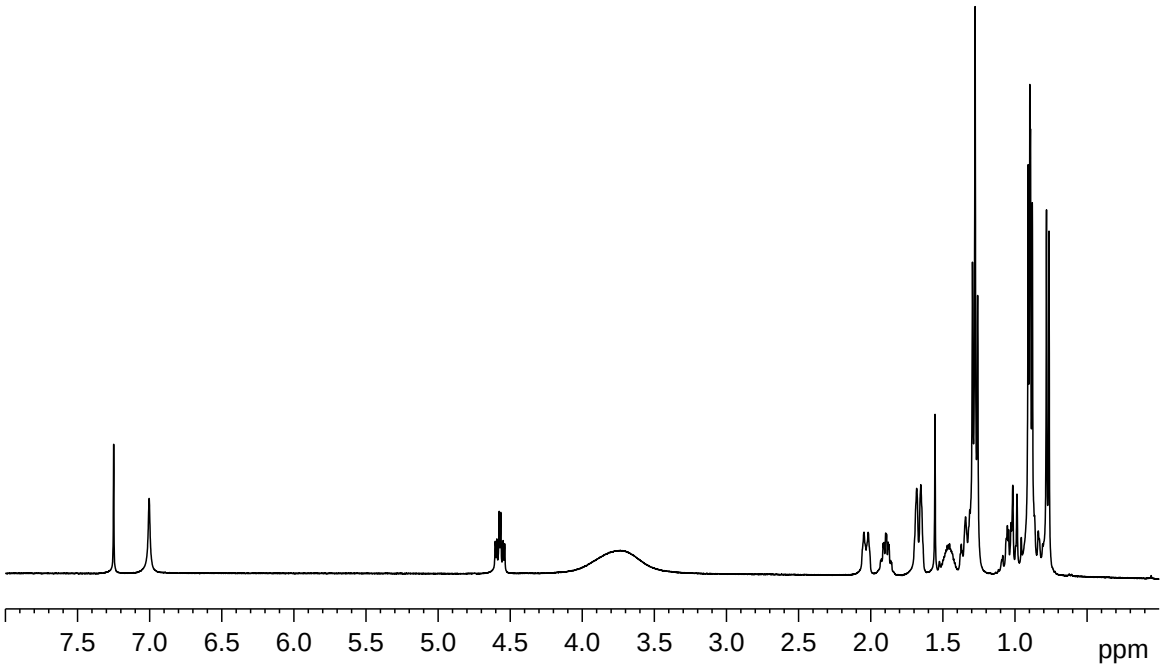

Figure 3.11: ^{1}H NMR spectrum for the *N,N*-diethyl-*N'*-(-)-(3*R*)-menthyloxycarbonylthiourea (**HL4**) at 30°C in $CDCl_3$.

3.3.4.4 Crystal structure of N,N-diethyl-N'-(-)-(3R)-menthyloxycarbonylthiourea (HL4)

Crystals of *N,N*-diethyl-*N'*-(-)-(3*R*)-menthyloxycarbonylthiourea (**HL4**) suitable for X-ray structure determination were obtained by recrystallisation from ethanol. The structure was determined by Dr. S. Otto from the University of the Orange Free State, South Africa. To the best of our knowledge this is the first crystal structure of an *N*-alkoxycarbonyl-*N',N'*-dialkylthiourea. All the relevant crystallographic data are given in Table 3.7. The structure of **HL4** consists of two discrete molecules per asymmetric unit; thus there are four chemically equivalent molecules in the unit cell. The molecular structure of *N,N*-diethyl-*N'*-(-)-(3*R*)-menthyloxycarbonylthiourea is shown in Figure 3.12, together with the atom numbering scheme. The conformations of the two molecules differ as illustrated in Figure 3.13, wherein the two molecules are superimposed on one

another. Selected bond lengths and angles for the two conformers are given in Table 3.8. A complete list of bond lengths and angles are given in Appendix A.

Table 3.7: Crystallographic data for *N,N*-diethyl-*N'*-(-)-(3*R*)-menthyloxycarbonyl-thiourea (**HL4**).

Empirical formula	$C_{32}H_{60}N_4O_4S_2$
Formula weight	628.96
Temperature	293(2) K
Wavelength	0.71073 Å
Crystal system, space group	Monoclinic, $P2_1$
Unit cell dimensions	a = 8.889(2) Å α = 90°
	b = 13.207(3) Å β = 100.51(3)°
	c = 16.911(3) Å γ = 90°
Volume	1952.0(7) $Å^3$
Z	2
μ	0.172 mm^{-1}
F(000)	688
Theta range for data collection	1.97 to 26.02°
Index ranges	$0 \le h \le 10$, $-16 \le k \le 0$, $-20 \le l \le 20$
Reflections collected/unique	2910/2770 [R(int) = 0.031]
Refinement method	Full-matrix least-squares on F^2
Goodness-of-fit on F^2	1.058
Final R indices [$I>2\sigma(I)$]	R^a = 0.0385, Rw^b = 0.0925
Absolute structure parameter [68]	0.18(11)

[a] $R = [(\Sigma\Delta F)/(\Sigma F_0)]$ [b] $Rw = \Sigma[w(F_0^2 - F_c^2)^2]/\Sigma[w(F_0^2)^2]^{1/2}$

Table 3.8: Selected bond lengths (Å) and angles (°) for the two conformers of *N,N*-diethyl-*N'*-(-)-(3*R*)-menthyloxycarbonylthiourea (**HL4**).

Molecule 1		Molecule 2	
S(1)-C(11)	1.677(4)	S(2)-C(21)	1.673(4)
O(11)-C(12)	1.200(5)	O(21)-C(22)	1.186(5)
O(12)-C(12)	1.333(5)	O(22)-C(22)	1.343(5)
N(11)-C(12)	1.370(5)	N(21)-C(22)	1.382(5)
N(11)-C(11)	1.399(5)	N(21)-C(21)	1.396(5)
N(11)-H(1)	0.69(4)	N(21)-H(2)	0.92(4)
C(15)-C(16)	1.514(6)	C(25)-C(26)	1.487(6)
C(12)-N(11)-C(11)	125.6(4)	C(22)-N(21)-C(21)	122.3(3)
C(12)-N(11)-H(1)	113(3)	C(22)-N(21)-H(2)	115(2)
C(11)-N(11)-H(1)	113(3)	C(21)-N(21)-H(2)	116(2)
C(11)-N(12)-C(13)	120.1(4)	C(21)-N(22)-C(23)	123.5(3)
C(11)-N(12)-C(15)	123.8(3)	C(21)-N(22)-C(25)	120.0(4)
N(12)-C(13)-C(14)	112.9(3)	N(22)-C(23)-C(24)	114.4(4)
O(11)-C(12)-O(12)-C(1A)	4.7(7)	O(21)-C(22)-O(22)-C(2A)	3.3(6)
C(1G)-C(1F)-C(1A)-O(12)	59.2(5)	C(2G)-C(2F)-C(2A)-O(22)	58.8(5)
O(11)-C(12)-C(11)-S(1)	115.0(4)	O(21)-C(22)-C(21)-S(2)	-109.3(4)

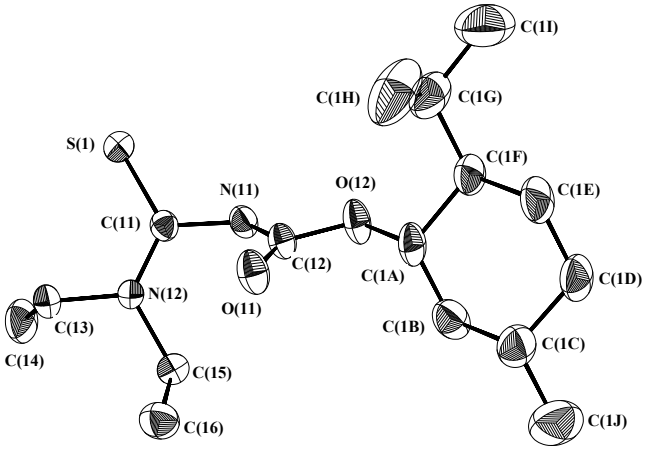

Figure 3.12: Molecular structure showing the numbering scheme and displacement ellipsoids (30% probability) for *N,N*-diethyl-*N'*-(-)-(3*R*)-menthyloxycarbonylthiourea. Hydrogen atoms have been omitted for clarity.

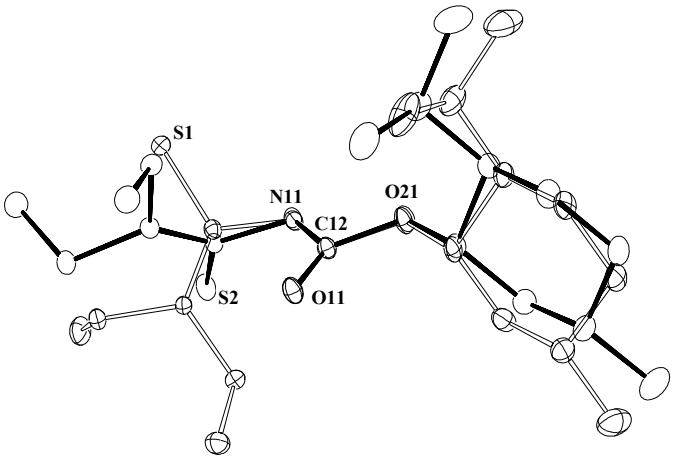

Figure 3.13: Molecular structures of molecules 1 and 2 of *N,N*-diethyl-*N'*-(-)-(3*R*)-menthyloxycarbonyl-thiourea superimposed. Molecule 2 is numbered with the first digit referring to the number of the molecule and the second to the number of the atom. Hydrogen atoms have been omitted for clarity.

The main difference between the two molecules concerns the orientation of sulfur [S(1) and S(2)] and carbonyl groups [C(12)–O(11) and C(22)–O(21)] with respect to one another, as illustrated by the torsion angles O(11)–C(12)–C(11)–S(1) and O(21)–C(22)–C(21)–S(2) of 115.0(4) and –109.3(4)°, respectively. The C–N bond lengths range from 1.326(6) to 1.399(5) Å and are significantly shorter than that expected for a C–N single bond length of 1.479 Å, [57] thus showing varying degrees of double bond character. The partial double bond character of the C(11)–N(12) bond is further manifested by the magnetic inequivalence of the methylene protons adjacent to the nitrogen atom of the diethylamino moiety. Since there are no examples of crystal structures of *N*-alkoxycarbonyl-*N',N'*-dialkylthioureas, the bond lengths of **HL4** are compared with the bond lengths generally found in *N*-acyl-*N',N'*-dialkylthioureas (Table 3.9). As seen in Table 3.9, the thiocarbonyl C(11/21)–S(1/2), thioamide C(11/21)–N(11/21) and amide C(12/22)–N(11/21) bond lengths fall within the range found for *N*-acyl-*N',N'*-dialkylthioureas. The carbonyl bond length C(12/22)–O(11/21) in **HL4** is significantly shorter than carbonyl bond length observed in *N*-acyl-*N',N'*-dialkylthiourea ligands, which may be due to the electron-withdrawing properties of the ester oxygen atom, O(12/22).

Table 3.9: Comparison of selected bond lengths (Å) of *N*-acyl-*N',N'*-dialkylthioureas [13, 15, 41–45] with the bond lengths obtained for *N,N*-diethyl-*N'*-(-)-(3*R*)-menthyloxycarbonyl-thiourea (**HL4**).

Bond	*N*-acyl-*N',N'*-disubstituted thiourea/ Å	**HL4**/ Å
Thiocarbonyl		
C(11)–S(1)	1.656–1.674	1.677(4)
C(21)–S(2)		1.673(4)
Carbonyl		
C(12)–O(11)	1.211–1.223	1.200(5)
C(22)–O(21)		1.186(5)
Amide		
C(12)–N(11)	1.360–1.407	1.370(5)
C(22)–N(21)		1.382(5)
Thioamide		
C(11)–N(11)	1.391–1.432	1.399(5)
C(21)–N(21)		1.396(5)

3.4 Conclusion

A series of *N,N*-dialkyl-*N'*-(3-*R*-benzoyl)thiourea and *N*-(3-*R*-benzoyl)-*N'*-morpholino-thiourea ligands, where R = NO_2, Cl, H, CH_3 and OCH_3, were prepared and characterised by ^{1}H NMR and infrared spectroscopy and elemental analyses. The electron-withdrawing and donating properties of the R-group and the amine moiety could possibly have an affect on the acidity of the amide N–H bond, because in the ^{1}H NMR spectra, the R-groups and amine moiety had a distinct effect on the chemical shift of the NH resonance. The NH signals in ligands containing nitro-groups (**HL1c**, **HL2c** and **HL3c**) are significantly more deshielded, suggesting that these protons may be more acidic.

Four novel chiral *N*-alkoxycarbonyl-*N',N'*-dialkylthiourea ligands were prepared and fully characterised. The X-ray crystal structure of *N,N*-diethyl-*N'*-(-)-(3*R*)-menthyloxy-carbonylthiourea (**HL4**) was also determined. To the best of our knowledge this is the first reported crystal structure of an *N*-alkoxycarbonyl-*N',N'*-dialkylthiourea.

3.5 Experimental

3.5.1 Materials

The adipoyl chloride (Fluka), benzoyl chloride (SaArchem), 3-substituted benzoyl chlorides (Aldrich) and menthyl chloroformates (Aldrich) were used as received. The diethylamine, morpholine and acetone were dried over 4Å molecular sieves, and were freshly distilled before use. The di(2-hydroxyethyl)amine was dried over 4Å molecular sieves. The potassium thiocyanate (SaArchem) was dried under high vacuum before use. All other solvents were commercial grade and used as received.

3.5.2 Crystal structure determination

The X-ray crystal structure of **HL4** was solved by Dr S Otto from the University of the Orange Free State, South Africa. The three dimensional intensity data were collected on a Syntex P-1. All reflections were corrected for Lorentz and polarisation effects. The structure of **HL4** was solved by the direct method (SHELXS 97 [69] and SHELXL 97 [70]). The crystal of **HL4** was covered with Canada Balsam after signs of decay were detected, hence a data reduction was done to eliminate weak reflections and identical reflections were merged. Data reduction was performed using Profit. [71] All hydrogen atoms were included in calculated positions with fixed isotropic parameters, except for the amine hydrogen's of **HL4** that were detected from the Fourier map. The molecular graphics were produced using ORTEP. [72] The crystallographic data has been deposited with the Cambridge Crystallographic Data Centre (CCDC) and entered into the Cambridge Structural Database (CCDC reference number 186/2253) and are also given in Appendix A.

3.5.3 Preparation of *N,N*-dialkyl-*N'*-(3-*R*-benzoyl)thiourea and *N*-(3-*R*-benzoyl)-*N'*-morpholinothiourea ligands

N-benzoyl-*N',N'*-diethylthiourea (L1a)

To a solution of dry potassium thiocyanate (4.86 g, 50.0 mmol) in dry acetone (50 ml), was added dropwise an equimolar amount of benzoyl chloride (7.03 g, 50.0 mmol). The

solution was refluxed under nitrogen for 30 minutes. Diethylamine (3.69 g, 50.0 mmol) was then added to the cooled reaction mixture and the solution was refluxed for a further 30 minutes. The solution was cooled to room temperature and then added to ice-water (200 ml). The solution was then placed in a refrigerator (4°C) overnight. The precipitate was collected by filtration, washed with water and recrystallised from ethanol to yield a crystalline product. The crystals were collected by filtration and dried *in vacuo* over silica gel. The filtrate was concentrated using a rotary-evaporator and then placed in the refrigerator (4°C) to yield a second crop of the product.

[**HL1a**]: Yield (6.48 g, 55%). IR (KBr pellet, cm^{-1}): 3213 (vs, br), 3084 (w), 3033 (m), 2988 (m), 2972 (s, sh), 2932 (m – s, sh), 2869 (m), 1678 (vs), 1649 (m, sh), 1597 (s, sh), 1579 (s, sh), 1536 (vs, br), 1454 (vs), 1424 (vs), 1380 (s), 1358 (s), 1342 (s, sh), 1309 (s), 1283 (vs), 1269 (vs), 1226 (vs), 1173 (vs), 1132 (vs), 1100 (s, sh), 1063 (vs), 1025 (s, sh), 1005 (m), 988 (w – m, sh), 948 (w – m, sh), 924 (s, sh), 864 (s, sh), 796 (s, sh), 714 (s, sh), 692 (s, sh), 650 (s), 616 (s, sh), 534 (m, sh), 506 (w), 471 (w – m, sh), 444 (w), 404 (w – m, sh), 395 (w), 385 (w), 376 (w). TLC [silica gel, $CHCl_3$/EtOAc (3:1)]: R_f 0.76.

***N,N*-diethyl-*N'*-(3-nitrobenzoyl)thiourea (HL1c)**

To a solution of dry potassium thiocyanate (1.05 g, 10.8 mmol) in dry acetone (50 ml), was added dropwise an equimolar amount of 3-nitrobenzoyl chloride (2.01 g, 10.8 mmol). The solution was refluxed under nitrogen for 2 hours. Diethylamine (0.792 g, 10.8 mmol) was then added to the cooled reaction mixture and the solution was refluxed for a further 2 hours. The solution was cooled to room temperature and then added to ice-water (120 ml). The solution was then placed in a refrigerator (4°C) overnight. The yellow precipitate was collected by filtration, washed with water and recrystallised from ethanol to yield a crystalline yellow product. The crystals were collected by filtration and dried *in vacuo* over silica gel. The filtrate was concentrated using a rotary-evaporator and then placed in a refrigerator (4°C) to yield a second crop of the product.

[**HL1c**]: Yield (1.87 g, 62%). IR (KBr pellet, cm^{-1}): 3285 (vs, br), 3083 (m – s, sh), 3073 (m – s, sh), 2993 (m – s, sh), 2977 (m – s, sh), 2942 (m, sh), 2927 (m – s, shld), 2880 (m), 3870 (w, sh), 1743 (w – m, sh), 1736 (w – m, sh), 1662 (vs, sh), 1615 (s, sh),

1527 (vs, br), 1485 (vs, br), 1462 (vs, br), 1431 (vs, br), 1383 (s, sh), 1350 (vs, sh), 1293 (s), 1277 (s), 1268 (s), 1229 (vs, sh), 1134 (s, sh), 1100 (s), 1076 (s, sh), 1014 (m), 1001 (m), 942 (m, sh), 932 (m, sh), 899 (m, sh), 848 (w – m, sh), 822 (m, sh), 801 (m), 782 (m, sh), 765 (m, sh), 746 (s, sh), 717 (vs, sh), 674 (s), 647 (m), 608 (m), 546 (w – m), 510 (w – m), 467 (w), 452 (w, sh), 423 (w – m, sh), 398 (w, sh). TLC [silica gel, $CHCl_3$/EtOAc (3:1)]: R_f 0.82.

_N,N_-diethyl-_N'_-(3-methylbenzoyl)thiourea (HL1e)

To a solution of dry potassium thiocyanate (1.16 g, 11.9 mmol) in dry acetone (50 ml), was added dropwise an equimolar amount of 3-methylbenzoyl chloride (1.85 g, 12.0 mmol). The solution was refluxed under nitrogen for an hour. Diethylamine (0.874 g, 11.9 mmol) was then added to the cooled reaction mixture and the solution was refluxed for a further hour. The solution was cooled to room temperature and then added to ice-water (100 ml). The solution was then placed in a refrigerator (4°C) overnight. The white precipitate was collected by filtration, washed with water and recrystallised from ethanol to yield a crystalline product. The crystals were collected by filtration and dried *in vacuo* over silica gel. The filtrate was concentrated using a rotary-evaporator and then placed in a refrigerator (4°C) to yield a second crop of the product.

[**HL1e**]: Yield (1.66 g, 55%). IR (KBr pellet, cm^{-1}): 3048 (w), 2999 (w), 2981 (w – m), 2971 (w – m), 2934 (w – m), 2874 (w – m), 1646 (s, sh), 1607 (m, sh), 1586 (m, sh), 1561 (w – m, sh), 1524 (s, sh), 1510 (m), 1475 (vs, sh), 1449 (m), 1431 (m), 1384 (m, sh), 1356 (m, sh), 1343 (m, sh), 1307 (w – m), 1282 (s, sh), 1232 (s, sh), 1205 (m – s, sh), 1183 (w), 1137 (m – s, sh), 1103 (m, sh), 1077 (m), 1068 (m), 1003 (w), 938 (w – m), 899 (w – m, sh), 829 (w – m, sh), 807 (w – m, sh), 791 (w – m, sh), 742 (m, sh), 705 (w), 688 (w – m, sh), 657 (w), 608 (w), 555 (w), 537 (w), 503 (w), 450 (w – m, sh). TLC [silica gel, $CHCl_3$/EtOAc (3:1)]: R_f 0.81.

***N,N*-Adipoylbis(*N',N'*-diethylthiourea) (HL1f)**

To a solution of dry potassium thiocyanate (3.87 g, 39.8 mmol) in dry acetone (50 ml), was added dropwise an equimolar amount of adipoyl chloride (3.68 g, 20.1 mmol). The solution was refluxed under nitrogen for 30 minutes. Diethylamine (2.92 g, 39.9 mmol) was then added to the cooled reaction mixture and the solution was refluxed for a further 30 minutes. The solution was cooled to room temperature and then added to ice-water (200 ml). The solution was then placed in a refrigerator (4°C) overnight. The precipitate was collected by filtration, washed with water and recrystallised twice from ethanol to yield a crystalline product. The crystals were collected by filtration and dried *in vacuo* over silica gel.

[**HL1f**]: Yield (1.45 g, 19%). IR (KBr pellet, cm^{-1}): 3251 (s, sh), 2981 (m, sh), 2966 (m, sh), 2935 (m, sh), 2871 (w), 1669 (vs, sh), 1523 (vs, sh), 1466 (m), 1459 (m), 1428 (s, sh), 1380 (m, sh), 1352 (m – s, sh), 1334 (m – s, sh), 1311 (m, sh), 1268 (m – s), 1239 (s), 1157 (m, sh), 1146 (m, sh), 1125 (s, sh), 1082 (m – s, sh), 957 (w – m, sh), 936 (w), 916 (w), 869 (w – m, sh), 800 (w), 719 (w – m, sh), 692 (w), 614 (w), 490 (w). ^{1}H NMR (400 MHz, $CDCl_3$): 8.32 (2H, s, NH), 3.93 (4H, br s, $2CH_2$), 3.52 (4H, br s, $2CH_2$), 2.38 (4H, t, $2CH_2$), 1.71 (4H, t, $2CH_2$), 1.27 (12H, s, $4CH_3$). TLC [silica gel, $CHCl_3$/EtOAc (3:1)]: R_f 0.10.

***N*-(3-*R*-benzoyl)-*N'*-morpholinothiourea (HL2a–e)**

To a solution of dry potassium thiocyanate (10.3 mmol) in dry acetone (50 ml), was added dropwise an equimolar amount of 3-R-benzoyl chloride (10.3 mmol). The solution was refluxed under nitrogen for 2 hours. Morpholine (10.3 mmol) was then added to the cooled reaction mixture and the solution was refluxed for a further 2 hours. The solution was cooled to room temperature and then added to ice water (100 ml). The cloudy solution was concentrated, and placed in a refrigerator (4°C) overnight. The yellow crystalline precipitate was collected by filtration, washed with water, ice-cold ether and dried *in vacuo* over silica gel.

[**HL2a**]: Yield (1.72 g, 57%). IR (KBr pellet, cm^{-1}): 3297 (s, shld), 3249 (s, br), 2971 (m – s, sh), 2925 (m – s, sh), 2856 (m – s, shld), 2849 (m – s, sh), 1667 (vs, sh), 1602

(m – s, sh), 1581 (m – s, sh), 1526 (vs), 1493 (s), 1456 (vs, sh), 1442 (vs), 1427 (vs), 1357 (s, sh), 1303 (s), 1285 (s, shld), 1269 (vs, sh), 1242 (vs), 1224 (vs), 1201 (vs, sh), 1149 (vs, sh), 1116 (vs), 1063 (s, sh), 1037 (s, sh), 1002 (m – s, sh), 958 (s, sh), 875 (s, sh), 848 (m – s, sh), 796 (m), 711 (vs, sh), 689 (s), 658 (s – vs), 617 (m – s, sh), 588 (m – s), 513 (w – m), 499 (w – m), 461 (m, sh). TLC [silica gel, $CHCl_3$/EtOAc (3:1)]: R_f 0.47.

[**HL2b**]: Yield (1.46 g, 49%). IR (KBr pellet, cm^{-1}): 3257 (s, sh), 3094 (w), 3045 (w), 2995 (w), 2982 (w), 2935 (w – m), 2909 (w – m), 2871 (w – m), 1752 (w), 1735 (w), 1718 (w), 1698 (vs, sh), 1655 (w – m), 1638 (w), 1596 (w), 1572 (m), 1560 (m), 1527 (vs), 1510 (s), 1500 (m), 1492 (m), 1458 (vs), 1432 (vs), 1389 (w – m), 1356 (w), 1304 (w – m, sh), 1281 (m – s, shld), 1273 (s, sh), 1246 (vs, sh), 1227 (vs, sh), 1202 (s, sh), 1151 (s, sh), 1114 (m – s, sh), 1101 (s, sh), 1063 (m), 1031 (s, sh), 1001 (w), 986 (w), 961 (m – s, sh), 913 (w), 884 (m, sh), 843 (m – s, sh), 801 (m – s, sh), 766 (s, sh), 745 (s, sh), 694 (m – s), 670 (w – m), 661 (w – m), 614 (m, sh), 553 (m, sh), 497 (w – m, sh), 473 (vw), 457 (w – m, sh), 392 (w – m, sh). TLC [silica gel, $CHCl_3$/EtOAc (3:1)]: R_f 0.42.

[**HL2c**]: Yield (1.37 g, 45%). IR (KBr pellet, cm^{-1}): 3188 (s, br), 3057 (s), 3001 (m – s, sh), 2970 (m – s, sh), 2940 (m – s), 2868 (s, sh), 1699 (vs, sh), 1617 (m – s, sh), 1530 (vs, br), 1482 (s), 1454 (vs), 1424 (vs), 1386 (s, sh), 1352 (vs, sh), 1299 (s, sh), 1253 (vs, br), 1223 (vs, sh), 1201 (vs, sh), 1156 (vs, sh), 1120 (vs, sh), 1066 (s), 1044 (s, sh), 963 (s), 902 (s, sh), 863 (m – s, sh), 834 (s, sh), 817 (m – s, sh), 770 (w), 741 (m – s, sh), 713 (vs, sh), 684 (s), 663 (s), 650 (s), 624 (m), 601 (m), 506 (m, sh), 460 (w – m), 444 (w – m). TLC [silica gel, $CHCl_3$/EtOAc (3:1)]: R_f 0.30.

[**HL2d**]: Yield (1.41 g, 47%). IR (KBr pellet, cm^{-1}): 3136 (s), 3033 (m – s), 3015 (m – s), 2981 (m – s), 2967 (s), 2930 (m – s), 2905 (m – s), 2865 (m – s, sh), 1652 (vs, sh), 1591 (s, sh), 1524 (vs), 1492 (s, sh), 1459 (s, sh), 1436 (s, sh), 1423 (s, sh), 1389 (w – m, sh), 1360 (w – m, sh), 1329 (m – s, sh), 1305 (m – s, sh), 1269 (vs, sh), 1246 (vs, sh), 1238 (vs), 1205 (s, sh), 1183 (w – m, sh), 1148 (m – s, sh), 1115 (s, sh), 1063 (w – m, sh), 1035 (s, sh), 993 (w), 960 (m – s, sh), 932 (w), 881 (w – m, sh), 860 (m, sh), 824 (m, sh), 804 (m, sh), 749 (s, sh), 726 (m), 688 (m), 621 (w – m, sh), 568 (w – m, sh), 556 (w, shld), 500 (w – m, sh), 465 (w – m, sh), 452 (w), 421 (w), 404 (w). TLC [silica gel, $CHCl_3$/EtOAc (3:1)]: R_f 0.42.

[**HL2e**]: Yield (2.18 g, 73%). IR (KBr pellet, cm^{-1}): 3150 (m), 3042 (w – m, shld), 3035 (w – m, shld), 2973 (m, sh), 2896 (w – m), 2858 (m, sh), 1719 (w, sh), 1657 (vs, sh), 1587 (m), 1529 (s, sh), 1465 (s), 1458 (s, sh), 1424 (s, sh), 1365 (w), 1303 (m), 1274 (s, sh), 1249 (s, sh), 1232 (m – s, sh), 1206 (m – s, sh), 1152 (m), 1115 (s, sh), 1080 (w – m), 1041 (m), 963 (m, sh), 928 (w), 905 (w), 859 (m, sh), 820 (m), 804 (m, sh), 738 (s, sh), 725 (m), 705 (m), 688 (w – m), 670 (w), 662 (w), 616 (m, sh), 541 (w), 502 (w), 474 (w), 455 (w), 412 (w). TLC [silica gel, $CHCl_3$/EtOAc (3:1)]: R_f 0.44.

_N_-(3-_R_-benzoyl)-_N'_,_N'_-di(2-hydroxyethyl)thiourea (HL3a–e)

To a solution of dry potassium thiocyanate (5.61 mmol) in dry acetone (50 ml), was added dropwise an equimolar amount of 3-R-benzoyl chloride (5.61 mmol). The solution was refluxed under nitrogen for an hour. Diethanolamine (5.77 mmol) was then added dropwise to the cooled reaction mixture and the solution was refluxed for a further hour. The solution was cooled to room temperature and the KCl precipitate was filtered. The filtrate was concentrated under reduced pressure and added to ice water (100 ml) and placed in a refrigerator (4°C) for several days. The precipitate was collected by filtration, washed with water, chloroform and dried *in vacuo* over silica gel. The aqueous layer was concentrated further using a rotary-evaporator, resulting in the isolation of a further crop of the product.

[**HL3b**]: Yield (1.30 g, 69%). IR (KBr pellet, cm^{-1}): 3180 (s, br), 2944 (s), 2927 (m – s), 2878 (m), 1693 (vs, sh), 1656 (w), 1598 (m, sh), 1551 (vs, br), 1500 (s),1468 (m), 1460 (m, sh), 1433 (m), 1409 (s, sh), 1357 (s, sh), 1345 (s, sh), 1302 (vs, sh), 1285 (vs), 1274 (vs), 1217 (vs), 1157 (m – s, sh), 1097 (m, sh), 1071 (s, sh), 1060 (vs, sh), 1000 (m, sh), 914 (m, sh), 893 (w – m), 880 (w, sh), 853 (w), 834 (w – m, sh), 806 (w), 774 (w – m), 740 (vs, sh), 697 (w), 670 (w), 652 (w), 630 (w), 572 (w), 419 (w). TLC [RP-$C18F_{254}S$, MeOH/H_2O (5:1)]: R_f 0.83.

[**HL3c**]: Yield (0.86 g, 70%). IR (KBr pellet, cm^{-1}): 3175 (vs, br), 2954 (s), 2918 (s), 2883 (s), 1697 (vs, sh), 1614 (s, sh), 1562 (vs, br), 1555 (vs, br), 1526 (vs), 1498 (s), 1474 (s), 1460 (s), 1440 (s, sh), 1406 (s, sh), 1364 (s), 1348 (vs), 1322 (s, sh), 1299 (s), 1277 (s), 1254 (s), 1213 (s), 1160 (m – s, sh), 1098 (m, sh), 1073 (vs, sh), 1056 (vs, sh), 1000

(m, sh), 932 (m, sh), 907 (m – s, sh), 887 (m, sh), 861 (m, sh), 851 (m – s, sh), 834 (m, sh), 749 (m – s, sh), 713 (vs, sh), 687 (m – s, sh), 650 (m, sh), 577 (w – m), 519 (w), 418 (m – s, sh). TLC [RP-C18F_{254}S, MeOH/H_2O (5:1)]: R_f 0.83.

[**HL3d**]: Yield (0.44 g, 77%). IR (KBr pellet, cm^{-1}): 3232 (vs, br), 3001 (s, sh), 2971 (s, sh), 2953 (s, sh), 2924 (s, sh), 2879 (s, sh), 2838 (s, sh), 1688 (vs, sh), 1606 (vs, sh), 1544 (vs, sh), 1503 (vs, sh), 1483 (vs, sh), 1468 (vs, sh), 1460 (vs, sh), 1412 (s), 1356 (s), 1345 (s), 1281 (vs, sh), 1237 (vs, sh), 1152 (m – s, sh), 1095 (m – s, sh), 1068 (vs), 1051 (vs), 1036 (vs), 925 (m, sh), 881 (m, sh), 857 (s, sh), 837 (s, sh), 750 (s, sh), 711 (s), 658 (m), 629 (m), 568 (m), 538 (w – m), 512 (w – m), 463 (w), 445 (w), 418 (w). TLC [RP-C18F_{254}S, MeOH/H_2O (5:1)]: R_f 0.77.

[**HL3e**]: Yield (1.51 g, 75%). IR (KBr pellet, cm^{-1}): 3192 (s, br), 3058 (m), 2999 (m), 2948 (s, sh), 2925 (m), 2879 (m), 2741 (w), 1693 (vs, sh), 1607 (m, sh), 1588 (m, sh), 1551 (vs), 1500 (s), 1433 (m), 1410 (m), 1356 (s, sh), 1345 (m), 1304 (s), 1278 (vs, sh), 1257 (vs), 1218 (vs), 1159 (w – m), 1100 (m), 1074 (s, sh), 1062 (s, sh), 1053 (s, sh), 1004 (m), 931 (w – m), 883 (m, sh), 837 (m, sh), 739 (s, sh), 680 (w), 660 (w – m, sh), 631 (w), 571 (w), 534 (w), 515 (w), 486 (w), 415 (w – m, sh). TLC [RP-C18F_{254}S, MeOH/H_2O (5:1)]: R_f 0.79.

3.5.4 Preparation of *N,N*-dialkyl-*N'*-menthyloxycarbonylthiourea and *N*-menthyloxycarbonyl-*N'*-morpholinothiourea ligands

N,N-diethyl-*N'*-(-)-(3*R*)-menthyloxycarbonylthiourea (HL4) and *N,N*-diethyl-*N'*-(+)-(3*S*)-menthyloxycarbonylthiourea (HL5)

To a solution of dry potassium thiocyanate (9.53 mmol) in dry acetone (50 ml), was added dropwise an equimolar amount of menthyl chloroformate (9.57 mmol). The solution was refluxed under nitrogen for 2 hours. Diethylamine (9.58 mmol) was then added dropwise to the cooled reaction mixture and the solution was refluxed for a further 2 hours. The solution was cooled to room temperature. KCl was removed by filtration and the filtrate was concentrated to half the volume under reduced pressure. Water (100 ml) was added, whereupon a yellow oil formed. The aqueous layer was decanted and the oil was extracted into ether (40 ml). The aqueous layer was extracted twice with

ether (40 ml). The ethereal fractions were combined, dried over anhydrous $MgSO_4$ and evaporated to dryness under reduced pressure to yield a yellow oil. The oil was dissolved in a small volume of ethanol and the solution was placed in a freezer. Colourless crystals were collected by filtration, washed with water, ethanol and dried *in vacuo* over silica gel.

[**HL4**]: Yield (0.76 g, 26%). IR (KBr pellet, cm^{-1}): 3179 (s, sh), 3061 (m), 2958 (vs), 2927 (vs), 2871 (s), 1737 (vs, sh), 1536 (vs, sh), 1479 (vs), 1433 (vs), 1386 (m, sh), 1378 (m, sh), 1361 (m, sh), 1349 (w – m,), 1309 (w – m), 1287 (s), 1251 (vs, br), 1221 (vs), 1180 (s), 1133 (s, sh), 1102 (m, sh), 1080 (m, sh), 1064 (m, sh), 1030 (s, sh), 984 (m), 942 (m), 900 (m), 880 (w, sh), 846 (w, sh), 802 (w – s), 768 (m), 757 (m), 715 (w – m), 689 (w – m, br), 617 (w), 596 (w), 569 (w), 546 (w), 511 (w), 491 (w), 469 (w), 416 (w – m, sh). $[\alpha]_D^{25}$ = - 42.4° (c = 0.5 acetone). TLC [Silica gel, $CHCl_3$/EtOH (2%)]: R_f 0.70.

[**HL5**]: Yield (0.96 g, 32%). IR (KBr pellet, cm^{-1}): 3179 (s, sh), 3061 (m), 2958 (vs), 2927 (vs), 2871 (s), 1737 (vs, sh), 1536 (vs, sh), 1479 (vs), 1433 (vs), 1386 (m, sh), 1378 (m, sh), 1361 (m, sh), 1349 (w – m,), 1309 (w – m), 1287 (s), 1251 (vs, br), 1221 (vs), 1180 (s), 1133 (s, sh), 1102 (m, sh), 1080 (m, sh), 1064 (m, sh), 1030 (s, sh), 984 (m), 942 (m), 900 (m), 880 (w, sh), 846 (w, sh), 802 (w – s), 768 (m), 757 (m), 715 (w – m), 689 (w – m, br), 617 (w), 596 (w), 569 (w), 546 (w), 511 (w), 491 (w), 469 (w), 416 (w – m, sh). $[\alpha]_D^{25}$ = + 36.5° (c = 0.4 acetone). TLC [Silica gel, $CHCl_3$/EtOH (2%)]: R_f 0.70.

_N_-(-)-(3_R_)-menthyloxycarbonyl-_N'_-morpholinothiourea (HL6)

To a solution of dry potassium thiocyanate (0.893 g, 9.19 mmol) in dry acetone (50 ml), was added dropwise an equimolar amount of (-)-menthyl chloroformate (2.01 g, 9.20 mmol). The solution was refluxed under nitrogen for 2 hours. Morpholine (0.782 g, 9.29 mmol) was then added dropwise to the cooled reaction mixture and the solution was refluxed for a further 2 hours. The solution was cooled to room temperature and the KCl was removed by filtration. The filtrate was concentrated to half the volume under reduced pressure and then water (80 ml) was added, whereupon a yellow oil formed. The

mixture was placed in a refrigerator (4°C) overnight, whereupon the oil solidified. The yellow crystals were collected, washed with water and ether. A large majority of the crystals dissolved in the ether. The ethereal layer was evaporated to dryness under reduced pressure to yield colourless crystals. The residual crystals were recrystallised from ethanol. The aqueous layers were combined, concentrated under reduced pressure with addition of ethanol. The aqueous layer was placed in a refrigerator (4°C) for several days. The filtrate from recrystallisation was left to evaporate at room temperature to yield a further crop. Colourless crystals were collected by filtration, washed with ice-cold ethanol and dried *in vacuo* over silica gel.

[**HL6**]: Yield (1.28 g, 42%). IR (KBr pellet, cm^{-1}): 3204 (s, br), 3059 (m), 2988 (m), 2953 (s), 2925 (s), 2873 (s), 2862 (s), 1736 (vs, sh), 1541 (s, br), 1473 (s), 1436 (s), 1390 (m, sh), 1374 (m, sh), 1354 (m), 1327 (m, sh), 1308 (m), 1280 (m – s, sh), 1246 (vs, br), 1223 (vs), 1203 (vs), 1183 (m – s, sh), 1164 (m – s), 1110 (s), 1082 (m, sh), 1066 (m, sh), 1026 (s), 984 (s, sh), 946 (m), 918 (m), 908 (m), 856 (m – s), 847 (m – s), 815 (m), 801 (m), 736 (w), 712 (w – m), 640 (m – s), 596 (m), 555 (m – s), 515 (m – s), 500 (m, sh), 466 (w – m), 419 (w), 398 (w), 377 (w), 370 (w). $[\alpha]_D^{25}$ = -45.8 (c = 0.7). TLC [Silica gel, $CHCl_3$/EtOH (2%)]: R_f 0.73

_N_-(+)-(3_S_)-menthyloxycarbonyl-_N'_-morpholinothiourea (HL7)

To a solution of dry potassium thiocyanate (0.888 g, 9.14 mmol) in dry acetone (50 ml), was added dropwise an equimolar amount of (+)-menthyl chloroformate (2.00 g, 9.15 mmol). The solution was refluxed under nitrogen for 2 hours. Morpholine (0.772 g, 9.18 mmol) was then added dropwise to the cooled reaction mixture and the solution was refluxed for a further 2 hours. The solution was cooled to room temperature and the KCl was removed by filtration. The filtrate was concentrated to half the volume under reduced pressure and then water (120 ml) was added, whereupon a yellow oil formed. The mixture was placed in a refrigerator (4°C) for 2 days. The oil was extracted twice into ether (50 ml), and the organic layer was dried over $MgSO_4$ and evaporated to dryness under reduced pressure to yield an orange oil. A little ether was added to the orange oil whereupon the oil solidified. The product was recrystallised from ethanol. Colourless

crystals were collected by filtration, washed with water, ice-cold ethanol and dried *in vacuo* over silica gel.

[**HL7**]: Yield (1.25 g, 42%). IR (KBr pellet, cm^{-1}): 3204 (s, br), 3059 (m), 2988 (m), 2953 (s), 2925 (s), 2873 (s), 2862 (s), 1736 (vs, sh), 1541 (s, br), 1473 (s), 1436 (s), 1390 (m, sh), 1374 (m, sh), 1354 (m), 1327 (m, sh), 1308 (m), 1280 (m – s, sh), 1246 (vs, br), 1223 (vs), 1203 (vs), 1183 (m – s, sh), 1164 (m – s), 1110 (s), 1082 (m, sh), 1066 (m, sh), 1026 (s), 984 (s, sh), 946 (m), 918 (m), 908 (m), 856 (m – s), 847 (m – s), 815 (m), 801 (m), 736 (w), 712 (w – m), 640 (m – s), 596 (m), 555 (m – s), 515 (m – s), 500 (m, sh), 466 (w – m), 419 (w), 398 (w), 377 (w), 370 (w). $[\alpha]_D^{25}$ = + 45.4 (c = 0.6). TLC [Silica gel, $CHCl_3$/EtOH (2%)]: R_f 0.73

3.6 References

1. M. Schuster, *Fresenius' J. Anal. Chem.*, 1992, **342**, 791.
2. L. Beyer, E. Hoyer, J. Liebscher, H. Hartmann, *Z. Chem*., 1981, **21**, 81.
3. S. Schmidt, F. Dietze, E. Hoyer, *Z. Anorg. Allg. Chem*., 1991, **603**, 33.
4. J. Sieler, R. Richter, E. Hoyer, L. Beyer, R. Köhler, *Z. Anorg. Allg. Chem*., 1991, **603**, 25.
5. E. Kleinpeter, S. Behrendt, L. Beyer, *Z. Anorg. Allg. Chem*., 1982, **495**, 105.
6. L. Beyer, R. Kirmse, J. Stach, R. Szargan, E. Hoyer, *Z. Anorg. Allg. Chem*., 1981, **476**, 7.
7. E. Uhlemann, H. Bukowsky, L. Beyer, F. Dietze, E. Hoyer, , *Z. Anorg. Allg. Chem*., 1980, **470**, 177.
8. F. Dietze, J. Lerchner, S. Schmidt, L. Beyer, R. Köhler, *Z. Anorg. Allg. Chem*., 1991, **600**, 37.
9. U. Braun, R. Richter, J. Sieler, A. I. Yanovsky, Y. T. Struchkov, *Z. Anorg. Allg. Chem*., 1985, **529**, 201.
10. R. Richter, F. Dietze, S. Schmidt, E. Hoyer, D. Mootz, *Z. Anorg. Allg. Chem*., 1997, **623**, 135.
11. R. Richter, J. Sieler, R. Köhler, E. Hoyer, L. Beyer, L. K. Hansen, *Z. Anorg. Allg. Chem*., 1989, **578**, 191.
12. R. Richter, L. Beyer, J. Kaiser, *Z. Anorg. Allg. Chem*., 1980, **461**, 67.
13. K. R. Koch, C. Sacht, S. Bourne, *Inorg. Chim. Acta*, 1995, **232**, 109.
14. O. Seidelmann, L. Beyer, *Polyhedron*, 1998, **17**, 1601.
15. O. Seidelmann, L. Beyer, G. Zdobinsky, R. Kirmse, F. Dietze, R. Richter, *Z. Anorg. Allg. Chem*., 1996, **622**, 692.
16. E. Unterreitmaier, M. Schuster, *Anal. Chim. Acta*, 1995, **309**, 339.
17. M. Šandor, F. Geistmann, M. Schuster, *Anal. Chim. Acta*, 1999, **388**, 19.
18. F. Dietze, S. Schmidt, E. Hoyer, L. Beyer, *Z. Anorg. Allg. Chem*., 1991, **595**, 35.
19. A. Mohamadou, I. Déchamps-Olivier, J. –P. Barbier, *Polyhedron*, 1994, **13**, 1363.
20. A. Mohamadou, I. Déchamps-Olivier, J. –P. Barbier, *Polyhedron*, 1994, **13**, 3277.
21. J. Sieler, R. Richter, E. Hoyer, L. Beyer, O. Lindqvist, L. Andersen, *Z. Anorg. Allg. Chem*., 1990, **580**, 167.

22. K. R. Koch, S. A. Bourne, A. Coetzee, J. Miller, *J. Chem. Soc., Dalton Trans*., 1999, 3157.
23. K. –H. König, M. Kuge, L. Kaul, H. –J. Pletsch, *Chem. Ber*., 1987, **120**, 1251.
24. J. Stach, R. Herzschuh, R. Kirmse, L. Beyer, J. Hartung, *Z. Anorg. Allg. Chem*., 1984, **514**, 223.
25. M. Schuster, E. Unterreitmaier, *Fresenius' J. Anal. Chem*., 1993, **346**, 630.
26. R. Loos, D. K. Breitinger, *J. Mol. Struct*., 1999, **482–483**, 137.
27. M. Schuster, K. –H. König, *Fresenius' Z. Anal. Chem*., 1987, **327**, 102.
28. M. Schuster, K. –H. König, *Fresenius' Z. Anal. Chem*., 1988, **331**, 383.
29. M. Schuster, B. Kugler, K. –H. König, *Fresenius' J. Anal. Chem*., 1990, **338**, 717.
30. M. Schuster, *Fresenius' Z. Anal. Chem*., 1986, **324**, 127.
31. K. R. Koch, Y. Wang, A. Coetzee, *J. Chem. Soc., Dalton Trans.*, 1999, 1013.
32. K. R. Koch, C. Sacht, T. Grimmbacher, S. Bourne, *S. Afr. J. Chem*., 1995, **48**, 71.
33. D. –C. Zhang, Y. –Q. Zhang, Y. Cao, B. Zhao, *Acta Crystallogr*., *Sect. C*, 1996, **52**, 1716.
34. Y. Cao, B. Zhao, Y. –Q. Zhang, D. –C. Zhang, *Acta Crystallogr.*, *Sect. C*, 1996, **52**, 1772.
35. A. Dago, M. A. Simonov, E. A. Pobedimskaya, A. Martin, A. Masias, *Kristallografiya*, 1987, **32**, 1024.
36. A. Dago, A. Martin, A. Macias, *Rev. Cienc. Quim.,* 1985, **16**, 145.
37. P. D. Beer, M. G. B. Drew, D. K. Smith, *J. Organomet. Chem*., 1997, **543**, 259.
38. J. –T. Wang, Y. –F. Yuan, Y. –M. Xu, Y. –W. Zhang, R. –J. Wang, H. –G. Wang, *J. Organomet. Chem*., 1994, **211**, 481.
39. S. Bourne, K. R. Koch, *J. Chem. Soc., Dalton Trans.*, 1993, 2071.
40. J. L. Bricks, K. Rurack, R. Radeglia, G. Reck, B. Schulz, H. Sonnenschein, U. Resch-Genger, *J. Chem. Soc., Perkin Trans*. 2., 2000, 1209.
41. R. A. Bailey, K. L. Rothaupt, R. K. Kullnig, *Inorg. Chim. Acta*, 1988, **147**, 233.
42. L. Beyer, R. Richter, O. Seidelmann, *J. Organomet. Chem*., 1998, **561**, 199.
43. Y. –F. Yuan, S. –M. Ye, L. –Y. Zhang, J. –T. Wang, H. –G. Wang, *Polyhedron*, 1997, **16**, 2271.
44. A. D. Morales, S. Garcia-Granda, Y. R. Esteva, A. P. Stevens, G. A. A. Crespo, *Acta Crystallogr., Sect. C*, 1997, **53**, 9700019.
45. R. Richter, O. Seidelmann, L. Beyer, H. Plenio, *J. Organomet. Chem*., 1996, **525**, 199.

46. F. Leβmann, L. Beyer, R. Richter, R. Meusinger, *Z. Naturforsch*., *B*, 1998, **53**, 981.
47. K. R. Koch, T. Grimmbacher, C. Sacht., *Polyhedron*, 1998, **17**, 267.
48. K. R. Koch, S. Bourne, *J. Mol. Struct*., 1998, **441**, 11.
49. S. E. Livingstone, in *Comprehensive Coordination Chemistry*, Editor-in-chief. G. Wilkinson, Pergamon Press, Oxford, 1987, vol. 2, ch. 16.6, pp. 639–660.
50. G. Kemp, A. Roodt, W. Purcell, K. R. Kock, *J. Chem. Soc., Dalton. Trans*., 1997, 4481.
51. K. R. Koch, M. C. Matoetoe, *Magn. Reson. Chem*., 1991, **29**, 1158.
52. K. R. Koch, J. du Toit, M. R. Caira, C. Sacht, *J. Chem. Soc.,Dalton Trans*., 1994, 785.
53. R. Köhler, R. Kirmse, R. Richter, J. Sieler, E. Hoyer, L. Beyer, *Z. Anorg. Allg. Chem*., 1986, **537**, 133.
54. E. Guillon, A. Mohamadou, I. Déchamps-Olivier, J. –P. Barbier, *Polyhedron*, 1996, **15**, 947.
55. X. Shen, B. –S. Kang, Y. Lui, L. –Q. Gu, X. –Y. Huang, J. Sun, Q. –T. Lui, *J. Coord. Chem*., 1999, **46**, 397.
56. X. Shen, T. –B. Wen, Q. –T. Lui, X. –Y. Huang, B. –S. Kang, X. –L. Wu, Z. –S. Huang, L. – Q. Gu, *Polyhedron*, 1997, **16**, 2605.
57. *Handbook of Chemistry and Physics*, ed. R. C. Weast, CRC Press, Inc., 61st ed., Boca Raton, Fl. 33431, pp. F-218, 1980–1981.
58. K. –H. König, H. –J. Pletsch, M. Schuster, *Fresenius' Z. Anal. Chem*., 1984, **319**, 66.
59. P. D. Beer, P. A. Gale, G. Z. Chen, *J. Chem. Soc., Dalton Trans*., 1999, 1897.
60. T. Seshadri, H. –J. Haupt, *J. Mater.Chem.*, 1998, **8**, 1345.
61. C. Djerassi, K. Undheim, A. –M. Weidler, *Acta Chem. Scand*., 1962, **16**, 1147.
62. I. B. Douglass, F. B. Dains, *J. Am. Chem. Soc*., 1934, **56**, 719.
63. A. Takamizawa, K. Hirai, K. Matsui, *Bull. Chem. Soc. Jpn.*, 1963, **36**, 1214.
64. R. Esmail, F. Kurzer, *Synthesis*, 1975, 301.
65. P. Mühl, K. Gloe, F. Dietze, E. Hoyer, L. Beyer, *Z. Chem*., 1986, **26**, 81.
66. E. Breitmaier, W. Voelter, in *Carbon-13 NMR Spectroscopy*, VCH, Weinheim, 1990, vol. 5, pp. 83 and 328.

67. J. K. M. Sanders, B. K. Hunter, in *Modern NMR Spectroscopy*, Oxford University Press, Oxford, 1989, ch. 5.2, pp. 147–149.
68. H. D. Flack, *Acta Crystallogr*., *Sect. A*, 1983, **39**, 876.
69. G. M. Sheldrick, SHELXS97, *Program for Solving Crystal Structures*, University of Göttingen, Germany, 1997.
70. G. M. Sheldrick, SHELXTL97, *Program for Solving Crystal Structures*, University of Göttingen, Germany, 1995.
71. V. A. Streltsov, V. E. Savodnik, *Kristallographia*, 1989, **34**, 1369.
72. C. K. Johnson, *ORTEPII*, Report ORNL-5138. Oak Ridge National Laboratory, Tennessee, USA, 1976.

CHAPTER 4: PART A

SYNTHESIS AND CHARACTERISATION OF [Pt(ACYLTHIOUREATO)Cl(RR'SO)] COMPLEXES

4.1 Introduction

This chapter is concerned with the synthesis and characterisation of complexes of the type [PtCl(L)(RR'SO)], where HL = acylthiourea or alkoxycarbonylthiourea ligand and RR'SO = sulfoxide. The acylthiourea and alkoxycarbonylthiourea ligand systems showed distinctly different coordination chemistry towards platinum(II), therefore the results and discussion will be presented as follows:

i) Part A: Synthesis and characterisation of [Pt(acylthioureato)Cl(RR'SO)] complexes.
ii) Part B: Synthesis and characterisation of [Pt(alkoxycarbonylthioureato)Cl-(RR'SO)] complexes.
iii) Part C: Comparison of the coordination chemistry of alkoxycarbonylthioureato and acylthioureato ligand systems.

PART A

4.2 Results and Discussion

4.2.1 Synthesis of [Pt(acylthioureato)Cl(RR'SO)] complexes

The [PtCl(L)(RR'SO)] complexes were prepared using RR'SO = dimethylsulfoxide (DMSO), (*S*)-(-)-methyl(*p*-tolyl)sulfoxide ((*S*)-MTSO), (*R*)-(+)methyl(*p*-tolyl)sulfoxide ((*R*)-MTSO), methylphenylsulfoxide (MPSO) and HL = *N*-(3-*R*-benzoyl)-*N',N'*-diethylthiourea (**HL1a–e**), *N*-(3-*R*-benzoyl)-*N'*-morpholinothiourea (**HL2a–e**) and *N*-(3-*R*-benzoyl)-*N',N'*-di(2-hydroxyethyl)thiourea (**HL3a–e**). A dinuclear complex, [{Pt(DMSO)Cl}$_2$L] was also prepared, where HL = *N,N*-adipoylbis(*N',N'*-diethylthiourea) (**HL1f**). Dimethylsulfoxide complexes were prepared using all the ligands, while complexes containing unsymmetrical sulfoxides were prepared using *N*-benzoyl-*N',N'*-diethylthiourea (**HL1a**) only. The structural formulae and atom numbering scheme adopted for NMR assignments for the proposed structures of the [Pt(acylthioureato)Cl(RR'SO)] complexes are shown in Figure 4.1 and Figure 4.2.

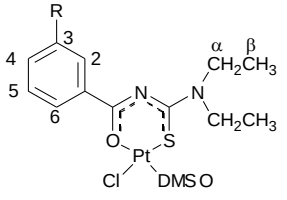

1a: R = H
1b: R = Cl
1c: R = NO_2
1d: R = OCH_3
1e: R = CH_3

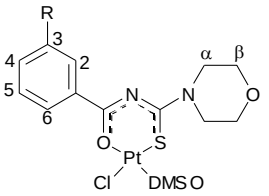

2a: R = H
2b: R = Cl
2c: R = NO_2
2d: R = OCH_3
2e: R = CH_3

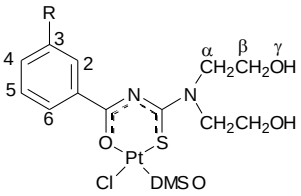

3a: R = H
3b: R = Cl
3c: R = NO_2
3d: R = OCH_3
3e: R = CH_3

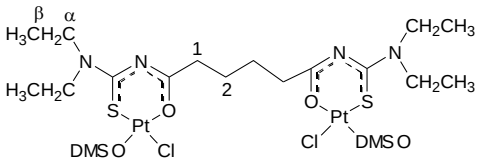

1f

Figure 4.1: Structural formulae and atom numbering scheme adopted for NMR assignments for the *cis*-(S,S)-[PtCl(DMSO)(L)] complexes, where L = *N,N*-dialkyl-*N'*-(3-*R*-benzoyl)thioureato, *N*-(3-*R*-benzoyl)-*N'*-morpholinothioureato and *N,N*-adipoylbis(*N',N'*-diethylthioureato) ligands.

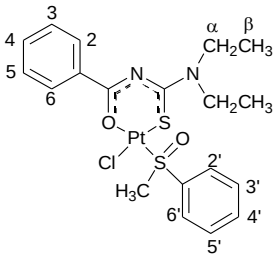

4: *cis*-(S,S)-[PtCl(L1a)(MPSO)]

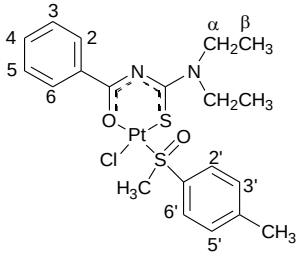

5: *cis*-(S,S)-[PtCl(L1a)((*R*)-MTSO)]

6: *cis*-(S,S)-[PtCl(L1a)((*S*)-MTSO)]

Figure 4.2: Structural formulae and atom numbering scheme adopted for NMR assignments for the *cis*-(S,S)-[PtCl(L)(RR'SO)] complexes, where L = *N*-benzoyl-*N',N'*-diethylthioureato and RR'SO = (*S*)-MTSO, (*R*)-MTSO and MPSO.

The complexes were prepared according to the general method described by equations (**4 – 1**) and (**4 – 2**), where HL represents an acylthiourea ligand and RR'SO is a sulfoxide. A detailed description of the preparation of these complexes is given in the experimental section (Section 4.11.4).

$$K_2PtCl_4 + 3\ RR'SO \longrightarrow cis\text{-}[PtCl_2(RR'SO)_2] \qquad (\mathbf{4-1})$$

$$cis\text{-}[PtCl_2(RR'SO)_2] + HL \xrightarrow{NaOAc} cis\text{-}(S,S)\text{-}[PtCl(L)(RR'SO)] + cis\text{-}[PtL_2] \qquad (\mathbf{4-2})$$

The synthesis of the *cis*-(S,S)-[PtCl(L)(RR'SO)] complexes involves the addition of an acylthiourea ligand to *cis*-[$PtCl_2$(RR'SO)$_2$] in the presence of approximately 1.5 times excess of sodium acetate to facilitate the deprotonation of the acylthiourea ligand and bidentate chelation via the thiocarbonyl and carbonyl groups. All the reactions were carried out at room temperature. Characterisation of the complexes revealed that only the *cis*-(S,S)-[PtCl(L)(RR'SO)] isomers were obtained. The *cis*-(S,S) notation indicates that the sulfoxide sulfur donor atom is in a *cis* arrangement to the sulfur donor atom of the acylthioureato ligand chelate. The *cis*-[$PtCl_2$((*S*)-MTSO)$_2$] and *cis*-[$PtCl_2$((*R*)-MTSO)$_2$] complexes were prepared using the optically pure sulfoxides. The known *cis*-[$PtCl_2$(RR'SO)$_2$] complexes were prepared according to a modified literature procedure. [1] The analytical and spectroscopic data for the *cis*-[$PtCl_2$(RR'SO)$_2$] complexes are given in the experimental section (Section 4.11.3). The sign and handedness of the optically pure free sulfoxides changes upon complexation to platinum(II) and the *R* and *S* assignments used throughout this study refer to the sign of the sulfoxide when coordinated to platinum(II).

As shown by equations (**4 – 1**) and (**4 – 2**), it was found for ligands **HL1a–e** and **HL2a–e**, that in addition to the formation of the desired complex, *cis*-(S,S)-[PtCl(L)(RR'SO)], the neutral *cis*-[PtL_2] complex was also formed. This was evident from both the TLC and the ^{1}H NMR spectra of the crude products. Integration of the proton resonances indicated that the *cis*-[PtL_2] complexes were present as minor products (*ca*. 5–15%). The *cis*-[PtL_2] complexes have higher mobility on silica gel (R_f *ca.* 0.8) compared to the *cis*-(S,S)-[PtCl(L)(RR'SO)] complexes (R_f *ca.* 0.5–0.6) and consequently the complexes were readily separated using flash or molecular exclusion chromatography. The platinum dimethylsulfoxide complexes containing *N*-(3-*R*-benzoyl)-*N',N'*-di(2-hydroxyethyl)-thiourea ligands (**3a–e**) were isolated by filtration free of the *cis*-[PtL_2] complexes. This is most likely due to the *cis*-[PtL_2] complexes being more hydrophilic than the *cis*-(S,S)-[PtCl(DMSO)(L)] complexes and thus remaining in solution. Conclusive evidence that the major *cis*-(S,S)-[PtCl(DMSO)(L)] and minor *cis*-[PtL_2] products are formed was provided by X-ray crystallography. The crystal and molecular structures of *cis*-(S,S)-

[PtCl(DMSO)(L1a)] (**1a**), *cis*-(S,S)-[PtCl(L1a)(MPSO)] (**4**) and *cis*-[Pt(L1a)$_2$] (**7**) have been determined and are shown in Figures 4.4–4.6, respectively

4.2.2 Characterisation of [Pt(acylthioureato)Cl(RR'SO)] complexes

The platinum(II) sulfoxide complexes were characterised using IR and NMR spectroscopy, elemental analyses and in some cases by X-ray crystallography. The analytical data, ^{195}Pt NMR chemical shifts and principal infrared bands are given in Tables 4.1–4.2. The analytical and spectroscopic data are consistent with the structural formulae shown in Figure 4.1 and Figure 4.2.

4.2.2.1 Infrared spectra

The IR spectra of the platinum(II) sulfoxide complexes are very similar. Notable features of the infrared spectra of the platinum complexes are the disappearance of the ν(NH) stretching frequency and the shift of the ν(CO) stretching frequency to higher frequencies upon complexation of the acylthiourea ligands. A shift to higher frequencies should also be observed for the ν(C=S) stretching vibration, but this vibration could not be assigned unambiguously. The strong IR band in the 1130–1155 cm^{-1} region is assigned to the ν(SO) stretching frequency. The ν(SO) peak is shifted to a higher frequency upon complexation to platinum, relative to the uncoordinated sulfoxide, which is indicative of a sulfoxide bonded through the sulfur donor atom. [1–3]

4.2.2.2 NMR spectra

The ^{1}H NMR chemical shift data for the *cis*-(S,S)-[Pt(acylthioureato)Cl(RR'SO)] complexes are summarised in Tables 4.3–4.4. For convenience, the ^{1}H NMR data for the dinuclear complex, *cis*-(S,S)-[{Pt(DMSO)Cl}$_2$(L1f)] (**1f**), are given in the experimental section (Section 4.11.4). The ^{1}H NMR spectra are assigned according to the numbering scheme given in Figure 4.1 and Figure 4.2. The assignments of the ^{1}H NMR spectra of the *cis*-(S,S)-[Pt(acylthioureato)Cl(RR'SO)] complexes were straightforward, except for the assignments of the H_4 and H_6 aromatic protons which were confirmed by HMBC

experiments. Proton H_6 shows a correlation with the carbonyl carbon, while proton H_4 does not. A representative ^{1}H NMR spectrum is shown in Figure 4.3

In accordance with the IR spectra, the NH signal, observed for the ligands in the 8–12 ppm region, disappears upon complexation. A downfield shift is observed for the H_2 and H_6 aromatic protons and an upfield shift for the H_3, H_4 and H_5 proton resonances relative to that of the free ligand, with the exception of the H_4 proton resonances for complexes **1c**, **2c** and **3a–e**, which undergo downfield shifts.

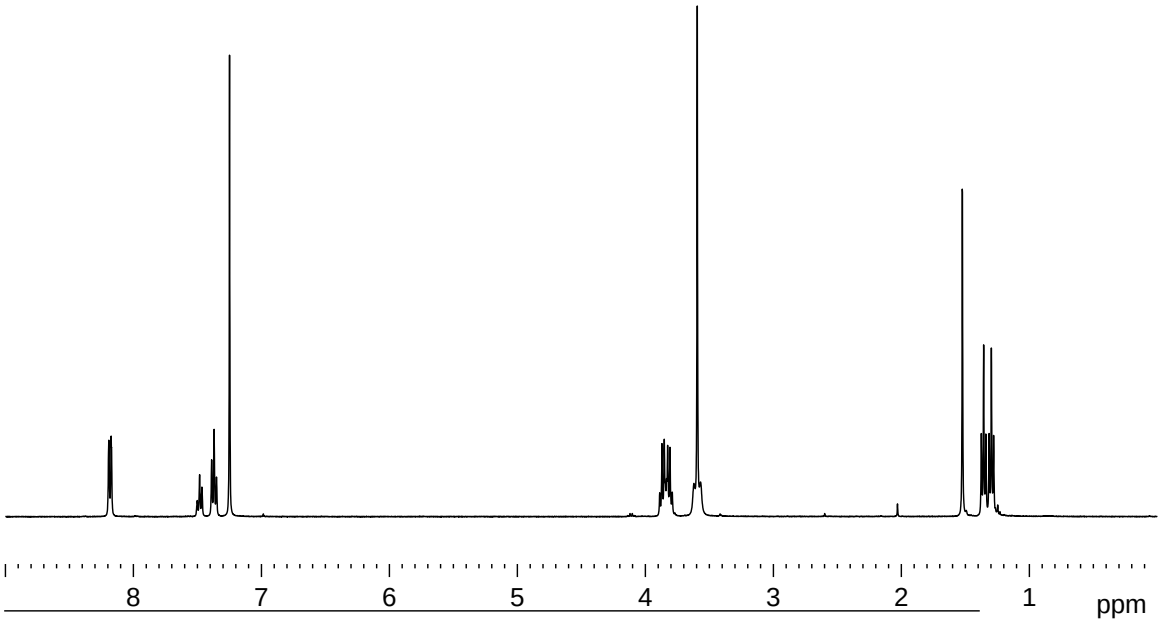

Figure 4.3: ^{1}H NMR spectrum of *cis*-(S,S)-[PtCl(DMSO)(L1a)] (**1a**) in $CDCl_3$ at 30°C.

The ^{1}H NMR chemical shift for the methyl protons of the coordinated sulfoxides are shifted approximately 1 ppm downfield relative to the free sulfoxide, which is typical for sulfur-bonded sulfoxides. [1] The assignment of the mode of coordination of the sulfoxide was further supported by the presence of platinum satellites due to vicinal coupling of the methyl protons of the sulfoxide with the platinum centre, ^{195}Pt (33.7%, I = ½). The ^3J(PtH) coupling constants are approximately 23 Hz, which is the same order of magnitude found for sulfur-bonded sulfoxides. [1, 4] The coordination geometry and mode of binding of the sulfoxide is consistent with the crystal structures of *cis*-(S,S)-[PtCl(DMSO)(L1a)], (Figure 4.4), and *cis*-(S,S)-[PtCl(L1a)(MPSO)], (Figure 4.5), in

which the DMSO and MPSO are sulfur-bonded to the platinum and *cis* to the sulfur donor atom of the *N*-benzoyl-*N',N'*-diethylthioureato ligand.

Table 4.1: Analytical and selected spectroscopic data for *cis*-(S,S)-[PtCl(DMSO)(L)] complexes.

Complex	R(C_6H_4)-	Mp/ °C [a]	Yield/ %	Analytical data (% C/H/N/S)[b]	ν(S=O)/ cm^{-1}	^{195}Pt NMR/ ppm [d]
1a	H	139–141	72	31.8; 3.9; 5.2; 11.7 (30.9; 3.9; 5.15; 11.8)	1139	-3256 -3229[c]
1b	Cl	160–162	78	29.5; 3.5; 4.8; 11.1 (29.1; 3.5; 4.8; 11.1)	1144	-3250
1c	NO_2	187–190	60	28.6; 3.3; 6.9; 10.7 (28.55; 3.4; 7.1; 10.9)	1153	-3242
1d	OCH_3	138–140	80	31.5; 4.1; 4.9; 11.1 (31.4; 4.0; 4.9; 11.2)	1137	-3256
1e	CH_3	109–111	45	32.6; 4.2; 4.9; 11.2 (32.3; 4.15; 5.0; 11.5)	1137	-3257
1f	[e]	> 230	93	24.5; 4.1; 5.7; 12.7 (22.4; 4.2; 5.8; 13.3)	1138	-3256
2a	H	197–dec[a]	51	30.9; 3.5; 4.8; 10.8 (30.1; 3.4; 5.0; 11.5)	1147	-3231[c]
2b	Cl	165–dec[a]	89	28.5; 3.0; 4.8; 11.1 (28.4; 3.1; 4.7; 10.8)	1148	-3224[c]
2c	NO_2	208–dec[a]	94	28.4; 3.1; 6.9; 10.65 (27.9; 3.0; 7.0; 10.6)	1145	-3219[c]
2d	OCH_3	189–dec[a]	49	31.0; 3.6; 4.7; 10.9 (30.6; 3.6; 4.8; 10.9)	1150	-3230[c]
2e	CH_3	187–dec[a]	86	31.6; 3.65; 5.0; 11.3 (31.5; 3.7; 4.9; 11.2)	1147	-3232[c]
3a	H	139–140	75	29.2; 3.7; 4.8; 11.05 (29.2; 3.7; 4.9; 11.1)	1146	-3229[c]
3b	Cl	130–132	77	28.2; 3.3; 4.8; 10.4 (27.5; 3.3; 4.6; 10.5)	1138	-3223[c]
3c	NO_2	152–154	68	27.4; 3.3; 6.8; 10.2 (27.1; 3.25; 6.8; 10.3)	1146	-3219[c]
3d	OCH_3	145–147	69	30.1; 4.0; 4.9; 10.4 (29.7; 3.8; 4.6; 10.6)	1148	-3228[c]
3e	CH_3	127–129	35	30.7; 3.9; 4.8; 10.8 (30.5; 3.9; 4.75; 10.9)	1149	-3231[c]

[a] Melting points determined by DSC. [b] Calculated values are given in parentheses. [c] Spectra recorded in DMSO–d_6. [d] ^{195}Pt NMR spectra were recorded at 30°C in $CDCl_3$, unless otherwise stated. [e] *N,N*-adipoylbis(*N',N'*-diethyl-thiourea).

Table 4.2: Analytical and selected spectroscopic data for *cis*-(S,S)-[PtCl(L1a)(RR'SO)] complexes, where RR'SO = MPSO, (*S*)-MTSO and (*R*)-MTSO.

Complex	RR'SO	Mp/ °C	Yield/ %	$[\alpha]_D^{25}$	Analytical data (% C/H/N/S)[a]	ν(S=O)/ cm^{-1}	^{195}Pt NMR/ ppm [b]
4	MPSO	64–67	10	-	37.85; 3.9; 4.6; 10.6 (37.65; 3.8; 4.6; 10.6)	1141	-3277
5	(*R*)-MTSO	70–74	39	+ 61.3	39.2; 4.1; 4.6; 10.3 (38.7; 4.1; 4.5; 10.3)	1145	-3273
6	(*S*)-MTSO	72–74	14	- 61.7	39.0; 4.1; 4.6; 10.3 (38.7; 4.1; 4.5; 10.3)	1145	-3273

[a] Calculated values are given in parentheses.

[b] ^{195}Pt NMR spectra were recorded at 30°C in $CDCl_3$.

Table 4.3: ^{1}H NMR data for *cis*-(S,S)-[PtCl(L1a)(RR'SO)] complexes, where RR'SO = MPSO, (*S*)-MTSO and (*R*)-MTSO.

Complex	$\delta H_{2,6}$	$\delta H_{3,5}$	δH_4	$\delta H_{4'}$	$\delta H_{2',6'}$	$\delta H_{3',5'}$	δH_{ArCH3}	δH_α	δH_β	δH_{SMe}
4	8.194	7.370	7.481	7.575	8.194	7.575	-	3.796	1.247	3.749
5	8.076	7.369	7.479	-	8.195	7.369	2.444	3.807	1.282	3.728
6	8.076	7.369	7.479	-	8.195	7.369	2.444	3.807	1.282	3.728

Table 4.4: ^{1}H NMR data for *cis*-(S,S)-[PtCl(DMSO)(L)] complexes, where HL= *N,N*-dialkyl-*N'*-(3-*R*-benzoyl)thiourea and *N*-(3-*R*-benzoyl)-*N'*-morpholinothiourea. The spectra were recorded at 30°C in $CDCl_3$, unless otherwise stated.

Complex	δH_2	δH_3	δH_4	δH_5	δH_6	δH_α	δH_β	δH_γ	δH_{SMe}	δH_R
1a	8.181	7.370	7.484	7.370	8.181	1.357	3.829		3.595	
						1.296				
1b	8.116		7.455	7.312	8.070	1.361	3.825		3.598	
						1.301				
1c	8.968		8.336	7.580	8.522	1.362	3.843		3.608	
1d	7.739		7.038	7.279	7.789	1.355	3.822		3.594	3.833
						1.299				
1e	7.911		7.238	7.192	7.911	1.276	3.749		3.596	2.313
						1.212				
2a	8.164	7.376	7.503	7.376	8.164	4.205	3.799		3.602	
						4.093				
2b	8.089		7.472	7.318	8.056	4.183	3.809		3.604	
						4.096				
2c	8.917		8.352	7.587	8.507	4.228	3.833		3.614	
						4.118				
2d	7.705		7.054	7.285	7.765	4.197	3.789		3.600	3.837
						4.090				
2e	7.959		7.313	7.254	7.959	4.200	3.803		3.601	2.384
						4.092				
3a [a]	8.069	7.441	7.602	7.441	8.069	4.008	3.772	5.052	[b]	
						3.921	3.696	4.936		
3b [a]	7.985		7.678	7.526	8.014	4.005	3.780	5.060	[b]	
						3.924	3.689	4.944		
3c [a]	8.759		8.445	7.794	8.445	4.042	3.789	5.077	[b]	
						3.939	3.717	4.957		
3d [a]	7.594		7.176	7.397	7.651	3.993	3.785	5.052	[b]	3.792
						3.913	3.709	4.932		
3e [a]	7.870		7.416	7.361	7.870	4.001	3.775	5.048	[b]	2.366
						3.917	3.694	4.930		

[a] Spectra were recorded in DMSO-d_6.

[b] Coordinated sulfoxide resonance not observed due to exchange with deuterated DMSO-d_6.

Variation of the electronic properties of the benzoyl and amine moieties appears to have a small effect on the ^{1}H NMR chemical shift ($\Delta\delta \approx 0.01$ ppm) of the methyl protons of the coordinated sulfoxide. As the electron-withdrawing properties of the 3-R-benzoyl moiety increases, the sulfoxide signal shifts downfield. The sulfoxide signal of the *cis*-(S,S)-[PtCl(DMSO)(L2)] complexes (**2a–e**) are more deshielded than the corresponding *cis*-(S,S)-[PtCl(DMSO)(L1)] complexes (**1a–e**). No coordinated sulfoxide resonances were observed for complexes **3a–e**, due to exchange with deuterated DMSO-d_6.

As seen in Table 4.4, the complexes generally exhibit separate resonances for the methylene protons (H_α) and distinct signals for the hydroxyl groups (H_γ) for complexes, **3a–e**, were observed in the ^{1}H NMR spectra. The magnetic inequivalence of the methylene and hydroxyl protons is ascribed to the restricted rotation around the C–N bond between the thiocarbonyl and the amine nitrogen, due to the partial double bond character of this bond. [5–9] The partial double bond character of the thioamide bond is consistent with the extensive delocalisation of the electrons in the chelate ring observed in the crystal structures of *cis*-(S,S)-[PtCl(DMSO)(L1a)] and *cis*-(S,S)-[PtCl(L1a)(MPSO)].

The ^{195}Pt NMR chemical shift for *cis*-[Pt(L1a)$_2$] (**7**) of –2723 ppm is identical to that reported in the literature. [3] All the *cis*-(S,S)-[Pt(acylthioureato)Cl(RR'SO)] complexes show ^{195}Pt chemical shifts in the –3200 to –3300 ppm region, which correspond to the chemical shift range for sulfur-bonded sulfoxides and are in agreement with the expected ^{195}Pt chemical shift positions for a [PtSOSCl] coordination sphere. [2, 10] The 3-substitution of the benzoyl moiety of these complexes results in a small but significant difference in the ^{195}Pt chemical shifts for the *cis*-(S,S)-[Pt(acylthioureato)Cl(DMSO)] complexes, demonstrating the sensitivity of the ^{195}Pt nucleus to subtle electronic changes on the benzoyl moiety. The electron-withdrawing effect of the nitro- and chloro-substituents results in notable downfield shifts of the ^{195}Pt signal: NO_2 ($\Delta\delta$: 10–14 ppm) > Cl ($\Delta\delta$: 6–7 ppm) > $OCH_3 \approx H \approx CH_3$, which is consistent with the mesomeric/inductive effects [11] expected for a 3-substituted benzoyl group. This parallels the general trend observed in the ^{1}H NMR data. No significant effect was observed on variation of the thioamide moiety.

For the *cis*-(S,S)-[PtCl(L1a)(RR'SO)] complexes the ^{195}Pt chemical shift positions for *cis*-(S,S)-[PtCl(L1a)(MPSO)] (-3277 ppm), *cis*-(S,S)-[PtCl(L1a)((*S*)-MTSO)] (-3273 ppm) and *cis*-(S,S)-[PtCl(L1a)((*R*)-MTSO)] (-3273 ppm) are upfield relative to the *cis*-(S,S)-[PtCl(DMSO)(L1a)] (-3256 ppm) complex. A similar trend has been observed for the mono-anionic K[$PtCl_3$(RR'SO)] series and has been attributed to the phenyl substituent conferring better donor ability on the sulfoxide. [12] This can be explained by considering the canonical forms of a sulfoxide, which is generally represented as:

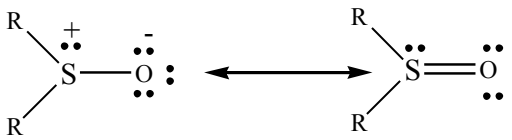

I **II**

Both forms (**I**) and (**II**) are considered to contribute to metal binding. The replacement of alkyl by aryl substituents results in a decrease in the net positive charge on the free sulfoxide. This decrease in positive charge favours forms (**II**) over form (**I**) in metal-sulfoxide binding, thus strengthening the sulfur-bonding through form (**II**), which is reflected in a more shielded environment for the platinum nucleus. [13]

The sensitivity of the ^{195}Pt NMR signal to changes in the benzoyl and sulfoxide substituents indicates that these groups influence the electron density at the platinum centre and are therefore expected to have an influence on the substitution reaction kinetics of these complexes. A detailed discussion of the substitution reaction kinetics of the *cis*-(S,S)-[PtCl(*N,N*-dialkyl-*N'*-(3-*R*-benzoyl)thioureato)(RR'SO)] complexes with various neutral and charged nucleophiles is given in Chapter 5.

4.2.2.3 Reaction of cis-(S,S)-[PtCl(DMSO)(L1a)] and cis-(S,S)-[PtCl(DMSO)(L2a)] with PPh_3

The *cis*-(S,S)-[PtCl(DMSO)(L1a)] and *cis*-(S,S)-[PtCl(DMSO)(L2a)] complexes were reacted with one equivalent of PPh_3, according to equation (**4 – 3**), to determine the substitution products of these reactions and to further highlight the difference in the coordination chemistry of the acylthiourea and alkoxycarbonylthiourea ligand systems.

$$cis\text{-(S,S)-[PtCl(DMSO)(L)]} \xrightarrow{PPh_3} cis\text{-(S,P)-[PtCl(L)(PPh}_3\text{)]} + \text{DMSO} \quad (\mathbf{4-3})$$

where L = L1a and L2a.

Upon addition of one equivalent of PPh_3 to *cis*-(S,S)-[PtCl(DMSO)(L1a)] and *cis*-(S,S)-[PtCl(DMSO)(L2a)] in $CDCl_3$, the proton resonance of the coordinated sulfoxide disappeared and a signal due to free dimethylsulfoxide was observed in the ^{1}H NMR spectra, suggesting that upon addition of one equivalent of PPh_3, the dimethylsulfoxide ligand is substituted. Structural analysis of the substitution product, *cis*-(S,P)-[PtCl(L1a)(PPh_3)] (**8**), proves conclusively that the dimethylsulfoxide ligand is substituted upon addition of one equivalent of PPh_3 to complexes of the type *cis*-(S,S)-[PtCl(DMSO)(L)], where L = acylthioureato ligand. The crystal and molecular structure of *cis*-(S,P)-[PtCl(L1a)(PPh_3)] is shown in Figure 4.7. The ^{31}P NMR spectra of *cis*-(S,P)-[PtCl(L1a)(PPh_3)] and *cis*-(S,P)-[PtCl(L2a)(PPh_3)], each consist of singlet at 8.137 and 7.729 ppm with ^1J(PtP) coupling constants of 4040 and 4033 Hz, respectively. A detailed ^{31}P NMR study of the reaction of *cis*-(S,S)-[PtCl(DMSO)(L1a)] and *cis*-(S,S)-[PtCl(DMSO)(L2a)] with triphenylphosphine is given in Section 4.8.

4.2.2.4 Crystallographic study

The crystallographic data for *cis*-(S,S)-[PtCl(DMSO)(L1a)], *cis*-(S,S)-[PtCl(L1a)(MPSO)], *cis*-[Pt(L1a)$_2$] and *cis*-(S,P)-[PtCl(L1a)(PPh_3)] are given in Table 4.5. Bond distances within the platinum(II) coordination sphere for *cis*-(S,S)-[PtCl(DMSO)(L1a)], *cis*-(S,S)-[PtCl(L1a)(MPSO)] and *cis*-[Pt(L1a)$_2$] are compared to bond distances in related compounds in the literature, and are discussed with respect to the *trans*-influence of the different donor atoms, in Section 4.9. A complete list of bond lengths and angles are given in Appendix A.

Table 4.5: Crystallographic data for *cis*-(S,S)-[PtCl(DMSO)(L1a)], *cis*-(S,S)-[PtCl(L1a)(MPSO)], *cis*-[Pt(L1a)$_2$] and *cis*-(S,P)-[PtCl(L1a)(PPh$_3$)].

	cis-(S,S)-[PtCl(DMSO)(L1a)] (**1a**)	*cis*-(S,S)-[PtCl(L1a)(MPSO)] (**4**)	*cis*-(Pt(L1a)$_2$] (**7**)	*cis*-(S,P)-[PtCl(L1a)(PPh$_3$)] (**8**)
Empirical formula	$C_{14}H_{21}ClN_2O_2PtS_2$	$C_{19}H_{23}ClN_2O_2PtS_2$	$C_{24}H_{30}N_4O_2PtS_2$	$C_{30}H_{30}ClN_2OPPtS$
Formula weight	543.99	606.05	665.73	728.13
Temperature	293(2) K	293(2) K	293(2) K	293(2) K
Wavelength	0.71073 Å	0.71073 Å	0.71073 Å	0.71073 Å
Crystal system, space group	Triclinic, P $\bar{1}$	Triclinic, P $\bar{1}$	Monoclinic, $P2_1/n$	Orthorhombic, $P2_12_12_1$
Unit cell dimensions	a = 8.7436(4) Å α = 76.263(10)°	a = 8.612(2) Å α = 115.11(2)°	a = 9.926(2) Å α = 90°	a = 10.1271(5) Å α = 90°
	b = 10.0717(5) Å β = 89.207(10)°	b = 11.776(2) Å β = 86.44(2)°	b = 12.265(3) Å β = 91.00(2)°	b = 16.4174(8) Å β = 90°
	c = 11.5723(6) Å γ = 68.205(10)°	c = 13.374(3) Å γ = 66.25(2)°	c = 21.168(5) Å γ = 90°	c = 17.7317(8) Å γ = 90°
Volume	916.05(8) Å^3	1078.8(4) Å^3	2576.7(10) Å^3	2948.1(2) Å^3
Z, Calculated density	2, 1.979 Mg/m^3	2, 1.866 Mg/m^3	4, 1.700 Mg/m^3	4, 1.641 Mg/m^3
μ	8.039 mm^{-1}	6.837 mm^{-1}	5.636 mm^{-1}	5.001 mm^{-1}
F(000)	524	588	1287	1432
Crystal size	0.30 x 0.30 x 0.08 mm	0.42 x 0.34 x 0.30 mm	0.35 × 0.32 × 0.21 mm	0.40 × 0.30 × 0.20 mm
Theta range for data collection	5.75 to 28.32°	1.75 to 25.05°	1.92 to 25.07°	1.69 to 28.27°
Index ranges	$-11 \le h \le 11$, $-13 \le k \le 13$, $-15 \le l \le 15$	$0 \le h \le 10$, $-12 \le k \le 14$, $-15 \le l \le 15$	$-10 \le h \le 9$, $0 \le k \le 14$, $0 \le l \le 24$	$12 \le h \le 11$, $-14 \le k \le 21$, $-23 \le l \le 23$
Reflections collected	9904	3450	3803	19304
Independent reflections	4433	2918	3454	6755
R_{int}	0.0365	0.0327	0.0215	0.0254
Goodness-of-fit on F^2	1.072	1.120	1.140	1.126
Final R indices [$I>2\sigma(I)$]	R^a = 0.0299, Rw^b = 0.0725	R^a = 0.0613, Rw^b = 0.1535	R^a = 0.0358, Rw^b = 0.0926	R^a = 0.0220, Rw^b = 0.0460
Largest diff. peak and hole	1.233 and –1.249 e.Å^{-3}	3.141 and –3.613 e.Å^{-3}	0.750 and –1.664 e.Å^{-3}	0.337 and –0.994 e.Å^{-3}

[a] $R = [(\Sigma\Delta F)/(\Sigma F_0)]$.

[b] $Rw = [\Sigma[w(F_o^2 - F_c^2)^2]/\Sigma[w(F_0^2)^2]]^{1/2}$.

Crystal structure of *cis*-(S,S)-[PtCl(DMSO)(L1a)] (**1a**)

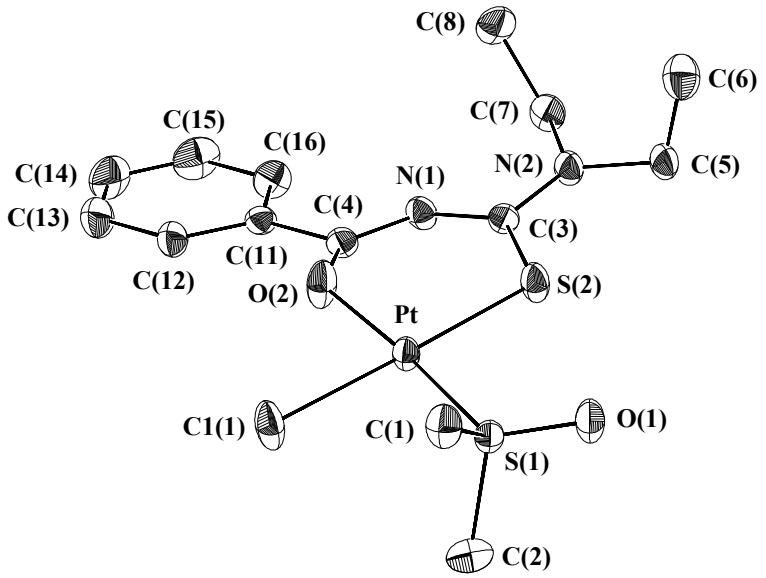

Figure 4.4: Molecular structure showing the atom numbering scheme and displacement ellipsoids (30% probability) for *cis*-(S,S)-[PtCl(DMSO)(L1a)]. Hydrogen atoms have been omitted for clarity.

The molecular structure of *cis*-(S,S)-[PtCl(DMSO)(L1a)] is shown in Figure 4.4, together with the atom numbering scheme. Selected bond lengths and angles for *cis*-(S,S)-[PtCl(DMSO)(L1a)] are given in Table 4.6. The complex displays the expected square-planar configuration around the platinum atom and confirms that the sulfoxide is sulfur-bonded to the platinum(II) and is coordinated *cis* to the sulfur atom of the acylthioureato ligand.

The dimensions of the sulfoxide compare well with previously reported structural results. [14] The phenyl ring of the acylthioureato ligand is almost planar (6.2(6)°) to the chelate ring of the acylthioureato ligand. The bond lengths of the thiocarbonyl [C(3)–S(2) = 1.735(4) Å] and the carbonyl [C(4)–O(2) = 1.271(5) Å] bonds are longer than the average C=S and C=O bond lengths of 1.71 and 1.23 Å, respectively, while the C–N bonds in the chelate ring are all shorter than the average C–N single bond lengths of 1.479 Å, [4] indicating extensive delocalisation of electrons in the chelate ring. The bond lengths and angles compare well with those reported for *cis*-bis(*N*-benzoyl-*N',N'*-di(*n*-butyl)-

thioureato)platinum(II), [15] *cis*-(S,S)-[PtCl(L1a)(MPSO)] (**4**), *cis*-[Pt(L1a)$_2$] (**7**) and *cis*-(S,S)-[PtCl(L1a)(PPh$_3$)] (**8**).

Table 4.6: Selected bond lengths (Å) and angles (°) for *cis*-(S,S)-[PtCl(DMSO)(L1a)].

Bond		Angle	
Pt-O(2)	2.010(3)	O(2)-Pt-S(1)	175.38(10)
Pt-S(1)	2.1885(10)	O(2)-Pt-S(2)	93.75(10)
Pt-S(2)	2.2586(11)	S(1)-Pt-S(2)	90.87(4)
Pt-Cl(1)	2.3337(11)	O(2)-Pt-Cl(1)	84.94(10)
S(1)-C(2)	1.759(5)	S(1)-Pt-Cl(1)	90.44(4)
N(1)-C(4)	1.312(6)	S(2)-Pt-Cl(1)	178.64(4)
N(1)-C(3)	1.348(5)		
N(2)-C(3)	1.335(5)		
N(2)-C(7)	1.472(6)		

Symmetry transformations used to generate equivalent atoms.

Crystal structure of *cis*-(S,S)-[PtCl(L1a)(MPSO)] (**4**)

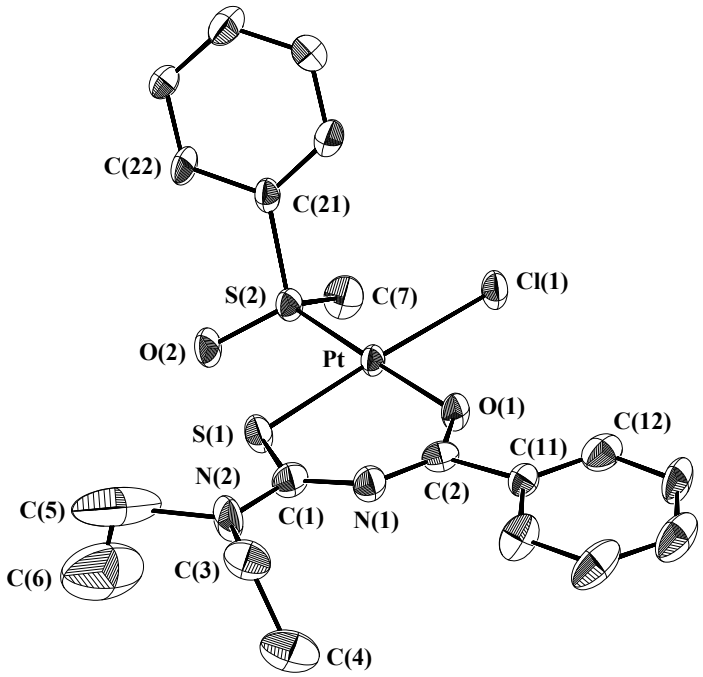

Figure 4.5: Molecular structure showing the atom numbering scheme and displacement ellipsoids (30% probability) for *cis*-(S,S)-[PtCl(L1a)(MPSO)]. Hydrogen atoms have been omitted for clarity.

The molecular structure of *cis*-(S,S)-[PtCl(L1a)(MPSO)] is shown in Figure 4.5, together with the atom numbering scheme. Selected bond lengths and angles for *cis*-(S,S)-[PtCl(L1a)(MPSO)] are given in Table 4.7. The complex displays the expected square-planar configuration around the platinum atom and the structure determination confirms that the sulfoxide is sulfur-bonded to the platinum(II) and coordinated *cis* to the sulfur donor atom of the acylthioureato ligand.

The structure shows discrete *cis*-(S,S)-[PtCl(L1a)(MPSO)] molecules with *R* and *S* configurations at the chiral sulfoxide sulfur atom. The dimensions of the sulfoxide compare well with previously reported structural results. [14] The phenyl ring of the sulfoxide lies almost perpendicular (111°) to the platinum(II) coordination plane. The bond lengths and angles compare well with those reported for *cis*-bis(*N*-benzoyl-*N',N'*-di(*n*-butyl)thioureato)platinum(II), [15] *cis*-[Pt(L1a)$_2$] (**7**), *cis*-(S,S)-[PtCl(DMSO)(L1a)] (**1a**) and *cis*-(S,S)-[PtCl(L1a)(PPh$_3$)] (**8**). The bond lengths of the thiocarbonyl [C(1)–S(1) = 1.736(14) Å] and the carbonyl [C(2)–O(1) = 1.26(2) Å] bonds are longer than the average C=S and C=O bond lengths of 1.71 and 1.23 Å, respectively. The C–N bonds in the chelate ring are all shorter than the average C–N single bond lengths of 1.479 Å, [4] indicating extensive delocalisation of electrons within the chelate ring.

Table 4.7: Selected bond lengths (Å) and angles (°) for *cis*-(S,S)-[PtCl(L1a)(MPSO)].

Bond		Angle	
Pt-O(1)	2.016(9)	O(1)-Pt-S(2)	177.2(3)
Pt-S(2)	2.192(3)	O(1)-Pt-S(1)	93.3(3)
Pt-S(1)	2.257(4)	S(2)-Pt-S(1)	89.09(13)
Pt-Cl(1)	2.334(3)	O(1)-Pt-Cl(1)	84.1(3)
S(1)-C(1)	1.736(14)	S(2)-Pt-Cl(1)	93.48(13)
N(1)-C(2)	1.28(2)	S(1)-Pt-Cl(1)	177.24(13)
N(1)-C(1)	1.35(2)		
N(2)-C(1)	1.34(2)		
N(2)-C(3)	1.48(2)		

Symmetry transformations used to generate equivalent atoms.

Crystal structure of *cis*-[Pt(L1a)$_2$] (**7**)

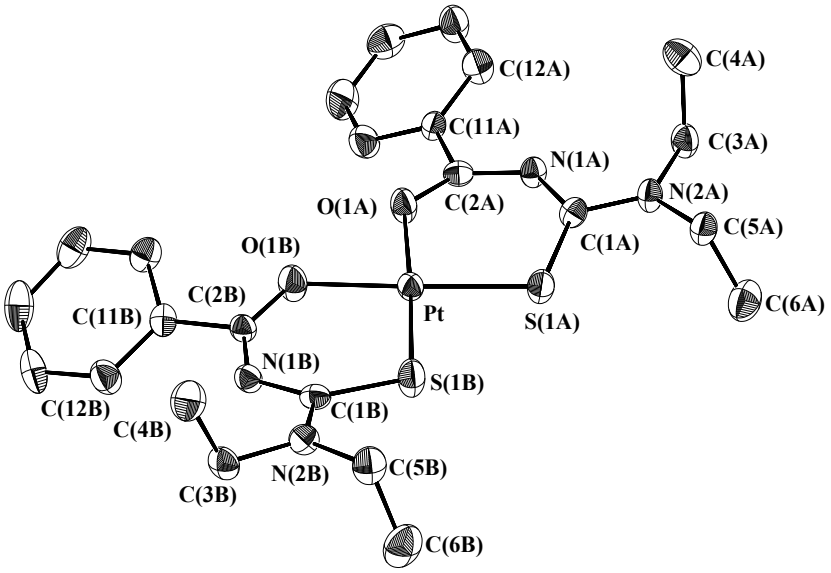

Figure 4.6: Molecular structure showing the atom numbering scheme and displacement ellipsoids (30% probability) for *cis*-[Pt(L1a)$_2$]. Hydrogen atoms have been omitted for clarity.

The molecular structure of *cis*-[Pt(L1a)$_2$] is shown in Figure 4.6, together with the atom numbering scheme. Selected bond lengths and angles for *cis*-[Pt(L1a)$_2$] are given in Table 4.8. The overall structure is consistent with that of *cis*-bis(*N*-benzoyl-*N',N'*-di(*n*-butyl)thioureato)platinum(II) and related complexes in that the ligands are coordinated in a *cis* configuration. [15, 16] The bond lengths and angles for the *cis*-[Pt(L1a)$_2$] complex compare well with those reported for *cis*-bis(*N,N*-di(*n*-butyl)-*N'*-benzoylthioureato)-platinum(II). [15] The bond lengths of the thiocarbonyl [C(1A)–S(1A) = 1.731(7); C(1B)–S(1B) = 1.723(7) Å] and the carbonyl [C(2A)–O(1A) = 1.271(8); C(2B)–O(1B) = 1.262(8) Å] bonds are longer than the average C=S and C=O bond lengths of 1.71 and 1.23 Å, respectively. The C–N bonds in the chelate ring are all shorter than the average C–N single bond length of 1.479 Å, [4] indicating extensive delocalisation of electrons within the chelate ring of the *cis*-[Pt(L1a)$_2$] complex. All other bond lengths fall within the expected range. [4]

Table 4.8: Selected bond lengths (Å) and angles (°) for *cis*-[Pt(L1a)$_2$].

Bond			Angle		
	ligand A	Ligand B		Ligand A	Ligand B
Pt-O(1)	2.018(5)	2.023(6)	O(1)-Pt-S(1)	94.8(2)	94.4(2)
Pt-S(1)	2.231(2)	2.233(2)	O(1A)-Pt-S(1B)	177.1(2)	
N(1)-C(1)	1.341(9)	1.350(9)	O(1B)-Pt-S(1A)	177.5(2)	
N(1)-C(2)	1.313(9)	1.319(9)	S(1A)-Pt-S(1B)	88.10(7)	
N(2)-C(1)	1.350(9)	1.336(9)	O(1A)-Pt-O(1B)	82.7(2)	
S(1)-C(1)	1.731(7)	1.723(7)			
O(1)-C(2)	1.271(8)	1.262(8)			

Symmetry transformations used to generate equivalent atoms.

Crystal structure of *cis*-(S,P)-[PtCl(L1a)(PPh$_3$)] (**8**)

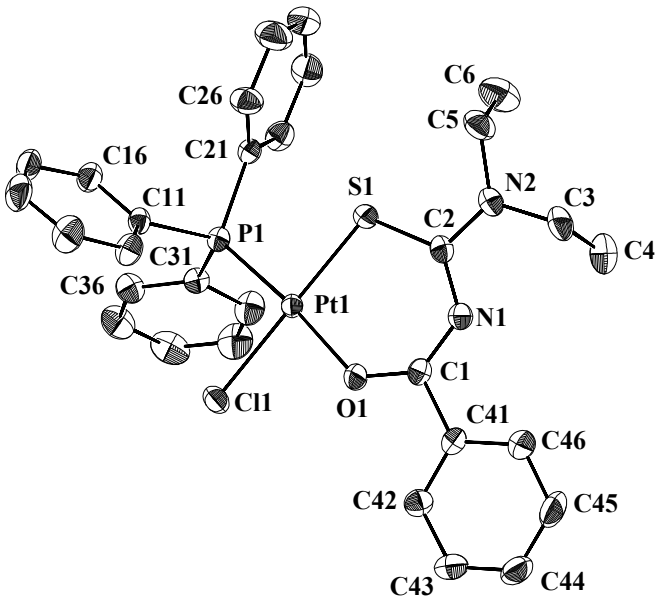

Figure 4.7: Molecular structure showing the numbering scheme and displacement ellipsoids (30% probability) of *cis*-(S,P)-[PtCl(L1a)(PPh$_3$)]. The phenyl ring is numbered with the first digit referring to the number of the ring (1–4) and the second digit refers to the number of the atoms in the ring (1–6). Hydrogen atoms are omitted for clarity.

The molecular structure of *cis*-(S,P)-[PtCl(L1a)(PPh_3)] is shown in Figure 4.7, together with the atom numbering scheme. Selected bond lengths and angles for *cis*-(S,P)-[PtCl(L1a)(PPh_3)] are given in Table 4.9. The bond lengths of the thiocarbonyl [C(2)–S(1) = 1.731(4) Å] and the carbonyl [C(1)–O(1) = 1.267(4) Å] bonds are longer than the average C=S and C=O bond lengths of 1.71 and 1.23 Å, respectively, while the C–N bonds in the chelate ring are all shorter than the average C–N single bond length of 1.479 Å, [4] indicating extensive delocalisation of electrons within the chelate ring of the *cis*-(S,P)-[PtCl(L1a)(PPh_3)] (**8**) complex. All the other bond lengths fall within the expected range. [4] The phenyl ring of the acylthioureato ligand deviates from the plane of the acylthioureato chelate slightly by, N(1)–C(1)–C(41)–C(46) = 8.3(6)°. No solvent molecules were incorporated in the crystal lattice. Selected bond lengths of the coordination sphere of *cis*-(S,P)-[PtCl(L1a)(PPh_3)] and some (S,O)-chelating phosphine complexes reported in the literature, are given in Table 4.10.

Table 4.9: Selected bond lengths (Å) and angles (°) for *cis*-(S,P)-[PtCl(L1a)(PPh_3)].

Bond lengths		Bond angles	
Pt(1)-P(1)	2.2159(9)	O(1)-Pt(1)-P(1)	173.72(7)
Pt(1)-O(1)	2.044(3)	S(1)-Pt(1)-Cl(1)	178.16(3)
Pt(1)-Cl(1)	2.3335(8)	O(1)-Pt(1)-S(1)	93.19(7)
Pt(1)-S(1)	2.2448(8)	P(1)-Pt(1)-S(1)	92.60(3)
S(1)-C(2)	1.731(4)	O(1)-Pt(1)-Ol(1)	85.58(7)
C(2)-N(1)	1.340(5)	P(1)-Pt(1)-Cl(1)	88.69(3)
N(1)-C(1)	1.316(4)		
C(1)-O(1)	1.267(4)		

Symmetry transformations used to generate equivalent atoms.

Table 4.10: Bond lengths of some selected platinum(II) complexes. [a]

Bond	*Trans* atom	Bond length/ Å	Complex	Ref.
Pt–Cl	acylthioureato-S	2.3337(11)	**1a**	This work
	acylthioureato-S	2.334(3)	**4**	This work
	acylthioureato-S	2.3335(8)	**8**	This work
Pt–P	benzenethiol-S	2.310(4)	$[Pt(TIPT)_2(PPh_3)_2]^{2+}$	17
		2.335(4)		
	benzenethiol-S	2.286(7)	$[PtCl(TIPT)(PPh_3)_2]^{+}$	17
	monothio-β-diketone-S	2.247(1)	$[PtEt(sacac)(PPh_3)]$	18
	monothio-β-diketone-S	2.267(2)	$[Pt(MeCO)(Bzsac)(PPh_3)]$	19
	thiosalicylic acid-S	2.3027(11)	$[Pt(PPh_3)_2(TSA)]^{+}$	20
	alkoxy-thioether-S	2.297(2)	$[Pt(PPh_3)_2(CH_3SCH_2C(CF_3)_2O)]^{+}$	21
Pt–P	acylthioureato-O	2.2159(9)	**8**	This work
	β-diketone-O	2.182(2)	$[PtEt(acac)(PPh_3)]$	18
	thiosalicylic acid-O	2.2501(11)	$[Pt(PPh_3)_2(TSA)]^{+}$	20
	thiosalicylic acid-O	2.231(3)	$[Pt(PPh_3)(py)(TSA)]$	22
	alkoxy-thioether-O	2.251(3)	$[Pt(PPh_3)_2(CH_3SCH_2C(CF_3)_2O)]^{+}$	21
Pt–O	PPh_3	2.044(3)	**8**	This work
	PPh_3	2.064(5)	$[PtEt(acac)(PPh_3)]$	18
	PPh_3	2.109(3)	$[Pt(PPh_3)_2(TSA)]^{+}$	20
	PPh_3	2.054(9)	$[Pt(PPh_3)(py)(TSA)]$	22
	PPh_3	2.041(5)	$[Pt(PPh_3)_2(CH_3SCH_2C(CF_3)_2O)]^{+}$	21
	DMSO	2.010(3)	**1a**	This work
	MPSO	2.016(9)	**4**	This work

[a] TIPT = 2,4,6-triisopropylbenzenethiol, sacac = monothioacetylacetonate, Bzsac = 3-mercapto-1-phenyl-but-2-en-1-onate, TSA = thiosalicylic acid, acac = acetylacetonate.

There are no significant differences in the Pt–Cl, C–N, C–S and C–O bond lengths in complexes **1a**, **4** and **8**. As seen in Table 4.10, the Pt–P bonds *trans* to sulfur donor atoms range from 2.247(1) to 2.335(4) Å, while the Pt–P bonds *trans* to oxygen donor atoms range from 2.182(2) to 2.251(3) Å. This is consistent with the greater *trans*-influence of sulfur relative to oxygen. For *cis*-(S,P)-[PtCl(L1a)(PPh_3)], the Pt–P bond (2.2159(9) Å) *trans* to oxygen lies on the lower side of this range. The *N*-benzoyl-*N',N'*-diethylthioureato oxygen donor atom appears to have a greater *trans*-influence than the β-diketone ligands, but has a significantly smaller *trans*-influence than the thiosalicylic acid

oxygen or alkoxy-thioether oxygen donor atoms. As seen in Table 4.10, the Pt–O bond lengths *trans* to PPh_3 [2.041(5)–2.109(3) Å] are significantly longer than the Pt–O bond lengths *trans* to a sulfoxide sulfur donor. The Pt–O bond lengths in (**1a**) and (**4**) are 2.010(3) and 2.016(9) Å, respectively. This is in agreement with PPh_3 having a greater *trans*-influence than a sulfoxide. [23]

4.3 Summary

Complexes of the type [PtCl(L)(RR'SO)] can be readily prepared by the reaction of *cis*-$[PtCl_2(RR'SO)_2]$ with an acylthiourea ligand in the presence of sodium acetate. ^{1}H NMR and IR spectroscopy indicated that the sulfoxides are sulfur-bonded. ^{1}H and ^{195}Pt NMR and IR spectroscopy indicated that only one species was present in solution. The coordination sphere of these complexes was confirmed by X-ray crystallography. X-ray crystal structures of *cis*-(S,S)-[PtCl(DMSO)(L1a)] and *cis*-(S,S)-[PtCl(L1a)(MPSO)] were determined, confirming that the sulfoxide ligand is coordinated through the sulfur atom, and bonded *cis* to the sulfur donor atom of the acylthioureato chelate. Only the *cis*-isomers were obtained for complexes of the type [PtCl(L)(RR'SO)], where HL = *N,N*-dialkyl-*N'*-(3-*R*-benzoyl)thiourea and *N*-(3-*R*-benzoyl)-*N'*-morpholinothiourea ligands. The ^{195}Pt NMR spectra of all the *cis*-(S,S)-[Pt(acylthioureato)Cl(DMSO)] complexes consisted of a single resonance with the chemical shift dependent on the electronic properties of the 3-R-benzoyl substituent. ^{1}H NMR indicated that the reaction of *cis*-(S,S)-[PtCl(DMSO)(L1a)] and *cis*-(S,S)-[PtCl(DMSO)(L2a)] with an equivalent of PPh_3 result in sulfoxide substitution to form complexes of the type *cis*-(S,P)-[Pt(acylthioureato)Cl(PPh_3)]. The ^{31}P NMR spectra of *cis*-(S,P)-[PtCl(L1a)(PPh_3)] and *cis*-(S,P)-[PtCl(L2a)(PPh_3)] are consistent with the phosphorus atom coordinated *trans* to the oxygen donor atom of the acylthioureato chelate. The substitution pattern for the reaction of *cis*-(S,S)-[PtCl(DMSO)(L1a)] with PPh_3 was also confirmed by X-ray crystallography, as single crystals of the product, *cis*-(S,P)-[PtCl(L1a)(PPh_3)], were obtained from the reaction.

CHAPTER 4: PART B

SYNTHESIS AND CHARACTERISATION OF [Pt(ALKOXYCARBONYLTHIOUREATO)Cl(RR'SO)] COMPLEXES

4.4 Results and Discussion

4.4.1 Synthesis of [Pt(alkoxycarbonylthioureato)Cl(RR'SO)] complexes

The alkoxycarbonylthioureato platinum(II) complexes were prepared following a procedure similar to that used for the acylthioureato complexes, described by equations (**4 – 4**) and (**4 – 5**), where HL = alkoxycarbonylthiourea ligand and RR'SO = sulfoxide. A detailed description of the preparation of these complexes is given in the experimental section (Section 4.11.5).

$$K_2PtCl_4 + 3\ RR'SO \longrightarrow \textit{cis}\text{-}[PtCl_2(RR'SO)_2] \qquad (\mathbf{4-4})$$

$$\textit{cis}\text{-}[PtCl_2(RR'SO)_2] + HL \xrightarrow{NaOAc} \textit{cis}\text{-}(S,S)\text{-}[PtCl(L)(RR'SO)] \qquad (\mathbf{4-5})$$

$$+$$

$$\textit{trans}\text{-}(S,S)\text{-}[PtCl(L)(RR'SO)] + [Pt(L)_2]$$

The [PtCl(L)(RR'SO)] were prepared using RR'SO = dimethylsulfoxide (DMSO) and (*S*)-(-)-methyl(*p*-tolyl)sulfoxide ((*S*)-MTSO) and HL = *N*-alkoxycarbonyl-*N',N'*-dialkyl-thiourea (**HL4** and **HL5**) and *N*-alkoxycarbonyl-*N'*-morpholinothiourea (**HL6** and **HL7**) ligands. Dimethylsulfoxide complexes were prepared using all the ligands, while complexes containing unsymmetrical sulfoxides were prepared using *N,N*-diethyl-*N'*-(-)-(3*R*)-menthyloxycarbonylthiourea (**HL4**) only. The structural formulae and atom numbering scheme adopted for NMR assignments are shown in Figures 4.8.

Characterisation of the [Pt(alkoxycarbonylthioureato)Cl(RR'SO)] complexes prepared in this study, revealed that they exist as both the *cis*-(S,S)- and *trans*-(S,S)-isomers. The *cis*-(S,S) and *trans*-(S,S) notation indicates that the sulfoxide sulfur donor atom is in a *cis* or *trans* arrangement to the sulfur donor atom of the alkoxycarbonylthioureato ligand.

TLC indicated that the [PtL_2] complexes were also formed in the reaction involving the alkoxycarbonylthiourea ligands. The [PtL_2] complexes were separated from the desired [Pt(alkoxycarbonylthioureato)Cl(RR'SO)] complexes using flash chromatography, but were not characterised or studied further.

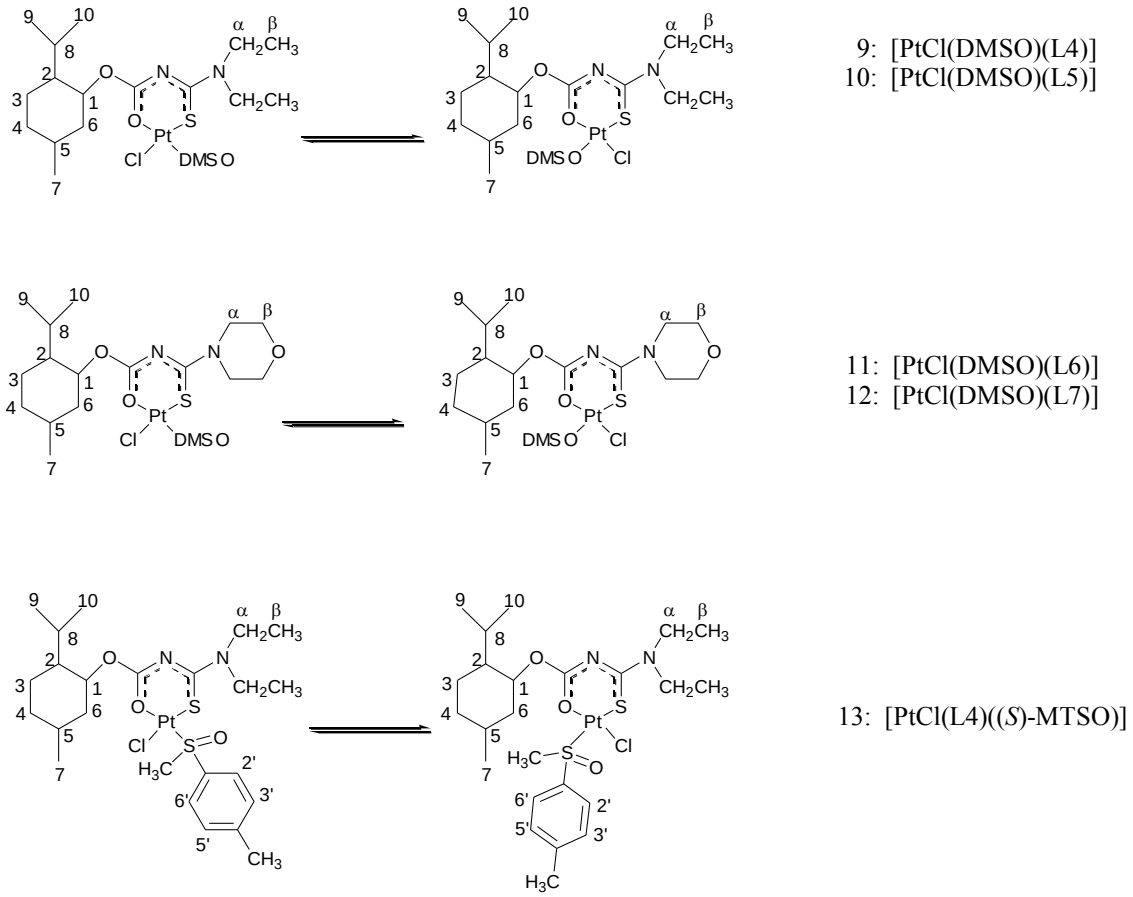

Figure 4.8: Structural formulae and atom numbering scheme adopted for NMR assignments for [PtCl(L)(RR'SO)] complexes, where L = *N,N*-diethyl-*N'*-menthyloxycarbonylthioureato and *N*-menthyloxycarbonyl-*N'*-morpholinothioureato and RR'SO = DMSO and (*S*)-MTSO.

4.4.2 Characterisation of [Pt(alkoxycarbonylthioureato)Cl(RR'SO)] complexes

The [Pt(alkoxycarbonylthioureato)Cl(RR'SO)] complexes were characterised using IR and NMR spectroscopy, elemental analyses and the structure of *cis*-(S,S)-[PtCl(DMSO)(L7)] (**12**) was determined by X-ray crystallography. The analytical data and principal infrared bands are given in Table 4.11. The analytical and spectroscopic data are consistent with the structural formulae shown in Figure 4.8.

Table 4.11: Analytical data for platinum(II) sulfoxide complexes.

Complex	Mp/ °C	Yield/ %	Analytical Data (% C/H/N/S)[a]	ν(SO)/ cm^{-1}
9	72–75	29	35.1; 5.8; 4.5; 10.25 (34.75; 5.7; 4.5; 10.3)	1142
10	74–80	64	35.1; 5.8; 4.5; 10.5 (34.75; 5.7; 4.5; 10.3)	1142
11	200–dec	75	34.2; 5.3; 4.6; 10.0 (34.0; 5.2; 4.4; 10.1)	1154
12	200–dec	80	34.3; 5.2; 4.5; 9.95 (34.0; 5.2; 4.4; 10.1)	1154
13	170 – 171	48	41.1; 6.1; 4.0; 9.1 (41.3; 5.6; 4.0; 9.2)	1138

[a] Required values are given in parentheses.

4.4.2.1 IR spectroscopy

The strong IR band in the 1135–1155 cm^{-1} region is assigned to the ν(SO) stretching frequency (Table 4.11). The ν(SO) peak is shifted to a higher frequency upon complexation, which is indicative of sulfur-bonded sulfoxides. [1, 24] Separate ν(SO) stretching frequencies due to the *cis*-(S,S)- and *trans*-(S,S)-isomers were not observed. Upon complexation of the alkoxycarbonylthiourea ligands there is a disappearance of the NH stretching vibrations and the ligand ν(CO) stretching frequency shifts to higher frequencies. Large shifts to higher frequencies should also be observed for the ν(C=S) stretch frequency, but this vibration could not be assigned unambiguously.

4.4.2.2 NMR spectroscopy

The ^{1}H and ^{195}Pt NMR chemical shift data for the platinum(II) sulfoxide complexes are summarised in Table 4.12. The ^{1}H NMR spectra are assigned according to the numbering schemes given in Figure 4.8. In the ^{1}H NMR spectra for the complexes two proton resonances for the methyl protons of the sulfoxide ligand are observed in the 3.6–3.4 ppm region. These are shifted 1 ppm downfield relative to the free sulfoxide and are thus

typical for sulfur-bonded sulfoxides. [25] Moreover, the signals due to the methyl protons of the sulfoxide, in cases where there were no overlapping peaks, show a ^{195}Pt satellite doublet with a ^{3}J(PtH) coupling constant of about 23 Hz, due to vicinal coupling with the platinum centre, ^{195}Pt (33.7%, I = ½), which is the same order of magnitude as found for sulfur-bonded sulfoxide complexes. The presence of two resonances for the sulfoxide ligand was unexpected, as it suggests that there are two sulfur-bonded sulfoxide species present in solution, or that that the methyl protons of the coordinated sulfoxide are in different magnetic environments due to hindered rotation about the Pt–S(sulfoxide) bond. This phenomenon is not observed for the corresponding complexes with acylthiourea ligands. The possibility that the methyl groups of the coordinated sulfoxide are in different magnetic environments was ruled out, because the two sulfoxide resonances did not coalesce upon heating the NMR sample. ^{195}Pt NMR spectroscopy provided evidence for the presence of both the *cis*-(S,S)- and *trans*-(S,S)-isomers in solution. It is well known that the ^{195}Pt chemical shift is sensitive to the coordination sphere of the metal centre and it is generally accepted that the chemical shifts of *cis*-isomers are upfield relative to those of the *trans*-isomers. [2, 26, 27] All the alkoxycarbonylthiourea complexes prepared showed two ^{195}Pt NMR signals at equilibrium, with an approximate *cis*-(S,S):*trans*-(S,S) ratio of 1:2. The *trans*-(S,S)-isomer is the thermodynamically favoured isomer in $CDCl_3$ in all the complexes prepared.

Separation of the two sulfoxide species by NP-HPLC (1/1 EtOAc:Hexane) was unsuccessful. Although two fractions were obtained with relative peak heights of 1.66:1, the ^{1}H NMR spectra of the fractions were identical to that of the original spectrum with two sulfoxide resonances. This suggests that the separated species equilibrated to give both isomers in solution.

^{1}H NMR of the [PtCl(DMSO)(L4)] (**9**) and [PtCl(DMSO)(L5)] (**10**) complexes in $CDCl_3$, immediately after addition of solvent, indicated that both *cis*-(S,S)- and *trans*-(S,S)-isomers were present in solution in a *cis*-(S,S):*trans*-(S,S) ratio of 1:2. The [PtCl(DMSO)(L6)] (**11**) and [PtCl(DMSO)(L7)] (**12**) complexes were isolated as predominately *cis*-(S,S)-isomers (greater than 90%), while the [PtCl(L4)((*S*)-MTSO)] (**13**) complex was isolated as predominately the *trans*-(S,S)-isomer, as indicted by the integral intensities in the ^{195}Pt NMR and ^{1}H NMR spectra. The ^{1}H and ^{195}Pt NMR spectra of [PtCl(DMSO)(L4)] are shown in Figure 4.9 and Figure 4.10, respectively.

Table 4.12: ^{1}H and ^{195}Pt NMR data for platinum(II) sulfoxide complexes.

Complex	δH_1	δH_2	δH_3	δH_4	δH_5	δH_6	δH_7	δH_8	δH_9	δH_{10}	δH_α	δH_β	δH_{Sme}	δH_{Tolyl}	$\delta^{195}Pt$
9	4.572	1.265	1.640	1.640	1.419	2.061	0.864	2.061	0.747 [a]	0.864	3.604	1.265	3.557 [a]		-3282
			1.015	0.864		1.015			0.742 [b]			1.172	3.402 [b]		-3239
10	4.572	1.265	1.640	1.640	1.419	2.061	0.864	2.061	0.747 [a]	0.864	3.604	1.265	3.557 [a]		-3281
			1.015	0.864		1.015			0.742 [b]			1.172	3.402 [b]		-3239
11	4.603 [a]	1.437	1.645	1.645	1.437	2.086	0.891	1.938	0.772 [a]	0.865	3.693	3.971	3.566 [a]		-3281
	4.511 [b]		1.041	0.825		1.041			0.735 [b]				3.411 [b]		-3227
12	4.603 [a]	1.437	1.645	1.645	1.437	2.086	0.891	1.938	0.772 [a]	0.865	3.693	3.971	3.566 [a]		-3281
	4.511 [b]		1.041	0.825		1.041			0.735 [b]				3.411 [b]		-3227
13	4.558	1.311	1.623	1.623	1.420	2.058	0.921	2.158	0.749	0.905	3.428	1.251	3.675 [a]	7.989	-3299
			1.000	0.870		1.000							3.518 [b]	7.337	-3248
														2.434	

[a] *Cis*-isomer.
[b] *Trans*-isomer.

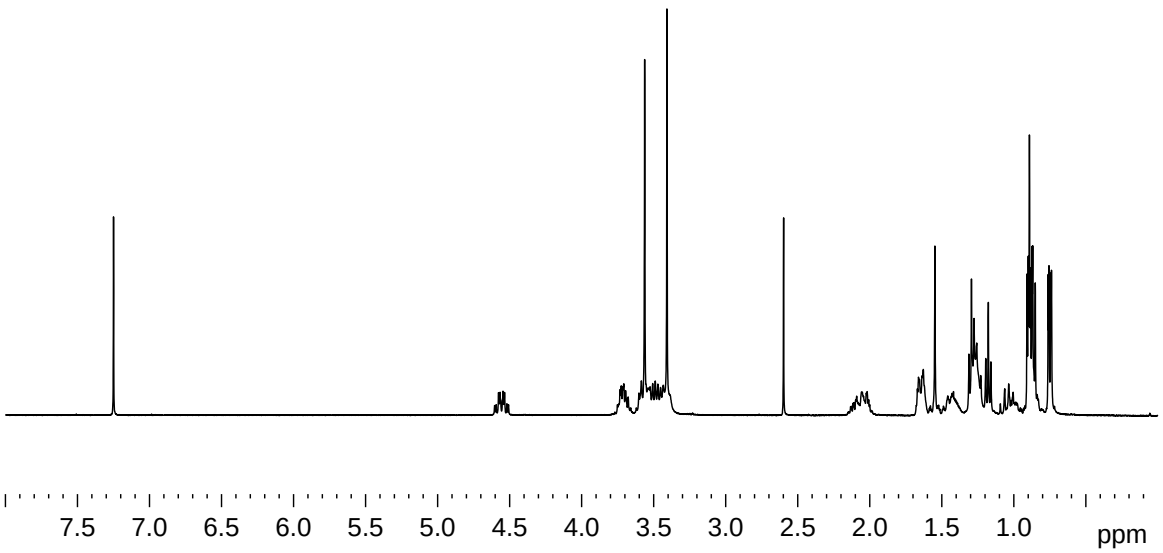

Figure 4.9: ^{1}H NMR spectrum of [PtCl(DMSO)(L4)] in $CDCl_3$ at 30°C.

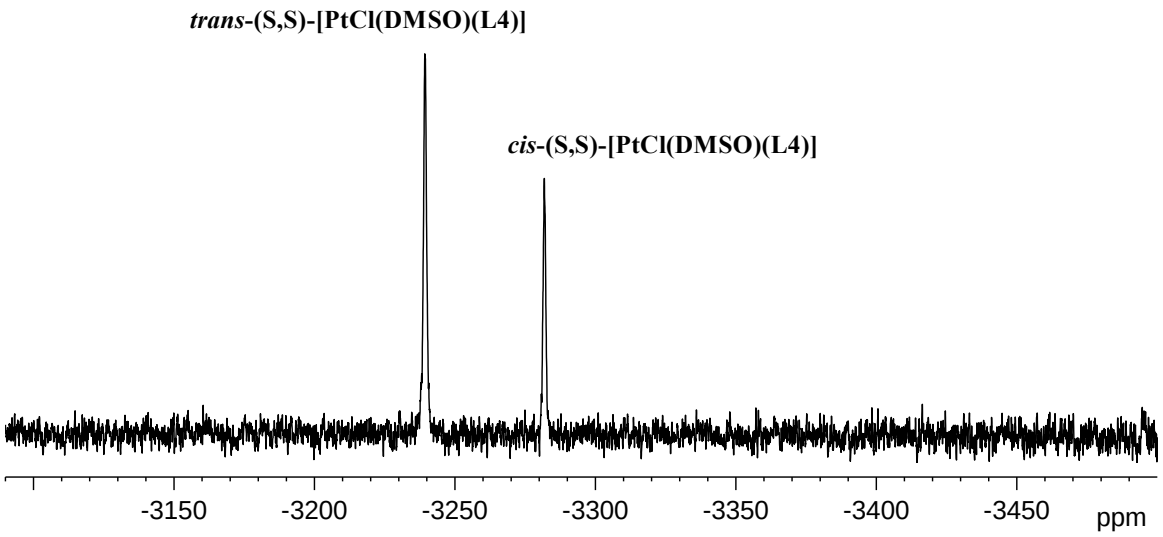

Figure 4.10: ^{195}Pt NMR spectrum of [PtCl(DMSO)(L4)] in $CDCl_3$ at 30°C.

4.4.2.3 Solvent study

The effect of solvent polarity on the isomerisation of the complexes was studied in acetone, dimethylsulfoxide, methanol and chloroform. The [PtCl(DMSO)(L7)] complex was placed in a NMR tube and the respective solvents added. The ^{1}H NMR spectra were recorded immediately (*ca*. 10 minutes) and again after 9 hours. The relative ratios of the *cis*-(S,S)- and *trans*-(S,S)-isomers were determined by integration of the well-resolved H_1 proton signal in the 4.6–4.3 ppm region. The equilibrium constants for the isomerisation could not be determined accurately, because on addition of coordinating solvents, exchange of the coordinated dimethylsulfoxide was observed in the ^{1}H NMR spectra. The amount of free dimethylsulfoxide continued to increase with time. No sulfoxide exchange was observed for benzene, hence only the equilibrium constant ($K_{eq} \approx 1.1$, K_{eq} = *trans*-(S,S)/*cis*-(S,S)) in this solvent could be determined. It is noteworthy to mention that comparison of the amount of free dimethylsulfoxide present in the ^{1}H NMR spectra of [PtCl(DMSO)(L7)] and *cis*-(S,S)-[PtCl(DMSO)(L1a)] in deuterated methanol and acetone, suggests that the sulfoxide ligand in the alkoxycarbonylthioureato complexes is significantly more labile than in the acylthioureato complexes.

4.4.2.4 Crystallographic study

Crystal structure of *cis*-(S,S)-[PtCl(DMSO)(L7)] (**12**)

The crystallographic data for *cis*-(S,S)-[PtCl(DMSO)(L7)] are given in Table 4.13. The molecular structure of *cis*-(S,S)-[PtCl(DMSO)(L7)] is shown in Figure 4.11, together with the atom numbering scheme. Selected bond lengths and angles for *cis*-(S,S)-[PtCl(DMSO)(L7)] are given in Table 4.14. A complete list of bond lengths and angles is given in Appendix A.

Table 4.13: Crystallographic data for *cis*-(S,S)-[PtCl(DMSO)(L7)].

Empirical formula	$C_{18}H_{35}ClN_2O_4PtS_2$
Formula weight	638.14
Temperature	293(2) K
Wavelength	0.71073 Å
Crystal system, space group	Orthorhombic, $P2_12_12_1$
Unit cell dimensions	a = 9.8964(6) Å α = 90° b = 13.2721(8) Å β = 90° c = 18.0016(11) Å γ = 90°
Volume	2364.4(2) Å^3
Z, Calculated density	4, 1.793 Mg/m^3
Absorption coefficient	6.249 mm^{-1}
F(000)	1264
Crystal size	0.40 × 0.20 × 0.08 mm
Theta range for data collection	1.91 to 28.30°
Index ranges	$-13 \le h \le 13$, $-10 \le k \le 17$, $-23 \le l \le 23$
Reflections collected	15355
Independent reflections	5462
R_{int}	0.0369
Refinement method	Full-matrix least-squares on F^2
Data /restraints/parameters	5462 / 0 / 259
Goodness-of-fit on F^2	1.040
Final R indices [$I>2\sigma(I)$]	R^a = 0.0296, Rw^b = 0.0535
Absolute structure parameter [28]	0.013(6)
Largest diff. peak and hole	0.499 and –0.882 e.Å^{-3}

[a] $R = [(\Sigma\Delta F)/(\Sigma F_0)]$.

[b] $Rw = [\Sigma[w(F_o^2 - F_c^2)^2]/\Sigma[w(F_0^2)^2]]^{1/2}$.

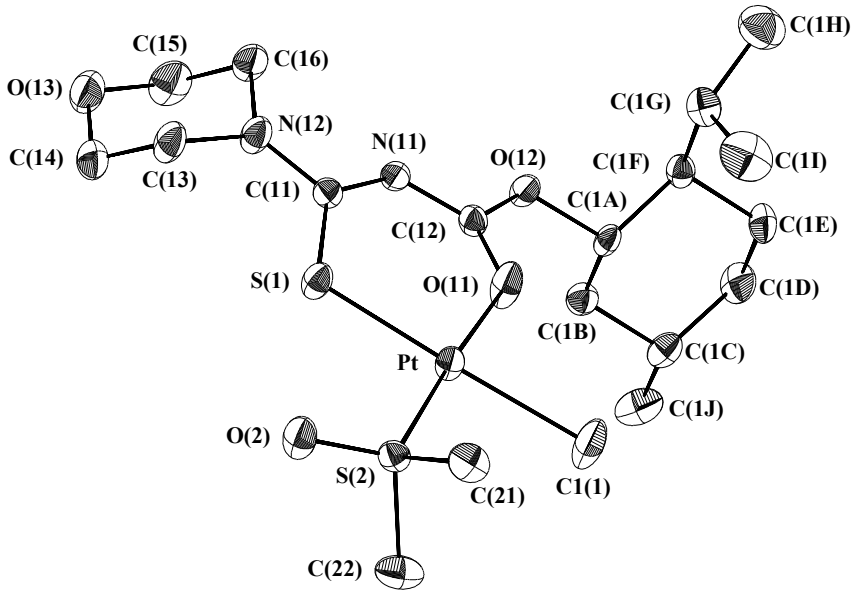

Figure 4.11: Molecular structure showing the atom numbering scheme and displacement ellipsoids (30% probability) for *cis*-(S,S)-[PtCl(DMSO)(L7)]. Hydrogen atoms have been omitted for clarity.

The complex displays the expected square-planar configuration around the platinum atom and the sulfoxide is sulfur-bonded to the platinum(II) and coordinated *cis* to the sulfur donor atom of the *N*-(+)-(3*S*)-menthyloxycarbonyl-*N'*-morpholinothioureato ligand. The ^{1}H NMR spectrum of the crystals of *cis*-(S,S)-[PtCl(DMSO)(L7)] is in agreement with the ^{1}H NMR assignments of *cis*-(S,S)-[PtCl(DMSO)(L7)] reported in Table 4.12.

The dimensions of the sulfoxide compare well with previously reported structural results.[14] The menthyl moiety lies almost perpendicular (98.4(5)°) to the alkoxy-carbonylthiourea chelate. The bond lengths of the thiocarbonyl [C(11)–S(1) = 1.734(5) Å] and the carbonyl [C(12)–O(11) = 1.254(5) Å] bonds are longer than the average C=S and C=O bond length of 1.71 and 1.23 Å, respectively, while the C–N bonds in the chelate ring are all shorter than the average C–N single bond length of 1.479 Å,[4] indicating extensive delocalisation in the chelate ring. The morpholine moiety is in a stable chair conformation and is virtually planar (3.4(7)°) with the chelate ring. The bond lengths and angles compare well with those reported for *cis*-bis(*N*-benzoyl-*N',N'*-di(*n*-butyl)thioureato)platinum(II),[15] *cis*-(S,S)-[PtCl(DMSO)(L1a)], *cis*-(S,S)-[PtCl(L1a)(MPSO)] and *cis*-[Pt(L1a)$_2$]. Bond distances within the platinum(II) coordination sphere for *cis*-(S,S)-[PtCl(DMSO)(L7)] are compared to bond distances of

related compounds in the literature, and are discussed with respect to the *trans*-influence of the different donor atoms, in Section 4.9.

Table 4.14: Selected bond lengths (Å) and angles (°) for *cis*-(S,S)-[PtCl(DMSO)(L7)].

Bond		Angle	
Pt-O(11)	2.018(3)	O(11)-Pt-S(2)	176.40(11)
Pt-S(2)	2.1839(12)	O(11)-Pt-S(1)	92.66(10)
Pt-S(1)	2.2595(13)	S(2)-Pt-S(1)	90.71(4)
Pt-Cl(1)	2.3276(14)	O(11)-Pt-Cl(1)	86.00(10)
N(11)-C(12)	1.309(5)	S(2)-Pt-Cl(1)	90.66(5)
N(11)-C(11)	1.345(6)	S(1)-Pt-Cl(1)	178.15(6)
N(12)-C(11)	1.343(6)		

Symmetry transformations used to generate equivalent atoms.

4.4.2.5 Reaction of [PtCl(DMSO)(L5)] and [PtCl(DMSO)(L7)] with PPh_3

The [PtCl(DMSO)(L5)] and [PtCl(DMSO)(L7)] complexes were reacted with PPh_3 according to equation (**4 – 6**), to compare the substitution products obtained with the corresponding acylthioureato complexes.

$$[PtCl(DMSO)(L)] \xrightarrow{PPh_3} \begin{array}{l} \textit{cis}\text{-(S,P)-}[PtCl(L)(PPh_3)] + DMSO \\ + \\ \textit{trans}\text{-(S,P)-}[PtCl(L)(PPh_3)] \end{array} \qquad \textbf{(4 – 6)}$$

where L = L5 and L7.

Upon addition of one equivalent of PPh_3 to [PtCl(DMSO)(L5)] and [PtCl(DMSO)(L7)] in $CDCl_3$, the proton resonance of the coordinated sulfoxides disappeared and a signal due to free dimethylsulfoxide was observed in the ^1H NMR spectra, suggesting that upon addition of one equivalent of PPh_3, the dimethylsulfoxide ligand is substituted. No shift in the coordinated sulfoxide signals in the ^1H NMR spectra was observed, suggesting that upon addition of one equivalent of PPh_3, the dimethylsulfoxide ligand is substituted. The ^{31}P NMR spectra of [PtCl(L5)(PPh_3)] and [PtCl(L7)(PPh_3)] each consist of two singlets with satellites, suggesting that each complex exists as two geometric isomers, *cis*-(S,P)-

and *trans*-(S,P)-[PtCl(L)(PPh_3)]. The ^{31}P NMR spectra of [PtCl(L5)(PPh_3)] and [PtCl(L7)(PPh_3)] consist of signals at 8.001 (4181 Hz) and 5.704 (3974 Hz) ppm, and 7.769 (4189 Hz) and 5.381 (3956 Hz) ppm, respectively. The presence of two species in solution is consistent with the ^{195}Pt NMR data discussed above. A detailed ^{31}P NMR study of the reaction [PtCl(DMSO)(L5)] and [PtCl(DMSO)(L7)] with triphenylphosphine is given in Section 4.8.

4.5 Summary

The reaction of *cis*-[$PtCl_2$(RR'SO)$_2$] with an alkoxycarbonylthiourea ligand in the presence of sodium acetate yielded [Pt(alkoxycarbonylthioureato)Cl(RR'SO)] complexes that were found to undergo *cis*/*trans*-isomerisation in solution. Two signals were observed in the ^{195}Pt NMR spectra of these complexes, consistent with complexes of the type *cis*-(S,S)-[PtCl(L)(RR'SO)] and *trans*-(S,S)-[PtCl(L)(RR'SO)], where HL = alkoxycarbonylthiourea. The ^{31}P NMR study provides further evidence that two species are present in solution. ^{1}H NMR and IR spectroscopy indicated that the sulfoxides are sulfur-bonded. The X-ray crystal structure of *cis*-(S,S)-[PtCl(DMSO)(L7)] was determined, confirming that the sulfoxide ligand is coordinated through the sulfur atom and *cis* to the sulfur donor atom of the alkoxycarbonylthioureato chelate. The crystal structure of *cis*-(S,S)-[PtCl(DMSO)(L7)] is the first example of an alkoxycarbonylthioureato platinum(II) sulfoxide complex and provides the first structural details of complexes of this type.

CHAPTER 4: PART C

COMPARISON OF THE COORDINATION CHEMISTRY OF ALKOXYCARBONYLTHIOUREA AND ACYLTHIOUREA LIGAND SYSTEMS

4.6 Introduction

The coordination chemistry of the acylthiourea and alkoxycarbonylthiourea ligand systems will now be discussed, highlighting the differences in the their complexation behaviour.

For convenience, the following notation is used to distinguish the possible binding modes of the ligands. A deprotonated chelating ligand coordinated to a metal through both the sulfur and oxygen donor atoms, is represented as (L-S,O), a protonated ligand that is bonded to the metal via the sulfur donor atom only is represented by (HL-S) and a deprotonated ligand that is only coordinated through the thiocarbonyl is represented by (L-S).

Studies in the literature have shown that protonation of *cis*-[Pt(L-S,O)$_2$] complexes, where (L-S,O) = *N,N*-dialkyl-*N'*-benzoylthioureato ligands, with HCl results in the formation of *cis*- and *trans*-[PtCl$_2$(HL-S)$_2$] complexes, in which the chloride anion substitutes the amidic oxygen donor of the ligand from the coordination sphere of the metal. [26, 29, 30] This displacement has also been confirmed by X-ray crystallography. [29] Upon deprotonation of the *cis*- and *trans*-[PtCl$_2$(HL-S)$_2$] complexes, only the *cis*-[Pt(L-S,O)$_2$] complexes are formed. In the present study similar protonation studies were carried out on selected [PtCl(DMSO)(L)] complexes. The [PtCl(DMSO)(L)] complexes were protonated with hydrochloric acid, to yield complexes of the type [PtCl$_2$(DMSO)(HL-S)]. These complexes were characterised by ^{195}Pt and ^{1}H NMR spectroscopy to determine if they undergo *cis*/*trans*-isomerisation, as noted for the [PtCl$_2$(HL-S)$_2$] complexes reported in the literature. The deprotonation of the [PtCl$_2$(DMSO)(HL-S)] complexes was also evaluated to determine if both *cis*-(S,S)- and *trans*-(S,S)-isomers are formed upon ring-closure of the ligand, as this could shed light on the mechanism of the isomerisation of the alkoxycarbonylthioureato complexes. Therefore, to gain a better understanding of the coordination chemistry of alkoxycarbonylthioureato and acylthioureato ligand systems, a protonation study of [PtCl(DMSO)(L5)] and *cis*-(S,S)-[PtCl(DMSO)(L1a)] was carried out using ^{195}Pt and ^{1}H NMR spectroscopy (Section 4.7).

As mentioned previously, the reaction of the [Pt(alkoxycarbonylthioureato)Cl(DMSO)] complexes with PPh_3 provided additional evidence for the presence of both *cis*-(S,S)- and *trans*-(S,S)-isomers in solution. Complexes of the type $[PtCl(L)(PPh_3)]$ and $[Pt(L)(PPh_3)_2]^+$, where L = L1a, L2a, L5 and L7, were prepared and evaluated by ^{31}P NMR spectroscopy to determine the relative *trans*-influences of the sulfur and oxygen donor atoms, to compare the coordination chemistry of the acylthioureato and alkoxycarbonylthioureato ligand systems (Section 4.8).

Bond distances within the platinum(II) coordination sphere for *cis*-(S,S)-[PtCl(DMSO)(L1a)], *cis*-(S,S)-[PtCl(L1a)(MPSO)], *cis*-(S,S)-[PtCl(DMSO)(L7)] and *cis*-$[Pt(L1a)_2]$ are compared to bond distances in related compounds in the literature, and are discussed with respect to the *trans*-influence of the different donor atoms (Section 4.9).

4.7 Protonation studies

4.7.1 Effect of protonation of *cis*-(S,S)-[PtCl(DMSO)(L1a-S,O)]

The ^1H NMR spectrum of *cis*-(S,S)-[PtCl(DMSO)(L1a-S,O)] in $CDCl_3$, shows a single sharp dimethylsulfoxide signal at 3.58 ppm. The ^1H NMR spectrum is consistent with a single unprotonated species in solution, as confirmed by the absence of an amido NH resonance. The corresponding ^{195}Pt NMR spectrum consists of a single resonance at –3256 ppm. Addition of 50 µl of concentrated HCl directly to the NMR tube containing the complex as described in the experimental section (Section 4.11.2), in $CDCl_3$, gave a ^1H NMR spectrum showing the presence of a single species, characterised by a single NH resonance at 10.74 ppm and a single sulfoxide signal at 3.35 ppm. The NH resonance clearly indicates protonation of the coordinated ligand by the HCl. The ^{195}Pt NMR spectrum of this solution shows a single resonance at –3469 ppm (Figure 4.12). Based on this data and the close correlation of the ^{195}Pt NMR chemical shift with that of *cis*-$[PtCl_2(DMSO)_2]$ (-3452 ppm), this protonated species has been assigned as *cis*-$[PtCl_2(DMSO)(HL1a\text{-}S)]$. No isomerisation of this species was observed. After addition of excess base, NaOAc, and removal of residual water from the $CDCl_3$ solution, the ^1H NMR spectrum was again recorded. Two sulfoxide resonances were observed at 3.35 and 3.58 ppm, corresponding to *cis*-$[PtCl_2(DMSO)(HL1a\text{-}S)]$ and *cis*-(S,S)-

[PtCl(DMSO)(L1a-S,O)], respectively. No other sulfoxide species appeared to be present in solution. The intensity of the ^{1}H NMR signal at 3.58 ppm increased with time, with a corresponding decrease of the signal at 3.35 ppm. The ^{1}H NMR spectra for the deprotonation of *cis*-[$PtCl_2$(DMSO)(HL1a-S)] are shown in Figure 4.13. The ^{195}Pt NMR spectrum consists of a single resonance at –3256 ppm, corresponding to the starting complex *cis*-(S,S)-[PtCl(DMSO)(L1a-S,O)]. The ^{195}Pt NMR spectra for the protonation/deprotonation of *cis*-(S,S)-[PtCl(DMSO)(L1a)] are shown in Figure 4.12. The downfield shift of the ^{195}Pt NMR signal is consistent with oxygen coordination. Similar downfield shifts of the ^{195}Pt NMR signal for some glycine platinum(II) complexes upon oxygen coordination have been observed. [2]

Protonatipon study [PtCl(DMSO)(L1)Cl

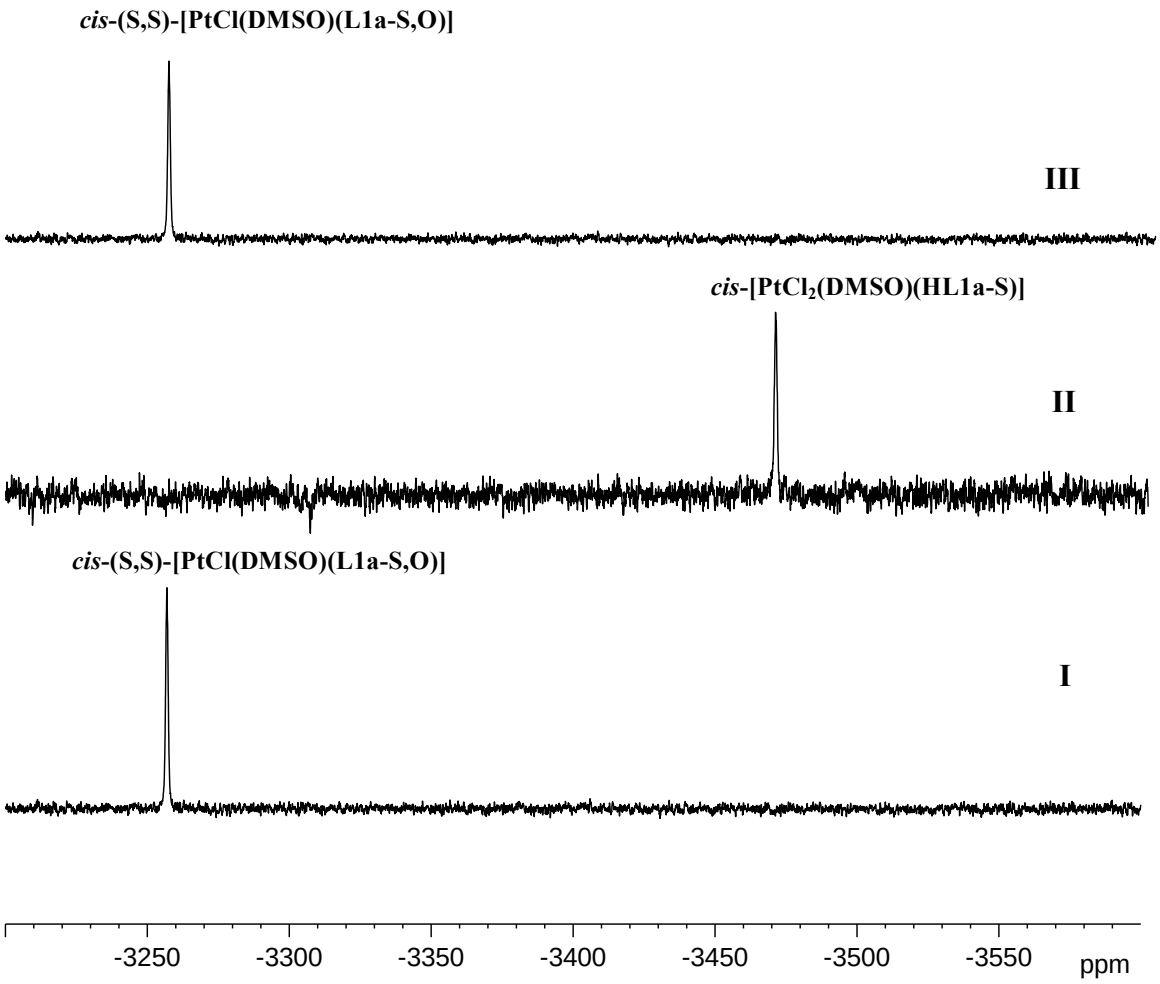

Figure 4.12: ^{195}Pt NMR spectra acquired during the protonation/deprotonation of *cis*-(S,S)-[PtCl(DMSO)(L1a-S,O)] in $CDCl_3$ at 30°C. I = spectrum of *cis*-(S,S)-[PtCl(DMSO)(L1a-S,O)], II = spectrum after addition of 50 µl HCl and III = spectrum after addition of sodium acetate.

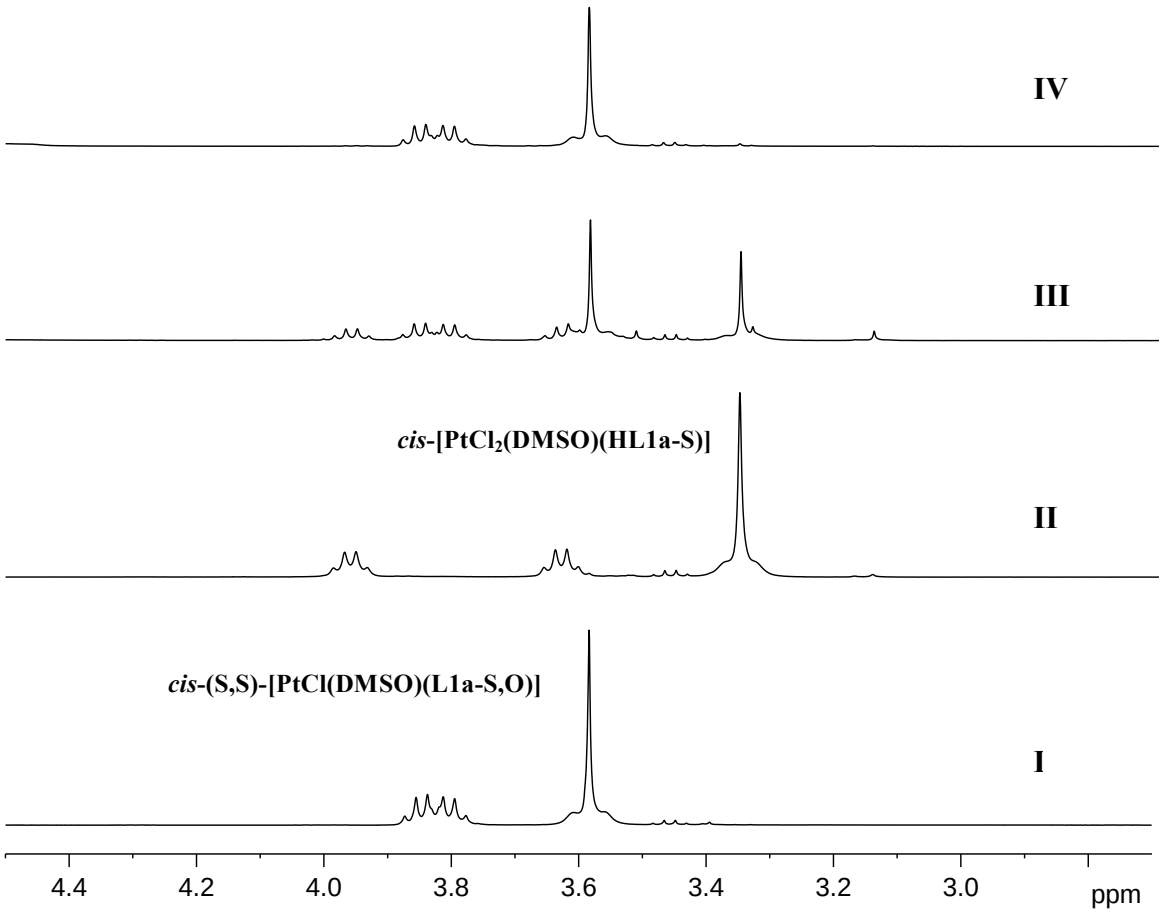

Figure 4.13: Partial ^{1}H NMR spectra showing the protonation/deprotonation of *cis*-(S,S)-[PtCl(DMSO)(L1a-S,O)] in $CDCl_3$ at 30°C. I = spectrum of *cis*-(S,S)-[PtCl(DMSO)(L1a-S,O)], II = spectrum after addition of 50 µl HCl, III = spectrum after addition of sodium acetate and IV = spectrum after 3.5 hours after adding sodium acetate.

4.7.2 Effect of protonation of [PtCl(DMSO)(L5-S,O)]

The ^{1}H NMR spectrum of [PtCl(DMSO)(L5-S,O)] in $CDCl_3$ shows two sulfoxide resonances at 3.56 and 3.41 ppm. The corresponding ^{195}Pt NMR spectrum (Figure 4.14) consists of two resonances at –3239 and –3282 ppm, which have been assigned to the *trans*-(S,S)- and *cis*-(S,S)-isomers, respectively. Addition of concentrated HCl to [PtCl(DMSO)(L5-S,O)] yields a ^{1}H NMR spectrum that suggests the presence of only one species in solution. The ^{1}H NMR spectrum consists of a single NH resonance at 9.43 ppm and a doublet at 3.45 ppm, which corresponds to a sulfur-bound sulfoxide. Further evidence for the presence of one species in solution was obtained from the ^{195}Pt NMR spectrum which consists of a signal at –3469 ppm (Figure 4.14), which has been assigned as *cis*-[$PtCl_2$(DMSO)(HL5-S)]. It is unclear why the sulfoxide signal in the ^{1}H NMR

spectrum is split into a doublet. It is unlikely that both the *cis*- and *trans*-isomers of the protonated complex are present in solution as these would be expected to give two well separated ^{195}Pt NMR signals.

Upon addition of base to the *cis*-[$PtCl_2$(DMSO)(HL5-S)] complex in the NMR tube, two single sulfoxide signals appeared in the ^{1}H NMR spectrum, at 3.56 and 3.41 ppm. The intensity of the new sulfoxide signals, which correspond to the *cis*-(S,S)- and *trans*-(S,S)-[PtCl(DMSO)(L5-S,O)] species, respectively, continued to increase with time, and there was a corresponding decrease in the intensity of the signal for the *cis*-[$PtCl_2$(DMSO)(HL5-S)] complex. After about an hour, the *cis*-(S,S):*trans*-(S,S) ratio was approximately 2:1, with the *cis*-(S,S)-isomer predominant in solution, but with time the *cis*-(S,S):*trans*-(S,S) ratio became 1:2, in which the *trans*-(S,S)-isomer was predominant. The ^{195}Pt NMR spectrum of this equilibrated solution was identical to that of the starting complex, [PtCl(DMSO)(L5-S,O)]. The ^{195}Pt NMR data for the protonation/deprotonation of [PtCl(DMSO)(L5-S,O)] and *cis*-(S,S)-[PtCl(DMSO)(L1a-S,O)] are summarised in Table 4.15. The ^{195}Pt NMR spectra for the protonation/deprotonation of [PtCl(DMSO)(L5-S,O)] are shown in Figure 4.14.

The foregoing results suggest that the reaction of *cis*-[$PtCl_2$(RR'SO)$_2$] (**1**) with an *N*-acyl-*N',N'*-dialkylthiourea or *N*-alkoxycarbonyl-*N',N'*-dialkylthiourea (**2**) results in the formation of the neutral *cis*-[$PtCl_2$(HL-S)(RR'SO)] complex (**3**) in which a sulfoxide ligand is replaced. Deprotonation of complex (**3**) and subsequent ring-closure of the ligand results in the formation of *cis*-(S,S)-[PtCl(L)(RR'SO)] (**5**). In the case of the alkoxycarbonylthioureato complexes, the *cis*-(S,S)-[PtCl(L)(RR'SO)] (**5**) complexes then isomerises to the *trans*-(S,S)-isomer (**6**). The proposed mechanism for the formation of [PtCl(L)(RR'SO)] complexes is shown in Figure 4.15. The rate of ring-closure appears to be faster than the rate of isomerisation, because upon addition of base to *cis*-[$PtCl_2$(DMSO)(HL5-S)], the *cis*-(S,S)-isomer initially predominates in solution

Table 4.15: ^{195}Pt NMR data for the protonation/deprotonation of complexes of the type [PtCl(DMSO)(L)], where HL = *N*-benzoyl-*N',N'*-diethylthiourea (**HL1a**) and *N,N*-diethyl-*N'*-(+)-(3*S*)-menthyloxycarbonylthiourea (**HL5**) at 30°C in $CDCl_3$.

Protonatipon study [PtCl(DMSO)(L5)Cl

Complex	^{195}Pt NMR/ ppm
cis-(S,S)-[PtCl(DMSO)(L1a-S,O)]	-3256
cis-[$PtCl_2$(DMSO)(HL1a-S)]	-3469
[PtCl(DMSO)(L5-S,O)]	-3239, -3282
cis-[$PtCl_2$(DMSO)(HL5-S)]	-3469
cis-[$PtCl_2(DMSO)_2$]	-3452

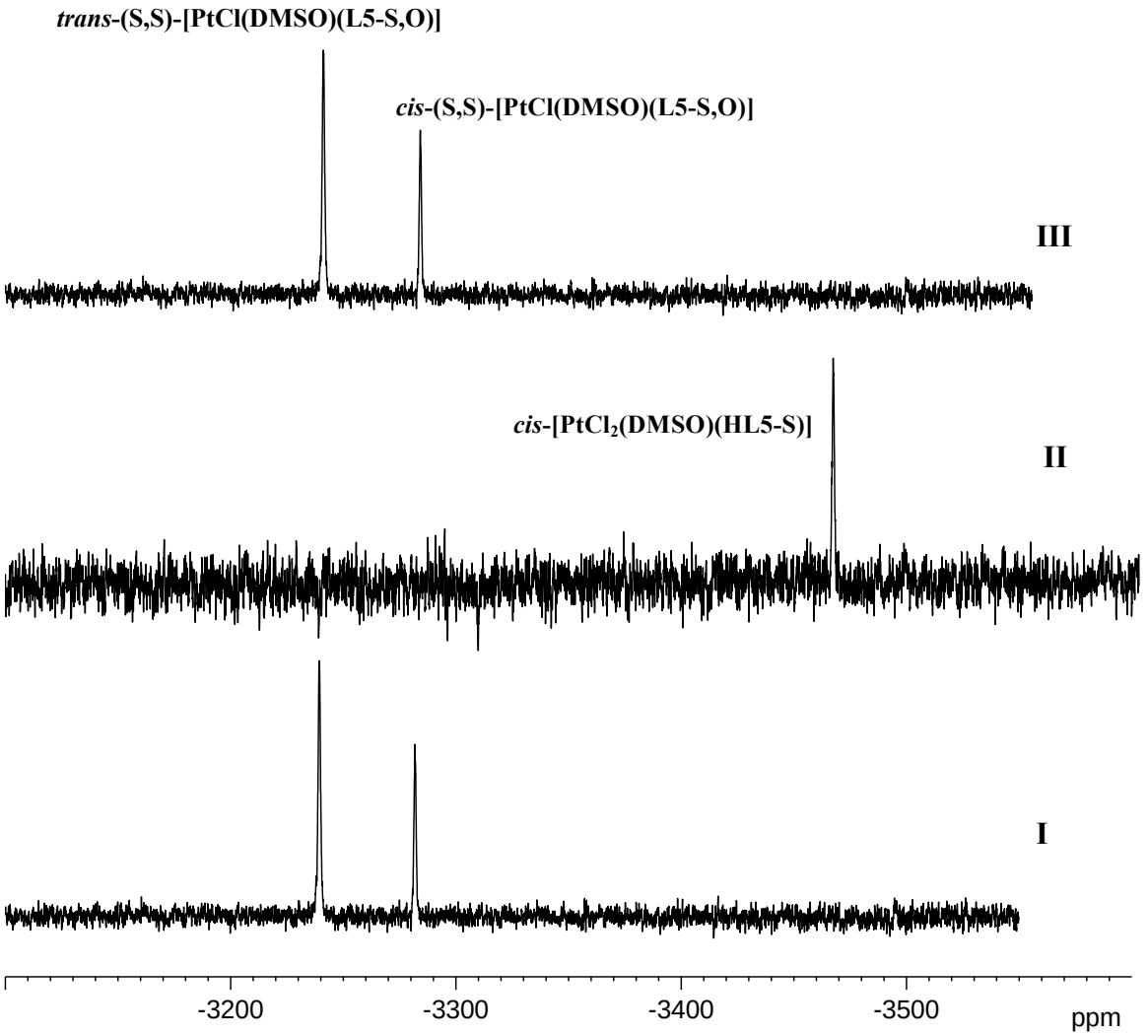

Figure 4.14: ^{195}Pt NMR spectra acquired during the protonation/deprotonation of [PtCl(DMSO)(L5-S,O)] in $CDCl_3$ at 30°C. I = spectrum of [PtCl(DMSO)(L5-S,O)], II = spectrum after addition of 50 µl HCl and III = spectrum after addition of sodium acetate.

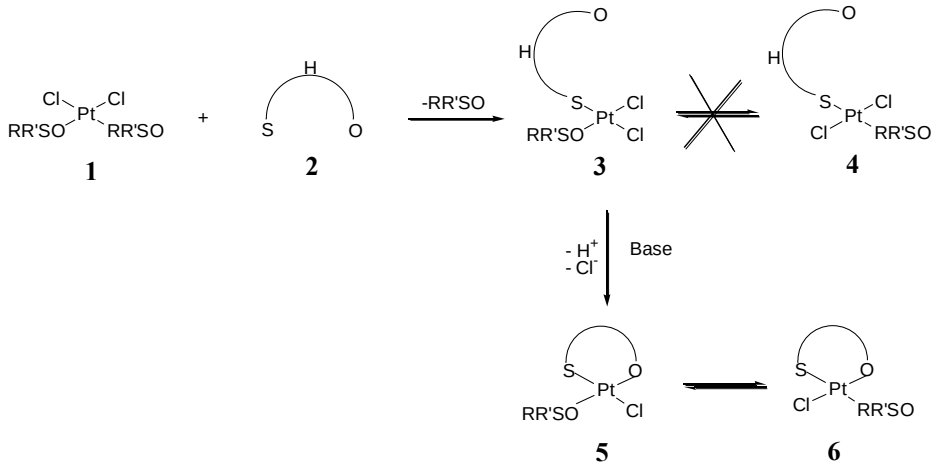

Figure 4.15: Proposed mechanism for the formation of [PtCl(L)(RR'SO)] complexes.

4.8 Reactions of [PtCl(DMSO)(L)] complexes with PPh_3

Further evidence for the difference in the coordination chemistry of the acylthiourea and alkoxycarbonylthiourea ligands was obtained by substitution of the bound sulfoxide and chloride ligands by PPh_3 from the [PtCl(DMSO)(L)] complexes, to form complexes of the type $[PtCl(L)(PPh_3)]$ and $[Pt(L)(PPh_3)_2]^+$, according to equations (**4 – 7**) and (**4 – 8**).

$$[PtCl(DMSO)(L)] \xrightarrow{PPh_3} [PtCl(L)(PPh_3)] + DMSO \qquad (\mathbf{4-7})$$

$$[PtCl(DMSO)(L)] \xrightarrow{2\ PPh_3} [Pt(L)(PPh_3)_2]^+ + DMSO + Cl^- \qquad (\mathbf{4-8})$$

The phosphine studies were carried out by adding stoichiometric amounts of triphenylphosphine to a solution of [PtCl(DMSO)(L)], where L = L1a, L2a, L5 and L7, in $CDCl_3$ at 30°C in an NMR tube. The mixture was shaken vigorously and then the ^1H and ^{31}P NMR spectra were recorded.

The substitution pattern of the dimethylsulfoxide and chloride ligand leaving groups from the [PtCl(DMSO)(L)] complexes were confirmed by ^1H NMR spectroscopy. Upon addition of an equivalent of PPh_3 to the platinum(II) sulfoxide complexes in $CDCl_3$ the methyl proton resonances of the bound sulfoxide disappeared and a resonance due to free

dimethylsulfoxide was observed. This suggests that upon the addition of one equivalent of PPh_3, the dimethylsulfoxide ligand is substituted and further addition of PPh_3 results in the substitution of the chloride ligand.

4.8.1 Reaction of *cis*-(S,S)-[PtCl(DMSO)(L1a)] and *cis*-(S,S)-[PtCl(DMSO)(L2a)] with one equivalent of PPh_3

The ^{31}P NMR spectra for the *cis*-(S,P)-[PtCl(L1a)(PPh_3)] and *cis*-(S,P)-[PtCl(L2a)(PPh_3)] complexes, each show a single resonance at 8.137 and 7.729 ppm with ^{1}J(PtP) coupling constants of 4040 and 4033 Hz, respectively. The large ^{1}J(PtP) coupling constants are consistent with a phosphorus atom *trans* to oxygen. [18, 19] The X-ray crystal structure of *cis*-(S,P)-[PtCl(L1a)(PPh_3)] confirms that the phosphorus atom is coordinated *trans* to the oxygen donor atom of the acylthioureato ligand (Figure 4.7).

4.8.2 Reaction of [PtCl(DMSO)(L5)] and [PtCl(DMSO)(L7)] with one equivalent of PPh_3

The ^{31}P NMR spectrum for the reaction of [PtCl(DMSO)(L5)] with one equivalent of PPh_3 consists of two singlets at 8.001 (*ca*. 62%) and 5.704 (*ca*. 35%) ppm with ^{1}J(PtP) coupling constants of 4181 and 3974 Hz, respectively. These signals can be unequivocally assigned to the *cis*-(S,P)- or *trans*-(S,P)-isomers, respectively, because it is generally accepted that for complexes of the type $[PtX_2(PR_3)_2]$ that the *cis*-isomers have significantly larger ^{1}J(PtP) coupling constants than the corresponding *trans*-isomers. [27, 31, 32] Moreover, the large coupling constants observed for the *cis*-(S,P)-isomers compared to the *trans*-(S,P)-isomers, are in agreement with the greater *trans*-influence of sulfur compared to oxygen. These results are also consistent with the work reported by Cavell *et al.* on platinum(II) complexes with monothio-β-diketone and phosphine ligands. [18, 19] A singlet with unresolved satellites was also observed at 15.562 (*ca.* 3%) ppm and is tentatively assigned as *cis*-$[PtCl_2(PPh_3)]$.

The ^{31}P NMR spectrum for the reaction of [PtCl(DMSO)(L7)] with one equivalent of PPh_3 consists of two singlets at 7.769 (*ca*. 36%) and 5.381 (*ca*. 54%) ppm with ^{1}J(PtP) coupling constants of 4189 and 3956 Hz, respectively. The signals at 7.769 and 5.381

ppm are consistent with *cis*-(S,P)- and *trans*-(S,P)-[Pt(Cl)(L7)(PPh_3)], respectively. A signal at 15.574 ppm [^1J(PtP) 3674 Hz; *ca*. 10%] was also observed, but was formed in larger quantities than with the [PtCl(DMSO)(L5)] complex. The signal at 15.574 ppm has been assigned to *cis*-[$PtCl_2(PPh_3)_2$]. The ^1J(PtP) coupling constant of this signal is similar to that reported for *cis*-[$PtCl_2(PPh_3)_2$] in the literature. [33] This assignment has also been confirmed by preparing *cis*-[$PtCl_2(PPh_3)_2$]. The ^{31}P NMR chemical shift and the coupling constant are in good agreement. The ^{31}P NMR data for the [PtCl(L)(PPh_3)] complexes are summarised in Table 4.16.

Table 4.16: ^{31}P NMR data for the [PtCl(L)(PPh_3)] complexes. [a]

Complex	^{31}P NMR/ ppm	^1J(PtP)/ Hz
cis-(S,P)-[PtCl(L1a)(PPh_3)]	8.137	4040
cis-(S,P)-[PtCl(L2a)(PPh_3)]	7.729	4033
cis-(S,P)-[PtCl(L5)(PPh_3)]	8.001	4181
trans-(S,P)-[PtCl(L5)(PPh_3)]	5.704	3974
cis-(S,P)-[PtCl(L7)(PPh_3)]	7.769	4189
trans-(S,P)-[PtCl(L7)(PPh_3)]	5.381	3956

[a] Spectra were recorded at 30°C in $CDCl_3$, relative to 85% H_3PO_4.

Integration of the *cis*-(S,P)- and *trans*-(S,P)-[PtCl(L5)(PPh_3)] signals gives rise to a *cis*-(S,P):*trans*-(S,P) ratio of approximately 2:1. The opposite is observed for the sulfoxide complexes, where the *trans*-(S,S)-isomers are favoured. This may to be due to the higher basicity and π-acceptor properties of PPh_3 compared to that of DMSO.

The ^1J(PtP) coupling constants of *cis*-(S,P)-[PtCl(L1a)(PPh_3)] and *cis*-(S,P)-[PtCl(L5)(PPh_3)] are 4040 and 4181 Hz, respectively. The increase in the ^1J(PtP) coupling constant by 141 Hz, on going from an acylthiourea to an alkoxycarbonylthiourea ligand, suggests an increase in the Pt–P bond strength *trans* to the carbonyl oxygen donor atom of the alkoxycarbonylthiourea ligand. This implies that for the monophosphine complexes the acylthiourea carbonyl oxygen donor atom is relatively softer and therefore has a greater *trans*-influence than the carbonyl oxygen donor atom of the alkoxycarbonylthiourea ligand, which is in agreement with the crystallographic data discussed in Section 4.9. Similar results were obtained for the morpholine containing

complexes, except that the *cis*-(S,P):*trans*-(S,P) ratio for the [PtCl(L7)(PPh_3)] complex is approximately 1:2. The inversion of the *cis*-(S,P):*trans*-(S,P) ratio for the morpholine containing complexes is as yet not clearly understood.

4.8.3 Reaction of *cis*-(S,S)-[PtCl(DMSO)(L1a)] and *cis*-(S,S)-[PtCl(DMSO)(L2a)] with two equivalents of PPh_3

In the ^{31}P NMR spectrum of $[Pt(L1a)(PPh_3)_2]^+$ two doublets are observed at 21.912 and 11.371 ppm, with ^1J(PtP) coupling constants of 3088 and 3836 Hz, respectively. The reaction of *cis*-(S,S)-[PtCl(DMSO)(L1a)] with two equivalents of PPh_3 is shown schematically in Figure 4.16. Similarly, two doublets are observed in the ^{31}P NMR spectrum of $[Pt(L2a)(PPh_3)_2]^+$ at 22.249 and 10.493 ppm, with ^1J(PtP) coupling constants of 3129 and 3835 Hz, respectively. The $[Pt(L1a)(PPh_3)_2]^+$ and $[Pt(L2a)(PPh_3)_2]^+$ complexes have ^2J(PP) coupling constants of 26 and 25 Hz, respectively. This data is consistent with the formation of a $[Pt(L)(PPh_3)_2]^+$ complex, in which the phosphorus atoms are arranged *cis* to each other. Unreacted PPh_3 was also observed in the ^{31}P NMR spectra, for both complexes, suggesting that an equilibrium may be present for the formation of the $[Pt(L)(PPh_3)_2]^+$ complexes. This observation is consistent with the kinetic data obtained for the reaction of *cis*-(S,S)-[PtCl(DMSO)(L1a)] with PPh_3 (Chapter 5). The reaction of *cis*-(S,S)-[PtCl(DMSO)(L2a)] with two equivalents of PPh_3 is shown schematically in Figure 4.17.

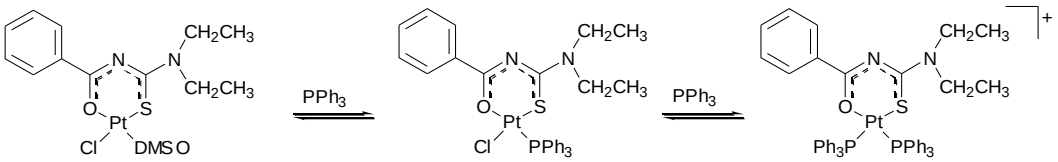

Figure 4.16: Reaction of *cis*-(S,S)-[PtCl(DMSO)(L1a)] with two equivalents of PPh_3.

A significant difference between the $[Pt(L1a)(PPh_3)_2]^+$ and $[Pt(L2a)(PPh_3)_2]^+$ complexes is that while the former complex is stable in solution the latter is not, as manifested by the changes in the ^{31}P NMR spectrum of $[Pt(L2a)(PPh_3)_2]^+$ with time. When the spectrum of $[Pt(L2a)(PPh_3)_2]^+$ was recorded again after 12 hours, a complicated spectrum was obtained. The intensity of the doublets at 22.249 and 10.493 ppm, for $[Pt(L2a)(PPh_3)_2]^+$, decreased dramatically and the solution only contained *ca*. 10% of the original complex.

This decrease in intensity of the doublets was accompanied by the appearance of singlets at 15.550 ppm [^{1}J(PtP) 3674 Hz; *ca*. 21%] and 7.720 ppm [^{1}J(PtP) 4030 Hz; *ca*. 21%], two singlets with no platinum satellites at 30.169 ppm (*ca*. 12%) and 44.582 ppm (*ca*. 22%), as well as two doublets at 12.553 and 20.096 ppm [^{2}J(PP) 20 Hz; *ca*. 8%] with unresolved platinum satellites. The signals at 7.720, 15,550 and 30.169 ppm have been assigned as *cis*-(S,P)-[PtCl(L2a)(PPh_3)], *cis*-[$PtCl_2(PPh_3)_2$] and triphenylphosphine oxide, respectively. The signal for triphenylphosphine oxide was confirmed by recording the ^{31}P NMR spectrum of the pure compound. The signal at 44.582 ppm appears to be due to the reaction of the deprotonated ligand with triphenylphosphine. This was established by recording the ^{31}P NMR spectrum of PPh_3 in the presence of protonated/deprotonated acylthiourea and alkoxycarbonylthiourea ligands. The PPh_3 could be binding to the oxygen or sulfur donor atoms of the ligands, as it is well known that trivalent phosphorus compounds are known to react with oxygen and sulfur bonds with significant double bond character. [34] The doublets at 20.096 and 12.553 ppm have been tentatively assigned to the ring-opened product [PtCl(L2a-S)(PPh_3)$_2$]$^+$, as the chemical shift position and ^{2}J(PP) value of 20 Hz corresponds to the ring-opened species of [Pt(L7)(PPh_3)$_2$]$^+$ discussed below. The ^{31}P NMR spectrum of the reaction of *cis*-(S,S)-[PtCl(DMSO)(L2a)] with two equivalents of PPh_3 is shown in Figure 4.18.

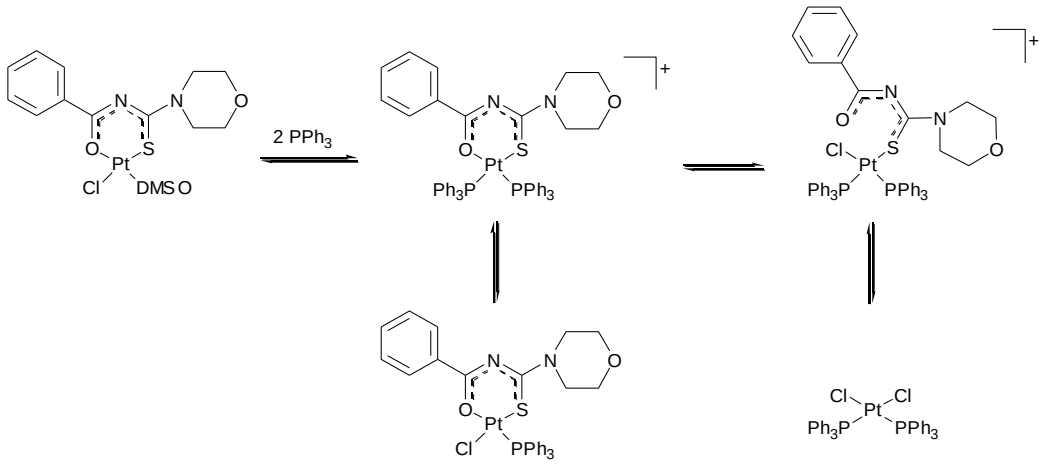

Figure 4.17 Reaction of *cis*-(S,S)-[PtCl(DMSO)(L2a)] with two equivalents of PPh_3.

4.8.4 Reaction of [PtCl(DMSO)(L5)] and [PtCl(DMSO)(L7)] with two equivalents of PPh_3

The reaction of [PtCl(DMSO)(L5)] with two equivalents of PPh_3 yielded a ^{31}P NMR spectrum that consists of three singlets at 8.001 ppm [^{1}J(PtP) 4181; *ca*. 11%], 5.704 ppm (*ca*. 7%) and 15.562 ppm (*ca*. 4%). The ^{1}J(PtP) coupling constants for the signals at 5.704 and 15.562 ppm could not be resolved due to overlapping peaks. Two sets of broad doublets are also observed at 22.010 and 10.512 ppm [^{1}J(PtP) 3064 and 3945 Hz; *ca*. 39%] and 15.562 and 8.855 ppm [^{1}J(PtP) 3346 and 3512 Hz; *ca*. 13%]. The two sets of doublets have ^{2}J(PP) coupling constants of 25 and 20 Hz, respectively. Based on the chemical shift positions and the ^{1}J(PtP) coupling constants observed for $[Pt(L1a)(PPh_3)_2]^+$, the doublets at 22.010 and 10.512 ppm have been assigned to $[Pt(L5)(PPh_3)_2]^+$. It is important to note that the difference in the coupling constants for the one set of doublets (881 Hz) is far greater compared to that observed for the other set of signals (166 Hz). Since the ^{1}J(PtP) coupling is diagnostic of the *trans* ligand, this

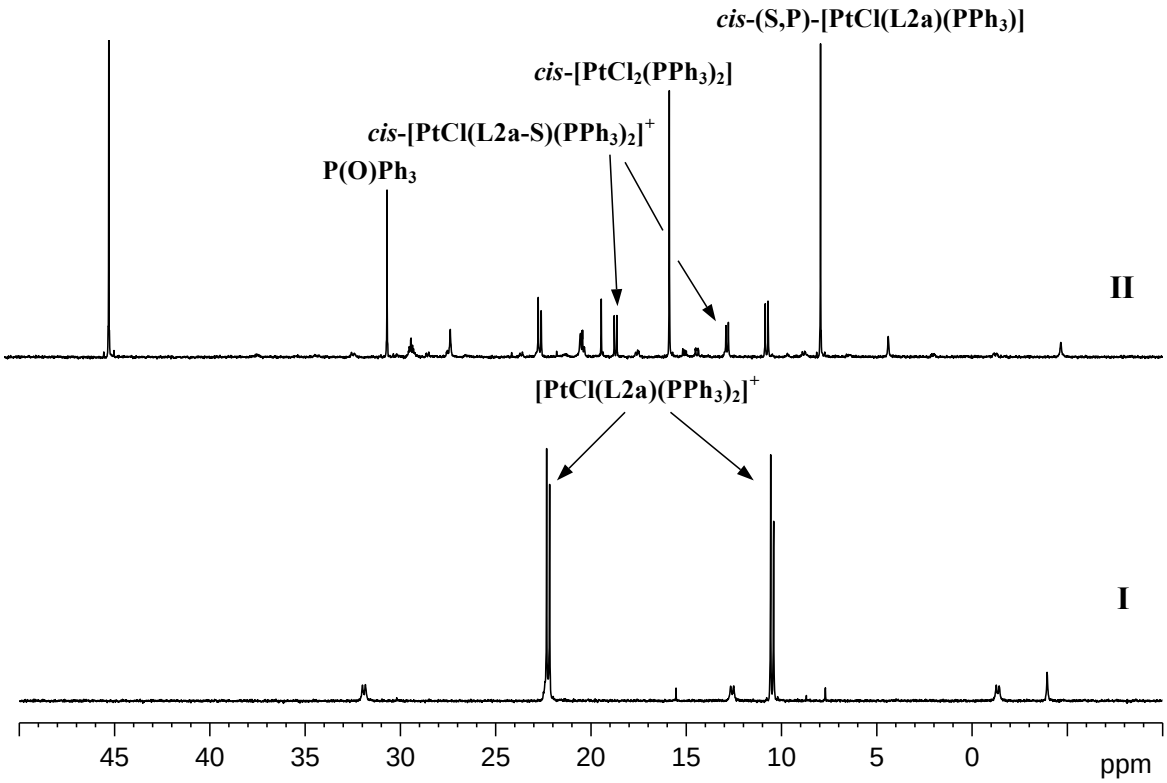

Figure 4.18: ^{31}P NMR spectrum for the reaction of *cis*-(S,S)-[PtCl(DMSO)(L2a)] with two equivalents of PPh_3 in $CDCl_3$ at 30°C.

suggests that the difference in the *trans*-influence of the two donor atoms *trans* to the phosphine ligands in the latter complex is much smaller than the difference in the *trans*-influence of the oxygen and sulfur donor atoms in the chelated ligand. Moreover, the increase in the coupling constant from 3064 to 3346 Hz for the signal at 15.562 ppm implies that a donor atom with a greater *trans*-influence than oxygen has replaced the oxygen donor atom of the chelated ligand. These results suggest that ring-opening has occurred and that the second set of doublets corresponds to a *cis*-$[PtCl(L5\text{-}S)(PPh_3)_2]^+$ complex, where (L5-S) represents the ring-opened ligand. The signals at 8.001 and 5.704 ppm are the same products formed with one equivalent of PPh_3 and have been assigned as *cis*-(S,P)- and *trans*-(S,P)-$[PtCl(L5)(PPh_3)]$, respectively. The singlet at 15.562 ppm has been assigned previously as *cis*-$[PtCl_2(PPh_3)_2]$. On the basis of the ^{31}P NMR spectral data the reaction of [PtCl(DMSO)(L5)] with two equivalents of PPh_3 could be represented by the scheme shown in Figure 4.19.

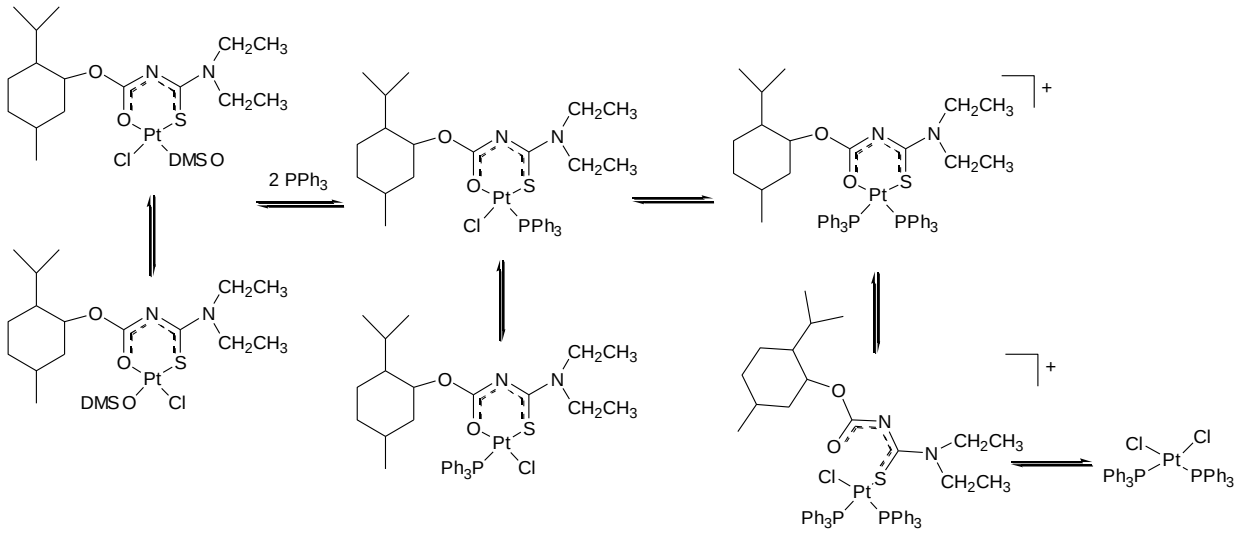

Figure 4.19: Reaction of [PtCl(DMSO)(L5)] with two equivalents of PPh_3.

The reaction of [PtCl(DMSO)(L7)] with two equivalents of PPh_3 yielded a ^{31}P NMR spectrum that consists of three singlets at 7.766 ppm [^1J(PtP) 4189 Hz; *ca*. 13%], 5.381 ppm [^1J(PtP) 3956 Hz; *ca*. 16%] and 15.572 ppm [^1J(PtP) 3673 Hz; *ca*. 37%] and only one set of doublets at 20.083 and 12.971 ppm [^1J(PtP) 3135 and 3477 Hz; ^2J(PP); 20 Hz; *ca*. 15%]. Since the difference in the ^1J(PtP) coupling constants is 242 Hz, the set of doublets at 20.083 and 12.971 ppm has been assigned as *cis*-$[PtCl(L7\text{-}S)(PPh_3)_2]^+$, where (L7-S) represents the ring-opened ligand. The three singlets at 7.766, 5.381 and 15.572

ppm have been assigned to *cis*-(S,P)- and *trans*-(S,P)-[PtCl(L7)(PPh_3)] and *cis*-[$PtCl_2(PPh_3)_2$], respectively. The signals due to [Pt(L7)(PPh_3)$_2$]$^+$ were not detected in the spectrum, implying that the *N*-menthyloxycarbonyl-*N'*-morpholinothioureato ligand is weakly bound to the platinum(II) ion. The ^{31}P NMR spectrum of the reaction of [PtCl(DMSO)(L7)] with two equivalents of PPh_3 is shown in Figure 4.20. Based on the ^{31}P NMR spectral data, the reaction of [PtCl(DMSO)(L7)] with two equivalents of PPh_3 could be represented by the scheme shown in Figure 4.21. The ^{31}P NMR data for the [PtCl(L)(PPh_3)] and *cis*-[PtCl(L-S)(PPh_3)$_2$]$^+$ complexes are summarised in Table 4.17.

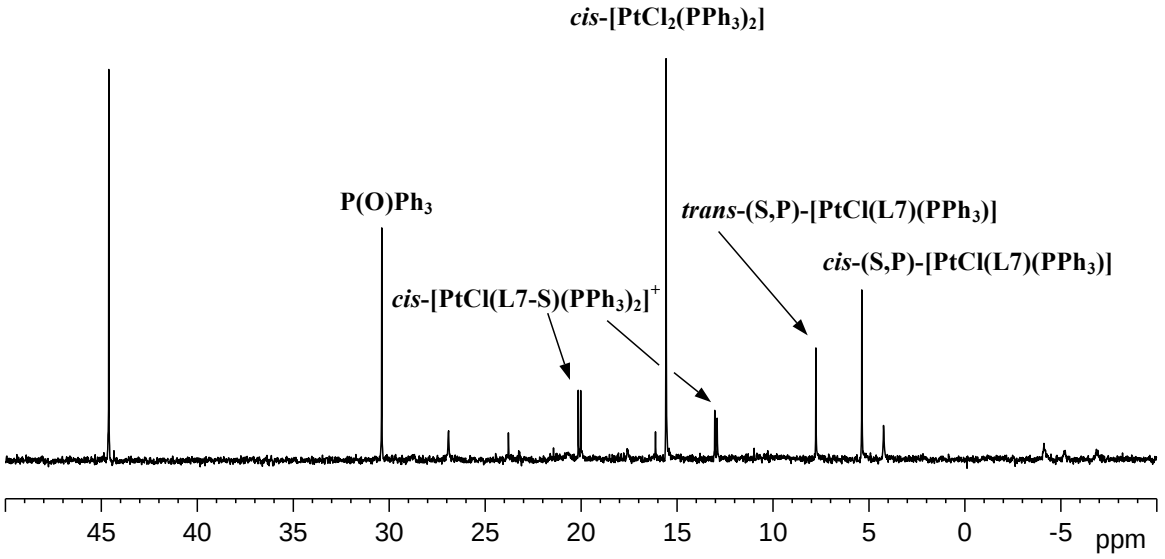

Figure 4.20: ^{31}P NMR spectrum for the reaction of [PtCl(DMSO)(L7)] with two equivalents of PPh_3 in $CDCl_3$ at 30°C.

[Ptmenmorph)Cl(DMSO) + 2 PPh3

Ptmenmor31Prep (2)

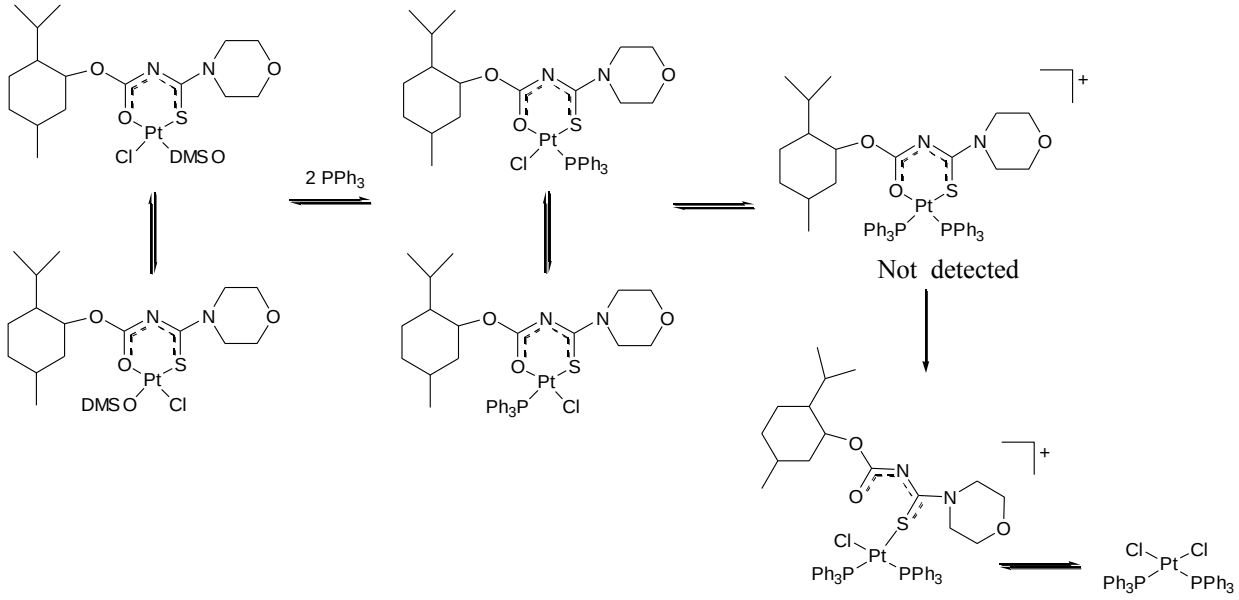

Figure 4.21: Reaction of [PtCl(DMSO)(L7)] with two equivalents of PPh_3.

Table 4.17: ^{31}P NMR data for the $[PtCl(L\text{-}S)(PPh_3)_2]^+$ and $[Pt(L)(PPh_3)_2]^+$ complexes. [a]

Complex	^{31}P NMR/ ppm [b]	^2J(PP)/ Hz
$[Pt(L1a)(PPh_3)_2]^+$	21.912 (3088)	26
	11.371 (3836)	
$[Pt(L2a)(PPh_3)_2]^+$	22.249 (3129)	25
	10.493 (3835)	
$[Pt(L5)(PPh_3)_2]^+$	22.010 (3064)	25
	10.512 (3945)	
$[Pt(L7)(PPh_3)_2]^+$	not detected	-
cis-$[PtCl(L2a\text{-}S)(PPh_3)_2]^+$	12.553 [c]	20
	20.096 [c]	
cis-$[PtCl(L5\text{-}S)(PPh_3)_2]^+$	15.562 (3346)	20
	8.855 (3512)	
cis-$[PtCl(L7\text{-}S)(PPh_3)_2]^+$	20.083 (3135)	20
	12.971 (3477)	

[a] Spectra were recorded at 30°C in $CDCl_3$, relative to 85% H_3PO_4.

[b] ^1J(PtP) coupling constants are given in parentheses.

[c] ^1J(PtP) coupling constants were not resolved.

In summary, the phosphine study highlights the difference in the coordination chemistry of the acylthiourea and alkoxycarbonylthiourea ligands illustrating that geometric isomers are formed when using the latter ligand systems and that these ligands bind less strongly to the platinum(II) ion. The *N*-benzoyl-*N',N'*-diethylthioureato carbonyl oxygen donor atom is relatively softer and therefore has a greater *trans*-influence than the carbonyl oxygen donor atom of the *N,N*-diethyl-*N'*-menthyloxycarbonylthioureato ligand. Moreover, the morpholine derivatives for both ligand systems appear to bind less tightly to the metal ion. These results are in agreement with the stability constant measurements reported by Beyer *et al*. which show that the Ni(II), Zn(II), Cd(II) and Co(II) complexes of **HL1a** are more stable than the corresponding complexes of **HL2a**. [35]

4.9 Crystallographic studies

The bond lengths within the coordination spheres of *cis*-(S,S)-[PtCl(DMSO)(L1a)] (**1a**), *cis*-(S,S)-[PtCl(L1a)(MPSO)] (**4**), *cis*-[Pt(L1a)$_2$] (**7**), *cis*-(S,S)-[PtCl(DMSO)(L7)] (**12**) and of related compounds in the literature are compared and discussed with respect to the *trans*-influence of the different donor atoms. The X-ray crystal structures of *cis*-(S,S)-[PtCl(DMSO)(L1a)] and *cis*-(S,S)-[PtCl(DMSO)(L7)] have also been compared to further highlight the differences in the coordination chemistry of acylthiourea and alkoxycarbonylthiourea ligands with platinum(II).

4.9.1 Correlation of the Pt–X bond distances in complexes (1a), (4), (7) and (12)

A summary of relevant Pt–S, Pt–Cl and Pt–O bond distance ranges for *cis*-(S,S)-[PtCl(DMSO)(L1a)] (**1a**), *cis*-(S,S)-[PtCl(L1a)(MPSO)] (**4**), *cis*-(S,S)-[PtCl(DMSO)-(L7)] (**12**), *cis*-[Pt(L1a)$_2$] (**7**) and related complexes are given in Table 4.18.

For complexes **1a**, **4** and **12**, the Pt–S(sulfoxide) bond distances of 2.1885(10), 2.192(3), and 2.1839(12) Å all fall within the range 2.168(2)–2.257(8) Å found for complexes with only one sulfur-bonded sulfoxide. [14] The Pt–MPSO bond length [2.192(3) Å] in complex **4** shows a tendency to slight elongation (although not statistically significant) compared to the Pt–DMSO bond length [2.1885(10) Å] in complex **1a**. This is in agreement with the expected labilities of the coordinated sulfoxides, in which MPSO is more labile than

DMSO. The effect of the *trans* ligand is shown in Table 4.18, where the Pt–S(sulfoxide) bond distances *trans* to an oxygen donor atom range from 2.174(2)–2.217(2) Å, while in bis(sulfoxide) complexes the Pt–S(sulfoxide) bonds *trans* to a chloride atom range from 2.188(4)–2.244(3) Å. The longest bonds in this latter range are found in complexes containing sulfoxides bulkier than DMSO or with π-accepting ligands in the *cis* position. [14] In the present study, the Pt-S(sulfoxide) bond distances are significantly shorter than those found in *cis*-[$PtCl_2(MPSO)_2$] [2.241(1), 2.245(1) Å] [12, 36] and *cis*-[$PtCl_2(DMSO)_2$] [2.244(2), 2.229(2) Å], [37] presumably because the Pt–S bond in the latter complexes is *trans* to chloride whereas in the present structures the Pt–S bond is *trans* to the acylthioureato or alkoxycarbonylthioureato oxygen donor atom.

Similarly, the Pt–S(acylthioureato) [2.257(4), 2.2586(11) Å] and Pt–S(alkoxycarbonylthioureato) [2.2595(13) Å] bond distances are found on the lower side of the range [spanning 2.243(1)–2.292(6) Å] for Pt(II) complexes containing bis(thioether) ligands as given in Table 4.18, and is also shorter than the Pt–S bond distance reported for *cis*-dichlorobis(*N,N*-dimethyl-*O*-ethylthiocarbamate)platinum(II) as well as *cis*-bis(*N*-benzoyl-*N'*-propylthioureato)dichloroplatinum(II) which ranges from 2.278(2)–2.291(4) Å. The Pt–S(acylthioureato) and Pt–S(alkoxycarbonylthioureato) bond lengths shown in Table 4.18, are however longer compared to the Pt–S bond lengths for *cis*-[$Pt(L1a)_2$] [2.232(2) Å] and *cis*-bis(*N*-benzoyl-*N',N'*-di(*n*-butyl)thioureato)-platinum(II) [2.230(2)–2.233(2) Å], [15] presumably because this bond is *trans* to Cl whereas in *cis*-[$Pt(L1a)_2$] and *cis*-bis(*N*-benzoyl-*N',N'*-di(*n*-butyl)thioureato)platinum(II) the Pt–S bonds are *trans* to oxygen donor atoms.

The Pt–Cl bond distances found in complexes **1a**, **4** and **12** lie at the longer side of the range, spanning 2.289(3)–2.337(5) Å, for platinum(II) complexes containing Pt–Cl bonds *trans* to sulfoxide ligands given in Table 4.18. It is therefore interesting to note that the sulfur donor atom of the bidentate acylthiourea ligand displays a larger *trans*-influence than the sulfur donor atoms of the thioether, *N,N*-dimethyl-*O*-ethylthiocarbamate, *N*-benzoyl-*N*-propylthiourea, *N*-menthyloxycarbonyl-*N'*-morpholinothiourea and most sulfoxide ligands listed in Table 4.18, which is indicative of significant σ-bonding. This is also in agreement with the observed trend that sulfur-bonded sulfoxides display a fairly weak *trans*-influence on chloride, nitrogen and oxygen ligands.

The Pt–O(acylthioureato) bond lengths in complex **4** (2.016(9) Å) and **1a** (2.010(3) Å) are not significantly different from those found complex **7** and **12**, and fall within the range 1.994(7)–2.033(7) Å found for Pt(II) sulfoxide complexes where Pt–O bonds are *trans* to the sulfoxide sulfur donor atom. It seems that the tendency of elongation, observed for the Pt–Cl bond mentioned above, is not reflected in the Pt–O bonds, which again follows the observed trend that sulfur-bonded sulfoxides display a fairly weak *trans*-influence on oxygen ligands.

A comparison of the Pt–O, Pt–Cl and Pt–S bond lengths in complex **1a** and **12**, further highlights the difference in the coordination chemistry of the acylthioureato and alkoxycarbonylthioureato ligand systems. Both the Pt–Cl and Pt–S(sulfoxide) bond lengths in complex **12**, [2.3276(14) and 2.1839(12) Å, respectively] are significantly shorter than in complex **1a**, that is 2.3337(11) and 2.1885(10) Å, respectively. The opposite however holds (although not statistically significant, the tendency is observed) for the corresponding sulfur and oxygen donor atoms of the bidentate ligands as manifested in the Pt–S(1) and Pt–O(11) distances of 2.2595(13) and 2.018(3) Å in complex **12** compared to 2.2586(11) and 2.010(3) Å for complex **1a**, respectively. This implies that the sulfur and oxygen donor atoms of ligand **HL1a** have larger *trans*-influences than the corresponding donor atoms in ligand **HL7**. In general this implies further that the $(\mathbf{L1a})^{-1}$ ligand is more strongly bound than the $(\mathbf{L7})^{-1}$ moiety, which is in excellent agreement with what is observed from the NMR experiments described in Section 4.8. Small differences exist in the bond angles of the chelate in complex **12** and **1a**, but these may be due to packing effects and are thus not discussed further.

4.10 Conclusion

Crystallographic and ^{31}P NMR studies suggest that the acylthiourea ligands bind more strongly to the platinum centre than the alkoxycarbonylthiourea ligands. This is consistent with the stability constants reported for Ni(II) complexes with *N,N*-diethyl-*N'*-propionylthiourea (log β_2 = 15.0) and *N*-ethoxycarbonyl-*N',N'*-diethylthiourea (log β_2 = 13.5) ligands, which suggest that the acylthiourea ligands form more stable complexes than the alkoxycarbonylthiourea ligands. [38] Furthermore, the morpholine derivatives of

the acylthiourea and alkoxycarbonylthiourea ligand systems appear to bind less tightly than the diethyl derivatives.

Based on the fact that ring-opened species of the alkoxycarbonylthioureato complexes were identified and the difference in binding strength of the acylthioureato and alkoxycarbonylthioureato ligands, it is tentatively proposed that the isomerisation of the [Pt(alkoxycarbonylthioureato)Cl(RR'SO)] complexes may occur via a ring-opened species.

Table 4.18: Correlation of literature Pt–X bond distances in analogous Pt(II) complexes (X = S, O, Cl).

Bond	Donor atom	*Trans* atom	Bond ranges/ Å	Ref.	Bond/ Å	Complex
Pt-S	sulfoxide-S	oxygen	2.174(2)-2.217(2)	39–42	-	-
	sulfoxide-S	*N*-benzoyl-*N',N'*-diethylthioureato-O	-	This study	2.192(3)	**4**
	sulfoxide-S	*N*-alkoxycarbonyl-*N'*-morpholinothioureato-O		This study	2.1839(12)	**12**
	sulfoxide-S	*N*-benzoyl-*N',N'*-diethylthioureato-O	-	This study	2.1885(10)	**1a**
	sulfoxide-S	chloride	2.188(4)-2.244(2)	14, 43	-	-
	thioether-S	chloride	2.243(1)-2.292(6)	44–47	-	-
	N,N-dimethyl-*O*-ethylthiocarbamate-S	chloride	2.285(4)-2.291(4)	48	-	-
	N-benzoyl-*N'*-propylthioureato-S	chloride	2.278(6)	49	-	-
	N-alkoxycarbonyl-*N'*-morpholino-thioureato-S	chloride	-	This study	2.2595(13)	**12**
	N-benzoyl-*N',N'*-diethylthioureato-S	chloride	-	This study	2.2586(11)	**1a**
	N-benzoyl-*N',N'*-diethylthioureato-S	chloride	-	This study	2.257(4)	**4**
	N-benzoyl-*N',N'*-dibutylthioureato-S	acylthioureato-O	2.230(2)-2.233(2)	15	2.232(2)	**7**
	N,N-dibutyl-*N'*-naphtholylthioureato-S	acylthioureato-S	2.250(4)	9	-	-
Pt-Cl	-	sulfoxide-S	2.289(3)-2.337(5)	14	-	-
	-	thioether-S	2.298(7)-2.327(2)	44–47	-	-
	-	*N*-alkoxycarbonyl-*N'*-morpholinothioureato-S	-	This study	2.3276(14)	**12**
	-	*N*-benzoyl-*N',N'*-diethylthioureato-S	-	This study	2.3337(11)	**1a**
	-	*N*-benzoyl-*N',N'*-diethylthioureato-S	-	This study	2.334(3)	**4**
	-	*N*-benzoyl-*N'*-propylthioureato-S	2.307(4)-2.324(5)	49	-	-
	-	*N,N*-dimethyl-*O*-ethylthiocarbamate-S	2.320(4)-2.321(4)	48	-	-
Pt-O	N-O and O-O chelate ligands	sulfoxide-S	1.994(7)-2.033(7)	39–42		
	N-benzoyl-*N',N'*-dibutylthioureato-S	acylthioureato-O	2.017(5)-2.026(4)	15	2.021(6)	**7**
	N,N-dibutyl-*N'*-naphtholylthioureato-S	acylthioureato-S	1.98(1)	9	-	-
	N-benzoyl-*N',N'*-diethylthioureato-O	sulfoxide-S	-	This study	2.010(3)	**1a**
	N-alkoxycarbonyl-*N'*-morpholinothioureato-O	sulfoxide-S	-	This study	2.018(3)	**12**
	N-benzoyl-*N',N'*-diethylthioureato-O	sulfoxide-S	-	This study	2.016(9)	**4**

4.11 Experimental

4.11.1 Crystal structure determination

All the platinum(II) complexes crystal structures were determined by Dr S. Otto from the University of the Orange Free State, South Africa. The three dimensional intensity data (Mo-Kα radiation, λ = 0.71073 Å) for *cis*-[Pt(L1a)$_2$] (**7**) and *cis*-(S,S)-[PtCl(L1a)(MPSO)] (**4**) were collected on a Nicolet P3 Diffractometer. All reflections were corrected for Lorenz and polarisation effects. The structures were solved by Patterson [50] and successive Fourier syntheses (SHELXL 97). [51] The crystals of complex **4** were extensively twinned and showed signs of decomposition. These were therefore covered with a thin layer of Canada Balsam thus no absorption corrections were applied. This resulted in residual electron density peaks corresponding to *ca*. 3 e Å^{-3}. All the relevant structural data and refinement parameters are given in Table 4.6. The hydrogen atom positions were calculated riding on the adjacent carbon atom (phenyl C–H = 0.92 Å and methyl C–H = 0.98 Å, [51] and were refined with an overall isotropic thermal parameter. The crystallographic data has been deposited with the Cambridge Crystallographic Data Centre (CCDC) and entered into the Cambridge Structural Database (CCDC reference number 186/1811) and are also given in Appendix A.

The three dimensional intensity data for *cis*-(S,S)-[PtCl(DMSO)(L1a)] (**1a**), *cis*-(S,P)-[PtCl(L1a)(PPh$_3$)] (**8**) and *cis*-(S,S)-[PtCl(DMSO)(L7)] (**12**) were collected on a Bruker SMART CCD Diffractometer. All reflections were corrected for Lorentz and polarisation effects. Data reduction for **1a**, **8** and **12** were performed using SHELXTL. [52] Absorption corrections on the data for **1a**, **8** and **12** were done using SADABS. [53] The structures of **1a**, **8** and **12** were solved by Patterson and successive Fourier syntheses (SHELXS 97 [54] and SHELXL 97 [51]). All hydrogen atoms were included in calculated positions with fixed isotropic thermal parameters. All the relevant structural data and refinement parameters for complex **1a** and **8** are given in Table 4.6. All the relevant structural data and refinement parameters for complex **12** are given in Table 4.15. The molecular graphics for all the complexes were produced using ORTEP. [55] The crystallographic data has been deposited with the Cambridge Crystallographic Data Centre (CCDC) and

entered into the Cambridge Structural Database (CCDC reference number 186/2253) and is also given in Appendix A.

4.11.2 Protonation study

All ^{1}H NMR and ^{195}Pt NMR spectra were recorded in $CDCl_3$ at 30°C. The following experimental procedure was performed.

i) Between 10–15 mg of the respective [PtCl(DMSO)(L-S,O)] complexes were dissolved in 0.6 ml $CDCl_3$, to give a clear, pale yellow solution. The ^{1}H and ^{195}Pt NMR spectra were then recorded.

ii) Concentrated hydrochloric acid (50 μl) was added to the NMR tube containing the [PtCl(DMSO)(L-S,O)] complex in $CDCl_3$. The tube was shaken vigorously for a few minutes. The solution was passed through *Extrelut*® to remove excess water, resulting in a clear yellow solution prior to spectra acquisition. The ^{1}H and ^{195}Pt NMR spectra were then recorded.

iii) Excess NaOAc in water was added to the NMR tube. After vigorous shaking and filtration through *Extrelut*® the ^{1}H NMR spectra were recorded at suitable time intervals in order to follow the deprotonation and subsequent ring closure of the ligand.

iv) After the reaction was complete the ^{195}Pt NMR spectrum was acquired.

4.11.3 Platinum dichloride complexes

The *cis*-$[PtCl_2(RR'SO)_2]$ complexes were prepared according to a modified literature procedure. [1] The *cis*-$[PtCl_2((S)\text{-}MTSO)_2]$ and *cis*-$[PtCl_2((R)\text{-}MTSO)_2]$ complexes were prepared using the optically pure sulfoxides. The sign and handedness of the optically pure free sulfoxides changes upon complexation to platinum(II) and the *R* and *S* assignments refer to the sign of the sulfoxide when coordinated to platinum(II).

***cis*-$[PtCl_2(RR'SO)_2]$**

A three times excess of the respective sulfoxides (3.6 mmol) was added to an aqueous solution of K_2PtCl_4 (1.2 mmol) in water (4 ml). The solution was stirred for 2 days. The

resulting precipitate was collected by filtration, washed with water and a little ethanol and dried *in vacuo* over silica gel.

cis-[$PtCl_2(DMSO)_2$]

Yield (75%). IR (KBr pellet, cm^{-1}): 1158 (s), 1136 (s), 1022 (w), 982 (w), 434 (m), 382 (m).

cis-[$PtCl_2(MPSO)_2$]

The *cis*-[$PtCl_2(MPSO)_2$] complex was found to be a mixture of *RS*/*SR* and *RR*/*SS* diastereomers, in the ratio 0.66:1. The ratio was determined by integrating the discrete methyl sulfoxide resonances observed for the diastereomers. The composition is in agreement with that observed by Antolini *et al*.. [36] Yield (91%), mp 170–183°C. IR (KBr pellet, cm^{-1}): 3090 (w), 3050 (w), 3010 (w), 2916 (w – m), 1469 (w – m), 1442 (s), 1400 (w – m), 1304 (w – m), 1155, 1145 (s, pr), 1065 (m), 950 (m – s), 740 (m), 705 (m), 675 (m), 507 (s), 400 (w – m), 350 (w – m). ^1H NMR (400 MHz, $CDCl_3$): 8.060 (4H, m, C_6H_5), 7.636 (4H, m, C_6H_5), 7.459 (1H, t, C_6H_5), 7.333 (1H, t, C_6H_5), 3.567 (6H, s, $S_{Me\ (meso)}$), 3.494 (6H, s, $S_{Me\ (RR/SS)}$) ppm.

cis-[$PtCl_2(MTSO)_2$]

Yield (90%), mp 156–158°C. IR (KBr pellet, cm^{-1}): 3005 (m, sh), 2920 (m, sh), 1645 (w), 1595 (m), 1555 (w), 1500 (m – s, sh), 1445 (m), 1400 (m – s), 1304 (m), 1145 (vs, br), 1115 (s), 1080 (s), 1030 (m), 795 (s), 705 (m), 620 (w – m), 610 (m), 510 (m), 500 (m – s), 495 (m), 413 (m), 335 (s). ^1H NMR (400 MHz, $CDCl_3$): 7.945 (2H, d, C_6H_5), 7.401 (2H, d, C_6H_5), 3.469 (6H, s, S_{Me}), 2.465 (3H, s, CH_3) ppm.

cis-[$PtCl_2(PPh_3)_2$]

A solution of K_2PtCl_4 (0.201 g, 0.48 mmol) in water (25 ml), was added slowly to a refluxing solution of finely powdered triphenylphosphine (0.286 g, 1.09 mmol) in degassed ethanol (15 ml) and under a nitrogen atmosphere to prevent formation of Ph_3PO.

A white precipitate was observed after several minutes. The solution was allowed to cool to room temperature and was stirred for an hour under nitrogen. The white precipitate was collected by centrifugation, washed with a little methanol and ether and dried *in vacuo* over silica gel. Yield (0.333 g, 87%). ^{31}P NMR (400 MHz, $CDCl_3$): 15.562 (s), ^{1}J(PtP) = 3673 Hz.

4.11.4 Platinum acylthiourea complexes

cis-(S,S)-[PtCl(DMSO)(L1a)] (1a)

A solution of *N*-benzoyl-*N',N'*-diethylthiourea (0.130 g, 0.55 mmol) in acetonitrile (20 ml) was added dropwise to a stirred solution of *cis*-[$PtCl_2(DMSO)_2$] (0.234 g, 0.55 mmol) in acetonitrile/dimethylsulfoxide (6 ml, 1:1 v/v). 1.5 equivalents of sodium acetate in water (1.5 ml) was then added. The solution was allowed to stir for 48 hours. Water (100 ml) was added to the solution whereupon a precipitate formed. The mixture was placed in a refrigerator (4°C) overnight. The yellow precipitate was extracted into chloroform (50 ml) and the organic extract dried over anhydrous $MgSO_4$. ^{1}H NMR and TLC of the organic extract showed that it consisted of *cis*-(S,S)-[PtCl(DMSO)(L1a)] and *cis*-[$Pt(L1a)_2$]. The desired complex was obtained after purification by flash chromatography [eluant: $CHCl_3$/EtOAc (3:1)]. Crystals suitable for X-ray crystallography were obtained by a double layer diffusion method, using chloroform and hexane as solvents. IR (KBr pellet, cm^{-1}): 2980 (w), 2930 (w), 1520 (m), 1500 (s, sh), 1140 (m), 1410 (s, sh), 1375 (w – m), 1352 (m), 1305; 1295 (w – m, pr), 1248 (m), 1200 (m, sh), 1139 (m – s), 1095 (w), 1084 (w), 1069 (w), 1025 (m), 880 (w – m), 810 (w – m), 702 (m), 680 (m), 445 (m). TLC [Silica gel, $CHCl_3$/EtOAc (3:1)]: R_f 0.41.

cis-[$Pt(L1a)_2$] (7)

This complex was isolated from the above-mentioned reaction by flash chromatography (yield 14 mg, 5%). mp 170–172°C. Crystals suitable for X-ray crystallography were obtained by slow evaporation of a chloroform solution of the complex. (Found: C, 42.7; H, 4.5; N, 8.2; S, 9.4. Calc for $C_{24}H_{30}N_4O_2S_2Pt$: C, 43.3; H, 4.5; N, 8.4; S, 9.6%). IR (KBr pellet, cm^{-1}): 3062 (w), 2960 (w), 2930 (m), 2850 (w), 1585 (m – s), 1525 (s), 1505 (s), 1410 (s), 1370 (w), 1349 (m – s), 1296 (w – m), 1250 (m – s), 1205 (w – m), 1170

(w – m), 1136 (m), 1100 (m), 1027 (w – m), 1036 (w – m), 1020 (w), 1005 (w), 974 (w), 881 (w – m), 810 (w – m), 781 (w), 769 (w), 708 (m), 680 (w – m, sh), 690 (w – m, sh), 665 (w – m, sh), 465 (w), 351 (w), 325 (w), 302 (w), 245 (w – m). ^{1}H NMR (400 MHz, $CDCl_3$): 8.25 (4H, d, C_6H_5) 7.50 (2H, t, C_6H_5), 7.41 (4H, t, C_6H_5), 3.84 (4H, q, $2CH_2$), 3.77 (4H, q, $2CH_2$), 1.33 (6H, t, $2CH_3$), 1.28 (6H, t, $2CH_3$). TLC [Silica gel, $CHCl_3$/EtOAc (3:1)]: R_f 0.78.

cis-(S,S)-[PtCl(DMSO)(L1b)] (1b)

A solution of *N*-(3-chlorobenzoyl)-*N',N'*-diethylthiourea (0.155 g, 0.57 mmol) in acetonitrile (20 ml) was added dropwise to a stirred solution of *cis*-$[PtCl_2(DMSO)_2]$ (0.271 g, 0.57 mmol) in acetonitrile/dimethylsulfoxide (6 ml, 1:1 v/v). Sodium acetate (0.075 g, 0.91 mmol) in water (1.5 ml) was then added. The solution was allowed to stir for 48 hours. Water (100 ml) was added and the solution became opaque. The opaque solution was placed in a refrigerator (4°C) overnight, whereupon a yellow precipitate separated out from the solution. The yellow precipitate was extracted into chloroform (40 ml) and the organic layer was dried over $MgSO_4$. The pure product was obtained by flash chromatography [eluant: $CHCl_3$/EtOAc (3:1)]. IR (KBr pellet, cm^{-1}): 3067 (w), 3014 (w), 2998 (w), 2976 (w), 2934 (w), 2914 (w), 2873 (w), 1525 (s), 1507 (s, sh), 1459 (m, sh), 1424 (vs, sh), 1357 (s, sh), 1319 (w – m, sh), 1299 (w – m, sh), 1268 (w, sh), 1252 (w – m, sh), 1209 (w – m, sh), 1144 (s, sh), 1113 (w), 1072 (w), 1030 (m, sh), 989 (w), 948 (w), 923 (w), 910 (w), 900 (w), 841 (w), 791 (w), 761 (m, sh), 733 (m – s, sh), 697 (w – m, sh), 669 (w), 650 (w), 456 (w – m, sh). TLC [silica gel, $CHCl_3$/EtOAc (3:1)]: R_f 0.54.

cis-(S,S)-[PtCl(DMSO)(L1c)] (1c)

A solution of *N,N*-diethyl-*N'*-(3-nitrobenzoyl)thiourea (0.142 g, 0.50 mmol) in acetonitrile (20 ml) was added dropwise to a stirred solution of *cis*-$[PtCl_2(DMSO)_2]$ (0.214 g, 0.51 mmol) in acetonitrile/dimethylsulfoxide (6 ml, 1:1 v/v). Sodium acetate (0.064 g, 0.78 mmol) in water (1.5 ml) was then added. The solution was allowed to stir for 48 hours. On stirring for a few minutes a yellow precipitate was observed. Water (100 ml) was added to the solution and the solution became opaque. The opaque solution

was placed in a refrigerator (4°C) overnight, whereupon a yellow precipitate was observed. The yellow precipitate was collected by filtration, washed with water and ethanol. The desired complex was obtained after purification by flash chromatography [eluant: $CHCl_3$/EtOAc (18:1)]. IR (KBr pellet, cm^{-1}): 3012 (w - m, sh), 2975 (w – m, sh), 2929 (w – m, sh), 1587 (m, sh), 1534 (vs, sh), 1525 (vs, sh), 1510 (vs, sh), 1458 (m, sh), 1436 (vs), 1418 (vs, shld), 1407 (vs, sh), 1379 (m), 1347 (vs, sh), 1321 (m), 1305 (m), 1272 (m, sh), 1248 (m, sh), 1153 (s, sh), 1096 (m, sh), 1077 (m – s, sh), 1033 (m – s, sh), 1002 (w – m), 980 (w – m, sh), 939 (w), 918 (w – m, sh), 870 (w), 825 (m, sh), 817 (m, sh), 766 (w), 741 (m – s, sh), 717 (s, sh), 967 (m, sh), 670 (w), 660 (w), 649 (w), 577 (w), 541 (w), 452 (w – m, sh), 400 (vw), 379 (w – m, sh). TLC [silica gel, $CHCl_3$/EtOAc (18:1)]: R_f 0.42.

cis-(S,S)-[PtCl(DMSO)(L1d)] (1d)

This complex was prepared using a similar procedure to that described for *cis*-(S,S)-[PtCl(DMSO)(L1c)] above, except for the following. The yellow precipitate was extracted into chloroform (40 ml). The aqueous phase was extracted with chloroform (10 ml). The organic layers were combined and dried over $MgSO_4$. The desired complex was obtained by flash chromatography [eluant: $CHCl_3$/EtOAc (3:1)]. IR (KBr pellet, cm^{-1}): 3019 (w), 2996 (w), 2977 (w), 2950 (w), 2933 (w), 2920 (w), 2912 (w), 2869 (w), 2829 (w), 1599 (w, sh), 1521 (s, sh), 1498 (s, sh), 1459 (m, sh), 1453 (m, sh), 1427 (s, sh), 1400 (s, sh), 1354 (m), 1331 (w), 1283 (w – m, sh), 1260 (w – m, sh), 1236 (m, sh), 1201 (w, sh), 1182 (w, sh), 1156 (m, sh), 1137 (m, sh), 1097 (w), 1081 (w), 1074 (w), 1031 (m, sh), 983 (w, sh), 943 (w), 918 (w), 866 (w – m, sh), 801 (w – m, sh), 752 (m, sh), 734 (w), 697 (w, sh), 659 (w), 576 (w), 449 (w – m, sh), 378 (w – m, sh). TLC [silica gel, $CHCl_3$/EtOAc (3:1)]: R_f 0.50

cis-(S,S)-[PtCl(DMSO)(L1e)] (1e)

This complex was prepared using a similar procedure to that described for *cis*-(S,S)-[PtCl(DMSO)(L1c)] above, except that the yellow precipitate was extracted into chloroform (20 ml). IR (KBr pellet, cm^{-1}): 3015 (w), 2999 (w, sh), 2980 (w, sh), 2936 (w), 2917 (w, sh), 2874 (w), 1524 (s, sh), 1499 (vs, sh), 1429 (vs, sh), 1412 (vs, sh), 1358

(m), 1303 (w), 1260 (m, sh), 1221 (w), 1186 (w), 1137 (s, sh), 1097 (w), 1084 (w), 1026 (w – m, sh), 983 (w – m), 949 (w), 865 (w), 803 (w – m, sh), 739 (m, sh), 698 (w – m, sh), 685 (w – m, sh), 670 (w, sh), 655 (w), 452 (w – m, sh), 421 (w), 400 (w), 381 (w). TLC [silica gel, $CHCl_3$/EtOAc (3:1)]: R_f 0.73.

cis-(S,S)-[{PtCl(DMSO)}$_2$(L1f)] (1f)

A solution of *N,N*-adipoylbis(*N',N'*-diethylthiourea) (0.134 g, 0.36 mmol) in acetonitrile (10 ml) was added to a solution of *cis*-[$PtCl_2(DMSO)_2$] (0.30 g, 0.71 mmol) in acetonitrile/dimethylsulfoxide (6 ml, 1:1 v/v). Sodium acetate (0.105 g, 1.28 mmol) in water (2 ml) was added and the solution was stirred at room temperature for 2 days. Water (100 ml) was added and the mixture was placed in a refrigerator (4°C) for 10 days. The resultant yellow precipitate was collected by centrifugation and dried in an oven (64°C). IR (KBr pellet, cm^{-1}): 2980 (w), 2935 (w), 1525 (m, shld), 1522 (s, shld), 1502 (s), 1428 (s), 1378 (w), 1356 (m), 1290 (m), 1242 (w – m), 1193 (w), 1138 (m – s, sh), 1095 (w), 1078 (w), 1022 (m), 978 (w – m), 920 (w), 900 (w), 842 (w), 781 (w), 734 (w), 693 (w – m, sh), 671 (w), 652 (w), 449 (w – m), 400 (w), 383 (w). ^{1}H NMR (400 MHz, $CDCl_3$): 3.71 (8H, m, $4CH_2$), 3.54 (12H, s, ^3J(PtH) 24 Hz, $4CH_3$), 2.40 (4H, t, $2CH_3$), 1.67 (4H, m, $2CH_2$), 1.30 (6H, t, $2CH_3$), 1.18 (6H, t, $2CH_3$). TLC [Silica gel, $CHCl_3$/EtOAc (3:1 v/v)]: R_f 0.23.

cis-(S,S)-[PtCl(DMSO)(L2a)] (2a)

A solution of *N*-benzoyl-*N'*-morpholinothiourea (0.130 g, 0.52 mmol) in acetonitrile (10 ml) was added dropwise to a stirred solution of *cis*-[$PtCl_2(DMSO)_2$] (0.221 g, 0.52 mmol) in 1.5 ml acetonitrile/2.5 ml dimethylsulfoxide. Sodium acetate (0.066 g, 0.81 mmol) in water (1.5 ml) was then added. The solution was allowed to stir for 48 hours. On stirring for a few minutes a yellow precipitate was observed. Water (100 ml) was added and the solution became opaque. The opaque solution was placed in a refrigerator (4°C) overnight, whereupon a yellow precipitate separated out of solution. The yellow precipitate was collected by filtration, washed with water and ethanol. The product was purified using flash chromatography [eluant: $CHCl_3$/EtOAc (2.3:1)]. IR (KBr pellet, cm^{-1}): 3006 (w, sh), 2967 (w, sh), 2916 (w, sh), 2864 (w, sh), 2527 (s, sh), 1511 (m – s),

1492 (m – s, sh), 1447 (m – s), 1417(vs, sh), 1355 (w – m, sh), 1312 (w), 1293 (w), 1264 (w – m, sh), 1229 (m, sh), 1192 (w), 1147 (m, sh), 1118 (m, sh), 1068 (w), 1030 (m, sh), 937 (w – m, sh), 929 (w – m), 908 (w – m, sh), 834 (w), 819 (w), 800 (w), 757 (w), 718 (m, sh), 706 (m, sh), 694 (m, sh), 647 (w), 615 (w), 563 (w), 508 (w), 485 (w), 449 (w – m, sh). TLC [silica gel, $CHCl_3$/EtOAc (2.3:1)]: R_f 0.31.

cis-(S,S)-[PtCl(DMSO)(L2b)] (2b)

A solution of *N*-(3-chlorobenzoyl)-*N'*-morpholinothiourea (0.145 g, 0.51 mmol) was dissolved in a solvent mixture of 12 ml acetonitrile/14 ml ethanol and then added dropwise to a stirred solution of *cis*-$[PtCl_2(DMSO)_2]$ (0.215 g, 0.51 mmol) in 1.5 ml acetonitrile/2.5 ml dimethylsulfoxide. Sodium acetate (0.062 g, 0.76 mmol) in water (1.5 ml) was added. Upon stirring for a few minutes a yellow precipitate was observed. The solution was allowed to stir for 48 hours. Water (100 ml) was added and the solution became opaque. The opaque solution was placed in a refrigerator (4°C) overnight, whereupon a yellow precipitate separated out from solution. The yellow precipitate was collected by filtration, washed with water, ethanol and dried *in vacuo* over silica gel. IR (KBr pellet, cm^{-1}): 1523 (s, sh), 1508 (s), 1491 (s), 1482 (s), 1431 (vs, sh), 1354 (m, sh), 1305 (w – m), 1294 (w – m), 1259 (m, sh), 1229 (m, sh), 1187 (w, sh), 1148 (m, sh), 1115 (s, sh), 1071 (w), 1028 (m, sh), 981 (w), 942 (w), 913 (w), 870 (w), 829 (w), 760 (m, sh), 741 (m – s, sh), 695 (w), 675 (w), 700 (w), 651 (w, sh), 613 (w), 564 (w), 509 (w), 448 (w – m, sh), 381 (w, sh). TLC [silica gel, $CHCl_3$/EtOAc (3:1)]: R_f 0.36.

cis-(S,S)-[PtCl(DMSO)(L2c)] (2c)

This complex was prepared using a similar procedure to that described for *cis*-(S,S)-[PtCl(DMSO)(L2b)] above, except that the *N*-morpholino-*N'*-(3-nitrobenzoyl)thiourea ligand was dissolved in 10 ml acetonitrile/15 ml ethanol/1 ml dimethylsulfoxide. IR (KBr pellet, cm^{-1}): 3082 (w), 3017 (w, sh), 3006 (w), 2971 (w), 2955 (w, sh), 2918 (w, sh), 2868 (w), 2856 (w), 1612 (w – m), 1586 (w – m, sh), 1525 (vs, sh), 1493 (s, sh), 1482 (s), 1426 (vs), 1346 (vs, sh), 1322 (w – m, sh), 1302 (w – m, sh), 1264 (m, sh), 1230 (m – s, sh), 1211 (w – m), 1189 (w), 1145 (s, sh), 1114 (m – s, sh), 1083 (w – m), 1065 (w – m), 1030 (s, sh), 993 (m, sh), 948 (m, sh), 928 (w – m), 885 (w – m), 769 (w), 743 (m – s, sh),

716 (s, sh), 699 (m, sh), 661 (w – m, sh), 648 (w – m, sh), 612 (w), 567 (w), 505 (w), 453 (m, sh), 378 (w – m, sh). TLC [silica gel, $CHCl_3$/EtOAc (3:1)]: R_f 0.28.

cis-(S,S)-[PtCl(DMSO)(L2d)] (2d)

This complex was prepared using a similar procedure to that described for *cis*-(S,S)-[PtCl(DMSO)(L2b)] above, except that the *N*-(3-methoxylbenzoyl)-*N'*-morpholinothiourea ligand was dissolved in acetonitrile (10 ml). The product was purified by flash chromatography [eluant: $CHCl_3$/EtOAc (6:1)]. IR (KBr pellet, cm^{-1}): 3009 (w, sh), 2964 (w, sh), 2934 (w, shld), 2918 (w), 2865 (w, sh), 1599 (w), 1524 (vs, sh), 1420 (vs, sh), 1412 (vs, sh), 1355 (m, sh), 1321 (w – m, sh), 1281 (w – m, sh), 1267 (m, sh), 1239 (m, sh), 1226 (m, sh), 1189 (w), 1169 (w – m), 1150 (m, sh), 1116 (m, sh), 1032 (m, sh), 988 (w, sh), 949 (w – m, sh), 885 (w – m, sh), 851 (w), 797 (w – m, sh), 751 (m, sh), 695 (w – m), 683 (w – m), 653 (w – m), 620 (w), 509 (w), 450 (w – m, sh), 377 (w). TLC [silica gel, $CHCl_3$/EtOAc (6:1)]: R_f 0.29.

cis-(S,S)-[PtCl(DMSO)(L2e)] (2e)

This complex was prepared using a similar procedure to that described for *cis*-(S,S)-[PtCl(DMSO)(L2b)] above, except that the *N*-(3-methylbenzoyl)-*N'*-morpholinothiourea ligand was dissolved in acetonitrile (10 ml). IR (KBr pellet, cm^{-1}): 3014 (w – m, sh), 3001 (w – m, sh), 2966 (w – m, sh), 2916 (w – m, sh), 2864 (w – m, sh), 1521 (vs, sh), 1482 (s), 1431 (vs, sh), 1355 (m, sh), 1321 (w – m), 1310 (w – m), 1266 (m, sh), 1233 (s, sh), 1147 (m – s, sh), 1118 (m – s, sh), 1032 (m), 985 (w – m), 949 (m, sh), 922 (w), 849 (w), 796 (w – m), 739 (m – s, sh), 693 (w – m), 650 (w – m, sh), 619 (w), 563 (w), 527 (w, sh), 508 (w, sh), 450 (m, sh), 376 (m, sh). TLC [silica gel, $CHCl_3$/EtOAc (3:1)]: R_f 0.34.

cis-(S,S)-[PtCl(DMSO)(L3a)] (3a)

A solution of *N*-benzoyl-*N',N'*-di(2-hydroxyethyl)thiourea (0.45 mmol) in acetonitrile (10 ml) was added dropwise to a stirred solution of *cis*-[$PtCl_2(DMSO)_2$] (0.45 mmol) in acetonitrile/dimethylsulfoxide (4 ml, 1:1 v/v). Sodium acetate (0.60 mmol) in water (1 ml) was then added, and the solution was stirred for 25 hours. A large excess of water

(130 ml) was added whereupon a yellow precipitate formed. The solution was placed in a refrigerator (4°C) for 70 hours. The yellow precipitate was collected by filtration, recrystallised from ethanol and dried in an oven (64°C). IR (KBr pellet, cm^{-1}): 3495 (m), 3387 (m), 3003 (w), 2943 (w), 2919 (w), 2878 (w), 1541 (w), 1525 (vs, sh), 1491 (vs, sh), 1447 (s, sh), 1408 (vs, sh), 1362 (s, sh), 1320 (w – m), 1209 (w – m), 1168 (w – m), 1146 (s, sh), 1070 (, sh), 1059 (m), 1032 (s, sh), 998 (w – m), 983 (w – m), 935 (w – m), 897 (w), 869 (w), 859 (w), 799 (w – m, sh), 715 (s, sh), 691 (m, sh), 653 (w), 570 (w), 519 (w), 450 (s, sh), 380 (w), 374 (w). TLC [RP-18F_{254}S, MeOH/H_2O (5:1)]: R_f 0.76.

***cis*-(S,S)-[PtCl(DMSO)(L3b)] (3b)**

A solution of *N*-(3-chlorobenzoyl)-*N',N'*-di(2-hydroxyethyl)thiourea (0.153 g, 0.50 mmol) in 10 ml acetonitrile/7 ml ethanol was added dropwise to a stirred solution of *cis*-[$PtCl_2(DMSO)_2$] (0.212 g, 0.50 mmol) in 1.5 ml acetonitrile/2.5 ml dimethylsulfoxide. Sodium acetate (0.063 g, 0.77 mmol) in water (1.5 ml) was added and the solution was allowed to stir for 48 hours. The yellow solution was concentrated to *ca*. 10 ml and water (40 ml) was added and the solution became opaque. The opaque solution was placed in a refrigerator (4°C) overnight, whereupon a yellow precipitate separated out from solution. The yellow precipitate was collected by filtration, washed with water, a little ethanol and dried *in vacuo* over silica gel. IR (KBr pellet, cm^{-1}): 3442 (m – s, br), 3069 (w), 3004 (m), 2918 (m), 2881 (w), 1528 (vs), 1497 (vs), 1424 (vs), 1355 (s, sh), 1320 (m, sh), 1297 (m), 1269 (w – m), 1259 (w – m), 1205 (m), 1175 (m), 1138 (m, sh), 1072 (s, sh), 1028 (s, sh), 983 (m), 936 (w – m, sh), 898 (w – m, sh), 859 (w), 811 (w – m, sh), 763 (m – s, sh), 743 (s, sh), 697 (m, sh), 677 (w – m), 668 (w – m), 654 (w – m), 574 (w), 521 (w), 508 (w), 473 (w), 451 (m, sh), 400 (w), 380 (w – m). TLC [RP-18F_{254}S, MeOH/H_2O (5:1)]: R_f 0.76.

***cis*-(S,S)-[PtCl(DMSO)(L3c)] (3c)**

This complex was prepared using a similar procedure to *cis*-(S,S)-[PtCl(DMSO)(L3b)], except that *N,N*-di(2-hydroxyethyl)-*N'*-(3-nitrobenzoyl)thiourea was dissolved in 10 ml acetonitrile/12 ml ethanol. IR (KBr pellet, cm^{-1}): 3428 (s, br), 3081 (w), 3015(w), 2924 (w), 2885 (w), 1611 (w – s, sh), 1580 (m, sh), 1524 (vs, sh), 1491 (vs, sh), 1412 (vs, sh),

1346 (vs, sh), 1207 (w – m), 1146 (s, sh), 1080 (m – s, sh), 1029 (s, sh), 983 (m, sh), 941 (w – m, sh), 924 (w – m), 854 (w), 814 (w, sh), 769 (w, sh), 742 (m – s, sh), 716 (s, sh), 695 (m – s, sh), 661 (w), 648 (w), 451 (m – s, sh), 419 (vw). TLC [RP-18F_{254}S, MeOH/H_2O (5:1)]: R_f 0.74.

cis-(S,S)-[PtCl(DMSO)(L3d)] (3d)

This complex was prepared using a similar procedure to *cis*-(SS)-[PtCl(DMSO)(L3b)] above, except that *N,N*-di(2-hydroxyethyl)-*N'*-(3-methoxybenzoyl)thiourea was dissolved in acetonitrile (10 ml). The yellow precipitate was collected by filtration, washed with water and ether. IR (KBr pellet, cm^{-1}): 3480 (m – s), 3392 (m – s), 3007 (m, sh), 2938 (m), 2921 (m), 2833 (w – m), 1598 (m, sh), 1527 (vs, sh), 1490 (vs), 1459 (s), 1449 (s), 1410 (vs), 1357 (s), 1325 (m – s), 1280 (m – s, sh), 1238 (m – s, sh), 1204 (m – s, sh), 1160 (m – s, shld), 1148 (s, sh), 1071 (s, sh), 1031 (s, sh), 996 (m, sh), 981 (m, sh), 942 (m), 903 (m, sh), 870 (m, sh), 836 (m, sh), 801 (w – m), 751 (s, sh), 732 (w – m), 693 (m, sh), 683 (m), 657 (w – m, sh), 575 (w), 546 (w), 447 (m – s, sh), 376 (m, sh). TLC [RP-18F_{254}S, MeOH/H_2O (5:1)]: R_f 0.75.

cis-(S,S)-[PtCl(DMSO)(L3e)] (3e)

This complex was prepared using a similar procedure to *cis*-(S,S)-[PtCl(DMSO)(L3b)] above, except that *N,N*-di(2-hydroxyethyl)-*N'*-(3-methylbenzoyl)thiourea was dissolved in 10 ml acetonitrile/5 ml ethanol. The yellow precipitate was collected by filtration, washed with water, ether and dried *in vacuo* over silica gel. IR (KBr pellet, cm^{-1}): 3455 (m), 3384 (m), 308 (w –m), 2920 (w – m), 2879 (w – m), 1524 (s, sh), 1491 (s, sh), 1412 (vs, sh), 1358 (m – s, sh), 1319 (w – m), 1215 (w – m), 1149 (m, sh), 1069 (m), 1027 (m), 998 (w – m, sh), 983 (w – m), 941 (w), 898 (w), 859 (w), 830 (w), 807 (w), 740 (m, sh), 691 (w – m), 654 (w), 571 (w), 529 (w), 504 (w), 474 (w), 449 (w – m, sh), 400 (w), 379 (w). TLC [RP-18F_{254}S, MeOH/H_2O (5:1)]: R_f 0.78.

cis-(S,S)-[PtCl(L1a)(MPSO)] (4)

A solution of *N*-benzoyl-*N',N'*-diethylthiourea (0.11 g, 0.47 mmol) in acetonitrile (10 ml) was added dropwise to a stirred solution of *cis*-[$PtCl_2(MPSO)_2$] (0.26 g, 0.47 mmol) in

acetonitrile/dichloromethane (10 ml, 1:1 v/v) followed by 1.5 equivalents of sodium acetate in water (1.5 ml). The reaction mixture was stirred for 66 hours at room temperature. The resulting orange solution was added to water (100 ml), whereupon the aqueous and organic phases separated. The aqueous phase was extracted with CH_2Cl_2 (10 ml) and the organic phases were combined and dried over anhydrous $MgSO_4$. The pure product was obtained by chromatography using Lipophilic Sephadex LH-20 [eluant: CH_2Cl_2]. Slow recystallisation from EtOH/$CHCl_3$ yielded crystals suitable for X-ray structure analysis. IR (KBr pellet, cm^{-1}): 3070 (m – s), 2985 (m, sh), 2940 (m), 2921 (m), 2875 (w – m), 1570 (m), 1501 (s sh), 1450 (m), 1418 (s), 1356 (m), 1300 (w), 1255 (w), 1206 (w), 1141 (m, sh), 1075 (w – m), 1025 (w), 1000 (w), 946 (w – m) 876 (w), 810 (w), 705 (m – s, sh), 695 (m), 680 (m), 520 (m), 315 (vw), 205 (vw). TLC [Silica gel, $CHCl_3$/EtOH (2%)]: R_f 0.65.

***cis*-(S,S)-[PtCl(L1a)((*R*)-MTSO)] (5)**

This complex was prepared using the same procedure as described for *cis*-(S,S)-[PtCl(DMSO)(L1a)] above, with exception of the following: a solution of *N*-benzoyl-*N',N'*-diethylthiourea in acetonitrile (10 ml) was added dropwise to a stirred solution of *cis*-[$PtCl_2$((*R*)-MTSO)$_2$] in acetonitrile (6 ml) and the solution was stirred for 66 hours. The pure complex was obtained by flash chromatography [eluant: $CHCl_3$/EtOH (2%)]. IR (KBr pellet, cm^{-1}): 2985 (w – m), 2940 (w – m), 1579 (w, sh), 1540 (s, shld), 1501 (vs, sh), 1450 (s), 1430 (s), 1415 (vs), 1380 (m), 1356 (s), 1310 (w – m), 1255 (m), 1210 (m), 1175 (w), 1145 (s, sh), 1125 (w), 1120 (w – m), 1100 (w), 1081 (m – s), 1075 (w), 944 (m), 880 (w – m), 810 (w – m), 795 (w – m), 705 (s), 698 (m, shld), 679 (m), 628 (w – m), 619 (w – m), 515 (m), 315 (w), 280 (w). TLC [Silica gel, $CHCl_3$/EtOAc (2%)]: R_f 0.64.

***cis*-(S,S)-[PtCl(L1a)((*S*)-MTSO)] (6)**

This complex was prepared using the same procedure as described for *cis*-(S,S)-[PtCl(DMSO)(L1a)] above, with exception of the following: a solution of *N*-benzoyl-*N',N'*-diethylthiourea in acetonitrile (10 ml) was added dropwise to a stirred solution of *cis*-[$PtCl_2$((*S*)-MTSO)$_2$] in acetonitrile (6 ml). The pure complex was obtained by flash chromatography [eluant: $CHCl_3$/EtOH (2%)]. IR (KBr pellet, cm^{-1}): 2985 (w – m), 2940

(w – m), 1579 (w, sh), 1540 (s, shld), 1501 (vs, sh), 1450 (s), 1430 (s), 1415 (vs), 1380 (m), 1356 (s), 1310 (w – m), 1255 (m), 1210 (m), 1175 (w), 1145 (s, sh), 1125 (w), 1120 (w – m), 1081 (m – s), 1100 (w), 1075 (w), 944 (m), 880 (w – m), 810 (w – m), 795 (w – m), 705 (s), 698 (m, shld), 679 (m), 628 (w – m), 619 (w – m), 515 (m), 315 (w), 280 (w). TLC [Silica gel, $CHCl_3$/EtOAc (2%)]: R_f 0.64.

4.11.5 Platinum alkoxycarbonylthiourea complexes

[PtCl(DMSO)(L4)] (9) and [PtCl(DMSO)(L5)] (10)

A solution of the respective ligand (0.48 mmol) in acetonitrile (10 ml), was added dropwise to a solution of *cis*-[$PtCl_2(DMSO)_2$] (0.48 mmol) in acetonitrile/ dimethylsulfoxide (6 ml, 1:1 v/v) followed by sodium acetate (0.74 mmol) in water (1.5 ml). The resulting solution was stirred for 3 days at room temperature. Water (100 ml) was then added to the bright yellow solution, whereupon a yellow oil formed. The mixture was placed in a refrigerator (4°C) overnight. The yellow oil was extracted into ether (40 ml), dried over $MgSO_4$ and evaporated to dryness under reduced pressure to yield a yellow precipitate. The precipitate was dried *in vacuo*.

[PtCl(DMSO)(L4)]: IR (KBr pellet, cm^{-1}): 2954 (s, sh), 2927 (s), 2867 (m – s, sh), 1688 (s, sh), 1557 (s), 1532 (s), 1502 (s), 1430 (s, sh), 1379 (m – s, shld), 1377 (m – s, shld), 1357 (s, sh), 1310 (m – s), 1301 (m – s), 1255 (s), 1206 (s, sh), 1208.8 (m – s, sh), 1184 (m – s, sh), 1139 (s, br), 1093 (s, shld), 1079 (s, sh), 1020 (s, sh), 978 (m – s), 961 (m – s, sh), 934 (w – m, sh), 921 (w – m), 862 (w), 840 (w), 774 (w – m, sh), 721 (w – m, sh), 693 (w – m, sh), 655 (w), 549 (w), 527 (w), 449 (m, sh), 379 (w – m, sh). TLC [Silica gel, $CHCl_3$/EtOH (2%)]: R_f 0.55.

[PtCl(DMSO)(L5)]: IR (KBr pellet, cm^{-1}): 2954 (s, sh), 2927 (s), 2867 (m – s, sh), 1688 (s, sh), 1557 (s), 1532 (s), 1502 (s), 1430 (s, sh), 1379 (m – s, shld), 1377 (m – s, shld), 1357 (s, sh), 1310 (m – s), 1301 (m – s), 1255 (s), 1206 (s, sh), 1208.8 (m – s, sh), 1184 (m – s, sh), 1139 (s, br), 1093 (s, shld), 1079 (s, sh), 1020 (s, sh), 978 (m – s), 961 (m – s, sh), 934 (w – m, sh), 921 (w – m), 862 (w), 840 (w), 774 (w – m, sh), 721

(w – m, sh), 693 (w – m, sh), 655 (w), 549 (w), 527 (w), 449 (m, sh), 379 (w – m, sh). TLC [Silica gel, $CHCl_3$/EtOH (2%)]: R_f 0.55.

[PtCl(DMSO)(L6)] (11) and [PtCl(DMSO)(L7)] (12)

A solution of the respective ligand (0.47 mmol) in acetonitrile (10 ml), was added dropwise to a solution of *cis*-[$PtCl_2(DMSO)_2$] (0.47 mmol) in acetonitrile/dimethylsulfoxide (6 ml, 1:1 v/v) followed by sodium acetate (0.72 mmol) in water (1.5 ml). After a few hours a yellow precipitate was observed. The resulting solution was stirred for 3 days at room temperature. Water (100 ml) was then added and the mixture was placed in a refrigerator (4°C) overnight. The yellow precipitate was collected by filtration, washed with water, ethanol and dried *in vacuo* over silica gel. Crystals of **12**, suitable for X-ray crystallography were obtained by a double layer diffusion method, using benzene and hexane as solvents.

[PtCl(DMSO)(L6)]: IR (KBr pellet, cm^{-1}): 3010 (m, sh), 2958 (s, sh), 2919 (s, sh), 2866 (s), 2849 (s), 1528 (vs, sh), 1493 (vs, sh), 1434 (vs, sh), 1403 (s), 1389 (m – s), 1378 (m – s), 1351 (m – s), 1330 (m – s), 1312 (vs, sh), 1298 (s, shld), 1260 (s, sh), 1227 (s, sh), 1210 (s, sh), 1178 (s, sh), 1154 (s, sh), 1110 (s, sh), 1081 (m), 1032 (s), 1022 (s), 1002 (m), 981 (m – s, sh), 959 (m – s, sh), 877 (w – m, sh), 773 (w – m), 726 (w – m), 697 (m, sh), 651 (w), 559 (w), 522 (w), 501 (w), 453 (m – s). TLC [Silica gel, $CHCl_3$/EtOH (2%)]: R_f 0.62.

[PtCl(DMSO)(L7)]: IR (KBr pellet, cm^{-1}): 3010 (m, sh), 2957 (s, sh), 2921 (s, sh), 2852 (s), 1531 (vs, sh), 1486 (vs, sh), 1444 (vs, sh), 1350 (m – s), 1312 (vs, sh), 1262 (s, sh), 1226 (s, sh), 1210 (s, sh), 1179 (s, sh), 1153 (s, sh), 1112 (s, sh), 1083 (m), 1062 (s), 1024 (s, sh), 982 (s, sh), 960 (s, sh), 878 (m, sh), 841 (w – m), 772 (m, sh), 726 (m – s, sh), 697 (m – s, sh), 650 (w, sh), 597 (vw), 559 (w), 523 (w – m), 502 (w), 453 (s, sh), 380 (m – s). TLC [Silica gel, $CHCl_3$/EtOH (2%)]: R_f 0.62.

[PtCl(L4)((*S*)-MTSO)] (13)

A solution of **HL4** (0.115 g, 0.364 mmol) in acetonitrile (10 ml), was added dropwise to a solution of *cis*-[$PtCl_2$((*S*)-$MTSO)_2$](0.209 g, 0.364 mmol) in acetonitrile (6 ml), followed by sodium acetate (0.045 g, 0.546 mmol) in water (1.5 ml). The resulting solution was stirred for 3 days at room temperature. Water (100 ml) was then added to the orange solution, whereupon a fine yellow precipitate formed. This mixture was placed in a refrigerator (4°C) for a week. The precipitate was extracted into $CHCl_3$ (40 ml), dried over $MgSO_4$ and evaporated to dryness under reduced pressure to yield a brown oil. The oil was dissolved in ethanol and placed in a freezer for several days. The resultant yellow precipitate was collected by filtration, washed with water, ethanol and dried *in vacuo* over silica gel. IR (KBr pellet, cm^{-1}): 2930 (m, sh), 2935 (m, sh), 2866 (m, sh), 1682 (vs, sh), 1561 (s), 1554 (s), 1492 (m), 1459 (m), 1405 (m), 1379 (m), 1368 (m), 1327 (m), 1265 (vs, sh), 1244 (vs, sh), 1183 (s, sh), 1140 (s, sh), 1116 (s, sh), 1078 (s), 1037 (w – m), 1017 (w - m), 1002 (w – m), 985 (w – m), 971 (w – m), 957 (m), 945 (m), 949 (w), 919 (m), 813 (m – s, sh), 749 (m), 723 (m), 627 (m), 626 (m), 510 (s, sh), 502 (s, shld), 417 (w), 387 (w). TLC [Silica gel, $CHCl_3$/EtOH (2%)]: R_f 0.58.

4.12 References

1. J. H. Price, A. N. Williamson, R. F. Schramm, B. B. Wayland, *Inorg. Chem*., 1972, **11**, 1280.
2. P. S. Pregosin, *Coord. Chem. Rev*., 1982, **44**, 247.
3. K. R. Koch, M. C. Matoetoe, *Magn. Reson. Chem*., 1991, **29**, 1158.
4. *Handbook of Chemistry and Physics*, ed. R. C. Weast, CRC Press, Inc., 61st ed., Boca Raton, Fl. 33431, pp. F-218, 1980–1981.
5. E. Kleinpeter, S. Behrendt, L. Beyer, *Z. Anorg. Allg. Chem*., 1982, **495**, 105.
6. S. Behrendt, L. Beyer, F. Dietze, E. Kleinpeter, E. Hoyer, E. Ludwig, E. Uhlemann, *Inorg. Chim. Acta*, 1980, **43**, 141.
7. L. Beyer, E. Hoyer, J. Liebscher, H. Hartmann, *Z. Chem*., 1981, **21**, 81.
8. J. Hartung, G. Weber, L. Beyer, R. Szargan, *Z. Anorg. Allg. Chem*., 1985, **523**, 153.
9. K. R. Koch, J. du Toit, M. R. Caira, C. Sacht, *J. Chem. Soc., Dalton Trans*., 1994, 785.
10. N. Farrell, D. M. Kiley, W. Schmidt, M. P. Hacker, *Inorg. Chem*., 1990, **29**, 397.
11. J. March, in *Advanced Organic Chemistry*, John Wiley & Sons, Inc. New York, 4th edn., 1992.
12. S. G. de Almeida, J. L. Hubbard, N. Farrell, *Inorg. Chim. Acta*, 1992, **193,** 149.
13. J. A. Davies, *Adv. Inorg. Chem. Radiochem*., 1981, **24**, 115.
14. M. Calligaris, O. Carugo, *Coord. Chem. Rev*., 1996, **153**, 83 and references therein.
15. A. Irving, K. R. Koch, M. Matoetoe, *Inorg. Chim. Acta*, 1993, **206**, 193.
16. K. R. Koch, C. Sacht, S. Bourne, *Inorg. Chim. Acta*, 1995, **232**, 109.
17. Q. Chen, F. Boeheim, J. Dabrowiak, J. Zubieta, *Inorg. Chim. Acta*, 1994, **216**, 83.
18. K. J. Cavell, H. Jin, B. W. Skelton, A. H. White, *J. Chem. Soc., Dalton Trans*., 1993, 1973.
19. K. J. Cavell, H. Jin, B. W. Skelton, A. H. White, *J. Chem. Soc., Dalton Trans*., 1992, 2923.
20. L. J. McCaffrey, W. Henderson, B. K. Nicholson, J. E. Mackay, M. B. Dinger, *J. Chem. Soc., Dalton Trans*., 1997, 2577.
21. R. T. Boeré, N. C. Payne, C. J. Willis, *Can. J. Chem*., 1986, **64**, 1474.

22. W. Henderson, L. J. McCaffrey, B. K. Nicholson, *J. Chem. Soc., Dalton Trans*., 2000, 2753.
23. M. L.Tobe and J. Burgess, in *Inorganic Reaction Mechanisms*, Addison Wesley Longman Ltd, New york, 1999.
24. W. Kitching, C. J. Moore, D. Doddrell, *Inorg. Chem*., 1970, **9**, 541.
25. N. Farrell, *Chem. Commun*., 1982, 331.
26. K. R. Koch, T. Grimmbacher, C. Sacht, *Polyhedron*, 1998, **17**, 267.
27. S. O. Grim, R. L. Keiter, W. McFarlane, *Inorg. Chem*., 1967, **6**, 1133.
28. H. D. Flack, *Acta Crystallogr*., *Sect. A*, 1983, **39**, 876.
29. K. R. Koch, S. Bourne, *J. Mol. Struct.*, 1998, **441**, 11.
30. K. R. Koch, Y. Wang, A. Coetzee, *J. Chem. Soc., Dalton Trans*., 1999, 1013.
31. A. Pidcock, R. E. Richards, L. M. Venanzi, *J. Chem. Soc*. (A), 1966, 1707.
32. R. Favez, R. Roulet, A. A. Pinkerton, D. Schwarzenbach, *Inorg. Chem*., 1980, **19**, 1356.
33. C. J. Cobley, P. G. Pringle, *Inorg. Chim. Acta*, 1997, **265**, 107.
34. J. Emsley, D. Hall, in *The Chemistry of Phosphorus*, Harper & Row, Publishers, New York, 1976, ch. 4, pp. 142–143.
35. P. Mühl, K. Gloe, F. Dietze, E. Hoyer, L. Beyer, *Z. Chem*., 1986, **26**, 81.
36. L. Antolini, U. Folli, D. Iarossi, L. Schenetti, F. Taddei, *J. Chem. Soc., Perkin Trans. 2*, 1991, 955.
37. R. Melanson, F. D. Rochon, *Can. J. Chem*., 1975, **53**, 2371.
38. M. Schuster, B. Kugler, K. –H. König, *Fresenius' J. Anal. Chem*., 1990, **338**, 717.
39. G. Annibale, L. Cattalini, L. Canovese, B. Pitteri, A. Tiripicchio, M. Tiripicchio Camellini, M. L. Tobe, *J. Chem. Soc., Dalton Trans*., 1986, 1101.
40. P. B. Viossat, A. Michelet, P. Khodadad, N. Rodier, *Acta Crystallogr., Sect. C*, 1990, **46**, 1733.
41. L. E. Erickson, G. S. Jones, J. L. Blanchard, K. J. Ahmed, *Inorg. Chem*., 1991, **30**, 3147.
42. F. D. Rochon, P. C. Kong, R. Melanson, *Inorg. Chem*., 1990, **29**, 2708.
43. K. Lövqvist, Ph.D. Dissertation, Lund University, Sweden, 1996.
44. G. Marangoni, B. Pitteri, V. Bertolasi, P. Gilli, *Inorg. Chim. Acta*, 1995, **234**, 173.
45. Z. Bugarcic, K. Lövqvist, Å. Oskarsson, *Acta Chem. Scand*., 1993, **47**, 554.
46. W. A. Spofford, E. L. Amma, C. V. Senoff, *Inorg. Chem*., 1971, **10**, 2309.

47. G. W. Horn, R. Kumar, A. W. Maverick, F. R. Fronczek, S. F. Watkins, *Acta Crystallogr., Sect. C*, 1990, **45**, 135.
48. R. Bardi, A. M. Piazzesi, L. Sindellari, *Inorg. Chim. Acta*, 1981, **47**, 225.
49. S. Bourne, K. R. Koch, *J. Chem. Soc., Dalton Trans*., 1993, 2071.
50. G. M. Sheldrick, SHELXS-86, *Program for Crystal Structure Determination*, University of Göttingen, Germany, 1986.
51. G. M. Sheldrick, SHELXL-97, *Program for Crystal Structure Determination*, University of Göttingen, Germany, 1997.
52. G. M. Sheldrick, SHELXTL, *Program for Solving Crystal Structures*, University of Göttingen, Germany, 1995.
53. G. M. Sheldrick, SADABS, *Program for Absorption Corrections of Area Detector Data*, University of Göttingen, Germany, 1996.
54. G. M. Sheldrick, SHELXS97, *Program for Solving Crystal Structures*, University of Göttingen, Germany, 1997.
55. C. K. Johnson, *ORTEP II*, Report ORNL-5138, Oak Ridge National Laboratory, TN, USA, 1976.

CHAPTER 5

SUBSTITUTION REACTION KINETICS OF ACYLTHIOUREATO PLATINUM(II) SULFOXIDE COMPLEXES

5.1 Introduction

The rate of substitution of the leaving groups have been shown to be related to the toxicity and bioactivity of some platinum(II) complexes. [1] Hence, an understanding of the basic substitution reaction kinetics of these complexes is important to aid in the interpretation of more complex substitution kinetics encountered with biomolecules and the study of their mode of action. Furthermore, an understanding of the rates of reaction of these complexes with different nucleophiles could aid in the development of a structure-reactivity relationship for these complexes.

This chapter is concerned with the substitution kinetics of the *cis*-(S,S)-[Pt(acylthioureato)Cl(RR'SO)] complexes in order to:

i) Evaluate the factors affecting the substitution reaction kinetics of these complexes.

ii) To make a novel contribution to the knowledge of dimethylsulfoxide substitution in platinum(II) complexes.

The substitution kinetics of the *cis*-(S,S)-[Pt(acylthioureato)Cl(RR'SO)] complexes are complicated by the fact that the complexes possess two distinct possible monodentate leaving groups, namely the chloride and sulfoxide ligands. The substitution pattern of all the nucleophiles was confirmed by ^{1}H NMR spectroscopy. Less than one equivalent of the respective nucleophile was added to a solution of *cis*-(S,S)-[PtCl(DMSO)(L1a)] in deuterated methanol-d_4. The substitution products were determined by monitoring the coordinated sulfoxide resonance. The anionic nucleophiles (azide, iodide and thiocyanate) substitute the chloride ligand in the first substitution step, because no free sulfoxide was observed in the ^{1}H NMR spectrum, suggesting that the coordinated sulfoxide is not being substituted by the incoming nucleophile. Chloride substitution was further indicated by the presence of a new sulfoxide signal either upfield/downfield of the original sulfoxide signal, depending on the incoming nucleophile. On addition of neutral nucleophiles (PPh_3, thiourea, DMAP and MBI), free dimethylsulfoxide was immediately observed in the ^{1}H NMR spectrum, suggesting that these nucleophiles substitute the sulfoxide initially.

The substitution kinetics of the anionic and neutral nucleophiles will be presented as follows:

i) Part A: Anionic nucleophiles.
ii) Part B: Neutral nucleophiles.
iii) Overall discussion.

As an introduction, some theoretical aspects of the substitution reaction kinetics involving square-planar platinum(II) complexes are considered.

5.1.1 Substitution reactions of square-planar metal complexes

In bimolecular, nucleophilic substitution reactions involving metal complexes, the composition of the metal's coordination sphere changes is depicted schematically in equation (**5 – 1**), (ignoring any equilibria and possible parallel pathways), where T and C are the ligands *trans* and *cis* to the leaving group X.

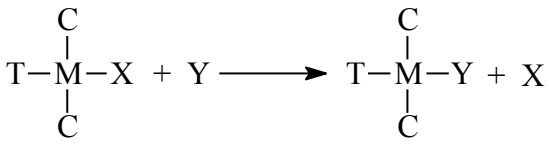

(**5 – 1**)

The *cis* and *trans* groups relative to the leaving group give rise to the *cis*- and *trans*-effects, respectively. [2] The substitution of X for Y is stereospecific and generally occurs via an associative mechanism.

The rates of substitution reactions vary from mixing times to years. Reactions with a half-life ($t_{½}$) of less than 30 seconds are usually termed labile and those with longer half-lives are termed inert. The study of the rates of slow reactions can be followed by conventional techniques such as UV/Vis spectrophotometry, while faster labile reactions require expensive and specialised equipment. Stopped-flow, P-jump and T-jump techniques are generally used for the study of fast reactions. [3]

Metal ions with d^8 configurations [Au(III), Ni(II), Pd(II), Pt(II), Rh(I) and Ir(I)] generally form square-planar complexes with strong-field ligands. A large number of kinetic

studies have been carried out on Pt(II), Pd(II) and Au(III) complexes due to these metal ions having moderate reaction rates that are conveniently followed by conventional methods. Pt(II) has a more stable oxidation state than Rh(I) and Ir(I) and always forms square-planar complexes. Fewer studies of substitution reactions of Ni(II), Rh(I) and Ir(I) complexes have been reported due to their exceptionally fast reaction rates. [3]

The direct result of a kinetic study is the rate of the reaction and this can be expressed in terms of factors affecting the rate of substitution such as temperature, pressure, solvent and as a function of the concentrations of the reactive species. The kinetic data can provide information concerning the reaction pathway through which the reaction proceeds. The thermodynamic data are concerned with the beginning and end of the reaction and not the reaction pathway. A more detailed reaction mechanism can be proposed using both the kinetic and thermodynamic data.

The substitution reaction kinetics of most d^8 transition metal complexes occur via an associative mode of activation (Figure 5.1), involving the formation of a five-coordinate trigonal bipyramidal transition-state complex rather than a dissociative mode of activation involving an unfavourable three-coordinate transition-state. This is due to the fact that d^8 metal complexes are coordinately unsaturated and have a classic 16-electron valence shell. The lack of steric crowding and the availability of an empty p_z-orbital perpendicular to the molecular plane, therefore, aids in the formation of a transition-state complex with a stable 18-electron valence shell. [4] Available kinetic evidence supports this mechanism, which is widely accepted. [5–11] Dissociative modes of activation are uncommon and were not reported until recently. The first clear demonstration of a dissociative mode of activation in square-planar d^8 metal complexes has been provided by studies of the substitution kinetics of sulfoxides and thioethers by chelating ligands in complexes of the type *cis*-$[PtR_2L_2]$, where R = Me, phenyl and L = DMSO, RR'S. [12–15]

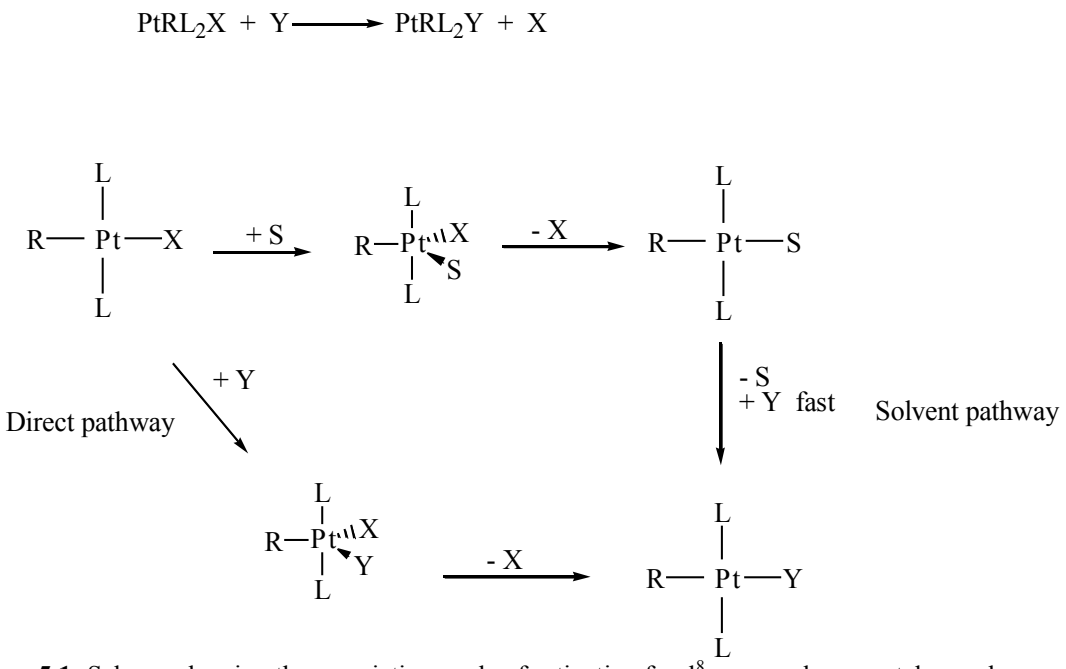

Figure 5.1: Scheme showing the associative mode of activation for d^8 square-planar metal complexes.

The rate of a reaction is determined by the slowest step (rate-determining step) in the overall reaction. The rate law of a reaction can be determined by monitoring either the formation of products or the disappearance of the reactants with time. For a simple reaction such as

$$\mathbf{A + B} \xrightarrow{k_1} \mathbf{C}$$

The rate is given by

$$\text{Rate} = R = \frac{\text{d[products]}}{\text{dt}} = -\frac{\text{d[reactants]}}{\text{dt}} = k_1[\text{A}]^{\text{M}}[\text{B}]^{\text{N}} \qquad \textbf{(5 – 2)}$$

where k_1 is the rate constant which relates the rate of reaction to the concentration of reactants. The values M and N represent the order of the reaction with respect to the concentration of A and B. The overall order of the reaction is given by M + N. These values can be difficult to determine experimentally, but this can be circumvented by making use of pseudo first-order reaction conditions, in which [B] >> [A], so that equation (**5 – 2**) becomes

$$\text{Rate} = k_{obs}[\text{A}] \text{ and } k_{obs} = k_1[\text{B}] \qquad \textbf{(5 – 3)}$$

where k_{obs} is the observed pseudo first-order rate constant and k_1 is the second-order rate constant.

Therefore, the general mechanism shown in Figure 5.1, gives rise to a two-term rate law (equation **5 – 4**) where k_y is the second-order rate constant for the direct pathway and k_s is the pseudo first-order rate constant for the solvent pathway.

$$\text{Rate} = (k_s + k_y[\text{Y}])[\text{ML}_3\text{X}] \qquad \textbf{(5 – 4)}$$

If the steps in the scheme shown in Figure 5.1 are reversible, the reaction may be represented as shown in Figure 5.2.

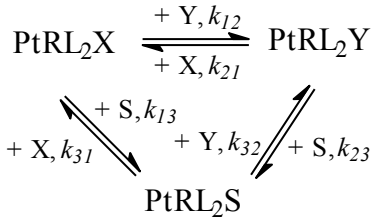

Figure 5.2: Schematic representation of a square-planar substitution reaction involving reversible steps.

To derive a rate equation for this scheme, the species depicted in Figure 5.2 were numbered in the following way: $PtRL_2X$ = 1, $PtRL_2Y$ = 2 and $PtRL_2S$ = 3 (S = solvent molecule). The subscripts of the rate constants denote the number of the species involved during the specific reaction, e.g. k_{12} describes the rate constant for the reaction going from 1 to 2.

The rate expression for the formation of $[PtRL_2Y]$ can be written as:

$$R = k_{12}[\text{Y}][PtRL_2X] + k_{32}[\text{Y}][PtRL_2S] - k_{21}[\text{X}][PtRL_2Y] - k_{23}[\text{S}][PtRL_2Y] \qquad \textbf{(5 – 5)}$$

For pseudo first-order conditions in both [X] and [Y], the steady-state approximation can be used for $[PtRL_2S]$, provided that $k_{32}[\text{Y}]k_{31}[\text{X}] >> k_{13}k_{23}$.

$$\frac{d[PtRL_2S]}{dt} = 0 = k_{13}[PtRL_2X] + k_{23}[PtRL_2Y] - k_{31}[X][PtRL_2S] - k_{32}[Y][PtRL_2S]$$

$$\therefore [PtRL_2S] = \frac{k_{13}[PtRL2X] + k_{23}[PtRL2Y]}{k_{31}[X] + k_{32}[Y]} \qquad (\mathbf{5-6})$$

Set $(\mathbf{5-6})$ in $(\mathbf{5-5})$:

$$R = k_{12}[Y][PtRL_2X] + \frac{k_{32}k_{13}[Y][PtRL_2X] + k_{23}k_{32}[Y][PtRL_2Y]}{k_{31}[X] + k_{32}[Y]} - k_{21}[X][PtRL_2Y] - k_{23}[S][PtRL_2Y]$$

$$R = k_{12}[Y][PtRL_2X] - k_{21}[X][PtRL_2Y] + \frac{k_{32}k_{13}[Y][PtRL_2X] + k_{23}k_{32}[Y][PtRL_2Y] - k_{23}k_{31}[X][PtRL_2Y] - k_{23}k_{32}[Y][PtRL_2Y]}{k_{31}[X] + k_{32}[Y]}$$

$$= k_{21}[Y][PtRL_2X] - k_{21}[X][PtRL_2Y] + \frac{k_{32}k_{13}[Y][PtRL_2X] - k_{23}k_{31}[X][PtRL_2Y]}{k_{31}[X] + k_{32}[Y]}$$

$$= k_{21}[Y][PtRL_2X] - k_{21}[X][PtRL_2Y] - \frac{k_{23}k_{31}[X][PtRL_2Y] - k_{32}k_{13}[Y][PtRL_2X]}{k_{31}[X] + k_{32}[Y]}$$

Integration gives :

$$k_{obs} = k_{12}[Y] + k_{21}[X] + \frac{k_{23}k_{31}[X] + k_{32}k_{13}[Y]}{k_{31}[X] + k_{32}[Y]} \qquad (\mathbf{5-7})$$

Also, at equilibrium, the direct and solvent routes are synchronised, giving :

$$K_{eq} = \frac{k_{12}}{k_{21}} = \frac{k_{13}k_{32}}{k_{23}k_{31}} \qquad (\mathbf{5-8})$$

Substitute for k_{21} and k_{23} from $(\mathbf{5-8})$ into $(\mathbf{5-7})$:

$$k_{obs} = k_{12}[Y]\frac{k_{12}}{K_{eq}}[X] + \frac{\frac{k_{13}}{K_{eq}}\frac{k_{32}}{k_{31}}k_{31}[X] + k_{32}k_{13}[Y]}{k_{31}[X] + k_{32}[Y]} \qquad (\mathbf{5-9})$$

If all steps are considered as non - equilibrium reactions :
K_{eq} = large and $k_{31} \approx k_{23} \approx 0$
Then (**5 – 9**) simplifies to:

$$k_{obs} = k_{12}[\mathrm{Y}] + 0[\mathrm{X}] + \frac{0[\mathrm{X}] + k_{32}k_{13}[\mathrm{Y}]}{0[\mathrm{X}] + k_{32}[\mathrm{Y}]}$$
$$= k_{12}[\mathrm{Y}] + k_{13} \qquad \textbf{(5 – 10)}$$

This is the typical rate law obtained for simple square-planar substitution kinetics (equation (**5 – 4**)). The rates of the direct and solvolytic pathways are described in terms of the rate constants k_{12} and k_{13}, $k_{12} = k_y$ and $k_{13} = k_s$ in equation (**5 – 4**), respectively.

5.1.2 Thermodynamic parameters

The effect of temperature on the rate of a chemical reaction is usually described by the Arrhenius equation (equation (**5 – 11**)), shown below, which relates the rate constant, *k*, to the absolute temperature, *T:*

$$k = A \exp(-E_a / RT) \qquad \textbf{(5 – 11)}$$

where A = pre-exponential factor, E_a = activation energy and R = universal gas constant.

A similar relationship is also derived from absolute reaction rate theory, which is used almost exclusively in the kinetics of reactions in solution. [16] Consider the following reaction.

$$\mathrm{A} + \mathrm{B} \overset{K_c^{\neq}}{\rightleftharpoons} (\mathrm{AB})^{\neq} \xrightarrow{k} \text{products}$$

The transition-state complex is assumed to be in equilibrium with the reactants A and B before the reaction occurs and a product is formed. The rate of the reaction, *R*, is given by the rate of decomposition of the transition-state complex into the product, and is expressed as the product of the equilibrium concentration of $(\mathrm{AB})^{\neq}$ and the specific rate constant (k).

$$k = \frac{k_b T}{h} K_c^{\neq} \qquad \textbf{(5 – 12)}$$

where k_b = Boltzmann's constant and h = Planck's constant

Furthermore, on the assumption that the formation of the transition-state complex may be regarded as an equilibrium process, the Gibbs free energy of activation ($\Delta G^{\neq}$), as well as the enthalpy of activation ($\Delta H^{\neq}$) and the entropy of activation ($\Delta S^{\neq}$) may be derived, as in normal thermodynamics,

$$\Delta G^{\neq} = -RT\ln K^{\neq}_c = \Delta H^{\neq} - T\Delta S^{\neq} \qquad \textbf{(5 – 13)}$$

leading to

$$k = \frac{k_b T}{h} \exp\left(\frac{-\Delta G^{\neq}}{RT}\right) = \frac{k_b T}{h} \exp\left(\frac{-\Delta H^{\neq}}{RT}\right) \exp\left(\frac{+\Delta S^{\neq}}{R}\right) \qquad \textbf{(5 – 14)}$$

Therefore

$$\ln\left(\frac{k}{T}\right) = \ln\left(\frac{k_b}{h}\right) + \left(\frac{\Delta S^{\neq}}{R}\right) - \left(\frac{-\Delta H^{\neq}}{RT}\right) \qquad \textbf{(5 – 15)}$$

Thus a plot of $\ln\left(\frac{k}{T}\right)$ against $\frac{1}{T}$ will give :

$$\text{a slope} = \frac{-\Delta H^{\neq}}{\mathrm{R}} \qquad \textbf{(5 – 16)}$$

$$\text{y-intercept} = \frac{\Delta S^{\neq}}{R} + \ln\left(\frac{K_b}{h}\right) \qquad \textbf{(5 – 17)}$$

This plot is referred to as an Eyring plot.

The enthalpy and entropy of activation derived from the temperature dependence of the rate constant can suggest the mode of activation for the reaction being studied. The entropy of activation reflects the amount of disorder in the transition-state complex. Therefore, large positive entropies of activation are highly suggestive of a dissociative

mechanism, whereas large negative entropies of activation reflect an associative mechanism.

It must be noted that care must be taken in the interpretation of the activation parameters, because, for example, if the reaction contains an equilibrium step preceding the activation step, the parameters obtained are a composite of all the steps up to and including the activation step. [17]

5.2 Kinetics of dimethylsulfoxide substitution

This section gives a short account of dimethylsulfoxide substitution from platinum(II) complexes. Emphasis will be placed on the factors affecting the rate and mechanism of the substitution reaction.

It is generally accepted that the substitution of a single sulfur-bonded sulfoxide is difficult, whereas the substitution of one sulfoxide from a complex containing two sulfoxide ligands *cis* to one another occurs more easily. Kinetic analyses of the substitution of two *cis*-sulfoxides in the complex, $[Pt(en)(DMSO)_2]^{2+}$, with various nucleophiles in methanol and water at 30°C, were carried out by Romeo *et al*.. [18] In aqueous and methanolic solutions, one dimethylsulfoxide was found to be readily substituted by the solvent or any other nucleophile studied, while the second remained bound even in the presence of an excess of a strong nucleophile such as thiourea. The lability of the dimethylsulfoxide was found to be comparable to that of water. The mutual labilisation of a pair of sulfoxides has been ascribed to the ability of sulfur-bonded sulfoxides to act as π-acceptors, which stabilises the five-coordinate transition-state complex.

The *cis*-effect [19] of sulfur-bonded dimethylsulfoxide was determined by evaluating the rates of chloride substitution in a series of ethylenediamine platinum(II) complexes of the type, $[PtCl(en)(L)]^+$, where L = DMSO or NH_3, in water with a variety of nucleophiles according to reactions (**5 – 18**) and (**5 – 19**) below.

$$[Pt(en)(DMSO)Cl]^{+} + X^{-} \longrightarrow [Pt(en)(DMSO)X]^{+} + Cl^{-} \qquad \textbf{(5 – 18)}$$

$$[Pt(en)(NH_3)Cl]^{+} + X^{-} \longrightarrow [Pt(en)(NH_3)X]^{+} + Cl^{-} \qquad \textbf{(5 – 19)}$$

Ring-opening of the ethylenediamine chelate was found to be not significant, with the rate-determining step being chloride displacement. No dimethylsulfoxide substitution was observed. The rates of chloride substitution were significantly different for the two complexes depicted in equations (**5 – 18**) and (**5 – 19**), with the chloride ligand *cis* to dimethylsulfoxide being more labile, by an order of magnitude, compared to the ammine complex.

Although the inertness of a single dimethylsulfoxide ligand is well known, studies have shown that there are a few cases in which a single dimethylsulfoxide can be readily substituted. For example, when the ethylenediamine ligand in the complex, $[Pt(en)(DMSO)Cl]^{+}$, is substituted for *N,N,N',N'*-tetramethylethylenediamine, labilisation of the bonded dimethylsulfoxide occurred in the solid state and in solution. [20] In solution the dimethylsulfoxide substitution was found to be solvent dependent. In solvents with low dielectric constants, such as chloroform and dichloromethane, dimethylsulfoxide liberation was observed, according to the following two-step reaction:

$$[Pt(Me_4en)(DMSO)Cl]^{+} + X^{-} \xrightarrow{\text{fast}} [Pt(Me_4en)(DMSO)X]^{+} + Cl^{-} \qquad \textbf{(5 – 20)}$$

$$[Pt(Me_4en)(DMSO)X]^{+} + X^{-} \xrightarrow{\text{slow}} [Pt(Me_4en)X_2] + DMSO \qquad \textbf{(5 – 21)}$$

where $X^{-} = Cl^{-}$, Br^{-} and I^{-}.

The first step involves the very fast displacement of the chloride ligand, followed by a slower rate-determining dimethylsulfoxide substitution step. In aqueous or protic solutions, the behaviour of $[Pt(Me_4en)(DMSO)Cl]^{+}$ resembled that of the $[Pt(en)(DMSO)Cl]^{+}$ complex discussed above. When $[Pt(Me_4en)(DMSO)Cl]^{+}$ is reacted with a series of nucleophiles (Br^{-}, I^{-}, $SeCN^{-}$ and thiourea) in aqueous solution only chloride substitution was observed, except that the reaction of the ethylenediamine complexes was approximately two orders of magnitude faster than that of the tetramethylated analogue. The authors explained that this might be due to steric crowding

of the transition-state complex by the bulky, substituted ethylenediamine ligand. Upon changing the solvent from water to chloroform and dichloromethane, liberation of dimethylsulfoxide was observed. This is not just a rate acceleration accompanying change of solvent, because, even in the presence of uncharged strong nucleophiles such as thiourea and triphenylphosphine, no dimethylsulfoxide substitution was observed in aqueous solution. The substitution of the dimethylsulfoxide in non-polar solvents was explained in terms of an ion-pair mechanism.

The above example clearly demonstrates that the lability of coordinated dimethylsulfoxide is dependent on the nature of the non-leaving group. Knowledge of the effect of the non-leaving group was extended further when Cattalini and Tobe [21] evaluated the substitution kinetics of complexes of the type $[Pt(N\text{-}N)(DMSO)X]^+$, where N-N is 1,10-phenanthroline, 2,2'-bipyridyl, or 2,2-bis(2'-pyridyl)-1,3-dioxolane, with excess halide X (Br^-, Cl^-) in methanol/water (95:5 (v/v)) at 25°C. α-Diimines were found to have a considerable labilising effect when compared to other nitrogen donors such as ethylenediamine or even *cis*-monodentate amines. In other words, the displacement of dimethylsulfoxide from $[Pt(N\text{-}N)(DMSO)X]^+$, where N-N is an α-diimine, is easier than from the corresponding ethylenediamine or monodentate amine complexes, in which no dimethylsulfoxide exchange was observed.

Comparison of the rates of isotopic exchange of the dimethylsulfoxide at 25°C in the two complexes shown below, also shows that ligands with π-bonding abilities have a labilising effect on the coordinated sulfoxide. [22]

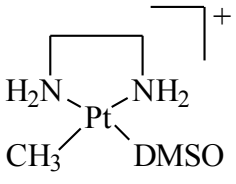

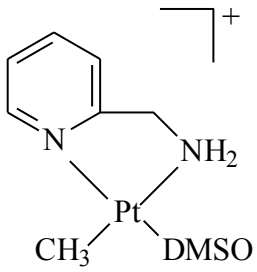

$k_y = (9.49 \pm 0.05) \times 10^{-6}\ M^{-1}\ s^{-1}$ $k_y = (3.5 \pm 0.3) \times 10^{-3}\ M^{-1}\ s^{-1}$

The rate of dimethylsulfoxide substitution in the ethylenediamine complex is about 300 times slower than in the 2-(aminomethyl)pyridine complex in which the pyridine moiety

is *trans* to the sulfoxide. Similar results were obtained for the substitution of water from complexes of the type $[Pt(N\text{-}N)(H_2O)]^{2+}$, where N-N is 1,10-phenanthroline or ethylenediamine. [23] The use of phenanthroline, instead of ethylenediamine, increased the substitution rate of the diaqua complexes by two orders of magnitude, thus confirming the *trans*-labilising nature of ligands with π-bonding properties.

There is also a dependence on the basicity of the non-leaving group. When the pK_a values of substituted phenanthrolines were varied in a series of complexes of the type $[Pt(R\text{-}phen)(CH_3)(DMSO)]^+$, there was a significant decrease in the rate of substitution with an increase in basicity. According to the authors, this decrease in reactivity is due to a decrease in electrophilicity of the metal centre. [22]

An extensive kinetic study was carried out to try and gain some insight into the affect of solvation on the rate of dimethylsulfoxide exchange. [24] An organometallic complex was prepared in which the only possible leaving group was the dimethylsulfoxide ligand and the substitution of dimethylsulfoxide from this cationic complex, $[Pt(phen)(CH_3)(DMSO)]^+$, by a series of uncharged and anionic nucleophiles, was determined in a wide range of solvents: methanol, water, ethanol, acetonitrile, acetone, *N*-methylformamide and methanol:water (19:1 (v/v)). [24] The rate of dimethylsulfoxide substitution was found to be strongly solvent dependent, with reactivities ranging over several orders of magnitude. The solvent contribution to the reactivity of $[Pt(phen)(CH_3)(DMSO)]^+$ arising from the solvolytic pathway was negligible, except for acetone and acetonitrile. No correlation between the rate of substitution and the ionizing power (dielectric constant), or the donor properties (Gutmann donor number), of the respective solvents could be found. On the other hand, correlations with parameters describing the electrophilicity or Lewis acidity (acceptor numbers, Dimroth-Reichart's ET and Taft's α) of the solvents were found. Furthermore, a good correlation was found with the change in the molar Gibbs free energies of transfer ($\Delta G_t°$) for chloride from acetonitrile to the other solvents. This linear free-energy relationship (LFER) suggests that the observed rate differences are due to differences in solvation energy of the chloride nucleophile in various solvents and are not due to the solvation of the cationic complex.

Similarly, the nucleophilic discrimination factor was also found to be dependent upon the solvent. In protic solvents, $[Pt(phen)(CH_3)(DMSO)]^+$ exhibited a high degree of nucleophilic discrimination, while in dichloromethane there was a loss of discrimination ability due to ion-pair formation.

In summary, the non-leaving group has a significant effect on the lability of sulfur-bonded sulfoxides. In aqueous or methanolic solutions of $[Pt(am)_2(Cl)(DMSO)]^+$, where am = diamine or monodentate amines, only chloride substitution was observed, with no dimethylsulfoxide substitution, except for when substituted ethylenediamines were used. Ligands with π-properties, such as 1,10-phenanthroline and 2,2'-bipyridine, have been shown to have a labilising effect on the coordinated sulfoxide. There is also a dependence of the rate of dimethylsulfoxide substitution on the basicity of the non-leaving group.

5.3 Experimental

5.3.1 Materials

Sodium thiocyanate (NaSCN), sodium azide (NaN_3), sodium iodide (NaI), thiourea, 4-(dimethylamino)pyridine (DMAP), (Aldrich), triphenylphosphine (PPh_3), (Fluka), 2-mercaptobenzimidazole (MBI), (Merck), and tetraphenylphosphonium chloride (Aldrich) were purchased in the highest purity grade commercially available. Dimethylsulfoxide (Merck) was dried over 3Å molecular sieves before use. All solvents were analytical grade and were dried and freshly distilled before use.

5.3.2 Physical methods

Preliminary kinetic traces were recorded on a Hitachi 150-20 spectrophotometer in the wavelength range 350–450 nm. The rates of reaction were followed by repetitive scanning of the spectrum at fixed wavelengths, where the difference in absorbance was the greatest. Kinetic measurements, unless otherwise stated, were carried out in methanol at 25°C. Final platinum concentrations, $[Pt]_F$, for all kinetic runs were kept at 0.5 mM, except for the reaction of *cis*-(S,P)-$[PtCl(L1a)(PPh_3)]$ with PPh_3, in which the $[Pt]_F$ = 0.25 mM due to the low solubility of this complex in methanol. All kinetic measurements

were performed under pseudo first-order conditions. Classic square-planar substitution kinetics was assumed unless otherwise stated and motivated. Pseudo first-order rate constants (k_{obs}/ s^{-1}) were obtained from a non-linear least-squares fit of the experimental data by $A_t = A_\infty + (A_0 - A_\infty)\exp(-k_{obs}t)$, with A_0, A_∞ and k_{obs} as parameters to be optimised, where A_0 = absorbance at $t = 0$ and A_∞ = absorbance at completion of reaction. For the labile reactions, each k_{obs} was determined as the average of at least four measurements. The rate constants for the direct pathway (k_y) and the solvent pathway (k_s) for the first substitution step, were determined from least-square fits of the plots of k_{obs} against concentration of incoming nucleophile, according to equation (**5 – 10**). The equilibrium constants for dimethylsulfoxide substitution by PPh_3 from *cis*-(S,S)-[PtCl(DMSO)(L1a)] were estimated using ^{1}H NMR, according to equation (**5 – 22**),

$$K_{eq} = [PtCl(L1a)(PPh_3)][DMSO]/[PtCl(DMSO)(L1a)][PPh_3] \qquad (\mathbf{5 - 22})$$

The rate constants and equilibrium constants for the second substitution step involving PPh_3 and DMAP were estimated according to equation (**5 – 9**). The pseudo first-order rate constants are given in Appendix B.

Chloride substitution from the respective platinum complexes by azide, iodide and thiocyanate was followed at 375 nm. Dimethylsulfoxide substitution by DMAP, MBI and thiourea was followed at 380 nm. Dimethylsulfoxide substitution by PPh_3 was followed at 370 or 357 nm. The second consecutive reactions (chloride substitution) for DMAP and PPh_3 were followed at 380 and 400 nm, respectively. The effect of the solvent on dimethylsulfoxide and chloride substitution by PPh_3 from *cis*-(S,S)-[PtCl(DMSO)(L1a)] was also evaluated in acetonitrile (380 nm), acetone (390 nm) and dichloromethane (380 nm). Selective variation of the leaving groups (chloride and dimethylsulfoxide) was also carried out to determine the possible influence thereof on the overall rate of the reaction.

The reaction with azide was initiated by mixing equal amounts of prethermostated solutions of the respective complexes and incoming nucleophile in a quartz cuvette in the thermostated cell compartment of a GBC UV-Vis 916 or CARY 50 Conc spectrophotometer. The kinetic traces were evaluated using the program Scientist for

Windows. [25] All the other reactions, were followed using a DURRUM 110 spectrophotometer or an Applied Photophysics SZ, 18 MV Stopped Flow System coupled to a TIDAS 16-500 J&M Diode Array System. The kinetic traces were evaluated using OLIS, [26] and an Applied Photophysics SZ, 18 MV Stopped Flow Reaction Analyser, respectively.

PART A: ANIONIC NUCLEOPHILES

5.4 Results

The substitution of the chloride ligand by various anionic nucleophiles from complexes of the type *cis*-(S,S)-[Pt(acylthioureato)Cl(RR'SO)], according to equation (**5 – 23**), will now be discussed.

cis-(S,S)-[PtCl(L)(RR'SO)] + Y^- ⟶ *cis*-(S,S)-[Pt(L)(RR'SO)(Y)] + Cl^- (**5 – 23**)

5.4.1 Effect of the incoming nucleophile

5.4.1.1 Substitution kinetics of cis-(S,S)-[PtCl(DMSO)(L1a)]

The substitution of the chloride ligand from *cis*-(S,S)-[PtCl(DMSO)(L1a)] by azide, iodide and thiocyanate, according to equation (**5 – 23**), gave linear plots of k_{obs} against [Y] and are shown in Figure 5.3. The first-order rate constant, $k_{13} = k_s$, for the solvolytic pathway and second-order rate constant, $k_{12} = k_y$, for the direct pathway were calculated from these plots according to equation (**5 – 10**), and are reported in Table 5.1.

Table 5.1: Rate constants for chloride substitution from *cis*-(S,S)-[PtCl(DMSO)(L1a)] by azide, iodide and thiocyanate in methanol at 25°C.

Nucleophile	k_y/ $M^{-1}s^{-1}$	k_s/ s^{-1}
N_3^-	0.0724(7)	0.00144(4)
I^-	1.16(3)	0.005(2)
SCN^-	4.47(15)	0.012(9)

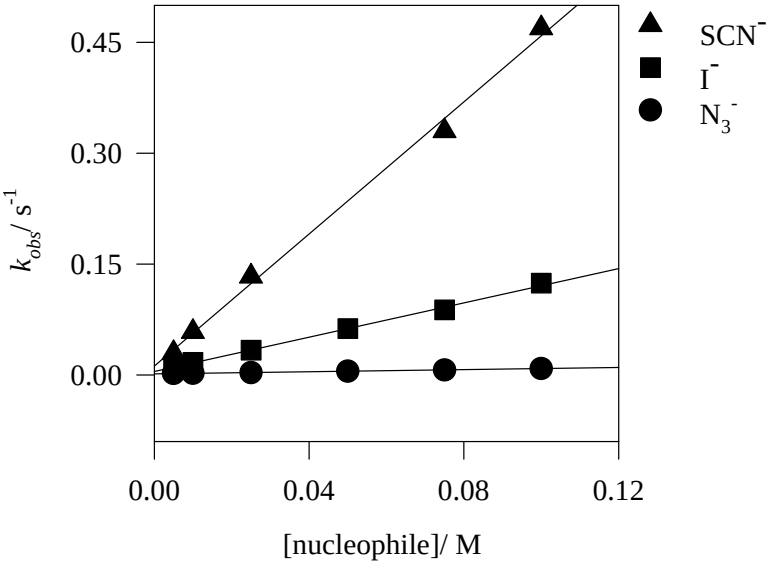

Figure 5.3: Concentration dependence for chloride substitution from *cis*-(S,S)-[PtCl(DMSO)(L1a)] by iodide, thiocyanate and azide in methanol at 25ºC. $[Pt]_F$ = 0.5 mM. λ = 375 nm. The pseudo first-order rate constants are given in Appendix B, Tables B1–3.

A relatively large dependence of the rate on the incoming anionic nucleophile (62 times) is observed. The order of reactivity was, $N_3^- < I^- < SCN^-$.

5.4.2 *cis*-Effect of the sulfoxide on chloride substitution

The *cis*-effect of the sulfoxide ligand on chloride substitution by azide in *cis*-(S,S)-[PtCl(L1a)(RR'SO)], where RR'SO = DMSO, (*S*)-MTSO and MPSO, was evaluated in methanol. Only the (*S*)-MTSO enantiomer was studied because the (*R*)-MTSO is expected to have the same kinetic properties. The plots of k_{obs} against [azide] in methanol at 25°C are given in Figure 5.4, for the *cis*-(S,S)-[PtCl(L1a)(RR'SO)] complexes, where RR'SO = DMSO, (*S*)-MTSO and MPSO. The rate constants for the solvolytic pathway, k_s, and for the direct pathway, k_y, were calculated from these plots and are reported in Table 5.2.

Table 5.2: Rate constants for chloride substitution by azide from *cis*-(S,S)-[PtCl(L1a)(RR'SO)] in methanol at 25°C.

RR'SO	k_y/ $M^{-1}s^{-1}$	k_s/ s^{-1}
DMSO	0.0724(7)	0.00144(4)
(*S*)-MTSO	0.078(2)	0.0013(1)
MPSO	0.099(6)	0.0008(3)

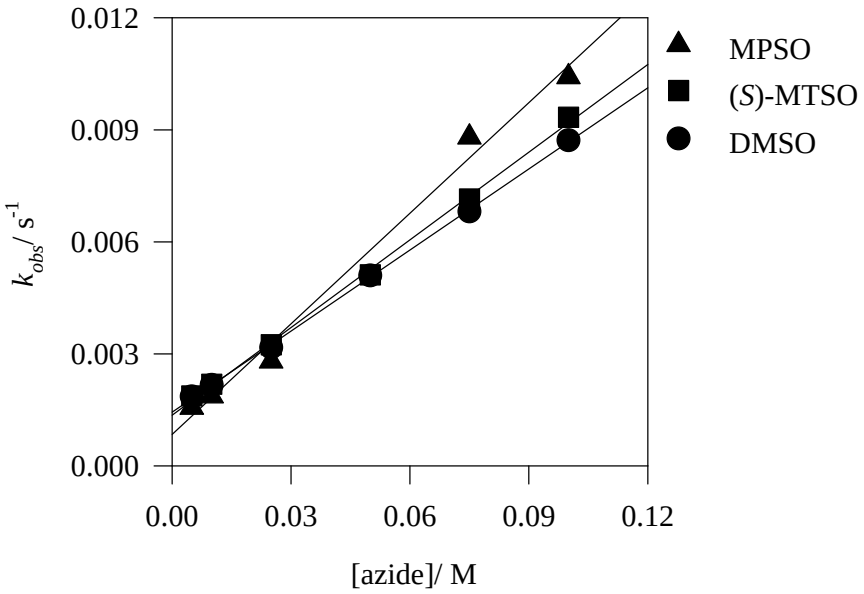

Figure 5.4: Concentration dependence for chloride substitution by azide from *cis*-(S,S)-[PtCl(L1a)(RR'SO)] in methanol at 25ºC. $[Pt]_F$ = 0.5 mM. λ = 375 nm. The pseudo first-order rate constants are given in Appendix B, Tables B1, B4 and B5.

The *cis*-effect of the respective sulfoxides on chloride substitution by azide from *cis*-(S,S)-[PtCl(L1a)(RR'SO)] decreases in the order, MPSO > (*S*)-MTSO > DMSO.

5.4.3 Electronic effects on chloride substitution

5.4.3.1 Effect of 3-benzoyl substitution

Various complexes with 3-substituted benzoyl moieties on the functionalised bidentate thiourea ligand (Figure 4.1) were prepared with electron-withdrawing and electron-donating groups, in order to evaluate how these electronic properties affect the substitution kinetics of these platinum(II) complexes. The substitution kinetics of *cis*-

(S,S)-[PtCl(DMSO)(L)], where HL = *N*-(3-*R*-benzoyl)-*N'*,*N'*-diethylthiourea (R = NO_2, Cl, H, OCH_3 and CH_3), with azide were studied in methanol at 25°C. The plots of k_{obs} against [azide] are given in Figure 5.5 and the rate constants are given in Table 5.3.

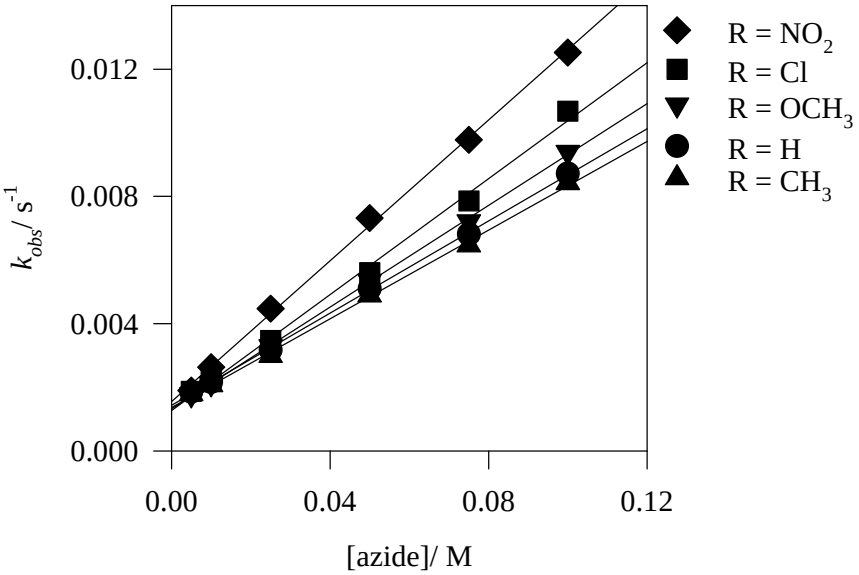

Figure 5.5: Concentration dependence for chloride substitution by azide from *cis*-(S,S)-[PtCl(DMSO)(L)], where L = *N*-(3-*R*-benzoyl)-*N'*,*N'*-diethylthioureato, in methanol at 25°C. $[Pt]_F$ = 0.5 mM. λ = 375 nm. The pseudo first-order rate constants are given in Appendix B, Table B6.

Table 5.3: Rate constants for chloride substitution by azide from *cis*-(S,S)-[PtCl(DMSO)(L)], where L = *N*-(3-*R*-benzoyl)-*N'*,*N'*-diethylthioureato, in methanol at 25°C.

R-Group	k_y/ M^{-1}s^{-1}	k_s/ s^{-1}
H	0.0724(7)	0.00144(4)
Cl	0.091(3)	0.0013(2)
NO_2	0.110(2)	0.0015(1)
CH_3	0.070(1)	0.00136(7)
OCH_3	0.0799(9)	0.00132(5)

For *cis*-(S,S)-[PtCl(DMSO)(L)] complexes, where HL = *N*-(3-*R*-benzoyl)-*N'*,*N'*-diethyl-thiourea, the chloride reactivity decreases in the order: R = NO_2 > Cl > OCH_3 ≈ H ≈ CH_3.

5.4.3.2 Effect of the amine

To evaluate the effect of the amine moiety on chloride substitution by azide in methanol at 25°C, complexes with diethylamine, morpholine and di(2-hydroxyethyl)amine functionalities on the bidentate ligand were introduced. Due to the low solubility of the *N*-benzoyl-*N'*-morpholinothiourea complex (**2a**) in methanol, kinetic data were only obtained for the *N*-benzoyl-*N',N'*-diethylthiourea (**1a**) and *N*-benzoyl-*N',N'*-di(2-hydroxyethyl)thiourea (**3a**) complexes. Only the initial chloride substitution reaction was studied. The kinetic behaviour of *cis*-(S,S)-[PtCl(DMSO)(L3a)] was analogous to that of *cis*-(S,S)-[PtCl(DMSO)(L1a)]. The plots of k_{obs} against [azide] are shown in Figure 5.6 and the rate constants are given in Table 5.4.

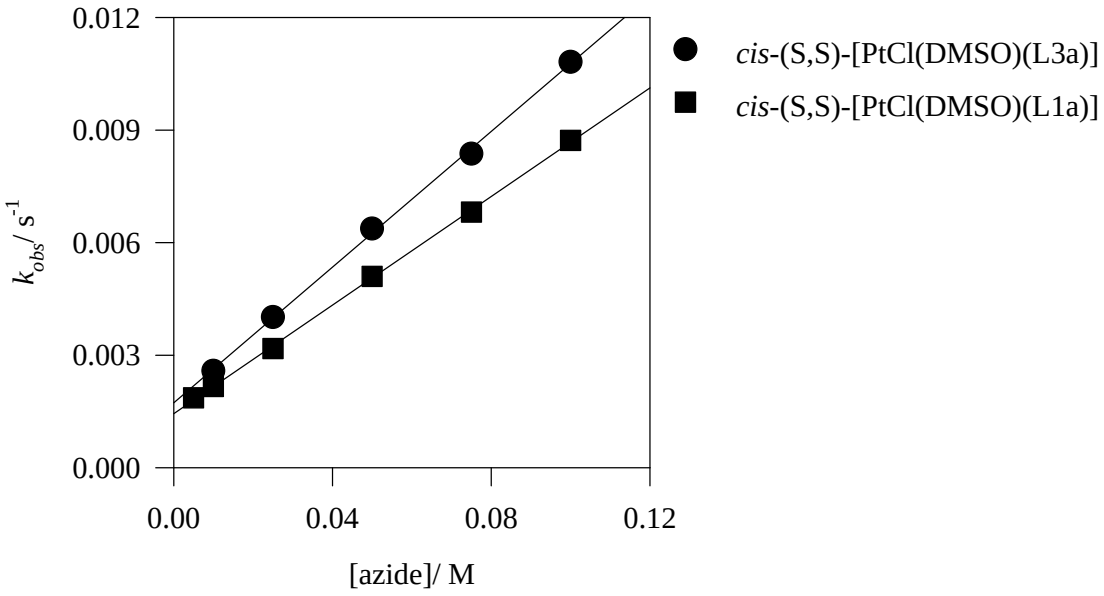

Figure 5.6: Concentration dependence for chloride substitution by azide from *cis*-(S,S)-[PtCl(DMSO)(L3a)] and *cis*-(S,S)-[PtCl(DMSO)(L1a)] in methanol at 25ºC. $[Pt]_F$ = 0.5 mM. λ = 375 nm. The pseudo first-order rate constants are given in Appendix B, Tables B1 and B7.

Table 5.4: Rate constants for chloride substitution by azide from *cis*-(S,S)-[PtCl(DMSO)(L3a)] and *cis*-(S,S)-[PtCl(DMSO)(L1a)] in methanol at 25°C.

Complex	k_y/ M^{-1}s^{-1}	k_s/ s^{-1}
cis-(S,S)-[PtCl(DMSO)(L1a)]	0.0724(7)	0.00144(4)
cis-(S,S)-[PtCl(DMSO)(L3a)]	0.090(2)	0.0017(1)

As seen in Table 5.4, variation of the amine moiety on the bidentate ligand has a small influence on the rate of chloride substitution by azide.

5.4.4 Thermodynamic parameters of chloride substitution

The *cis*-effect of the sulfoxide ligand on chloride substitution by azide from *cis*-(S,S)-[PtCl(L1a)(RR'SO)], where RR'SO = DMSO, (*S*)-MTSO and MPSO, was evaluated at three temperatures (40°C, 25°C and 10°C) to determine the activation parameters. The plots of k_{obs} against [azide] at various temperatures are given in Figures 5.7–5.9. The Eyring plots are shown in Figure 5.10, while the rate constants and activation parameters are given in Tables 5.5 and 5.6, respectively.

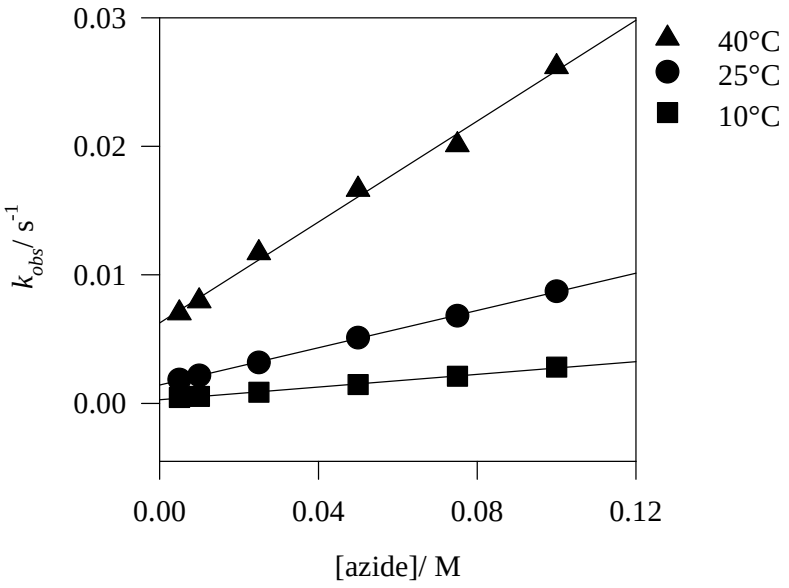

Figure 5.7: Temperature and concentration dependence for chloride substitution by azide from *cis*-(S,S)-[PtCl(DMSO)(L1a)] in methanol. $[Pt]_F$ = 0.5 mM. λ = 375 nm. The pseudo first-order rate constants are given in Appendix B, Table B1.

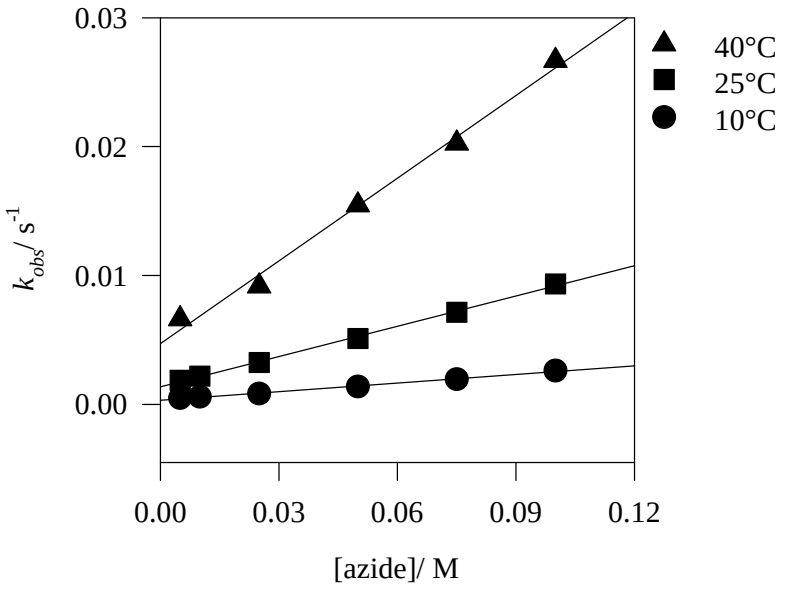

Figure 5.8: Temperature and concentration dependence for chloride substitution by azide from *cis*-(S,S)-[PtCl(L1a)((*S*)-MTSO)] in methanol. $[Pt]_F$ = 0.5 mM. λ = 375 nm. The pseudo first-order rate constants are given in Appendix B, Table B5.

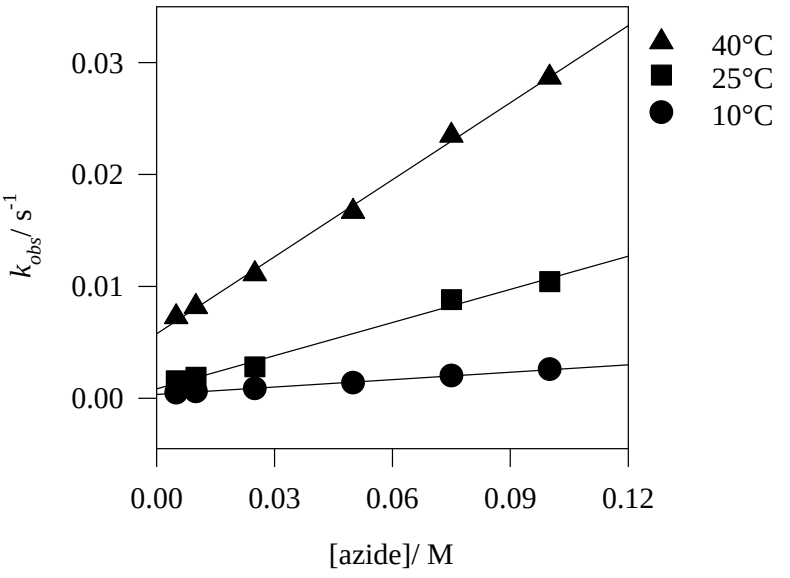

Figure 5.9: Temperature and concentration dependence for chloride substitution by azide from *cis*-(S,S)-[PtCl(L1a)(MPSO)] in methanol. $[Pt]_F$ = 0.5 mM. λ = 375 nm. The pseudo first-order rate constants are given in Appendix B, Table B4.

Table 5.5: Rate constants for chloride substitution by azide from *cis*-(S,S)-[PtCl(L1a)(RR'SO)] in methanol. The pseudo first-order rate constants are given in Appendix B, Tables B1, B4 and B5.

RR'SO	Temperature/ °C	k_y/ $M^{-1}s^{-1}$	k_s/ s^{-1}
DMSO	10.2	0.0230(3)	0.00031(1)
	25.0	0.0724(7)	0.00144(4)
	39.8	0.196(7)	0.0062(4)
MPSO	10.2	0.022(6)	0.0003(3)
	25.1	0.099(6)	0.0008(3)
	39.8	0.230(5)	0.0057(3)
(*S*)-MTSO	10.0	0.0223(7)	0.00032(4)
	25.0	0.078(2)	0.0013(1)
	39.8	0.214(11)	0.0047(7)

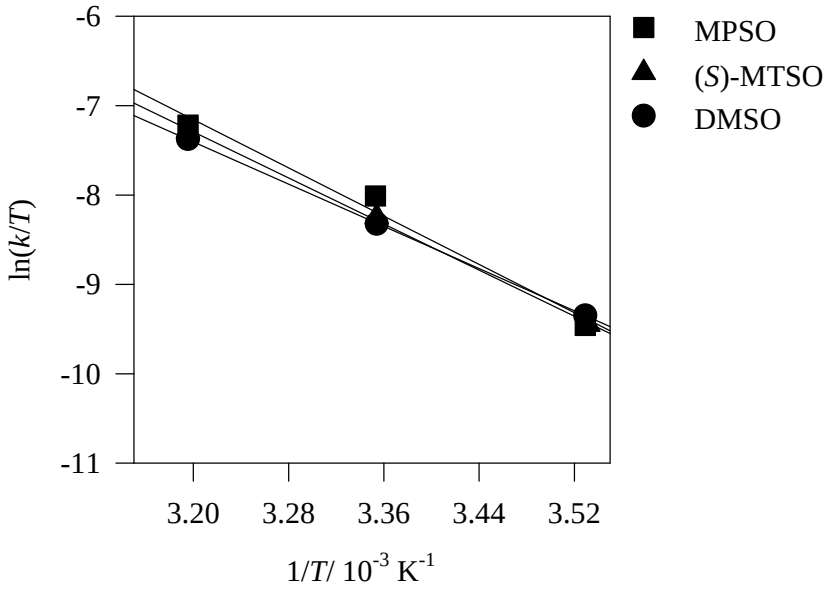

Figure 5.10: Eyring plots for chloride substitution by azide from *cis*-(S,S)-[PtCl(L1a)(RR'SO)] in methanol, where RR'SO = DMSO, MPSO and (*S*)-MTSO.

Table 5.6: Activation parameters for chloride substitution by azide from *cis*-(S,S)-[PtCl(L1a)(RR'SO)] in methanol.

RR'SO	$\Delta S^{\neq}$/ J $K^{-1}mol^{-1}$	$\Delta H^{\neq}$/ kJ mol^{-1}	$\Delta G^{\neq}$/ kJ mol^{-1} [a]
DMSO	-102(1)	+49.1(3)	+30(3)
(*S*)-MTSO	-87(6)	+53(2)	+26(6)
MPSO	-78(25)	+56(7)	+23(26)

[a] Calculated from $\Delta G^{\neq} = \Delta H^{\neq} - T\Delta S^{\neq}$, where T = 298 K.

The large negative entropies of activation for chloride substitution by azide from *cis*-(S,S)-[PtCl(L1a)(RR'SO)] suggest that the reaction occurs via an associative mechanism.

5.5 Discussion

5.5.1 Effect of the incoming nucleophile

5.5.1.1 Substitution kinetics of cis-(S,S)-[PtCl(DMSO)(L1a)]

As shown in Figure 5.3, a relatively large dependence of the rate on the incoming anionic nucleophile (62 times) is observed. The order of reactivity was, N_3^- < I^- < SCN^-. This order is in agreement with the nucleophilic reactivity index determined for the ligands from *trans*-[$PtCl_2(py)_2$]. [27–28] The large negative entropy of activation (Table 5.6) for chloride substitution by azide from *cis*-(S,S)-[PtCl(DMSO)(L1a)] and the dependence of the rate on the incoming nucleophile indicate that chloride substitution occurs via an associative mechanism.

Kinetic data for chloride substitution have been reported for a number of diamine complexes, but due to different experimental conditions (ionic strength, solvent), no quantitative comparisons can be made. However, the second-order rate constants, k_y, for the substitution of chloride by anionic nucleophiles are compared qualitatively with a range of literature examples. A summary of the relevant rate constants and Pt–Cl bond distance ranges found in the literature is given in Table 5.7.

Table 5.7: Selected bond lengths and second-order rate constants, k_y, for some platinum(II) sulfoxide complexes. The bold text indicates the leaving group.

Complex	Pt–Cl/ Å	k_y/ $M^{-1}s^{-1}$ [f]			Ref.
		N_3^-	I^-	SCN^-	
cis-(S,S)-[Pt**Cl**(DMSO)(L1a)][a]	2.337(11)	0.0724(7)	1.16(3)	4.47(15)	This work
[Pt**Cl**(dien)]$^+$	2.312(3)	0.0033	0.123	0.201	24, 29
[Pt**Cl**(en)(NH_3)]$^+$ [d]	-	0.0027	0.077	0.13	19
[Pt(DMSO)(en)(**H_2O**)]$^{2+}$ [c]	-	-	17500	3300	18
[Pt**Cl**(DMSO)(en)]$^+$ [d]	2.294(3)	0.033	2.71	2.35	19, 30
[Pt**Cl**(DMSO)(Me_4en)]$^+$ [e]	2.296(5)	-	0.00778(10)	-	20
[Pt(**DMSO**)(phen)Me]$^+$ [b]	-	0.162	59	45	24

[a] In methanol at 25°C.

[b] In methanol/ water (19:1 (v/v)) at 25°C; corrected to $\mu = 0$.

[c] In water at 30°C; corrected to $\mu = 0$.

[d] In water at 25°C; corrected to $\mu = 0$.

[e] In water at 25°C; $\mu = 0.10$ mol dm^{-3} ($LiClO_4$).

[f] Where no standard deviations are given, these have not been reported in the original paper.

As mentioned in Chapter 4, the Pt–Cl bond distance of *cis*-(S,S)-[PtCl(DMSO)(L1a)] is significantly longer than the Pt–Cl bond distances of the other platinum(II) sulfoxide complexes given in Table 5.7. This may be due to the greater *trans*-influence of the sulfur donor atom of the (S,O)-chelate relative to the amine nitrogen donors of the amine and α-diimine ligands. It was thus expected that the chloride ligand from *cis*-(S,S)-[PtCl(DMSO)(L1a)] would be easier to substitute than the chloride leaving group from complexes of the type [Pt(amine)$_2$Cl(DMSO)]$^+$ and [Pt(amine)$_3$Cl]$^+$, which according to the data and examples given in Table 5.7, was generally found to be the case. Depending on the incoming nucleophile, the rate of chloride substitution from *cis*-(S,S)-[PtCl(DMSO)(L1a)] is about one to two orders of magnitude larger than from [PtCl(en)(NH_3)]$^+$ and [PtCl(dien)]$^+$ and three orders of magnitude larger than chloride substitution from [PtCl(DMSO)(Me_4en)]$^+$. Interestingly, the rate of chloride substitution from *cis*-(S,S)-[PtCl(DMSO)(L1a)] is the same order of magnitude as from [PtCl(DMSO)(en)]$^+$. The rate of chloride substitution is three to four orders of magnitude smaller than water substitution from [Pt(DMSO)(en)(H_2O)]$^+$ and an order of magnitude smaller than dimethylsulfoxide substitution from [Pt(DMSO)(phen)Me]$^+$.

5.5.2 *cis*-Effect of the sulfoxide on chloride substitution

As seen in Table 5.2, the chloride leaving ability and, therefore, the *cis*-effect of the respective sulfoxides, decreases slightly in the order, MPSO > (*S*)-MTSO > DMSO. A similar order of lability is observed for sulfoxide substitution (Section 5.6.2). The large negative entropies of activation for all the complexes indicate that chloride substitution occurs via an associative mechanism.

Comparison of the Pt–Cl bond distances of *cis*-(S,S)-[PtCl(DMSO)(L1a)] and *cis*-(S,S)-[PtCl(L1a)(MPSO)] may provide evidence for the *cis*-influence (ground-state effect) of the sulfoxide on the bond order of the Pt–Cl bond adjacent to the sulfoxides. A detailed discussion of the crystal structures is given in Chapter 4. The Pt–Cl bond distances in *cis*-[PtCl(DMSO)(L1a)] and *cis*-(S,S)-[PtCl(L1a)(MPSO)] are 2.337(11) Å and 2.334(3) Å, respectively. The Pt–Cl bond lengths in the two complexes are similar, thus no effect is observed in the solid state to explain the increased lability of the chloride leaving group in *cis*-(S,S)-[PtCl(L1a)(MPSO)].

The observed *cis*-effect could possibly be due to steric or electronic effects. Because chloride substitution occurs via an associative pathway, the rate of the reaction is dependent on several factors:

i) Stability of the transition-state complex (TSC).
ii) Ease of approach of the incoming nucleophile (steric effects).
iii) Electrophilicity of the platinum centre.

All of these factors must be considered in order to explain the observed *cis*-effect. The more stable the TSC, the faster the reaction will proceed. If the TSC is destabilised for any reason a decrease in the rate constant will be observed.

The increase in steric bulk, on going from DMSO to (*S*)-MTSO, does not appear to have a significant effect on the rate of chloride substitution, while there is a larger increase in the rate of reaction for the MPSO complex. Because there is very little or no increase in bulkiness when (*S*)-MTSO is compared to MPSO, it is unlikely that steric bulkiness is responsible for the increase in the rate constant. In fact, the opposite should be observed, because a substantial increase in steric bulk is more likely to hinder attack of the

incoming nucleophile and may result in a possible destabilisation of the transition-state complex.

The electron-withdrawing properties of the three sulfoxides studied decrease in the order, MPSO > (*S*)-MTSO > DMSO. This is the same trend observed for the *cis*-effect on chloride substitution. Sulfoxides are moderate π-acceptors and are known to π-backbond to transition metals. [31–32] The observed *cis*-effect is proposed to be due to the tendency of the respective sulfoxide to π-backbond to the platinum(II) centre, thus aiding in the accommodation of the extra electron density brought by the anionic nucleophile on the metal. These π-properties would stabilise the TSC and facilitate nucleophilic attack by withdrawing electron density away from the platinum(II) centre making it more electrophilic. Additional evidence for this is provided from the thermodynamic activation parameters given in Table 5.6. On substituting the methyl group on DMSO for stronger electron-withdrawing groups such as phenyl and tolyl groups there is a tendency of an increase in the enthalpy of activation and a decrease in the entropy of activation. Small changes in the entropy and enthalpy of activation can result in large changes in the rate of a reaction. [33] The rate of these reactions are mainly controlled by the enthalpy of activation. As seen in Figure 5.6, the enthalpy appears to increase with an increase in the rate of reaction. However, due to the large experimental uncertainties on the enthalpy values coupled with very small enthalpy changes within the series, nothing conclusive may be said about the enthalpy of activation (reaction profile) of these complexes and the *cis*-effect observed.

The Gibbs free energy of activation ($\Delta G^{\neq}$) is the energy required to form the activated complex at a specific temperature. It is also a measure of the stability of the transition-state complex. The lower the $\Delta G^{\neq}$, the easier it is for the reaction to proceed, and hence the rate of the reaction will increase. Comparison of the calculated Gibbs free energies of activation (Table 5.6) for the different sulfoxide complexes at 298 K suggests that the MPSO complex has the lowest energy barrier followed by the (*S*)-MTSO and DMSO complex. Based on this $\Delta G^{\neq}$ data, the predicted rate of chloride substitution from the *cis*-(S,S)-[PtCl(L1a)(MPSO)] should be the fastest, while substitution from *cis*-(S,S)-[PtCl(DMSO)(L1a)] complex should be the slowest, with the MTSO complex being

intermediate, which is indeed observed. Unfortunately, the uncertainties in the $\Delta G^{\neq}$ values are too large to make any significant conclusions there from.

5.5.3 Electronic effects on chloride substitution

5.5.3.1 Effect of 3-benzoyl substitution

For *cis*-(S,S)-[PtCl(DMSO)(L)] complexes, where HL = *N*-(3-*R*-benzoyl)-*N'*,*N'*-diethylthiourea, and R = NO_2, Cl, OCH_3, H and CH_3, the chloride reactivity decreases in the order: NO_2 > Cl > OCH_3 ≈ H ≈ CH_3. These results are in agreement with the ^{195}Pt NMR data (Chapter 4) which provide evidence that electron-withdrawing substituents on the phenyl ring resulting in an increased positive charge on the platinum nucleus, thereby making it more susceptible to nucleophilic attack. The electron-withdrawing affect of the nitro and chloro groups result in notable downfield shifts in the ^{195}Pt signal. This is consistent with the mesomeric/inductive effect expected for 3-substituted benzoyl groups. This trend is also in agreement with the chemical shifts observed in the ^{1}H NMR spectra for the methyl protons of the sulfoxide resonances (Chapter 4) for the respective complexes.

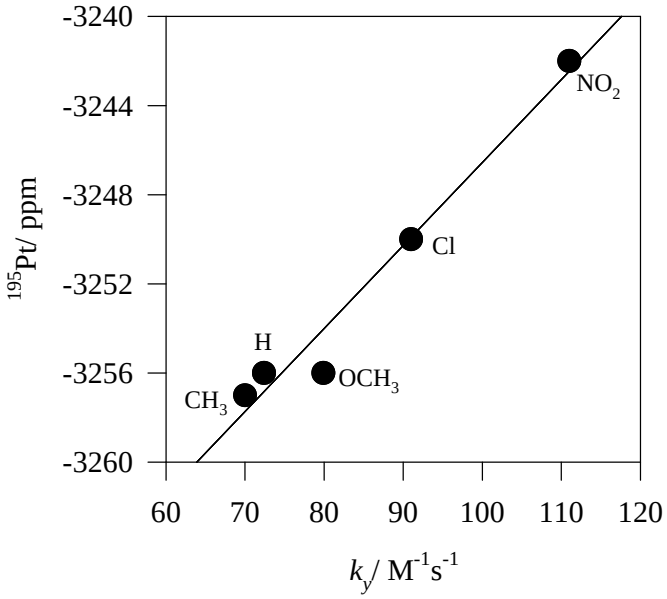

Figure 5.11: The dependence of the ^{195}Pt NMR chemical shifts on the second-order rate constants, k_y, for the substitution of chloride by azide from *cis*-(S,S)-[PtCl(DMSO)(L1a–e)] at 25°C. (r^2 = 0.9990).

The ^{195}Pt signal is a measure of the electron density at the platinum nucleus. Downfield shifts indicate that the platinum nucleus is deshielded and, therefore, more electron deficient (more electrophilic), while an upfield shift in the ^{195}Pt signal indicates that the platinum centre is less electrophilic. The ^{195}Pt NMR data shown in Figure 5.11, are consistent with the proposed associative mechanism for chloride substitution. For an associative mechanism, it is generally accepted that the rate of substitution is dependent on the nature of the incoming nucleophile. The linear dependence of the second-order rate constant on the ^{195}Pt NMR resonance (Figure 5.11) of the respective complexes indicates that the rate is also dependent on the electrophilic nature of the platinum centre. As the platinum nucleus becomes more electrophilic, the anionic nucleophile has a higher affinity for the electrophilic platinum centre and there is thus an increase in the rate of chloride substitution. The inductive/mesomeric effect of the phenyl substituents is most likely transferred to the platinum(II) nucleus via the conjugated system of the *N*,*N*-dialkyl-*N'*-(3-*R*-benzoyl)thiourea ligand.

5.5.3.2 Effect of the amine

Comparison of the rates of chloride substitution from *cis*-(S,S)-[PtCl(DMSO)(L1a)] and *cis*-(S,S)-[PtCl(DMSO)(L3a)] shows the effect of the amine moiety on chloride substitution. As seen in Table 5.4, variation of the amine moiety on the bidentate ligand for diethylamine and di(2-hydroxyethyl)amine had a small (but still significant) effect on chloride substitution by azide. This is not surprising because the amine is relatively far from the platinum nucleus and is not expected to affect the electron density at the metal centre via inductive/mesomeric effects.

Part B: NEUTRAL NUCLEOPHILES

5.6 Results

Dimethylsulfoxide and chloride substitution by various neutral nucleophiles from complexes of the type *cis*-(S,S)-[Pt(acylthioureato)Cl(RR'SO)], according to equation (**5 – 24**) and (**5 – 25**), will now be discussed,

$$[PtCl(L)(RR'SO)] + Y^- \longrightarrow [PtCl(L)(Y)] + RR'SO \qquad (\mathbf{5-24})$$

$$[PtCl(L)(Y)] + Y^- \longrightarrow [Pt(L)(Y)_2]^+ + RR'SO + Cl^- \qquad (\mathbf{5-25})$$

5.6.1 Effect of the incoming nucleophile

5.6.1.1 Substitution kinetics of cis-(S,S)-[PtCl(DMSO)(L1a)]

The substitution of dimethylsulfoxide from *cis*-(S,S)-[PtCl(DMSO)(L1a)] by 4-(dimethylamino)pyridine (DMAP), 2-mercaptobenzimidazole (MBI), thiourea and triphenylphosphine (PPh_3) was studied at 25°C in methanol.

The plot of k_{obs} against the concentration of incoming nucleophile, Y, is shown in Figure 5.12. The substitution of dimethylsulfoxide from *cis*-(S,S)-[PtCl(DMSO)(L1a)] with DMAP, thiourea and PPh_3 gave linear plots of k_{obs} against [Y], while the results for MBI deviate slightly from linearity. The first-order rate constants, k_s, for the solvolytic pathway and the second-order rate constants, k_y, for the direct pathway were calculated from these plots and are reported in Table 5.8.

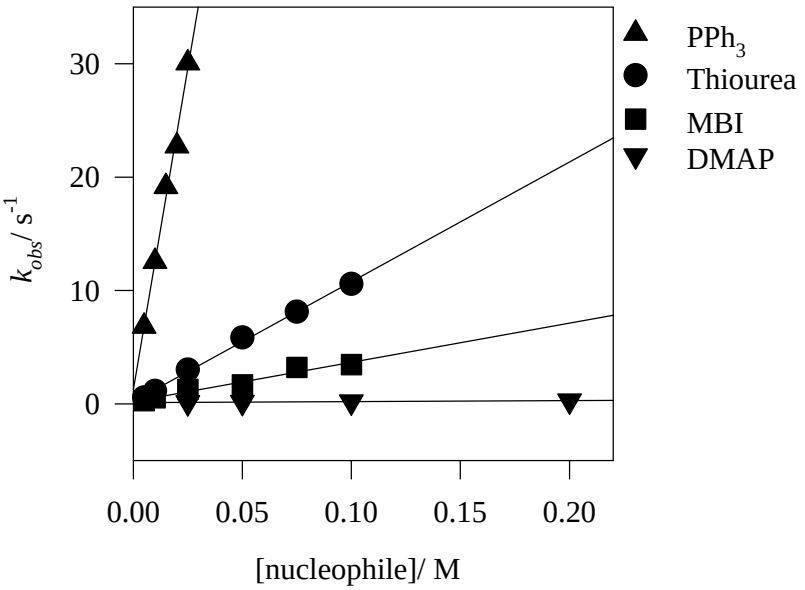

Figure 5.12: Concentration dependence for dimethylsulfoxide substitution from *cis*-(S,S)-[PtCl(DMSO)(L1a)] by PPh_3, MBI, thiourea and DMAP in methanol at 25ºC. $[Pt]_F$ = 0.5 mM. All the reactions were followed at λ = 380 nm, except for PPh_3 which was followed at λ = 370 nm. The pseudo first-order rate constants are given in Appendix B, Tables B8–11.

Table 5.8: Rate constants for dimethylsulfoxide substitution from *cis*-(S,S)-[PtCl(DMSO)(L1a)] by neutral nucleophiles in methanol at 25°C.

Nucleophile	k_y/ M^{-1} s^{-1}	k_s/ s^{-1}
DMAP	0.87(4)	0.100(6)
MBI [a]	42(1)	0
Thiourea [a]	107(1)	0
PPh_3 [a]	1203(23)	0

[a] k_s values have been fixed to zero due to a negligible observed solvent pathway contribution.

The slight decrease in the rate at high concentrations of MBI was assumed to be due to the low solubility of MBI in methanol, as a precipitate was observed with time in solutions of MBI. However, the non-linear tendencies at high concentrations in the plots of k_{obs} against [MBI], could also be due to the presence of equilibria. To check for the presence of equilibria the dimethylsulfoxide concentration was varied. The plot of k_{obs} against [MBI], in the presence of free dimethylsulfoxide, is given in Figure 5.13.

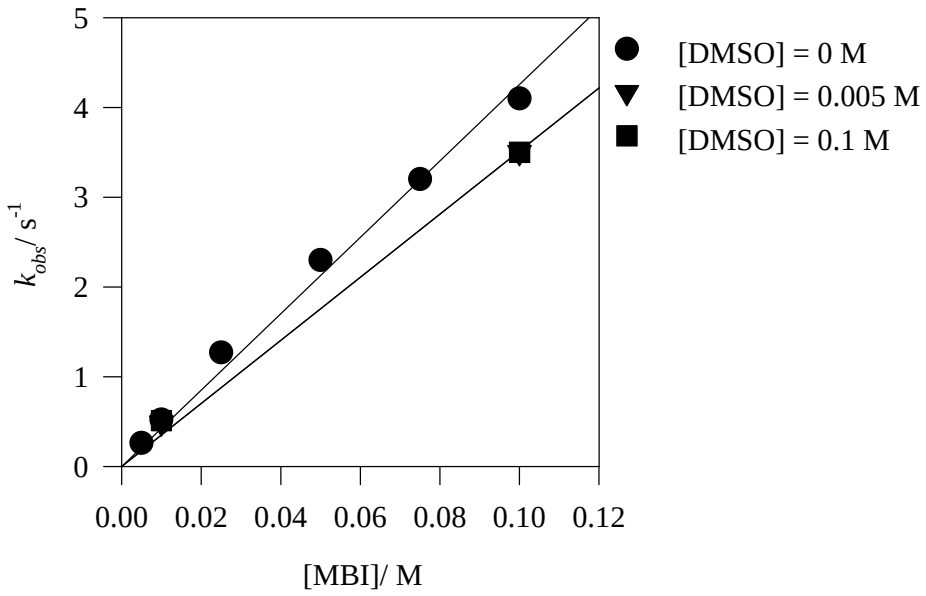

Figure 5.13: Concentration dependence for dimethylsulfoxide substitution from *cis*-(S,S)-[PtCl(DMSO)(L1a)] by MBI, in the presence of varying amounts of excess free dimethylsulfoxide. $[Pt]_F$ = 0.5 mM. λ = 380 nm. The pseudo first-order rate constants are given in Appendix B, Table B12.

The substitution reactions of dimethylsulfoxide from *cis*-(S,S)-[PtCl(DMSO)(L1a)] by DMAP and PPh_3 was also checked for possible equilibria by studying their rates in the presence of excess dimethylsulfoxide. The plots of k_{obs} against [DMAP], in the presence of free dimethylsulfoxide, are given in Figure 5.14, while the plots of k_{obs} against [PPh_3] in the presence of free dimethylsulfoxide are shown in Figure 5.15.

According to the data given in Table 5.8, the order of reactivity was found to be DMAP < MBI < thiourea < PPh_3. The data presented in Figures 5.13–5.15 have shown that the rate of dimethylsulfoxide substitution from *cis*-(S,S)-[PtCl(DMSO)(L1a)] by MBI, DMAP and PPh_3 is significantly affected by the presence of free dimethylsulfoxide, suggesting that equilibria are present in these reactions. However, due to the limited data, complete analysis of the effect of added dimethylsulfoxide was not pursued further

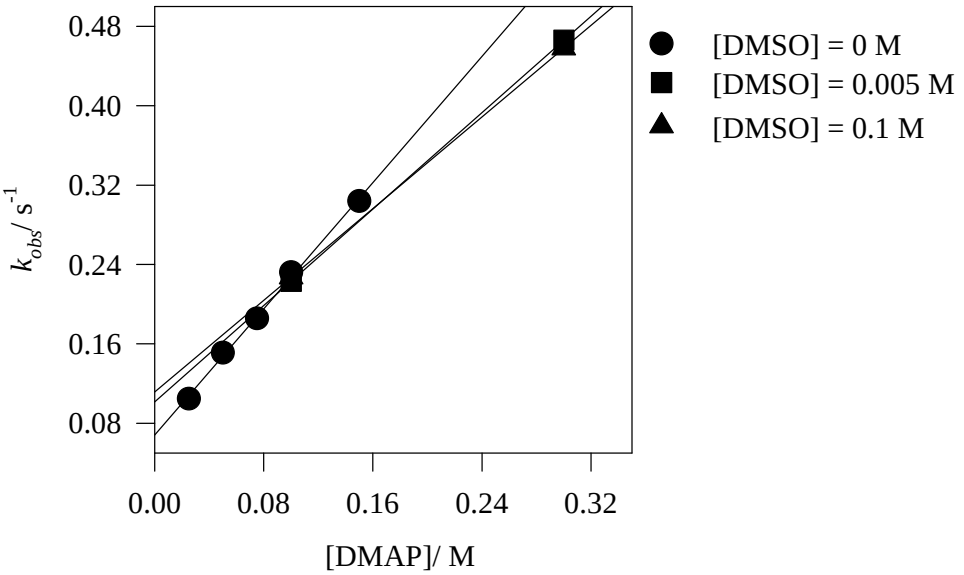

Figure 5.14: Concentration dependence for dimethylsulfoxide substitution by DMAP from *cis*-(S,S)-[PtCl(DMSO)(L1a)], in the presence of varying amounts of excess free dimethylsulfoxide. $[Pt]_F$ = 0.5 mM. λ = 380 nm. The pseudo first-order rate constants are given in Appendix B, Table B13.

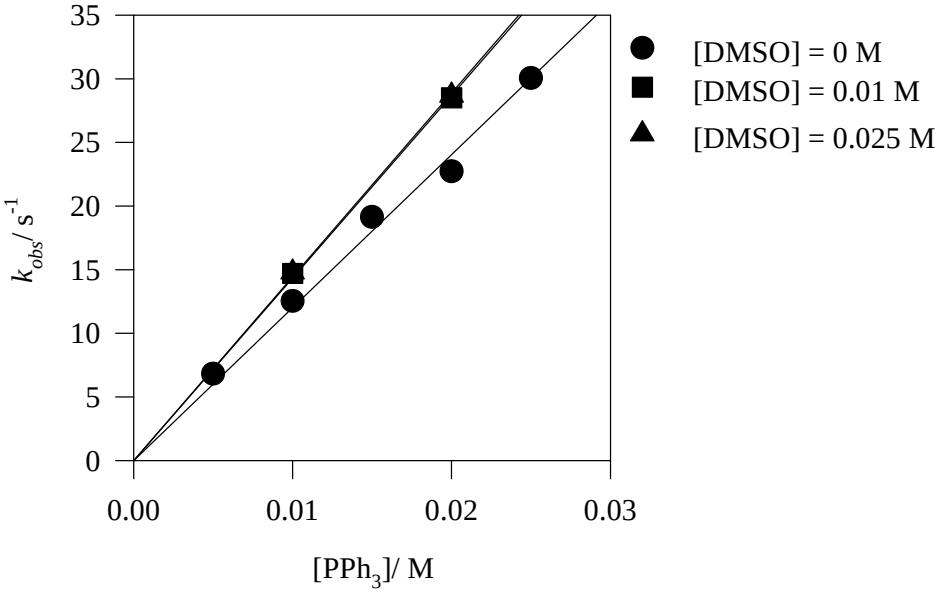

Figure 5.15: Concentration dependence for dimethylsulfoxide substitution by PPh_3 from *cis*-(S,S)-[PtCl(DMSO)(L1a)], in the presence of varying amounts of excess free dimethylsulfoxide. $[Pt]_F$ = 0.5 mM. λ = 357 nm. The pseudo first-order rate constants are given in Appendix B, Table B14.

5.6.2 Effect of the sulfoxide as a leaving group

A variety of sulfoxides with different electronic and steric properties were used to study their effect on sulfoxide substitution by MBI from *cis*-(S,S)-[PtCl(L1a)(RR'SO)], where RR'SO = DMSO, (*S*)-MTSO and MPSO, in methanol. Only the first substitution step according to equation (**5 – 24**) was studied. The observed rate constants were determined at, at least, five different concentrations of MBI. Linear plots of k_{obs} against [MBI] were obtained and are shown in Figure 5.16. The first-order rate constants, k_s, for the solvolytic pathway and second-order rate constants, k_y, for the direct pathway were calculated from these plots and are reported in Table 5.9.

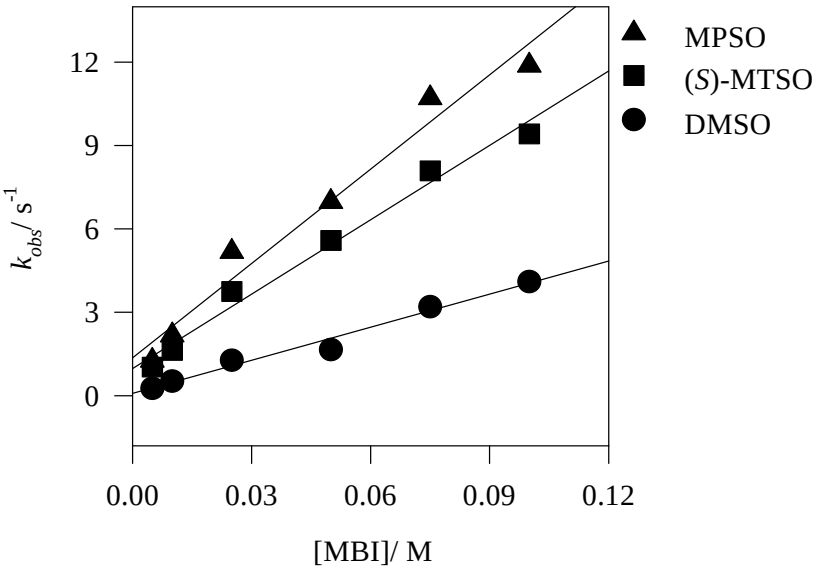

Figure 5.16: Concentration dependence for sulfoxide substitution by MBI from *cis*-(S,S)-[PtCl(L1a)(RR'SO)] in methanol at 25ºC, where RR'SO = DMSO, (*S*)-MTSO and MPSO. $[Pt]_F$ = 0.5 mM. λ = 380 nm. The pseudo first-order rate constants are given in Appendix B, Tables B9, B15 and B16.

Table 5.9: Rate constants for the sulfoxide substitution by MBI from *cis*-(S,S)-[PtCl(L1a)(RR'SO)] in methanol at 25ºC.

RR'SO	k_y/M^{-1}s^{-1}	k_s/s^{-1}
DMSO [a]	42(1)	0
(*S*)-MTSO	94(4)	0.9(2)
MPSO	121(8)	1.2(4)

[a] k_s values have been fixed to zero due to a negligible observed solvent pathway contribution.

According to the data in Table 5.9, the sulfoxide leaving ability decreases in the order, MPSO > (*S*)-MTSO > DMSO.

5.6.3 Electronic effects on dimethylsulfoxide substitution

5.6.3.1 Effect of the amine

Only the initial reactions according to equation (**5 – 24**) were studied. The plots of k_{obs} against [MBI] are shown in Figure 5.17 and the rate constants are given in Table 5.10.

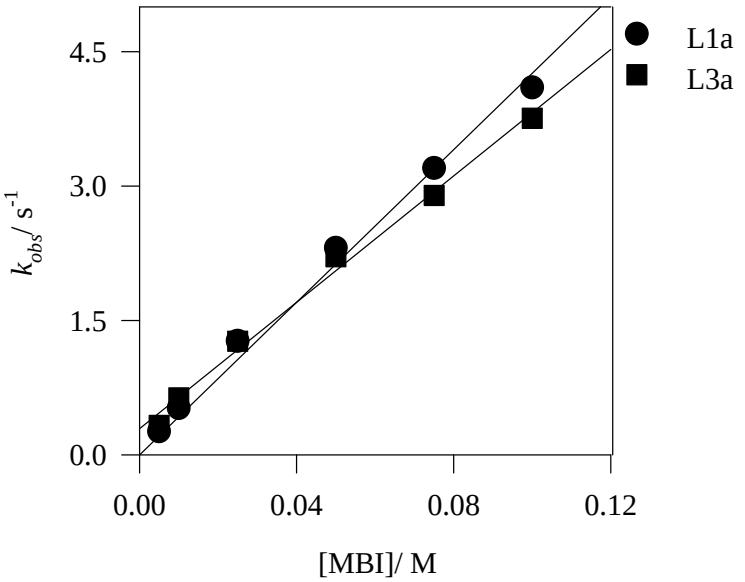

Figure 5.17: Concentration dependence for dimethylsulfoxide substitution by MBI from *cis*-(S,S)-[PtCl(DMSO)(L3a)] and *cis*-(S,S)-[PtCl(DMSO)(L1a)] in methanol at 25ºC. $[Pt]_F$ = 0.5 mM. λ = 380 nm. The pseudo first-order rate constants are given in Appendix B, Tables B9 and B17.

Table 5.10: Rate constants for the substitution of dimethylsulfoxide by MBI from *cis*-(S,S)-[PtCl(DMSO)(L3a)] and *cis*-(S,S)-[PtCl(DMSO)(L1a)] in methanol at 25°C.

Complex	k_y/ M^{-1}s^{-1}	k_s/ s^{-1}
cis-(S,S)-[PtCl(DMSO)(L1a)] [a]	42(1)	0
cis-(S,S)-[PtCl(DMSO)(L3a)]	35(1)	0.3(1)

[a] k_s values have been fixed to zero due to a negligible observed solvent pathway contribution.

As seen in Table 5.10, the dimethylsulfoxide ligand in *cis*-(S,S)-[PtCl(DMSO)(L1a)] is slightly more labile than in the *cis*-(S,S)-[PtCl(DMSO)(L3a)] complex.

5.6.4 Thermodynamic parameters of dimethylsulfoxide substitution

The reaction of *cis*-(S,S)-[PtCl(DMSO)(L1a)] with MBI was carried out at 40°C, 25°C and 10°C and with PPh_3 at 43°C, 25°C and 18°C, to determine the activation parameters for these reactions. The solvent pathway for both these nucleophiles was negligible (see Table 5.8), thus only one concentration of each nucleophile was necessary to study the temperature affect. The Eyring plots are shown in Figure 5.18. The rate constants and the activation parameters for the substitution of the dimethylsulfoxide ligand by MBI and by PPh_3 from *cis*-(S,S)-[PtCl(DMSO)(L1a)] are given in Table 5.11 and Table 5.12, respectively.

Table 5.11: Rate constants for dimethylsulfoxide substitution by PPh_3 from *cis*-(S,S)-[PtCl(DMSO)(L1a)] in methanol at various temperatures. [a] The pseudo first-order rate constants are given in Appendix B, Tables B18 and B19.

Nucleophile	Temperature/ °C	k_y/ $M^{-1}s^{-1}$
PPh_3	18.2	1020(100)
	25.0	1600(160)
	43.1	5600(400)
MBI	10.2	8(1)
	25.2	18(2)
	40.1	58(6)

[a] k_s values have been fixed to zero due to a negligible observed solvent pathway contribution.

Table 5.12: Activation parameters for dimethylsulfoxide substitution by PPh_3 and by MBI from *cis*-(S,S)-[PtCl(DMSO)(L1a)] in methanol.

Nucleophile	$\Delta S^{\neq}$/ J $K^{-1}mol^{-1}$	$\Delta H^{\neq}$/ kJ mol^{-1}
PPh_3	- 15(5)	50(1)
MBI	- 65(22)	46(6)

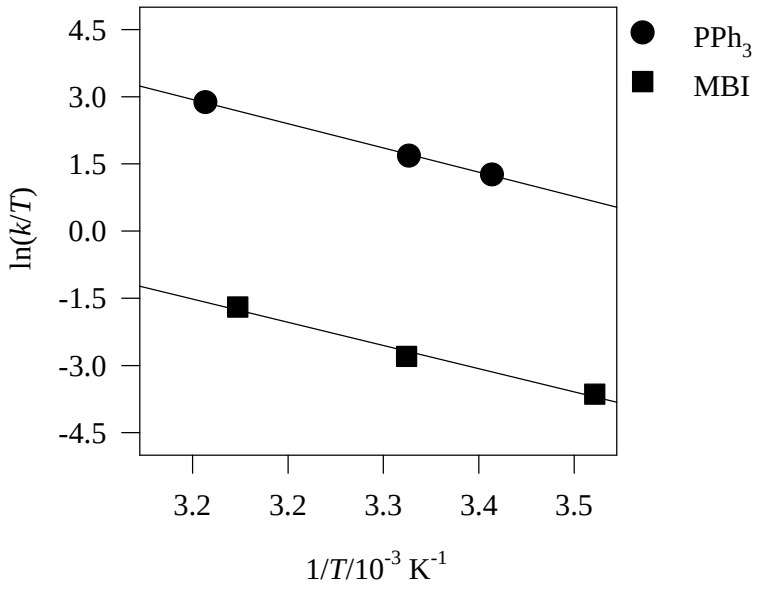

Figure 5.18: Eyring plot for dimethylsulfoxide substitution from *cis*-(S,S)-[PtCl(DMSO)(L1a)] in methanol by MBI and by PPh_3.

The negative entropy of activation for dimethylsulfoxide substitution from *cis*-(S,S)-[PtCl(DMSO)(L1a)] by MBI indicates that this reaction occurs via an associative mechanism. The large standard deviation in the entropy of activation for dimethylsulfoxide substitution from *cis*-(S,S)-[PtCl(DMSO)(L1a)] by PPh_3 makes a more detailed discussion not feasible. However, the activation entropy for PPh_3 is less negative than the usual square-planar substitution proceeding via an associative mechanism.

5.6.5 Effect of the solvent on dimethylsulfoxide substitution

The effect of the solvent on dimethylsulfoxide substitution by PPh_3 from *cis*-(S,S)-[PtCl(DMSO)(L1a)] was also evaluated. The plots of k_{obs} against [PPh_3] are shown in Figure 5.19 and the rate constants for the reactions in various solvents are given in Table 5.13.

Table 5.13: Rate constants for the substitution of dimethylsulfoxide by PPh_3 from *cis*-(S,S)-[PtCl(DMSO)(L1a)] at 25°C in various solvents.

Solvent	k_y/ $M^{-1}s^{-1}$	k_s/ s^{-1}	K_{eq} [b]	ε [c, e, f]	D_N [d,e]
Dichloromethane	161(13)	1.0(2)	≈ 0	8.9	-
Acetone [a]	203(2)	0	≈ 5	20.7	17
Acetonitrile [a]	480(14)	0	≈ 1	38	14.1
Methanol [a]	1203(23)	0	≈ 0.49	32.6	19

[a] k_s values have been fixed to zero due to a negligible observed solvent pathway contribution.

[b] Equilibrium constants were determined from ^{1}H NMR, according to equation (**5 – 22**).

[c] Dielectric constant.

[d] Donor number.

[e] From Ref. 24.

[f] From Ref. 34.

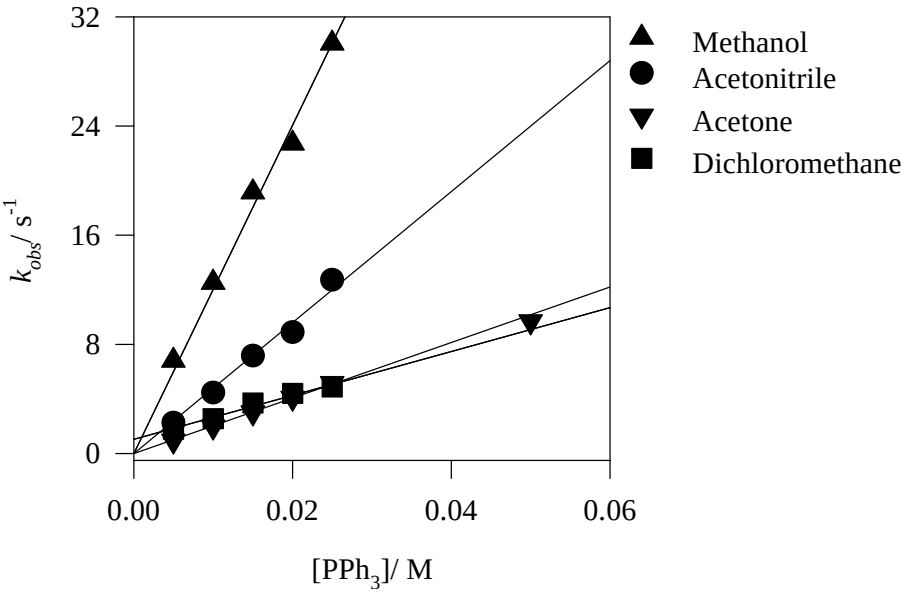

Figure 5.19: Concentration dependence for dimethylsulfoxide substitution by PPh_3 from *cis*-(S,S)-[PtCl(DMSO)(L1a)] in various solvents at 25ºC. $[Pt]_F$ = 0.5 mM. The reactions were followed in methanol (λ = 370 nm), acetonitrile (λ = 380 nm), acetone (λ = 390 nm) and dichloromethane (λ = 380 nm). The pseudo first-order rate constants are given in Appendix B, Tables B10 and B20–22.

As seen in Table 5.13, the rate of dimethylsulfoxide substitution by PPh_3 shows a strong solvent dependence, with the rates varying by an order of magnitude. The rate of dimethylsulfoxide substitution by PPh_3 increases in the order, dichloromethane < acetone

< acetonitrile < methanol, which is in agreement with a more polar transition-state complex which may be stabilised by more polar solvents.

5.6.6 The second consecutive reaction: chloride substitution

Preliminary studies of chloride ligand substitution from *cis*-(S,S)-[PtCl(DMSO)(L1a)] by PPh_3 and DMAP in methanol at 25°C were carried out, according to equation (**5 – 25**). In both cases limiting kinetics were obtained.

5.6.6.1 Chloride substitution by PPh_3 from cis-(S,S)-[PtCl(DMSO)(L1a)]

The plot of k_{obs} against [PPh_3] is shown in Figure 5.20. Although the data does not fit the calculated line that well, it is in reasonable agreement and should be interpreted in conjunction with the data shown in Figure 5.22 and Figure 5.23. The effects of excess chloride and of solvent on the substitution of the chloro ligand by PPh_3 from *cis*-(S,S)-[PtCl(DMSO)(L1a)] were also studied, to determine if any equilibria are present. The plot of k_{obs} against [PPh_3], in the presence of free chloride, is shown in Figure 5.21. The dependence of chloride substitution by PPh_3 on the solvent is shown in Figure 5.22.

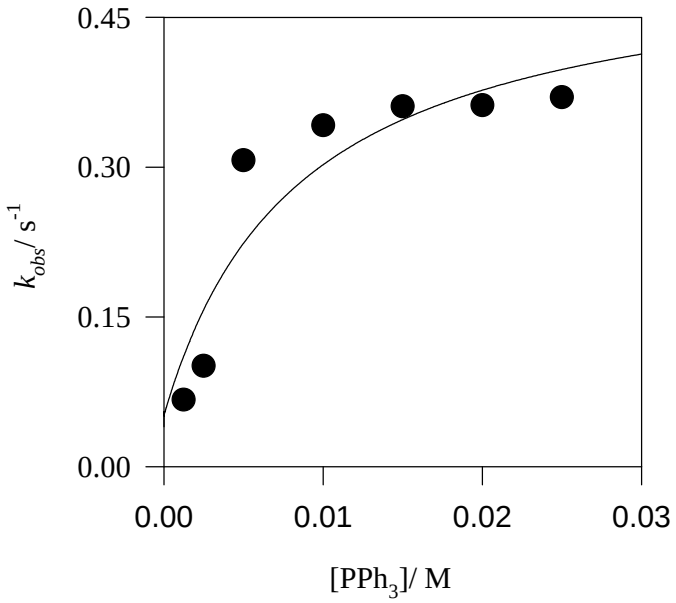

Figure 5.20: Concentration dependence for chloride substitution by PPh_3 from *cis*-(S,S)-[PtCl(DMSO)(L1a)] in methanol at 25ºC. Solid lines represent non-linear least squares fit using equation (**5 – 9**). $[Pt]_F$ = 0.5 mM. λ = 400 nm. The pseudo first-order rate constants are given in Appendix B, Table B23.

In the non-linear least squares fit using equation (**5 – 9**), shown in Figure 5.20, K_{eq} and k_{12} values had to be fixed at 0.6 and 0.1 $M^{-1}s^{-1}$, respectively, because these values were not well defined as a result of the limited data available at high [PPh_3] due to the limited solubility of PPh_3 in methanol. The rate constant for the solvolysis step (k_{13}) is however well defined and was found to be 0.51(9) s^{-1}. The discrimination factor (k_{32}/k_{31}) was determined to be 0.06(3), which is indicative of a substantial competition between the chloride and the entering PPh_3 for the solvento complex, with the chloride being favoured.

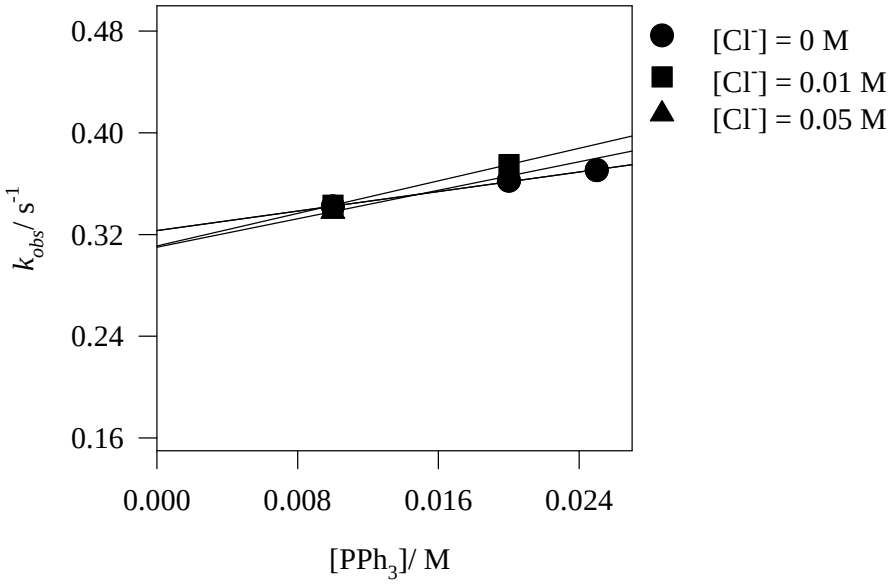

Figure 5.21: Concentration dependence for chloride substitution by PPh_3 from *cis*-(S,S)-[PtCl(DMSO)(L1a)] in the presence of excess chloride ions, in methanol at 25ºC. $[Pt]_F$ = 0.5 mM. λ = 400 nm. The pseudo first-order rate constants are given in Appendix B, Table B24.

As seen in Figure 5.21, the addition of excess chloride had no dramatic effect on the observed rate constants for chloride substitution by PPh_3 from *cis*-(S,S)-[PtCl(DMSO)(L1a)], and was therefore not investigated further.

Effect of the solvent on chloride substitution

The plots of k_{obs} against [PPh_3] are shown in Figure 5.22. The data points in Figure 5.22, for the reactions in various solvents, were fitted to equation (**5 – 9**), and the results are summarised in Table 5.14. Since equation (**5 – 9**) contains many parameters to be

determined, and only limited data was available, only estimated values for the rate constants and equilibrium constants could be obtained. A more detailed investigation can be carried out in the future.

Table 5.14: Table of rate and equilibrium constants for chloride substitution by PPh_3 from *cis*-(S,S)-[PtCl(DMSO)(L1a)] in various solvents.

Constant	Methanol	Acetonitrile	Acetone	Dichloromethane
k_{12}/ $M^{-1}s^{-1}$	0.1–10 [a]	6(3)	2.2(2)	1.75(2)
k_{13}/ s^{-1}	0.51(9)	0.32(15)	0.23(4)	0.011(2)
K_{eq}	0.6 [b]	0.7 [b]	0.7 [b]	0.7 [b]
k_{32}/k_{31}	0.06 [b]	0.0014 [b]	0.015(3)	0.019 [b]

[a] Value show the effect when varied between 0.1–10.

[b] Values were fixed due to limited data. The values indicated enabled the best fit to the data.

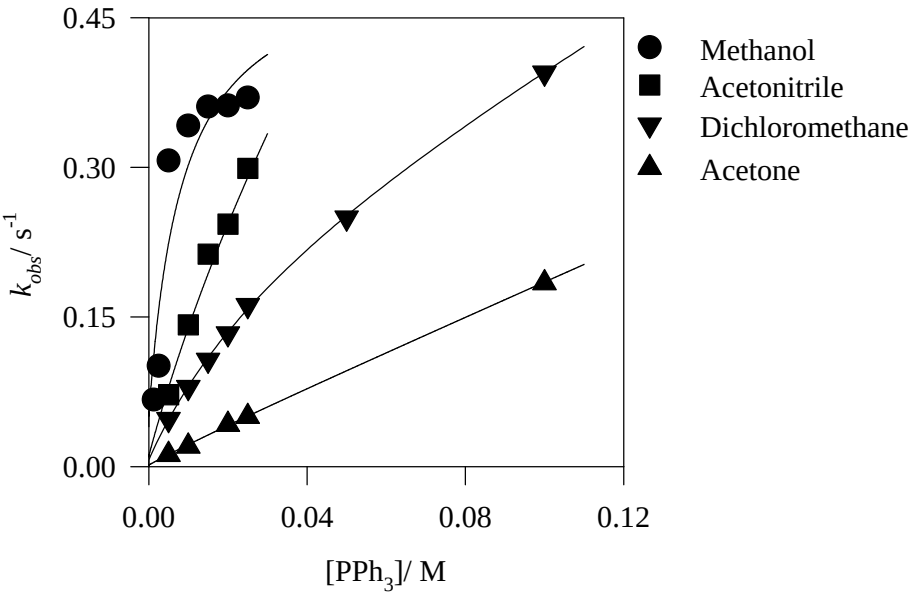

Figure 5.22: Concentration dependences for chloride substitution by PPh_3 from *cis*-(S,S)-[PtCl(DMSO)(L1a)] in various solvents at 25ºC. $[Pt]_F$ = 0.5 mM. The reactions were followed in methanol (λ = 400 nm), acetonitrile (λ = 380 nm), acetone (λ = 390 nm) and dichloromethane (λ = 380 nm). The pseudo first-order rate constants are given in Appendix B, Tables B23 and B25–27.

Both the discrimination factors (k_{32}/k_{31}) and the equilibrium constants reported in Table 5.14 were not well defined from these fits and were therefore fixed in the least-squares analyses. Even though the k_{12} values could not be accurately determined, there is a clear

tendency of increased reactivity with increasing polarity of the solvent. Similarly, a *ca.* fifty-fold decrease in magnitude of the solvolysis step is also observed, confirming the importance of solvent interaction in more coordinating solvents.

Substitution kinetics of *cis*-(S,P)-[PtCl(L1a)(PPh_3)] with PPh_3

The limiting kinetics observed for chloride substitution from *cis*-(S,S)-[PtCl(DMSO)(L1a)] by PPh_3 could possibly be caused by a fast pre-equilibrium in the first substitution step (dimethylsulfoxide substitution). In order to validate this, the intermediate *cis*-(S,P)-[PtCl(L1a)(PPh_3)] complex was prepared so that the second reaction could be evaluated without any interference from the first substitution step.

The complex *cis*-(S,P)-[PtCl(L1a)(PPh_3)] was prepared by the addition of one equivalent of PPh_3 to *cis*-(S,S)-[PtCl(DMSO)(L1a)] in dichloromethane. The solution was evaporated to dryness and the residue washed with water to remove the displaced dimethylsulfoxide. The residue was redissolved in dichloromethane, dried over $MgSO_4$ and evaporated to dryness, to yield the desired product. The ^1H NMR spectrum of the product is in agreement with the crystal structure of *cis*-(S,P)-[PtCl(L1a)(PPh_3)], shown in Figure 4.7. No coordinated or free dimethylsulfoxide signals were observed.

The substitution of the chloride ligand from *cis*-(S,P)-[PtCl(L1a)(PPh_3)] by PPh_3 was carried out in methanol at 25°C. Surprisingly, limiting kinetics in good agreement with that shown in Figure 5.20 (evaluating two consecutive reactions) were obtained for chloride substitution from *cis*-(S,P)-[PtCl(L1a)(PPh_3)] as shown in Figure 5.23. The rate constant and equilibrium constant were determined using equation (**5 – 9**), and are as follows: K_{eq} = 0.6 (fixed), k_{12} = 0.1 $M^{-1}s^{-1}$ (fixed), k_{13} = 0.54(2) s^{-1} and k_{32}/k_{31} = 0.050(8). These values are in good agreement with those given in Table 5.14.

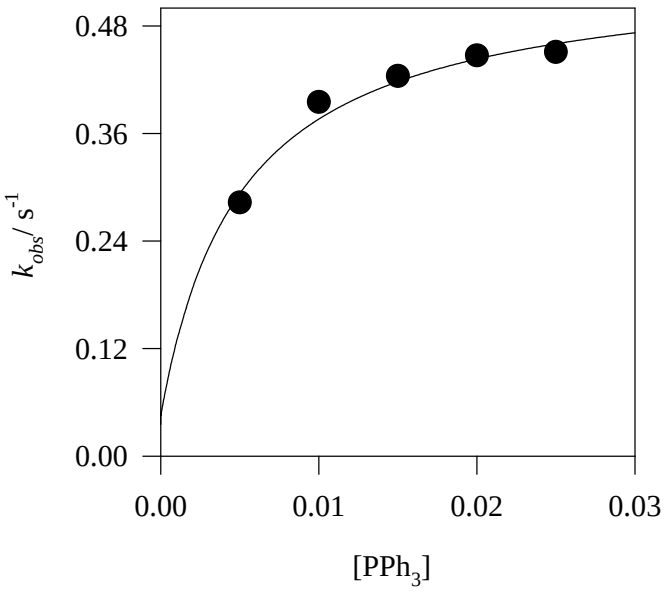

Figure 5.23: Concentration dependence for the reaction of *cis*-(S,P)-[PtCl(L1a)(PPh_3)] with PPh_3 in methanol at 25ºC. $[Pt]_F$ = 0.25 mM. λ = 400 nm. The pseudo first-order rate constants are given in Appendix B, Table B28.

It thus seems as if similar kinetics are obtained independently; a) starting from *cis*-(S,S)-[PtCl(DMSO)(L1a)], studying the second consecutive reaction (chloride substitution by PPh_3) or b) isolating the intermediate *cis*-(S,P)-[PtCl(L1a)(PPh_3)] complex and directly studying only chloride substitution. It is not completely clear why limiting kinetics are obtained for chloride substitution by PPh_3 from *cis*-(S,P)-[PtCl(L1a)(PPh_3)]. One reason could be that solvolysis might take place. The discrimination factor (k_{32}/k_{31}) of 0.050(8) is indicative of a substantial competition between the chloride and the entering PPh_3 for the solvento complex, in which the chloride is favoured. However, further investigation in this regard involves more detailed and complete analysis of the system, which was considered to be beyond the scope of this study.

5.6.6.2 Chloride substitution by DMAP from cis-(S,S)-[PtCl(DMSO)(L1a)]

Since it was also discovered that DMAP could substitute the chloride ligand in a consecutive step, a preliminary study was conducted to gain some knowledge of this reaction. The plot of k_{obs} against [DMAP] is shown in Figure 5.24. Limiting kinetics are obtained for chloride substitution from *cis*-(S,S)-[PtCl(DMSO)(L1a)] by DMAP. The rate constant, k_y, and equilibrium constant, K_{eq}, for chloride substitution by DMAP from

cis-(S,S)-[PtCl(DMSO)(L1a)] in methanol at 25°C were determined by fitting the data according to equation (**5 – 9**). The rate and equilibrium constants obtained were, K_{eq} = 200 (fixed), k_{12} = 0.009(2) $M^{-1}s^{-1}$, k_{13} = 0.0035(6) s^{-1} and k_{32}/k_{31} = 0.012(3).

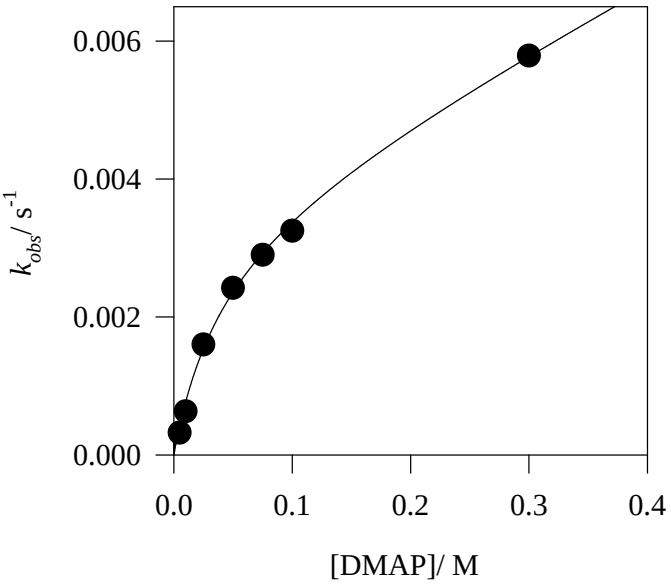

Figure 5.24: Concentration dependence for chloride substitution from *cis*-(S,S)-[PtCl(DMSO)(L1a)] by DMAP in methanol at 25ºC. $[Pt]_F$ = 0.25 mM. λ = 380 nm. The pseudo first-order rate constants are given in Appendix B, Table B29.

It is clear that a similar type of rate law for PPh_3 as entering nucleophile can be operative for DMAP upon substitution of the chloride ligand. Although the rate constant for chloride substitution by PPh_3 from *cis*-(S,P)-[PtCl(L1a)(PPh_3)] via the direct step (k_{12}) is not well defined, the estimated value is still at least two orders of magnitude larger (*ca.* 1 *vs* 0.009 $M^{-1}s^{-1}$, respectively) than for DMAP as entering ligand on the [PtCl(DMAP)(L1a)] complex. This also holds for the solvent step (k_{13} = 0.51(9) *vs* 0.0035(6) s^{-1}, respectively). In general this underlines the increased ability of PPh_3 as the entering ligand. It can also however be a reflection of the DMAP (when first already coordinated; good sigma donor), to increase the electron density at the platinum atom, thus opposing the entering of a second DMAP as entering nucleophile. In comparison, it is worth noting that the relative difference between PPh_3 and DMAP as entering nucleophiles in the first substitution step is more than three orders of magnitude ($k_y = k_{12}$ = 1138(46) *vs* 0.87(4) $M^{-1}s^{-1}$, respectively) and approximately two orders of magnitude

difference for the second step (*ca.* $k_y = k_{12} = 0.1$ *vs* 0.009(2) $M^{-1}s^{-1}$, respectively). A detailed investigation of this system was not explored, as it is considered beyond the scope of this study.

5.7 Discussion

5.7.1 Effect of the incoming nucleophile

5.7.1.1 Substitution kinetics of cis-(S,S)-[PtCl(DMSO)(L1a)]

According to the data given in Table 5.8, the order of reactivity was found to be: DMAP < MBI < thiourea < PPh_3, which is in agreement with the nucleophilic reactivity index determined for *trans*-$[PtCl_2(py)_2]$. [27–28] The overall order of reactivity for all the nucleophiles studied was: N_3^- < DMAP < I^- < SCN^- < MBI < thiourea < PPh_3. The rate for the first substitution step at 25°C varied by three orders of magnitude for the range of nucleophiles studied.

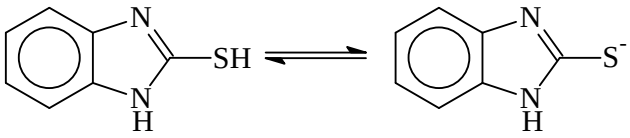

Thiol Thiolate anion

It is important to note that 2-mercaptobenzimidazole (MBI) can exist as either the thiol (RSH) or the thiolate anion (RS^-) as shown above. The thiol is expected to be less reactive than the thiolate anion as entering ligand. Comparison of the n_{Pt}° (nucleophilic reactivity constant) values for the nucleophiles studied was very informative and gave an indication as to which tautomer of MBI was reacting in methanol. Because no values for the nucleophilic reactivity constant exists for MBI, the value for thiophenol was used as a substitute. The series obtained in the literature [27–28] is as follows, N_3^- < RSH < I^- < SCN^- < RS^- ≈ thiourea < PPh_3. Based on the fact that MBI is more reactive than iodide and thiocyanate, and less reactive than thiourea, it is thus proposed that MBI is reacting as the thiolate anion (RS^-) in methanol. This may appear to be contrary to the observation that

the anionic nucleophiles initially substituted the chloride ligand, while for MBI the sulfoxide is substituted, but the thiolate anion has significant π-properties and is therefore expected to substitute the DMSO group.

5.7.2 Effect of sulfoxide as a leaving group

There is a distinct effect on sulfoxide substitution upon changing the electronic properties of the coordinating sulfoxide ligands. The rate of sulfoxide substitution is enhanced when the electron-withdrawing nature of the R and R' groups increases. As seen from Table 5.15, the labilising ability of the sulfoxides studied decreases in the order: MPSO > (*S*)-MTSO > DMSO. A similar order of lability was obtained by Farrell *et al.* for the substitution of the coordinated sulfoxide from $[PtCl(RR'SO)(diamine)]^+$ by chloride. [35]

Table 5.15: Second-order rate constants, k_y, for sulfoxide substitution by MBI from *cis*-(S,S)-[PtCl(L1a)(RR'SO)] in methanol at 25°C.

RR'SO	k_y/ $M^{-1}s^{-1}$	$k_{RR'SO}$/ k_{DMSO}
DMSO	42(1)	1
(*S*)-MTSO	94(4)	2.2
MPSO	121(8)	2.9

The Pt–S(sulfoxide) bond lengths of *cis*-(S,S)-[PtCl(DMSO)(L1a)] and *cis*-(S,S)-[PtCl(L1a)(MPSO)] are 2.1885(10) Å and 2.192(3) Å, respectively (Section 4.2.2.4). The Pt–S(sulfoxide) bond length for *cis*-(S,S)-[PtCl(DMSO)(L1a)] is slightly shorter than the Pt–S(sulfoxide) bond length for *cis*-(S,S)-[PtCl(L1a)(MPSO)], which is consistent the slower rate of sulfoxide substitution from *cis*-(S,S)-[PtCl(DMSO)(L1a)] compared to *cis*-(S,S)-[PtCl(L1a)(MPSO)].

For comparison, selected platinum(II) sulfoxide bond distances and second-order rate constants, k_y, for the substitution of dimethylsulfoxide and chloride by thiourea are given in Table 5.16. However, no direct quantitative comparison of the rate constants can be made due to the differences in charge and solvents. The rate constant for dimethylsulfoxide substitution by thiourea from *cis*-(S,S)-[PtCl(DMSO)(L1a)] is about five times smaller than from $[Pt(DMSO)(phen)Me]^+$. Interestingly, the rate constant for

dimethylsulfoxide substitution by thiourea from *cis*-(S,S)-[PtCl(DMSO)(L1a)] is of the same order of magnitude as the substitution of water from $[Pt(DMSO)(en)(H_2O)]^{2+}$, reflecting the lability of the sulfoxide in the *cis*-(S,S)-[PtCl(DMSO)(L1a)] complex. Dimethylsulfoxide substitution from *cis*-(S,S)-[PtCl(DMSO)(L1a)] by thiourea is an order of magnitude slower than from $[Pt(DMSO)_2(en)]^{2+}$. This is in agreement with the generally accepted trend that the substitution of a single sulfoxide is more difficult than the substitution of a single sulfoxide from two mutually *cis*-sulfoxides.

Table 5.16: Bond lengths of some platinum(II) sulfoxide complexes and second-order rate constants for the substitution of the sulfoxide or chloride by thiourea. The bold text indicates the leaving group.

Complex	Pt–S/ Å	k_y/ $M^{-1}s^{-1}$ [g]	Ref.
cis-(S,S)-[PtCl(**DMSO**)(L1a)] [a]	2.1885(10)	107(1)	This work
[Pt(**DMSO**)(phen)Me]$^{+}$ [b]	2.203(1)	539	24
[Pt(DMSO)(en) (**H_2O**)]$^{2+}$ [c]	-	640	18
[Pt(**DMSO**)$_2$(en)]$^{2+}$ [d]	2.249, 2.248	6650	18, 36
[Pt**Cl**(DMSO)(en)]$^{+}$ [e]	2.219(3)	4.48	19, 30
[Pt**Cl**(DMSO)(Me_4en)]$^{+}$ [f]	2.234(4)	0.00792(20)	20
[PtMe(dpa)((DMSO)]$^{+}$	2.197(1)	-	37
trans-[PtCl(DMSO)(NH_3)$_2$]$^{+}$	2.204(4)	-	38

[a] In methanol at 25°C.

[b] In methanol/ water (19:1 (v/v)) at 25°C; corrected to $\mu = 0$.

[c] In water at 30°C; corrected to $\mu = 0$.

[d] In methanol at 30°C; corrected to $\mu = 0$.

[e] In water at 25°C; corrected to $\mu = 0$.

[f] In water at 25°C; $\mu = 0.10$ mol dm^{-3} ($LiClO_4$).

[g] Where no standard deviations are given, these have not been reported in the original paper.

For *cis*-(S,S)-[PtCl(DMSO)(L1a)], the Pt–S(sulfoxide) bond distance of 2.1885(10) Å is significantly shorter than the range of Pt–S(sulfoxide) bond distances, 2.197–2.249 Å, given in Table 5.16. The fact that the Pt–S(sulfoxide) bond is stronger in *cis*-(S,S)-[PtCl(DMSO)(L1a)] than the diimine complexes is paralleled by its smaller rate constant.

5.7.3 Electronic effects on dimethylsulfoxide substitution

5.7.3.1 Effect of the amine

As seen from Table 5.10, comparison of dimethylsulfoxide substitution by MBI from *cis*-(S,S)-[PtCl(DMSO)(L3a)] and *cis*-(S,S)-[PtCl(DMSO)(L1a)] indicates that variation of the amine moiety for diethylamine and di(2-hydroxyethyl)amine has a small effect on the rate. This is not surprising because the amine is relatively far from the platinum nucleus and cannot affect the electron density at the metal centre via inductive/mesomeric effects.

5.7.4 Solvent effects

5.7.4.1 Effect of the solvent on dimethylsulfoxide substitution

The rate of dimethylsulfoxide substitution by PPh_3 showed a strong dependence on the solvent, with rates varying by an order of magnitude (Table 5.13). The rate of dimethylsulfoxide substitution by PPh_3 increased in the order: dichloromethane < acetone < acetonitrile < methanol. The increase in the rate of dimethylsulfoxide substitution corresponds to an increase in the donicity and dielectric constants of the various solvents. In all the solvents employed in this study, the contribution from the solvent pathway was found to be negligible, and therefore, the observed increase in the rate of reaction is not due to an increased contribution from the solvolytic pathway.

5.7.4.2 Effect of the solvent on chloride substitution

The strong solvent dependence of dimethylsulfoxide and chloride substitution by triphenylphosphine from *cis*-(S,S)-[PtCl(DMSO)(L1a)] suggests that both the first and second substitution steps are significantly affected by the solvents properties, especially an increase in polarity, which suggests a polar transition state, stabilised by the solvent.

5.7.5 Second consecutive reaction: chloride substitution

5.7.5.1 Chloride substitution by PPh_3 and by DMAP from cis-(S,S)-[PtCl(DMSO)(L1a)]

Limiting kinetics were observed for chloride substitution by PPh_3 and DMAP from *cis*-(S,S)-[PtCl(DMSO)(L1a)], and are shown in Figure 5.20 and Figure 5.24, respectively. The presence of excess chloride had a small and virtually negligible effect on the rate of chloride substitution from *cis*-(S,S)-[PtCl(DMSO)(L1a)] by PPh_3, (Figure 5.21).

5.7.5.2 Substitution kinetics of cis-(S,P)-[PtCl(L1a)(PPh_3)] with PPh_3

As mentioned previously, the limiting kinetics observed for chloride substitution from *cis*-(S,S)-[PtCl(DMSO)(L1a)] by PPh_3, (Figure 5.20), could possibly be caused by a fast pre-equilibrium in the first substitution step. In order to validate this, the intermediate *cis*-(S,P)-[PtCl(L1a)(PPh_3)] complex was prepared, so that the second reaction could be evaluated without any interference from the first substitution step. Surprisingly, limiting kinetics were again observed for chloride substitution from *cis*-(S,P)-[PtCl(L1a)(PPh_3)] by PPh_3. The two sets of rate and equilibrium constants for chloride substitution from *cis*-(S,S)-[PtCl(DMSO)(L1a)] and *cis*-(S,P)-[PtCl(L1a)(PPh_3)] are of the same order of magnitude, which suggests that these two reactions may be similar. As noted, the reason for observing similar reaction profiles is not completely clear. Further studies are therefore necessary to clarify this.

5.8 Overall discussion

5.8.1 Leaving group discrimination

As mentioned previously, ^{1}H NMR studies indicated that neutral nucleophiles substituted the sulfoxide ligand initially, while anionic nucleophiles were found to substitute the chloride ligand in the first substitution step.

As seen from Figure 5.25, the anionic and neutral nucleophiles have different intercepts, reflecting the different rates of solvolysis of the potential chloride and sulfoxide leaving

groups, suggesting that the anionic and neutral nucleophiles are substituting different leaving groups in the first substitution step. Further kinetic evidence for different substitution processes is obtained by the linear free-energy relationship (LFER) shown in Figure 5.26. Because no values for the nucleophilic reactivity index were available for DMAP and MBI in the literature, the values for pyridine and mercaptophenol (as thiolate) were used, respectively, and these resulted in a good linear relationship. The anionic and neutral nucleophiles show two distinct linear free-energy relationships, which indicates that the neutral and anionic nucleophiles are substituting different ligands.

5.8.2 Effect of the non-leaving group

As discussed previously (Section 5.2), the ancillary non-leaving group has a significant effect on the lability of sulfur-bonded sulfoxides. [20–22] In aqueous or methanolic solutions of $[Pt(am)(Cl)(DMSO)]^+$, where am = diamine or monodentate amines, only chloride substitution was observed, with no DMSO substitution except when substituted ethylenediamines were used. Ligands with π-properties have also been shown to have a labilising effect on the coordinated sulfoxide. These ligands include bipyridine and 1,10-phenathroline, in which the electrons are extensively delocalised.

^{1}H NMR and X-ray crystallographic studies (Chapter 4) have shown that the electrons in the acylthioureato chelate are extensively delocalised and possess significant double bond character. The ligands are also unusual because they contain donor atoms with both σ- and π-properties, namely the oxygen and sulfur donor atoms. Hence, the π-properties and extensive delocalisation of electrons in the acylthioureato chelate could result in the labilisation of the coordinated dimethylsulfoxide in an analogous manner to the 1,10-phenanthroline and bipyridine complexes.

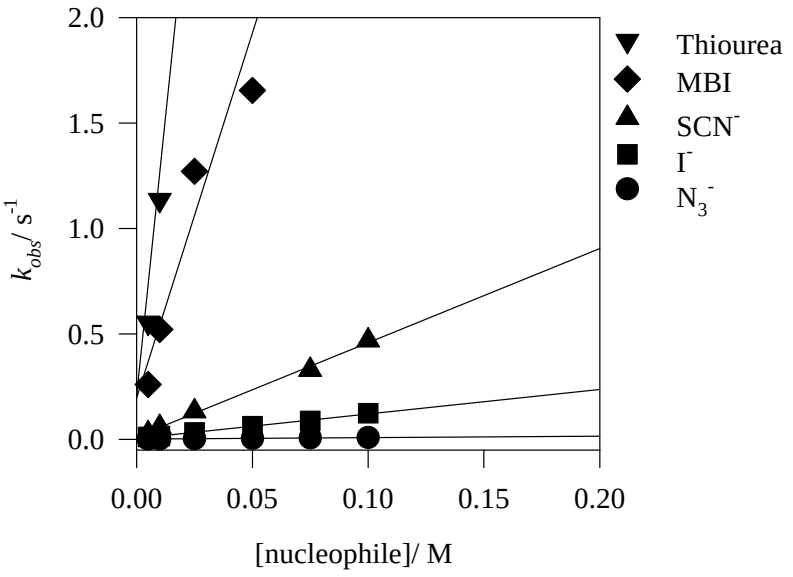

Figure 5.25: Concentration dependence for the reaction of *cis*-(S,S)-[PtCl(DMSO)(L1a)] with selected anionic and neutral nucleophiles, highlighting the different intercepts for the anionic and neutral nucleophiles.

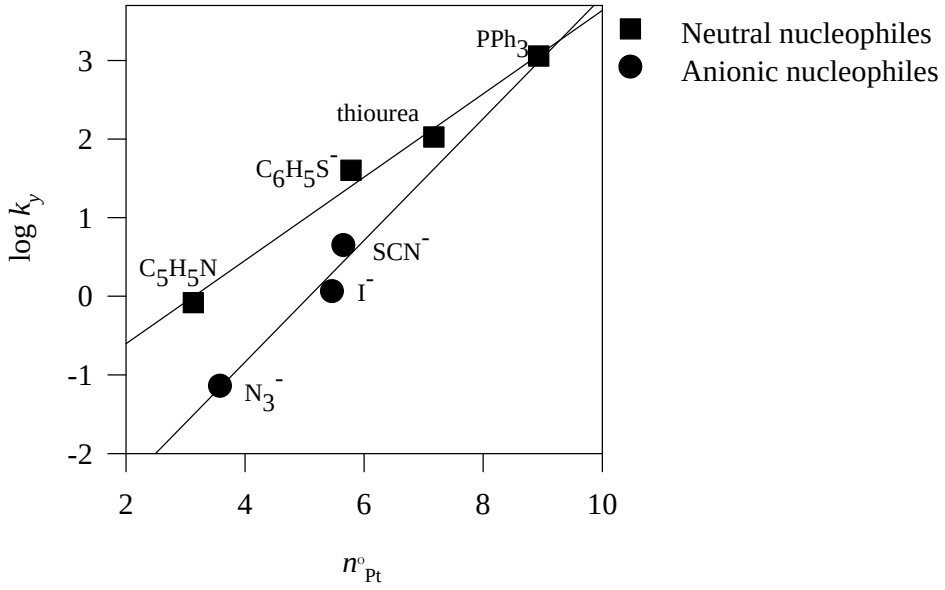

Figure 5.26: Effect of the incoming nucleophile on the linear relationship between log k_y and $n°_{Pt}$ for the initial substitution of dimethylsulfoxide and chloride from *cis*-(S,S)-[PtCl(DMSO)(L1a)] in methanol at 25°C.

5.8.3 Mechanistic implications

A more detailed mechanistic study with regard to the second consecutive chloride substitution step by neutral nucleophiles is beyond the scope of this thesis, but some important observations have been made which may have bearing on the mechanism of these reactions. The presence of excess dimethylsulfoxide had a significant effect on the rate of the first substitution step from *cis*-(S,S)-[PtCl(DMSO)(L1a)] by MBI, DMAP and PPh_3, suggesting that these reactions involve equilibria. The strong dependence of the rate of reaction with PPh_3 on the solvent is consistent with this observation. Similarly, the dependence of chloride substitution by PPh_3 from *cis*-(S,S)-[PtCl(DMSO)(L1a)] on the concentration of chloride and on the nature of the solvent also suggests that this step involves equilibria. This would be expected, because of the steric crowding in forming a complex with two large PPh_3 ligands in a *cis* arrangement. Furthermore, limiting kinetics were obtained for chloride substitution by PPh_3 and by DMAP from *cis*-(S,S)-[PtCl(DMSO)(L1a)].

The dependence of chloride substitution by PPh_3 and by DMAP from *cis*-(S,S)-[PtCl(DMSO)(L1a)] on the concentration of the incoming nucleophile may be due to the following:

i) The first substitution step involves a rapid pre-equilibrium.

ii) The complete square-planar substitution rate law (equation (**5 – 9**)) is operative. This rate law is applicable when significant equilibria are present.

Chloride substitution from *cis*-(S,P)-[PtCl(L1a)(PPh_3)] by PPh_3 showed a curved dependence on the concentration of PPh_3, suggesting that the second step is preceded by a rapid equilibrium. This is consistent with the observed solvent and chloride dependence of chloride substitution from *cis*-(S,S)-[PtCl(DMSO)(L1a)] by PPh_3. The small equilibrium constants determined from ^1H NMR and the solvent dependence of dimethylsulfoxide substitution from *cis*-(S,S)-[PtCl(DMSO)(L1a)] by PPh_3, indicate that an equilibrium exists in the first substitution step. It was thus concluded that the complete rate law (Section 5.1.1) should be used in the interpretation of these kinetics which complicates the isolation of the contributions by the different steps.

5.9 Conclusion

For the substitution reaction kinetics of complexes of the type *cis*-(S,S)-[Pt(acylthioureato)Cl(RR'SO)], two consecutive reactions were observed for all the nucleophiles studied: a fast first substitution step followed by a significantly slower second step. The substitution products were confirmed by ^{1}H NMR spectroscopy. Neutral nucleophiles, or nucleophiles with π-properties, were found to initially substitute the dimethylsulfoxide, while anionic nucleophiles, or nucleophiles with σ-properties, were found to substitute the chloride ligand. The substitution of the dimethylsulfoxide ligand, in the first substitution step of *cis*-(S,S)-[PtCl(DMSO)(L1a)] with PPh_3, was also confirmed by X-ray crystallography.

The present studies have also shown that there is a distinct effect on sulfoxide substitution upon changing the electronic properties of the coordinating sulfoxide ligand. The rate of sulfoxide substitution is enhanced when the electron-withdrawing nature of the R- and R'-groups increases. The sulfoxides also exhibited a significant *cis*-effect, decreasing in the order: MPSO > (*S*)–MTSO > DMSO.

Variation of the amine moiety had a small effect on chloride and dimethylsulfoxide substitution. Similarly, variation of the electronic properties of the benzoyl moiety also had a small but significant effect on the rate of chloride substitution.

In general, manipulation of electron density on the chelating moiety, as well as interchanging the sulfoxide did not alter the reactivity to a great extent. Thus, it is anticipated that variation of substituents to obtain optimum chemotherapeutic activity will not influence the kinetics of the system to a significant extent. Furthermore, the substitution of different leaving groups in these complexes are clearly possible, for example, sulfur donor sites *in vivo* are likely to substitute the dimethylsulfoxide ligand whereas more sigma orientated sites are likely to attack the chloride ligand.

5.10 References

1. E. L. M. Lempers, J. Reedijk, *Adv. Inorg. Chem*., 1991, **37**, 175.
2. F. R. Hartley, *Chem. Soc. Rev*., 1973, 163.
3. B. E. Douglas, D. H. McDaniel, J. J. Alexander, in *Concepts and Models of Inorganic Chemistry*, John Wiley & Sons, Inc., New York, 1994.
4. M. L. Tobe, J. Burgess, in *Inorganic Reaction Mechanisms*, Addison Wesley Longman Ltd., New York, 1999.
5. U. Belluco, M. Martelli, A. Orio, *Inorg. Chem.*, 1966, **5**, 582.
6. M. Kotowski, D. A. Palmer, H. Kelm, *Inorg. Chem.*, 1979, **18**, 2555.
7. U. Belluco, A. Orio, M. Martelli, *Inorg. Chem.*, 1966, **5**, 1370.
8. G. Faraone, V. Ricevuto, R. Romeo, M. Trozzi, *Inorg. Chem.*, 1970, **9**, 1525.
9. A. L. Odell, H. A. Raethel, *Chem. Commun.*, 1968, 1323.
10. A. L. Odell, H. A. Raethel, *Chem. Commun.*, 1969, 87.
11. L. Cattalini, A. Orio, A. Doni, *Inorg. Chem.*, 1966, **5**, 1517.
12. D. Minniti, G. Alibrandi, M. L. Tobe, R. Romeo, *Inorg. Chem.*, 1987, **26**, 3956.
13. S. Lanza, D. Minniti, P. Moore, J. Sachinidis, R. Romeo, M. L. Tobe, *Inorg. Chem.*, 1984, **23**, 4428.
14. U. Frey, L. Helm, A. E. Merbach, R. Romeo, *J. Am. Chem. Soc.*, 1989, **111**, 8161.
15. R. Romeo, A. Grassi, L. M. Scolaro, *Inorg. Chem.*, 1992, **31**, 4383.
16. R. G. Wilkins, in *Kinetics and Mechanisms of Reactions of Transition Metal Complexes*, VCH, New York, 2nd edn., 1991.
17. K. F. Purcell, J. C. Kotz, *Inorganic Chemistry*, W. B. Saunders Company, London, 1985.
18. S. Lanza, D. Minniti, R. Romeo, M. L. Tobe, *Inorg Chem.*, 1983, **22**, 2006.
19. M. Bonivento, L. Cattalini, G. Marangoni, G. Michelon, A. P. Schwab, M. L. Tobe, *Inorg. Chem.*, 1980, **19**, 1743.
20. G. Alibrandi, R. Romeo, L. M. Scolaro, M. L. Tobe, *Inorg. Chem.*, 1992, **31**, 5061.
21. G. Annibale, L. Canovese, G. Chessa, L. Cattalini, M. L. Tobe, *J. Chem. Soc., Dalton Trans.*, 1990, 401.
22. R. Romeo, L. M. Scolaro, N. Nastasi, G. Arena, *Inorg. Chem.*, 1996, **35**, 5087.
23. U. Fekl, R. van Eldik, *Eur. J. Chem.*, 1998, 389.

24. R. Romeo, G. Arena, L. M. Scolaro, M. R. Plutino, *Inorg. Chim. Acta*, 1995, **240**, 81.
25. Least-Squares Parameter Estimation, Version 4.00.950, MICROMATH, 1990.
26. On-line Instrument Systems Inc., Jefferson, Ga 30549.
27. R. G. Pearson, H. Sobel, J. Songstad, *J. Am. Chem. Soc.*, 1968, **90**, 319.
28. U. Belluco, L. Cattalini, F. Basolo, R. G. Pearson, A. Turco, *J. Am. Chem. Soc*., 1965, **87**, 241.
29. J. F. Britten, C. J. L. Lock, W. M. C. Pratt, *Acta Crystallogr., Sect. B*, 1982, **38**, 2148.
30. O. Clement, A. W. Roszak, E. Buncel, *Inorg. Chim. Acta*, 1996, **253**, 53.
31. M. Calligaris, O. Carugo, *Coord. Chem. Rev.*, 1996, **153**, 83.
32. J. A. Davies, *Adv. Inorg. Chem. Radiochem.*, 1981, **24**, 115.
33. L. Cattalini, in *Inorganic Reaction Mechanisms*: *Progress in Inorganic Chemsitry*, ed. J. O. Edwards, John Wiley & Sons, Inc., New York, 1970.
34. M. Casey, J. Leonard, B. Lygo, in *Advanced Practical Organic Chemistry*, Blackie Academic & Professional, London, 1993.
35. N. Farrell, D. M. Kiley, W. Schmidt, M. P. Hacker, *Inorg. Chem.*, 1990, **29**, 397.
36. G. Bruno, G. Bombieri, G. Alibrandi, S. Lanza, R. Romeo, *Cryst. Struct. Commun.*, 1982, **11**, 1369.
37. R. Romeo, N. Nastasi, L. M. Scolaro, M. R. Plutino, A. Albinati, A. Macchioni, *Inorg Chem*., 1998, **37**, 5460.
38. W. I. Sundquist, K. J. Ahmed, L. S. Hollis, S. J. Lippard, *Inorg. Chem.*, 1987, **26**, 1524.

CHAPTER 6

BIOLOGICAL STUDIES

6.1 Introduction

DNA contains the cell's genetic information and is responsible for the coding and regulation of proteins and enzymes that control cell growth and division, as well as the biosynthesis of necessary compounds that are required for cellular function. The regulation of these cellular processes is controlled by the interaction of regulatory proteins and small molecules with DNA in specific conformations. The binding of drugs or other molecules to DNA results in specific conformational changes in the DNA structure, which result in the activation and/or inactivation of DNA replication and gene regulation. Thus, considerable research effort has been applied to the identification and characterisation of the adducts of drugs with DNA in order to understand the relationship between DNA binding specificity and adduct formation with cytotoxicity, drug resistance, mutagenesis and carcinogenesis of these drugs. [1–15]

DNA binding studies may be carried out with bacterial closed circular supercoiled plasmid DNA because of the sensitivity with which small tertiary structural changes can be monitored and because their superhelical nature better mimics that of chromatin. [16] As shown in Figure 6.1, supercoiled plasmid DNA may exist in various conformations. The DNA may be in a random linear form (form III), an open circular form (form II) or a closed circular superhelical form (form I), (Figure 6.1). [2] DNA of different topological forms have different electrophoretic mobilities, which can be detected by gel electrophoresis. [17–18]

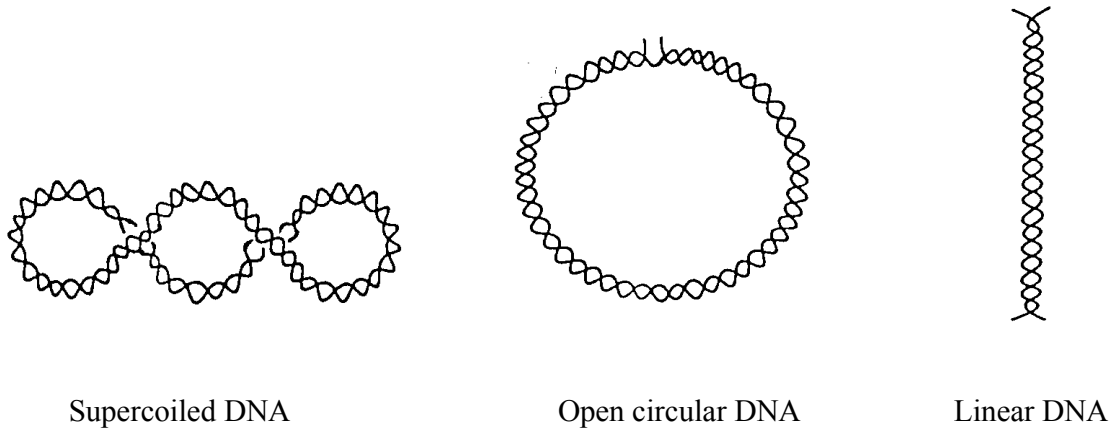

Figure 6.1: Schematic diagram of supercoiled (form I), open circular (form II) and linear (form III) forms of DNA. [2]

For closed circular DNA, the topology can be described by the link number, α, defined by equation (**6 – 1**), where β is the number of helical turns of the DNA molecule and τ is the number of superhelical turns. [17–19]

$$\alpha = \beta + \tau \qquad (\mathbf{6-1})$$

The linking number remains constant as long as the DNA molecule is not cleaved. A compound that unwinds the DNA decreases β. To keep the α value constant, τ, a negative number, must become more positive. The net effect is that the number of supercoils is reduced and the superhelical density decreases. This decease in superhelical density upon the unwinding of the DNA causes a decrease in the electrophoretic mobility of the DNA. [17–19] Closed supercoiled DNA (SC, form I) will migrate the fastest through the gel followed by the linear form (form III) with the open circular or nicked open circular (OC, form II) intermediate.

The cytotoxicity of the [PtCl(L)(RR'SO)] complexes (Chapter 4) prepared in this study were evaluated against a HeLa cell line, and some selected complexes were also evaluated against a MCF-7 cell line, by Prof. J. Seegers and Dr M. –L. Lottering, at the University of Pretoria, South Africa. Preliminary morphology studies were also carried out by Prof J. Seegers and Dr M. –L. Lottering, to determine if these platinum complexes induce apoptosis or necrosis in the HeLa cells. Preliminary DNA binding studies of selected *cis*-(S,S)-[Pt(acylthioureato)Cl(DMSO)] complexes were carried out with pBR322 plasmid DNA, using a gel mobility shift assay, to determine the binding properties of these complexes. The cytotoxicity of the ligand systems was evaluated at the National Cancer Institute (NCI, Bethesda, MA, USA) in their *in vitro* anticancer screening system.

6.2 Results

6.2.1 *In vitro* cytotoxicity studies

The ligand systems displayed no significant anticancer activity. *In vitro* cytotoxicity studies of all the [PtCl(L)(RR'SO)] complexes prepared were carried out against a HeLa

cell line. Only three complexes **1c**, **2c** and **2d** exhibited a concentration dependent anti-proliferative effect (Figure 6.3). The cytotoxicity of these three complexes was then evaluated against a MCF-7 cell line (Figure 6.4). These three complexes showed similar activity in the MCF-7 cell line. The plots of percentage HeLa cells against [complex] and percentage MCF-7 cells against [complex] are shown in Figure 6.3 and Figure 6.4, respectively, for the three complexes exhibiting biological activity. The structures of the three complexes exhibiting anticancer activity are shown in Figure 6.2.

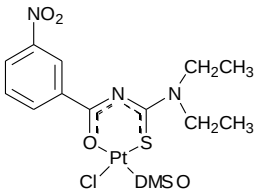

cis-(S,S)-[PtCl(DMSO)(L1c)] (**1c**)

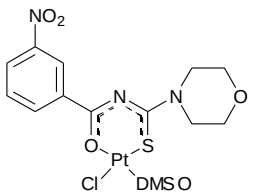

cis-(S,S)-[PtCl(DMSO)(L2c)] (**2c**)

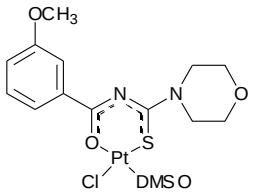

cis-(S,S)-[PtCl(DMSO)(L2d)] (**2d**)

Figure 6.2: Structures of complexes exhibiting a concentration dependent anti-proliferative effect against HeLa and MCF-7 cell lines.

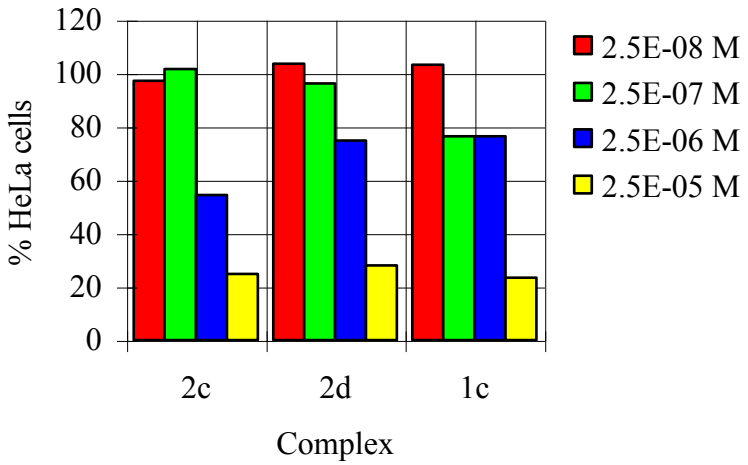

Figure 6.3: Percentage HeLa cells/control against concentration of the respective platinum complexes, *cis*-(S,S)-[Pt(DMSO)(L2c)] (**2c**), *cis*-(S,S)-[Pt(DMSO)(L2d)] (**2d**), and *cis*-(S,S)-[Pt(DMSO)(L1c)] (**1c**). The control was [DMSO] = 0.05% in all samples.

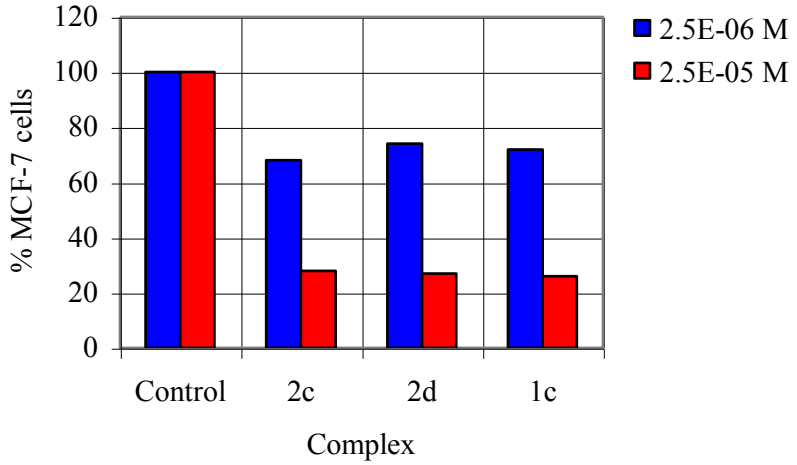

Figure 6.4: Percentage MCF-7 cells/control against concentration of the respective platinum complexes, *cis*-(S,S)-[Pt(DMSO)(L2c)] (**2c**), *cis*-(S,S)-[Pt(DMSO)(L2d)] (**2d**) and *cis*-(S,S)-[Pt(DMSO)(L1c)] (**1c**). The control was [DMSO] = 0.05% in all samples.

As seen from Figure 6.3 and Figure 6.4, complexes **1c**, **2c**, and **2d** display significant anticancer activity in HeLa and MCF-7 cell lines, but are less cytotoxic than cisplatin. Cisplatin has IC_{50} values of 7(5) and 0.74(14) μM in HeLa and MCF-7 cell lines, respectively.[20, 21] The IC_{50} value is the concentration of the platinum complex required to inhibit cell growth by 50% relative to a control.

6.2.1.1 Morphology studies

Preliminary morphology studies using the biologically active complexes were carried out against a HeLa cell line, to determine if the complexes **1c**, **2c** and **2d** induce cell death by apoptosis or necrosis. Selected pictures of the cells after exposure to the respective platinum complexes for 72 hours are shown in Figures 6.5–6.7.

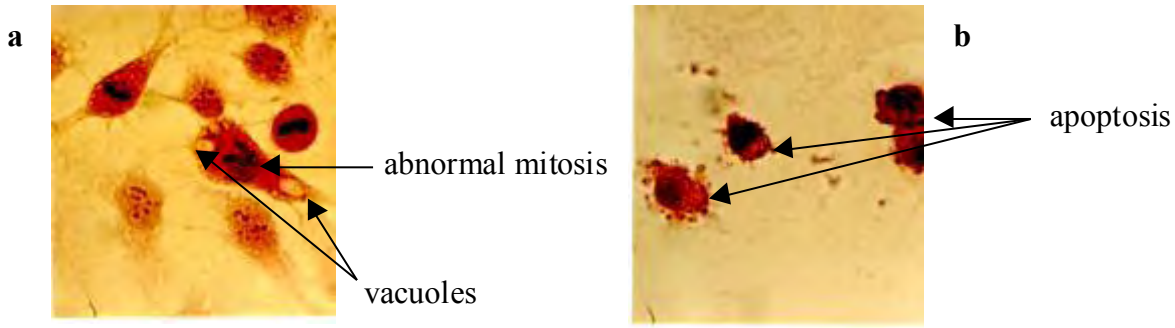

Figure 6.5: Pictures of HeLa cells after exposure for 72 hours, where **a** = *cis*-(S,S)-[Pt(DMSO)(L1c)] (**1c**), *ca*. 10^{-6} M and **b** = *cis*-(S,S)-[Pt(DMSO)(L1c)] (**1c**), *ca*. 10^{-5} M.

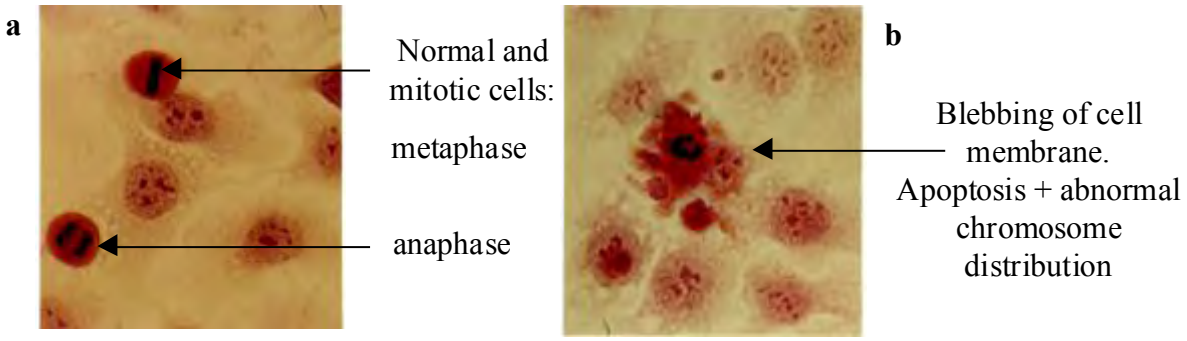

Figure 6.6: Pictures of cells after exposure for 72 hours. **a** = Control (DMSO, 0.05%). **b** = *cis*-(S,S)-[Pt(DMSO)(L2d)] (**2d**), *ca*. 10^{-5} M.

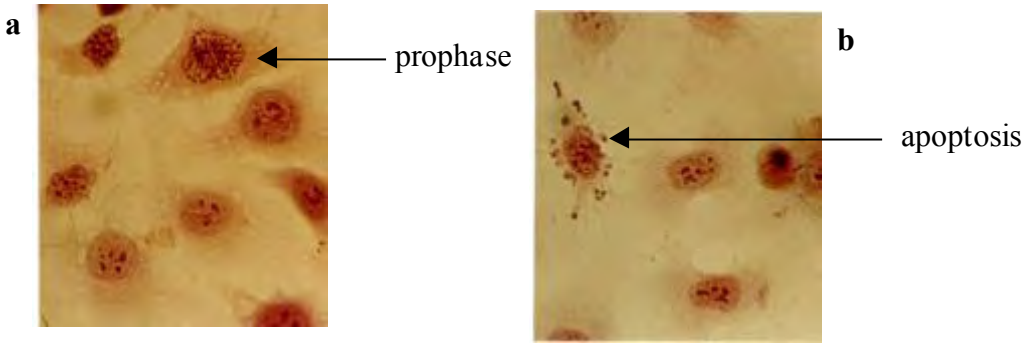

Figure 6.7: Pictures of cells after exposure for 72 hours. **a** = Control (DMSO, 0.05%). **b** = *cis*-(S,S)-[Pt(DMSO)(L2c)] (**2c**), *ca*. 10^{-5} M.

As shown in Figures 6.5–6.7, the presence of membrane blebbing and the formation of membrane bound vesicles (apoptotic bodies) clearly demonstrates that complexes **1c**, **2c** and **2d** induce cell death by apoptosis, which suggests that DNA is a major target for the binding of these complexes. Therefore, a preliminary plasmid DNA binding study was carried out to determine the mode of binding of these complexes to DNA.

6.2.2 Plasmid binding studies

6.2.2.1 Cisplatin

Gel mobility shift assays were carried out with cisplatin so that a direct comparison could be made with the covalent binders prepared in this study. The affect of cisplatin binding to pBR322 DNA, in the absence and presence of ethidium bromide, are shown in Figure 6.8 and Figure 6.9, respectively. The presence of ethidium bromide in the gel ensures that the DNA is wound into a net positively wound superhelix, suppressing the effect on the electrophoretic mobility upon changes in the superhelix density in regions of unbound platinum. [16] On binding to DNA, a decrease followed by a gradual increase in the electrophoretic mobility of the supercoiled (SC) DNA was observed (Figure 6.8), with increasing concentration of cisplatin, indicating that upon cisplatin binding to supercoiled DNA unwinding and winding of the DNA is observed. The supercoiled DNA is completely unwound in the 5 to 10 μM range. Upon bidentate coordination of cisplatin to DNA in the presence of ethidium bromide (Figure 6.9), there is a distinct increase in the mobility of both the supercoiled (SC) and open circular (OC) DNA, suggesting that the binding of cisplatin to DNA shortens and/or kinks the DNA structure. These results are in agreement with studies reported in the literature. [16, 22] The structural details of cisplatin-DNA adducts are given in Chapter 1.

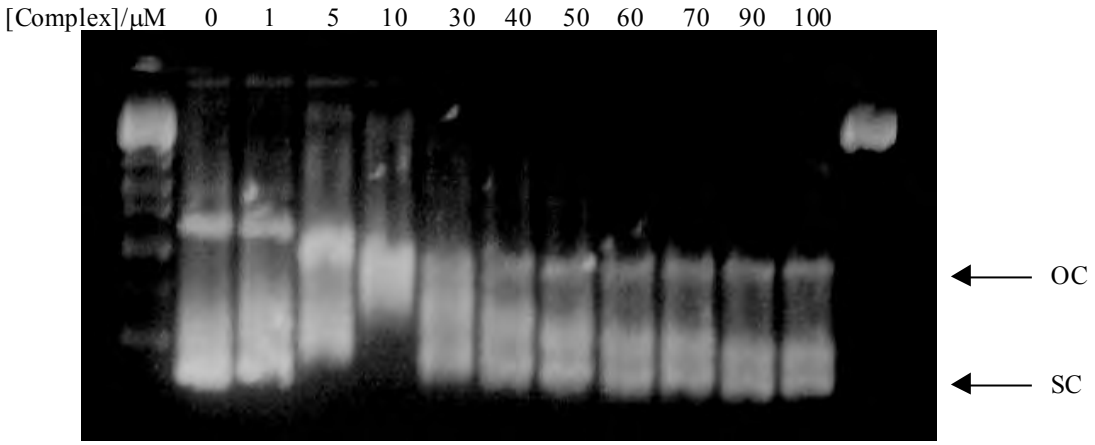

Figure 6.8: Electrophoresis in a 1% agarose gel of 0.4 μg of pBR322 incubated with various concentrations of cisplatin for 4 hours at 37°C.

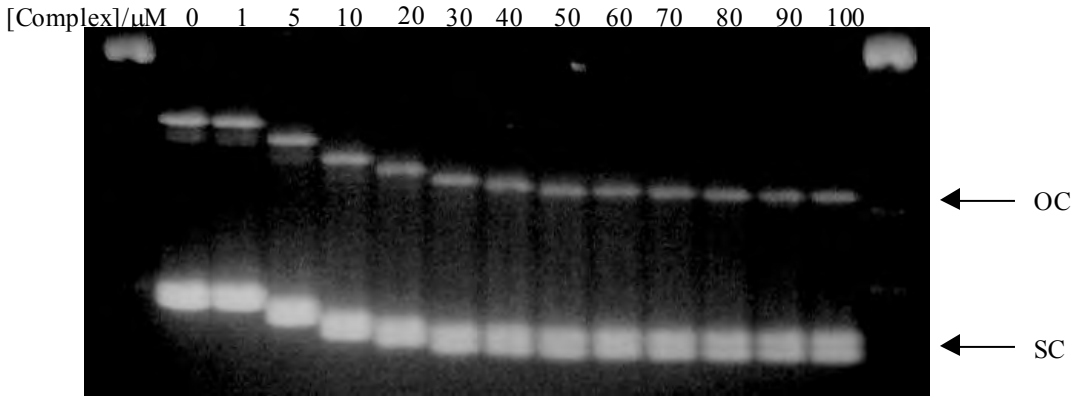

Figure 6.9: Electrophoresis in a 1% agarose gel containing 15 μl ethidium bromide, of 0.4 μg of pBR322 incubated with various concentrations of cisplatin for 4 hours at 37°C.

6.2.2.2 cis-(S,S)-*[PtCl(DMSO)(L3c)]* (***3c***) *and cis*-(S,S)-*[PtCl(DMSO)(L1c)]* (***1c***)

Complex **1c** showed a concentration dependent anti-proliferative effect against MCF-7 and HeLa cell lines, while complex **3c** was inactive. The DNA binding properties of these two complexes were evaluated to determine if the observed cytotoxicity was due to a different mode of binding to DNA. The gels showing the binding of *cis*-(S,S)-[PtCl(DMSO)(L3c)] (**3c**) and *cis*-(S,S)-[PtCl(DMSO)(L1c)] (**1c**) with pBR322 DNA are shown in Figure 6.10 and Figure 6.11, respectively.

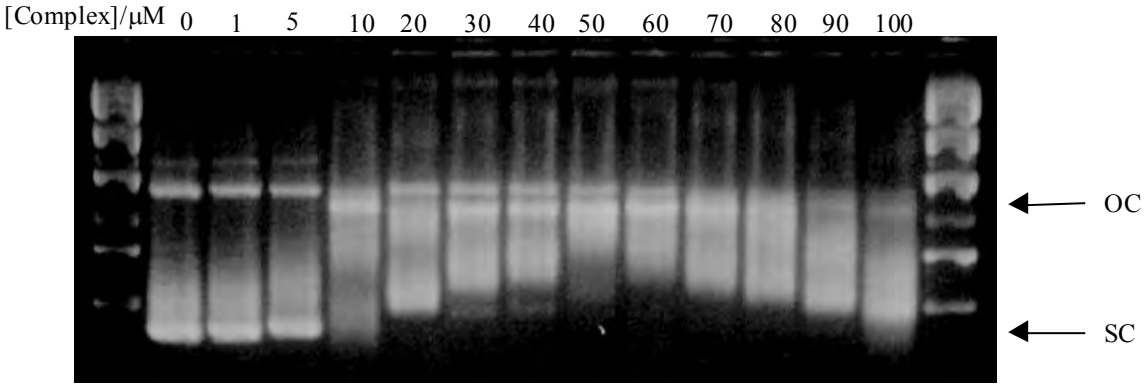

Figure 6.10: Electrophoresis in a 1% agarose gel of 0.4 μg of pBR322 incubated with various concentrations of *cis*-(S,S)-[PtCl(DMSO)(L3c)] (**3c**) for 4 hours at 37°C.

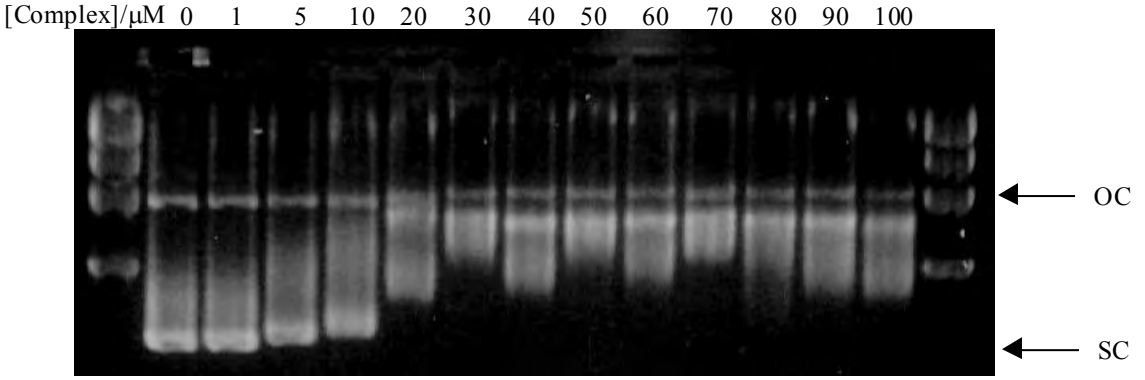

Figure 6.11: Electrophoresis in a 1% agarose gel of 0.4 μg of pBR322 incubated with various concentrations of *cis*-(S,S)-[PtCl(DMSO)(L1c)] (**1c**) for 4 hours at 37°C.

As shown in Figure 6.10 and Figure 6.11, the circular supercoiled DNA (SC) is completely unwound at approximately 10 and 30 μM, for complexes **3c** and **1c**, respectively. No recoiling of the open circular DNA (OC) is observed with increasing concentration of the respective complexes, although this is not clear due to extensive tailing observed for the binding of complex **3c** with pBR322 DNA. Comparison of the DNA binding properties of complexes **1c** and **3c** with the DNA binding properties of cisplatin (Figure 6.8), indicate that these complexes exhibit a different mode of binding to DNA compared to cisplatin. Cisplatin unwinds and winds the DNA with increasing concentrations of cisplatin, while complexes **1c** and **3c** do not rewind the DNA. [16, 22] The

topological changes induced by the binding of complexes **1c** and **3c** to positively supercoiled DNA are shown in Figure 6.12 and Figure 6.13, respectively.

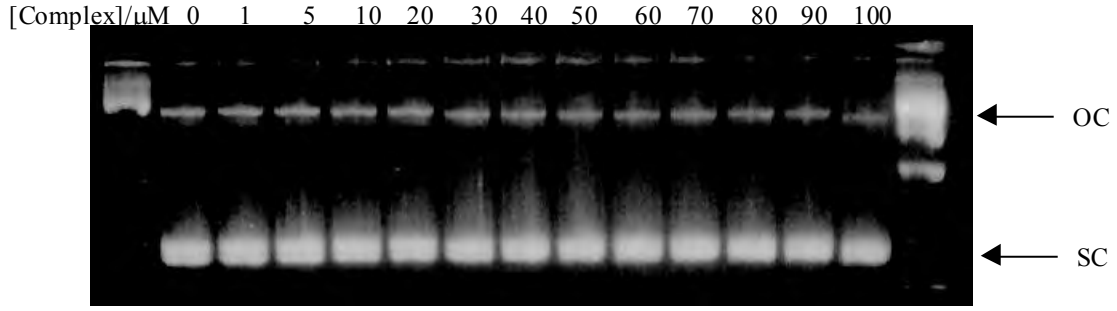

Figure 6.12: Electrophoresis in a 1% agarose gel containing 15 μl ethidium bromide, of 0.4 μg of pBR322 incubated with various concentrations of *cis*-(S,S)-[PtCl(DMSO)(L1c)] (**1c**) for 4 hours at 37°C.

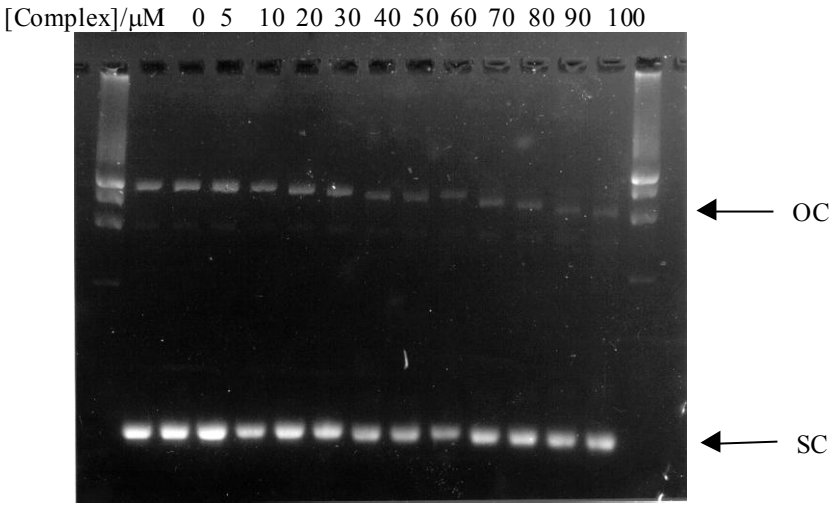

Figure 6.13: Electrophoresis in a 1% agarose gel containing 15 μl ethidium bromide, of 0.4 μg of pBR322 incubated with various concentrations of *cis*-(S,S)-[PtCl(DMSO)(L1c)] (**1c**) for 4 hours at 37°C.

As shown in Figure 6.12, no change in electrophoretic mobility of the supercoiled DNA was observed upon binding of complex **1c**, while a small increase in the electrophoretic mobility of the open circular DNA is observed with increasing concentration of complex **3c** (Figure 6.13). No change in the mobility of open circular DNA is observed with increasing concentration of complex **1c**. This suggests that the binding of complex **1c** and **3c** to DNA does not significantly shorten and/or kink the DNA molecule.

The binding of complex **1c** to DNA was probed further by carrying an enzymatic digestion assay. These studies provide information on the binding site and sequence selectivity of platinum binding, because the binding of the complex near or at the cutting site of a sequence selective restriction endonuclease may inhibit DNA cleavage. The restriction endonuclease *Bam*H1 was used as this enzyme makes a double-stranded cut at a single, unique -G/GATCC- sequence in pBR322 DNA, cleaving the DNA at the GG site. The enzyme converts plasmid form I and II into linear form III DNA. [16] As shown in Figure 6.14, with increasing concentration of complex **1c,** there is an increase in the amount of supercoiled DNA and a decrease in the quantity of linear DNA, suggesting that the platinum complex is binding at or near the cleavage site. It is interesting to note that, even at fairly high concentrations of complex **1c**, linear DNA is observed. This suggests that this complex is not efficient at inhibiting the activity of *Bam*H1. Lippard *et al*. have shown that cisplatin inhibits the cleavage of circular pBR322 DNA by *Bam*H1. [22]

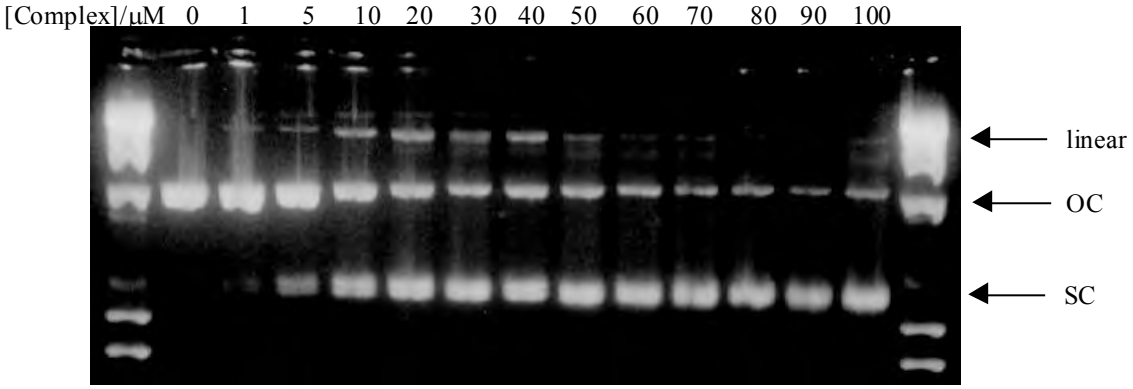

Figure 6.14: Electrophoresis in a 1% agarose gel containing 15 μl ethidium bromide, of 0.4 μg of pBR322 following treatment with *Bam*H1-digestion of platinated pBR322. The DNA was incubated with various concentrations of *cis*-(S,S)-[PtCl(DMSO)(L1c)] (**1c**) for 4 hours at 37°C.

The apparent lack of winding of platinated circular DNA and the small changes in electrophoretic mobility of positively supercoiled circular DNA, with increasing concentration of complex **1c** and **3c**, may be due to a slower rate of reaction with DNA compared to cisplatin. Therefore, a time-dependent study was carried out to determine if the mode of binding of these complexes changes with time. pBR322 DNA was incubated with two different concentrations of complex **1c**, i.e. 5 and 30 μM, for a total of 48 hours,

(Figure 6.15). The DNA starts to unwind at 5 μM and is fully unwound at 30 μM. No change in binding mode was observed over a period of 48 hours.

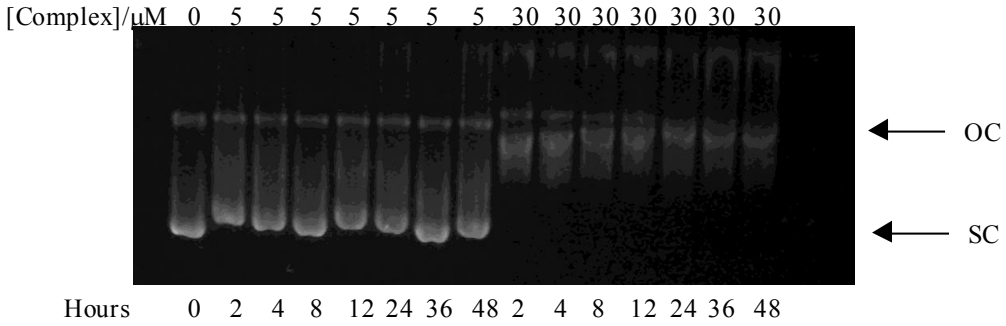

Figure 6.15: Electrophoresis in a 1% agarose gel of 0.4 μg of pBR322 incubated with *cis*-(S,S)-[PtCl(DMSO)(L1c)] (**1c**) at 5 and 30 μM, over a period of 48 hours at 37°C.

The lack of total inhibition of *Bam*H1 cleavage and the fact that small changes in electrophoretic mobility were observed on binding of complex **1c** and **3c** to positively supercoiled DNA, may possibly be explained by these complexes binding monofunctionally to pBR322 DNA. The X-ray crystal structures of *cis*-(S,S)-[PtCl(DMSO)(L1a)] (Figure 4.9) and *cis*-(S,S)-[PtCl(L1a)(MPSO)] (Figure 4.10) indicate that these complexes are relatively planar, hence an intercalative mode of binding cannot be excluded at this stage. An intercalative mode of binding may explain why no change in electrophoretic mobility of either the supercoiled or open circular DNA is observed in the presence of ethidium bromide.

6.2.2.3 cis-(S,S)-*[{PtCl(DMSO)}$_2$(L1f)] (**1f**)*

The binding of complex **1f** to pBR322 DNA was carried out in the absence and presence of ethidium bromide, as shown by the gels given in Figure 6.16 and Figure 6.17, respectively.

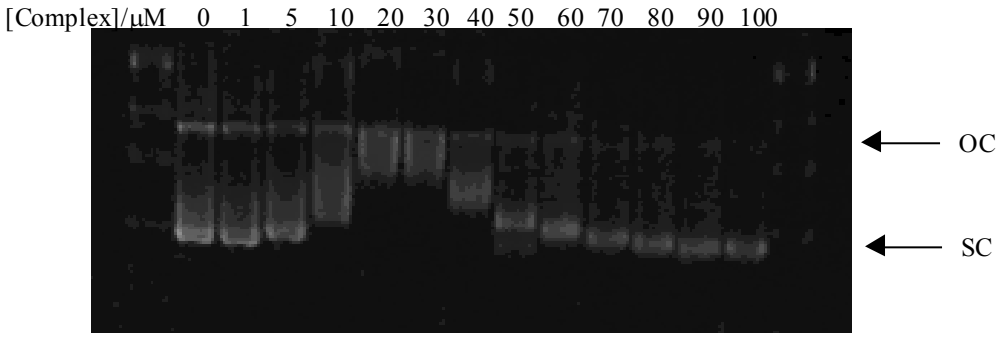

Figure 6.16: Electrophoresis in a 1% agarose gel of 0.4 μg of pBR322 incubated with various concentrations of *cis*-(S,S)-[{PtCl(DMSO)}$_2$(L1f)] (**1f**) for 4 hours at 37°C.

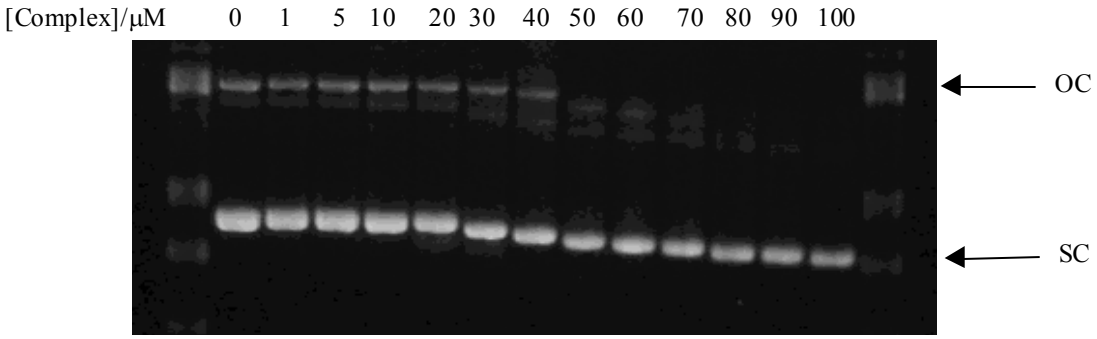

Figure 6.17 Electrophoresis in a 1% agarose gel containing 15 μl ethidium bromide, of 0.4 μg of pBR322 incubated with various concentrations of *cis*-(S,S)-[{PtCl(DMSO)}$_2$(L1f)] (**1f**) for 4 hours at 37°C.

The binuclear complex **1f**, forms different DNA adducts than complexes **1c** and **3c**. As shown in Figure 6.16, a decrease followed by an increase in electrophoretic mobility is observed upon DNA binding, with increasing concentration of complex **1f**. Distinct topological changes are observed upon binding of complex **1f** to positively supercoiled and open circular DNA (Figure 6.17). The binding of complex **1f** to positively supercoiled and open circular DNA showed an increase in mobility, with increasing concentration of complex **1f**. This suggests that this complex, even though biologically inactive, has a different mode of binding to DNA than the mononuclear complexes, **1c** and **3c**. The exact mode of binding of complexes **1c**, **3c** and **1f** are unknown.

6.3 Discussion

Only three platinum(II) sulfoxide complexes exhibited antineoplastic activity, which suggests that the ligand systems have a pronounced effect on the biological activity of the complexes, even though the ligand systems themselves exhibit no anticancer activity. The acylthioureato and alkoxycarbonylthioureato ligand systems may influence the biological activity of the complexes by:

i) Governing the extent of uptake of the complexes into the cell.
ii) Altering the reactivity of the complexes with cellular targets.
iii) Influencing the interactions with cellular targets, by possibly providing sites for hydrogen bonding or prohibiting certain modes of binding due to steric constraints imposed by the ligand systems.

Based on the fact that the *cis*-(S,S)-[Pt(acylthioureato)Cl(RR'SO)] complexes are all structurally similar, that variation of the 3-*R*-benzoyl substituent and amine moieties has a small effect on the rate of substitution of the chloride and sulfoxide ligands (Chapter 5), and that complexes **1c** and **3c** appear to have similar DNA binding properties, the biological activity of complexes **1c**, **2c** and **2d** may be due to the selective uptake of these complexes into the cell. The preliminary DNA binding studies showed that these complexes have a different mode of binding to DNA compared to cisplatin and this suggests that these complexes might exhibit a different spectrum of activity than cisplatin. However, to establish whether these complexes display a different spectrum of activity than cisplatin, cytotoxicity tests on a wide range of cell lines including cisplatin-resistant cell lines are essential. Further work is needed to establish the mode of action of these complexes and the biological activity of these complexes needs to be examined in more detail. Unfortunately, due to time constraints, no further studies could be carried out.

6.4 Experimental

6.4.1 Materials and physical methods

Dimethylformamide (spectroscopic grade, 99.8% purity), sodium hydrogenphosphate (≥ 99% purity), sodium chloride (≥ 99% purity), sodium phosphate, monobasic monohydate (≥ 98% purity), boric acid (99.99% purity), ethylenediaminetetraacetic acid (99.999% purity) and tris(hydroxymethyl)aminomethane (Tris), (≥ 99.9% purity), were purchased from Aldrich Chemical Company. Plasmid pBR322 DNA, *Bam*H1, DNA molecular weight marker II and agarose LE were purchased from Boehringer Mannheim (Germany). 10× TBE buffer (89 mM Tris, 89 mM boric acid, 2 mM EDTA, adjusted to pH 8.4) was purchased from Boehringer Mannheim (Germany) or was prepared. Ethidium bromide was purchased from Research Organics, Inc..

6.4.2 Plasmid binding studies

The plasmid binding studies were carried out using a modified methods described by Ushay *et al*.. [22]

Fresh stocks of the platinum complexes (322, 356 or 600 μM) were prepared in 2 ml dimethylformamide/8 ml water or 50:50 (v/v) dimethylformamide/water (depending on the solubility of the complex in water) were used for each assay to avoid hydrolysis. The platinum stock solutions were filtered through a 0.45 μm filter and made up to the appropriate concentrations in the 0–100 μM range. The samples for analysis were prepared by adding 11 μl of the respective concentration of platinum complex into an eppendorf tube containing plasmid pBR322 DNA (5 μl, 0.25 μg/ml H_2O) and sterilised buffer (4 μl, 3 mM NaCl, 1mM phosphate buffer, pH 7.4). 11 μl of sterilised water was added to the control tube. The sample tubes were gently pulse centrifuged to facilitate mixing and then incubated at 37°C in the dark for 4 hours. For the time dependant studies the samples were incubated over a period of 48 hours. The sample tubes were then placed in ice (0°C) to prevent any further reaction taking place.

6.4.3 *Bam*H1 restriction enzyme digestion

After the initial incubation period of the complexes with the DNA, a 10× restriction buffer B (3 μl, 10 mM Tris-HCl, 5 mM $MgCl_2$, 100 mM NaCl, 1 mM 2-mercaptoethanol, pH8.0) and *Bam*H1 (0.5 ml, activity 11U/μl) were added to each sample tube. Sterilised water was added such that the final volume in each sample tube was 30 μl. The tubes were incubated at 37°C for an hour to allow DNA digestion to take place. The tubes were rapidly cooled to 0°C to prevent any further reaction taking place.

6.4.4 Gel electrophoresis

Tracking dye (6 μl, 0.25% bromophenol blue, 0.25% xylene cyanol FF, 30% sucrose in water) was added to each sample tube and 20 μl portions were loaded on 1% agarose slab gels (20 cm × 15 cm) and electrophoretically chromatographed for 18 hours at 27 V. DNA molecular weight marker II (1μl in 6 μl tracking dye) was used as a standard and loaded into the first and last lanes of each gel. The agarose gels (1%) were prepared and run in 0.5× TBE buffer. Gels were run in the presence and absence of ethidium bromide (37.5 ng/ml). Gels run in the absence of ethidium bromide were stained with ethidium bromide after completion of electrophoresis, by immersing the gels in 0.025 μg/ml ethidium bromide for approximately 30 minutes. All the gels were rinsed with distilled water and photographed. Each gel was illuminated from below with UV light and photographed with a DS 34 Polaroid camera using a orange filter with Polaroid polapan ISO 3000 film or with a Kodak DC120 Digital Scientific Imaging System.

6.5 References

1. L. A. Marky, K. Alessi, D. Rentzeperis, in *Advances in DNA Sequence Specific Agents*, ed. L. H. Hurley, JAI Press Inc., London, 1996, vol. 2, pp. 4.
2. S. J. Lippard, *Acc. Chem. Res*., 1978, **11**, 211.
3. J. Holford, S. Y. Sharp, B. A. Murrer, M. Abrams, L. R. Kelland, *Br. J. Cancer*, 1998, **77**, 366.
4. C. F. O'Neill, L. Hunakova, L. R. Kelland, *Chem. -Biol. Interact*., 1999, **123**, 11.
5. S. G. Chaney, A. Sancar, *J. Natl. Cancer. Inst*., 1996, **88**, 1346.
6. M. Gosland, B. Lum, J. Schimmelpfennig, J. Baker, M. Doukas, *Pharmacotherapy*, 1996, **16**, 16.
7. P. M. Takahara, C. A. Frederick, S. J. Lippard, *J. Am. Chem. Soc*., 1996, **118**, 12309.
8. J. Reedijk, *Inorg. Chim. Acta*, 1992, **198–200**, 873.
9. E. L. M. Lempers, J. Reedijk, *Adv. Inorg. Chem.*, 1991, **37**, 175.
10. W. I. Sundquist, S. J. Lippard, *Coord. Chem. Rev*., 1990, **100**, 293.
11. S. J. Berners-Price, U. Frey, J. D. Ranford, P. J. Sadler, *J. Am. Chem. Soc*., 1993, **115**, 8649.
12. S. E. Sherman, S. J. Lippard, *Chem. Rev*., 1987, **87**, 1153.
13. S. J. Lippard, NATO ASI Series *Bioinorganic Chemistry: An Inorganic Perspective of Life*, ed. D. P. Kessissoglou, Kluwer Academic Publishers, The Netherlands, 1995, 131–140.
14. U. –M. Ohndorf, M. A. Rould, Q. He, C. O. Pabo, S. J. Lippard, *Nature*, 1999, **399**, 708.
15. S. Mazzini, R. Mondelli, E. Ragg, *J. Chem. Soc., Perkin Trans*. 2, 1998, 1983.
16. G. L. Cohen, W. R. Bauer, J. K. Barton, S. J. Lippard, *Science*, 1979, **203**, 1014.
17. W. Bauer, J. Vinograd, *J. Mol. Biol*., 1968, **33**, 141.
18. M. V. Keck, S. J. Lippard, *J. Am. Chem. Soc*., 1992, **114**, 3386.
19. J. C. Wang, *J. Mol. Biol*., 1974, **89**, 783.
20. A. G. Quiroga, J. M. Pérez, E. I. Montero, J. R. Masaguer, C. Alonso, C. Navarro-Ranninger, *J. Inorg. Biochem*., 1998, **70**, 117.
21. R. Köckerbauer, P. J. Bednarski, *J. Inorg. Biochem*., 1996, **62**, 281.
22. H. M. Ushay, T. D. Tullius, S. J. Lippard, *Biochemistry*, 1981, **20**, 3744.

CHAPTER 7

CONCLUDING REMARKS

Acylthiourea and alkoxycarbonylthiourea ligands and mixed-ligand platinum(II) complexes of the type [PtCl(L)(RR'SO)], where HL = acylthiourea or alkoxycarbonylthiourea, have been synthesised and characterised. The acylthioureato complexes are found to exist as only the *cis*-(S,S)-isomers, whereas the alkoxycarbonylthioureato complexes exist as *cis*-(S,S)- and *trans*-(S,S)-isomers, the *trans*-(S,S)-isomers being thermodynamically favoured. ^{31}P NMR and X-ray crystallographic studies suggest that the acylthioureato ligands bind more strongly to the platinum centre than the alkoxycarbonylthioureato ligands and that the acylthioureato carbonyl oxygen donor atom is relatively softer and therefore has a greater *trans*-influence than the carbonyl oxygen donor atom of the alkoxycarbonylthioureato ligands. Furthermore, it has been noted that the morpholine derivatives of the acylthioureato and alkoxycarbonylthioureato ligand systems appear to bind less tightly than the diethyl derivatives. It has been tentatively proposed that the weaker binding properties of the alkoxycarbonylthioureato ligands maybe responsible for the observed geometric isomerisation of these complexes and that the mechanism may involve a chelate ring-opening step.

The substitution kinetics of the *cis*-(S,S)-[Pt(acylthioureato)Cl(RR'SO)] complexes with a range of neutral and anionic nucleophiles are characterised by a fast first step followed by a significantly slower second step. Interestingly, it has been found that neutral nucleophiles initially substitute the sulfoxide ligand, while anionic nucleophiles substitute the chloride ligand. Variation of the electron-withdrawing properties of the 3-*R*-benzoyl, amine and sulfoxide moieties has a small influence on the reactivity of these complexes. Hence, these groups may be readily varied with biologically active groups or groups with different degrees of water solubility to try and increase the DNA binding specificity and chemotherapeutic efficacy of these novel complexes.

Three complexes, **1c**, **2c** and **2d,** exhibit significant anticancer activity against a HeLa and MCF-7 cell line, but were found to be less cytotoxic than cisplatin. The fact that the electronic properties of the acylthiourea ligands do not significantly effect the reactivity of the complexes, together with the fact that the ligands themselves are not cytotoxic, suggests that the biological activity of the complexes is most likely governed by the hydrophilicity/lipophilicity of the chelating ligand. Morphology studies show that these complexes induce cell death in a HeLa cell line by apoptosis. The induction of cell death

by apoptosis suggests that DNA is a major target for these complexes. Very importantly, preliminary plasmid DNA binding studies indicate that these biologically active complexes (**1c**, **2c** and **2d**) display a different mode of binding to DNA than cisplatin, suggesting that these complexes may display a different spectrum of activity compared to cisplatin. However, further studies are required to determine if these complexes are active in other cell lines, particularly in cisplatin-resistant cell lines, to establish if these complexes have a broader spectrum of activity and are less toxic than cisplatin and its analogues.

APPENDIX A

Crystallographic data for *N,N*-diethyl-*N'*-(-)-(3*R*)-menthyloxycarbonylthiourea

Crystallographic data for *cis*-(S,S)-[PtCl(DMSO)(L1a)]

Crystallographic data for *cis*-(S,S)-[PtCl(L1a)(MPSO)]

Table No.	Contents	Page

Crystallographic data for *cis*-(S,S)-[PtCl(DMSO)(L7)]

Table No.	Contents	Page

Crystallographic data for *cis*-[Pt(L1a)$_2$]

Crystallographic data for *cis*-(S,P)-[PtCl(L1a)(PPh$_3$)]

Table A1: Crystallographic data for *N,N*-diethyl-*N'*-(-)-(3*R*)-menthyloxycarbonyl-thiourea.

Empirical formula	$C_{32}H_{60}N_4O_4S_2$
Formula weight	628.96
Temperature	293(2) K
Wavelength	0.71073 Å
Crystal system, space group	Monoclinic, $P2_1$
Unit cell dimensions	a = 8.889(2) Å $\alpha = 90°$
	b = 13.207(3) Å $\beta = 100.51(3)°$
	c = 16.911(3) Å $\gamma = 90°$
Volume	1952.0(7) $Å^3$
Z	2, 1.070 Mg/m^3
μ	0.172 mm^{-1}
F(000)	688
Theta range for data collection	1.97 to 26.02°
Index ranges	$0 \le h \le 10, -16 \le k \le 0, -20 \le l \le 20$
Reflections collected/unique	2910/2770 [R(int) = 0.031]
Refinement method	Full-matrix least-squares on F^2
Goodness-of-fit on F^2	1.058
Final R indices [$I>2\sigma(I)$]	$R^a = 0.0385$, $Rw^b = 0.0925$
Absolute structure parameter	0.18(11)

[a] $R = [(\Sigma\Delta F)/(\Sigma F_0)]$.

[b] $Rw = \Sigma[w(F_0^2 - F_c^2)^2]/ \Sigma[w(F_0^2)^2]^{1/2}$.

Table A2: Bond lengths (Å) for *N,N*-diethyl-*N'*-(-)-(3*R*)-menthyloxycarbonylthiourea.

Molecule 1		Molecule 2	
S(1)-C(11)	1.677(4)	S(2)-C(21)	1.673(4)
O(11)-C(12)	1.200(5)	O(21)-C(22)	1.186(5)
O(12)-C(12)	1.333(5)	O(22)-C(22)	1.343(5)
O(12)-C(1A)	1.463(5)	O(22)-C(2A)	1.458(4)
N(11)-C(12)	1.370(5)	N(21)-C(22)	1.382(5)
N(11)-C(11)	1.399(5)	N(21)-C(21)	1.396(5)
N(11)-H(1)	0.69(4)	N(21)-H(2)	0.92(4)
N(12)-C(11)	1.329(6)	N(22)-C(21)	1.326(6)
N(12)-C(13)	1.463(5)	N(22)-C(23)	1.477(5)
N(12)-C(15)	1.483(5)	N(22)-C(25)	1.488(5)
C(13)-C(14)	1.501(6)	C(23)-C(24)	1.506(6)
C(13)-H(13A)	0.9700	C(23)-H(23A)	0.9700
C(13)-H(13B)	0.9700	C(23)-H(23B)	0.9700
C(14)-H(14A)	0.9600	C(24)-H(24A)	0.9600
C(14)-H(14B)	0.9600	C(24)-H(24B)	0.9600
C(14)-H(14C)	0.9600	C(24)-H(24C)	0.9600
C(15)-C(16)	1.514(6)	C(25)-C(26)	1.487(6)
C(15)-H(15A)	0.9700	C(25)-H(25A)	0.9700
C(15)-H(15B)	0.9700	C(25)-H(25B)	0.9700
C(16)-H(16A)	0.9700	C(26)-H(26A)	0.9600
C(16)-H(16B)	0.9600	C(26)-H(26B)	0.9600
C(16)-H(16C)	0.9600	C(26)-H(26C)	0.9600
C(1A)-C(1B)	1.483(7)	C(2A)-C(2B)	1.498(7)
C(1A)-C(1F)	1.524(7)	C(2A)-C(2F)	1.528(6)
C(1A)-H(1A)	0.9800	C(2A)-H(2A)	0.9800
C(1B)-C(1C)	1.520(6)	C(2B)-C(2C)	1.533(6)
C(1B)-H(1BA)	0.9700	C(2B)-H(2BA)	0.9700
C(1B)-H(1BB)	0.9700	C(2B)-H(2BB)	0.9700
C(1C)-C(1D)	1.522(7)	C(2C)-C(2D)	1.496(7)
C(1C)-C(1J)	1.508(8)	C(2C)-C(2J)	1.514(8)
C(1C)-H(1C)	0.9800	C(2C)-H(2C)	0.9800

C(1D)-C(1E)	1.508(7)	C(2D)-C(2E)	1.517(8)
C(1D)-H(1DA)	0.9700	C(2D)-H(2DA)	0.9700
C(1D)-H(1DB)	0.9700	C(2D)-H(2DB)	0.9700
C(1E)-C(1F)	1.536(6)	C(2E)-C(2F)	1.535(6)
C(1E)-H(1EA)	0.9700	C(2E)-H(2EA)	0.9700
C(1E)-H(1EB)	0.9700	C(2E)-H(2EB)	0.9700
C(1F)-C(1G)	1.526(7)	C(2F)-C(2G)	1.539(7)
C(1F)-H(1F)	0.9800	C(2F)-H(2F)	0.9800
C(1G)-C(1I)	1.504(11)	C(2G)-C(2H)	1.504(8)
C(1G)-C(1H)	1.527(9)	C(2G)-C(2I)	1.520(7)
C(1G)-H(1G)	0.9800	C(2G)-H(2G)	0.9800
C(1H)-H(1HA)	0.9600	C(2H)-H(2HA)	0.9600
C(1H)-H(1HB)	0.9600	C(2H)-H(2HB)	0.9600
C(1H)-H(1HC)	0.9600	C(2H)-H(2HC)	0.9600
C(1I)-H(1IA)	0.9600	C(2I)-H(2IA)	0.9600
C(1I)-H(1IB)	0.9600	C(2I)-H(2IB)	0.9600
C(1I)-H(1IC)	0.9600	C(2I)-H(2IC)	0.9600
C(1J)-H(1JA)	0.9600	C(2J)-H(2JA)	0.9600
C(1J)-H(1JB)	0.9600	C(2J)-H(2JB)	0.9600
C(1J)-H(1JC)	0.9600	C(2J)-H(2JC)	0.9600

Table A3: Bond angles (°) for *N,N*-diethyl-*N'*-(-)-(3*R*)-menthyloxycarbonylthiourea.

Molecule 1		Molecule 2	
C(12)-O(12)-C(1A)	117.2(3)	C(22)-O(22)-C(2A)	117.1(3)
C(12)-N(11)-C(11)	125.6(4)	C(22)-N(21)-C(21)	122.3(3)
C(12)-N(11)-H(1)	113(3)	C(22)-N(21)-H(2)	115(2)
C(11)-N(11)-H(1)	113(3)	C(21)-N(21)-H(2)	116(2)
C(11)-N(12)-C(13)	120.1(4)	C(21)-N(22)-C(23)	123.5(3)
C(11)-N(12)-C(15)	123.8(3)	C(21)-N(22)-C(25)	120.0(4)
C(13)-N(12)-C(15)	114.8(3)	C(23)-N(22)-C(25)	115.7(4)
N(12)-C(11)-N(11)	116.8(4)	N(22)-C(21)-N(21)	117.5(4)
N(12)-C(11)-S(1)	124.6(3)	N(22)-C(21)-S(2)	124.0(3)
N(11)-C(11)-S(1)	118.5(3)	N(21)-C(21)-S(2)	118.5(3)
O(11)-C(12)-O(12)	126.0(4)	O(21)-C(22)-O(22)	126.0(4)
O(11)-C(12)-N(11)	125.3(4)	O(21)-C(22)-N(21)	126.4(4)
O(12)-C(12)-N(11)	108.7(4)	O(22)-C(22)-N(21)	107.7(3)
N(12)-C(13)-C(14)	112.9(3)	N(22)-C(23)-C(24)	114.4(4)
N(12)-C(13)-H(13A)	109.0	N(22)-C(23)-H(23A)	108.7
C(14)-C(13)-H(13A)	109.0	C(24)-C(23)-H(23A)	108.7
N(12)-C(13)-H(13B)	109.0	N(22)-C(23)-H(23B)	108.7
C(14)-C(13)-H(13B)	109.0	C(24)-C(23)-H(23B)	108.7
H(13A)-C(13)-H(13B)	107.8	H(23A)-C(23)-H(23B)	107.6
C(13)-C(14)-H(14A)	109.5	C(23)-C(24)-H(24A)	109.5
C(13)-C(14)-H(14B)	109.5	C(23)-C(24)-H(24B)	109.5
H(14A)-C(14)-H(14B)	109.5	H(24A)-C(24)-H(24B)	109.5
C(13)-C(14)-H(14C)	109.5	C(23)-C(24)-H(24C)	109.5
H(14A)-C(14)-H(14C)	109.5	H(24A)-C(24)-H(24C)	109.5
H(14B)-C(14)-H(14C)	109.5	H(24B)-C(24)-H(24C)	109.5
N(12)-C(15)-C(16)	114.0(3)	C(26)-C(25)-N(22)	112.7(4)
N(12)-C(15)-H(15A)	108.8	N(22)-C(25)-H(25A)	109.0
C(16)-C(15)-H(15A)	108.8	C(26)-C(25)-H(25A)	109.0
N(12)-C(15)-H(15B)	108.8	N(22)-C(25)-H(25B)	109.0
C(16)-C(15)-H(15B)	108.8	C(26)-C(25)-H(25B)	109.0
H(15A)-C(15)-H(15B)	107.7	H(25A)-C(25)-H(25B)	107.8

C(15)-C(16)-H(16A)	109.5	C(25)-C(26)-H(26A)	109.5
C(15)-C(16)-H(16B)	109.5	C(25)-C(26)-H(26B)	109.5
H(16A)-C(16)-H(16B)	109.5	H(26A)-C(26)-H(26B)	109.5
C(15)-C(16)-H(16C)	109.5	C(25)-C(26)-H(26C)	109.5
H(16A)-C(16)-H(16C)	109.5	H(26A)-C(26)-H(26C)	109.5
H(16B)-C(16)-H(16C)	109.5	H(26B)-C(26)-H(26C)	109.5
O(12)-C(1A)-C(1B)	108.6(4)	O(22)-C(2A)-C(2B)	108.2(4)
O(12)-C(1A)-C(1F)	105.8(4)	O(22)-C(2A)-C(2F)	107.4(3)
C(1B)-C(1A)-C(1F)	113.2(4)	C(2B)-C(2A)-C(2F)	112.8(4)
O(12)-C(1A)-H(1A)	109.7	O(22)-C(2A)-H(2A)	109.5
C(1B)-C(1A)-H(1A)	109.7	C(2B)-C(2A)-H(2A)	109.5
C(1F)-C(1A)-H(1A)	109.7	C(2F)-C(2A)-H(2A)	109.5
C(1A)-C(1B)-C(1C)	112.6(4)	C(2A)-C(2B)-C(2C)	111.3(4)
C(1A)-C(1B)-H(1BA)	109.1	C(2A)-C(2B)-H(2BA)	109.4
C(1C)-C(1B)-H(1BA)	109.1	C(2C)-C(2B)-H(2BA)	109.4
C(1A)-C(1B)-H(1BB)	109.1	C(2A)-C(2B)-H(2BB)	109.4
C(1C)-C(1B)-H(1BB)	109.1	C(2C)-C(2B)-H(2BB)	109.4
H(1BA)-C(1B)-H(1BB)	107.8	H(2BA)-C(2B)-H(2BB)	108.0
C(1J)-C(1C)-C(1B)	112.9(5)	C(2J)-C(2C)-C(2B)	111.3(5)
C(1J)-C(1C)-C(1D)	111.6(5)	C(2D)-C(2C)-C(2J)	111.2(5)
C(1B)-C(1C)-C(1D)	107.8(4)	C(2D)-C(2C)-C(2B)	109.7(4)
C(1J)-C(1C)-H(1C)	108.1	C(2J)-C(2C)-H(2C)	108.2
C(1B)-C(1C)-H(1C)	108.1	C(2B)-C(2C)-H(2C)	108.2
C(1D)-C(1C)-H(1C)	108.1	C(2D)-C(2C)-H(2C)	108.2
C(1E)-C(1D)-C(1C)	111.8(4)	C(2C)-C(2D)-C(2E)	111.7(5)
C(1E)-C(1D)-H(1DA)	109.3	C(2E)-C(2D)-H(2DA)	109.3
C(1C)-C(1D)-H(1DA)	109.3	C(2C)-C(2D)-H(2DA)	109.3
C(1E)-C(1D)-H(1DB)	109.3	C(2E)-C(2D)-H(2DB)	109.3
C(1C)-C(1D)-H(1DB)	109.3	C(2C)-C(2D)-H(2DB)	109.3
H(1DA)-C(1D)-H(1DB)	107.9	H(2DA)-C(2D)-H(2DB)	107.9
C(1D)-C(1E)-C(1F)	112.8(4)	C(2D)-C(2E)-C(2F)	112.1(4)
C(1D)-C(1E)-H(1EA)	109.0	C(2D)-C(2E)-H(2EA)	109.2
C(1F)-C(1E)-H(1EA)	109.0	C(2F)-C(2E)-H(2EA)	109.2

C(1D)-C(1E)-H(1EB)	109.0	C(2D)-C(2E)-H(2EB)	109.2
C(1F)-C(1E)-H(1EB)	109.0	C(2F)-C(2E)-H(2EB)	109.2
H(1EA)-C(1E)-H(1EB)	107.8	H(2EA)-C(2E)-H(2EB)	107.9
C(1A)-C(1F)-C(1G)	113.9(4)	C(2A)-C(2F)-C(2G)	112.8(4)
C(1A)-C(1F)-C(1E)	107.5(4)	C(2A)-C(2F)-C(2E)	107.6(4)
C(1G)-C(1F)-C(1E)	114.3(4)	C(2E)-C(2F)-C(2G)	113.5(4)
C(1A)-C(1F)-H(1F)	106.9	C(2A)-C(2F)-H(2F)	107.5
C(1G)-C(1F)-H(1F)	106.9	C(2G)-C(F)-H(2F)	107.5
C(1E)-C(1F)-H(1F)	106.9	C(2E)-C(2F)-H(2F)	107.5
C(1I)-C(1G)-C(1F)	112.1(6)	C(2I)-C(2G)-C(2F)	110.6(5)
C(1I)-C(1G)-C(1H)	109.8(7)	C(2H)-C(2G)-C(2I)	110.2(5)
C(1F)-C(1G)-C(1H)	13.2(6)	C(2H)-C(2G)-C(2F)	114.6(5)
C(1I)-C(1G)-H(1G)	107.1	C(2I)-C(2G)-H(2G)	107.0
C(1F)-C(1G)-H(1G)	107.1	C(2F)-C(2G)-H(2G)	107.0
C(1H)-C(1G)-H(1G)	107.1	C(2H)-C(2G)-H(2G)	107.0
C(1G)-C(1H)-H(1HA)	109.5	C(2G)-C(2H)-H(2HA)	109.5
C(1G)-C(1H)-H(1HB)	109.5	C(2G)-C(2H)-H(2HB)	109.5
H(1HA)-C(1H)-H(1HB)	109.5	H(2HA)-C(2H)-H(2HB)	109.5
C(1G)-C(1H)-H(1HC)	109.5	C(2G)-C(2H)-H(2HC)	109.5
H(1HA)-C(1H)-H(1HC)	109.5	H(2HA)-C(2H)-H(2HC)	109.5
H(1HB)-C(1H)-H(1HC)	109.5	H(2HB)-C(2H)-H(2HC)	109.5
C(1G)-C(1I)-H(1IA)	109.5	C(2G)-C(2I)-H(2IA)	109.5
C(1G)-C(1I)-H(1IB)	109.5	C(2G)-C(2I)-H(2IB)	109.5
H(1IA)-C(1I)-H(1IB)	109.5	H(2IA)-C(2I)-H(2IB)	109.5
C(1G)-C(1I)-H(1IC)	109.5	C(2G)-C(2I)-H(2IC)	109.5
H(1IA)-C(1I)-H(1IC)	109.5	H(2IA)-C(2I)-H(2IC)	109.5
H(1IB)-C(1I)-H(1IC)	109.5	H(2IB)-C(2I)-H(2IC)	109.5
C(1C)-C(1J)-H(1JA)	109.5	C(2C)-C(2J)-H(2JA)	109.5
C(1C)-C(1J)-H(1JB)	109.5	C(2C)-C(2J)-H(2JB)	109.5
H(1JA)-C(1J)-H(1JB)	109.5	H(2JA)-C(2J)-H(2JB)	109.5
C(1C)-C(1J)-H(1JC)	109.5	C(2C)-C(2J)-H(2JC)	109.5
H(1JA)-C(1J)-H(1JC)	109.5	H(2JA)-C(2J)-H(2JC)	109.5
H(1JB)-C(1J)-H(1JC)	109.5	H(2JB)-C(2J)-H(2JC)	109.5

Symmetry transformations used to generate equivalent atoms.

Table A4: Atomic coordinates (x 10^4) and equivalent isotropic displacement parameters (Å^2 x 10^3) for *N,N*-diethyl-*N'*-(-)-(3*R*)-menthyloxycarbonylthiourea. U(eq) is defined as one third of the trace of the orthogonalized Uij tensor.

	X	Y	Z	U(eq)
S(1)	4316(1)	7056(1)	5524(1)	65(1)
O(11)	3582(3)	6448(3)	3005(2)	68(1)
O(12)	1915(3)	7753(2)	2889(2)	67(1)
N(11)	2592(4)	7038(3)	4072(2)	51(1)
N(12)	3393(3)	5461(3)	4596(2)	45(1)
C(11)	3426(4)	6459(3)	4695(2)	46(1)
C(12)	2780(5)	7026(4)	3286(2)	51(1)
C(13)	4354(4)	4809(3)	5181(3)	58(1)
C(14)	3548(6)	4444(5)	5834(3)	88(2)
C(15)	2203(5)	4920(3)	4020(3)	57(1)
C(16)	2837(6)	4228(5)	3446(3)	78(1)
C(1A)	1846(5)	7808(4)	2019(2)	65(1)
C(1B)	447(6)	7276(4)	1614(3)	79(1)
C(1C)	204(7)	7362(4)	703(3)	86(2)
C(1D)	155(7)	8482(4)	489(3)	88(2)
C(1E)	1577(6)	9028(5)	896(3)	86(2)
C(1F)	1850(5)	8932(4)	1816(2)	70(1)
C(1G)	3258(7)	9499(6)	2251(3)	106(2)
C(1H)	4732(7)	9189(9)	1971(4)	168(4)
C(1I)	3060(10)	10628(6)	2186(5)	165(4)
C(1J)	-1212(9)	6817(6)	288(4)	138(3)
S(2)	-922(1)	4249(1)	5569(1)	66(1)
O(21)	-1312(3)	4697(3)	3091(2)	66(1)
O(22)	-3232(3)	3557(2)	2917(1)	60(1)
N(21)	-2587(4)	4269(3)	4107(2)	49(1)
N(22)	-1575(4)	5822(3)	4591(2)	52(1)
C(21)	-1707(4)	4838(3)	4718(2)	45(1)
C(22)	-2266(4)	4227(4)	3338(2)	50(1)
C(23)	-2640(5)	6397(3)	3982(3)	59(1)

C(24)	-1881(6)	6977(5)	3396(3)	80(1)
C(25)	-483(5)	6441(4)	5167(3)	63(1)
C(26)	-1193(6)	6880(6)	5821(3)	99(2)
C(2A)	-3041(5)	3349(4)	2094(2)	58(1)
C(2B)	-2502(6)	2278(4)	2056(3)	78(1)
C(2C)	-2380(6)	1978(4)	1194(3)	84(1)
C(2D)	-3884(6)	2148(5)	649(3)	94(2)
C(2E)	-4426(6)	3232(5)	690(3)	86(2)
C(2F)	-4583(5)	3538(4)	1547(2)	67(1)
C(2G)	-5166(6)	4627(4)	1608(3)	88(2)
C(2H)	-4228(9)	5425(5)	1289(4)	128(2)
C(2I)	-6834(7)	4711(7)	1202(4)	140(3)
C(2J)	-1858(8)	891(5)	1155(4)	136(3)

Table A5: Anisotropic displacement parameters ($Å^2$ x 10^3) for *N,N*-diethyl-*N'*-(-)-(3*R*)-menthyloxycarbonylthiourea. The anisotropic displacement factor exponent takes the form: $-2\pi^2$ [$h^2 a^{*2}$ U11 + ... + 2 h k a* b* U12].

	U11	U22	U33	U23	U13	U12
S(1)	70(1)	53(1)	62(1)	-3(1)	-11(1)	0(1)
O(11)	79(2)	73(2)	57(2)	14(2)	24(2)	26(2)
O(12)	88(2)	71(2)	44(2)	18(2)	19(1)	33(2)
N(11)	61(2)	44(2)	48(2)	2(2)	9(2)	11(2)
N(12)	44(2)	43(2)	45(2)	5(2)	1(1)	1(2)
C(11)	40(2)	46(3)	53(2)	5(2)	9(2)	2(2)
C(12)	57(2)	52(3)	46(2)	13(2)	13(2)	9(2)
C(13)	54(2)	50(3)	66(3)	9(2)	-2(2)	8(2)
C(14)	89(3)	94(4)	76(3)	40(3)	1(3)	-5(3)
C(15)	55(2)	54(3)	58(3)	-2(2)	3(2)	-3(2)
C(16)	92(3)	67(3)	76(3)	-9(3)	14(3)	2(3)
C(1A)	83(3)	74(3)	37(2)	14(2)	10(2)	25(3)
C(1B)	112(4)	62(3)	64(3)	2(3)	20(3)	12(3)
C(1C)	104(4)	88(4)	63(3)	-8(3)	6(3)	13(3)
C(1D)	116(4)	94(4)	47(2)	9(3)	1(3)	22(3)
C(1E)	112(4)	89(4)	55(3)	28(3)	9(3)	7(3)
C(1F)	82(3)	77(3)	49(2)	14(2)	4(2)	5(3)
C(1G)	109(4)	136(6)	65(3)	26(3)	-4(3)	-35(4)
C(1H)	92(4)	277(12)	128(5)	51(7)	2(4)	-52(6)
C(1I)	221(9)	139(7)	126(6)	4(5)	3(6)	-87(7)
C(1J)	184(7)	131(6)	93(4)	-22(4)	10(4)	-31(6)
S(2)	80(1)	56(1)	52(1)	6(1)	-13(1)	-10(1)
O(21)	64(2)	76(2)	61(2)	-16(2)	21(1)	-27(2)
O(22)	70(2)	67(2)	40(1)	-7(2)	5(1)	-24(2)
N(21)	57(2)	50(2)	39(2)	-2(2)	4(1)	-12(2)
N(22)	54(2)	52(2)	49(2)	-1(2)	6(2)	-2(2)
C(21)	46(2)	50(3)	38(2)	-7(2)	5(2)	-3(2)
C(22)	49(2)	49(2)	48(2)	-1(2)	2(2)	0(2)
C(23)	62(2)	51(3)	61(3)	5(2)	7(2)	7(2)

C(24)	97(3)	64(3)	76(3)	17(3)	8(3)	5(3)
C(25)	67(3)	54(3)	63(3)	-9(2)	3(2)	-8(2)
C(26)	85(3)	109(5)	99(4)	-45(4)	7(3)	3(4)
C(2A)	66(3)	63(3)	44(2)	-4(2)	11(2)	-9(2)
C(2B)	81(3)	77(3)	71(3)	-7(3)	1(2)	7(3)
C(2C)	89(3)	77(3)	88(3)	-25(3)	23(3)	2(3)
C(2D)	107(4)	101(4)	73(3)	-42(3)	18(3)	-15(4)
C(2E)	100(4)	104(4)	49(3)	-18(3)	4(2)	-2(3)
C(2F)	74(3)	78(3)	44(2)	-6(2)	4(2)	-1(2)
C(2G)	114(4)	92(4)	55(3)	1(3)	6(3)	22(3)
C(2H)	193(7)	89(4)	99(5)	12(4)	14(5)	23(5)
C(2I)	134(5)	180(8)	100(4)	6(5)	3(4)	78(5)
C(2J)	164(6)	114(6)	138(6)	-33(5)	47(5)	33(5)

Table A6: Hydrogen coordinates (x 10^4) and isotropic displacement parameters ($Å^2$ x 10^3) for *N,N*-diethyl-*N'*-(-)-(3*R*)-menthyloxycarbonylthiourea.

	X	Y	Z	U(eq)
H(1)	2380(4)	7510(3)	4200(2)	33(12)
H(13A)	5263	5180	5422	103(2)
H(13B)	4677	4228	4903	103(2)
H(14A)	4155	3931	6144	103(2)
H(14B)	4166	4166	5598	103(2)
H(14C)	3404	5001	6177	103(2)
H(15A)	1537	5416	3710	103(2)
H(15B)	1585	4521	4322	103(2)
H(16A)	2007	3940	3071	103(2)
H(16B)	3421	3697	3744	103(2)
H(16C)	3483	4611	3160	103(2)
H(1A)	2752	7482	1878	103(2)
H(1BA)	-434	7558	1800	103(2)
H(1BB)	520	6566	1763	103(2)
H(1C)	1091	7060	523	103(2)
H(1DA)	52	8555	-89	103(2)
H(1DB)	-734	8789	650	103(2)
H(1EA)	1490	9739	751	103(2)
H(1EB)	2454	8755	701	103(2)
H(1F)	960	9233	1994	103(2)
H(1G)	3382	9325	2822	103(2)
H(1HA)	5588	9517	2300	103(2)
H(1HB)	4678	9387	1421	103(2)
H(1HC)	4856	8468	2017	103(2)
H(1IA)	3148	10844	1655	103(2)
H(1IB)	3836	10953	2572	103(2)
H(1IC)	2069	10809	2291	103(2)
H(1JA)	-1189	6129	473	103(2)
H(1JB)	-1246	6825	-283	103(2)
H(1JC)	-2103	7150	409	103(2)

H(2)	-3030(4)	3700(3)	4270(2)	54(12)
H(23A)	-3205	6870	4256	103(2)
H(23B)	-3373	5929	3683	103(2)
H(24A)	-2648	7277	2991	103(2)
H(24B)	-1263	6524	3146	103(2)
H(24C)	-1245	7499	3677	103(2)
H(25A)	377	6020	5404	103(2)
H(25B)	-93	6985	4877	103(2)
H(26A)	-435	7250	6186	103(2)
H(26B)	-1596	6345	6106	103(2)
H(26C)	-2007	7329	5593	103(2)
H(2A)	-2273	3810	1947	103(2)
H(2BA)	-3211	1827	2254	103(2)
H(2BB)	-1509	2205	2401	103(2)
H(2C)	-1618	2417	1016	103(2)
H(2DA)	-4641	1693	800	103(2)
H(2DB)	-3784	1991	101	103(2)
H(2EA)	-5409	3309	336	103(2)
H(2EB)	-3705	3682	501	103(2)
H(2F)	-5330	3081	1719	103(2)
H(2G)	-5121	4770	2180	103(2)
H(2HA)	-4629	6083	1376	103(2)
H(2HB)	-4270	5322	723	103(2)
H(2HC)	-3185	5382	1564	103(2)
H(2IA)	-7417	4189	1401	103(2)
H(2IB)	-6913	4636	631	103(2)
H(2IC)	-7224	5362	1317	103(2)
H(2JA)	-907	799	1521	103(2)
H(2JB)	-1718	740	618	103(2)
H(2JC)	-2616	446	1300	103(2)

Table A7: Crystallographic data for *cis*-(S,S)-[PtCl(DMSO)(L1a)].

	cis-(S,S)-[PtCl(DMSO)(L1a)]
Empirical formula	$C_{14}H_{21}ClN_2O_2PtS_2$
Formula weight	543.99
Temperature	293(2) K
Wavelength	0.71073 Å
Crystal system, space group	Triclinic, $P\bar{1}$
Unit cell dimensions	a = 8.7436(4) Å α = 76.263(10)°
	b = 10.0717(5) Å β = 89.207(10)°
	c = 11.5723(6) Å γ = 68.205(10)°
Volume	916.05(8) $Å^3$
Z, Calculated density	2, 1.979 Mg/m^3
Absorption coefficient	8.039 mm^{-1}
F(000)	524
Crystal size	0.30 x 0.30 x 0.08 mm
Theta range for data collection	5.75 to 28.32°
Index ranges	$-11 \le h \le 11$, $-13 \le k \le 13$, $-15 \le l \le 15$
Reflections collected/unique	9904/4433 [R(int) = 0.0365]
Refinement method	Full-matrix least-squares on F^2
Data/restraints/parameters	4433/0/204
Goodness-of-fit on F^2	1.072
Final R indices [$I>2\sigma(I)$]	R1[a]= 0.0299, R*w*[b] = 0.0725
Largest diff. peak and hole	1.233 and –1.249 e.$Å^{-3}$

[a] $R = [(\Sigma\Delta F)/(\Sigma F_0)]$.

[b] $Rw = \Sigma[w(F_0^2 - F_c^2)^2]/ \Sigma[w(F_0^2)^2]^{1/2}$.

Table A8: Atomic coordinates (x 10^4) and equivalent isotropic displacement parameters (Å^2 x 10^3) for *cis*-(S,S)-[PtCl(DMSO)(L1a)]. U(eq) is defined as one third of the trace of the orthogonalized Uij tensor.

	X	Y	Z	U(eq)
Pt	2059(1)	855(1)	3640(1)	37(1)
Cl(1)	2866(2)	-686(1)	5562(1)	64(1)
S(1)	1105(1)	2795(1)	4373(1)	37(1)
O(1)	293(5)	4255(4)	3560(3)	58(1)
S(2)	1285(2)	2300(1)	1763(1)	50(1)
O(2)	2995(6)	-1026(4)	3102(3)	59(1)
N(1)	3097(4)	-246(4)	1037(3)	39(1)
N(2)	1724(5)	1826(4)	-380(3)	41(1)
C(1)	-266(7)	2569(6)	5466(5)	54(1)
C(2)	2708(7)	2846(7)	5241(6)	63(1)
C(3)	2100(5)	1195(5)	785(3)	36(1)
C(4)	3451(5)	-1200(5)	2082(4)	37(1)
C(5)	623(7)	3385(5)	-863(4)	49(1)
C(6)	-1118(7)	3575(6)	-1178(6)	61(1)
C(7)	2364(7)	959(6)	-1264(4)	48(1)
C(8)	1470(8)	-49(6)	-1373(5)	57(1)
C(11)	4480(5)	-2764(4)	2087(4)	36(1)
C(12)	4755(6)	-3880(5)	3131(5)	46(1)
C(13)	5687(7)	-5337(6)	3139(6)	62(1)
C(14)	6347(7)	-5691(6)	2113(7)	70(2)
C(15)	6065(7)	-4591(7)	1076(6)	67(2)
C(16)	5147(6)	-3126(6)	1049(5)	50(1)

Table A9: Bond lengths (Å) and angles (°) for *cis*-(S,S)-[PtCl(DMSO)(L1a)].

Pt-O(2)	2.010(3)
Pt-S(1)	2.1885(10)
Pt-S(2)	2.2586(11)
Pt-Cl(1)	2.3337(11)
S(1)-C(2)	1.759(5)
S(1)-O(1)	1.462(3)
S(1)-C(1)	1.764(5)
S(2)-C(3)	1.735(4)
O(2)-C(4)	1.271(5)
N(1)-C(4)	1.312(6)
N(1)-C(3)	1.348(5)
N(2)-C(3)	1.335(5)
N(2)-C(7)	1.472(6)
N(2)-C(5)	1.477(6)
C(4)-C(11)	1.495(5)
C(5)-C(6)	1.501(8)
C(7)-C(8)	1.501(8)
C(11)-C(12)	1.394(7)
C(11)-C(16)	1.396(6)
C(12)-C(13)	1.386(7)
C(13)-C(14)	1.379(9)
C(14)-C(15)	1.379(10)
C(15)-C(16)	1.386(7)
O(2)-Pt-S(1)	175.38(10)
O(2)-Pt-S(2)	93.75(10)
S(1)-Pt-S(2)	90.87(4)
O(2)-Pt-Cl(1)	84.94(10)
S(1)-Pt-Cl(1)	90.44(4)
S(2)-Pt-Cl(1)	178.64(4)
O(1)-S(1)-C(2)	108.2(3)
O(1)-S(1)-C(1)	107.4(2)

C(2)-S(1)-C(1)	101.0(3)
O(1)-S(1)-Pt	119.13(15)
C(2)-S(1)-Pt	109.2(2)
C(1)-S(1)-Pt	110.36(18)
C(3)-S(2)-Pt	107.71(14)
C(4)-O(2)-Pt	128.7(3)
C(4)-N(1)-C(3)	127.3(4)
C(3)-N(2)-C(7)	120.6(4)
C(3)-N(2)-C(5)	123.3(4)
C(7)-N(2)-C(5)	116.1(3)
N(2)-C(3)-N(1)	113.8(4)
N(2)-C(3)-S(2)	117.4(3)
N(1)-C(3)-S(2)	128.8(3)
O(2)-C(4)-N(1)	130.3(4)
O(2)-C(4)-C(11)	113.7(4)
N(1)-C(4)-C(11)	116.0(4)
N(2)-C(5)-C(6)	113.1(4)
N(2)-C(7)-C(8)	113.8(4)
C(12)-C(11)-C(16)	119.4(4)
C(12)-C(11)-C(4)	119.9(4)
C(16)-C(11)-C(4)	120.7(4)
C(13)-C(12)-C(11)	120.3(5)
C(14)-C(13)-C(12)	120.1(6)
C(13)-C(14)-C(15)	119.7(5)
C(14)-C(15)-C(16)	121.2(5)
C(15)-C(16)-C(11)	119.3(5)

Symmetry transformations used to generate equivalent atoms

Table A10: Anisotropic displacement parameters ($Å^2$ x 10^3) for *cis*-(S,S)-[PtCl(DMSO)(L1a)]. The anisotropic displacement factor exponent takes the form: $-2\pi^2$ [$h^2 a^{*2}$ U11 + ... + 2 h k a* b* U12].

	U11	U22	U33	U23	U13	U12
Pt	55(1)	27(1)	25(1)	-7(1)	3(1)	-11(1)
Cl(1)	101(1)	37(1)	29(1)	-1(1)	4(1)	-5(1)
S(1)	54(1)	30(1)	28(1)	-9(1)	3(1)	-14(1)
O(1)	94(3)	31(2)	37(2)	-5(1)	0(2)	-12(2)
S(2)	80(1)	31(1)	28(1)	-7(1)	-1(1)	-9(1)
O(2)	104(3)	30(2)	33(2)	-11(1)	17(2)	-13(2)
N(1)	46(2)	38(2)	29(2)	-9(1)	1(1)	-11(2)
N(2)	57(2)	36(2)	28(2)	-5(1)	1(2)	-16(2)
C(1)	64(3)	47(3)	45(3)	-11(2)	14(2)	-15(2)
C(2)	66(3)	72(4)	67(4)	-32(3)	4(3)	-35(3)
C(3)	47(2)	36(2)	26(2)	-9(2)	3(2)	-17(2)
C(4)	44(2)	34(2)	34(2)	-14(2)	0(2)	-11(2)
C(5)	74(3)	36(2)	29(2)	0(2)	-6(2)	-19(2)
C(6)	55(3)	52(3)	68(3)	-8(3)	10(2)	-13(2)
C(7)	66(3)	52(3)	26(2)	-11(2)	10(2)	-24(2)
C(8)	89(4)	55(3)	40(3)	-23(2)	10(2)	-34(3)
C(11)	37(2)	34(2)	38(2)	-14(2)	-2(2)	-11(2)
C(12)	52(2)	33(2)	47(2)	-7(2)	-4(2)	-9(2)
C(13)	66(3)	37(2)	68(4)	-9(2)	-12(3)	-6(2)
C(14)	60(3)	43(3)	102(5)	-31(3)	0(3)	-4(2)
C(15)	61(3)	64(4)	84(4)	-45(3)	20(3)	-15(3)
C(16)	51(2)	47(3)	53(3)	-23(2)	11(2)	-12(2)

Table A11: Hydrogen coordinates (x 10^4) and isotropic displacement parameters ($Å^2$ x 10^3) for *cis*-(S,S)-[PtCl(DMSO)(L1a)].

	X	Y	Z	U(eq)
H(1A)	-513	3332	5883	72(4)
H(1B)	237	1622	6020	72(4)
H(1C)	-1269	2631	5087	72(4)
H(2A)	3517	3039	4732	72(4)
H(2B)	3218	1913	5813	72(4)
H(2C)	2265	3614	5652	72(4)
H(5A)	1062	3800	-1571	72(4)
H(5B)	613	3934	-277	72(4)
H(6A)	-1124	3065	-1780	72(4)
H(6B)	-1779	4606	-1474	72(4)
H(6C)	-1565	3174	-479	72(4)
H(7A)	3528	363	-1045	72(4)
H(7B)	2273	1633	-2038	72(4)
H(8A)	1684	-809	-646	72(4)
H(8B)	1858	-491	-2024	72(4)
H(8C)	303	517	-1518	72(4)
H(12)	4311	-3646	3825	72(4)
H(13)	5868	-6076	3839	72(4)
H(14)	6979	-6667	2119	72(4)
H(15)	6499	-4836	382	72(4)
H(16)	4977	-2393	346	72(4)

Table A12: Crystallographic data for *cis*-(S,S)-[PtCl(L1a)(MPSO)].

	cis-[PtCl(L1a)(MPSO)]
Empirical formula	$C_{19}H_{23}ClN_2O_2PtS_2$
Formula weight	606.05
Temperature	293(2) K
Wavelength	0.71073 Å
Crystal system, space group	Triclinic, $P\bar{1}$
Unit cell dimensions	a = 8.612(2) Å α = 115.11(2)°
	b = 11.776(2) Å β = 86.44(2)°
	c = 13.374(3) Å γ = 66.25(2)°
Volume	1078.8(4) $Å^3$
Z, Calculated density	2, 1.866 Mg/m^3
Absorption coefficient	6.837 mm^{-1}
F(000)	588
Crystal size	0.42 x 0.34 x 0.30 mm
Theta range for data collection	1.75 to 25.05°
Index ranges	$0 \le h \le 10$, $-12 \le k \le 14$, $-15 \le l \le 15$
Reflections collected/unique	3450/2918 [R(int) = 0.0327]
Refinement method	Full-matrix least-squares on F^2
Goodness-of-fit on F^2	1.120
Final R indices [$I>2\sigma(I)$]	R_a = 0.0613, Rw^b = 0.1535
Largest diff. peak and hole	3.141 and –3.613 $e.Å^{-3}$

[a] $R = [(\Sigma\Delta F)/(\Sigma F_0)]$.

[b] $Rw = \Sigma[w(F_0^2 - F_c^2)^2]/ \Sigma[w(F_0^2)^2]^{1/2}$.

Table A13: Atomic coordinates (x 10^4) and equivalent isotropic displacement parameters ($Å^2$ x 10^3) for *cis*-(S,S)-[PtCl(L1a)(MPSO)]. U(eq) is defined as one third of the trace of the orthogonalized Uij tensor.

	X	Y	Z	U(eq)
Pt	2323(1)	2536(1)	979(1)	38(1)
Cl(1)	2395(6)	364(4)	-183(3)	53(1)
S(1)	2312(6)	4631(4)	2025(3)	54(1)
S(2)	2209(5)	2291(4)	2514(3)	41(1)
O(1)	2496(14)	2657(10)	-479(8)	45(2)
O(2)	2696(16)	3163(12)	3458(8)	59(3)
N(1)	2019(18)	4947(14)	79(11)	54(3)
N(2)	1748(24)	6806(14)	1697(13)	74(5)
C(1)	2022(22)	5457(17)	1191(14)	55(4)
C(2)	2321(18)	3687(15)	-627(13)	43(3)
C(3)	1471(27)	7616(21)	1072(19)	73(5)
C(4)	3261(32)	7152(26)	291(24)	96(8)
C(5)	1249(49)	7890(57)	3183(40)	188(23)
C(6)	2546(59)	7868(59)	3240(40)	217(25)
C(7)	3540(26)	491(18)	2146(17)	69(5)
C(11)	2509(18)	3310(15)	-1876(12)	43(3)
C(12)	2785(20)	2015(21)	-2688(16)	64(5)
C(13)	3111(24)	1642(22)	-3826(14)	68(5)
C(14)	3150(26)	2569(28)	-4180(17)	86(7)
C(15)	2825(28)	3913(29)	-3350(19)	91(7)
C(16)	2519(23)	4295(19)	-2203(15)	64(5)
C(21)	102(19)	2568(14)	3089(11)	42(3)
C(22)	-655(22)	3383(18)	4274(12)	55(4)
C(23)	-2290(23)	3644(20)	4751(13)	61(4)
C(24)	-3225(25)	3118(21)	4056(15)	67(5)
C(25)	-2511(26)	2309(21)	2884(17)	78(6)
C(26)	-864(23)	2059(20)	2407(14)	65(5)

Table A14: Bond lengths (Å) and angles (°) for *cis*-(S,S)-[PtCl(L1a)(MPSO)].

Pt-O(1)	2.016(9)
Pt-S(2)	2.192(3)
Pt-S(1)	2.257(4)
Pt-Cl(1)	2.334(3)
S(1)-C(1)	1.736(14)
S(2)-O(2)	1.462(11)
S(2)-C(21)	1.77(2)
S(2)-C(7)	1.77(2)
O(1)-C(2)	1.26(2)
N(1)-C(2)	1.28(2)
N(1)-C(1)	1.35(2)
N(2)-C(1)	1.34(2)
N(2)-C(3)	1.48(2)
N(2)-C(5)	1.75(5)
C(2)-C(11)	1.51(2)
C(3)-C(4)	1.55(3)
C(5)-C(6)	1.11(4)
C(11)-C(12)	1.35(2)
C(11)-C(16)	1.41(2)
C(12)-C(13)	1.37(2)
C(13)-C(14)	1.37(3)
C(14)-C(15)	1.39(3)
C(15)-C(16)	1.38(3)
C(21)-C(26)	1.38(2)
C(21)-C(22)	1.39(2)
C(22)-C(23)	1.36(2)
C(23)-C(24)	1.38(3)
C(24)-C(25)	1.37(2)
C(25)-C(26)	1.38(2)
O(1)-Pt-S(2)	177.2(3)
O(1)-Pt-S(1)	93.3(3)

S(2)-Pt-S(1)	89.09(13)
O(1)-Pt-Cl(1)	84.1(3)
S(2)-Pt-Cl(1)	93.48(13)
S(1)-Pt-Cl(1)	177.24(13)
C(1)-S(1)-Pt	107.2(6)
O(2)-S(2)-C(21)	107.6(6)
O(2)-S(2)-C(7)	107.4(8)
C(21)-S(2)-C(7)	100.7(8)
O(2)-S(2)-Pt	117.4(4)
C(21)-S(2)-Pt	111.7(4)
C(7)-S(2)-Pt	110.7(6)
C(2)-O(1)-Pt	129.9(9)
C(2)-N(1)-C(1)	126.8(13)
C(1)-N(2)-C(3)	122(2)
C(1)-N(2)-C(5)	113(2)
C(3)-N(2)-C(5)	113(2)
N(2)-C(1)-N(1)	113.0(13)
N(2)-C(1)-S(1)	117.5(13)
O(1)-C(2)-N(1)	131.6(14)
N(1)-C(1)-S(1)	129.5(12)
O(1)-C(2)-C(11)	111.8(13)
N(1)-C(2)-C(11)	116.6(12)
N(2)-C(3)-C(4)	110(2)
C(6)-C(5)-N(2)	100(4)
C(12)-C(11)-C(16)	120(2)
C(12)-C(11)-C(2)	121.4(13)
C(16)-C(11)-C(2)	118.9(14)
C(11)-C(12)-C(13)	121(2)
C(12)-C(13)-C(14)	121(2)
C(13)-C(14)-C(15)	118(2)
C(16)-C(15)-C(14)	121(2)
C(15)-C(16)-C(11)	119(2)
C(26)-C(21)-C(22)	118.3(14)

C(26)-C(21)-S(2)	122.8(11)
C(22)-C(21)-S(2)	118.8(11)
C(23)-C(22)-C(21)	121(2)
C(22)-C(23)-C(24)	120(2)
C(25)-C(24)-C(23)	121(2)
C(24)-C(25)-C(26)	119(2)
C(25)-C(26)-C(21)	121(2)

Symmetry transformations used to generate equivalent atoms.

Table A15: Anisotropic displacement parameters ($Å^2$ x 10^3) for *cis*-(S,S)-[PtCl(L1a)(MPSO)]. The anisotropic displacement factor exponent takes the form: $-2\pi^2$ [$h^2 a^{*2}$ U11 + ... + 2 h k a* b* U12].

	U11	U22	U33	U23	U13	U12
Pt	56(1)	37(1)	23(1)	13(1)	-9(1)	-27(1)
Cl(1)	87(3)	40(2)	32(2)	12(2)	-10(2)	-37(2)
S(1)	92(3)	51(2)	35(2)	20(2)	-20(2)	-48(2)
S(2)	59(2)	45(2)	28(2)	19(2)	-14(2)	-31(2)
O(1)	74(7)	46(5)	28(5)	24(4)	-18(4)	-33(5)
O(2)	93(8)	72(7)	26(5)	21(5)	-22(5)	-54(7)
N(1)	77(9)	55(8)	40(7)	26(6)	-12(6)	-40(7)
N(2)	124(14)	41(7)	51(9)	8(7)	-11(9)	-52(9)
C(1)	74(11)	61(10)	45(9)	33(8)	-12(8)	-39(9)
C(2)	45(8)	47(8)	50(9)	36(8)	-13(6)	-22(7)
C(3)	82(13)	62(11)	94(15)	48(11)	-29(11)	-42(10)
C(4)	117(18)	102(17)	141(23)	95(18)	-53(17)	-73(15)
C(5)	117(26)	335(64)	267(57)	234(55)	-85(32)	-146(36)
C(6)	209(49)	387(79)	203(49)	216(57)	-96(40)	-188(54)
C(7)	88(13)	55(10)	66(12)	36(9)	-16(10)	-31(10)
C(11)	47(8)	47(8)	35(7)	22(7)	-11(6)	-21(7)
C(12)	43(9)	89(13)	58(11)	40(10)	-16(8)	-26(9)
C(13)	74(12)	89(13)	26(8)	25(9)	-14(8)	-30(10)
C(14)	63(12)	136(21)	45(11)	49(14)	-18(9)	-27(13)
C(15)	90(15)	122(19)	60(13)	66(15)	-4(11)	-29(14)
C(16)	75(11)	55(9)	54(10)	38(9)	-10(9)	-13(8)
C(21)	64(9)	38(7)	27(7)	15(6)	-12(6)	-29(7)
C(22)	73(11)	67(10)	21(7)	16(7)	-7(7)	-35(9)
C(23)	77(11)	81(12)	29(8)	19(8)	-3(8)	-51(10)
C(24)	65(11)	76(12)	45(10)	25(9)	1(8)	-28(10)
C(25)	80(13)	81(13)	64(12)	13(10)	-11(10)	-56(12)
C(26)	62(10)	81(12)	34(8)	12(8)	-5(7)	-37(9)

Table A16: Hydrogen coordinates (x 10^4) and isotropic displacement parameters ($Å^2$ x 10^3) for *cis*-(S,S)-[PtCl(L1)(MPSO)].

	X	Y	Z	U(eq)
H(3A)	920(27)	8627(21)	1620(19)	95(15)
H(3B)	686(27)	7449(21)	606(19)	95(15)
H(4A)	3059(35)	7660(110)	-131(90)	95(15)
H(4B)	3817(88)	6147(39)	-238(76)	95(15)
H(4C)	4015(70)	7361(126)	758(25)	95(15)
H(5A)	310(49)	8848(57)	3450(40)	95(15)
H(5B)	930(49)	7488(57)	3610(40)	95(15)
H(6A)	2573(89)	8227(145)	4027(41)	95(15)
H(6B)	8451(127)	8451(127)	2956(119)	95(15)
H(6C)	3482(60)	6906(61)	2785(94)	95(15)
H(7A)	3027(96)	-74(29)	1706(96)	95(15)
H(7B)	3610(143)	427(25)	2835(17)	95(15)
H(7C)	4706(56)	145(46)	1697(97)	95(15)
H(12)	2752(20)	1372(21)	-2469(16)	4706(56)
H(13)	3311(24)	742(22)	-4371(14)	95(15)
H(14)	3388(26)	2304(28)	-4956(17)	3311(24)
H(15)	4564(29)	4564(29)	-3573(19)	95(15)
H(16)	2320(23)	5192(19)	-1653(15)	95(15)
H(22)	-39(22)	3755(18)	4746(12)	95(15)
H(23)	-2775(23)	4176(20)	5545(13)	95(15)
H(24)	-4349(25)	3314(21)	4385(15)	95(15)
H(25)	-3132(26)	1936(21)	2418(17)	95(15)
H(26)	-392(23)	1537(20)	1612(14)	95(15)

Table A17: Crystallographic data for *cis*-(S,S)-[PtCl(DMSO)(L7)].

Empirical formula	$C_{18}H_{35}ClN_2O_4PtS_2$
Formula weight	638.14
Temperature	293(2) K
Wavelength	0.71073 Å
Crystal system, space group	Orthorhombic, $P2_12_12_1$
Unit cell dimensions	a = 9.8964(6) Å $\alpha = 90°$
	b = 13.2721(8) Å $\beta = 90°$
	c = 18.0016(11) Å $\gamma = 90°$
Volume	2364.4(2) $Å^3$
Z, Calculated density	4, 1.793 Mg/m^3
Absorption coefficient	6.249 mm^{-1}
F(000)	1264
Crystal size	0.40 × 0.20 × 0.08 mm
Theta range for data collection	1.91 to 28.30°
Index ranges	$-13 \le h \le 13$, $-10 \le k \le 17$, $-23 \le l \le 23$
Reflections collected/unique	15355/5462 [R(int) = 0.0369]
Refinement method	Full-matrix least-squares on F^2
Data/restraints/parameters	5462/0/259
Goodness-of-fit on F^2	1.040
Final R indices [$I>2\sigma(I)$]	Ra = 0.0296, Rw^b = 0.0535
Absolute structure parameter	0.013(6)
Largest diff. peak and hole	0.499 and –0.882 e.$Å^{-3}$

[a] $R = [(\Sigma\Delta F)/(\Sigma F_0)]$.

[b] $Rw = \Sigma[w(F_0^2 - F_c^2)^2]/ \Sigma[w(F_0^2)^2]^{1/2}$.

Table A18: Bond lengths (Å) and angles (°) for *cis*-(S,S)-[PtCl(DMSO)(L7)].

Pt(1)-O(11)	2.018(3)	O(2)-S(2)-C(22)	108.5(3)
Pt(1)-S(2)	2.1839(12)	C(21)-S(2)-C(22)	101.1(3)
Pt(1)-S(1)	2.2595(13)	O(2)-S(2)-Pt(1)	117.16(14)
Pt(1)-Cl(1)	2.3276(14)	C(21)-S(2)-Pt(1)	111.26(19)
S(1)-C(11)	1.734(5)	C(22)-S(2)-Pt(1)	109.1(2)
S(2)-O(2)	1.457(4)	C(12)-O(11)-Pt(1)	130.7(3)
S(2)-C(21)	1.752(5)	C(12)-O(12)-C(1A)	120.1(3)
S(2)-C(22)	1.775(5)	C(12)-N(11)-C(11)	125.0(4)
O(11)-C(12)	1.254(5)	C(11)-N(12)-C(13)	125.8(4)
O(12)-C(12)	1.329(5)	C(11)-N(12)-C(16)	122.5(4)
O(12)-C(1A)	1.464(5)	C(13)-N(12)-C(16)	111.2(4)
N(11)-C(12)	1.309(5)	N(12)-C(11)-N(11)	114.8(4)
N(11)-C(11)	1.345(6)	N(12)-C(11)-S(1)	115.3(4)
N(12)-C(11)	1.343(6)	N(11)-C(11)-S(1)	129.8(4)
N(12)-C(13)	1.465(6)	O(11)-C(12)-N(11)	132.6(4)
N(12)-C(16)	1.474(6)	O(11)-C(12)-O(12)	115.7(4)
C(13)-C(14)	1.511(8)	N(11)-C(12)-O(12)	111.7(4)
C(14)-O(13)	1.407(7)	N(12)-C(13)-C(14)	108.4(4)
O(13)-C(15)	1.418(7)	O(13)-C(14)-C(13)	112.5(5)
C(15)-C(16)	1.517(8)	C(14)-O(13)-C(15)	112.3(4)
C(1A)-C(1F)	1.519(6)	O(13)-C(15)-C(16)	111.3(5)
C(1A)-C(1B)	1.522(7)	N(12)-C(16)-C(15)	108.9(5)
C(1B)-C(1C)	1.538(7)	O(12)-C(1A)-C(1F)	108.1(4)
C(1C)-C(1D)	1.506(7)	O(12)-C(1A)-C(1B)	106.9(4)
C(1C)-C(1J)	1.508(8)	C(1F)-C(1A)-C(1B)	112.7(4)
C(1D)-C(1E)	1.515(7)	C(1A)-C(1B)-C(1C)	111.4(4)
C(1E)-C(1F)	1.538(7)	C(1D)-C(1C)-C(1J)	112.9(5)
C(1F)-C(1G)	1.542(7)	C(1D)-C(1C)-C(1B)	108.9(4)
C(1G)-C(1H)	1.516(8)	C(1J)-C(1C)-C(1B)	110.9(5)
C(1G)-C(1I)	1.520(8)	C(1C)-C(1D)-C(1E)	112.9(4)
O(11)-Pt(1)-S(2)	176.40(11)	C(1D)-C(1E)-C(1F)	112.7(4)
O(11)-Pt(1)-S(1)	92.66(10)	C(1A)-C(1F)-C(1E)	107.6(4)

S(2)-Pt(1)-S(1)	90.71(4)	C(1A)-C(1F)-C(1G)	113.1(4)
O(11)-Pt(1)-Cl(1)	86.00(10)	C(1E)-C(1F)-C(1G)	113.9(4)
S(2)-Pt(1)-Cl(1)	90.66(5)	C(1H)-C(1G)-C(1I)	112.0(5)
S(1)-Pt(1)-Cl(1)	178.15(6)	C(1H)-C(1G)-C(1F)	111.3(5)
C(11)-S(1)-Pt(1)	108.73(18)	C(1I)-C(1G)-C(1F)	113.5(5)
O(2)-S(2)-C(21)	108.4(3)		

Symmetry transformations used to generate equivalent atoms.

Table A19: Atomic coordinates (x 10^4) and equivalent isotropic displacement parameters ($Å^2$ x 10^3) for *cis*-(S,S)-[PtCl(DMSO)(L7)]. U(eq) is defined as one third of the trace of the orthogonalized Uij tensor.

	X	Y	Z	U(eq)
Pt(1)	8451(1)	1170(1)	1008(1)	36(1)
Cl(1)	7636(2)	-274(1)	426(1)	75(1)
S(1)	9292(1)	2540(1)	1593(1)	44(1)
S(2)	6391(1)	1709(1)	1184(1)	37(1)
O(11)	10310(3)	616(3)	794(2)	61(1)
O(12)	12491(3)	473(2)	627(2)	41(1)
O(2)	6231(3)	2665(3)	1572(2)	57(1)
N(11)	11861(4)	1789(3)	1268(2)	35(1)
N(12)	11677(4)	3198(3)	1970(3)	49(1)
C(11)	11040(5)	2459(4)	1600(3)	35(1)
C(12)	11458(4)	982(3)	913(3)	35(1)
C(13)	11030(5)	4065(4)	2327(3)	56(2)
C(14)	11484(7)	5011(4)	1932(4)	66(2)
O(13)	12899(4)	5113(3)	1921(3)	68(1)
C(15)	13545(6)	4273(5)	1587(4)	70(2)
C(16)	13161(5)	3299(4)	1974(4)	58(2)
C(21)	5402(5)	801(4)	1635(3)	52(1)
C(22)	5557(6)	1795(5)	314(3)	63(2)
C(1A)	12245(5)	-362(3)	114(3)	35(1)
C(1B)	12428(5)	51(4)	-668(3)	42(1)
C(1C)	12266(5)	-781(4)	-1256(3)	46(1)
C(1D)	13234(6)	-1624(4)	-1081(3)	54(1)
C(1E)	13074(6)	-2024(4)	-298(3)	49(1)
C(1F)	13238(4)	-1200(3)	295(2)	37(1)
C(1G)	13108(5)	-1588(4)	1100(3)	53(1)
C(1H)	14292(7)	-2255(5)	1309(4)	80(2)
C(1I)	11760(7)	-2093(5)	1259(4)	84(2)
C(1J)	12453(6)	-361(5)	-2028(3)	71(2)

Table A20: Anisotropic displacement parameters ($Å^2$ x 10^3) for *cis*-(S,S)-[PtCl(DMSO)(L7)]. The anisotropic displacement factor exponent takes the form: $-2\pi^2$ [$h^2 a^{*2}$ U11 + ... + 2 h k a* b* U12].

	U11	U22	U33	U23	U13	U12
Pt(1)	28(1)	33(1)	48(1)	-7(1)	6(1)	-2(1)
Cl(1)	53(1)	53(1)	120(2)	-41(1)	6(1)	-11(1)
S(1)	30(1)	41(1)	61(1)	-19(1)	4(1)	1(1)
S(2)	28(1)	38(1)	44(1)	2(1)	2(1)	0(1)
O(11)	27(2)	47(2)	109(4)	-34(2)	14(2)	-1(2)
O(12)	26(2)	40(2)	56(2)	-18(2)	-2(2)	4(2)
O(2)	32(2)	47(2)	92(3)	-20(2)	7(2)	3(2)
N(11)	29(2)	34(2)	41(2)	-5(2)	-2(2)	3(2)
N(12)	35(2)	43(2)	71(3)	-22(2)	-2(2)	3(2)
C(11)	39(3)	34(3)	34(3)	1(2)	-2(2)	2(2)
C(12)	29(2)	31(2)	43(3)	-3(2)	2(2)	4(2)
C(13)	44(3)	48(4)	76(4)	-30(3)	2(3)	6(2)
C(14)	62(4)	42(3)	93(5)	-18(3)	-17(4)	11(3)
O(13)	57(2)	49(2)	97(3)	-16(2)	-9(2)	-5(2)
C(15)	42(3)	75(4)	93(5)	-19(4)	7(4)	-6(3)
C(16)	30(3)	53(4)	93(5)	-21(3)	-10(3)	4(2)
C(21)	37(3)	56(3)	62(4)	17(3)	7(3)	-9(3)
C(22)	55(4)	83(5)	51(4)	17(3)	-10(3)	-1(3)
C(1A)	29(2)	33(3)	43(3)	-17(2)	2(2)	0(2)
C(1B)	39(3)	41(3)	46(3)	-4(2)	-2(2)	1(2)
C(1C)	43(3)	51(3)	4(2)	4(2)	4(2)	-6(2)
C(1D)	58(3)	53(3)	-20(3)	-20(3)	10(3)	11(3)
C(1E)	59(4)	31(3)	58(4)	-8(2)	2(3)	7(2)
C(1F)	32(2)	32(2)	47(3)	-3(2)	-1(2)	-1(2)
C(1G)	58(3)	44(3)	58(4)	3(3)	1(3)	3(2)
C(1H)	84(5)	79(5)	76(5)	18(4)	18(4)	18(4)
C(1I)	74(5)	97(5)	80(5)	31(4)	18(4)	-10(4)
C(1J)	61(4)	94(5)	57(4)	-13(4)	-8(3)	-8(4)

Table A21: Hydrogen coordinates (x 10^4) and isotropic displacement parameters ($Å^2$ x 10^3) for *cis*-(S,S)-[PtCl(DMSO)(L7)].

	X	Y	Z	U(eq)
H(13A)	11284	4095	2847	72(3)
H(13B)	10055	4001	2297	72(3)
H(14A)	11150	4999	1426	72(3)
H(14B)	11093	5592	2178	72(3)
H(15A)	14517	4362	1612	72(3)
H(15B)	13289	4235	1068	72(3)
H(16A)	13568	2731	1718	72(3)
H(16B)	13491	3305	2481	72(3)
H(21A)	5745	693	2127	72(3)
H(21B)	5436	180	1361	72(3)
H(21C)	4484	1031	1663	72(3)
H(22A)	4627	391	391	72(3)
H(22B)	5607	1157	64	72(3)
H(22C)	5986	2301	15	72(3)
H(1A)	11318	-609	176	72(3)
H(1B1)	13320	349	-712	72(3)
H(1B2)	11765	576	-757	72(3)
H(1C)	11345	-1047	-1220	72(3)
H(1D1)	14152	-1383	-1146	72(3)
H(1D2)	13089	-2170	-1430	72(3)
H(1E1)	13742	-2546	-213	72(3)
H(1E2)	12187	-2327	-248	72(3)
H(1F)	14149	-920	241	72(3)
H(1G)	13156	-995	1423	72(3)
H(1H1)	14267	-2391	1832	72(3)
H(1H2)	15122	-1918	1188	72(3)
H(1H3)	14238	-2877	1039	72(3)
H(1I1)	11704	-2715	989	72(3)
H(1I2)	11037	-1656	1108	72(3)
H(1I3)	11686	-2227	1782	72(3)

H(1J1)	11882	217	-2092	72(3)
H(1J2)	12217	-866	-2387	72(3)
H(1J3)	13380	-168	-2096	72(3)

Table A22: Crystallographic data for *cis*-[Pt(L1a)$_2$].

Empirical formula	$C_{24}H_{30}N_4O_2PtS_2$
Formula weight	665.73
Temperature	293(2) K
Wavelength	0.71073 Å
Crystal system, space group	monoclinic, $P2_1/n$
Unit cell dimensions	a = 9.926(2) Å $\alpha = 90°$
	b = 12.265(3) Å $\beta = 91.00(2)°$
	c = 21.168(5) Å $\gamma = 90°$
Volume	2576.7(10) Å^3
Z, Calculated density	4, 1.700 Mg/m^3
Absorption coefficient	5.635 mm^{-1}
F(000)	1287
Crystal size	0.35 × 0.32 × 0.21 mm
Theta range for data collection	1.92 to 25.07°
Index ranges	$-10 \le h \le 9$, $0 \le k \le 14$, $0 \le l \le 24$
Reflections collected/unique	3803/3454 [R(int) = 0.0215]
Refinement method	Full-matrix least-squares on F^2
Data/restraints/parameters	3454/0/303
Goodness-of-fit on F^2	1.140
Final R indices [$I>2\sigma(I)$]	Ra = 0.0358, R*w*^{b} = 0.0926
Largest diff. peak and hole	0.750 and -1.664 e.Å^{-3}

[a] $R = [(\Sigma\Delta F)/(\Sigma F_0)]$.

[b] $Rw = \Sigma[w(F_0^2 - F_c^2)^2]/ \Sigma[w(F_0^2)^2]^{1/2}$.

Table A23: Bond lengths (Å) and angles (°) for *cis*-[Pt(L1a)$_2$].

Bond		Angle	
Pt(1)-O(1)	2.018(5)	C(4)-S(2)-Pt(1)	108.1(3)
Pt(1)-O(2)	2.024(6)	C(1)-O(1)-Pt(1)	128.7(5)
Pt(1)-S(1)	2.232(2)	C(3)-O(2)-Pt(1)	128.2(5)
Pt(1)-S(2)	2.233(2)	C(1)-N(1)-C(2)	127.4(6)
S(1)-C(2)	1.731(7)	C(2)-N(2)-C(23)	120.9(6)
S(2)-C(4)	1.723(7)	C(2)-N(2)-C(21)	123.3(6)
O(1)-C(1)	1.271(8)	C(23)-N(2)-C(21)	115.8(6)
O(2)-C(3)	1.262(8)	C(3)-N(3)-C(4)	125.5(6)
N(1)-C(1)	1.313(9)	C(4)-N(4)-C(43)	123.3(7)
N(1)-C(2)	1.341(9)	C(4)-N(4)-C(41)	122.3(7)
N(2)-C(2)	1.349(9)	C(43)-N(4)-C(41)	114.4(6)
N(2)-C(23)	1.467(9)	O(1)-C(1)-N(1)	130.7(7)
N(2)-C(21)	1.471(9)	O(1)-C(1)-C(11)	115.2(6)
N(3)-C(3)	1.319(9)	N(1)-C(1)-C(11)	114.0(6)
N(3)-C(4)	1.350(9)	N(1)-C(2)-N(2)	114.8(6)
N(4)-C(4)	1.336(9)	N(1)-C(2)-S(1)	128.8(6)
N(4)-C(43)	1.476(11)	N(2)-C(2)-S(1)	116.3(5)
N(4)-C(41)	1.480(9)	O(2)-C(3)-N(3)	131.9(7)
C(1)-C(11)	1.491(10)	O(2)-C(3)-C(31)	112.7(7)
C(3)-C(31)	1.498(11)	N(3)-C(3)-C(31)	115.3(6)
C(11)-C(12)	1.369(10)	N(4)-C(4)-N(3)	114.2(6)
C(11)-C(16)	1.383(11)	N(4)-C(4)-S(2)	116.6(6)
C(12)-C(13)	1.375(11)	N(3)-C(4)-S(2)	129.2(5)
C(13)-C(14)	1.378(13)	C(12)-C(11)-C(16)	118.4(7)
C(14)-C(15)	1.347(13)	C(12)-C(11)-C(1)	121.7(7)
C(15)-C(16)	1.372(12)	C(16)-C(11)-C(1)	119.9(7)
C(21)-C(22)	1.487(11)	C(11)-C(12)-C(13)	120.8(8)
C(23)-C(24)	1.491(12)	C(12)-C(13)-C(14)	120.1(9)
C(31)-C(32)	1.386(11)	C(15)-C(14)-C(13)	119.2(9)
C(31)-C(36)	1.399(11)	C(14)-C(15)-C(16)	121.2(9)
C(32)-C(33)	1.392(12)	C(15)-C(16)-C(11)	120.2(8)

C(33)-C(34)	1.368(14)	N(2)-C(21)-C(22)	112.8(7)
C(34)-C(35)	1.380(14)	N(2)-C(23)-C(24)	111.9(6)
C(35)-C(36)	1.369(12)	C(32)-C(31)-C(36)	118.1(8)
C(41)-C(42)	1.499(11)	C(32)-C(31)-C(3)	121.8(7)
C(43)-C(44)	1.503(13)	C(36)-C(31)-C(3)	120.1(7)
		C(31)-C(32)-C(33)	121.3(9)
		C(34)-C(33)-C(32)	118.7(9)
		C(33)-C(34)-C(35)	121.2(9)
		C(36)-C(35)-C(34)	119.8(9)
		C(35)-C(36)-C(31)	120.7(8)
		N(4)-C(41)-C(42)	111.7(7)
		N(4)-C(43)-C(44)	111.8(8)
		O(1)-Pt(1)-O(2)	82.7(2)
		O(1)-Pt(1)-S(1)	94.8(2)
		O(2)-Pt(1)-S(1)	177.5(2)
		O(1)-Pt(1)-S(2)	177.1(2)
		O(2)-Pt(1)-S(2)	94.4(2)
		S(1)-Pt(1)-S(2)	88.10(7)
		C(2)-S(1)-Pt(1)	107.9(3)

Symmetry transformations used to generate equivalent atoms.

Table A24: Atomic coordinates (x 10^4) and equivalent isotropic displacement parameters ($Å^2$ x 10^3) for *cis*-[Pt(L1a)$_2$]. U(eq) is defined as one third of the trace of the orthogonalized Uij tensor.

	X	Y	Z	U(eq)
Pt(1)	5933(1)	4824(1)	3911(1)	39(1)
S(1)	7426(2)	4795(2)	4711(1)	53(1)
S(2)	7063(2)	6234(2)	3514(1)	61(1)
O(1)	4844(6)	3558(4)	4233(2)	54(1)
O(2)	4533(6)	4799(4)	3204(3)	58(2)
N(1)	6003(6)	3014(5)	5157(3)	40(1)
N(2)	8019(6)	3413(5)	5621(3)	43(2)
N(3)	5127(6)	6270(5)	2549(3)	40(1)
N(4)	7025(6)	7254(5)	2431(3)	44(1)
C(1)	4999(8)	3028(5)	4745(3)	39(2)
C(2)	7093(8)	3661(6)	5169(3)	40(2)
C(3)	4355(8)	5485(6)	2766(3)	39(2)
C(4)	6339(8)	6564(5)	2793(3)	40(2)
C(11)	3899(7)	2242(6)	4889(3)	39(2)
C(12)	4118(9)	1352(7)	5266(4)	55(2)
C(13)	3092(10)	635(8)	5391(4)	65(2)
C(14)	1815(10)	822(8)	5149(5)	66(3)
C(15)	1595(10)	1701(9)	4780(5)	72(3)
C(16)	2619(9)	2407(7)	4639(4)	58(2)
C(21)	9332(8)	3963(6)	5681(3)	48(2)
C(22)	9321(10)	4881(8)	6140(5)	73(3)
C(23)	7771(9)	2543(6)	6080(3)	51(2)
C(24)	8242(10)	1461(7)	5851(4)	69(3)
C(31)	3036(8)	5336(6)	2422(3)	43(2)
C(32)	2483(9)	6150(7)	2045(4)	58(2)
C(33)	1221(10)	6028(9)	1757(4)	73(3)
C(34)	552(10)	5062(10)	1826(5)	76(3)
C(35)	1098(10)	4223(9)	2182(4)	65(3)
C(36)	2316(9)	4362(7)	2484(4)	52(2)

C(41)	6499(9)	7642(6)	1813(3)	50(2)
C(42)	6917(10)	6909(8)	1285(4)	70(3)
C(43)	8379(9)	7669(7)	2603(4)	59(2)
C(44)	8307(11)	8696(9)	2989(5)	83(3)

Table A25: Anisotropic displacement parameters ($Å^2$ x 10^3) for *cis*-[Pt(L1a)$_2$]. The anisotropic displacement factor exponent takes the form: $-2\pi^2$ [$h^2 a^{*2}$ U11 + ... + 2 h k a* b* U12].

	U11	U22	U33	U23	U13	U12
Pt(1)	43(1)	38(1)	37(1)	6(1)	-3(1)	-4(1)
S(1)	61(1)	52(1)	46(1)	12(1)	-14(1)	-20(1)
S(2)	63(2)	65(1)	54(1)	22(1)	-21(1)	-25(1)
O(1)	54(4)	56(3)	52(3)	20(3)	-16(3)	-15(3)
O(2)	63(4)	60(3)	51(3)	20(3)	-12(3)	-18(3)
N(1)	32(4)	46(3)	41(3)	6(3)	-1(3)	-8(3)
N(2)	37(4)	54(4)	39(3)	6(3)	-5(3)	-9(3)
N(3)	39(4)	37(3)	44(3)	7(3)	-2(3)	-2(3)
N(4)	37(4)	43(3)	51(4)	4(3)	2(3)	-6(3)
C(1)	41(5)	33(3)	44(4)	1(3)	6(3)	-2(3)
C(2)	42(5)	46(4)	32(3)	-2(3)	5(3)	-4(3)
C(3)	47(5)	38(4)	32(3)	2(3)	-1(3)	4(3)
C(4)	49(5)	30(3)	42(4)	2(3)	5(3)	-2(3)
C(11)	38(4)	42(4)	35(3)	0(3)	-4(3)	-6(3)
C(12)	46(5)	57(5)	62(5)	17(4)	-2(4)	-14(4)
C(13)	60(6)	64(5)	70(6)	21(5)	-18(5)	-19(5)
C(14)	54(6)	62(6)	81(6)	-4(5)	7(5)	-18(5)
C(15)	39(6)	84(7)	94(7)	1(6)	-15(5)	-10(5)
C(16)	47(6)	53(5)	74(6)	8(4)	-13(4)	-2(4)
C(21)	44(5)	55(4)	45(4)	0(3)	-6(3)	-7(4)
C(22)	56(7)	90(8)	74(7)	-16(5)	-9(5)	-2(5)
C(23)	56(6)	58(5)	40(4)	9(3)	-8(4)	-6(4)
C(24)	70(7)	65(6)	71(6)	22(5)	8(5)	4(5)
C(31)	37(5)	55(5)	37(4)	-2(3)	0(3)	2(3)
C(32)	48(6)	57(5)	70(5)	12(4)	-10(4)	-1(4)
C(33)	59(7)	97(8)	61(6)	14(5)	-22(5)	13(6)
C(34)	36(6)	131(10)	60(6)	3(6)	-7(4)	-6(6)
C(35)	55(6)	84(7)	56(5)	-8(5)	5(4)	-25(5)

C(36)	47(5)	57(5)	50(4)	2(4)	4(4)	-16(4)
C(41)	58(6)	49(4)	44(4)	18(3)	1(4)	-5(4)
C(42)	77(7)	79(7)	53(5)	-3(5)	1(5)	0(5)
C(43)	53(6)	65(5)	61(5)	13(4)	-1(4)	-19(4)
C(44)	78(8)	84(7)	86(7)	2(6)	-7(6)	-34(6)

Table A26: Hydrogen coordinates (x 10^4) and isotropic displacement parameters ($Å^2$ x 10^3) for *cis*-[Pt(L1a)$_2$].

	X	Y	Z	U(eq)
H(12)	4971(9)	1230(7)	5441(4)	67(5)
H(13)	3259(10)	23(8)	5640(4)	67(5)
H(14)	1113(10)	347(8)	5239(5)	67(5)
H(15)	734(10)	1831(9)	4617(5)	67(5)
H(16)	2452(9)	2998(7)	4374(4)	67(5)
H(21A)	9585(8)	4240(6)	5270(3)	67(5)
H(21B)	10008(8)	3437(6)	5815(3)	67(5)
H(22A)	10167(22)	5258(28)	6130(19)	67(5)
H(22B)	9181(54)	4600(9)	6557(6)	67(5)
H(22C)	8606(35)	5376(24)	6030(15)	67(5)
H(23A)	6814(9)	2506(6)	6162(3)	67(5)
H(23B)	8234(9)	2717(6)	6475(3)	67(5)
H(24A)	7721(35)	1253(20)	5484(15)	67(5)
H(24B)	8132(50)	926(11)	6177(10)	67(5)
H(24C)	9176(16)	1508(13)	5744(23)	67(5)
H(32)	2966(9)	6790(7)	1982(4)	67(5)
H(33)	840(10)	6593(9)	1521(4)	67(5)
H(34)	-286(10)	4968(10)	1630(5)	67(5)
H(35)	639(10)	3565(9)	2216(4)	67(5)
H(36)	2669(9)	3803(7)	2733(4)	67(5)
H(41A)	6830(9)	8373(6)	1736(3)	67(5)
H(41B)	5523(9)	7673(6)	1823(3)	67(5)
H(42A)	6581(46)	7195(24)	890(5)	67(5)
H(42B)	6555(45)	6192(14)	1349(14)	67(5)
H(42C)	7882(10)	6870(34)	1276(16)	67(5)
H(43A)	8873(9)	7814(7)	2221(4)	67(5)
H(43B)	8865(9)	7116(7)	2842(4)	67(5)
H(44A)	9203(11)	8937(24)	3095(21)	67(5)
H(44B)	7825(47)	8554(14)	3369(13)	67(5)

Table A27: Crystallographic data for *cis*-(S,P)-[PtCl(L1a)(PPh_3)].

Empirical formula	$C_{30}H_{30}ClN_2OPPt\ S$
Formula weight	728.13
Temperature	293(2) K
Wavelength	0.71073 Å
Crystal system, space group	Orthorhombic, $P2_12_12_1$
Unit cell dimensions	a = 10.1271(5) Å $\alpha = 90°$
	b = 16.4174(8) Å $\beta = 90°$
	c = 17.7317(8) Å $\gamma = 90°$
Volume	2948.1(2) $Å^3$
Z, Calculated density	4, 1.641 Mg/m^3
Absorption coefficient	5.001 mm^{-1}
F(000)	1432
Crystal size	0.40 × 0.30 × 0.20 mm
Theta range for data collection	1.69 to 28.27°
Index ranges	$12 \le h \le 11, -14 \le k \le 21, -23 \le l \le 23$
Reflections collected/unique	19304/6755 [R(int) = 0.0254]
Refinement method	Full-matrix least-squares on F^2
Data/restraints/parameters	6755/0/337
Goodness-of-fit on F^2	1.126
Final R indices [$I>2\sigma(I)$]	R^a = 0.0220, Rw^b = 0.0460
Absolute structure parameter	-0.008(4)
Largest diff. peak and hole	0.337 and -0.994 e.$Å^{-3}$

[a] $R = [(\Sigma\Delta F)/(\Sigma F_0)]$.

[b] $Rw = \Sigma[w(F_0^2 - F_c^2)^2]/ \Sigma[w(F_0^2)^2]^{1/2}$.

Table A28: Atomic coordinates (x 10^4) and equivalent isotropic displacement parameters ($Å^2$ x 10^3) for *cis*-(S,P)-[PtCl(L1a)(PPh_3)]. U(eq) is defined as one third of the trace of the orthogonalized Uij tensor.

	X	Y	Z	U(eq)
Pt(1)	5394(1)	4913(1)	616(1)	33(1)
Cl(1)	4413(1)	5001(1)	1804(1)	51(1)
S(1)	6401(1)	4828(1)	-509(1)	45(1)
P(1)	4033(1)	5879(1)	219(1)	34(1)
O(1)	6499(3)	3994(2)	1071(1)	49(1)
N(1)	7635(3)	3433(2)	41(2)	43(1)
N(2)	8170(3)	3875(2)	-1122(2)	51(1)
C(1)	7182(3)	3458(2)	737(2)	38(1)
C(2)	7454(3)	3997(2)	-495(2)	39(1)
C(3)	8993(5)	3143(3)	-1211(3)	72(1)
C(4)	8192(7)	2381(4)	-1363(3)	100(2)
C(5)	8178(4)	4455(3)	-1759(2)	66(1)
C(6)	7209(6)	4266(5)	-2369(3)	95(2)
C(11)	4360(3)	6875(2)	625(2)	39(1)
C(12)	5383(4)	6966(2)	1145(2)	52(1)
C(13)	5654(5)	7730(3)	1444(3)	70(1)
C(14)	4904(5)	8387(3)	1244(3)	72(1)
C(15)	3910(5)	8306(2)	729(3)	62(1)
C(16)	3652(4)	7558(2)	406(2)	52(1)
C(21)	4091(3)	6088(2)	-796(2)	38(1)
C(22)	3236(4)	5726(3)	-1303(2)	4091(3)
C(23)	3403(5)	5867(3)	-2074(2)	68(1)
C(24)	4377(6)	6343(3)	-2327(3)	77(2)
C(25)	5220(6)	6700(3)	-1829(3)	84(2)
C(26)	5087(4)	6576(3)	-1063(2)	61(1)
C(31)	2333(3)	5605(2)	436(2)	39(1)
C(32)	1935(4)	4807(3)	278(2)	62(1)
C(33)	659(5)	4562(3)	455(3)	75(1)
C(34)	-208(4)	5086(4)	789(2)	72(1)

C(35)	183(4)	5861(4)	956(3)	68(1)
C(36)	1451(4)	6131(3)	781(2)	53(1)
C(41)	7538(3)	2744(2)	1225(2)	42(1)
C(42)	6942(4)	2651(3)	1915(2)	49(1)
C(43)	7214(5)	1969(3)	2351(2)	59(1)
C(44)	8072(5)	1402(3)	2117(3)	68(1)
C(45)	8676(6)	1484(3)	1427(3)	81(2)
C(46)	8425(5)	2158(3)	987(3)	65(1)

Table A29: Bond lengths (Å) and angles (°) for *cis*-(S,P)-[PtCl(L1a)(PPh_3)].

Pt(1)-O(1)	2.044(3)
Pt(1)-P(1)	2.2159(9)
Pt(1)-S(1)	2.2448(8)
Pt(1)-Cl(1)	2.3335(8)
S(1)-C(2)	1.731(4)
P(1)-C(11)	1.731(4)
P(1)-C(31)	1.820(3)
P(1)-C(21)	1.833(3)
O(1)-C(1)	1.267(4)
N(1)-C(1)	1.316(4)
N(1)-C(2)	1.316(4)
N(2)-C(2)	1.342(4)
N(2)-C(3)	1.472(6)
N(2)-C(5)	1.477(5)
C(1)-C(41)	1.477(5)
C(3)-C(4)	1.477(5)
C(5)-C(6)	1.493(7)
C(11)-C(16)	1.493(7)
C(11)-C(12)	1.395(5)
C(12)-C(13)	1.367(7)
C(13)-C(14)	1.367(7)
C(14)-C(15)	1.365(6)
C(15)-C(16)	1.383(5)
C(21)-C(26)	1.383(5)
C(21)-C(22)	1.383(5)
C(22)-C(23)	1.397(6)
C(23)-C(24)	1.336(7)
C(24)-C(25)	1.362(7)
C(25)-C(26)	1.379(6)
C(31)-C(36)	1.398(6)
C(31)-C(32)	1.398(6)
C(32)-C(33)	1.389(6)

C(33)-C(34)	1.365(7)
C(34)-C(35)	1.365(7)
C(35)-C(36)	1.393(6)
C(41)-C(42)	1.373(5)
C(41)-C(46)	1.382(6)
C(42)-C(43)	1.387(6)
C(43)-C(44)	1.376(6)
C(44)-C(45)	1.376(6)
C(45)-C(46)	1.376(6)

O(1)-Pt(1)-P(1)	173.72(7)
O(1)-Pt(1)-S(1)	93.19(7)
P(1)-Pt(1)-S(1)	92.60(3)
O(1)-Pt(1)-Cl(1)	88.69(3)
P(1)-Pt(1)-Cl(1)	88.69(3)
S(1)-Pt(1)-Cl(1)	178.16(3)
C(2)-S(1)-Pt(1)	108.46(12)
C(11)-P(1)-C(31)	108.16(16)
C(11)-P(1)-C(21)	106.48(16)
C(31)-P(1)-C(21)	106.48(16)
C(11)-P(1)-Pt(1)	113.89(12)
C(31)-P(1)-Pt(1)	110.14(13)
C(21)-P(1)-Pt(1)	126.6(3)
C(1)-O(1)-Pt(1)	126.6(3)
C(1)-N(1)-C(2)	126.6(3)
C(2)-N(2)-C(3)	122.7(3)
C(2)-N(2)-C(5)	122.7(3)
C(3)-N(2)-C(5)	116.2(3)
O(1)-C(1)-N(1)	130.5(3)
O(1)-C(1)-C(41)	115.7(3)
N(1)-C(1)-C(41)	115.7(3)
N(1)-C(2)-N(2)	114.3(3)
N(1)-C(2)-S(1)	116.0(3)

N(2)-C(2)-S(1)	116.0(3)
N(2)-C(3)-C(4)	112.9(4)
N(2)-C(5)-C(6)	114.6(4)
C(16)-C(11)-C(12)	118.9(3)
C(16)-C(11)-P(1)	121.5(3)
C(12)-C(11)-P(1)	119.6(3)
C(13)-C(12)-C(11)	119.7(4)
C(14)-C(13)-C(12)	120.2(4)
C(15)-C(14)-C(13)	120.5(4)
C(14)-C(15)-C(16)	120.3(4)
C(15)-C(16)-C(11)	120.3(4)
C(26)-C(21)-C(22)	119.1(3)
C(26)-C(21)-P(1)	118.2(3)
C(22)-C(21)-P(1)	122.5(3)
C(21)-C(22)-C(23)	119.3(4)
C(24)-C(23)-C(22)	121.0(4)
C(23)-C(24)-C(25)	119.8(4)
C(24)-C(25)-C(26)	120.9(5)
C(21)-C(26)-C(25)	119.9(4)
C(36)-C(31)-C(32)	119.1(3)
C(36)-C(31)-P(1)	123.3(3)
C(32)-C(31)-P(1)	117.6(3)
C(33)-C(32)-C(31)	119.7(4)
C(34)-C(33)-C(32)	119.7(4)
C(33)-C(34)-C(35)	119.7(4)
C(34)-C(35)-C(36)	121.0(4)
C(31)-C(36)-C(35)	121.6(3)
C(42)-C(41)-C(46)	121.6(3)
C(42)-C(41)-C(1)	121.6(3)
C(46)-C(41)-C(1)	121.6(3)
C(41)-C(42)-C(43)	119.9(4)
C(44)-C(43)-C(42)	121.1(4)
C(43)-C(44)-C(45)	119.8(4)

C(44)-C(45)-C(46)	120.0(5)
C(45)-C(46)-C(41)	120.4(4)

Symmetry transformations used to generate equivalent atoms.

Table A30: Anisotropic displacement parameters ($Å^2$ x 10^3) for *cis*-(S,P)-[PtCl(L1a)(PPh_3)]. The anisotropic displacement factor exponent takes the form: $-2\pi^2$ [$h^2 a^{*2}$ U11 + ... + 2 h k a* b* U12].

	U11	U22	U33	U23	U13	U12
Pt(1)	34(1)	32(1)	35(1)	-2(1)	2(1)	1(1)
Cl(1)	55(1)	60(1)	39(1)	-4(1)	9(1)	6(1)
S(1)	50(1)	45(1)	41(1)	5(1)	10(1)	7(1)
P(1)	30(1)	32(1)	41(1)	-2(1)	0(1)	-2(1)
O(1)	58(2)	48(2)	41(1)	2(1)	4(1)	21(1)
N(1)	40(2)	42(2)	46(2)	-1(1)	3(1)	4(1)
N(2)	51(2)	56(2)	46(2)	-5(2)	10(2)	6(2)
C(1)	33(2)	38(2)	43(2)	-2(2)	-3(2)	1(1)
C(2)	35(2)	42(2)	42(2)	-7(2)	5(1)	-4(1)
C(3)	73(3)	78(4)	64(3)	-10(3)	23(3)	25(3)
C(4)	145(6)	67(4)	87(4)	-24(3)	15(4)	17(4)
C(5)	64(3)	77(3)	56(2)	1(2)	22(2)	-5(2)
C(6)	98(4)	128(6)	60(3)	11(3)	0(3)	2(4)
C(11)	36(2)	34(2)	48(2)	-5(2)	5(2)	-3(1)
C(12)	49(2)	41(2)	67(2)	-7(2)	-8(2)	-10(2)
C(13)	73(3)	55(3)	82(3)	-15(2)	-16(3)	-18(2)
C(14)	79(3)	42(2)	94(4)	-19(2)	11(3)	-14(2)
C(15)	66(3)	39(2)	81(3)	-1(2)	16(3)	9(2)
C(16)	53(2)	41(2)	62(3)	-3(2)	3(2)	2(2)
C(21)	37(2)	36(2)	42(2)	1(1)	-2(1)	3(1)
C(22)	55(2)	51(3)	57(2)	0(2)	-12(2)	2(2)
C(23)	83(3)	70(3)	51(3)	-8(2)	-23(2)	11(3)
C(24)	108(4)	73(3)	51(3)	8(2)	5(3)	7(3)
C(25)	106(4)	82(4)	63(3)	8(3)	21(3)	-26(3)
C(26)	66(3)	63(3)	53(2)	5(2)	4(2)	-20(2)
C(31)	32(2)	43(2)	43(2)	2(2)	-1(1)	-2(2)
C(32)	49(2)	54(3)	83(3)	-6(2)	4(2)	-13(2)
C(33)	61(3)	66(3)	98(4)	-2(3)	-1(2)	-27(2)
C(34)	39(2)	105(4)	71(3)	2(3)	2(2)	-25(3)

C(35)	41(2)	94(4)	70(3)	-3(3)	11(2)	0(3)
C(36)	40(2)	61(3)	57(2)	-2(2)	4(2)	-4(2)
C(41)	42(2)	35(2)	0(2)	0(2)	-6(2)	1(2)
C(42)	43(2)	51(2)	52(2)	6(2)	-4(2)	1(2)
C(43)	68(3)	58(3)	52(2)	13(2)	-8(2)	-9(2)
C(44)	93(3)	47(3)	63(3)	11(2)	-15(3)	10(3)
C(45)	106(4)	52(3)	84(3)	0(3)	-9(3)	38(3)
C(46)	80(3)	60(3)	60(3)	7(2)	11(2)	23(2)

Table A31: Hydrogen coordinates (x 10^4) and isotropic displacement parameters ($Å^2$ x 10^3) for *cis*-(S,P)-[PtCl(L1a)(PPh_3)].

	X	Y	Z	U(eq)
H(3A)	9509	3063	-756	81(3)
H(3B)	9604	3227	-1625	81(3)
H(4A)	7576	2298	-959	81(3)
H(4B)	8773	1921	-1397	81(3)
H(4C)	7720	2443	-1829	81(3)
H(5A)	9057	4465	-1976	81(3)
H(5B)	7993	4996	-1566	81(3)
H(6A)	7364	3726	-2555	81(3)
H(6B)	7312	4651	-2773	81(3)
H(6C)	6328	4302	-2172	81(3)
H(12)	5883	6518	1290	81(3)
H(13)	6348	7794	1783	81(3)
H(14)	5071	8893	1460	81(3)
H(15)	3406	8757	595	81(3)
H(16)	3000	7512	39	81(3)
H(22)	2556	5393	-1132	81(3)
H(23)	2827	5626	-2416	81(3)
H(24)	4478	6430	-2842	81(3)
H(25)	5895	7033	-2007	81(3)
H(26)	5671	6822	-729	81(3)
H(32)	2520	4443	55	81(3)
H(33)	393	4032	346	81(3)
H(34)	-1062	4917	901	81(3)
H(35)	-405	6214	1192	81(3)
H(36)	1703	6662	894	81(3)
H(42)	6358	3044	2091	81(3)
H(43)	6792	1905	2813	81(3)
H(44)	8259	955	2420	81(3)
H(45)	9255	1085	1257	81(3)
H(46)	8855	2219	527	81(3)

APPENDIX B

Kinetic data

Table B1: Rate constants for the reaction of *cis*-(S,S)-[PtCl(DMSO)(L1a)] with azide in methanol. $[Pt]_F$ = 0.5 mM. λ = 375 nm.

Temperature/ °C	[Azide]/ M	$k_{obs}/10^{-3}$ s^{-1}	k_y/ $M^{-1}s^{-1}$	k_s/ s^{-1}
10.2	0.1	2.6(2)	0.0230(3)	0.00031(1)
	0.075	2.07(1)		
	0.05	1.462(5)		
	0.025	0.8642(2)		
	0.01	0.547(1)		
	0.005	0.442(1)		
25.0	0.1	8.72(3)	0.0724(7)	0.00144(4)
	0.075	6.812(2)		
	0.05	5.10(1)		
	0.025	3.167(5)		
	0.01	2.164(2)		
	0.005	1.856(3)		
39.8	0.1	26.2(2)	0.196(7)	0.0062(4)
	0.075	20.1(1)		
	0.05	16.6(3)		
	0.025	11.7(1)		
	0.01	7.95(1)		
	0.005	7.02(2)		

Table B2: Rate constants for the reaction of *cis*-(S,S)-[PtCl(DMSO)(L1a)] with iodide in methanol. λ = 375 nm, $[Pt]_F$ = 0.5 mM.

Temperature/ °C	$[I^-]$/ M	$k_{obs}/10^{-3}$ s^{-1}	k_y/ $M^{-1}s^{-1}$	k_s/ s^{-1}
25.1	0.1	128.3(1)	1.16(3)	0.005(2)
		121(1)		
		11(1)		
		129(1)		
		124(2)		
	0.075	100(1)		
		82(1)		
		82(1)		
		88(1)		
		88(2)		
	0.05	59.8(5)		
		57.7()		
		67.6(9)		
		59.9(6)		
		65.6(9)		
		65.3(8)		
		63(2)		
	0.025	32.1(2)		
		34.4(2)		
		34.3(2)		
		32.7(2)		
		33.3(4)		
	0.01	17.8(1)		
		10.3(1)		
		18.5(1)		
		020.8(2)		
		16.9(2)		
	0.005	11.47(1)		
		11.34(7)		
		10.87(7)		

12.5(1)

11.55(15)

Table B3: Rate constants for the reaction of *cis*-(S,S)-[PtCl(DMSO)(L1a)] with thiocyanate in methanol. λ = 375 nm, $[Pt]_F$ = 0.5 mM.

Temperature/ °C	$[SCN^-]$/ M	k_{obs}/ s^{-1}	k_y/ $M^{-1}s^{-1}$	k_s/ s^{-1}
25.0	0.1	0.412(5)	4.47(15)	0.012(9)
		0.458(8)		
		0.505(7)		
		0.502(8)		
		0.47(1)		
	0.075	0.332(7)		
		0.325(5)		
		0.334(7)		
		0.331(5)		
		0.33(1)		
	0.025	0.125(3)		
		0.142(3)		
		0.1330(20)		
		0.133(5)		
	0.01	0.0564(5)		
		0.0600(5)		
		0.0557(6)		
		0.0616(6)		
		0.058(1)		
	0.005	0.0349(3)		
		0.0288(4)		
		0.0250(4)		
		0.0304(5)		
		0.0298(8)		

Table B4: Rate constants for the reaction of *cis*-(S,S)-[PtCl(L1a)(MPSO)] with azide in methanol. λ = 375 nm, $[Pt]_F$ = 0.5 mM.

Temperature/ °C	[Azide]/ M	k_{obs}/ 10^{-3} s^{-1}	k_y/ 10^{-3} $M^{-1}s^{-1}$	k_s/ 10^{-3} s^{-1}
10.2	0.1	2.59(2)	22.0(6)	0.3(3)
	0.075	2.02(1)		
	0.05	1.38(1)		
	0.025	0.88(1)		
	0.01	0.61(1)		
	0.005	0.49(1)		
25.1	0.1	10.4(2)	99(6)	0.8(3)
	0.075	8.8(1)		
	0.025	2.8(3)		
	0.01	1.867(15)		
	0.005	1.56(1)		
39.8	0.1	28.67(5)	230(5)	5.7(3)
	0.075	23.5(1)		
	0.05	16.68(3)		
	0.025	11.10(2)		
	0.01	8.18(1)		
	0.005	7.25(1)		

Table B5: Rate constants for the reaction of *cis*-(S,S)-[PtCl(L1a)((*S*)-MTSO)] with azide in methanol. λ = 375 nm, $[Pt]_F$ = 0.5 mM.

Temperature/ °C	[Azide]/ M	k_{obs}/ 10^{-3} s^{-1}	k_y/ 10^{-3} $M^{-1}s^{-1}$	k_s/ 10^{-3} s^{-1}
10.0	0.1	2.617(15)	22.3(7)	0.32(4)
	0.075	1.953(1)		
	0.05	1.374(5)		
	0.025	0.829(2)		
	0.01	0.578(2)		
	0.005	0.487(2)		
25.0	0.1	9.33(8)	78(2)	1.3(1)
	0.075	7.14(6)		
	0.05	5.11(3)		
	0.025	3.24(2)		
	0.01	2.19(1)		
	0.005	1.87(1)		
39.8	0.1	26.7(1)	214(11)	4.7(7)
	0.075	20.25(5)		
	0.05	15.45(3)		
	0.025	9.2(3)		
	0.005	6.62(1)		

Table B6: Rate constants for the reaction of *cis*-(S,S)-[PtCl(DMSO)(L1aR)] with azide in methanol. λ = 375 nm, $[Pt]_F$ = 0.5 mM , T = 25.0°C.

R-Group	[Azide]/ M	k_{obs}/ 10^{-3} s^{-1}	k_y/ $M^{-1}s^{-1}$	k_s/ s^{-1}
H	0.1	8.72(3)	0.0724(7)	0.00144(4)
	0.075	6.812(2)		
	0.05	5.10(1)		
	0.025	3.167(5)		
	0.01	2.164(2)		
	0.005	1.856(3)		
Cl	0.1	10.7(2)	0.091(3)	0.0013(2)
	0.075	7.8(1)		
	0.05	5.60(6)		
	0.025	3.47(2)		
	0.01	2.28(1)		
	0.005	1.87(1)		
NO_2	0.1	12.5(3)	0.110(2)	0.0015(1)
	0.075	9.8(2)		
	0.05	7.3(1)		
	0.025	4.47(6)		
	0.01	2.63(5)		
	0.005	1.90(3)		
CH_3	0.1	8.42(9)	0.070(1)	0.00136(7)
	0.075	6.47(6)		
	0.05	4.89(5)		
	0.025	3.00(2)		
	0.01	2.08(1)		
	0.005	1.79(1)		
OCH_3	0.1	9.39(6)	0.0799(9)	0.00132(5)
	0.075	7.21(4)		
	0.05	5.34(3)		
	0.025	3.28(2)		
	0.01	2.12(1)		
	0.005	1.78(1)		

Table B7: Rate constants for the reaction of *cis*-(S,S)-[PtCl(DMSO)(L3a)] with azide in methanol. λ = 375 nm, $[Pt]_F$ = 0.5 mM.

Temperature/ °C	[Azide]/ M	k_{obs}/ 10^{-3} s^{-1}	k_y/ 10^{-3} $M^{-1}s^{-1}$	k_s/ 10^{-3} s^{-1}
25.2	0.1	10.8(1)	90(2)	1.7(1)
	0.075	8.37(4)		
	0.05	6.4(2)		
	0.025	4.01(1)		
	0.01	2.583(7)		

Table B8: Rate constants for the reaction of *cis*-(S,S)-[PtCl(DMSO)(L1a)] with thiourea in methanol. λ = 380 nm, $[Pt]_F$ = 0.5 mM.

Temperature/ °C	[Thiourea]/ M	k_{obs}/ s^{-1}	k_y/ $M^{-1}s^{-1}$	k_s/ s^{-1}
25.1	0.1	10.78(15)	107(1)	0
		10.63(16)		
		10.58(14)		
		10.34(16)		
		10.6(3)		
	0.075	7.64(7)		
		7.98(7)		
		8.34(7)		
		8.54(6)		
		8.1(1)		
	0.025	2.931(14)		
		3.018(12)		
		3.019(13)		
		2.992(15)		
		3.056(17)		
		3.00(3)		
	0.01	1.139(5)		
		1.125(5)		
		1.144(5)		
		1.136(4)		
		1.136(9)		
	0.005	0.5461(7)		
		0.550(3)		
		0.5613(25)		
		0.588(3)		
		0.554(5)		

Table B9: Rate constants for the reaction of *cis*-(S,S)-[PtCl(DMSO)(L1a)] with MBI in methanol. λ = 380 nm, $[Pt]_F$ = 0.5 mM.

Temperature/ °C	[MBI]/ M	k_{obs}/ s^{-1}	k_y/ $M^{-1}s^{-1}$	k_s/ s^{-1}
25.0	0.1	4.26(4)	42(1)	0
		3.94(3)		
		3.89(3)		
		4.38(4)		
		4.03(3)		
		4.10(8)		
	0.075	3.101(21)		
		3.213(20)		
		3.238(21)		
		3.148(18)		
		3.301(19)		
		3.20(4)		
	0.05	2.31(3)		
		2.33(2)		
		2.26(2)		
		2.33(3)		
		2.31(5)		
	0.025	1.255(5)		
		1.271(5)		
		1.288(5)		
		1.271(5)		
		1.272(5)		
		1.27(1)		
	0.01	0.5173(21)		
		0.5180(23)		
		0.5223(23)		
		0.5219(23)		
		0.5237(23)		
		0.5247(23)		
		0.521(5)		

	0.005	0.2603(8)
		0.2601(9)
		0.2614(9)
		0.2608(9)
		0.2605(8)
		0.261(2)

Table B10: Rate constants for the first reaction of *cis*-(S,S)-[PtCl(DMSO)(L1a)] with PPh_3 in methanol. λ = 370 nm, $[Pt]_F$ = 0.5 mM (Chloride Substitution).

Temperature/ °C	$[PPh_3]$/ M	k_{obs}/ s^{-1}	k_y/ $M^{-1}s^{-1}$	k_s/ s^{-1}
25.1	0.025	24.6(9)	1203(23)	0
		34.5(8)		
		34.6(7)		
		21.8(5)		
		34.8(8)		
		30(2)		
	0.02	22.7(1)		
		23(1)		
		22.5(1)		
		23(1)		
	0.015	21.0(5)		
		17.5(5)		
		20.7(5)		
		20.2(5)		
		20.7(6)		
		14.3(4)		
		19(1)		
	0.01	12.16(14)		
		12.25(12)		
		12.72(11)		
		12.73(12)		
		12.81(14)		
		12.5(3)		
	0.005	6.64(5)		
		6.68(4)		
		6.88(4)		
		7.02(5)		
		6.66(5)		
		7.07(4)		
		6.8(1)		

Table B11: Rate constants for the first reaction of *cis*-(S,S)-[PtCl(DMSO)(L1a)] with DMAP in methanol. λ = 380 nm, $[Pt]_F$ = 0.5 mM.

Temperature/ °C	[DMAP]/ M	k_{obs}/ s^{-1}	k_y/ $M^{-1}s^{-1}$	k_s/ s^{-1}
25.1°C	0.3	0.362(2)	0.87(4)	0.100(6)
		0.363(2)		
		0.370(2)		
		0.377(1)		
		0.368(3)		
25.1°C	0.2	0.267(1)		
		0.271(1)		
		0.278(1)		
		0.2376(15)		
		0.263(2)		
25.1°C	0.1	0.1752(8)		
		0.1726(5)		
		0.1883(5)		
		0.1911(5)		
		0.1882(5)		
		0.183(1)		
	0.05	0.1443(7)		
		0.1418(6)		
		0.1473(7)		
		0.1460(7)		
		0.1469(7)		
		0.1405(6)		
		0.1427(6)		
		0.144(2)		
	0.025	0.1235(7)		
		0.1242(7)		
		0.1264(8)		
		0.1227(6)		
		0.1276(6)		
		0.1392(9)		

	0.1229(8)
	0.127(2)
0.01	0.1384(9)
	0.1281(7)
	0.1254(9)
	0.1342(9)
	0.1256(9)
	0.1361(9)
	0.1224(9)
	0.130(2)
0.005	0.150(3)
	0.160(3)
	0.155(3)
	0.161(3)
	0.156(6)

Table B12: Rate constants for the reaction of *cis*-(S,S)-[PtCl(DMSO)(L1a)] with MBI in methanol. DMSO variation at constant [MBI]. λ = 380 nm, $[Pt]_F$ = 0.5 mM.

Temperature/ °C	[MBI]/ M	[DMSO]/ M	k_{obs}/ s^{-1}
25.0	0.01	0.1	0.486(4)
			0.515(2)
			0.515(2)
			0.515(2)
			0.516(2)
			0.509(6)
		0.005	0.479(4)
			0.487(3)
			0.478(3)
			0.484(3)
			0.493(3)
			0.494(3)
			0.497(3)
			0.487(8)
25.1	0.1	0.1	3.98(6)
			3.34(5)
			3.71(6)
			3.24(5)
			3.81(6)
			3.16(5)
			3.5(1)
		0.005	3.29(8)
			3.63(5)
			3.71(5)
			3.53(3)
			3.51(3)
			3.5(1)

Table B13: Rate constants for the first reaction of *cis*-(S,S)-[PCl(DMSO)(L1a)] with DMAP in methanol. λ = 380 nm, $[Pt]_F$ = 0.5 mM T = 25°C (DMSO variation, constant [DMAP]).

[DMAP]/ M	[DMSO]/ M	k_{obs}/ s^{-1}
0.1	0.005	0.2133(2)
		0.2186(3)
		0.2223(3)
		0.2248(3)
		0.2278(3)
		0.2321(3)
		0.2231(6)
	0.1	0.2383(4)
		0.2325(3)
		0.2340(3)
		0.2263(3)
		0.2231(3)
		0.2195(3)
		0.2164(3)
		0.2271(9)
0.3	0.005	0.4643(8)
		0.4716(9)
		0.47400(1)
		0.464(1)
		0.465(1)
		0.465(1)
		0.461(1)
		0.466(2)
	0.1	0.4505(6)
		0.4531(7)
		0.4567(8)
		0.4598(8)
		0.4623(6)
		0.4652(5)

0.458(2)

Table B14: Rate constants for the first reaction of *cis*-(S,S)-[PtCl(DMSO)(L1a)] with PPh_3 in methanol. DMSO variation at constant [PPh_3]. λ = 357 nm, $[Pt]_F$ = 0.5 mM, T = 25°C.

[PPh_3]/ M	[DMSO]/ M	k_{obs}/ s^{-1}
0.02	0.025	28.3(3)
		29.2(2)
		29.1(2)
		28.4(2)
		28.6(2)
		28.7(2)
		28.7(6)
	0.01	28.6(2)
		28.6(2)
		28.8(2)
		28.4(2)
		28.2(2)
		28.5(5)
0.01	0.025	14.9(1)
		14.9(1)
		15.0(1)
		14.8(1)
		14.7(1)
		14.8(3)
	0.01	14.4(2)
		15.0(2)
		14.7(2)
		14.7(2)
		14.5(2)
		14.7(5)

Table B15: Rate constants for the reaction of *cis*-(S,S)-[PtCl(MPSO)(L1a)] with MBI in methanol. λ = 380 nm, $[Pt]_F$ = 0.5 mM.

Temperature/ °C	[MBI]/ M	k_{obs}/ s^{-1}	k_y/ $M^{-1}s^{-1}$	k_s/ s^{-1}
25.1	0.1	12.47(11)	121(8)	1.2(4)
		13.16(13)		
		13.19(20)		
		13.00(16)		
		12.58(12)		
		12.9(3)		
	0.075	10.24(7)		
		10.63(7)		
		11.13(8)		
		10.85(8)		
		10.71(15)		
	0.05	7.02(6)		
		6.89(5)		
		6.99(5)		
		7.11(5)		
		6.87(5)		
		7.0(1)		
	0.025	5.34(3)		
		5.41(4)		
		5.08(4)		
		5.00(4)		
		5.18(4)		
		5.05(4)		
		5.18(9)		
	0.01	2.469(19)		
		2.174(18)		
		2.012(16)		
		2.230(19)		
		1.987(17)		
		2.17(4)		

	0.005	1.337(11)
		1.192(9)
		1.249(1)
		1.276(11)
		1.247(12)
		1.26(2)

Table B16: Rate constants for the reaction of *cis*-(S,S)-[PtCl(L1a)((*S*)-MTSO)] with MBI in methanol. λ = 380 nm, $[Pt]_F$ = 0.5 mM.

Temperature/ °C	[MBI]/ M	k_{obs}/ s^{-1}	k_y/ $M^{-1}s^{-1}$	k_s/ s^{-1}
25.0	0.1	10.05(9)	94(4)	0.9(2)
		10.00(6)		
		10.08(11)		
		10.04(15)		
	0.075	7.84(5)		
		8.31(5)		
		7.98(5)		
		8.21(5)		
		8.1(1)		
	0.05	5.55(4)		
		5.38(5)		
		5.55(4)		
		5.75(5)		
		5.67(5)		
		5.6(1)		
	0.025	3.758(21)		
		3.754(20)		
		3.713(19)		
		3.771(21)		
		3.75(4)		
	0.01	1.661(1)		
		1.622(1)		
		1.617(1)		
		1.604(9)		
		1.593(10)		
		1.63(1)		
	0.005	0.999(8)		
		0.989(8)		
		1.11(1)		
		1.01(1)		

1.0101)

1.03(2)

Table B17: Rate constants for the reaction of *cis*-(S,S)-[PtCl(DMSO)(L3a)] with MBI in methanol. λ = 380 nm, $[Pt]_F$ = 0.5 mM.

Temperature/ °C	[MBI]/ M	k_{obs}/ s^{-1}	k_y/ $M^{-1}s^{-1}$	k_s/ s^{-1}
25.0	0.1	3.46(3)	35(1)	0.3(1)
		3.63(3)		
		3.94(3)		
		3.99(3)		
		3.75(6)		
	0.075	2.64(3)		
		3.12(3)		
		2.89(3)		
		2.927(25)		
		2.89(6)		
	0.05	2.28(6)		
		2.22(4)		
		2.229(19)		
		2.112(17)		
		2.21(8)		
	0.025	1.305(15)		
		1.313(15)		
		1.222(9)		
		1.231(3)		
		1.27(3)		
	0.01	0.632(3)		
		0.634(3)		
		0.642(3)		
		0.633(3)		
		0.635(6)		
	0.005	0.3370(16)		
		0.3256(16)		
		0.3214(19)		
		0.3212(16)		
		0.3353(19)		

0.328(4)

Table B18: Rate constants for the reaction of *cis*-(S,S)-[PtCl(DMSO)(L1a)] with MBI in methanol at various temperatures. λ = 380 nm, $[Pt]_F$ = 0.5 mM.

Temperature/ °C	[MBI]/ M	k_{obs}/ s^{-1}
10.2	0.025	0.18(1)
		0.19(1)
		0.19(1)
		0.19(1)
		0.19(2)
25.2		0.45(2)
		0.45(2)
		0.47(2)
		0.45(2)
		0.45(4)
40.1		1.46(7)
		1.41(7)
		1.44(7)
		1.43(7)
		1.45(7)
		1.44(16)

Table B19: Rate constants for the first reaction of *cis*-(S,S)-[PtCl(DMSO)(L1a)] with PPh_3 in methanol at various temperatures. λ = 357 nm, $[Pt]_F$ = 0.5 mM.

Temperature/ °C	$[PPh_3]$/ M	k_{obs}/ s^{-1}
10.2	0.005	3.5(2)
		3.4(2)
		3.4(2)
		3.4(2)
		3.4(4)
18.2	0.005	5.1(2)
		4.9(2)
		5.2(3)
		5.3(3)
		5.1(5)
25.0	0.005	8.1(4)
		8.0(4)
		8.0(4)
		8.0(4)
		8.0(8)
43.1	0.005	29(1)
		26(1)
		28(1)
		30(1)
		28(2)

Table B20: Rate constants for the first reaction of *cis*-(S,S)-[PtCl(DMSO)(L1a)] with PPh_3 in acetonitrile. λ = 380 nm, $[Pt]_F$ = 0.5 mM , T = 25°C.

$[PPh_3]$/ M	k_{obs}/ s^{-1}	k_y/ $M^{-1}s^{-1}$	k_s/ s^{-1}
0.025	12.53(18)	480(14)	0
	12.08(14)		
	12.36(15)		
	12.82(14)		
	12.80(15)		
	13.37(14)		
	13.19(15)		
	12.7(4)		
0.02	9.14(8)		
	8.71(7)		
	8.81(6)		
	9.11(7)		
	8.70(5)		
	8.9(1)		
0.015	7.11(8)		
	7.28(9)		
	7.40(10)		
	7.17(6)		
	7.25(8)		
	7.2(2)		
0.01	4.48(4)		
	4.37(4)		
	4.56(4)		
	4.50(4)		
	4.72(4)		
	4.35(4)		
	4.50(4)		
	4.5(1)		
0.005	2.26(2)		
	2.29(2)		

2.32(2)
2.28(2)
2.26(2)
2.26(2)
2.20(2)
2.19(2)
2.26(6)

Table B21: Rate constants for the first reaction of *cis*-(S,S)-[PtCl(DMSO)(L1a)] with PPh_3 in acetone. λ = 390 nm, $[Pt]_F$ = 0.5 mM , T = 25°C.

$[PPh_3]$/ M	k_{obs}/ s^{-1}	k_y/ $M^{-1}s^{-1}$	k_s/ s^{-1}
0.1	20.4(2)	203(2)	0
	20.9(2)		
	20.5(2)		
	20.2(1)		
	20.9(1)		
	20.6(4)		
0.05	9.63(6)		
	9.67(5)		
	9.53(6)		
	9.71(6)		
	9.73(6)		
	9.80(6)		
	9.64(7)		
	9.67(16)		
0.025	5.00(2)		
	4.98(2)		
	5.25(2)		
	5.21(2)		
	5.24(2)		
	5.20(2)		
	5.21(2)		
	5.15(6)		
0.02	4.06(2)		
	4.08(2)		
	4.05(2)		
	4.00(2)		
	4.15(2)		
	4.10(2)		
	4.15(2)		
	4.02(2)		

	4.08(6)
0.015	3.02(1)
	3.04(1)
	2.91(1)
	3.02(1)
	3.00(1)
	3.00(1)
	3.04(1)
	3.01(3)
0.01	1.986(9)
	1.94(1)
	1.99(1)
	1.99(1)
	1.96(1)
	1.97(2)
0.005	0.90(1)
	0.95(1)
	0.90(1)
	0.95(1)
	0.97(1)
	0.98(1)
	0.94(1)
	0.93(1)
	0.93(2)
	0.93(2)
	0.94(4)

Table B22: Rate constants for the first reaction of *cis*-(S,S)-[PtCl(DMSO)(L1a)] with PPh_3 in dichloromethane. λ = 380 nm, $[Pt]_F$ = 0.5 mM , T = 25°C.

$[PPh_3]$/ M	k_{obs}/ s^{-1}	k_y/ $M^{-1}s^{-1}$	k_s/ s^{-1}
0.025	7.80(1)	161(13)	1.0(2)
	4.92(10)		
	4.89(10)		
	4.87(16)		
0.02	4.13(10)		
	4.75(3)		
	3.92(5)		
	3.99(5)		
	5.25(4)		
	4.4(1)		
0.015	4.31(8)		
	3.70(3)		
	3.21(2)		
	3.32(3)		
	3.94(2)		
	3.70(10)		
0.01	1.93(1)		
	3.31(7)		
	2.48(2)		
	2.540(15)		
	2.47(2)		
	2.54(8)		
0.005	2.13(1)		
	1.60(1)		
	1.83(2)		
	1.52(1)		
	1.65(2)		
	1.94(2)		
	1.78(3)		

Table B23: Rate constants for the second reaction of *cis*-(S,S)-[PtCl(DMSO)(L1a)] with PPh_3 in methanol. $\lambda = 400$ nm, $[Pt]_F = 0.5$ mM.

Temperature/ °C	$[PPh_3]$/ M	k_{obs}/ s^{-1}
25.1	0.025	0.370(1)
		0.371(1)
		0.372(1)
		0.369(1)
		0.371(1)
		0.370(1)
		0.370(3)
	0.02	0.358(2)
		0.3617(15)
		0.3659(15)
		0.362(1)
		0.363(1)
		0.362(3)
	0.015	0.366(1)
		0.3612(1)
		0.3588(15)
		0.358(1)
		0.359(1)
		0.361(2)
	0.01	0.343(1)
		0.347(1)
		0.3399(1)
		0.3347(9)
		0.340(1)
		0.342(2)
	0.005	0.3172(7)
		0.3042(8)
		0.3049(7)
		0.3043(6)
		0.3066(6)

	0.3055(6)
	0.307(2)
0.0025	0.1063(1)
	0.1084(1)
	0.0920(15)
	0.107(2)
	0.092(2)
	0.101(3)
0.00124	0.0662(7)
	0.0738(6)
	0.0673(7)
	0.0669(4)
	0.0627(5)
	0.0652(7)
	0.067(1)

Table B24: Rate constants for the second reaction of *cis*-(S,S)-[PtCl(DMSO)(L1a)] with PPh_3 in methanol. Chloride variation at constant [PPh_3]. λ = 400 nm, $[Pt]_F$ = 0.5 mM, T = 25°C.

[PPh_3]/ M	[Cl^-]/ M	k_{obs}/ s^{-1}
0.02	0.05	0.3504(9)
		0.360(1)
		0.3598(9)
		0.361(1)
		0.367(1)
		0.367(1)
		0.375(1)
		0.366(2)
	0.01	0.373(1)
		0.373(1)
		0.372(1)
		0.368(1)
		0.384(1)
		0.385(1)
		0.375(3)
0.01	0.05	0.3300(8)
		0.3330(7)
		0.3392(8)
		0.3343(7)
		0.3428(7)
		0.3454(8)
		0.3403(7)
		0.338(2)
	0.01	0.3548(10)
		0.3448(9)
		0.3403(8)
		0.3404(9)
		0.3394(10)
		0.3397(8)

0.343(2)

Table B25: Rate constants for the second reaction of *cis*-(S,S)-[PtCl(DMSO)(L1a)] with PPh_3 in acetonitrile. λ = 380 nm, $[Pt]_F$ = 0.5 mM , T = 25.1°C.

$[PPh_3]$/ M	k_{obs}/ s^{-1}
0.025	0.294(2)
	0.296(2)
	0.305(2)
	0.304(2)
	0.299(4)
0.02	0.248(1)
	0.247(1)
	0.249(1)
	0.238(1)
	0.235(1)
	0.243(2)
0.015	0.2140(8)
	0.2124(7)
	0.2121(8)
	0.2153(8)
	0.2114(7)
	0.213(2)
0.01	0.1401(7)
	0.1431(7)
	0.1380(7)
	0.1453(7)
	0.1432(7)
	0.142(1)
0.005	0.0760(5)
	0.0667(5)
	0.0730(5)
	0.0725(5)
	0.0747(5)
	0.072(1)

Table B26: Rate constants for the second reaction of *cis*-(S,S)-[PtCl(DMSO)(L1a)] with PPh_3 in acetone. λ = 390 nm, $[Pt]_F$ = 0.5 mM , T = 25°C.

$[PPh_3]$/ M	k_{obs}/ s^{-1}
0.1	0.3906(4)
	0.3934(4)
	0.3911(3)
	0.3997(5)
	0.3970(4)
	0.3995(4)
	0.395(1)
0.05	0.2500(1)
	0.2486(1)
	0.2475(2)
	0.2478(2)
	0.2449(2)
	0.2530(1)
	0.2558(1)
	0.2496(4)
0.025	0.1615(1)
	0.1641(1)
	0.1620(1)
	0.1611(1)
	0.1603(1)
	0.1618(2)
0.02	0.1307(1)
	0.1319(1)
	0.1326(1)
	0.1334(1)
	0.1349(1)
	0.1358(1)
	0.1344(1)
	0.1336(1)
	0.1334(3)

0.015	0.1073(1)
	0.1056(1)
	0.1059(1)
	0.1062(1)
	0.1067(1)
	0.1076(1)
	0.1096(1)
	0.1070(2)
0.01	0.0798(1)
	0.0815(1)
	0.0815(1)
	0.08052(6)
	0.07881(6)
	0.07782(6)
	0.07791(6)
	0.07878(7)
	0.0796(2)
0.005	0.04857(5)
	0.04779(5)
	0.04864(5)
	0.04905(4)
	0.04851(5)
	0.04768(4)
	0.0459(1)
	0.0451(1)
	0.0458(1)
	0.0474(2)

Table B27: Rate constants for the second reaction of *cis*-(S,S)-[PtCl(DMSO)(L1a)] with PPh_3 in dichloromethane. λ = 380 nm, $[Pt]_F$ = 0.5 mM , T = 25°C.

$[PPh_3]$/ M	k_{obs}/ s^{-1}
0.1	0.183(1)
	0.199(1)
	0.177(1)
	0.179(1)
	0.180(1)
	0.187(1)
	0.184(3)
0.025	0.0536(4)
	0.0472(5)
	0.0484(4)
	0.0517(4)
	0.0487(4)
	0.0499(9)
0.02	0.0471(2)
	0.0433(3)
	0.0438(3)
	0.0371(4)
	0.0387(4)
	0.0420(7)
0.015	0.0330(3)
	0.0310(2)
	0.0319(2)
	0.0319(2)
	0.0319(5)
0.01	0.0220(1)
	0.0198(1)
	0.0196(1)
	0.0201(1)
	0.0199(1)
	0.0203(3)

0.005	0.0146(2)
	0.0094(1)
	0.0118(1)
	0.0113(1)
	0.0118(3)

Table B28: Rate constants for the second reaction of *cis*-(S,P)-[PtCl(L1a)(PPh_3)] with PPh_3 in methanol. λ = 400 nm, $[Pt]_F$ = 0.25 mM , T = 25°C.

$[PPh_3]$/ M	k_{obs}/ s^{-1}
0.025	0.452(1)
	0.447(1)
	0.447(1)
	0.454(1)
	0.456(1)
	0.451(3)
0.02	0.435(1)
	0.448(1)
	0.445(1)
	0.445(1)
	0.446(1)
	0.450(1)
	0.448(1)
	0.458(1)
	0.447(4)
0.015	0.420(1)
	0.428(1)
	0.428(1)
	0.428(1)
	0.422(1)
	0.422(1)
	0.424(3)
0.01	0.3897(5)
	0.4001(6)
	0.392(1)
	0.390(1)
	0.394(1)
	0.403(1)
	0.395(5)
0.005	0.2731(7)

0.2772(7)
0.2794(7)
0.2794(8)
0.2945(9)
0.2973(9)
0.283(2)

Table B29: Rate constants for the second reaction of *cis*-(S,S)-[PtCl(DMSO)(L1a)] with DMAP in methanol. λ = 380 nm, $[Pt]_F$ = 0.5 mM.

Temperature/ °C	[DMAP]/ M	k_{obs}/ 10^{-3} s^{-1}
25.0	0.3	5.788(5)
	0.1	3.25(15)
	0.075	2.9(1)
	0.05	2.42(7)
	0.025	1.6(1)
	0.01	0.63(3)
	0.005	0.32(2)

Table A1: Crystallographic data for *N,N*-diethyl-*N'*-(-)-(3*R*)-menthyloxycarbonyl-thiourea (**HL4**).

Empirical formula	$C_{32}H_{60}N_4O_4S_2$
Formula weight	628.96
Temperature	293(2) K
Wavelength	0.71073 Å
Crystal system, space group	Monoclinic, $P2_1$
Unit cell dimensions	a = 8.889(2) Å α = 90°
	b = 13.207(3) Å β = 100.51(3)°
	c = 16.911(3) Å γ = 90°
Volume	1952.0(7) $Å^3$
Z	2, 1.070 Mg/m^3
μ	0.172 mm^{-1}
F(000)	688
Theta range for data collection	1.97 to 26.02°
Index ranges	$0 \le h \le 10$, $-16 \le k \le 0$, $-20 \le l \le 20$
Reflections collected/unique	2910/2770 [R(int) = 0.031]
Refinement method	Full-matrix least-squares on F^2
Goodness-of-fit on F^2	1.058
Final R indices [$I>2\sigma(I)$]	R^a = 0.0385, Rw^b = 0.0925
Absolute structure parameter	0.18(11)

[a] $R = [(\Sigma\Delta F)/(\Sigma F_0)]$.

[b] $Rw = \Sigma[w(F_0^2 - F_c^2)^2]/\Sigma[w(F_0^2)^2]^{1/2}$.

Table A2: Bond lengths (Å) for *N,N*-diethyl-*N'*-(-)-(3*R*)-menthyloxycarbonyl-thiourea (**HL4**).

Molecule 1		Molecule 2	
S(1)-C(11)	1.677(4)	S(2)-C(21)	1.673(4)
O(11)-C(12)	1.200(5)	O(21)-C(22)	1.186(5)
O(12)-C(12)	1.333(5)	O(22)-C(22)	1.343(5)
O(12)-C(1A)	1.463(5)	O(22)-C(2A)	1.458(4)
N(11)-C(12)	1.370(5)	N(21)-C(22)	1.382(5)
N(11)-C(11)	1.399(5)	N(21)-C(21)	1.396(5)
N(11)-H(1)	0.69(4)	N(21)-H(2)	0.92(4)
N(12)-C(11)	1.329(6)	N(22)-C(21)	1.326(6)
N(12)-C(13)	1.463(5)	N(22)-C(23)	1.477(5)
N(12)-C(15)	1.483(5)	N(22)-C(25)	1.488(5)
C(13)-C(14)	1.501(6)	C(23)-C(24)	1.506(6)
C(13)-H(13A)	0.9700	C(23)-H(23A)	0.9700
C(13)-H(13B)	0.9700	C(23)-H(23B)	0.9700
C(14)-H(14A)	0.9600	C(24)-H(24A)	0.9600
C(14)-H(14B)	0.9600	C(24)-H(24B)	0.9600
C(14)-H(14C)	0.9600	C(24)-H(24C)	0.9600
C(15)-C(16)	1.514(6)	C(25)-C(26)	1.487(6)
C(15)-H(15A)	0.9700	C(25)-H(25A)	0.9700
C(15)-H(15B)	0.9700	C(25)-H(25B)	0.9700
C(16)-H(16A)	0.9700	C(26)-H(26A)	0.9600
C(16)-H(16B)	0.9600	C(26)-H(26B)	0.9600
C(16)-H(16C)	0.9600	C(26)-H(26C)	0.9600
C(1A)-C(1B)	1.483(7)	C(2A)-C(2B)	1.498(7)
C(1A)-C(1F)	1.524(7)	C(2A)-C(2F)	1.528(6)
C(1A)-H(1A)	0.9800	C(2A)-H(2A)	0.9800
C(1B)-C(1C)	1.520(6)	C(2B)-C(2C)	1.533(6)
C(1B)-H(1BA)	0.9700	C(2B)-H(2BA)	0.9700
C(1B)-H(1BB)	0.9700	C(2B)-H(2BB)	0.9700

Table A2 continued.

C(1C)-C(1D)	1.522(7)	C(2C)-C(2D)	1.496(7)
C(1C)-C(1J)	1.508(8)	C(2C)-C(2J)	1.514(8)
C(1C)-H(1C)	0.9800	C(2C)-H(2C)	0.9800
C(1D)-C(1E)	1.508(7)	C(2D)-C(2E)	1.517(8)
C(1D)-H(1DA)	0.9700	C(2D)-H(2DA)	0.9700
C(1D)-H(1DB)	0.9700	C(2D)-H(2DB)	0.9700
C(1E)-C(1F)	1.536(6)	C(2E)-C(2F)	1.535(6)
C(1E)-H(1EA)	0.9700	C(2E)-H(2EA)	0.9700
C(1E)-H(1EB)	0.9700	C(2E)-H(2EB)	0.9700
C(1F)-C(1G)	1.526(7)	C(2F)-C(2G)	1.539(7)
C(1F)-H(1F)	0.9800	C(2F)-H(2F)	0.9800
C(1G)-C(1I)	1.504(11)	C(2G)-C(2H)	1.504(8)
C(1G)-C(1H)	1.527(9)	C(2G)-C(2I)	1.520(7)
C(1G)-H(1G)	0.9800	C(2G)-H(2G)	0.9800
C(1H)-H(1HA)	0.9600	C(2H)-H(2HA)	0.9600
C(1H)-H(1HB)	0.9600	C(2H)-H(2HB)	0.9600
C(1H)-H(1HC)	0.9600	C(2H)-H(2HC)	0.9600
C(1I)-H(1IA)	0.9600	C(2I)-H(2IA)	0.9600
C(1I)-H(1IB)	0.9600	C(2I)-H(2IB)	0.9600
C(1I)-H(1IC)	0.9600	C(2I)-H(2IC)	0.9600
C(1J)-H(1JA)	0.9600	C(2J)-H(2JA)	0.9600
C(1J)-H(1JB)	0.9600	C(2J)-H(2JB)	0.9600
C(1J)-H(1JC)	0.9600	C(2J)-H(2JC)	0.9600

Table A3: Bond angles (°) for *N,N*-diethyl-*N'*-(-)-(3*R*)-menthyloxycarbonyl-thiourea (**HL4**).

Molecule 1		Molecule 2	
C(12)-O(12)-C(1A)	117.2(3)	C(22)-O(22)-C(2A)	117.1(3)
C(12)-N(11)-C(11)	125.6(4)	C(22)-N(21)-C(21)	122.3(3)
C(12)-N(11)-H(1)	113(3)	C(22)-N(21)-H(2)	115(2)
C(11)-N(11)-H(1)	113(3)	C(21)-N(21)-H(2)	116(2)
C(11)-N(12)-C(13)	120.1(4)	C(21)-N(22)-C(23)	123.5(3)
C(11)-N(12)-C(15)	123.8(3)	C(21)-N(22)-C(25)	120.0(4)
C(13)-N(12)-C(15)	114.8(3)	C(23)-N(22)-C(25)	115.7(4)
N(12)-C(11)-N(11)	116.8(4)	N(22)-C(21)-N(21)	117.5(4)
N(12)-C(11)-S(1)	124.6(3)	N(22)-C(21)-S(2)	124.0(3)
N(11)-C(11)-S(1)	118.5(3)	N(21)-C(21)-S(2)	118.5(3)
O(11)-C(12)-O(12)	126.0(4)	O(21)-C(22)-O(22)	126.0(4)
O(11)-C(12)-N(11)	125.3(4)	O(21)-C(22)-N(21)	126.4(4)
O(12)-C(12)-N(11)	108.7(4)	O(22)-C(22)-N(21)	107.7(3)
N(12)-C(13)-C(14)	112.9(3)	N(22)-C(23)-C(24)	114.4(4)
N(12)-C(13)-H(13A)	109.0	N(22)-C(23)-H(23A)	108.7
C(14)-C(13)-H(13A)	109.0	C(24)-C(23)-H(23A)	108.7
N(12)-C(13)-H(13B)	109.0	N(22)-C(23)-H(23B)	108.7
C(14)-C(13)-H(13B)	109.0	C(24)-C(23)-H(23B)	108.7
H(13A)-C(13)-H(13B)	107.8	H(23A)-C(23)-H(23B)	107.6
C(13)-C(14)-H(14A)	109.5	C(23)-C(24)-H(24A)	109.5
C(13)-C(14)-H(14B)	109.5	C(23)-C(24)-H(24B)	109.5
H(14A)-C(14)-H(14B)	109.5	H(24A)-C(24)-H(24B)	109.5
C(13)-C(14)-H(14C)	109.5	C(23)-C(24)-H(24C)	109.5
H(14A)-C(14)-H(14C)	109.5	H(24A)-C(24)-H(24C)	109.5
H(14B)-C(14)-H(14C)	109.5	H(24B)-C(24)-H(24C)	109.5
N(12)-C(15)-C(16)	114.0(3)	C(26)-C(25)-N(22)	112.7(4)
N(12)-C(15)-H(15A)	108.8	N(22)-C(25)-H(25A)	109.0
C(16)-C(15)-H(15A)	108.8	C(26)-C(25)-H(25A)	109.0

Table A3 continued.

Molecule 1		Molecule 2	
N(12)-C(15)-H(15B)	108.8	N(22)-C(25)-H(25B)	109.0
C(16)-C(15)-H(15B)	108.8	C(26)-C(25)-H(25B)	109.0
N(12)-C(15)-H(15B)	108.8	N(22)-C(25)-H(25B)	109.0
C(16)-C(15)-H(15B)	108.8	C(26)-C(25)-H(25B)	109.0
H(15A)-C(15)-H(15B)	107.7	H(25A)-C(25)-H(25B)	107.8
C(15)-C(16)-H(16A)	109.5	C(25)-C(26)-H(26A)	109.5
C(15)-C(16)-H(16B)	109.5	C(25)-C(26)-H(26B)	109.5
H(16A)-C(16)-H(16B)	109.5	H(26A)-C(26)-H(26B)	109.5
C(15)-C(16)-H(16C)	109.5	C(25)-C(26)-H(26C)	109.5
H(16A)-C(16)-H(16C)	109.5	H(26A)-C(26)-H(26C)	109.5
H(16B)-C(16)-H(16C)	109.5	H(26B)-C(26)-H(26C)	109.5
O(12)-C(1A)-C(1B)	108.6(4)	O(22)-C(2A)-C(2B)	108.2(4)
O(12)-C(1A)-C(1F)	105.8(4)	O(22)-C(2A)-C(2F)	107.4(3)
C(1B)-C(1A)-C(1F)	113.2(4)	C(2B)-C(2A)-C(2F)	112.8(4)
O(12)-C(1A)-H(1A)	109.7	O(22)-C(2A)-H(2A)	109.5
C(1B)-C(1A)-H(1A)	109.7	C(2B)-C(2A)-H(2A)	109.5
C(1F)-C(1A)-H(1A)	109.7	C(2F)-C(2A)-H(2A)	109.5
C(1A)-C(1B)-C(1C)	112.6(4)	C(2A)-C(2B)-C(2C)	111.3(4)
C(1A)-C(1B)-H(1BA)	109.1	C(2A)-C(2B)-H(2BA)	109.4
C(1C)-C(1B)-H(1BA)	109.1	C(2C)-C(2B)-H(2BA)	109.4
C(1A)-C(1B)-H(1BB)	109.1	C(2A)-C(2B)-H(2BB)	109.4
C(1C)-C(1B)-H(1BB)	109.1	C(2C)-C(2B)-H(2BB)	109.4
H(1BA)-C(1B)-H(1BB)	107.8	H(2BA)-C(2B)-H(2BB)	108.0
C(1J)-C(1C)-C(1B)	112.9(5)	C(2J)-C(2C)-C(2B)	111.3(5)
C(1J)-C(1C)-C(1D)	111.6(5)	C(2D)-C(2C)-C(2J)	111.2(5)
C(1B)-C(1C)-C(1D)	107.8(4)	C(2D)-C(2C)-C(2B)	109.7(4)
C(1J)-C(1C)-H(1C)	108.1	C(2J)-C(2C)-H(2C)	108.2
C(1B)-C(1C)-H(1C)	108.1	C(2B)-C(2C)-H(2C)	108.2
C(1D)-C(1C)-H(1C)	108.1	C(2D)-C(2C)-H(2C)	108.2

Table A3 continued.

Molecule 1		Molecule 2	
C(1E)-C(1D)-C(1C)	111.8(4)	C(2C)-C(2D)-C(2E)	111.7(5)
C(1E)-C(1D)-H(1DA)	109.3	C(2E)-C(2D)-H(2DA)	109.3
C(1C)-C(1D)-H(1DA)	109.3	C(2C)-C(2D)-H(2DA)	109.3
C(1E)-C(1D)-H(1DB)	109.3	C(2E)-C(2D)-H(2DB)	109.3
C(1C)-C(1D)-H(1DB)	109.3	C(2C)-C(2D)-H(2DB)	109.3
H(1DA)-C(1D)-H(1DB)	107.9	H(2DA)-C(2D)-H(2DB)	107.9
C(1D)-C(1E)-C(1F)	112.8(4)	C(2D)-C(2E)-C(2F)	112.1(4)
C(1D)-C(1E)-H(1EA)	109.0	C(2D)-C(2E)-H(2EA)	109.2
C(1F)-C(1E)-H(1EA)	109.0	C(2F)-C(2E)-H(2EA)	109.2
C(1D)-C(1E)-H(1EB)	109.0	C(2D)-C(2E)-H(2EB)	109.2
C(1F)-C(1E)-H(1EB)	109.0	C(2F)-C(2E)-H(2EB)	109.2
H(1EA)-C(1E)-H(1EB)	107.8	H(2EA)-C(2E)-H(2EB)	107.9
C(1A)-C(1F)-C(1G)	113.9(4)	C(2A)-C(2F)-C(2G)	112.8(4)
C(1A)-C(1F)-C(1E)	107.5(4)	C(2A)-C(2F)-C(2E)	107.6(4)
C(1G)-C(1F)-C(1E)	114.3(4)	C(2E)-C(2F)-C(2G)	113.5(4)
C(1A)-C(1F)-H(1F)	106.9	C(2A)-C(2F)-H(2F)	107.5
C(1G)-C(1F)-H(1F)	106.9	C(2G)-C(F)-H(2F)	107.5
C(1E)-C(1F)-H(1F)	106.9	C(2E)-C(2F)-H(2F)	107.5
C(1I)-C(1G)-C(1F)	112.1(6)	C(2I)-C(2G)-C(2F)	110.6(5)
C(1I)-C(1G)-C(1H)	109.8(7)	C(2H)-C(2G)-C(2I)	110.2(5)
C(1F)-C(1G)-C(1H)	13.2(6)	C(2H)-C(2G)-C(2F)	114.6(5)
C(1I)-C(1G)-H(1G)	107.1	C(2I)-C(2G)-H(2G)	107.0
C(1F)-C(1G)-H(1G)	107.1	C(2F)-C(2G)-H(2G)	107.0
C(1H)-C(1G)-H(1G)	107.1	C(2H)-C(2G)-H(2G)	107.0
C(1G)-C(1H)-H(1HA)	109.5	C(2G)-C(2H)-H(2HA)	109.5
C(1G)-C(1H)-H(1HB)	109.5	C(2G)-C(2H)-H(2HB)	109.5
H(1HA)-C(1H)-H(1HB)	109.5	H(2HA)-C(2H)-H(2HB)	109.5
C(1G)-C(1H)-H(1HC)	109.5	C(2G)-C(2H)-H(2HC)	109.5
H(1HA)-C(1H)-H(1HC)	109.5	H(2HA)-C(2H)-H(2HC)	109.5

Table A3 continued.

Molecule 1		Molecule 2	
H(1HB)-C(1H)-H(1HC)	109.5	H(2HB)-C(2H)-H(2HC)	109.5
C(1G)-C(1I)-H(1IA)	109.5	C(2G)-C(2I)-H(2IA)	109.5
C(1G)-C(1I)-H(1IB)	109.5	C(2G)-C(2I)-H(2IB)	109.5
H(1IA)-C(1I)-H(1IB)	109.5	H(2IA)-C(2I)-H(2IB)	109.5
C(1G)-C(1I)-H(1IC)	109.5	C(2G)-C(2I)-H(2IC)	109.5
H(1IA)-C(1I)-H(1IC)	109.5	H(2IA)-C(2I)-H(2IC)	109.5
H(1IB)-C(1I)-H(1IC)	109.5	H(2IB)-C(2I)-H(2IC)	109.5
C(1C)-C(1J)-H(1JA)	109.5	C(2C)-C(2J)-H(2JA)	109.5
C(1C)-C(1J)-H(1JB)	109.5	C(2C)-C(2J)-H(2JB)	109.5
H(1JA)-C(1J)-H(1JB)	109.5	H(2JA)-C(2J)-H(2JB)	109.5
C(1C)-C(1J)-H(1JC)	109.5	C(2C)-C(2J)-H(2JC)	109.5
H(1JA)-C(1J)-H(1JC)	109.5	H(2JA)-C(2J)-H(2JC)	109.5
H(1JB)-C(1J)-H(1JC)	109.5	H(2JB)-C(2J)-H(2JC)	109.5

Symmetry transformations used to generate equivalent atoms.

Table A4: Atomic coordinates (x 10^4) and equivalent isotropic displacement parameters (Å^2 x 10^3) for *N,N*-diethyl-*N'*-(-)-(3*R*)-menthyloxycarbonylthiourea (**HL4**). $U_{(eq)}$ is defined as one third of the trace of the orthogonalized U_{ij} tensor.

	x	*y*	*z*	$U_{(eq)}$
S(1)	4316(1)	7056(1)	5524(1)	65(1)
O(11)	3582(3)	6448(3)	3005(2)	68(1)
O(12)	1915(3)	7753(2)	2889(2)	67(1)
N(11)	2592(4)	7038(3)	4072(2)	51(1)
N(12)	3393(3)	5461(3)	4596(2)	45(1)
C(11)	3426(4)	6459(3)	4695(2)	46(1)
C(12)	2780(5)	7026(4)	3286(2)	51(1)
C(13)	4354(4)	4809(3)	5181(3)	58(1)
C(14)	3548(6)	4444(5)	5834(3)	88(2)
C(15)	2203(5)	4920(3)	4020(3)	57(1)
C(16)	2837(6)	4228(5)	3446(3)	78(1)
C(1A)	1846(5)	7808(4)	2019(2)	65(1)
C(1B)	447(6)	7276(4)	1614(3)	79(1)
C(1C)	204(7)	7362(4)	703(3)	86(2)
C(1D)	155(7)	8482(4)	489(3)	88(2)
C(1E)	1577(6)	9028(5)	896(3)	86(2)
C(1F)	1850(5)	8932(4)	1816(2)	70(1)
C(1G)	3258(7)	9499(6)	2251(3)	106(2)
C(1H)	4732(7)	9189(9)	1971(4)	168(4)
C(1I)	3060(10)	10628(6)	2186(5)	165(4)
C(1J)	-1212(9)	6817(6)	288(4)	138(3)
S(2)	-922(1)	4249(1)	5569(1)	66(1)
O(21)	-1312(3)	4697(3)	3091(2)	66(1)
O(22)	-3232(3)	3557(2)	2917(1)	60(1)
N(21)	-2587(4)	4269(3)	4107(2)	49(1)
N(22)	-1575(4)	5822(3)	4591(2)	52(1)
C(21)	-1707(4)	4838(3)	4718(2)	45(1)

Table A4 continued.

C(22)	-2266(4)	4227(4)	3338(2)	50(1)
C(23)	-2640(5)	6397(3)	3982(3)	59(1)
C(24)	-1881(6)	6977(5)	3396(3)	80(1)
C(25)	-483(5)	6441(4)	5167(3)	63(1)
C(26)	-1193(6)	6880(6)	5821(3)	99(2)
C(2A)	-3041(5)	3349(4)	2094(2)	58(1)
C(2B)	-2502(6)	2278(4)	2056(3)	78(1)
C(2C)	-2380(6)	1978(4)	1194(3)	84(1)
C(2D)	-3884(6)	2148(5)	649(3)	94(2)
C(2E)	-4426(6)	3232(5)	690(3)	86(2)
C(2F)	-4583(5)	3538(4)	1547(2)	67(1)
C(2G)	-5166(6)	4627(4)	1608(3)	88(2)
C(2H)	-4228(9)	5425(5)	1289(4)	128(2)
C(2I)	-6834(7)	4711(7)	1202(4)	140(3)
C(2J)	-1858(8)	891(5)	1155(4)	136(3)

Table A5: Anisotropic displacement parameters ($Å^2$ x 10^3) for *N,N*-diethyl-*N'*-(-)-(3*R*)-menthyloxycarbonylthiourea (**HL4**). The anisotropic displacement factor exponent takes the form: $-2\pi^2 [h^2 a^{*2} U11 + ... + 2 h k a^* b^* U12]$.

	*U*11	*U*22	*U*33	*U*23	*U*13	*U*12
S(1)	70(1)	53(1)	62(1)	-3(1)	-11(1)	0(1)
O(11)	79(2)	73(2)	57(2)	14(2)	24(2)	26(2)
O(12)	88(2)	71(2)	44(2)	18(2)	19(1)	33(2)
N(11)	61(2)	44(2)	48(2)	2(2)	9(2)	11(2)
N(12)	44(2)	43(2)	45(2)	5(2)	1(1)	1(2)
C(11)	40(2)	46(3)	53(2)	5(2)	9(2)	2(2)
C(12)	57(2)	52(3)	46(2)	13(2)	13(2)	9(2)
C(13)	54(2)	50(3)	66(3)	9(2)	-2(2)	8(2)
C(14)	89(3)	94(4)	76(3)	40(3)	1(3)	-5(3)
C(15)	55(2)	54(3)	58(3)	-2(2)	3(2)	-3(2)
C(16)	92(3)	67(3)	76(3)	-9(3)	14(3)	2(3)
C(1A)	83(3)	74(3)	37(2)	14(2)	10(2)	25(3)
C(1B)	112(4)	62(3)	64(3)	2(3)	20(3)	12(3)
C(1C)	104(4)	88(4)	63(3)	-8(3)	6(3)	13(3)
C(1D)	116(4)	94(4)	47(2)	9(3)	1(3)	22(3)
C(1E)	112(4)	89(4)	55(3)	28(3)	9(3)	7(3)
C(1F)	82(3)	77(3)	49(2)	14(2)	4(2)	5(3)
C(1G)	109(4)	136(6)	65(3)	26(3)	-4(3)	-35(4)
C(1H)	92(4)	277(12)	128(5)	51(7)	2(4)	-52(6)
C(1I)	221(9)	139(7)	126(6)	4(5)	3(6)	-87(7)
C(1J)	184(7)	131(6)	93(4)	-22(4)	10(4)	-31(6)
S(2)	80(1)	56(1)	52(1)	6(1)	-13(1)	-10(1)
O(21)	64(2)	76(2)	61(2)	-16(2)	21(1)	-27(2)
O(22)	70(2)	67(2)	40(1)	-7(2)	5(1)	-24(2)
N(21)	57(2)	50(2)	39(2)	-2(2)	4(1)	-12(2)
N(22)	54(2)	52(2)	49(2)	-1(2)	6(2)	-2(2)
C(21)	46(2)	50(3)	38(2)	-7(2)	5(2)	-3(2)

Table A5 continued.

C(22)	49(2)	49(2)	48(2)	-1(2)	2(2)	0(2)
C(23)	62(2)	51(3)	61(3)	5(2)	7(2)	7(2)
C(24)	97(3)	64(3)	76(3)	17(3)	8(3)	5(3)
C(25)	67(3)	54(3)	63(3)	-9(2)	3(2)	-8(2)
C(26)	85(3)	109(5)	99(4)	-45(4)	7(3)	3(4)
C(2A)	66(3)	63(3)	44(2)	-4(2)	11(2)	-9(2)
C(2B)	81(3)	77(3)	71(3)	-7(3)	1(2)	7(3)
C(2C)	89(3)	77(3)	88(3)	-25(3)	23(3)	2(3)
C(2D)	107(4)	101(4)	73(3)	-42(3)	18(3)	-15(4)
C(2E)	100(4)	104(4)	49(3)	-18(3)	4(2)	-2(3)
C(2F)	74(3)	78(3)	44(2)	-6(2)	4(2)	-1(2)
C(2G)	114(4)	92(4)	55(3)	1(3)	6(3)	22(3)
C(2H)	193(7)	89(4)	99(5)	12(4)	14(5)	23(5)
C(2I)	134(5)	180(8)	100(4)	6(5)	3(4)	78(5)
C(2J)	164(6)	114(6)	138(6)	-33(5)	47(5)	33(5)

Table A6: Hydrogen coordinates (x 10^4) and isotropic displacement parameters ($Å^2$ x 10^3) for *N,N*-diethyl-*N'*-(-)-(3*R*)-menthyloxycarbonylthiourea (**HL4**).

	x	*y*	*z*	$U_{(eq)}$
H(1)	2380(4)	7510(3)	4200(2)	33(12)
H(13A)	5263	5180	5422	103(2)
H(13B)	4677	4228	4903	103(2)
H(14A)	4155	3931	6144	103(2)
H(14B)	4166	4166	5598	103(2)
H(14C)	3404	5001	6177	103(2)
H(15A)	1537	5416	3710	103(2)
H(15B)	1585	4521	4322	103(2)
H(16A)	2007	3940	3071	103(2)
H(16B)	3421	3697	3744	103(2)
H(16C)	3483	4611	3160	103(2)
H(1A)	2752	7482	1878	103(2)
H(1BA)	-434	7558	1800	103(2)
H(1BB)	520	6566	1763	103(2)
H(1C)	1091	7060	523	103(2)
H(1DA)	52	8555	-89	103(2)
H(1DB)	-734	8789	650	103(2)
H(1EA)	1490	9739	751	103(2)
H(1EB)	2454	8755	701	103(2)
H(1F)	960	9233	1994	103(2)
H(1G)	3382	9325	2822	103(2)
H(1HA)	5588	9517	2300	103(2)
H(1HB)	4678	9387	1421	103(2)
H(1HC)	4856	8468	2017	103(2)
H(1IA)	3148	10844	1655	103(2)
H(1IB)	3836	10953	2572	103(2)
H(1IC)	2069	10809	2291	103(2)
H(1JA)	-1189	6129	473	103(2)

Table A6 continued.

H(1JB)	-1246	6825	-283	103(2)
H(1JC)	-2103	7150	409	103(2)
H(2)	-3030(4)	3700(3)	4270(2)	54(12)
H(23A)	-3205	6870	4256	103(2)
H(23B)	-3373	5929	3683	103(2)
H(24A)	-2648	7277	2991	103(2)
H(24B)	-1263	6524	3146	103(2)
H(24C)	-1245	7499	3677	103(2)
H(25A)	377	6020	5404	103(2)
H(25B)	-93	6985	4877	103(2)
H(26A)	-435	7250	6186	103(2)
H(26B)	-1596	6345	6106	103(2)
H(26C)	-2007	7329	5593	103(2)
H(2A)	-2273	3810	1947	103(2)
H(2BA)	-3211	1827	2254	103(2)
H(2BB)	-1509	2205	2401	103(2)
H(2C)	-1618	2417	1016	103(2)
H(2DA)	-4641	1693	800	103(2)
H(2DB)	-3784	1991	101	103(2)
H(2EA)	-5409	3309	336	103(2)
H(2EB)	-3705	3682	501	103(2)
H(2F)	-5330	3081	1719	103(2)
H(2G)	-5121	4770	2180	103(2)
H(2HA)	-4629	6083	1376	103(2)
H(2HB)	-4270	5322	723	103(2)
H(2HC)	-3185	5382	1564	103(2)
H(2IA)	-7417	4189	1401	103(2)
H(2IB)	-6913	4636	631	103(2)
H(2IC)	-7224	5362	1317	103(2)
H(2JA)	-907	799	1521	103(2)

Table A6 continued.

H(2JB)	-1718	740	618	103(2)
H(2JC)	-2616	446	1300	103(2)

Table A7: Crystallographic data for *cis*-(S,S)-[PtCl(DMSO)(L1a)] (**1a**).

	cis-(S,S)-[PtCl(DMSO)(L1a)]
Empirical formula	$C_{14}H_{21}ClN_2O_2PtS_2$
Formula weight	543.99
Temperature	293(2) K
Wavelength	0.71073 Å
Crystal system, space group	Triclinic, $P\bar{1}$
Unit cell dimensions	a = 8.7436(4) Å α = 76.263(10)°
	b = 10.0717(5) Å β = 89.207(10)°
	c = 11.5723(6) Å γ = 68.205(10)°
Volume	916.05(8) Å^3
Z, Calculated density	2, 1.979 Mg/m^3
Absorption coefficient	8.039 mm^{-1}
F(000)	524
Crystal size	0.30 x 0.30 x 0.08 mm
Theta range for data collection	5.75 to 28.32°
Index ranges	$-11 \le h \le 11$, $-13 \le k \le 13$, $-15 \le l \le 15$
Reflections collected/unique	9904/4433 [R(int) = 0.0365]
Refinement method	Full-matrix least-squares on F^2
Data/restraints/parameters	4433/0/204
Goodness-of-fit on F^2	1.072
Final R indices [$I>2\sigma(I)$]	$R1$[a]= 0.0299, Rw[b] = 0.0725
Largest diff. Peak and hole	1.233 and –1.249 e.Å^{-3}

[a] $R = [(\Sigma\Delta F)/(\Sigma F_0)]$.

[b] $Rw = \Sigma[w(F_0^2 - F_c^2)^2]/\Sigma[w(F_0^2)^2]^{1/2}$.

Table A8: Atomic coordinates (x 10^4) and equivalent isotropic displacement parameters (Å^2 x 10^3) for *cis*-(S,S)-[PtCl(DMSO)(L1a)] (**1a**). $U_{(eq)}$ is defined as one third of the trace of the orthogonalized U_{ij} tensor.

	x	*y*	*z*	$U_{(eq)}$
Pt	2059(1)	855(1)	3640(1)	37(1)
Cl(1)	2866(2)	-686(1)	5562(1)	64(1)
S(1)	1105(1)	2795(1)	4373(1)	37(1)
O(1)	293(5)	4255(4)	3560(3)	58(1)
S(2)	1285(2)	2300(1)	1763(1)	50(1)
O(2)	2995(6)	-1026(4)	3102(3)	59(1)
N(1)	3097(4)	-246(4)	1037(3)	39(1)
N(2)	1724(5)	1826(4)	-380(3)	41(1)
C(1)	-266(7)	2569(6)	5466(5)	54(1)
C(2)	2708(7)	2846(7)	5241(6)	63(1)
C(3)	2100(5)	1195(5)	785(3)	36(1)
C(4)	3451(5)	-1200(5)	2082(4)	37(1)
C(5)	623(7)	3385(5)	-863(4)	49(1)
C(6)	-1118(7)	3575(6)	-1178(6)	61(1)
C(7)	2364(7)	959(6)	-1264(4)	48(1)
C(8)	1470(8)	-49(6)	-1373(5)	57(1)
C(11)	4480(5)	-2764(4)	2087(4)	36(1)
C(12)	4755(6)	-3880(5)	3131(5)	46(1)
C(13)	5687(7)	-5337(6)	3139(6)	62(1)
C(14)	6347(7)	-5691(6)	2113(7)	70(2)
C(15)	6065(7)	-4591(7)	1076(6)	67(2)
C(16)	5147(6)	-3126(6)	1049(5)	50(1)

Table A9: Bond lengths (Å) and angles (°) for *cis*-(S,S)-[PtCl(DMSO)(L1a)] (**1a**).

Pt-O(2)	2.010(3)
Pt-S(1)	2.1885(10)
Pt-S(2)	2.2586(11)
Pt-Cl(1)	2.3337(11)
S(1)-C(2)	1.759(5)
S(1)-O(1)	1.462(3)
S(1)-C(1)	1.764(5)
S(2)-C(3)	1.735(4)
O(2)-C(4)	1.271(5)
N(1)-C(4)	1.312(6)
N(1)-C(3)	1.348(5)
N(2)-C(3)	1.335(5)
N(2)-C(7)	1.472(6)
N(2)-C(5)	1.477(6)
C(4)-C(11)	1.495(5)
C(5)-C(6)	1.501(8)
C(7)-C(8)	1.501(8)
C(11)-C(12)	1.394(7)
C(11)-C(16)	1.396(6)
C(12)-C(13)	1.386(7)
C(13)-C(14)	1.379(9)
C(14)-C(15)	1.379(10)
C(15)-C(16)	1.386(7)
O(2)-Pt-S(1)	175.38(10)
O(2)-Pt-S(2)	93.75(10)
S(1)-Pt-S(2)	90.87(4)
O(2)-Pt-Cl(1)	84.94(10)
S(1)-Pt-Cl(1)	90.44(4)
S(2)-Pt-Cl(1)	178.64(4)

Table A9 continued.

O(1)-S(1)-C(2)	108.2(3)
O(1)-S(1)-C(1)	107.4(2)
C(2)-S(1)-C(1)	101.0(3)
O(1)-S(1)-Pt	119.13(15)
C(2)-S(1)-Pt	109.2(2)
C(1)-S(1)-Pt	110.36(18)
C(3)-S(2)-Pt	107.71(14)
C(4)-O(2)-Pt	128.7(3)
C(4)-N(1)-C(3)	127.3(4)
C(3)-N(2)-C(7)	120.6(4)
C(3)-N(2)-C(5)	123.3(4)
C(7)-N(2)-C(5)	116.1(3)
N(2)-C(3)-N(1)	113.8(4)
N(2)-C(3)-S(2)	117.4(3)
N(1)-C(3)-S(2)	128.8(3)
O(2)-C(4)-N(1)	130.3(4)
O(2)-C(4)-C(11)	113.7(4)
N(1)-C(4)-C(11)	116.0(4)
N(2)-C(5)-C(6)	113.1(4)
N(2)-C(7)-C(8)	113.8(4)
C(12)-C(11)-C(16)	119.4(4)
C(12)-C(11)-C(4)	119.9(4)
C(16)-C(11)-C(4)	120.7(4)
C(13)-C(12)-C(11)	120.3(5)
C(14)-C(13)-C(12)	120.1(6)
C(13)-C(14)-C(15)	119.7(5)
C(14)-C(15)-C(16)	121.2(5)
C(15)-C(16)-C(11)	119.3(5)

Symmetry transformations used to generate equivalent atoms

Table A10: Anisotropic displacement parameters ($Å^2$ x 10^3) for *cis*-(S,S)-[PtCl(DMSO)(L1a)] (**1a**). The anisotropic displacement factor exponent takes the form: $-2\pi^2 [h^2 a^{*2} U11 + ... + 2 h k a^* b^* U12]$.

	*U*11	*U*22	*U*33	*U*23	*U*13	*U*12
Pt	55(1)	27(1)	25(1)	-7(1)	3(1)	-11(1)
Cl(1)	101(1)	37(1)	29(1)	-1(1)	4(1)	-5(1)
S(1)	54(1)	30(1)	28(1)	-9(1)	3(1)	-14(1)
O(1)	94(3)	31(2)	37(2)	-5(1)	0(2)	-12(2)
S(2)	80(1)	31(1)	28(1)	-7(1)	-1(1)	-9(1)
O(2)	104(3)	30(2)	33(2)	-11(1)	17(2)	-13(2)
N(1)	46(2)	38(2)	29(2)	-9(1)	1(1)	-11(2)
N(2)	57(2)	36(2)	28(2)	-5(1)	1(2)	-16(2)
C(1)	64(3)	47(3)	45(3)	-11(2)	14(2)	-15(2)
C(2)	66(3)	72(4)	67(4)	-32(3)	4(3)	-35(3)
C(3)	47(2)	36(2)	26(2)	-9(2)	3(2)	-17(2)
C(4)	44(2)	34(2)	34(2)	-14(2)	0(2)	-11(2)
C(5)	74(3)	36(2)	29(2)	0(2)	-6(2)	-19(2)
C(6)	55(3)	52(3)	68(3)	-8(3)	10(2)	-13(2)
C(7)	66(3)	52(3)	26(2)	-11(2)	10(2)	-24(2)
C(8)	89(4)	55(3)	40(3)	-23(2)	10(2)	-34(3)
C(11)	37(2)	34(2)	38(2)	-14(2)	-2(2)	-11(2)
C(12)	52(2)	33(2)	47(2)	-7(2)	-4(2)	-9(2)
C(13)	66(3)	37(2)	68(4)	-9(2)	-12(3)	-6(2)
C(14)	60(3)	43(3)	102(5)	-31(3)	0(3)	-4(2)
C(15)	61(3)	64(4)	84(4)	-45(3)	20(3)	-15(3)
C(16)	51(2)	47(3)	53(3)	-23(2)	11(2)	-12(2)

Table A11: Hydrogen coordinates (x 10^4) and isotropic displacement parameters (Å^2 x 10^3) for *cis*-(S,S)-[PtCl(DMSO)(L1a)] (**1a**).

	x	*y*	*z*	$U_{(eq)}$
H(1A)	-513	3332	5883	72(4)
H(1B)	237	1622	6020	72(4)
H(1C)	-1269	2631	5087	72(4)
H(2A)	3517	3039	4732	72(4)
H(2B)	3218	1913	5813	72(4)
H(2C)	2265	3614	5652	72(4)
H(5A)	1062	3800	-1571	72(4)
H(5B)	613	3934	-277	72(4)
H(6A)	-1124	3065	-1780	72(4)
H(6B)	-1779	4606	-1474	72(4)
H(6C)	-1565	3174	-479	72(4)
H(7A)	3528	363	-1045	72(4)
H(7B)	2273	1633	-2038	72(4)
H(8A)	1684	-809	-646	72(4)
H(8B)	1858	-491	-2024	72(4)
H(8C)	303	517	-1518	72(4)
H(12)	4311	-3646	3825	72(4)
H(13)	5868	-6076	3839	72(4)
H(14)	6979	-6667	2119	72(4)
H(15)	6499	-4836	382	72(4)
H(16)	4977	-2393	346	72(4)

Table A12: Crystallographic data for *cis*-(S,S)-[PtCl(L1a)(MPSO)] (**4**).

	cis-[PtCl(L1a)(MPSO)]
Empirical formula	$C_{19}H_{23}ClN_2O_2PtS_2$
Formula weight	606.05
Temperature	293(2) K
Wavelength	0.71073 Å
Crystal system, space group	Triclinic, $P\bar{1}$
Unit cell dimensions	a = 8.612(2) Å α = 115.11(2)°
	b = 11.776(2) Å β = 86.44(2)°
	c = 13.374(3) Å γ = 66.25(2)°
Volume	1078.8(4) Å^3
Z, Calculated density	2, 1.866 Mg/m^3
Absorption coefficient	6.837 mm^{-1}
F(000)	588
Crystal size	0.42 x 0.34 x 0.30 mm
Theta range for data collection	1.75 to 25.05°
Index ranges	$0 \le h \le 10$, $-12 \le k \le 14$, $-15 \le l \le 15$
Reflections collected/unique	3450/2918 [R(int) = 0.0327]
Refinement method	Full-matrix least-squares on F^2
Goodness-of-fit on F^2	1.120
Final R indices [$I>2\sigma(I)$]	R^a = 0.0613, Rw^b = 0.1535
Largest diff. peak and hole	3.141 and –3.613 e.Å^{-3}

[a] $R = [(\Sigma\Delta F)/(\Sigma F_0)]$.

[b] $Rw = \Sigma[w(F_0^2 - F_c^2)^2]/\Sigma[w(F_0^2)^2]^{1/2}$.

Table A13: Atomic coordinates (x 10^4) and equivalent isotropic displacement parameters (Å^2 x 10^3) for *cis*-(S,S)-[PtCl(L1a)(MPSO)] (**4**). $U_{(eq)}$ is defined as one third of the trace of the orthogonalized U_{ij} tensor.

	x	*y*	*z*	$U_{(eq)}$
Pt	2323(1)	2536(1)	979(1)	38(1)
Cl(1)	2395(6)	364(4)	-183(3)	53(1)
S(1)	2312(6)	4631(4)	2025(3)	54(1)
S(2)	2209(5)	2291(4)	2514(3)	41(1)
O(1)	2496(14)	2657(10)	-479(8)	45(2)
O(2)	2696(16)	3163(12)	3458(8)	59(3)
N(1)	2019(18)	4947(14)	79(11)	54(3)
N(2)	1748(24)	6806(14)	1697(13)	74(5)
C(1)	2022(22)	5457(17)	1191(14)	55(4)
C(2)	2321(18)	3687(15)	-627(13)	43(3)
C(3)	1471(27)	7616(21)	1072(19)	73(5)
C(4)	3261(32)	7152(26)	291(24)	96(8)
C(5)	1249(49)	7890(57)	3183(40)	188(23)
C(6)	2546(59)	7868(59)	3240(40)	217(25)
C(7)	3540(26)	491(18)	2146(17)	69(5)
C(11)	2509(18)	3310(15)	-1876(12)	43(3)
C(12)	2785(20)	2015(21)	-2688(16)	64(5)
C(13)	3111(24)	1642(22)	-3826(14)	68(5)
C(14)	3150(26)	2569(28)	-4180(17)	86(7)
C(15)	2825(28)	3913(29)	-3350(19)	91(7)
C(16)	2519(23)	4295(19)	-2203(15)	64(5)
C(21)	102(19)	2568(14)	3089(11)	42(3)
C(22)	-655(22)	3383(18)	4274(12)	55(4)
C(23)	-2290(23)	3644(20)	4751(13)	61(4)
C(24)	-3225(25)	3118(21)	4056(15)	67(5)
C(25)	-2511(26)	2309(21)	2884(17)	78(6)
C(26)	-864(23)	2059(20)	2407(14)	65(5)

Table A14: Bond lengths (Å) and angles (°) for *cis*-(S,S)-[PtCl(L1a)(MPSO)] (**4**).

Pt-O(1)	2.016(9)
Pt-S(2)	2.192(3)
Pt-S(1)	2.257(4)
Pt-Cl(1)	2.334(3)
S(1)-C(1)	1.736(14)
S(2)-O(2)	1.462(11)
S(2)-C(21)	1.77(2)
S(2)-C(7)	1.77(2)
O(1)-C(2)	1.26(2)
N(1)-C(2)	1.28(2)
N(1)-C(1)	1.35(2)
N(2)-C(1)	1.34(2)
N(2)-C(3)	1.48(2)
N(2)-C(5)	1.75(5)
C(2)-C(11)	1.51(2)
C(3)-C(4)	1.55(3)
C(5)-C(6)	1.11(4)
C(11)-C(12)	1.35(2)
C(11)-C(16)	1.41(2)
C(12)-C(13)	1.37(2)
C(13)-C(14)	1.37(3)
C(14)-C(15)	1.39(3)
C(15)-C(16)	1.38(3)
C(21)-C(26)	1.38(2)
C(21)-C(22)	1.39(2)
C(22)-C(23)	1.36(2)
C(23)-C(24)	1.38(3)
C(24)-C(25)	1.37(2)
C(25)-C(26)	1.38(2)
O(1)-Pt-S(2)	177.2(3)

Table A14 continued.

O(1)-Pt-S(1)	93.3(3)
S(2)-Pt-S(1)	89.09(13)
O(1)-Pt-Cl(1)	84.1(3)
S(2)-Pt-Cl(1)	93.48(13)
S(1)-Pt-Cl(1)	177.24(13)
C(1)-S(1)-Pt	107.2(6)
O(2)-S(2)-C(21)	107.6(6)
O(2)-S(2)-C(7)	107.4(8)
C(21)-S(2)-C(7)	100.7(8)
O(2)-S(2)-Pt	117.4(4)
C(21)-S(2)-Pt	111.7(4)
C(7)-S(2)-Pt	110.7(6)
C(2)-O(1)-Pt	129.9(9)
C(2)-N(1)-C(1)	126.8(13)
C(1)-N(2)-C(3)	122(2)
C(1)-N(2)-C(5)	113(2)
C(3)-N(2)-C(5)	113(2)
N(2)-C(1)-N(1)	113.0(13)
N(2)-C(1)-S(1)	117.5(13)
O(1)-C(2)-N(1)	131.6(14)
N(1)-C(1)-S(1)	129.5(12)
O(1)-C(2)-C(11)	111.8(13)
N(1)-C(2)-C(11)	116.6(12)
N(2)-C(3)-C(4)	110(2)
C(6)-C(5)-N(2)	100(4)
C(12)-C(11)-C(16)	120(2)
C(12)-C(11)-C(2)	121.4(13)
C(16)-C(11)-C(2)	118.9(14)
C(11)-C(12)-C(13)	121(2)
C(12)-C(13)-C(14)	121(2)

Table A14 continued.

C(13)-C(14)-C(15)	118(2)
C(16)-C(15)-C(14)	121(2)
C(15)-C(16)-C(11)	119(2)
C(26)-C(21)-C(22)	118.3(14)
C(26)-C(21)-S(2)	122.8(11)
C(22)-C(21)-S(2)	118.8(11)
C(23)-C(22)-C(21)	121(2)
C(22)-C(23)-C(24)	120(2)
C(25)-C(24)-C(23)	121(2)
C(24)-C(25)-C(26)	119(2)
C(25)-C(26)-C(21)	121(2)

Symmetry transformations used to generate equivalent atoms.

Table A15: Anisotropic displacement parameters ($Å^2$ x 10^3) for *cis*-(S,S)-[PtCl(L1a)(MPSO)] (**4**). The anisotropic displacement factor exponent takes the form: $-2\pi^2 [h^2 a^{*2} U11 + ... + 2 h k a^* b^* U12]$.

	*U*11	*U*22	*U*33	*U*23	*U*13	*U*12
Pt	56(1)	37(1)	23(1)	13(1)	-9(1)	-27(1)
Cl(1)	87(3)	40(2)	32(2)	12(2)	-10(2)	-37(2)
S(1)	92(3)	51(2)	35(2)	20(2)	-20(2)	-48(2)
S(2)	59(2)	45(2)	28(2)	19(2)	-14(2)	-31(2)
O(1)	74(7)	46(5)	28(5)	24(4)	-18(4)	-33(5)
O(2)	93(8)	72(7)	26(5)	21(5)	-22(5)	-54(7)
N(1)	77(9)	55(8)	40(7)	26(6)	-12(6)	-40(7)
N(2)	124(14)	41(7)	51(9)	8(7)	-11(9)	-52(9)
C(1)	74(11)	61(10)	45(9)	33(8)	-12(8)	-39(9)
C(2)	45(8)	47(8)	50(9)	36(8)	-13(6)	-22(7)
C(3)	82(13)	62(11)	94(15)	48(11)	-29(11)	-42(10)
C(4)	117(18)	102(17)	141(23)	95(18)	-53(17)	-73(15)
C(5)	117(26)	335(64)	267(57)	234(55)	-85(32)	-146(36)
C(6)	209(49)	387(79)	203(49)	216(57)	-96(40)	-188(54)
C(7)	88(13)	55(10)	66(12)	36(9)	-16(10)	-31(10)
C(11)	47(8)	47(8)	35(7)	22(7)	-11(6)	-21(7)
C(12)	43(9)	89(13)	58(11)	40(10)	-16(8)	-26(9)
C(13)	74(12)	89(13)	26(8)	25(9)	-14(8)	-30(10)
C(14)	63(12)	136(21)	45(11)	49(14)	-18(9)	-27(13)
C(15)	90(15)	122(19)	60(13)	66(15)	-4(11)	-29(14)
C(16)	75(11)	55(9)	54(10)	38(9)	-10(9)	-13(8)
C(21)	64(9)	38(7)	27(7)	15(6)	-12(6)	-29(7)
C(22)	73(11)	67(10)	21(7)	16(7)	-7(7)	-35(9)
C(23)	77(11)	81(12)	29(8)	19(8)	-3(8)	-51(10)
C(24)	65(11)	76(12)	45(10)	25(9)	1(8)	-28(10)
C(25)	80(13)	81(13)	64(12)	13(10)	-11(10)	-56(12)
C(26)	62(10)	81(12)	34(8)	12(8)	-5(7)	-37(9)

Table A16: Hydrogen coordinates (x 10^4) and isotropic displacement parameters (Å^2 x 10^3) for *cis*-(S,S)-[PtCl(L1)(MPSO)] (**4**).

	x	*y*	*z*	$U_{(eq)}$
H(3A)	920(27)	8627(21)	1620(19)	95(15)
H(3B)	686(27)	7449(21)	606(19)	95(15)
H(4A)	3059(35)	7660(110)	-131(90)	95(15)
H(4B)	3817(88)	6147(39)	-238(76)	95(15)
H(4C)	4015(70)	7361(126)	758(25)	95(15)
H(5A)	310(49)	8848(57)	3450(40)	95(15)
H(5B)	930(49)	7488(57)	3610(40)	95(15)
H(6A)	2573(89)	8227(145)	4027(41)	95(15)
H(6B)	8451(127)	8451(127)	2956(119)	95(15)
H(6C)	3482(60)	6906(61)	2785(94)	95(15)
H(7A)	3027(96)	-74(29)	1706(96)	95(15)
H(7B)	3610(143)	427(25)	2835(17)	95(15)
H(7C)	4706(56)	145(46)	1697(97)	95(15)
H(12)	2752(20)	1372(21)	-2469(16)	4706(56)
H(13)	3311(24)	742(22)	-4371(14)	95(15)
H(14)	3388(26)	2304(28)	-4956(17)	3311(24)
H(15)	4564(29)	4564(29)	-3573(19)	95(15)
H(16)	2320(23)	5192(19)	-1653(15)	95(15)
H(22)	-39(22)	3755(18)	4746(12)	95(15)
H(23)	-2775(23)	4176(20)	5545(13)	95(15)
H(24)	-4349(25)	3314(21)	4385(15)	95(15)
H(25)	-3132(26)	1936(21)	2418(17)	95(15)
H(26)	-392(23)	1537(20)	1612(14)	95(15)

Table A17: Crystallographic data for *cis*-(S,S)-[PtCl(DMSO)(L7)] (**12**).

Empirical formula	$C_{18}H_{35}ClN_2O_4PtS_2$
Formula weight	638.14
Temperature	293(2) K
Wavelength	0.71073 Å
Crystal system, space group	Orthorhombic, $P2_12_12_1$
Unit cell dimensions	a = 9.8964(6) Å α = 90°
	b = 13.2721(8) Å β = 90°
	c = 18.0016(11) Å γ = 90°
Volume	2364.4(2) Å^3
Z, Calculated density	4, 1.793 Mg/m^3
Absorption coefficient	6.249 mm^{-1}
F(000)	1264
Crystal size	0.40 × 0.20 × 0.08 mm
Theta range for data collection	1.91 to 28.30°
Index ranges	$-13 \le h \le 13$, $-10 \le k \le 17$, $-23 \le l \le 23$
Reflections collected/unique	15355/5462 [R(int) = 0.0369]
Refinement method	Full-matrix least-squares on F^2
Data/restraints/parameters	5462/0/259
Goodness-of-fit on F^2	1.040
Final R indices [$I>2\sigma(I)$]	R^a = 0.0296, Rw^b = 0.0535
Absolute structure parameter	0.013(6)
Largest diff. peak and hole	0.499 and –0.882 e.Å^{-3}

[a] $R = [(\Sigma\Delta F)/(\Sigma F_0)]$.

[b] $Rw = \Sigma[w(F_0^2 - F_c^2)^2]/\Sigma[w(F_0^2)^2]^{1/2}$.

Table A18: Bond lengths (Å) and angles (°) for *cis*-(S,S)-[PtCl(DMSO)(L7)] (**12**).

Pt(1)-O(11)	2.018(3)	O(2)-S(2)-C(22)	108.5(3)
Pt(1)-S(2)	2.1839(12)	C(21)-S(2)-C(22)	101.1(3)
Pt(1)-S(1)	2.2595(13)	O(2)-S(2)-Pt(1)	117.16(14)
Pt(1)-Cl(1)	2.3276(14)	C(21)-S(2)-Pt(1)	111.26(19)
S(1)-C(11)	1.734(5)	C(22)-S(2)-Pt(1)	109.1(2)
S(2)-O(2)	1.457(4)	C(12)-O(11)-Pt(1)	130.7(3)
S(2)-C(21)	1.752(5)	C(12)-O(12)-C(1A)	120.1(3)
S(2)-C(22)	1.775(5)	C(12)-N(11)-C(11)	125.0(4)
O(11)-C(12)	1.254(5)	C(11)-N(12)-C(13)	125.8(4)
O(12)-C(12)	1.329(5)	C(11)-N(12)-C(16)	122.5(4)
O(12)-C(1A)	1.464(5)	C(13)-N(12)-C(16)	111.2(4)
N(11)-C(12)	1.309(5)	N(12)-C(11)-N(11)	114.8(4)
N(11)-C(11)	1.345(6)	N(12)-C(11)-S(1)	115.3(4)
N(12)-C(11)	1.343(6)	N(11)-C(11)-S(1)	129.8(4)
N(12)-C(13)	1.465(6)	O(11)-C(12)-N(11)	132.6(4)
N(12)-C(16)	1.474(6)	O(11)-C(12)-O(12)	115.7(4)
C(13)-C(14)	1.511(8)	N(11)-C(12)-O(12)	111.7(4)
C(14)-O(13)	1.407(7)	N(12)-C(13)-C(14)	108.4(4)
O(13)-C(15)	1.418(7)	O(13)-C(14)-C(13)	112.5(5)
C(15)-C(16)	1.517(8)	C(14)-O(13)-C(15)	112.3(4)
C(1A)-C(1F)	1.519(6)	O(13)-C(15)-C(16)	111.3(5)
C(1A)-C(1B)	1.522(7)	N(12)-C(16)-C(15)	108.9(5)
C(1B)-C(1C)	1.538(7)	O(12)-C(1A)-C(1F)	108.1(4)
C(1C)-C(1D)	1.506(7)	O(12)-C(1A)-C(1B)	106.9(4)
C(1C)-C(1J)	1.508(8)	C(1F)-C(1A)-C(1B)	112.7(4)
C(1D)-C(1E)	1.515(7)	C(1A)-C(1B)-C(1C)	111.4(4)
C(1E)-C(1F)	1.538(7)	C(1D)-C(1C)-C(1J)	112.9(5)
C(1F)-C(1G)	1.542(7)	C(1D)-C(1C)-C(1B)	108.9(4)
C(1G)-C(1H)	1.516(8)	C(1J)-C(1C)-C(1B)	110.9(5)
C(1G)-C(1I)	1.520(8)	C(1C)-C(1D)-C(1E)	112.9(4)

Table A18 continued.

O(11)-Pt(1)-S(2)	176.40(11)	C(1D)-C(1E)-C(1F)	112.7(4)
O(11)-Pt(1)-S(1)	92.66(10)	C(1A)-C(1F)-C(1E)	107.6(4)
S(2)-Pt(1)-S(1)	90.71(4)	C(1A)-C(1F)-C(1G)	113.1(4)
O(11)-Pt(1)-Cl(1)	86.00(10)	C(1E)-C(1F)-C(1G)	113.9(4)
S(2)-Pt(1)-Cl(1)	90.66(5)	C(1H)-C(1G)-C(1I)	112.0(5)
S(1)-Pt(1)-Cl(1)	178.15(6)	C(1H)-C(1G)-C(1F)	111.3(5)
C(11)-S(1)-Pt(1)	108.73(18)	C(1I)-C(1G)-C(1F)	113.5(5)
O(2)-S(2)-C(21)	108.4(3)		

Symmetry transformations used to generate equivalent atoms.

Table A19: Atomic coordinates (x 10^4) and equivalent isotropic displacement parameters (Å^2 x 10^3) for *cis*-(S,S)-[PtCl(DMSO)(L7)] (**12**). $U_{(eq)}$ is defined as one third of the trace of the orthogonalized U_{ij} tensor.

	x	*y*	*z*	$U_{(eq)}$
Pt(1)	8451(1)	1170(1)	1008(1)	36(1)
Cl(1)	7636(2)	-274(1)	426(1)	75(1)
S(1)	9292(1)	2540(1)	1593(1)	44(1)
S(2)	6391(1)	1709(1)	1184(1)	37(1)
O(11)	10310(3)	616(3)	794(2)	61(1)
O(12)	12491(3)	473(2)	627(2)	41(1)
O(2)	6231(3)	2665(3)	1572(2)	57(1)
N(11)	11861(4)	1789(3)	1268(2)	35(1)
N(12)	11677(4)	3198(3)	1970(3)	49(1)
C(11)	11040(5)	2459(4)	1600(3)	35(1)
C(12)	11458(4)	982(3)	913(3)	35(1)
C(13)	11030(5)	4065(4)	2327(3)	56(2)
C(14)	11484(7)	5011(4)	1932(4)	66(2)
O(13)	12899(4)	5113(3)	1921(3)	68(1)
C(15)	13545(6)	4273(5)	1587(4)	70(2)
C(16)	13161(5)	3299(4)	1974(4)	58(2)
C(21)	5402(5)	801(4)	1635(3)	52(1)
C(22)	5557(6)	1795(5)	314(3)	63(2)
C(1A)	12245(5)	-362(3)	114(3)	35(1)
C(1B)	12428(5)	51(4)	-668(3)	42(1)
C(1C)	12266(5)	-781(4)	-1256(3)	46(1)
C(1D)	13234(6)	-1624(4)	-1081(3)	54(1)
C(1E)	13074(6)	-2024(4)	-298(3)	49(1)
C(1F)	13238(4)	-1200(3)	295(2)	37(1)
C(1G)	13108(5)	-1588(4)	1100(3)	53(1)
C(1H)	14292(7)	-2255(5)	1309(4)	80(2)
C(1I)	11760(7)	-2093(5)	1259(4)	84(2)

Table A19 continued.

C(1J)	12453(6)	-361(5)	-2028(3)	71(2)

Table A20: Anisotropic displacement parameters ($Å^2$ x 10^3) for *cis*-(S,S)-[PtCl(DMSO)(L7)] (**12**). The anisotropic displacement factor exponent takes the form: $-2\pi^2 [h^2 a^{*2} U11 + ... + 2 h k a^* b^* U12]$.

	*U*11	*U*22	*U*33	*U*23	*U*13	*U*12
Pt(1)	28(1)	33(1)	48(1)	-7(1)	6(1)	-2(1)
Cl(1)	53(1)	53(1)	120(2)	-41(1)	6(1)	-11(1)
S(1)	30(1)	41(1)	61(1)	-19(1)	4(1)	1(1)
S(2)	28(1)	38(1)	44(1)	2(1)	2(1)	0(1)
O(11)	27(2)	47(2)	109(4)	-34(2)	14(2)	-1(2)
O(12)	26(2)	40(2)	56(2)	-18(2)	-2(2)	4(2)
O(2)	32(2)	47(2)	92(3)	-20(2)	7(2)	3(2)
N(11)	29(2)	34(2)	41(2)	-5(2)	-2(2)	3(2)
N(12)	35(2)	43(2)	71(3)	-22(2)	-2(2)	3(2)
C(11)	39(3)	34(3)	34(3)	1(2)	-2(2)	2(2)
C(12)	29(2)	31(2)	43(3)	-3(2)	2(2)	4(2)
C(13)	44(3)	48(4)	76(4)	-30(3)	2(3)	6(2)
C(14)	62(4)	42(3)	93(5)	-18(3)	-17(4)	11(3)
O(13)	57(2)	49(2)	97(3)	-16(2)	-9(2)	-5(2)
C(15)	42(3)	75(4)	93(5)	-19(4)	7(4)	-6(3)
C(16)	30(3)	53(4)	93(5)	-21(3)	-10(3)	4(2)
C(21)	37(3)	56(3)	62(4)	17(3)	7(3)	-9(3)
C(22)	55(4)	83(5)	51(4)	17(3)	-10(3)	-1(3)
C(1A)	29(2)	33(3)	43(3)	-17(2)	2(2)	0(2)
C(1B)	39(3)	41(3)	46(3)	-4(2)	-2(2)	1(2)
C(1C)	43(3)	51(3)	4(2)	4(2)	4(2)	-6(2)
C(1D)	58(3)	53(3)	-20(3)	-20(3)	10(3)	11(3)
C(1E)	59(4)	31(3)	58(4)	-8(2)	2(3)	7(2)
C(1F)	32(2)	32(2)	47(3)	-3(2)	-1(2)	-1(2)
C(1G)	58(3)	44(3)	58(4)	3(3)	1(3)	3(2)
C(1H)	84(5)	79(5)	76(5)	18(4)	18(4)	18(4)
C(1I)	74(5)	97(5)	80(5)	31(4)	18(4)	-10(4)

Table A20 continued.

C(1J)	61(4)	94(5)	57(4)	-13(4)	-8(3)	-8(4)

Table A21: Hydrogen coordinates (x 10^4) and isotropic displacement parameters (Å^2 x 10^3) for *cis*-(S,S)-[PtCl(DMSO)(L7)] (**12**).

	x	*y*	*z*	$U_{(eq)}$
H(13A)	11284	4095	2847	72(3)
H(13B)	10055	4001	2297	72(3)
H(14A)	11150	4999	1426	72(3)
H(14B)	11093	5592	2178	72(3)
H(15A)	14517	4362	1612	72(3)
H(15B)	13289	4235	1068	72(3)
H(16A)	13568	2731	1718	72(3)
H(16B)	13491	3305	2481	72(3)
H(21A)	5745	693	2127	72(3)
H(21B)	5436	180	1361	72(3)
H(21C)	4484	1031	1663	72(3)
H(22A)	4627	391	391	72(3)
H(22B)	5607	1157	64	72(3)
H(22C)	5986	2301	15	72(3)
H(1A)	11318	-609	176	72(3)
H(1B1)	13320	349	-712	72(3)
H(1B2)	11765	576	-757	72(3)
H(1C)	11345	-1047	-1220	72(3)
H(1D1)	14152	-1383	-1146	72(3)
H(1D2)	13089	-2170	-1430	72(3)
H(1E1)	13742	-2546	-213	72(3)
H(1E2)	12187	-2327	-248	72(3)
H(1F)	14149	-920	241	72(3)
H(1G)	13156	-995	1423	72(3)
H(1H1)	14267	-2391	1832	72(3)
H(1H2)	15122	-1918	1188	72(3)
H(1H3)	14238	-2877	1039	72(3)
H(1I1)	11704	-2715	989	72(3)

Table A21 continued.

H(1I2)	11037	-1656	1108	72(3)
H(1I3)	11686	-2227	1782	72(3)
H(1J1)	11882	217	-2092	72(3)
H(1J2)	12217	-866	-2387	72(3)
H(1J3)	13380	-168	-2096	72(3)

Table A22: Crystallographic data for *cis*-[Pt(L1a)$_2$] (**7**).

Empirical formula	$C_{24}H_{30}N_4O_2PtS_2$
Formula weight	665.73
Temperature	293(2) K
Wavelength	0.71073 Å
Crystal system, space group	monoclinic, $P2_1/n$
Unit cell dimensions	a = 9.926(2) Å α = 90°
	b = 12.265(3) Å β = 91.00(2)°
	c = 21.168(5) Å γ = 90°
Volume	2576.7(10) Å^3
Z, Calculated density	4, 1.700 Mg/m^3
Absorption coefficient	5.635 mm^{-1}
F(000)	1287
Crystal size	0.35 × 0.32 × 0.21 mm
Theta range for data collection	1.92 to 25.07°
Index ranges	$-10 \le h \le 9$, $0 \le k \le 14$, $0 \le l \le 24$
Reflections collected/unique	3803/3454 [R(int) = 0.0215]
Refinement method	Full-matrix least-squares on F^2
Data/restraints/parameters	3454/0/303
Goodness-of-fit on F^2	1.140
Final R indices [$I>2\sigma(I)$]	R^a = 0.0358, Rw^b = 0.0926
Largest diff. peak and hole	0.750 and -1.664 e.Å^{-3}

[a] $R = [(\Sigma\Delta F)/(\Sigma F_0)]$.

[b] $Rw = \Sigma[w(F_0^2 - F_c^2)^2]/\Sigma[w(F_0^2)^2]^{1/2}$.

Table A23: Bond lengths (Å) and angles (°) for *cis*-[Pt(L1a)$_2$] (**7**).

Bond		Angle	
Pt(1)-O(1)	2.018(5)	C(4)-S(2)-Pt(1)	108.1(3)
Pt(1)-O(2)	2.024(6)	C(1)-O(1)-Pt(1)	128.7(5)
Pt(1)-S(1)	2.232(2)	C(3)-O(2)-Pt(1)	128.2(5)
Pt(1)-S(2)	2.233(2)	C(1)-N(1)-C(2)	127.4(6)
S(1)-C(2)	1.731(7)	C(2)-N(2)-C(23)	120.9(6)
S(2)-C(4)	1.723(7)	C(2)-N(2)-C(21)	123.3(6)
O(1)-C(1)	1.271(8)	C(23)-N(2)-C(21)	115.8(6)
O(2)-C(3)	1.262(8)	C(3)-N(3)-C(4)	125.5(6)
N(1)-C(1)	1.313(9)	C(4)-N(4)-C(43)	123.3(7)
N(1)-C(2)	1.341(9)	C(4)-N(4)-C(41)	122.3(7)
N(2)-C(2)	1.349(9)	C(43)-N(4)-C(41)	114.4(6)
N(2)-C(23)	1.467(9)	O(1)-C(1)-N(1)	130.7(7)
N(2)-C(21)	1.471(9)	O(1)-C(1)-C(11)	115.2(6)
N(3)-C(3)	1.319(9)	N(1)-C(1)-C(11)	114.0(6)
N(3)-C(4)	1.350(9)	N(1)-C(2)-N(2)	114.8(6)
N(4)-C(4)	1.336(9)	N(1)-C(2)-S(1)	128.8(6)
N(4)-C(43)	1.476(11)	N(2)-C(2)-S(1)	116.3(5)
N(4)-C(41)	1.480(9)	O(2)-C(3)-N(3)	131.9(7)
C(1)-C(11)	1.491(10)	O(2)-C(3)-C(31)	112.7(7)
C(3)-C(31)	1.498(11)	N(3)-C(3)-C(31)	115.3(6)
C(11)-C(12)	1.369(10)	N(4)-C(4)-N(3)	114.2(6)
C(11)-C(16)	1.383(11)	N(4)-C(4)-S(2)	116.6(6)
C(12)-C(13)	1.375(11)	N(3)-C(4)-S(2)	129.2(5)
C(13)-C(14)	1.378(13)	C(12)-C(11)-C(16)	118.4(7)
C(14)-C(15)	1.347(13)	C(12)-C(11)-C(1)	121.7(7)
C(15)-C(16)	1.372(12)	C(16)-C(11)-C(1)	119.9(7)
C(21)-C(22)	1.487(11)	C(11)-C(12)-C(13)	120.8(8)
C(23)-C(24)	1.491(12)	C(12)-C(13)-C(14)	120.1(9)
C(31)-C(32)	1.386(11)	C(15)-C(14)-C(13)	119.2(9)

Table A23 continued.

C(31)-C(36)	1.399(11)	C(14)-C(15)-C(16)	121.2(9)
C(32)-C(33)	1.392(12)	C(15)-C(16)-C(11)	120.2(8)
C(33)-C(34)	1.368(14)	N(2)-C(21)-C(22)	112.8(7)
C(34)-C(35)	1.380(14)	N(2)-C(23)-C(24)	111.9(6)
C(35)-C(36)	1.369(12)	C(32)-C(31)-C(36)	118.1(8)
C(41)-C(42)	1.499(11)	C(32)-C(31)-C(3)	121.8(7)
C(43)-C(44)	1.503(13)	C(36)-C(31)-C(3)	120.1(7)
		C(31)-C(32)-C(33)	121.3(9)
		C(34)-C(33)-C(32)	118.7(9)
		C(33)-C(34)-C(35)	121.2(9)
		C(36)-C(35)-C(34)	119.8(9)
		C(35)-C(36)-C(31)	120.7(8)
		N(4)-C(41)-C(42)	111.7(7)
		N(4)-C(43)-C(44)	111.8(8)
		O(1)-Pt(1)-O(2)	82.7(2)
		O(1)-Pt(1)-S(1)	94.8(2)
		O(2)-Pt(1)-S(1)	177.5(2)
		O(1)-Pt(1)-S(2)	177.1(2)
		O(2)-Pt(1)-S(2)	94.4(2)
		S(1)-Pt(1)-S(2)	88.10(7)
		C(2)-S(1)-Pt(1)	107.9(3)

Symmetry transformations used to generate equivalent atoms.

Table A24: Atomic coordinates (x 10^4) and equivalent isotropic displacement parameters (Å^2 x 10^3) for *cis*-[Pt(L1a)$_2$] (**7**). $U_{(eq)}$ is defined as one third of the trace of the orthogonalized U_{ij} tensor.

	x	*y*	*z*	$U_{(eq)}$
Pt(1)	5933(1)	4824(1)	3911(1)	39(1)
S(1)	7426(2)	4795(2)	4711(1)	53(1)
S(2)	7063(2)	6234(2)	3514(1)	61(1)
O(1)	4844(6)	3558(4)	4233(2)	54(1)
O(2)	4533(6)	4799(4)	3204(3)	58(2)
N(1)	6003(6)	3014(5)	5157(3)	40(1)
N(2)	8019(6)	3413(5)	5621(3)	43(2)
N(3)	5127(6)	6270(5)	2549(3)	40(1)
N(4)	7025(6)	7254(5)	2431(3)	44(1)
C(1)	4999(8)	3028(5)	4745(3)	39(2)
C(2)	7093(8)	3661(6)	5169(3)	40(2)
C(3)	4355(8)	5485(6)	2766(3)	39(2)
C(4)	6339(8)	6564(5)	2793(3)	40(2)
C(11)	3899(7)	2242(6)	4889(3)	39(2)
C(12)	4118(9)	1352(7)	5266(4)	55(2)
C(13)	3092(10)	635(8)	5391(4)	65(2)
C(14)	1815(10)	822(8)	5149(5)	66(3)
C(15)	1595(10)	1701(9)	4780(5)	72(3)
C(16)	2619(9)	2407(7)	4639(4)	58(2)
C(21)	9332(8)	3963(6)	5681(3)	48(2)
C(22)	9321(10)	4881(8)	6140(5)	73(3)
C(23)	7771(9)	2543(6)	6080(3)	51(2)
C(24)	8242(10)	1461(7)	5851(4)	69(3)
C(31)	3036(8)	5336(6)	2422(3)	43(2)
C(32)	2483(9)	6150(7)	2045(4)	58(2)
C(33)	1221(10)	6028(9)	1757(4)	73(3)
C(34)	552(10)	5062(10)	1826(5)	76(3)

Table A24 continued.

C(35)	1098(10)	4223(9)	2182(4)	65(3)
C(36)	2316(9)	4362(7)	2484(4)	52(2)
C(41)	6499(9)	7642(6)	1813(3)	50(2)
C(42)	6917(10)	6909(8)	1285(4)	70(3)
C(43)	8379(9)	7669(7)	2603(4)	59(2)
C(44)	8307(11)	8696(9)	2989(5)	83(3)

Table A25: Anisotropic displacement parameters ($Å^2$ x 10^3) for *cis*-[Pt(L1a)$_2$] (**7**). The anisotropic displacement factor exponent takes the form: $-2\pi^2$ [$h^2 a^{*2} U11$ + ... + 2 $h k a^* b^* U12$].

	*U*11	*U*22	*U*33	*U*23	*U*13	*U*12
Pt(1)	43(1)	38(1)	37(1)	6(1)	-3(1)	-4(1)
S(1)	61(1)	52(1)	46(1)	12(1)	-14(1)	-20(1)
S(2)	63(2)	65(1)	54(1)	22(1)	-21(1)	-25(1)
O(1)	54(4)	56(3)	52(3)	20(3)	-16(3)	-15(3)
O(2)	63(4)	60(3)	51(3)	20(3)	-12(3)	-18(3)
N(1)	32(4)	46(3)	41(3)	6(3)	-1(3)	-8(3)
N(2)	37(4)	54(4)	39(3)	6(3)	-5(3)	-9(3)
N(3)	39(4)	37(3)	44(3)	7(3)	-2(3)	-2(3)
N(4)	37(4)	43(3)	51(4)	4(3)	2(3)	-6(3)
C(1)	41(5)	33(3)	44(4)	1(3)	6(3)	-2(3)
C(2)	42(5)	46(4)	32(3)	-2(3)	5(3)	-4(3)
C(3)	47(5)	38(4)	32(3)	2(3)	-1(3)	4(3)
C(4)	49(5)	30(3)	42(4)	2(3)	5(3)	-2(3)
C(11)	38(4)	42(4)	35(3)	0(3)	-4(3)	-6(3)
C(12)	46(5)	57(5)	62(5)	17(4)	-2(4)	-14(4)
C(13)	60(6)	64(5)	70(6)	21(5)	-18(5)	-19(5)
C(14)	54(6)	62(6)	81(6)	-4(5)	7(5)	-18(5)
C(15)	39(6)	84(7)	94(7)	1(6)	-15(5)	-10(5)
C(16)	47(6)	53(5)	74(6)	8(4)	-13(4)	-2(4)
C(21)	44(5)	55(4)	45(4)	0(3)	-6(3)	-7(4)
C(22)	56(7)	90(8)	74(7)	-16(5)	-9(5)	-2(5)
C(23)	56(6)	58(5)	40(4)	9(3)	-8(4)	-6(4)
C(24)	70(7)	65(6)	71(6)	22(5)	8(5)	4(5)
C(31)	37(5)	55(5)	37(4)	-2(3)	0(3)	2(3)
C(32)	48(6)	57(5)	70(5)	12(4)	-10(4)	-1(4)
C(33)	59(7)	97(8)	61(6)	14(5)	-22(5)	13(6)

Table A25 continued.

C(34)	36(6)	131(10)	60(6)	3(6)	-7(4)	-6(6)
C(35)	55(6)	84(7)	56(5)	-8(5)	5(4)	-25(5)
C(36)	47(5)	57(5)	50(4)	2(4)	4(4)	-16(4)
C(41)	58(6)	49(4)	44(4)	18(3)	1(4)	-5(4)
C(42)	77(7)	79(7)	53(5)	-3(5)	1(5)	0(5)
C(43)	53(6)	65(5)	61(5)	13(4)	-1(4)	-19(4)
C(44)	78(8)	84(7)	86(7)	2(6)	-7(6)	-34(6)

Table A26: Hydrogen coordinates (x 10^4) and isotropic displacement parameters (Å^2 x 10^3) for *cis*-[Pt(L1a)$_2$] (**7**).

	x	*y*	*z*	$U_{(eq)}$
H(12)	4971(9)	1230(7)	5441(4)	67(5)
H(13)	3259(10)	23(8)	5640(4)	67(5)
H(14)	1113(10)	347(8)	5239(5)	67(5)
H(15)	734(10)	1831(9)	4617(5)	67(5)
H(16)	2452(9)	2998(7)	4374(4)	67(5)
H(21A)	9585(8)	4240(6)	5270(3)	67(5)
H(21B)	10008(8)	3437(6)	5815(3)	67(5)
H(22A)	10167(22)	5258(28)	6130(19)	67(5)
H(22B)	9181(54)	4600(9)	6557(6)	67(5)
H(22C)	8606(35)	5376(24)	6030(15)	67(5)
H(23A)	6814(9)	2506(6)	6162(3)	67(5)
H(23B)	8234(9)	2717(6)	6475(3)	67(5)
H(24A)	7721(35)	1253(20)	5484(15)	67(5)
H(24B)	8132(50)	926(11)	6177(10)	67(5)
H(24C)	9176(16)	1508(13)	5744(23)	67(5)
H(32)	2966(9)	6790(7)	1982(4)	67(5)
H(33)	840(10)	6593(9)	1521(4)	67(5)
H(34)	-286(10)	4968(10)	1630(5)	67(5)
H(35)	639(10)	3565(9)	2216(4)	67(5)
H(36)	2669(9)	3803(7)	2733(4)	67(5)
H(41A)	6830(9)	8373(6)	1736(3)	67(5)
H(41B)	5523(9)	7673(6)	1823(3)	67(5)
H(42A)	6581(46)	7195(24)	890(5)	67(5)
H(42B)	6555(45)	6192(14)	1349(14)	67(5)
H(42C)	7882(10)	6870(34)	1276(16)	67(5)
H(43A)	8873(9)	7814(7)	2221(4)	67(5)
H(43B)	8865(9)	7116(7)	2842(4)	67(5)
H(44A)	9203(11)	8937(24)	3095(21)	67(5)

Table A26 continued.

H(44B)	7825(47)	8554(14)	3369(13)	67(5)

Table A27: Crystallographic data for *cis*-(S,P)-[PtCl(L1a)(PPh_3)] (**8**).

Empirical formula	$C_{30}H_{30}ClN_2OPPt\ S$
Formula weight	728.13
Temperature	293(2) K
Wavelength	0.71073 Å
Crystal system, space group	Orthorhombic, $P2_12_12_1$
Unit cell dimensions	a = 10.1271(5) Å α = 90°
	b = 16.4174(8) Å β = 90°
	c = 17.7317(8) Å γ = 90°
Volume	2948.1(2) $Å^3$
Z, Calculated density	4, 1.641 Mg/m^3
Absorption coefficient	5.001 mm^{-1}
F(000)	1432
Crystal size	0.40 × 0.30 × 0.20 mm
Theta range for data collection	1.69 to 28.27°
Index ranges	$12 \le h \le 11$, $-14 \le k \le 21$, $-23 \le l \le 23$
Reflections collected/unique	19304/6755 [R(int) = 0.0254]
Refinement method	Full-matrix least-squares on F^2
Data/restraints/parameters	6755/0/337
Goodness-of-fit on F^2	1.126
Final R indices [$I>2\sigma(I)$]	R^a = 0.0220, Rw^b = 0.0460
Absolute structure parameter	-0.008(4)
Largest diff. peak and hole	0.337 and -0.994 e.$Å^{-3}$

[a] $R = [(\Sigma\Delta F)/(\Sigma F_0)]$.

[b] $Rw = \Sigma[w(F_0^2 - F_c^2)^2]/\Sigma[w(F_0^2)^2]^{1/2}$.

Table A28: Atomic coordinates (x 10^4) and equivalent isotropic displacement parameters (Å^2 x 10^3) for *cis*-(S,P)-[PtCl(L1a)(PPh_3)] (**8**). $U_{(eq)}$ is defined as one third of the trace of the orthogonalized U_{ij} tensor.

	x	*y*	*z*	$U_{(eq)}$
Pt(1)	5394(1)	4913(1)	616(1)	33(1)
Cl(1)	4413(1)	5001(1)	1804(1)	51(1)
S(1)	6401(1)	4828(1)	-509(1)	45(1)
P(1)	4033(1)	5879(1)	219(1)	34(1)
O(1)	6499(3)	3994(2)	1071(1)	49(1)
N(1)	7635(3)	3433(2)	41(2)	43(1)
N(2)	8170(3)	3875(2)	-1122(2)	51(1)
C(1)	7182(3)	3458(2)	737(2)	38(1)
C(2)	7454(3)	3997(2)	-495(2)	39(1)
C(3)	8993(5)	3143(3)	-1211(3)	72(1)
C(4)	8192(7)	2381(4)	-1363(3)	100(2)
C(5)	8178(4)	4455(3)	-1759(2)	66(1)
C(6)	7209(6)	4266(5)	-2369(3)	95(2)
C(11)	4360(3)	6875(2)	625(2)	39(1)
C(12)	5383(4)	6966(2)	1145(2)	52(1)
C(13)	5654(5)	7730(3)	1444(3)	70(1)
C(14)	4904(5)	8387(3)	1244(3)	72(1)
C(15)	3910(5)	8306(2)	729(3)	62(1)
C(16)	3652(4)	7558(2)	406(2)	52(1)
C(21)	4091(3)	6088(2)	-796(2)	38(1)
C(22)	3236(4)	5726(3)	-1303(2)	4091(3)
C(23)	3403(5)	5867(3)	-2074(2)	68(1)
C(24)	4377(6)	6343(3)	-2327(3)	77(2)
C(25)	5220(6)	6700(3)	-1829(3)	84(2)
C(26)	5087(4)	6576(3)	-1063(2)	61(1)
C(31)	2333(3)	5605(2)	436(2)	39(1)
C(32)	1935(4)	4807(3)	278(2)	62(1)

Table A28 continued.

C(33)	659(5)	4562(3)	455(3)	75(1)
C(34)	-208(4)	5086(4)	789(2)	72(1)
C(35)	183(4)	5861(4)	956(3)	68(1)
C(36)	1451(4)	6131(3)	781(2)	53(1)
C(41)	7538(3)	2744(2)	1225(2)	42(1)
C(42)	6942(4)	2651(3)	1915(2)	49(1)
C(43)	7214(5)	1969(3)	2351(2)	59(1)
C(44)	8072(5)	1402(3)	2117(3)	68(1)
C(45)	8676(6)	1484(3)	1427(3)	81(2)
C(46)	8425(5)	2158(3)	987(3)	65(1)

Table A29: Bond lengths (Å) and angles (°) for *cis*-(S,P)-[PtCl(L1a)(PPh_3)] (**8**).

Pt(1)-O(1)	2.044(3)
Pt(1)-P(1)	2.2159(9)
Pt(1)-S(1)	2.2448(8)
Pt(1)-Cl(1)	2.3335(8)
S(1)-C(2)	1.731(4)
P(1)-C(11)	1.731(4)
P(1)-C(31)	1.820(3)
P(1)-C(21)	1.833(3)
O(1)-C(1)	1.267(4)
N(1)-C(1)	1.316(4)
N(1)-C(2)	1.316(4)
N(2)-C(2)	1.342(4)
N(2)-C(3)	1.472(6)
N(2)-C(5)	1.477(5)
C(1)-C(41)	1.477(5)
C(3)-C(4)	1.477(5)
C(5)-C(6)	1.493(7)
C(11)-C(16)	1.493(7)
C(11)-C(12)	1.395(5)
C(12)-C(13)	1.367(7)
C(13)-C(14)	1.367(7)
C(14)-C(15)	1.365(6)
C(15)-C(16)	1.383(5)
C(21)-C(26)	1.383(5)
C(21)-C(22)	1.383(5)
C(22)-C(23)	1.397(6)
C(23)-C(24)	1.336(7)
C(24)-C(25)	1.362(7)
C(25)-C(26)	1.379(6)
C(31)-C(36)	1.398(6)

Table A29 continued.

C(31)-C(32)	1.398(6)
C(32)-C(33)	1.389(6)
C(33)-C(34)	1.365(7)
C(34)-C(35)	1.365(7)
C(35)-C(36)	1.393(6)
C(41)-C(42)	1.373(5)
C(41)-C(46)	1.382(6)
C(42)-C(43)	1.387(6)
C(43)-C(44)	1.376(6)
C(44)-C(45)	1.376(6)
C(45)-C(46)	1.376(6)
O(1)-Pt(1)-P(1)	173.72(7)
O(1)-Pt(1)-S(1)	93.19(7)
P(1)-Pt(1)-S(1)	92.60(3)
O(1)-Pt(1)-Cl(1)	88.69(3)
P(1)-Pt(1)-Cl(1)	88.69(3)
S(1)-Pt(1)-Cl(1)	178.16(3)
C(2)-S(1)-Pt(1)	108.46(12)
C(11)-P(1)-C(31)	108.16(16)
C(11)-P(1)-C(21)	106.48(16)
C(31)-P(1)-C(21)	106.48(16)
C(11)-P(1)-Pt(1)	113.89(12)
C(31)-P(1)-Pt(1)	110.14(13)
C(21)-P(1)-Pt(1)	126.6(3)
C(1)-O(1)-Pt(1)	126.6(3)
C(1)-N(1)-C(2)	126.6(3)
C(2)-N(2)-C(3)	122.7(3)
C(2)-N(2)-C(5)	122.7(3)
C(3)-N(2)-C(5)	116.2(3)

Table A29 continued.

O(1)-C(1)-N(1)	130.5(3)
O(1)-C(1)-C(41)	115.7(3)
N(1)-C(1)-C(41)	115.7(3)
N(1)-C(2)-N(2)	114.3(3)
N(1)-C(2)-S(1)	116.0(3)
N(2)-C(2)-S(1)	116.0(3)
N(2)-C(3)-C(4)	112.9(4)
N(2)-C(5)-C(6)	114.6(4)
C(16)-C(11)-C(12)	118.9(3)
C(16)-C(11)-P(1)	121.5(3)
C(12)-C(11)-P(1)	119.6(3)
C(13)-C(12)-C(11)	119.7(4)
C(14)-C(13)-C(12)	120.2(4)
C(15)-C(14)-C(13)	120.5(4)
C(14)-C(15)-C(16)	120.3(4)
C(15)-C(16)-C(11)	120.3(4)
C(26)-C(21)-C(22)	119.1(3)
C(26)-C(21)-P(1)	118.2(3)
C(22)-C(21)-P(1)	122.5(3)
C(21)-C(22)-C(23)	119.3(4)
C(24)-C(23)-C(22)	121.0(4)
C(23)-C(24)-C(25)	119.8(4)
C(24)-C(25)-C(26)	120.9(5)
C(21)-C(26)-C(25)	119.9(4)
C(36)-C(31)-C(32)	119.1(3)
C(36)-C(31)-P(1)	123.3(3)
C(32)-C(31)-P(1)	117.6(3)
C(33)-C(32)-C(31)	119.7(4)
C(34)-C(33)-C(32)	119.7(4)

Table A29 continued.

C(33)-C(34)-C(35)	119.7(4)
C(34)-C(35)-C(36)	121.0(4)
C(31)-C(36)-C(35)	121.6(3)
C(42)-C(41)-C(46)	121.6(3)
C(42)-C(41)-C(1)	121.6(3)
C(46)-C(41)-C(1)	121.6(3)
C(41)-C(42)-C(43)	119.9(4)
C(44)-C(43)-C(42)	121.1(4)
C(43)-C(44)-C(45)	119.8(4)
C(44)-C(45)-C(46)	120.0(5)
C(45)-C(46)-C(41)	120.4(4)

Symmetry transformations used to generate equivalent atoms.

Table A30: Anisotropic displacement parameters ($Å^2$ x 10^3) for *cis*-(S,P)-[PtCl(L1a)(PPh_3)] (**8**). The anisotropic displacement factor exponent takes the form: $-2\pi^2 [h^2 a^{*2} U11 + ... + 2 h k a^* b^* U12]$.

	*U*11	*U*22	*U*33	*U*23	*U*13	*U*12
Pt(1)	34(1)	32(1)	35(1)	-2(1)	2(1)	1(1)
Cl(1)	55(1)	60(1)	39(1)	-4(1)	9(1)	6(1)
S(1)	50(1)	45(1)	41(1)	5(1)	10(1)	7(1)
P(1)	30(1)	32(1)	41(1)	-2(1)	0(1)	-2(1)
O(1)	58(2)	48(2)	41(1)	2(1)	4(1)	21(1)
N(1)	40(2)	42(2)	46(2)	-1(1)	3(1)	4(1)
N(2)	51(2)	56(2)	46(2)	-5(2)	10(2)	6(2)
C(1)	33(2)	38(2)	43(2)	-2(2)	-3(2)	1(1)
C(2)	35(2)	42(2)	42(2)	-7(2)	5(1)	-4(1)
C(3)	73(3)	78(4)	64(3)	-10(3)	23(3)	25(3)
C(4)	145(6)	67(4)	87(4)	-24(3)	15(4)	17(4)
C(5)	64(3)	77(3)	56(2)	1(2)	22(2)	-5(2)
C(6)	98(4)	128(6)	60(3)	11(3)	0(3)	2(4)
C(11)	36(2)	34(2)	48(2)	-5(2)	5(2)	-3(1)
C(12)	49(2)	41(2)	67(2)	-7(2)	-8(2)	-10(2)
C(13)	73(3)	55(3)	82(3)	-15(2)	-16(3)	-18(2)
C(14)	79(3)	42(2)	94(4)	-19(2)	11(3)	-14(2)
C(15)	66(3)	39(2)	81(3)	-1(2)	16(3)	9(2)
C(16)	53(2)	41(2)	62(3)	-3(2)	3(2)	2(2)
C(21)	37(2)	36(2)	42(2)	1(1)	-2(1)	3(1)
C(22)	55(2)	51(3)	57(2)	0(2)	-12(2)	2(2)
C(23)	83(3)	70(3)	51(3)	-8(2)	-23(2)	11(3)
C(24)	108(4)	73(3)	51(3)	8(2)	5(3)	7(3)
C(25)	106(4)	82(4)	63(3)	8(3)	21(3)	-26(3)
C(26)	66(3)	63(3)	53(2)	5(2)	4(2)	-20(2)
C(31)	32(2)	43(2)	43(2)	2(2)	-1(1)	-2(2)
C(32)	49(2)	54(3)	83(3)	-6(2)	4(2)	-13(2)

Table A30 continued.

C(33)	61(3)	66(3)	98(4)	-2(3)	-1(2)	-27(2)
C(34)	39(2)	105(4)	71(3)	2(3)	2(2)	-25(3)
C(35)	41(2)	94(4)	70(3)	-3(3)	11(2)	0(3)
C(36)	40(2)	61(3)	57(2)	-2(2)	4(2)	-4(2)
C(41)	42(2)	35(2)	0(2)	0(2)	-6(2)	1(2)
C(42)	43(2)	51(2)	52(2)	6(2)	-4(2)	1(2)
C(43)	68(3)	58(3)	52(2)	13(2)	-8(2)	-9(2)
C(44)	93(3)	47(3)	63(3)	11(2)	-15(3)	10(3)
C(45)	106(4)	52(3)	84(3)	0(3)	-9(3)	38(3)
C(46)	80(3)	60(3)	60(3)	7(2)	11(2)	23(2)

Table A31: Hydrogen coordinates (x 10^4) and isotropic displacement parameters (Å^2 x 10^3) for *cis*-(S,P)-[PtCl(L1a)(PPh_3)] (**8**).

	x	*y*	*z*	$U_{(eq)}$
H(3A)	9509	3063	-756	81(3)
H(3B)	9604	3227	-1625	81(3)
H(4A)	7576	2298	-959	81(3)
H(4B)	8773	1921	-1397	81(3)
H(4C)	7720	2443	-1829	81(3)
H(5A)	9057	4465	-1976	81(3)
H(5B)	7993	4996	-1566	81(3)
H(6A)	7364	3726	-2555	81(3)
H(6B)	7312	4651	-2773	81(3)
H(6C)	6328	4302	-2172	81(3)
H(12)	5883	6518	1290	81(3)
H(13)	6348	7794	1783	81(3)
H(14)	5071	8893	1460	81(3)
H(15)	3406	8757	595	81(3)
H(16)	3000	7512	39	81(3)
H(22)	2556	5393	-1132	81(3)
H(23)	2827	5626	-2416	81(3)
H(24)	4478	6430	-2842	81(3)
H(25)	5895	7033	-2007	81(3)
H(26)	5671	6822	-729	81(3)
H(32)	2520	4443	55	81(3)
H(33)	393	4032	346	81(3)
H(34)	-1062	4917	901	81(3)
H(35)	-405	6214	1192	81(3)
H(36)	1703	6662	894	81(3)
H(42)	6358	3044	2091	81(3)
H(43)	6792	1905	2813	81(3)
H(44)	8259	955	2420	81(3)

Table A31 continued.

H(45)	9255	1085	1257	81(3)
H(46)	8855	2219	527	81(3)

APPENDIX A

Crystallographic data for *N,N*-diethyl-*N'*-(-)-(3*R*)-menthyloxycarbonylthiourea (HL4)

Crystallographic data for *cis*-(S,S)-[PtCl(DMSO)(L1a)] (1a)

Crystallographic data for *cis*-(S,S)-[PtCl(L1a)(MPSO)] (4)

Crystallographic data for *cis*-(S,S)-[PtCl(DMSO)(L7)] (12)

Crystallographic data for *cis*-[Pt(L1a)$_2$] (7)

Crystallographic data for *cis*-(S,P)-[PtCl(L1a)(PPh_3)] (8)

Table B1: Rate constants for the reaction of *cis*-(S,S)-[PtCl(DMSO)(L1a)] with azide in methanol. $[Pt]_F$ = 0.5 mM. λ = 375 nm.

Temperature/ °C	[Azide]/ M	$k_{obs}/10^{-3}$ s^{-1}	k_y/ $M^{-1}s^{-1}$	k_s/ s^{-1}
10.2	0.1	2.6(2)	0.0230(3)	0.00031(1)
	0.075	2.07(1)		
	0.05	1.462(5)		
	0.025	0.8642(2)		
	0.01	0.547(1)		
	0.005	0.442(1)		
25.0	0.1	8.72(3)	0.0724(7)	0.00144(4)
	0.075	6.812(2)		
	0.05	5.10(1)		
	0.025	3.167(5)		
	0.01	2.164(2)		
	0.005	1.856(3)		
39.8	0.1	26.2(2)	0.196(7)	0.0062(4)
	0.075	20.1(1)		
	0.05	16.6(3)		
	0.025	11.7(1)		
	0.01	7.95(1)		
	0.005	7.02(2)		

Table B2: Rate constants for the reaction of *cis*-(S,S)-[PtCl(DMSO)(L1a)] with iodide in methanol. λ = 375 nm, $[Pt]_F$ = 0.5 mM.

Temperature/ °C	$[I^-]$/ M	$k_{obs}/10^{-3}$ s^{-1}	k_y/ $M^{-1}s^{-1}$	k_s/ s^{-1}
25.1	0.1	128.3(1)	1.16(3)	0.005(2)
		121(1)		
		11(1)		
		129(1)		
		124(2)		
	0.075	100(1)		
		82(1)		
		82(1)		
		88(1)		
		88(2)		
	0.05	59.8(5)		
		57.7()		
		67.6(9)		
		59.9(6)		
		65.6(9)		
		65.3(8)		
		63(2)		
	0.025	32.1(2)		
		34.4(2)		
		34.3(2)		
		32.7(2)		
		33.3(4)		
	0.01	17.8(1)		
		10.3(1)		
		18.5(1)		
		020.8(2)		
		16.9(2)		

Table B2 continued.

	0.005	11.47(1)
		11.34(7)
		10.87(7)
		12.5(1)
		11.55(15)

Table B3: Rate constants for the reaction of *cis*-(S,S)-[PtCl(DMSO)(L1a)] with thiocyanate in methanol. λ = 375 nm, $[Pt]_F$ = 0.5 mM.

Temperature/ °C	$[SCN^-]$/ M	k_{obs}/ s^{-1}	k_y/ $M^{-1}s^{-1}$	k_s/ s^{-1}
25.0	0.1	0.412(5)	4.47(15)	0.012(9)
		0.458(8)		
		0.505(7)		
		0.502(8)		
		0.47(1)		
	0.075	0.332(7)		
		0.325(5)		
		0.334(7)		
		0.331(5)		
		0.33(1)		
	0.025	0.125(3)		
		0.142(3)		
		0.1330(20)		
		0.133(5)		
	0.01	0.0564(5)		
		0.0600(5)		
		0.0557(6)		
		0.0616(6)		
		0.058(1)		
	0.005	0.0349(3)		
		0.0288(4)		
		0.0250(4)		
		0.0304(5)		
		0.0298(8)		

Table B4: Rate constants for the reaction of *cis*-(S,S)-[PtCl(L1a)(MPSO)] with azide in methanol. λ = 375 nm, $[Pt]_F$ = 0.5 mM.

Temperature/ °C	[Azide]/ M	k_{obs}/ 10^{-3} s^{-1}	k_y/ 10^{-3} $M^{-1}s^{-1}$	k_s/ 10^{-3} s^{-1}
10.2	0.1	2.59(2)	22.0(6)	0.3(3)
	0.075	2.02(1)		
	0.05	1.38(1)		
	0.025	0.88(1)		
	0.01	0.61(1)		
	0.005	0.49(1)		
25.1	0.1	10.4(2)	99(6)	0.8(3)
	0.075	8.8(1)		
	0.025	2.8(3)		
	0.01	1.867(15)		
	0.005	1.56(1)		
39.8	0.1	28.67(5)	230(5)	5.7(3)
	0.075	23.5(1)		
	0.05	16.68(3)		
	0.025	11.10(2)		
	0.01	8.18(1)		
	0.005	7.25(1)		

Table B5: Rate constants for the reaction of *cis*-(S,S)-[PtCl(L1a)((*S*)-MTSO)] with azide in methanol. λ = 375 nm, $[Pt]_F$ = 0.5 mM.

Temperature/ °C	[Azide]/ M	k_{obs}/ 10^{-3} s^{-1}	k_y/ 10^{-3} $M^{-1}s^{-1}$	k_s/ 10^{-3} s^{-1}
10.0	0.1	2.617(15)	22.3(7)	0.32(4)
	0.075	1.953(1)		
	0.05	1.374(5)		
	0.025	0.829(2)		
	0.01	0.578(2)		
	0.005	0.487(2)		
25.0	0.1	9.33(8)	78(2)	1.3(1)
	0.075	7.14(6)		
	0.05	5.11(3)		
	0.025	3.24(2)		
	0.01	2.19(1)		
	0.005	1.87(1)		
39.8	0.1	26.7(1)	214(11)	4.7(7)
	0.075	20.25(5)		
	0.05	15.45(3)		
	0.025	9.2(3)		
	0.005	6.62(1)		

Table B6: Rate constants for the reaction of *cis*-(S,S)-[PtCl(DMSO)(L1aR)] with azide in methanol. λ = 375 nm, $[Pt]_F$ = 0.5 mM , T = 25.0°C.

R-Group	[Azide]/ M	k_{obs}/ 10^{-3} s^{-1}	k_y/ $M^{-1}s^{-1}$	k_s/ s^{-1}
H	0.1	8.72(3)	0.0724(7)	0.00144(4)
	0.075	6.812(2)		
	0.05	5.10(1)		
	0.025	3.167(5)		
	0.01	2.164(2)		
	0.005	1.856(3)		
Cl	0.1	10.7(2)	0.091(3)	0.0013(2)
	0.075	7.8(1)		
	0.05	5.60(6)		
	0.025	3.47(2)		
	0.01	2.28(1)		
	0.005	1.87(1)		
NO_2	0.1	12.5(3)	0.110(2)	0.0015(1)
	0.075	9.8(2)		
	0.05	7.3(1)		
	0.025	4.47(6)		
	0.01	2.63(5)		
	0.005	1.90(3)		
CH_3	0.1	8.42(9)	0.070(1)	0.00136(7)
	0.075	6.47(6)		
	0.05	4.89(5)		
	0.025	3.00(2)		
	0.01	2.08(1)		
	0.005	1.79(1)		
OCH_3	0.1	9.39(6)	0.0799(9)	0.00132(5)
	0.075	7.21(4)		
	0.05	5.34(3)		
	0.025	3.28(2)		

Table B6 continued.

0.01	2.12(1)
0.005	1.78(1)

Table B7: Rate constants for the reaction of *cis*-(S,S)-[PtCl(DMSO)(L3a)] with azide in methanol. λ = 375 nm, $[Pt]_F$ = 0.5 mM.

Temperature/ °C	[Azide]/ M	k_{obs}/ 10^{-3} s^{-1}	k_y/ 10^{-3} $M^{-1}s^{-1}$	k_s/ 10^{-3} s^{-1}
25.2	0.1	10.8(1)	90(2)	1.7(1)
	0.075	8.37(4)		
	0.05	6.4(2)		
	0.025	4.01(1)		
	0.01	2.583(7)		

Table B8: Rate constants for the reaction of *cis*-(S,S)-[PtCl(DMSO)(L1a)] with thiourea in methanol. λ = 380 nm, $[Pt]_F$ = 0.5 mM.

Temperature/ °C	[Thiourea]/ M	k_{obs}/ s^{-1}	k_y/ $M^{-1}s^{-1}$	k_s/ s^{-1}
25.1	0.1	10.78(15)	107(1)	0
		10.63(16)		
		10.58(14)		
		10.34(16)		
		10.6(3)		
	0.075	7.64(7)		
		7.98(7)		
		8.34(7)		
		8.54(6)		
		8.1(1)		
	0.025	2.931(14)		
		3.018(12)		
		3.019(13)		
		2.992(15)		
		3.056(17)		
		3.00(3)		
	0.01	1.139(5)		
		1.125(5)		
		1.144(5)		
		1.136(4)		
		1.136(9)		
	0.005	0.5461(7)		
		0.550(3)		
		0.5613(25)		
		0.588(3)		
		0.554(5)		

Table B9: Rate constants for the reaction of *cis*-(S,S)-[PtCl(DMSO)(L1a)] with MBI in methanol. λ = 380 nm, $[Pt]_F$ = 0.5 mM.

Temperature/ °C	[MBI]/ M	k_{obs}/ s^{-1}	k_y/ $M^{-1}s^{-1}$	k_s/ s^{-1}
25.0	0.1	4.26(4)	42(1)	0
		3.94(3)		
		3.89(3)		
		4.38(4)		
		4.03(3)		
		4.10(8)		
	0.075	3.101(21)		
		3.213(20)		
		3.238(21)		
		3.148(18)		
		3.301(19)		
		3.20(4)		
	0.05	2.31(3)		
		2.33(2)		
		2.26(2)		
		2.33(3)		
		2.31(5)		
	0.025	1.255(5)		
		1.271(5)		
		1.288(5)		
		1.271(5)		
		1.272(5)		
		1.27(1)		

Table B9 continued.

	0.01	0.5173(21)
		0.5180(23)
		0.5223(23)
		0.5219(23)
		0.5237(23)
		0.5247(23)
		0.521(5)
	0.005	0.2603(8)
		0.2601(9)
		0.2614(9)
		0.2608(9)
		0.2605(8)
		0.261(2)

Table B10: Rate constants for the first reaction of *cis*-(S,S)-[PtCl(DMSO)(L1a)] with PPh_3 in methanol. λ = 370 nm, $[Pt]_F$ = 0.5 mM (DMSO substitution).

Temperature/ °C	$[PPh_3]$/ M	k_{obs}/ s^{-1}	k_y/ $M^{-1}s^{-1}$	k_s/ s^{-1}
25.1	0.025	24.6(9)	1203(23)	0
		34.5(8)		
		34.6(7)		
		21.8(5)		
		34.8(8)		
		30(2)		
	0.02	22.7(1)		
		23(1)		
		22.5(1)		
		23(1)		
	0.015	21.0(5)		
		17.5(5)		
		20.7(5)		
		20.2(5)		
		20.7(6)		
		14.3(4)		
		19(1)		
	0.01	12.16(14)		
		12.25(12)		
		12.72(11)		
		12.73(12)		
		12.81(14)		
		12.5(3)		

Table B10 continued.

	0.005	6.64(5)
		6.68(4)
		6.88(4)
		7.02(5)
		6.66(5)
		7.07(4)
		6.8(1)

Table B11: Rate constants for the first reaction of *cis*-(S,S)-[PtCl(DMSO)(L1a)] with DMAP in methanol. λ = 380 nm, $[Pt]_F$ = 0.5 mM.

Temperature/ °C	[DMAP]/ M	k_{obs}/ s^{-1}	k_y/ $M^{-1}s^{-1}$	k_s/ s^{-1}
25.1°C	0.3	0.362(2)	0.87(4)	0.100(6)
		0.363(2)		
		0.370(2)		
		0.377(1)		
		0.368(3)		
25.1°C	0.2	0.267(1)		
		0.271(1)		
		0.278(1)		
		0.2376(15)		
		0.263(2)		
25.1°C	0.1	0.1752(8)		
		0.1726(5)		
		0.1883(5)		
		0.1911(5)		
		0.1882(5)		
		0.183(1)		
	0.05	0.1443(7)		
		0.1418(6)		
		0.1473(7)		
		0.1460(7)		
		0.1469(7)		
		0.1405(6)		
		0.1427(6)		
		0.144(2)		

Table B11 continued.

	0.025	0.1235(7)
		0.1242(7)
		0.1264(8)
		0.1227(6)
		0.1276(6)
		0.1392(9)
		0.1229(8)
		0.127(2)
	0.01	0.1384(9)
		0.1281(7)
		0.1254(9)
		0.1342(9)
		0.1256(9)
		0.1361(9)
		0.1224(9)
		0.130(2)
	0.005	0.150(3)
		0.160(3)
		0.155(3)
		0.161(3)
		0.156(6)

Table B12: Rate constants for the reaction of *cis*-(S,S)-[PtCl(DMSO)(L1a)] with MBI in methanol. DMSO variation at constant [MBI]. λ = 380 nm, $[Pt]_F$ = 0.5 mM.

Temperature/ °C	[MBI]/ M	[DMSO]/ M	k_{obs}/ s^{-1}
25.0	0.01	0.1	0.486(4)
			0.515(2)
			0.515(2)
			0.515(2)
			0.516(2)
			0.509(6)
		0.005	0.479(4)
			0.487(3)
			0.478(3)
			0.484(3)
			0.493(3)
			0.494(3)
			0.497(3)
			0.487(8)
25.1	0.1	0.1	3.98(6)
			3.34(5)
			3.71(6)
			3.24(5)
			3.81(6)
			3.16(5)
			3.5(1)
		0.005	3.29(8)
			3.63(5)
			3.71(5)
			3.53(3)
			3.51(3)
			3.5(1)

Table B13: Rate constants for the first reaction of *cis*-(S,S)-[PCl(DMSO)(L1a)] with DMAP in methanol. λ = 380 nm, $[Pt]_F$ = 0.5 mM, T = 25°C (DMSO variation, constant [DMAP]).

[DMAP]/ M	[DMSO]/ M	k_{obs}/ s^{-1}
0.1	0.005	0.2133(2)
		0.2186(3)
		0.2223(3)
		0.2248(3)
		0.2278(3)
		0.2321(3)
		0.2231(6)
	0.1	0.2383(4)
		0.2325(3)
		0.2340(3)
		0.2263(3)
		0.2231(3)
		0.2195(3)
		0.2164(3)
		0.2271(9)
0.3	0.005	0.4643(8)
		0.4716(9)
		0.47400(1)
		0.464(1)
		0.465(1)
		0.465(1)
		0.461(1)
		0.466(2)

Table B13 continued.

	0.1	0.4505(6)
		0.4531(7)
		0.4567(8)
		0.4598(8)
		0.4623(6)
		0.4652(5)
		0.458(2)

Table B14: Rate constants for the first reaction of *cis*-(S,S)-[PtCl(DMSO)(L1a)] with PPh_3 in methanol. DMSO variation at constant [PPh_3]. λ = 357 nm, $[Pt]_F$ = 0.5 mM, T = 25°C.

[PPh_3]/ M	[DMSO]/ M	k_{obs}/ s^{-1}
0.02	0.025	28.3(3)
		29.2(2)
		29.1(2)
		28.4(2)
		28.6(2)
		28.7(2)
		28.7(6)
	0.01	28.6(2)
		28.6(2)
		28.8(2)
		28.4(2)
		28.2(2)
		28.5(5)
0.01	0.025	14.9(1)
		14.9(1)
		15.0(1)
		14.8(1)
		14.7(1)
		14.8(3)
	0.01	14.4(2)
		15.0(2)
		14.7(2)
		14.7(2)
		14.5(2)
		14.7(5)

Table B15: Rate constants for the reaction of *cis*-(S,S)-[PtCl(MPSO)(L1a)] with MBI in methanol. λ = 380 nm, $[Pt]_F$ = 0.5 mM.

Temperature/ °C	[MBI]/ M	k_{obs}/ s^{-1}	k_y/ $M^{-1}s^{-1}$	k_s/ s^{-1}
25.1	0.1	12.47(11)	121(8)	1.2(4)
		13.16(13)		
		13.19(20)		
		13.00(16)		
		12.58(12)		
		12.9(3)		
	0.075	10.24(7)		
		10.63(7)		
		11.13(8)		
		10.85(8)		
		10.71(15)		
	0.05	7.02(6)		
		6.89(5)		
		6.99(5)		
		7.11(5)		
		6.87(5)		
		7.0(1)		
	0.025	5.34(3)		
		5.41(4)		
		5.08(4)		
		5.00(4)		
		5.18(4)		
		5.05(4)		
		5.18(9)		

Table B15 continued.

	0.01	2.469(19)
		2.174(18)
		2.012(16)
		2.230(19)
		1.987(17)
		2.17(4)
	0.005	1.337(11)
		1.192(9)
		1.249(1)
		1.276(11)
		1.247(12)
		1.26(2)

Table B16: Rate constants for the reaction of *cis*-(S,S)-[PtCl(L1a)((*S*)-MTSO)] with MBI in methanol. λ = 380 nm, $[Pt]_F$ = 0.5 mM.

Temperature/ °C	[MBI]/ M	k_{obs}/ s^{-1}	k_y/ $M^{-1}s^{-1}$	k_s/ s^{-1}
25.0	0.1	10.05(9)	94(4)	0.9(2)
		10.00(6)		
		10.08(11)		
		10.04(15)		
	0.075	7.84(5)		
		8.31(5)		
		7.98(5)		
		8.21(5)		
		8.1(1)		
	0.05	5.55(4)		
		5.38(5)		
		5.55(4)		
		5.75(5)		
		5.67(5)		
		5.6(1)		
	0.025	3.758(21)		
		3.754(20)		
		3.713(19)		
		3.771(21)		
		3.75(4)		
	0.01	1.661(1)		
		1.622(1)		
		1.617(1)		
		1.604(9)		
		1.593(10)		
		1.63(1)		

Table B16 continued.

	0.005	0.999(8)
		0.989(8)
		1.11(1)
		1.01(1)
		1.0101)
		1.03(2)

Table B17: Rate constants for the reaction of *cis*-(S,S)-[PtCl(DMSO)(L3a)] with MBI in methanol. λ = 380 nm, $[Pt]_F$ = 0.5 mM.

Temperature/ °C	[MBI]/ M	k_{obs}/ s^{-1}	k_y/ $M^{-1}s^{-1}$	k_s/ s^{-1}
25.0	0.1	3.46(3)	35(1)	0.3(1)
		3.63(3)		
		3.94(3)		
		3.99(3)		
		3.75(6)		
	0.075	2.64(3)		
		3.12(3)		
		2.89(3)		
		2.927(25)		
		2.89(6)		
	0.05	2.28(6)		
		2.22(4)		
		2.229(19)		
		2.112(17)		
		2.21(8)		
	0.025	1.305(15)		
		1.313(15)		
		1.222(9)		
		1.231(3)		
		1.27(3)		
	0.01	0.632(3)		
		0.634(3)		
		0.642(3)		
		0.633(3)		
		0.635(6)		

Table B17 continued.

	0.005	0.3370(16)
		0.3256(16)
		0.3214(19)
		0.3212(16)
		0.3353(19)
		0.328(4)

Table B18: Rate constants for the reaction of *cis*-(S,S)-[PtCl(DMSO)(L1a)] with MBI in methanol at various temperatures. λ = 380 nm, $[Pt]_F$ = 0.5 mM.

Temperature/ °C	[MBI]/ M	k_{obs}/ s^{-1}
10.2	0.025	0.18(1)
		0.19(1)
		0.19(1)
		0.19(1)
		0.19(2)
25.2		0.45(2)
		0.45(2)
		0.47(2)
		0.45(2)
		0.45(4)
40.1		1.46(7)
		1.41(7)
		1.44(7)
		1.43(7)
		1.45(7)
		1.44(16)

Table B19: Rate constants for the first reaction of *cis*-(S,S)-[PtCl(DMSO)(L1a)] with PPh_3 in methanol at various temperatures. λ = 357 nm, $[Pt]_F$ = 0.5 mM.

Temperature/ °C	$[PPh_3]$/ M	k_{obs}/ s^{-1}
10.2	0.005	3.5(2)
		3.4(2)
		3.4(2)
		3.4(2)
		3.4(4)
18.2	0.005	5.1(2)
		4.9(2)
		5.2(3)
		5.3(3)
		5.1(5)
25.0	0.005	8.1(4)
		8.0(4)
		8.0(4)
		8.0(4)
		8.0(8)
43.1	0.005	29(1)
		26(1)
		28(1)
		30(1)
		28(2)

Table B20: Rate constants for the first reaction of *cis*-(S,S)-[PtCl(DMSO)(L1a)] with PPh_3 in acetonitrile. $\lambda = 380$ nm, $[Pt]_F = 0.5$ mM, $T = 25°C$.

$[PPh_3]$/ M	k_{obs}/ s^{-1}	k_y/ $M^{-1}s^{-1}$	k_s/ s^{-1}
0.025	12.53(18)	480(14)	0
	12.08(14)		
	12.36(15)		
	12.82(14)		
	12.80(15)		
	13.37(14)		
	13.19(15)		
	12.7(4)		
0.02	9.14(8)		
	8.71(7)		
	8.81(6)		
	9.11(7)		
	8.70(5)		
	8.9(1)		
0.015	7.11(8)		
	7.28(9)		
	7.40(10)		
	7.17(6)		
	7.25(8)		
	7.2(2)		
0.01	4.48(4)		
	4.37(4)		
	4.56(4)		
	4.50(4)		
	4.72(4)		
	4.35(4)		
	4.50(4)		
	4.5(1)		

Table B20 continued.

0.005	2.26(2)
	2.29(2)
	2.32(2)
	2.28(2)
	2.26(2)
	2.26(2)
	2.20(2)
	2.19(2)
	2.26(6)

Table B21: Rate constants for the first reaction of *cis*-(S,S)-[PtCl(DMSO)(L1a)] with PPh_3 in acetone. $\lambda = 390$ nm, $[Pt]_F = 0.5$ mM, $T = 25$°C.

$[PPh_3]$/ M	k_{obs}/ s^{-1}	k_y/ $M^{-1}s^{-1}$	k_s/ s^{-1}
0.1	20.4(2)	203(2)	0
	20.9(2)		
	20.5(2)		
	20.2(1)		
	20.9(1)		
	20.6(4)		
0.05	9.63(6)		
	9.67(5)		
	9.53(6)		
	9.71(6)		
	9.73(6)		
	9.80(6)		
	9.64(7)		
	9.67(16)		
0.025	5.00(2)		
	4.98(2)		
	5.25(2)		
	5.21(2)		
	5.24(2)		
	5.20(2)		
	5.21(2)		
	5.15(6)		

Table B21 continued.

0.02	4.06(2)
	4.08(2)
	4.05(2)
	4.00(2)
	4.15(2)
	4.10(2)
	4.15(2)
	4.02(2)
	4.08(6)
0.015	3.02(1)
	3.04(1)
	2.91(1)
	3.02(1)
	3.00(1)
	3.00(1)
	3.04(1)
	3.01(3)
0.01	1.986(9)
	1.94(1)
	1.99(1)
	1.99(1)
	1.96(1)
	1.97(2)

Table B21 continued.

0.005	0.90(1)
	0.95(1)
	0.90(1)
	0.95(1)
	0.97(1)
	0.98(1)
	0.94(1)
	0.93(1)
	0.93(2)
	0.93(2)
	0.94(4)

Table B22: Rate constants for the first reaction of *cis*-(S,S)-[PtCl(DMSO)(L1a)] with PPh_3 in dichloromethane. $\lambda = 380$ nm, $[Pt]_F = 0.5$ mM, $T = 25°C$.

$[PPh_3]$/ M	k_{obs}/ s^{-1}	k_y/ $M^{-1}s^{-1}$	k_s/ s^{-1}
0.025	7.80(1)	161(13)	1.0(2)
	4.92(10)		
	4.89(10)		
	4.87(16)		
0.02	4.13(10)		
	4.75(3)		
	3.92(5)		
	3.99(5)		
	5.25(4)		
	4.4(1)		
0.015	4.31(8)		
	3.70(3)		
	3.21(2)		
	3.32(3)		
	3.94(2)		
	3.70(10)		
0.01	1.93(1)		
	3.31(7)		
	2.48(2)		
	2.540(15)		
	2.47(2)		
	2.54(8)		

Table B22 continued.

0.005	2.13(1)
	1.60(1)
	1.83(2)
	1.52(1)
	1.65(2)
	1.94(2)
	1.78(3)

Table B23: Rate constants for the second reaction of *cis*-(S,S)-[PtCl(DMSO)(L1a)] with PPh_3 in methanol. λ = 400 nm, $[Pt]_F$ = 0.5 mM.

Temperature/ °C	$[PPh_3]$/ M	k_{obs}/ s^{-1}
25.1	0.025	0.370(1)
		0.371(1)
		0.372(1)
		0.369(1)
		0.371(1)
		0.370(1)
		0.370(3)
	0.02	0.358(2)
		0.3617(15)
		0.3659(15)
		0.362(1)
		0.363(1)
		0.362(3)
	0.015	0.366(1)
		0.3612(1)
		0.3588(15)
		0.358(1)
		0.359(1)
		0.361(2)
	0.01	0.343(1)
		0.347(1)
		0.3399(1)
		0.3347(9)
		0.340(1)
		0.342(2)

Table B23 continued.

0.005	0.3172(7)
	0.3042(8)
	0.3049(7)
	0.3043(6)
	0.3066(6)
	0.3055(6)
	0.307(2)
0.0025	0.1063(1)
	0.1084(1)
	0.0920(15)
	0.107(2)
	0.092(2)
	0.101(3)
0.00124	0.0662(7)
	0.0738(6)
	0.0673(7)
	0.0669(4)
	0.0627(5)
	0.0652(7)
	0.067(1)

Table B24: Rate constants for the second reaction of *cis*-(S,S)-[PtCl(DMSO)(L1a)] with PPh_3 in methanol. Chloride variation at constant $[PPh_3]$. λ = 400 nm, $[Pt]_F$ = 0.5 mM, T = 25°C.

$[PPh_3]$/ M	$[Cl^-]$/ M	k_{obs}/ s^{-1}
0.02	0.05	0.3504(9)
		0.360(1)
		0.3598(9)
		0.361(1)
		0.367(1)
		0.367(1)
		0.375(1)
		0.366(2)
	0.01	0.373(1)
		0.373(1)
		0.372(1)
		0.368(1)
		0.384(1)
		0.385(1)
		0.375(3)
0.01	0.05	0.3300(8)
		0.3330(7)
		0.3392(8)
		0.3343(7)
		0.3428(7)
		0.3454(8)
		0.3403(7)
		0.338(2)

Table B24 continued.

0.01	0.3548(10)
	0.3448(9)
	0.3403(8)
	0.3404(9)
	0.3394(10)
	0.3397(8)
	0.343(2)

Table B25: Rate constants for the second reaction of *cis*-(S,S)-[PtCl(DMSO)(L1a)] with PPh_3 in acetonitrile. $\lambda = 380$ nm, $[Pt]_F = 0.5$ mM, $T = 25.1$°C.

$[PPh_3]$/ M	k_{obs}/ s^{-1}
0.025	0.294(2)
	0.296(2)
	0.305(2)
	0.304(2)
	0.299(4)
0.02	0.248(1)
	0.247(1)
	0.249(1)
	0.238(1)
	0.235(1)
	0.243(2)
0.015	0.2140(8)
	0.2124(7)
	0.2121(8)
	0.2153(8)
	0.2114(7)
	0.213(2)
0.01	0.1401(7)
	0.1431(7)
	0.1380(7)
	0.1453(7)
	0.1432(7)
	0.142(1)

Table B25 continued.

0.005	0.0760(5)
	0.0667(5)
	0.0730(5)
	0.0725(5)
	0.0747(5)
	0.072(1)

Table B26: Rate constants for the second reaction of *cis*-(S,S)-[PtCl(DMSO)(L1a)] with PPh_3 in acetone. $\lambda = 390$ nm, $[Pt]_F = 0.5$ mM, $T = 25$°C.

$[PPh_3]$/ M	k_{obs}/ s^{-1}
0.1	0.3906(4)
	0.3934(4)
	0.3911(3)
	0.3997(5)
	0.3970(4)
	0.3995(4)
	0.395(1)
0.05	0.2500(1)
	0.2486(1)
	0.2475(2)
	0.2478(2)
	0.2449(2)
	0.2530(1)
	0.2558(1)
	0.2496(4)
0.025	0.1615(1)
	0.1641(1)
	0.1620(1)
	0.1611(1)
	0.1603(1)
	0.1618(2)

Table B26 continued.

0.02	0.1307(1)
	0.1319(1)
	0.1326(1)
	0.1334(1)
	0.1349(1)
	0.1358(1)
	0.1344(1)
	0.1336(1)
	0.1334(3)
0.015	0.1073(1)
	0.1056(1)
	0.1059(1)
	0.1062(1)
	0.1067(1)
	0.1076(1)
	0.1096(1)
	0.1070(2)
0.01	0.0798(1)
	0.0815(1)
	0.0815(1)
	0.08052(6)
	0.07881(6)
	0.07782(6)
	0.07791(6)
	0.07878(7)
	0.0796(2)

Table B26 continued.

0.005	0.04857(5)
	0.04779(5)
	0.04864(5)
	0.04905(4)
	0.04851(5)
	0.04768(4)
	0.0459(1)
	0.0451(1)
	0.0458(1)
	0.0474(2)

Table B27: Rate constants for the second reaction of *cis*-(S,S)-[PtCl(DMSO)(L1a)] with PPh_3 in dichloromethane. $\lambda = 380$ nm, $[Pt]_F = 0.5$ mM, $T = 25°C$.

$[PPh_3]$/ M	k_{obs}/ s^{-1}
0.1	0.183(1)
	0.199(1)
	0.177(1)
	0.179(1)
	0.180(1)
	0.187(1)
	0.184(3)
0.025	0.0536(4)
	0.0472(5)
	0.0484(4)
	0.0517(4)
	0.0487(4)
	0.0499(9)
0.02	0.0471(2)
	0.0433(3)
	0.0438(3)
	0.0371(4)
	0.0387(4)
	0.0420(7)
0.015	0.0330(3)
	0.0310(2)
	0.0319(2)
	0.0319(2)
	0.0319(5)

Table B27 continued.

0.01	0.0220(1)
	0.0198(1)
	0.0196(1)
	0.0201(1)
	0.0199(1)
	0.0203(3)
0.005	0.0146(2)
	0.0094(1)
	0.0118(1)
	0.0113(1)
	0.0118(3)

Table B28: Rate constants for the second reaction of *cis*-(S,P)-[PtCl(L1a)(PPh_3)] with PPh_3 in methanol. λ = 400 nm, $[Pt]_F$ = 0.25 mM, T = 25°C.

$[PPh_3]$/ M	k_{obs}/ s^{-1}
0.025	0.452(1)
	0.447(1)
	0.447(1)
	0.454(1)
	0.456(1)
	0.451(3)
0.02	0.435(1)
	0.448(1)
	0.445(1)
	0.445(1)
	0.446(1)
	0.450(1)
	0.448(1)
	0.458(1)
	0.447(4)
0.015	0.420(1)
	0.428(1)
	0.428(1)
	0.428(1)
	0.422(1)
	0.422(1)
	0.424(3)

Table B28 continued.

0.01	0.3897(5)
	0.4001(6)
	0.392(1)
	0.390(1)
	0.394(1)
	0.403(1)
	0.395(5)
0.005	0.2731(7)
	0.2772(7)
	0.2794(7)
	0.2794(8)
	0.2945(9)
	0.2973(9)
	0.283(2)

Table B29: Rate constants for the second reaction of *cis*-(S,S)-[PtCl(DMSO)(L1a)] with DMAP in methanol. λ = 380 nm, $[Pt]_F$ = 0.5 mM.

Temperature/ °C	[DMAP]/ M	k_{obs}/ 10^{-3} s^{-1}
25.0	0.3	5.788(5)
	0.1	3.25(15)
	0.075	2.9(1)
	0.05	2.42(7)
	0.025	1.6(1)
	0.01	0.63(3)
	0.005	0.32(2)